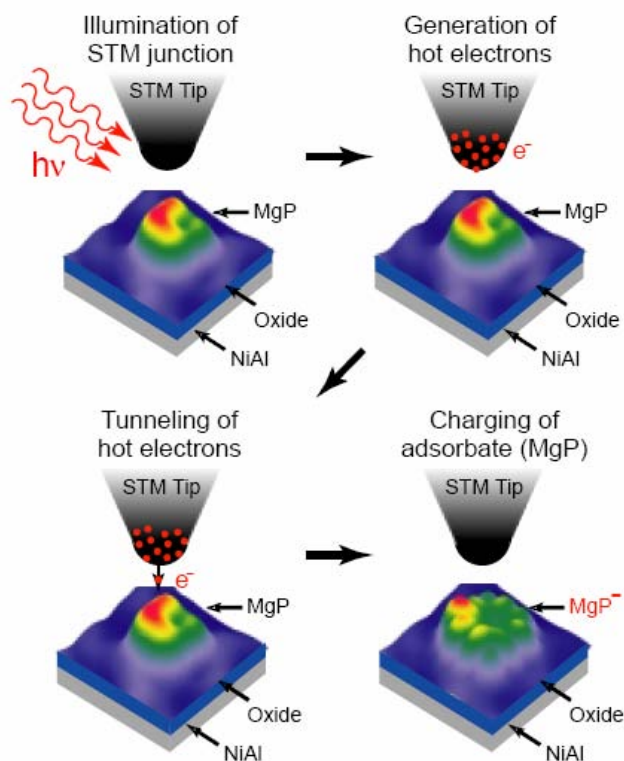
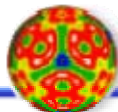


2006 Condensed Phase and Interfacial Molecular Science Research Meeting



Airlie Conference Center Warrenton,
Virginia October 22-25, 2006



Office of Basic Energy Sciences

Chemical Sciences, Geosciences & Biosciences Division

Cover

Sequential steps for photo-induced transfer of an electron to a single molecule of magnesium porphine adsorbed on a 5 Å thick Al₂O₃ grown on NiAl(110) substrate. To enable the experiment, the power of the laser is stabilized to 0.1% to avoid temperature drifts and fluctuations. The laser generates hot electrons in the tip. The excited electrons tunnel more efficiently due to the lower barrier. The negatively charged molecule (MgP⁻) is stabilized on the oxide surface. The atomic scale resolution is inherent in the mechanism of photo-induced tunneling, resonant in this case with the molecular orbital state.

Wilson Ho

Department of Physics & Astronomy and Department of Chemistry
University of California, Irvine

**This document was produced under contract number DE-AC05-06OR23100
between the U.S. Department of Energy and Oak Ridge Associated Universities.**

Foreword

This volume summarizes the scientific content of the 2006 Research Meeting on Condensed Phase and Interfacial Molecular Science (CPIMS) sponsored by the U. S. Department of Energy (DOE), Office of Basic Energy Sciences (BES). This marks the third meeting of CPIMS—the fourth of the regular Contractors' Meetings within the Fundamental Interactions Team.

In keeping with the notion that CPIMS makes connections across BES research programs based on common topical interests, one of the main themes of this year's meeting will be the molecular-level, detailed understanding of physics and chemistry relevant to solid-liquid interfaces in the environment. To emphasize the theme of interfacial environmental science, four investigators who are funded under the BES Geosciences Program will be featured on the agenda: James De Yoreo (Lawrence Livermore National Laboratory), Paul Fenter (Argonne National Laboratory), Dimitri Sverjensky (The Johns Hopkins University), and David Wesolowski (Oak Ridge National Laboratory). We hope that the blending of these external experts in geosciences with the CPIMS principal investigators who have expertise in surface and cluster science will provide an interesting and useful cross fertilization of ideas and concepts that benefits both groups.

The contributions of this year's speakers for their investment of time and for their willingness to share their ideas with the meeting participants are most gratefully acknowledged. Thanks also go to Nick Woodward for consultations regarding the Geosciences program, and to Frank Tully for advice in assembling the meeting agenda. Finally, this meeting would not be possible without the excellent logistical support it receives from Diane Marceau from our Division, Sophia Kitts from the Oak Ridge Institute of Science and Education, and the staff of the Airlie Conference Center.

Greg Fiechtner and Dick Hilderbrandt
Fundamental Interactions Team
Chemical Sciences, Geosciences and Biosciences Division
Office of Basic Energy Sciences
September 2006

Agenda

**U. S. Department of Energy
Office of Basic Energy Sciences
2006 Meeting on Condensed Phase and Interfacial Molecular Sciences**

Sunday, October 22

3:00-6:00 pm **** Registration ****
6:00 pm **** Reception at the Pub (No Host) ****
7:00 pm **** Dinner ****

Monday, October 23

7:00 am **** Breakfast ****
8:30 am *Introductory Remarks*
Greg Fiechtner, DOE Basic Energy Sciences

Session I *Chair: Mark Stockman, Georgia State University*

8:45 am *Nanoscale Kondo Physics and Nanomechanics of Metallic Systems from First Principles*

Emily A. Carter, Princeton University

9:15 am *Computational Nanophotonics: Modeling Optical Interactions and Transport in Tailored Nanosystem Architectures*

George C. Schatz, Northwestern University

9:45 am **** Break ****

10:15 am *Nanoscale Complexity at the Oxide-Water Interface*

David J. Wesolowski, Oak Ridge National Laboratory

10:45 am *Controlling the Growth Kinetics and Morphology of Crystal Surfaces Through Bio-molecular Interactions*

Jim J. De Yoreo, Lawrence Livermore National Laboratory

11:15 am *Direct Visualization of Structures and Processes at Mineral-Water Interfaces*

Paul Fenter, Argonne National Laboratory

12:15 pm **** Lunch ****

5:00 pm **** Reception on the Rooftop Terrace (No Host) ****

6:00 pm **** Dinner ****

Session II *Chair: Andrei Tokmakoff, Massachusetts Institute of Technology*

7:00 pm *Prediction of Inorganic and Organic Anionic Speciation at the Oxide-Electrolyte-Water Interface*

Dimitri A. Sverjensky, Johns Hopkins University

7:30 pm *Radiation Chemistry at Water Ceramic Oxide Interfaces*

Jay A. LaVerne, University of Notre Dame

8:00 pm *Ion Solvation in Nonuniform Aqueous Environments*

Phillip L. Geissler, Lawrence Berkeley Laboratory

Tuesday, October 24

7:00 am **** Breakfast ****

Session III Chair: **Lai-Sheng Wang**, *Pacific Northwest National Laboratory*

8:30 am *The Effect of Crystallization on the Proton Pump Function of Bacteriorhodopsin and New Studies on Nanomedicine*

Mostafa El-Sayed, *Georgia Tech*

9:00 am *Influence of Co-Solvents and Temperature on Nanoscale Self-Assembly of Biomaterials*

Teresa Head-Gordon, *Lawrence Berkeley Laboratory*

9:30 am *Fluctuations in Macromolecules Studied Using Time-Resolved, Multi-Spectral Single Molecule Imaging*

Carl Hayden, *Sandia National Laboratories*

10:00 am **** Break ****

10:30 am *Investigating Atoms to Aerosols with Vacuum Ultraviolet Radiation*

Musahid Ahmed, *Lawrence Berkeley Laboratory*

11:00 am *Spectroscopy of Organometallic Radicals*

Michael D. Morse, *University of Utah*

11:30 am *Electronic Structure of Transition Metal Clusters, and Actinide Complexes, and Their Reactivities*

Krishnan Balasubramanian, *California State University East Bay*

12:00 pm **** Lunch ****

Session IV Chair: **Ken Jordan**, *University of Pittsburgh*

4:30 pm *Molecular Theory & Modeling: Reactions of Ions and Radicals in Aqueous Systems*

Bruce C. Garrett, *Pacific Northwest National Laboratory*

5:00 pm *Computational Studies of Radiolytic Species and Processes in Water*

Daniel M. Chipman, *University of Notre Dame*

5:30 pm *First Principles Investigations: Spectroscopy and Reactions in Aqueous Systems*

Michel Dupuis, *Pacific Northwest National Laboratory*

6:15 pm **** Reception at the Pavilion (No Host) ****

7:00 pm **** Banquet Dinner at the Pavilion ****

Wednesday, October 25

- 7:00 am **** Breakfast ****
- Session V** Chair: **Michael D. Fayer**, *Stanford University*
- 8:30 am *Molecular Theory & Modeling: Nucleation in Solution*
Shawn M. Kathmann, *Pacific Northwest National Laboratory*
- 9:00 am *New Ultrafast Techniques for Electron Radiolysis Studies*
Robert A. Crowell, *Argonne National Laboratory*
- 9:30 am *Surface Chemical Dynamics*
Nicholas Camillone III, *Brookhaven National Laboratory*
- 10:00 am **** Break ****
- 10:15 am *Experimental and Computational Studies of Ultrafast Electronic Relaxation
and Charge Transfer in Molecular Systems of Importance to Chemistry*
Edward C. Lim, *The University of Akron*
- 10:45 am *Rapid Bond-Breaking and Bond Making in Radical Ions*
John R. Miller, *Brookhaven National Laboratory*
- 11:15 am *Closing Remarks*
Greg Fiechtner, DOE Basic Energy Sciences
- 11:45 pm **** Lunch ****
(Optional boxed lunches available)

Table of Contents

Invited Presentations (Ordered by Agenda)

Nanoscale Kondo Physics and Nanomechanics of Metallic Systems From First Principles
Emily A. Carter.....1

Computational Nanophotonics: Modeling Optical Interactions and Transport in Tailored Nanosystem Architectures
George C. Schatz.....5

Nanoscale Complexity at the Oxide-Water Interface
David J. Wesolowski.....8

Controlling the Growth Kinetics and Morphology of Crystal Surfaces Through Biomolecular Interactions
Jim J. De Yoreo.....9

Direct Visualization of Structures and Processes at Mineral-Water Interfaces
Paul Fenter10

Prediction of Inorganic and Organic Anionic Speciation at the Oxide-Electrolyte-Water Interface
Dimitri A. Sverjensky11

Radiation Chemistry at Water Ceramic Oxide Interfaces
Jay A. LaVerne.....12

Ion Solvation in Nonuniform Aqueous Environments
Phillip L. Geissler.....16

The Effect of Crystallization on the Proton Pump Function of Bacteriorhodopsin and New Studies on Nanomedicine
Mostafa El-Sayed18

Influence of Co-Solvents and Temperature on Nanoscale Self-Assembly of Biomaterials
Teresa Head-Gordon22

Fluctuations in Macromolecules Studied Using Time-Resolved, Multi-Spectral Single Molecule Imaging
Carl Hayden26

Investigating Atoms to Aerosols With Vacuum Ultraviolet Radiation
Musahid Ahmed.....30

Spectroscopy of Organometallic Radicals
Michael D. Morse.....34

<i>Electronic Structure of Transition Metal Clusters, and Actinide Complexes, and Their Reactivities</i> Krishnan Balasubramanian	38
<i>Molecular Theory & Modeling: Reactions of Ions and Radicals in Aqueous Systems</i> Bruce C. Garrett	42
<i>Computational Studies of Radiolytic Species and Processes in Water</i> Daniel M. Chipman	46
<i>First Principles Investigations: Spectroscopy and Reactions in Aqueous Systems</i> Michel Dupuis	50
<i>Molecular Theory & Modeling: Nucleation in Solution</i> Shawn M. Kathmann	52
<i>New Ultrafast Techniques for Electron Radiolysis Studies</i> Robert A. Crowell	56
<i>Surface Chemical Dynamics</i> Nicholas Camillone III	60
<i>Experimental and Computational Studies of Ultrafast Electronic Relaxation and Charge Transfer in Molecular Systems of Importance to Chemistry</i> Edward C. Lim	64
<i>Rapid Bond-Breaking and Bond Making in Radical Ion</i> John R. Miller	68
Research Summaries (Alphabetically by First PI)	
<i>Model Catalysis by Size-Selected Cluster Deposition</i> Scott Anderson ,	72
<i>Thermochemistry and Reactivity of Transition Metal Clusters and Their Oxides</i> Peter B. Armentrout	76
<i>Role of Solvent: Reactions in Supercritical Fluids</i> David M. Bartels	80

<i>Clusters: Unraveling Fundamental Oxygen Transfer Reaction Mechanisms Effected by Heterogeneous Catalysts</i> A. W. Castleman, Jr.	84
<i>An Exploration of Catalytic Chemistry on Au/Ni(111)</i> Syvia T. Ceyer	88
<i>Theory of Dynamics in Complex Systems</i> David Chandler	91
<i>Excited States of Benzoquinone Radical Anion, New Ultrafast Single-Shot Detection at LEAF, and Non-Exponential Charge Capture.</i> Andrew R. Cook	93
<i>Chemical Kinetics and Dynamics at Interfaces</i> James P. Cowin	97
<i>Computational Studies of Liquid Interfaces</i> Liem X. Dang	101
<i>Infrared Spectroscopy of Transition Metal-Molecular Interactions in the Gas Phase</i> Michael A. Duncan	106
<i>Photochemistry at Interfaces</i> Kenneth B. Eisenthal	110
<i>Interfacial Oxidation of Complex Organic Molecules</i> G. Barney Ellison	114
<i>Modeling of Cooperative Phenomena in Surface Reaction Processes</i> Jim Evans	116
<i>Liquid and Chemical Dynamics in Nanoscopic Environments</i> Michael D. Fayer	120
<i>Electronic Structure Theory: Surface Chemistry, Solvent Effects, and Catalysis</i> Mark S. Gordon	124
<i>Computational Nanophotonics: Modeling Optical Interactions and Transport in Tailored Nanosystem Architectures</i> Stephen K. Gray	128
<i>Dynamics of Electrons at Interfaces on Ultrafast Timescales</i> Charles B. Harris	135

<i>Catalysis at Metal Surfaces Studied by Non-Equilibrium and STM Methods</i> Ian Harrison	139
<i>Electronic Structure and Optical Response of Nanostructures</i> Martin Head-Gordon	143
<i>Chemical Kinetics and Dynamics at Interfaces</i> Wayne P. Hess	147
<i>Optical Spectroscopy at the Spatial Limit</i> Wilson Ho	151
<i>Theory of the Reaction Dynamics of Small Molecules on Metal Surfaces</i> Bret E. Jackson	155
<i>Understanding the Electron-Water Interaction at the Molecular Level: Integrating Theory and Experiment in the Cluster Regime</i> Kenneth D. Jordan and Mark A. Johnson	159
<i>Chemical Kinetics and Dynamics at Interfaces: Structure and Reactivity of Ices, Oxides, and Amorphous Materials</i> Bruce D. Kay	163
<i>Chemical Kinetics and Dynamics at Interfaces: Non-Thermal Reactions at Surfaces and Interfaces</i> Greg A. Kimmel	167
<i>Single-Molecule Kinetics and Dynamics in the Condensed Phase and at Interfaces</i> H. Peter Lu	171
<i>Reactivity of Nitrogen Oxides, Oxoacids, and Oxoanions in Aqueous Solution</i> Sergei V. Lymar	175
<i>Metallic Nanoparticles Under Irradiation</i> Dan Meisel	179
<i>Laser Dynamic Studies of Photoreactions on Single-Crystal and Nanostructured Surfaces</i> Richard Osgood	182
<i>Optical Manipulation of Ultrafast Electron and Nuclear Motion on Metal Surfaces</i> Hrvoje Petek	186
<i>X-Ray Spectroscopy of Volatile Liquids and their Surfaces</i> Richard J. Saykally	190
<i>Molecular Theory & Modeling Development of Statistical Mechanical Techniques for Complex Condensed-Phase Systems</i> Gregory K. Schenter	194

<i>Reactive Intermediates in High Energy Chemistry</i> Ilya A. Shkrob	198
<i>Generation, Detection and Characterization of Gas-Phase Transition Metal Containing Molecules</i> Timothy C. Steimle	202
<i>Computational Nanophotonics: Model Optical Interactions and Transport in Tailored Nanosystem Architectures</i> Mark Stockman	206
<i>Understanding Nanoscale Confinement Effects in Solvent-Driven Chemical Reactions</i> Ward H. Thompson	210
<i>Structural Dynamics in Complex Liquids Studied with Multidimensional Vibrational Spectroscopy</i> Andrei Tokmakoff	214
<i>The Role of Electronic Excitations on Chemical Reaction Dynamics at Metal, Semiconductor and Nanoparticle Surfaces</i> John C. Tully	218
<i>Chemical Kinetics and Dynamics at Interfaces</i> Lai-Sheng Wang	222
<i>Ionic Liquids: Radiation Chemistry, Solvation Dynamics and Reactivity Patterns</i> James F. Wishart	226
<i>Electronically Non-Adiabatic Interactions at the Gas-Solid Interface</i> Alec M. Wodtke	230
<i>Molecular Theory & Modeling Structural and Thermodynamic Properties of Liquid Water and Ice</i> Sotiris S. Xantheas	231
<i>Experimental and Theoretical Studies of Conformational Dynamics of Proteins and Nonequilibrium Steady State of Biochemical Reactions</i> Sunney Xie	235

Invited Presentations
(ordered by agenda)

Nanoscale Kondo Physics and Nanomechanics of Metallic Systems from First Principles

Patrick Huang, Gregory S. Ho, Vincent Lignères, and Emily A. Carter
*Department of Mechanical and Aerospace Engineering and Program in Applied and
Computational Mathematics, Princeton University, Princeton, NJ 08544-5263*

Kohn-Sham density functional theory (DFT) is a powerful, well-established tool for the study of condensed phase electronic structure. However, there are still a number of situations where its applicability is limited. The basic theme of our research is the development of first principles electronic structure approaches for condensed matter that goes beyond what can currently be done with standard implementations of Kohn-Sham DFT. Our efforts to this end have focused on two classes of methods. The first addresses the well-known inability of DFT to handle strong, many-body electron correlation effects. Our approach is a DFT-based embedding theory, to treat localized features (e.g. impurity, adsorbate, vacancy, etc.) embedded in a periodic, metallic crystal. A description for the embedded region is provided by explicitly correlated, ab initio wave function methods. DFT, as a formally ground state theory, does not give a good description of excited states; an additional feature of our approach is the ability to obtain excitations localized in this region. We apply our method to a first-principles study of the adsorption of a single magnetic Co adatom on non-magnetic Cu(111), a known Kondo system whose behavior is governed by strong electron correlation.

The second class of methods that we are developing is an orbital-free density functional theory (OFDFT), which addresses the speed limitations of Kohn-Sham DFT. OFDFT is a powerful, $O(N)$ scaling method for electronic structure calculations.^{1,2,3} Unlike Kohn-Sham DFT, OFDFT goes back to the original Hohenberg-Kohn idea of directly optimizing an energy functional which is an *explicit* functional of the density, without invoking an orbital description. This eliminates the need to manipulate orbitals, which leads to $O(N^3)$ scaling in the Kohn-Sham approach. The speed of OFDFT allows direct electronic structure calculations on large systems on the order of thousands to tens of thousands of atoms, an expensive feat within Kohn-Sham. Due to our incomplete knowledge of the exact, universal energy density functional, this speedup comes at the cost of some accuracy with respect to Kohn-Sham methods. However, OFDFT has been shown to be remarkably accurate with respect to Kohn-Sham when used in the study of nearly-free-electron-like metals, e.g., Al, for which good density functionals have been derived. Examples of past applications of OFDFT include the prediction of properties of bulk crystals, surfaces, vacancies, vacancy clusters, nanoclusters, and dislocations, as well as OFDFT-based multiscale simulations of nanoindentation in Al and Al-Mg alloys.^{2,4,5,6,7,8,9}

Localized electron correlation in metals: application to the many-body Kondo state

We have been advancing a density-based embedding theory developed in our group, whose goal is to provide an accurate description of localized features embedded in periodic, metallic crystals.¹⁰ The procedure begins with a plane-wave, Kohn-Sham DFT calculation for the total periodic system, to obtain the total density ρ_{tot} . This quantity is then partitioned as $\rho_{\text{tot}} = \rho_I + \rho_{\text{II}}$, where ρ_I and ρ_{II} are the embedded region and the background densities, respectively. The embedded region is chosen as a finite cluster containing the inhomogeneity of interest and a few surrounding atoms from the host, and should be large enough to capture the essential physics.

The problem is recast as a cluster in the presence of an effective, one-electron embedding potential v_{emb} , whose role is to represent the periodic, metallic background. We employ a DFT model for the potential v_{emb} , which is regarded as a functional of the total system and cluster densities, i.e.

$$v_{\text{emb}}[\rho_{\text{tot}}, \rho_I] = (v_{\text{Ts}}[\rho_{\text{tot}}] - v_{\text{Ts}}[\rho_I]) + (v_{\text{J}}[\rho_{\text{tot}}] - v_{\text{J}}[\rho_I]) + (v_{\text{xc}}[\rho_{\text{tot}}] - v_{\text{xc}}[\rho_I]) + v_{\text{ion}}^{\text{II}}.$$

Here, v_{Ts} , v_{J} , and v_{xc} denote the kinetic, Hartree, and exchange-correlation potentials, respectively, and $v_{\text{ion}}^{\text{II}}$ is the electron-ion potential due to the background region ions. In general, the exact form for v_{Ts} and

ν_{xc} are not known; well-known local models (Thomas-Fermi λ -von Weizsäcker for ν_{Ts} , the local density approximation for ν_{xc}) are employed in this work. The embedded cluster problem can now be treated with the standard hierarchy of ab initio quantum chemistry methods that explicitly include electron correlation. For a given choice of ab initio theory, ρ_I and $\nu_{emb}[\rho_{tot}, \rho_I]$ are solved self-consistently, and localized excitations are subsequently evaluated in the presence of this converged ν_{emb} .

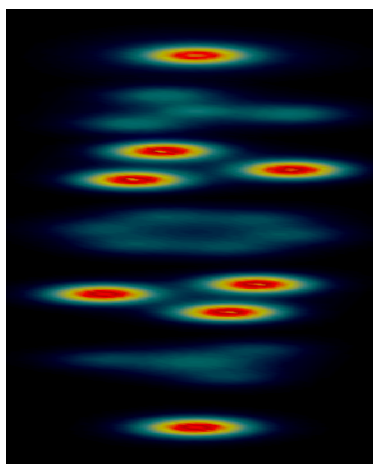
We have made important advances in the embedding methodology, allowing for the treatment of non-trivial, realistic systems. The first is the consistent incorporation of ultrasoft pseudopotentials to represent the relatively inert core electrons in transition metals. Previous implementations of the embedding theory relied solely on norm-conserving potentials. The ultrasoft formulation significantly reduces the computational expense in the plane-wave Kohn-Sham DFT calculations;¹¹ however, non-standard modifications in the ultrasoft potentials were necessary to ensure consistency in the embedding. The net gain is the capability to treat transition metal systems, at a more reasonable cost in the plane-wave calculations. A second advance was made in the self-consistent search for the embedded cluster density ρ_I and embedding potential $\nu_{emb}[\rho_{tot}, \rho_I]$. Our early work with the embedding encountered difficulties due to numerical divergences in the von Weizsäcker functional, and thus the kinetic energy contributions ν_{Ts} were frozen at some initial value. We now have a new strategy for the self-consistent search, which begins with an estimate for the background density ρ_{II} . This ρ_{II} is frozen in the embedding model, consistent with the notion that the background should be relatively inert. At each iteration of the self-consistent search, a new total density ρ_{tot}' is evaluated as $\rho_{tot}' = \rho_I' + \rho_{II}$, and the embedding potential is updated as $\nu_{emb} = \nu_{emb}[\rho_{tot}', \rho_I']$. This leads to a larger local cancellation of errors in the potential, and a more numerically stable procedure. In our current work, *all* terms in the embedding potential are allowed to update, leading to a fully self-consistent ν_{emb} .

A challenging application of the embedding methodology is the long-standing Kondo problem. The prototypical Kondo system consists of localized a magnetic impurity in a non-magnetic, metallic environment. At a material-dependent temperature T_K , an anomalous minimum in the resistivity is observed. In the Kondo picture, below T_K the conduction electrons of the host are thought to align their spins against the impurity moment, leading to an extended, open-shell singlet. The effect is thought to arise from strong many-body correlations involving the impurity moment and the conduction electrons, which is not correctly described by DFT with its approximate mean-field exchange-correlation.

Scanning tunneling microscopy (STM) experiments in 1998 reported the first direct probe of the Kondo state due to a *single* impurity moment. These experiments examined a single magnetic adatom on the (111) surface of a non-magnetic metal [Co on Au(111) and Ce on Ag(111)], and subsequent work have also explored various combinations of first-row magnetic transition metals on the (111) and (001) cuts of Cu, Ag, and Au. The STM signature ascribed to the Kondo state was found to be localized within $\sim 10 - 60 \text{ \AA}$ of the magnetic adatom.

Up until now, our understanding of Kondo physics derives primarily from simple model Hamiltonians, i.e. the Anderson impurity model, which includes a few select interactions characterized by adjustable parameters. However, the STM experiments have opened up a whole new set of questions regarding this old problem. Given the ability to experimentally probe the Kondo state on atomic length scales, the first question that arises is: what is the detailed electronic structure of the Kondo singlet? Next, what is the nature of the low-lying excitations? How is this affected by variations in the local chemical environment? What is the role, if any, of surface states?

We have applied the embedded CI theory to examine a single Co adatom on Cu(111).¹² Correlation effects in the embedded cluster were explicitly treated using multireference single and double excitation configuration interaction (MRSDCI) theory, with the embedding theory yielding the correct singlet ground state. Note that no spin compensation is observed in a standard application of Kohn-Sham DFT, exhibiting the qualitative failure of DFT noted above. Analysis of the embedded CI ground state wave function indicates that the quenching of the Co moment is due to the formation of metal-metal bonds between Co and the neighboring Cu ions. The usual Anderson model approach does not allow for strong hybridization, i.e. bond formation, between the impurity state and conduction states, whereas our first-principles approach fully accounts for all local interactions. Thus, our work provides an alternative, chemical interpretation on the nature of the Kondo ground state.



Many-body singlet ground state electron density of the embedded CoCu_7 cluster. Red denotes region of high density, corresponding to localized d-electrons, and blue denotes low density regions associated with metal s-electrons. Density cuts are taken along planes parallel to the $\text{Cu}(111)$ surface, starting with the top plane passing through the Co adatom.

Future work on the Kondo problem will explore how the Co d-orbital occupations vary with changes in the local chemical environment. The lineshape of the STM Kondo resonance is due to two interfering tunneling pathways between the STM tip and 1) the localized Co d-state, and 2) the host conduction states. The experiments reveal qualitative differences in the tunneling spectra of Co on $\text{Cu}(111)$ versus $\text{Cu}(001)$, which was attributed to the different relative probabilities of the two pathways. In addition, an increase in the Kondo temperature T_K was seen in going from the (111) to (001) cut (from 54 K to 88 K). A first-principles estimate for the Co d-orbital populations would tell us whether it is reasonable to expect tunneling onto the Co d-levels, and a comparison of the excited states would provide insight into the scaling in T_K .

Development of new OFDFT code and application to nanowires

We have developed a second generation code to perform electronic structure calculations within the OFDFT formalism. This new code is capable of optimizing electron density, ion coordinates, and cell lattice vectors. In addition, this code is capable of finding transition state pathways using the Climbing-Image Nudged Elastic Band method.

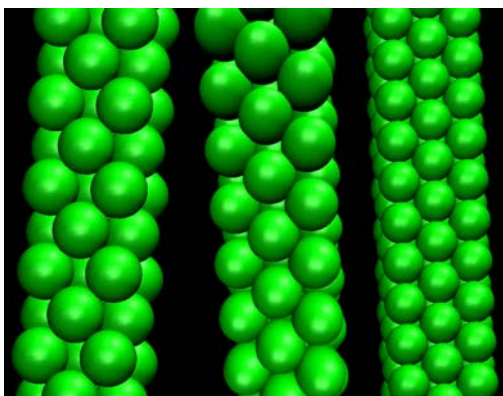
An important new aspect of this code is the ability to handle a variety of boundary conditions. Within fully periodic boundary conditions, we have implemented the Thomas-Fermi (TF), von Weizsäcker (VW), Wang-Teter (WT) and the Wang-Govind-Carter (WGC) kinetic energy functionals.^{1,2} The WGC is the most complicated, but also the most accurate OFDFT kinetic energy functional available today. Both the GGA-PBE and LDA exchange-correlation functionals are available within periodic boundary conditions.

Within free-space (aperiodic) boundary conditions, we have implemented the TF, VW, and WT kinetic energy functionals, along with the LDA exchange-correlation functional. Implementation of the WT functional presented special challenges, since the form of the response kernel is known only in reciprocal space. The WT kernel had to be decomposed into a term short-ranged in q -space, which is obtained in real-space via a Hankel transform, and a term long-ranged in q -space, which is transformed analytically.¹³ Once the kernel is available in real-space, the WT energy is then obtained using a fast Fourier transform to perform a real-space convolution.

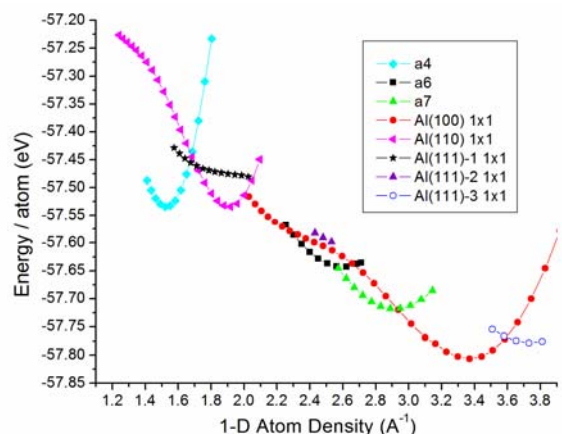
Fast algorithms to minimize the energy with respect to the electron density are critical for a useful code. We have therefore added a variety of minimization algorithms. The most useful algorithms include a nonlinear conjugate gradient algorithm, a Hessian-free truncated Newton algorithm, and a multigrid (FMG-FAS) algorithm. Previously, we have been minimizing with respect to the electron density; a major advance this year was to move to using the absolute value of the square root of the density as the relevant minimization variable, making the minimization much more stable and efficient. In addition, we are currently examining the use of other possible variables, such as the logarithm of the density.

We are now using our new OFDFT code to study properties of Al nanowires. Such wires are of interest because of their potential use in polarizing grids, biosensors, molecular electronics, and fuel cells.

Recently, Gulseren et al. [Phys. Rev. Lett. **80**, 3775 (1998)] used empirical potential molecular dynamics (EPMD) to propose exotic, noncrystalline, stable atomic structures in ultrathin Al nanowires for wire radii below a critical value, which they proposed to be on the order of a few atomic spacings. Makita et al. [J. Chem. Phys. **119**, 538 (2003)] later performed Kohn-Sham DFT calculations to examine the stability and properties of seven of the smallest of those exotic structures, and proposed that one such structure could be used to create a nanoscale fuel cell. We are in the process of comparing OFDFT and KS-DFT results for the ultrathin nanowire structures examined by Makita et al. in order to verify the accuracy of OFDFT in this context. We then will move on to examine the larger exotic structures proposed by EPMD, which OFDFT can easily calculate while KS-DFT cannot, in order to develop a more complete phase diagram of aluminum nanowires as a function of wire diameter, as well as uniaxial expansion and compression.



Left: [100]-oriented aluminum nanowire under 10% uniaxial tension. **Right:** Identical nanowire subject to 34% compression undergoes a phase transition to a close-packed surface structure; phase transition onset occurs at 18% compression (**middle**).



Energy per atom as a function of atomic density along the wire for various possible wire structures calculated via OFDFT. Structure labels are consistent with Gulseren et al. Phase transitions are predicted to occur as the wire is compressed and expanded.

Lastly, we are improving several aspects of the second generation code. The entire code is being parallelized, allowing for the distribution of memory to multiple nodes, so that nanosystems with more than 10,000 atoms will be accessible to study with OFDFT. Also, to reduce unwanted image effects, we would like to study nanowires with free space, or even mixed boundary conditions. This requires work in two directions: first, mixed boundary conditions must be allowed for, which presents its own set of unique challenges. Second, the more accurate but also more complex WGC kinetic energy functional must be implemented within these conditions. We also may implement local refinement within the multigrid minimizer, to improve accuracy in regions of interest.

¹ Y. A. Wang, N. Govind, and E. A. Carter, Phys. Rev. B **58**, 13465 (1998).

² Y. A. Wang, N. Govind, and E. A. Carter, Phys. Rev. B **60**, 16350 (1999).

³ V. Lignères and E. A. Carter, in *Handbook of Materials Modeling*, S. Yip (Ed.) p.137-148, (2005); Y. A. Wang and E. A. Carter, in “Theoretical Methods in Condensed Phase Chemistry,” S. D. Schwartz, Ed., within the series “Progress in Theoretical Chemistry and Physics,” Kluwer, 117-84 (2000).

⁴ S. C. Watson and E. A. Carter, Comp. Phys. Comm. **128**, 67 (2000).

⁵ G. S. Ho, M. T. Ong, K. J. Caspersen, and E. A. Carter, to be submitted.

⁶ N. Choly, G. Lu, W. E, and E. Kaxiras, Phys. Rev. B **71**, 094101 (2005).

⁷ R. L. Hayes, G. S. Ho, M. Ortiz, and E. A. Carter, Phil. Mag. **86**, 2343 (2006).

⁸ R. L. Hayes, M. Fago, M. Ortiz, and E. A. Carter, Multiscale Mod. Sim. **4** 359 (2005).

⁹ M. Fago, R. L. Hayes, E. A. Carter, and M. Ortiz, Phys. Rev. B **70**, 100102(R) (2004).

¹⁰ P. Huang and E. A. Carter, J. Chem. Phys. **125**, 084102 (2006).

¹¹ V. Cocula, C. J. Pickard, and E. A. Carter, J. Chem. Phys., **123**, 214101 (2005).

¹² P. Huang and E. A. Carter, Nano Lett. **6**, 1146 (2006), cover article.

¹³ C.J. García-Cervera, Comm. Comp. Phys., submitted (2006).

Computational nanophotonics: modeling optical interactions and transport in tailored nanosystem architectures

George C. Schatz and Mark A. Ratner
Department of Chemistry
Northwestern University
Evanston, IL 60208-3113
schatz@chem.northwestern.edu
ratner@chem.northwestern.edu

Research by Schatz and Ratner is concerned with the interaction of light with noble metal nanoparticles, with arrays of nanoparticles, with metal films that contain nanosize holes and with nanoparticles and holes that occur in electronic devices. The goal of this project is to develop theory and computational methods that enable a quantitative description of these particle/hole systems and, from this, understanding of the physical phenomena that are taking place, including the description of experiments being done by our collaborators. We expect to use the methods developed in this research to aid in the design of new classes of particle/hole devices that will be of use in electronics and optics. Also, we are developing methods that combine quantum descriptions of the optical response of parts of system of interest with continuum electrostatics for the rest.

Recent Progress

Our work in this project has been divided between two kinds of computational electrostatics theory: the discrete dipole approximation (DDA) and the finite difference time domain (FDTD) method. DDA is a frequency domain method while FDTD is a time domain method. Both methods provide the ability to describe light interacting with particles or holes with dimensions up to microns, and with or without periodic boundary conditions. The methods have overlapping capabilities, but in specific applications it is often the case that one will be more convenient or more accurate. Also, we are developing an interface between classical electrostatics and quantum chemistry so that we can study the coupling of molecules to enhanced electromagnetic fields on metal particle surfaces.

Our DDA applications have been concerned with triangular prisms, cubes and other anisotropic nanoparticle structures. Previously we teamed up with the Mirkin group at Northwestern to study gold triangular prisms that they have synthesized with wet chemistry methods, leading to the first observation of quadrupole resonance effects for this particle shape. In addition, we characterized the properties of higher multipole resonances for this particle shape. More recently we have studied pyramid-shaped gold particles that the Odom group has fabricated using a soft lithography approach. These are relatively large particles, so there are complex multipolar excitations, but the calculated results are in good qualitative agreement with experiment. A unique contribution from this work has been the characterization of the wave vector dependence of the plasmon resonance wavelength of one of the quadrupolar resonances, which is something that has not been done before for localized surface plasmon resonances.

With the FDTD method we have been studying the interaction of light with holes in metal films, including the contrast between plasmon excitation in particles versus holes, and the influence of

plasmon excitation on the transmission of light through the holes. For isolated holes we have demonstrated plasmon enhanced transmission, however the enhancement effects from these studies are quite modest (factors of $<10\%$). Larger enhancements (transmissions of 4) are obtained when each hole is surrounded by circular grooves, or is in an array with the appropriate spacing. We have also characterized SERS enhancement factors, which we find to be similar in size to that for a sphere ($|E|^2 \sim 10^2$) for isolated holes, and larger ($|E|^2 \sim 10^3$) for holes surrounded by optimal grooves. The large values are such that nonresonant SERS measurements should be possible.

We are continuing our study of the forces acting on metallic nanoparticles interacting with strong radiation fields. There are significant issues here both at the fundamental level (the relative importance of the three terms that act on the particles, arising from different terms in the Maxwell equations, the importance of conservative and nonconservative forces, and the magnitudes and directions of the forces on two neighboring nanoparticles) and for applications (how can these radiation forces be used to form particular geometric patterns). This is a new direction in the group, but one paper was published this year that was concerned with fundamental issues about how radiation forces are defined.

Future Plans

Continuing our work with the Odom group concerning the gold pyramids, we have identified a new type of plasmon resonance mode that involves a magnetic dipole transition moment. We are now working to identify this mode in the experiments. Our work on the hole structures has shifted to studying the effect of a dielectric substrate on the plasmon wavelengths and SERS enhancements.

We are developing a new 2D FDTD code that uses hexagonal grid elements. This code is superior in its convergence properties to the equivalent square grid code, so we hope to use this to characterize “hard” problems, such as particles with sharp points and very large ($>1 \mu\text{m}$) structures. We are also developing 2D and 3D finite element-based codes.

We have initiated a study of nonlinear optical phenomena associated with metal nanoparticles. Initial activity in this area has been concerned with metal nanoparticles that are embedded in a Kerr nonlinear medium. Additional nonlinear optical properties such as second harmonic generation for metal particles will be examined.

The work on forces arising from the radiative interactions will be extended to deal with molecule/metal conjugates, specifically to investigate that possible formation of geometries in which or earlier studies indicate that single-molecule Raman spectra might be observable.

Finally, we continue to develop methods in which electrodynamics methods are combined with quantum mechanics to model enhanced infrared, Raman and nonlinear optical scattering processes.

Publications

- Surface plasmons at single nanoholes in Au-films. L. Yin, V. K. Vlasko-Vlasov, A. Rydh, J. Pearson, U. Welp, S. -H. Chang, S. K. Gray, G. C. Schatz, D. E. Brown, C. W. Kimball, *Applied Phys. Lett.* 85 467-469 (2004).
- Near-field photochemical imaging of noble metal nanostructures, C. Hubert. A. Romyantseva, G. Lerondel, J. Grand, S. Kostcheev, A. Vial, R. Bachelot, P. Royer, S. -H. Chang, S. K. Gray, G. P. Wiederrecht, and G. C. Schatz, *Science, Nano Letters*, 5, 615-19 2005.
- Observation of the Quadrupole Plasmon Mode for a Colloidal Solution of Gold Nanoprisms, J. E. Millstone, S. Park, K. L. Shuford, L. Qin, G. C. Schatz and C. A. Mirkin, *J. Am. Chem. Soc.*, 127, 5312-5313 (2005).
- Surface plasmon generation and light transmission by isolated nanoholes and arrays of nanoholes in thin metal films, S-H. Chang, S. K. Gray and G. C. Schatz, *Optics Express*, 13, 3150-65 (2005).
- Electrodynamics simulations of surface plasmon behavior in metallic nanostructures, S. K. Gray. T. -W. Lee, S. -H. Chang and G. C. Schatz, *SPIE Proceedings (Plasmonics: Metallic Nanostructures and Their Optical Properties III)* Ed. M. I. Stockman, 5927, 96-101 (2005)
- Multipolar Excitation in Triangular Nanoprisms, Kevin L. Shuford, Mark. A. Ratner and George C. Schatz, *J. Chem. Phys.*, 123(11), 114713/1-114713/9 (2005).
- Surface Plasmon Standing Waves in Large-Area Subwavelength Hole Arrays, Eun-Soo Kwak, Joel Henzie, Shih-Hui Chang, Stephen K. Gray, George C. Schatz, and Teri W. Odom, *Nano Letters*, 5(10), 1963-1967 (2005).
- Multipole plasmon resonances in gold nanorods, Emma K. Payne, Kevin L. Shuford, Sungho Park, George C. Schatz and Chad A. Mirkin, *J. Phys. Chem. B* 110(5), 2150-2154. (2006).
- Finite-difference time-domain studies of light transmission through nanohole structures, K. L. Shuford, Mark A. Ratner, Stephen K. Gray and George C. Schatz, *Appl. Phys. B*, 84, 11-18 (2006).
- Electric Field Enhancement and Light Transmission in Cylindrical Nanoholes, Kevin Shuford, Mark A. Ratner, Stephen K. Gray, and George C. Schatz, *Journal of Computational and Theoretical Nanoscience*, in press (2006).
- Manipulating the optical properties of pyramidal nanoparticle arrays, J. Henzie, K. L. Shuford, E. -S. Kwak, G. C. Schatz and T. W. Odom, *J. Phys. Chem. B* 110, 14028-31 (2006).
- Gradient and nongradient contributions to plasmon-enhanced optical forces on silver nanoparticles, Vance Wong and Mark. A. Ratner, *Phys. Rev. B*, 73, 075416/1-/6 (2006).
- Ultrafast pulse excitation of a metallic nanosystem containing a Kerr nonlinear material, X. Yang, G. C. Schatz and Stephen K. Gray, *Phys. Rev. B*, submitted (2006).

Nanoscale Complexity at the Oxide-Water Interface

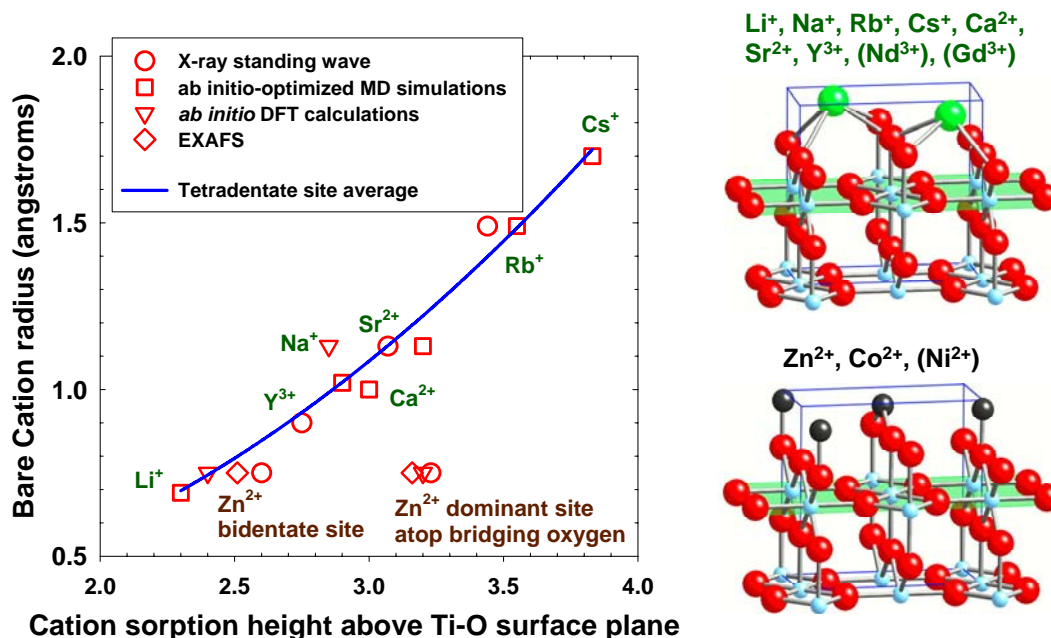
David J. Wesolowski

Oak Ridge National Laboratory, P.O. Box 2008, Oak Ridge, TN 37831-6110

Phone: 865-574-6903; Email: wesolowskid@ornl.gov

Abstract: Phenomena occurring at solid-solution interfaces are central to understanding a wide range of industrial and subsurface geological processes, including contaminant transport, mineral dissolution/precipitation rates, nanomaterials synthesis and self-assembly, corrosion, nutrient bioavailability and fluid-mediated biological processes. This talk summarizes a highly-integrated team effort involving scientists at ORNL, Argonne National Lab, Penn State, Vanderbilt, the University of Illinois and international collaborators. The approaches employed include: 1.) Unique high temperature pH monitoring and microelectrophoresis instrumentation that permit determination of the proton-induced surface charge and zeta potential, and the pH-dependent sorption of dissolved ions on nanoparticle and macroscopic powder suspensions at temperatures of 10-290°C and pressures up to several hundred atmospheres; 2.) Synchrotron X-ray standing wave (XSW), crystal-truncation-rod (CTR) and absorption fine structure (EXAFS) studies of the detailed structure of the interfacial region at sub-angstrom resolution; 3.) Neutron small angle (SANS) and quasi-elastic scattering (QENS) studies of interfacial structure and dynamics at nanoparticle surfaces; 4.) *ab initio* molecular dynamics (AIMD), density functional theory (DFT), classical molecular dynamics simulations (MD) and macroscopic bond-valence calculations of interfacial structure, dynamics and ion adsorption affinities. All of these approaches are being fully integrated and applied in detailed studies of idealized systems, such as the (110) crystallographic surfaces of the isostructural minerals rutile (α -TiO₂) and cassiterite (SnO₂), which have surprisingly-different surface chemistries. The figure below is an example of the excellent agreement obtained among various X-ray and computational determinations of the structure of sorbed ions on the rutile (110) surface at room temperature.

Remarkable agreement between *ab initio*-optimized MD Simulations and 3-D X-ray imaging of ion sorption sites and water structure at the interface between TiO₂ (rutile) surfaces and aqueous solutions points the way toward fundamental understanding of ion and particulate migration



Controlling the Growth Kinetics and Morphology of Crystal Surfaces through Bio-molecular Interactions

ABSTRACT

2006 Meeting on Condensed Phase and Interfacial Molecular Science (CPIMS)
October 22-25, 2006, Warrenton, Virginia

Jim J. De Yoreo, Roger Qiu, Jonathan R.I. Lee, Yong Han
Lawrence Livermore National Laboratory, Livermore, California

Patricia Dove, Selim Elhadj, Dongbo Wang, Virginia Tech, Blacksburg, Virginia
Dan Morse, Germaine Fu, University of California at Santa Barbara, Santa Barbara, California
Andrzej Wierzbicki, Alan Salter, South Alabama University, Mobile, Alabama

The complex shapes and hierarchical designs of bio-mineralized nanostructures arise from bio-molecular controls over crystallization. One prevailing view is that mineral-associated macromolecules are responsible for nucleating and stabilizing non-equilibrium polymorphs and morphologies through interactions at crystal surfaces. But, a quantitative picture of molecular interactions between modifiers and crystal surfaces and the changes in growth mechanism induced by those interactions has been lacking. Here we report results of *in situ* AFM, X-ray absorption, and molecular modeling investigations of calcite nucleation and growth in the presence of acidic amino acids, polypeptides, and proteins associated with bio-mineral formation. We find that small molecules, organic modifiers, and proteins exhibit a wide range of control mechanisms, but in all cases crystal shape is driven kinetically by stereo-chemical recognition of the modifiers for the atomic structure at step edges on the crystal faces. We also show that the conventional analysis of mineral growth from aqueous solutions based on application of the Gibbs-Thomson effect cannot be applied to sparingly soluble systems like those found in bio-mineral structures because of the rarity of kinks along the step edges. The results call into question the basic Gibbs-Thomson requirement that the thermal fluctuations of steps on the crystal face are always fast enough to assure that steps propagate at a rate controlled just by molecular incorporation at kinks. Rather, the generation of kinks by so-called "1D nucleation" becomes the rate-limiting step. Finally, we look at the phenomenon of templated nucleation at self-assembled mono-layers and show that, in the case of OH-terminated surfaces, although there is complete control over the orientation of the crystals that nucleate, the pathway to this templated state first passes through an ACC phase. Moreover, the film itself, while initially displaying a high degree of orientational order, becomes completely disordered prior to the ACC-to-crystal transformation. Thus, if there is an epitaxial or stereo-chemical relationship between film and crystal as is generally assumed, one must view crystal templating in this system as a cooperative phenomenon where solid phase and organic film order one another.

This work was performed under the auspices of the U.S. Department of Energy by the University of California, Lawrence Livermore National Laboratory under contract No. W-7405-Eng-48.

Direct Visualization of Structures and Processes at Mineral-Water Interfaces*

Paul Fenter
Chemistry Division
Argonne National Laboratory
9700 South Cass Avenue
Argonne IL 60439
Fenter@anl.gov

The mineral-water interface is the primary site of low-temperature geochemical processes and exerts a strong influence over the near-surface environment. A fundamental understanding of even elementary aspects of mineral-water interface structure and associated processes (e.g., adsorption, dissolution, and growth) has been limited by the intrinsic complexity of these systems and the associated inability to directly observe these interfaces in-situ through an aqueous phase with molecular-scale resolution. I will discuss new insights in this area derived from observations of mineral-water interfaces using advanced interfacial X-ray scattering techniques that incorporate elemental and chemical sensitivities with surface specificity and Å-scale resolution, including high resolution X-ray reflectivity, X-ray standing waves, and resonant anomalous reflectivity. Recent advances with these techniques allow model-independent images of interfacial and element-specific structures at mineral-water interfaces to be obtained directly from the experimental data. Selected examples of recent work will be discussed including observations of: ordered “interfacial water” immediately adjacent to mineral-water interfaces [1]; the distribution of ions at charged mineral-water interfaces (i.e., electrical double layer structure) [2,3,4]; and the heterogeneous growth and stability of mineral films in supersaturated solutions (i.e., the ‘dolomite problem’). I will conclude by describing a recent advance that enables the direct and non-invasive imaging of interfacial topography with X-ray reflection interface microscopy [5].

References:

- [1] P. Fenter and N. C. Sturchio, *Progress in Surface Science*, **77**, 171-258 (2004).
- [2] Z. Zhang et al., *Surf. Sci. Lett.* **554** L95-L100 (2004).
- [3] C. Park et al., *Phys. Rev. Lett.* **97**, 016101(1-4) (2006)
- [4] Z. Zhang et al., *Langmuir* **20** 4954-4969 (2004).
- [5] P. Fenter, C. Park, and Z. Zhang, Y. Wang, *Nature Physics*, in press (2006).

*This work was supported by the Geoscience Research Program, Office of Basic Energy Sciences, Office of Science, Department of Energy, both directly and through its support for the Advanced Photon Source at Argonne National Laboratory under contract W-31-109-ENG-38.

Department of Energy, Office of Basic Energy Sciences, Division of Chemical Sciences, Geosciences and Biosciences, Geosciences Research Program.

Dimitri A. Sverjensky
Professor of Geochemistry
Dept. of Earth and Planetary Sciences
Johns Hopkins University
Baltimore, MD 21218
sver@jhu.edu

Prediction of inorganic and organic anionic speciation at the oxide-electrolyte-water interface

Adsorption of aqueous anions such as sulfate, selenate, arsenite, arsenate and oxalate to oxide surfaces is important in the mobility of toxic metals and metalloids in the environment, but predicting the surface speciation as a function of environmental parameters is a major challenge. Recent *in situ* ATR-FTIR spectroscopic studies and X-ray standing-wave and reflectivity studies have defined surface speciations for these anions that typically involve multiple surface species (e.g. inner- vs. outer-sphere). These results must be integrated with a surface complexation model (SCM) in order to predict surface speciation under environmental conditions. SCMs combine mass action and mass and charge balance equations with an electric double-layer model, but have often had difficulty using the spectroscopically defined surface species to fit macroscopic adsorption data. Even when this is possible, the models do not predict the correct speciation trends with environmental parameters such as pH, ionic strength, and surface loading defined by the spectroscopic studies. The present study describes a new approach to this problem.

Inner-sphere anion adsorption by the ligand exchange mechanism with surface functional groups on metal oxides is thought to involve desorption of water dipoles chemisorbed to the surface metal ions. For example, when sulfate adsorbs as a monodentate-mononuclear complex to one Fe-octahedron on iron oxide, one water is released. When arsenite adsorbs as a bidentate complex bridging two Fe-octahedra, two waters are released. SCMs have traditionally neglected the electrostatic work associated with this desorption of water dipoles from a charged surface. Taking this effect into account in the extended triple-layer model of surface complexation (ETLM) permits close quantitative description of anion adsorption data using a combination of inner- and outer-sphere (or H-bonded) species identified by spectroscopic studies. Furthermore, the model anion surface speciation predicted as a function of pH, ionic strength and surface coverage is in agreement with qualitative trends from *in situ* ATR-FTIR and X-ray results. Finally, variations in the model equilibrium constants for anion adsorption from one metal oxide to another can be explained with the aid of Born solvation theory. This permits the prediction of the equilibrium constants of inner- and outer-sphere surface species of adsorbed anions on all oxides.

Radiation Chemistry at Water Ceramic Oxide Interfaces

Jay A. LaVerne
Radiation Laboratory, University of Notre Dame
Notre Dame, IN 46556
laverne.1@nd.edu

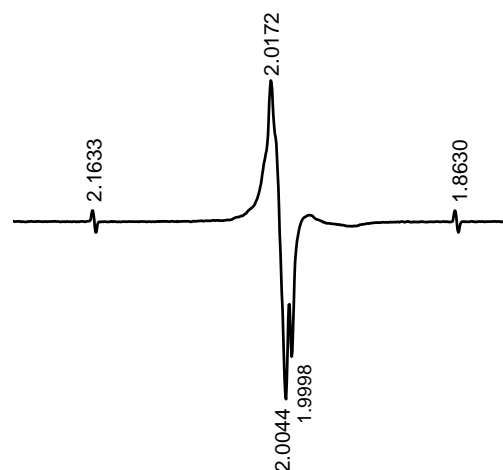
Program Scope

This program examines the fundamental species formed in the irradiation of multi-phase systems consisting of water and aqueous solutions in association with ceramic oxides such as ZrO_2 , SiO_2 , MgO , BeO , and Al_2O_3 . The research focuses on the radiation chemistry of liquid water and how it is affected by the liquid – solid interface. Radiation induced reactions at the water – solid interface and the transport of energy and matter through the interface are examined for different ceramic oxides, particle sizes, and morphologies. Gas evolution and the formation of interfacial species at ambient temperatures and pressures are measured using a variety of analytical techniques. Virtually nothing is known about the intermediate species involved or the mechanisms for product formation under conditions commonly encountered in typical applications involving liquid – solid interfaces in radiation fields. The fundamental physical and chemical information obtained in this program will find wide application in a wide variety of science and technology fields including: nano-technology, nuclear power plant operation, radioactive waste cleanup and management, environmental remediation, and health physics.

Recent Progress

Experimental studies have determined H_2 production in the radiolysis of water adsorbed on CeO_2 , ZrO_2 , and UO_2 particles,^{1,2} and more recently on SiO_2 , MgO , and BeO . In all cases, the transport of energy from the oxide results in a larger H_2 yield than expected from energy deposition in the water alone. For instance, a few monolayers of water on a MgO particle of 100 nm diameter amounts to only about one percent of the total weight. Energy absorbed by each component of a system is essentially equal to its fraction of electron density so virtually all of the energy is located initially in the solid particle. The H_2 yield is determined to be 0.28 molecule/100 eV of total energy absorbed by the $\text{MgO}/\text{H}_2\text{O}$ system. The radiolysis of pure water would result in a H_2 yield of 0.45 molecule/100 eV. A significant fraction of the energy initially deposited within the solid oxide reaches the surface and induces the production of H_2 . Variation of the H_2 yields with layers of adsorbed water show that H_2 can be observed down to the lowest water loading.^{1,2} The results suggest that surface reactions of physisorbed water are responsible for much of the H_2 production and that these processes can be very dependent on particle type. The reason for this phenomenon is uncertain, but may involve the migration of excitons in the bulk and their coupling to bound surface water.³ The nature of the chemisorbed water molecules on the oxide surface will also play an important role. Significant differences are found in the H_2 yields from water adsorbed on ZrO_2 , SiO_2 , MgO and BeO that cannot be explained by known factors. In all of the experimental studies performed to date, H_2 production is not accompanied by the formation of stoichiometric O_2 . This result suggests that oxygen species remain on the particle surface. Identification of these species will aid in determination of the water decomposition mechanism, which is also of extreme technological importance. For instance, adsorbed oxygen species may affect the water chemistry of reactors or it may incorporate into the surface leading to radiation induced corrosion or dissolution.

Recent experimental studies were performed to characterize the chemisorbed water species on the oxide surface using reflective FTIR and Raman spectroscopy. The nature of the oxygen species remaining on the surface of ceramic oxide particles following radiolysis was examined using EPR spectroscopy. Various ceramic oxides were dried and a controlled amount of water added to their surface. Irradiations were performed with γ -rays at room temperature and at 77 K. The latter experiments were designed to trap surface H atoms that may be produced in the radiolysis thereby giving some insight to the mechanism involved. The



EPR of γ -irradiated water on ZrO_2 particles at 77K.

Figure shows the formation of H atoms with g-factors of 1.863 and 2.163 in the γ -radiolysis of water on ZrO_2 . An oxygen radical species adsorbed on the surface gives rise to the central spectrum. Surface studies have been performed in which ZrO_2 was reduced at high temperatures under a vacuum and then treated with O_2 .⁴ The EPR spectrum from that study is very similar to the one observed in this work and the species responsible is identified as the O_2^- radical. Further characterization of this species and those on other ceramic oxides are underway.

Studies will also be performed to determine the oxygen species remaining on the surface following reaction with H_2O_2 . Extensive studies on the decomposition of H_2O_2 at ceramic oxide interfaces were able to determine that the process occurs at the liquid – solid interface,⁵ but were unable to elucidate the mechanism. EPR studies will be performed on ceramic oxides in aqueous H_2O_2 solutions in order to identify interfacial species.

Future Plans

Experimental measurements of the dependence of H_2 production on the number of water layers on SiO_2 , ZrO_2 , CeO_2 , and UO_2 suggest that radiolytic water decomposition occurs mainly at the surface. Of these oxides, water in association with ZrO_2 seems to be the most efficient system for the radiolytic formation of H_2 . Many oxides have been examined for H_2 production and a number of these have been found to be more efficient than ZrO_2 , but those studies have very little control on the amount of water loading.⁶ An examination of the effects of water loading will be performed for a variety of ceramic oxides. Correlation of the yield of H_2 with oxide band gap suggests that there may be a resonance process at about 5 eV in which an exciton formed in the bulk oxide efficiently couples with the interfacial water to produce H_2 .³ However, band gap energy alone is not sufficient to lead to efficient H_2 production. Some oxides with band gap energy of 5 eV are not found to give enhanced H_2 yields. Furthermore, there is no known water energy band at 5 eV. Dissociative electron attachment, DEA, has been observed in the radiolysis of water with low energy electrons, which can lead to H_2 formation.⁷ However, the DEA energy band is broad from about 7 to 10 eV and does not match the suggested band gap resonance energy. The dependence of H_2 formation on the energy levels of the oxides is

not understood and will be probed.

Recent EPR examinations of the interfacial species produced in the radiolysis of chemisorbed water observed the formation of oxygen containing species and H atoms. These studies suggest that the oxygen species formed in the radiolysis of water adsorbed on the ZrO₂ surface is the O₂⁻ radical. This finding agrees with surface science studies in which O₂ was adsorbed onto ZrO₂ surfaces previously reduced.⁴ Those same studies found that the same species was formed when H₂O₂ was placed in contact with ZrO₂. This finding is difficult to accept considering that experiments show no formation of O₂ from irradiated water on ZrO₂. There is clearly a large discrepancy in the results that must be resolved. EPR and FTIR techniques will be used to examine the species involved in the decomposition of H₂O₂ at a ceramic oxide surface. Emphasis will be placed on ZrO₂, TiO₂, and Al₂O₃ because of their importance as construction materials and because they have the most ancillary information on processes occurring at their surface. Solutions of H₂O₂ and oxide will be dried at various temperatures to establish thermal effects on the peroxide degradation.

References

- (1) LaVerne, J. A.; Tandon, L. "H₂ Production in the Radiolysis of Water on CeO₂ and ZrO₂", *J. Phys. Chem. B* **2002**, *106*, 380.
- (2) LaVerne, J. A.; Tandon, L. "H₂ Production in the Radiolysis of Water on UO₂ and Other Oxides", *J. Phys. Chem. B* **2003**, *107*, 13623.
- (3) Petrik, N. G.; Alexandrov, A. B.; Vall, A. I. "Interfacial Energy Transfer During Gamma Radiolysis of Water on the Surface of ZrO₂ and Some other Oxides", *J. Phys. Chem. B* **2001**, *105*, 5935.
- (4) Anpo, M.; Che, M.; Garrone, E.; Giamello, E.; Paganini, M. C. "Generation of Superoxide Ions at Oxide Surfaces", *Topics in Catalysis* **1999**, *8*, 189.
- (5) Hiroki, A.; LaVerne, J. A. "Decomposition of Hydrogen Peroxide at Water-Ceramic Oxide Interfaces", *J. Phys. Chem. B* **2005**, *109*, 3364.
- (6) Aleksandrov, A. B.; Byakov, A. Y.; Vall, A. I.; Petrik, N. G. "Radiolysis of Adsorbed Substances on Oxide Surfaces", *Russ. J. Phys. Chem.* **1991**, *65*, 847.
- (7) Rowntree, P.; Parenteau, L.; Sanche, L. "Electron Stimulated Desorption via Dissociative Attachment in Amorphous H₂O", *J. Chem. Phys.* **1991**, *94*, 8570.

DOE Sponsored Publications in 2003-2006

K. Enomoto, J. A. LaVerne and S. M. Pimblott, "Products of the Triplet Excited State Produced in the Radiolysis of Liquid Benzene" *J. Phys. Chem. A* **2006**, *110*, 4124-4130.

K. Enomoto, et al., "Formation and Decay of the Triplet Excited State of Pyridine" *J. Phys. Chem. A* **2006**, *110*, 9874-9879.

S. M. Pimblott, B. H. Milosavljevic and J. A. LaVerne, "Radiolysis of Aqueous Solutions of 1,1- and 1,2-Dichloroethane" *J. Phys. Chem. A* **2005**, *109*, 10294-10301.

B. M. Milosavljevic and J. A. LaVerne, "Pulse Radiolysis of Aqueous Thiocyanate Solution" *J. Phys. Chem. A* **2005**, *109*, 165-168.

B. H. Milosavljevic, J. A. LaVerne and S. M. Pimblott, "Rate coefficient measurements of hydrated electrons and hydroxyl radicals with chlorinated ethanes in aqueous solutions" *J. Phys. Chem. A* **2005**, 109, 7751-7756.

J. A. LaVerne, et al., "Heavy Ion Radiolysis of Methylene Blue" *Radiat. Phys. Chem.* **2005**, 72, 143-147.

J. A. LaVerne and L. Tandon, "H₂ and Cl₂ Production in the Radiolysis of Calcium and Magnesium Chlorides and Hydroxides" *J. Phys. Chem. A* **2005**, 109, 2861-2865.

J. A. LaVerne, I. Stefanic and S. M. Pimblott, "Hydrated Electron Yields in the Heavy Ion Radiolysis of Water" *J. Phys. Chem. A* **2005**, 109, 9393-9401.

J. A. LaVerne, I. Stefanic and S. M. Pimblott, "Hydrated Electron Yields in the Proton Radiolysis of Water" *Jpn. J. Radiat. Chem.* **2005**, 79, 9-12.

J. A. LaVerne, I. Carmichael and M. S. Araos, "Radical Production in the Radiolysis of Liquid Pyridine" *J. Phys. Chem. A* **2005**, 109, 461-465.

J. A. LaVerne, "H₂ Formation from the Radiolysis of Liquid Water with Zirconia" *J. Phys. Chem. B* **2005**, 109, 5395-5397.

A. Hiroki and J. A. LaVerne, "Decomposition of Hydrogen Peroxide at Water-Ceramic Oxide Interfaces" *J. Phys. Chem. B.* **2005**, 109, 3364-3370.

B. C. Garrett, et al., "The Role of Water on Electron-Initiated Processes and Radical Chemistry: Issues and Scientific Advances" *Chem. Rev.* **2005**, 105, 355-389.

J. A. LaVerne, I. Stefanic and S. M. Pimblott, Hydrated Electron Yields in the Radiolysis of Water with Protons. Proceedings of the Japanese Society for Radiation Chemistry, Hokkaido University, Soporro, Japan **2004**.

J. A. LaVerne, "Hydrogen Generation in Transuranic Waste Storage Containers" in Proceedings of the International Atomic Energy Agency Workshop on "Advances in Radiation Chemistry of Polymers". IAEA Press: Vienna. **2004** 15-20.

J. A. LaVerne, "Radiation Chemical Effects of Heavy Ions" in Charged Particle and Photon Interactions with Matter. A. Mozumder and Y. Hatano. Marcel Dekker, Inc: New York. **2004** 403-429.

J. A. LaVerne and S. E. Tonnie, "H₂ Production in the Radiolysis of Aqueous SiO₂ Suspensions and Slurries" *J. Phys. Chem. B* **2003**, 107, 7277-7280.

J. A. LaVerne and L. Tandon, "H₂ Production in the Radiolysis of Water on UO₂ and Other Oxides" *J. Phys. Chem. B.* **2003**, 107, 13623-13628.

Ion Solvation in Nonuniform Aqueous Environments

Principal Investigator
Phillip L. Geissler

Faculty Scientist, Physical Biosciences & Materials Sciences Divisions

Mailing address of PI:
Lawrence Berkeley National Laboratory
1 Cyclotron Road
Mailstop: HILDEBRAND
Berkeley, CA, 94720

Email: geissler@cchem.berkeley.edu

Research in this program applies computational and theoretical tools to determine structural and dynamical features of aqueous salt solutions. It focuses specifically on heterogeneous environments, such as liquid-substrate interfaces and crystalline lattices, that figure prominently in the chemistry of energy conversion. In these situations conventional pictures of ion solvation, though quite accurate for predicting bulk behavior, appear to fail dramatically, e.g., for predicting the spatial distribution of ions near interfaces. We develop, simulate, and analyze reduced models to clarify the chemical physics underlying these anomalies. We also scrutinize the statistical mechanics of intramolecular vibrations in nonuniform aqueous systems, in order to draw concrete connections between spectroscopic observables and evolving intermolecular structure. Together with experimental collaborators we aim to make infrared and Raman spectroscopy a quantitative tool for probing molecular arrangements in these solutions.

Our work on these issues thus far has focused on establishing quantitative interpretations for Raman spectra of liquid water and salt solutions. The temperature dependence of the neat liquid spectrum exhibits an isosbestic point, a vibrational frequency whose scattering intensity does not change over nearly the entire range from freezing to boiling. This feature has long been used to motivate and justify two-state models of local structure in the liquid, implying that broken hydrogen bonds exist as a distinct chemical species. Using straightforward principles of statistical mechanics we have shown that isosbestic behavior can plausibly arise from the temperature dependence of thermal frequency distributions alone. This consequence of Boltzmann weighting applies very generally, suggesting that many inferences of two-state equilibrium from isosbestic behavior should be reconsidered.

We have also examined the Raman spectra of salt solutions, which have been used to classify various anions as “structure makers” (enhancing the degree and strength of hydrogen bonds among nearby water molecules) or “structure breakers” (distorting or breaking nearby hydrogen bonds). These classifications have further served as a basis for rationalizing the affinity of ions for interfaces. Our computer simulations of empirical water models have achieved almost quantitative agreement with newly measured spectra.

These calculations indicate that spectroscopic changes across the halide series arise primarily from electric fields experienced by OH groups adjacent to an anion. Raman spectra thus say little about hydrogen bond network reorganization, i.e., changes in spatial relationships *among* water molecules. Our simulations do not exhibit substantial reorganization, suggesting a remarkable ability of the hydrogen bond network to accommodate perturbations imposed by solvation structure.

We have begun to explore interfacial phenomena more directly for ions in polar liquids. Computer simulations of individual ions in a schematic polar solvent will unambiguously determine whether affinity of polarizable anions for liquid water-vapor interfaces originates in the chemical physics of hydrogen bonding. Results of these calculations will direct subsequent work to generalize dielectric continuum theory for heterogeneous environments. Possible avenues include incorporating directionality and nonuniform polarizability in lattice dielectric models, accounting for molecular granularity with integral equation theory, and constructing a molecular field theory to examine correlations among ions at finite concentration. We plan similar theoretical treatments of ionic solutes in ice, aiming to explain the unusually low solubility of ions in the bulk and the unusually high conductivity of interfaces with vapor.

The Effect of Crystallization on the Proton Pump Function of Bacteriorhodopsin and New Studies on Nanomedicine

Mostafa El-Sayed (mostafa.el-sayed@chemistry.gatech.edu)
Laser Dynamics Laboratory, Georgia Tech, Atlanta, GA-30332-0400

1. Program Scope: The past studies conducted with DOE support have focused on understanding the mechanism of the proton pump function of bacteriorhodopsin, the other photosynthetic system in nature besides chlorophyll. The last few years, our group has also been examining the properties of nanoparticles with NSF support. We began to study the applications of these properties to biological systems starting with use of plasmonic nanoparticles in detecting and destroying cancer cells. Now that we have expertise in the field of nanoparticles as well as biological systems, we are just beginning a program to combine our expertise in the two areas of nanotechnology and bacteriorhodopsin to determine the effect of introducing nanoparticles into bacteriorhodopsin on its proton pump function.

2. Recent Progress:

A. The Effect of crystallization on the Proton Pump Function of Bacteriorhodopsin: Bacteriorhodopsin ("bR"), is a retinal protein with 248-amino acid, 26 kDa transmembrane protein first discovered in the purple membrane (cell membrane) of the salt-marsh bacterium *Halobacterium salinarium* by Oesterhelt and Stoeckenius in 1971.¹ Upon light absorption, retinal isomerizes. This is followed by a dark cycle of intermediates resulting in the deprotonation of the Schiff base (to form the M-intermediate) and the pumping of protons to the surface of the cell membrane. This created proton gradient is latter used in the formation of ATP, the fuel of life processes.

In 2002, a novel crystallization method published by Bowie and Farham² resulted in an unusual antiparallel monomeric packing structure of bicelle bacteriorhodopsin (bcbR) crystals the spectroscopic properties of which had not been studied. Last couple of years, we investigated these bcbR crystals to better understand how the changes in the protein tertiary structure affect the function. Specifically: Can the retinal Schiff base isomerize in this unusual protein packing structure? Does the protein following crystallization retain the ability to undergo the photocycle and pump protons? If so, how are the rates of the deprotonation/reprotonation of the Schiff base affected by the antiparallel monomer packing structure of the protein? Is Asp85 still the proton acceptor during the deprotonation process of the photocycle? In this work, visible, Raman, FTIR, and single-wavelength transient absorption spectroscopies have been used to answer these questions.

A mass of hydrated bcbR crystals in their detergent matrix was investigated by visible spectroscopy. Reversible changes in the absorption maximum upon exposure to light suggest that the photo-isomerization of the retinal Schiff base is still possible in the bcbR crystals.

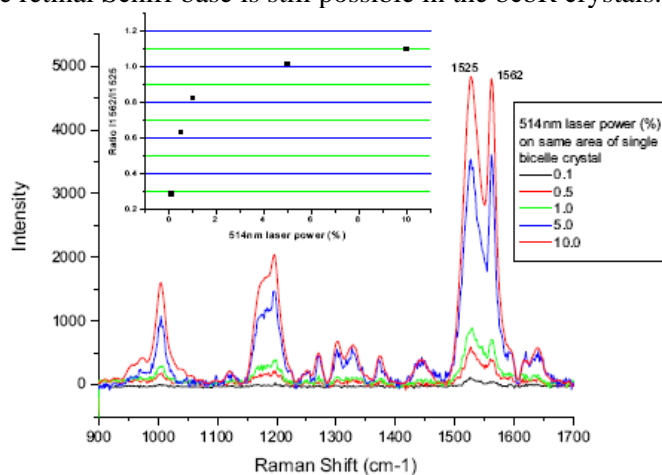


Fig. 1: Increasing the power of the 514 nm Raman laser on a hydrated single bcbR crystal increases the intensity ratio (inset) between the 1562 nm band (M intermediate) and the 1525 nm band (parent) nonlinearly. This is the first indication that the bcbR crystals are capable of making the M intermediate photochemically, and that the deprotonated Schiff base is caused by photochemical formation of the M intermediate and not by thermal dehydration of the parent.

Single-crystal Raman spectroscopy using the 514 nm incident wavelength was used to detect bands belonging to the deprotonated M intermediate in single hydrated bcbR crystals. Raman bands belonging to both the parent and the M intermediate were observed in the hydrated bcbR crystals. To demonstrate that the new bands appearing are actually due to the photochemical formation of the M intermediate and not simply due to resonance enhancement of a thermally formed M analogue, Raman band intensities were monitored as a function of 514 nm laser power. In these studies the intensities of the Raman bands increased nonlinearly with increasing laser power, confirming that the M intermediate is being formed photochemically (Fig. 1).

Single-wavelength transient absorption spectroscopy (flash photolysis) was used to monitor the rise and decay kinetics of the M intermediate in bcbR crystals in both H₂O and D₂O. In these studies, the M intermediate rise time in bcbR crystals in H₂O was found to be three times faster compared to that of native bR and cbR crystals, with a decay time that was seven times slower than in either native bR (see Fig. 2a, 2b) or the previously-published *in-cubo* (cbR) crystals.³

Finally, FTIR difference spectroscopy was used to monitor both the changes in the protein *and* the surrounding amino acids during the proton transfer time scale. It was found that Asp85 was the proton acceptor during the formation of the M intermediate in bcbR crystals, indicated by the appearance of a positive carbonyl band at 1760 cm⁻¹ assigned to Asp85.

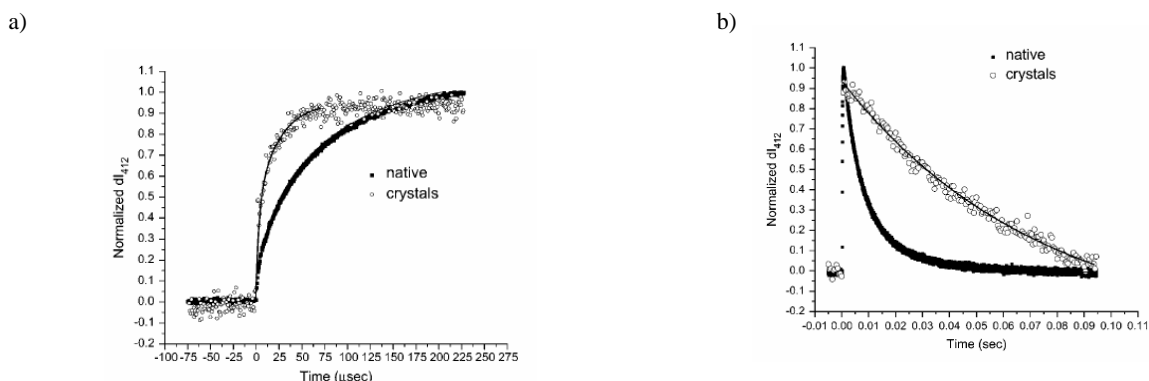


Fig. 2. a) Comparison of M rise kinetics in DDW, expressed as the intensity of the 412 nm absorption. Both the native and the bicelle crystals fit to a biexponential rise, with an average rise time for the native sample of 83 ms and an average rise time for the crystals of 24 ms. The crystals have a rise time for the M intermediate that is three times faster relative to the M rise in the native sample. b) Comparison of M decay kinetics in DDW, expressed as the intensity of the 412 nm absorption. The M decay for the native solution fits best to a biexponential expression with an average decay time of 10 ms, whereas that for the bicelle crystals fits best to a monoexponential expression with an average decay time of 73 ms—a decay time which is over seven times slower than observed in native bR.

B. Nanobiology and Nanomedicine: Metal nanoparticles have the ability to strongly scatter and absorb visible and near-infrared light due to the phenomenon of surface plasmon resonance (SPR).⁴ Further, nanoparticles composed of gold are biocompatible, potentially non-cytotoxic, easily synthesized and conjugated to a variety of biomolecular ligands, antibodies and other targeting moieties. This makes them suitable for use in biochemical labeling, sensing and detection, medical diagnostics and therapeutic applications.⁵ The strongly enhanced SPR scattering of gold nanoparticles can be employed for optical imaging of cells and tissues of interest with potential applications in biomedicine.

In a recent study, our group in collaboration with Dr. Ivan El-Sayed at UCSF demonstrated the differentiation of cancerous cells from non-cancerous cells by the simple and inexpensive dark field light scattering-imaging and absorption spectroscopy of gold nanospheres immunotargeted to epidermal growth factor receptor (EGFR) over-expressed on cancer cells. Gold nanospheres (~35 nm in diameter) were prepared by the well-known citrate reduction of chloroauric acid and conjugated to monoclonal anti-EGFR antibodies. The antibody-conjugated gold nanoparticles were incubated with cell cultures from a non-cancerous epithelial cell line (HaCaT) and two cancerous epithelial cell lines (HOC 313 clone 8 and HSC 3). SPR scattering images (Fig. 3) of the cell lines were recorded using dark-field optical microscopy on an Olympus IX70 microscope with a U-DCW illumination condenser and 100x/1.35 oil Iris Ph3 UPLANAPO objective. It was seen that the HaCaT non-cancerous cells were poorly labeled by the nanoparticles and the cells could not be identified individually in the light-scattering images (Fig. 3, left column). In the case of

the HOC (Fig. 3, middle column) and HSC (Fig. 3, right column) cancerous cells incubated with the conjugated nanoparticles, the nanoparticles are found to be on the surface of the cells and the scattering from the nanoparticles clearly defines individual cells. This difference between cancerous and non-cancerous cells is due to the specific binding of anti-EGFR antibodies on the gold nanoparticle surface to EGFR over-expressed on the cancer cells.

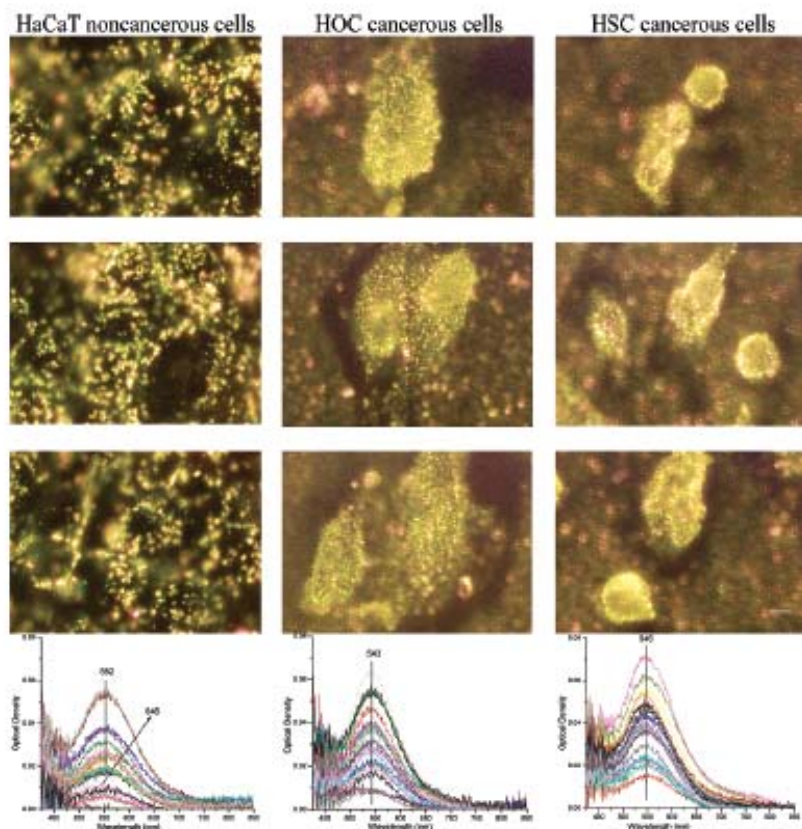


Fig. 3. Light scattering images and microabsorption spectra of HaCaT noncancerous cells (left column), HOC cancerous cells (middle column), and HSC cancerous cells (right column) after incubation with anti-EGFR antibody conjugated gold nanoparticles. Three different images of each kind of cells are shown to test reproducibility. The absorption spectra were measured for 25 different single cells. The figure shows clearly distinguished difference for the scattering images from the noncancerous cells (left column) and the cancerous cells (right two columns). The conjugated nanoparticles bind specifically with high concentrations to the surface of the cancer cells (right two columns). Conjugated nanoparticles did not show aggregation tendency (no long wavelength broad tail is observed). Scale bar: 10 μ m for all images.

SPR absorption spectra (Fig. 3, bottom panel) of the labeled cells were also obtained for the three cell lines using a SEE1100 micro-spectrometer under 20x magnification. The nanoparticles bound to HOC and HSC cancer cells have similar absorption maxima around 545 nm, which is 9 nm red shifted from that of the isolated anti-EGFR/Au solutions at 536 nm. This red shift is due to the specific binding of the anti-EGFR antibodies on the gold surface to EGFR on the cell surface. It also could be due to the interparticle interaction resulting from the arrangement of the conjugates on the cell surface in two dimensions. The specific and homogeneous binding of the antibody-conjugated nanoparticles to the cell surface is also found to give a relatively sharper SPR absorption band for the cancerous cells as compared to that of the non-cancerous cells, where the nanoparticles are distributed non-homogeneously. Based on the absorbance of the labeled cells at the SPR wavelength maximum, it was concluded that the anti-EGFR antibody conjugated nanoparticles specifically and homogeneously bind to the surface of the cancer type cells with 600% greater affinity than to the non-cancerous cells. In summary, the results suggest that SPR scattering imaging or SPR absorption spectroscopy generated from antibody conjugated gold nanoparticles can be useful for the diagnosis and investigation of oral cancer cells.

The ability of gold nanoparticles to efficiently convert absorbed light into localized heat can be readily employed for cancer therapy based on the selective laser photothermal damage of cancer cells and tissue. In a recent work, we employed the strong photoabsorption of anti-EGFR conjugated gold nanoparticles

immunotargeted to cancer cells for their selective photothermal destruction using Argon-ion CW laser irradiation. The specific binding of the anti-EGFR-conjugated gold nanoparticles to the surface EGFR on the cancer cells selectively lowered the laser energy necessary to photodamage oral cancer cells (150 mW for HOC cells and 200 mW for HSC cells) compared to that needed to damage non-cancerous HaCaT cells (450 mW) *in vitro*. These results demonstrate the potential of immunotargeted gold nanospheres in the selective therapy of surface type/skin cancers. The method can also be extended to the therapy of tumors *in vivo* by using gold nanorods having strong absorption in the near-infrared region of the biological spectral window.⁶

References:

- (1) Oesterhelt, D.; Stoerkenius, W. *Nature (London), New Biology* **1971**, 233, 149.
- (2) Bowie, J.; Farham, S. *Journal of Molecular Biology* **2002**, 316, 1; Farham, S.; Yang, D.; Bare, E.; Yohannan, S.; Whitelegge, J. P.; Bowie, J. U. *Journal of Molecular Biology* **2004**, 335, 297.
- (3) Heberle, J.; Buldt, G.; Koglin, E.; Rosenbusch, J. P.; Landau, E. M. *Journal of Molecular Biology* **1998**, 281, 587; le Coutre, J.; Gerwert, K. *FEBS letters* **1996**, 398, 333.
- (4) Link, S.; El-Sayed, M. A. *J. Phys. Chem. B* **1999**, 103, 8410; Mostafa A. El-Sayed *Acc. Chem. Res.* **2001**, 34 (4), 257.
- (5) Katz, E.; Willner, I. *Angew. Chem., Int. Ed.* **2004**, 43, 6042.
- (6) Huang, X.; El-Sayed, I. H.; Qian, W.; El-Sayed, M. A. *J. Am. Chem. Soc.* **2006**, 128, 2115.

3. Future Directions: At the moment, many studies have been carried out that involve the introduction of nanoparticles into biological systems. What is the effect of this on the biological function is what we would like to know. We do understand a great deal about bacteriorhodopsin function and the mechanism of the proton pump is reasonably understood. What we would like to do in our future DOE-supported studies is to examine in details the effect of the proton pump function when silver or gold nanoparticles are introduced into the bacterium, attached to its surface or adsorbed into its tissues.

4. DOE supported publications (2003-)

1. Colin D. Heyes, Mostafa A. El-Sayed, "Thermal Properties of Bacteriorhodopsin", *Journal of Physical Chemistry B*, 107, 44, 12045-12053, (2003).
2. Colin D. Heyes, Mostafa A. El-Sayed, "Proton Transfer Reactions in Native and Deionized Bacteriorhodopsin Upon Delipidation and Monomerization," *Biophysical Journal*, 85, 426-434, (2003).
3. Colin D. Heyes, Keith B. Reynolds, Mostafa A. El-Sayed, "Eu³⁺ Binding to Europium-Regenerated Bacteriorhodopsin upon Delipidation and Monomerization", *FEBS Letters*, 562 (2004) 207-210.
4. R.M. Donlan; J.A. Piede; C.D. Heyes; L. Sanii; R. Murga; P. Edmonds; I. El-Sayed; M.A. El-Sayed, "Model System for Growing and Quantifying *Streptococcus Pneumoniae* Biofilms in Situ and in Real Time," *Appl. Environ. Microbiol.* 70(8), 4980-4988, (2004).
5. Garczarek, Florian; Wang, Jianping; El-Sayed, Mostafa A.; Gerwert, Klaus, "The Assignment of the Different Infrared Continuum Absorbance Changes Observed in the 3000-1800-cm⁻¹ Region During the Bacteriorhodopsin Photocycle," *Biophysical Journal* 87 (4), 2676-2682, (2004).
6. Laurie S. Sanii; Alex W. Schill; Cristin E. Moran; Mostafa A. El-Sayed, "The Protonation-Deprotonation Kinetics of the Protonated Schiff Base in Bicelle Bacteriorhodopsin Crystals", *Biophysical Journal* 89, 444-451 (2005).
7. Laurie S. Sanii; Mostafa A. El-Sayed, "Partial Dehydration of the Retinal Binding Pocket and Proof for Photochemical Deprotonation of the Retinal Schiff Base in Bicelle Bacteriorhodopsin Crystals", *Photochemistry and Photobiology*, 81 (6), 1356-1360 (2005).
8. Laurie S. Sanii; Mostafa A. El-Sayed, "Partial Dehydration of the Retinal Binding Pocket and Proof for Photochemical Deprotonation of the Retinal Schiff Base in Bicelle Bacteriorhodopsin Crystals", *Photochemistry and Photobiology*, 81 (6), 1356-1360 (2005).
9. Ivan El-Sayed, Xiaohua Huang, Mostafa A. El-Syed, "Surface Plasmon Resonance Scattering and Absorption of anti-EGFR Antibody Conjugated Gold Nanoparticles in Cancer Diagnostics; Applications in Oral Cancer," *Nano Letters*, 4(5), 829-834, (2005).

Influence of Co-Solvents and Temperature on Nanoscale Self-Assembly of Biomaterials

Teresa Head-Gordon
Department of Bioengineering, UC Berkeley
Physical Biosciences Division, Lawrence Berkeley National Laboratory
TLHead-Gordon@lbl.gov

Program Scope

Synthesis of tailor-made biomaterials requires a detailed understanding of the effect of solvent on structure, stability, and dynamics. How these physical quantities develop during self-assembly will be affected by the nature of the solvent, as evidenced by the fact that biopolymers such as proteins can be denatured or stabilized by various additives. Non-aqueous solvents such as guanadinium hydrochloride and urea are used to denature proteins.[1,2] Additions of trifluoro-ethanol or methanol can lead to specific stabilization of certain structural motifs, [3] whereas other organic solvents such as acetone, formamide, and DMSO are known to destabilize protein native states. The formulation of effective co-solvents is important in biopharmaceutical production of peptide and proteins to improve their long-term storage and delivery.[4] In principle, molecular switches can be created by control over protein function and reactivity through their solvent environment; such a possibility was recently demonstrated by embedding hemoglobin in a glassy solid of low water content trehalose solutions to reduce the protein conformational transitions and thereby turn off function [5]. Clearly, solvent interactions mediate the thermodynamics and kinetics of protein conformations that in turn influence their self-assembly and co-assembly properties. Understanding solvent environmental influences may lead to the ability to exploit not only differences in monomer composition but solvent composition, to create polymers, both biological and non-biological, with desired properties.

Recent Progress

Hydration Dynamics Near Peptide Interfaces [6]. We have completed quasi-elastic neutron scattering experiments at two resolutions that probe timescales of picoseconds to nanoseconds for the hydration dynamics of water near a concentrated solution of N-acetyl-leucine-methylamide (NALMA) peptides in water over a temperature range of 248K to 310K. The two QENS resolutions used allow for a clean separation of two observable translational components, and ultimately two very different relaxation processes that become evident when analyzed under a combination of the jump diffusion model, intermediate scattering function, as well as the relaxation cage model. The first translational motion is a localized β -relaxation process of the bound surface water, and exhibits an Arrhenius temperature dependence and a large activation energy of ~ 8 kcal/mole. The second non-Arrhenius translational component is a dynamical signature of the α -relaxation of more fluid water, exhibiting a glass transition temperature of ~ 128 K when fit to the Volger Fulcher Tamman functional form. For these peptide-water systems the Arrhenius β -relaxation is the slower translational process as

temperature is lowered, until a cross-over temperature is reached at 160K, at which point it becomes the much faster motion relative to the α -relaxation. This peptide system suggests the possibility that the recently observed fragile-to-strong transition in water dynamics near protein surfaces may instead be interpreted as a transition from bulk water to bound water dynamics due to the rapid disappearance of the α -relaxation process on the timescale of the QENS experiment in this temperature sensitive range, although lower temperature data is required to bolster this preliminary conclusion.

Consequence of Chain Networks on Water's Thermodynamic Properties [7]. There is a wealth of thermodynamic, structural, and dielectric data on water that together provides a global view of the liquid that seems to emphasize its tetrahedral hydrogen-bonding network as the unifying molecular connection to its global (and sometimes anomalous) properties. Recently the classification of water as a tetrahedral liquid has been challenged based on x-ray absorption (XAS) experiments on liquid water, which have been interpreted to show a hydrogen-bonding network that replaces tetrahedral structure with chains or large rings of water molecules. We examine the consequences of tetrahedral vs. chain networks using three different modified water models that exhibit a local hydrogen-bonding environment of two hydrogen-bonds and therefore networks of chains. Using these very differently parameterized models we evaluate their bulk densities, enthalpies of vaporization, heat capacities, isothermal compressibilities, thermal expansion coefficients, and dielectric constants, over the temperature range of 235K-323K. We compare the results from the modified water models to the recently developed TIP4P-EW model that exhibits tetrahedral structure consistent with x-ray and neutron scattering, and shows good agreement with experiment for the same thermodynamic and dynamic properties over the same temperature range.

Coarse-Grained Water Models and Their Anomalies [8]. We have examined the coarse-graining of the multi-site TIP4P-Ew water model to a series of simpler isotropic single-site potential by an inversion of the oxygen-oxygen radial distribution function at each characterized state point. We focus on water because many of its well-characterized structural and thermodynamic anomalies, which are postulated to be related to its strong orientational order. One might therefore expect that integrating out these orientational degrees of freedom to derive an isotropic pair potential would be a worst-case scenario, and a useful foil to highlight coarse-graining pitfalls. Our main finding is that although the pair structure is correctly reproduced at each state point, thermodynamic properties like the virial pressure and the internal energy are poorly rendered. However, we observe both anomalies in structural order (decreasing order under compression) and anomalous trends in dynamical properties (exhibiting maxima in the self diffusion coefficient as a function of density at temperature isotherms below the TMD), and possibly thermodynamic anomalies (density decreases upon cooling) like that of the TIP4P-EW model, suggesting that coarse-graining procedures are robust for reproducing water's well known anomalies.

Hydrophobic Solvation at Small Lengthscales in Modified Water Models [9]. We have characterized the solvation of small hydrophobic solutes, modeled as hard spheres or Lennard-Jones particles, in several modified water liquids. In the hybrid family of liquids the SPC/E model is partially transformed to a Lennard-Jones liquid with the same number density. In this family, hydrophobic solutes become less soluble as the liquid structure becomes more close packed. In the bent family of models the network structure is altered by geometrical

changes from SPC/E that increases the solubility of hydrophobic groups. Solvophobicity in the isotropic model, which has the same radial distribution function as SPC/E water by construction, is greater than in SPC/E water. This shows the importance of three body correlations. In addition to excess chemical potentials, we also evaluated the Gaussian model for hydrophobic solvation which was found to be a poor theory for describing excess chemical potentials of our model liquids with tight network structures. For solvation of polar solutes, we find that the dielectric constant of water is lower than many of our modified models.

Future Plans

We plan to pursue a number of studies on water and aqueous solutions, but we detail one particular project here- the relation between the solvent and protein dynamical transition and their coupling. The dynamical transition in bulk water is based on the observation that extrapolated relaxation timescales appear to diverge at a temperature of $\sim 228\text{K}$. This dynamical transition in the supercooled state has been postulated to drive a corresponding dynamical transition for proteins, for the reason that the restoration of anharmonic protein motions appear above a critical temperature (and more controversially a critical hydration level) which activates motions of surface hydration water. A number of simulation studies have now shown that it is likely the translational (vs. rotational) motions of surface hydration water in particular that drives the protein dynamical transition. Most recently quasi-elastic neutron scattering (QENS) and NMR measurements of the average translational relaxation time of surface water near lysozyme report an observation of a fragile to strong transition, i.e. the avoidance of the translational relaxation divergence in which the hydration dynamics transitions from a non-Arrhenius to Arrhenius temperature dependence at temperatures near $\sim 225\text{K}$, and several other heterogeneous systems are also reported to show a fragile-to-strong transition such as surface water near CeO_2 , and water in highly confined nanopores of silica glass.

In these heterogeneous systems it is undoubtedly important to sort out the confluence of water dynamics near the interface that may mask the desired anomalous water dynamics. The benefit of our studies using two QENS resolutions and multiple models for dynamical analysis on the peptide-water systems is that it has allowed us to isolate the localized β -relaxation process of the bound surface water from what we believe is a dynamical signature of the α -relaxation of more fluid water. For these peptide-water systems the Arrhenius β -relaxation is the slower translational process as temperature is lowered, until a cross-over temperature is reached, at which point it becomes the much faster motion relative to the second translational motion attributed to α -relaxation. The incredible slowing down of the non-Arrhenius translational process in water over a narrow range at low temperatures would coincide with a rapidly increasing demand on the resolution of the experimental instrument to quantify the transition from fragile-to-strong behavior in the α -relaxation. The demands on instrument resolution are correspondingly lighter for the β -relaxation process, at least for this peptide-water system. This therefore opens the possibility that the fragile-to-strong transition in water dynamics that have been observed in heterogeneous environments may instead be interpreted as a transition from bulk water to bound water dynamics due to the rapid disappearance of the α -relaxation process on the timescale of the experiment in this temperature sensitive range,

allowing only the observation of a dynamics that arises strictly from water's strong interactions with the interface.

We wish to emphasize that these conclusions are only a possibility, since our experimental temperature range of 298-248K has not yet reached low enough temperatures to be definitive. In fact it is possible that we might see a fragile-to-strong transition in the α -relaxation for our system at a higher temperature than the crossover temperature at which point the β -relaxation process dominates, thus eliminating the worry of dynamical interference from the interface. Over the next year we will return to NIST to perform even lower temperature studies (200-250K) to look for this possibility. We also will analyze these results further with a molecular dynamics study using polarizable force fields that we find necessary to reproduce the correct trends with temperature.

1. C. N. Pace (1986). *Methods in Enzymology* 131, 266.
2. G. I. Makhatadze (1999). *J. Phys. Chem. B*, 103, 4781.
3. M. Buck (1998). *Quarterly Reviews of Biophysics* 31, 297.
4. L. N. Bell (1997). *Biotechnology Progress* 13, 342.
5. D. S. Gottfried (1996). *J. Phys. Chem.* 100, 12034.
6. C. Maladier-Jugroot, D. Russo, J. R.D. Copley, T. Head-Gordon (2006). In preparation,
7. T. Head-Gordon and S. Rick (2006). In preparation
8. M. E. Johnson, T. Head-Gordon, A.A. Louis (2006). In preparation
9. R. M. Lynden-Bell and T. Head-Gordon (2006). *Mol. Phys.*, *in press*.

Fluctuations in Macromolecules Studied Using Time-Resolved, Multi-spectral Single Molecule Imaging

Carl Hayden
Sandia National Laboratories
P. O. Box 969, MS 9055
Livermore, CA 94551-0969
CCHAYDE@SANDIA.GOV

Haw Yang
Department of Chemistry
University of California at Berkeley
Berkeley, CA
hawyang@uclink.berkeley.edu

Program Scope

This is a newly started research program to study macromolecule dynamics using single molecule spectroscopy. The goal of this program is to study the fluctuations in the local chemical environments of macromolecules using simultaneous, time-resolved measurements of the full set of fluorescence properties from probe fluorophores in single macromolecules. An important aspect of this work will be the development of new data analysis methods that will extract the maximum information about the macromolecule fluctuations from the experimental record of photons.

One of the distinguishing characteristics of macromolecules is that their conformation, along with their chemical composition, creates distinct local chemical environments, such as binding sites, that govern much of their important chemistry. Unique chemical environments, such as the interior of proteins, have long been investigated by placing environmentally sensitive fluorophores within them and measuring the resulting fluorescence properties including intensity, spectrum, lifetime, and polarization anisotropy. More recently, the use of fluorescent probes has been extended to the level of single molecules where the fluorescence from one fluorophore must be detected. Time dependent measurements of fluorescence from single molecules can reveal chemical dynamics, such as conformational fluctuations, that are not evident in measurements on ensembles of molecules because the actions of multiple molecules are not synchronized.^{1,2} Studies on single molecules can also reveal the sequence of events in complex chemical or biological processes. In bulk samples the averaging of many fluctuations makes the system essentially time independent and hence the fluorescence properties can usually be measured sequentially. In contrast, to determine the time-dependent behavior of a fluorophore within a single macromolecule the relevant fluorescence properties must be measured simultaneously, with the sensitivity to detect single fluorophores. Development of methods to make and analyze simultaneous measurements of multiple fluorescence properties on single molecules is a primary aim of our research.

While probe fluorophores enable the investigation of single molecule dynamics, many factors determine their fluorescence properties, including chemical properties of the local environment around the fluorophore, the orientation of the fluorophore in the macromolecule and relative to the excitation laser polarization, the environmental sensitivity of electronic states of the fluorophore, and energy transfer from the excited fluorophore to a nearby quencher or acceptor fluorophore. Applying single molecule spectroscopy to probing fluctuations in the

conformations and local chemical environments around macromolecules requires relating changes in fluorophore fluorescence properties to fluctuations in the macromolecule. In many cases multiple fluorescence properties will fluctuate at the same time, thus the ability to interpret the result will be enhanced by measurements that reveal correlations between multiple fluorescence properties.

Recent Progress:

Time-resolved multispectral microscope

Recently we have developed a time-resolved, multi-spectral, confocal microscope with single molecule sensitivity. This instrument records the wavelength, emission time relative to excitation, and absolute detection time for each detected fluorescence photon so that correlations among all the fluorescence properties are maintained. From the record of detected photons, simultaneous, time-dependent fluorescence intensity, spectra and lifetimes can be extracted. The capability of the apparatus to measure correlated single molecule fluorescence spectra and lifetimes with excellent signal to noise ratios is demonstrated in Figure 1, where an image of single molecules and their corresponding spectra and lifetimes are shown. In preliminary experiments we have used this apparatus to measure the time dependent spectral properties of single molecules and quantum dots embedded in polymer matrices and attached to surfaces. We have also measured the full temporal and spectral fluorescence characteristics of single-pair fluorescence resonance energy transfer (FRET) systems.³

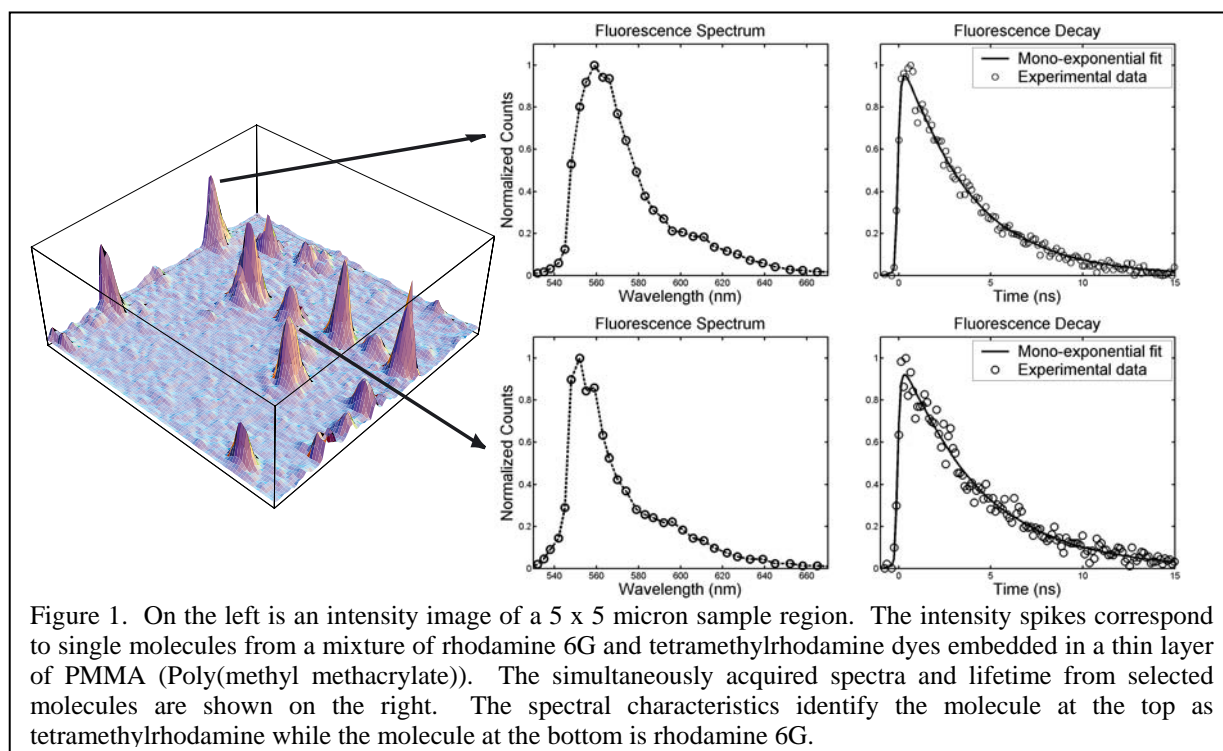


Figure 1. On the left is an intensity image of a 5 x 5 micron sample region. The intensity spikes correspond to single molecules from a mixture of rhodamine 6G and tetramethylrhodamine dyes embedded in a thin layer of PMMA (Poly(methyl methacrylate)). The simultaneously acquired spectra and lifetime from selected molecules are shown on the right. The spectral characteristics identify the molecule at the top as tetramethylrhodamine while the molecule at the bottom is rhodamine 6G.

The time-resolved multi-spectral microscope couples a confocal fluorescence microscope to a new custom photon detection system. In the confocal microscope fluorescence is excited by a high repetition rate mode-locked laser focused through a high numerical aperture objective lens to form a ~250 nm spot on the sample plane. The fluorescence emission from the laser spot on the sample is collected through the same objective and imaged confocally through a pinhole. An

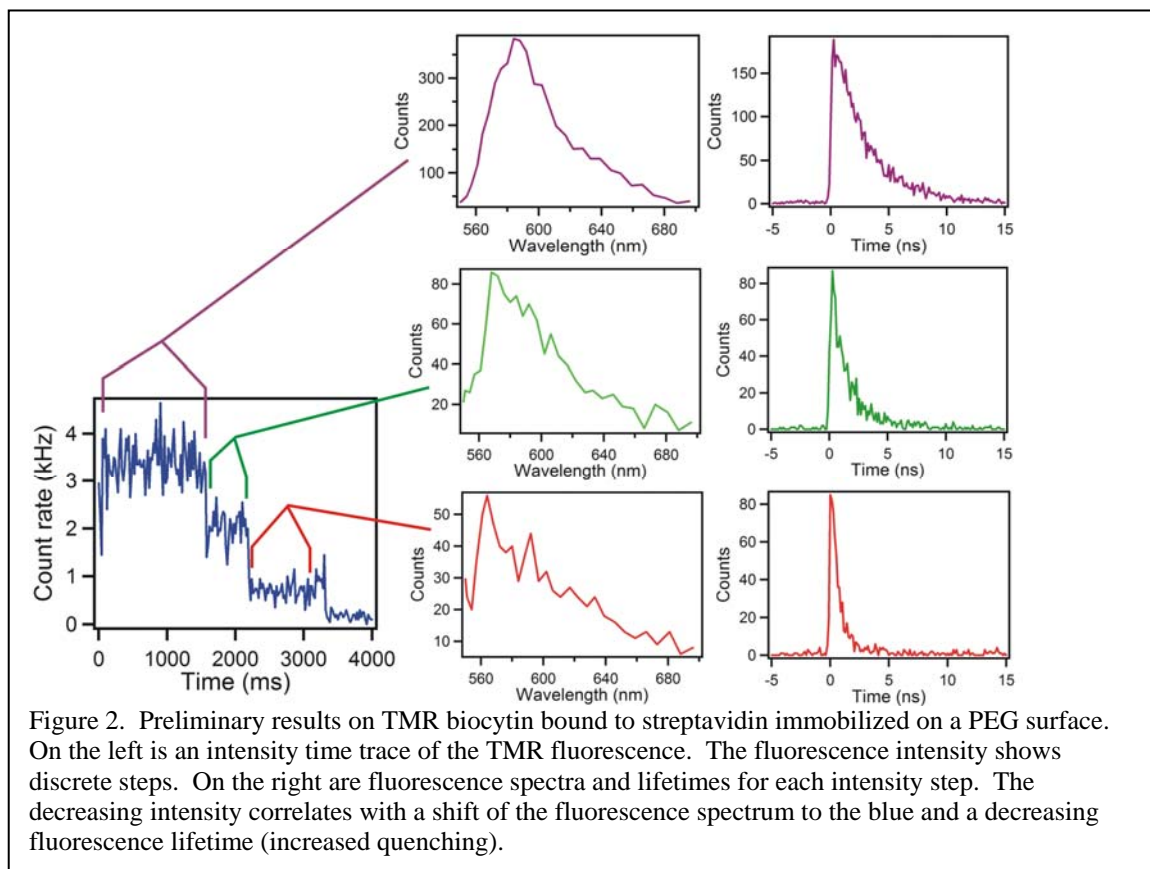
image is created by raster scanning the sample through the excitation laser focal spot. These components comprise a fairly conventional confocal microscope.

The novel aspect of the apparatus is the detection system. In our system the pinhole is imaged through a dispersing optical system onto a photon-counting time- and position-sensitive detector. The fluorescence signal is spectrally dispersed so the position on the detector where the photon strikes is determined by the wavelength of the photon, while the measurement of arrival time of the photon relative to the excitation laser pulse enables us to determine the emission time. The present detection system is based on a high-quantum-efficiency, cooled, 32-anode photomultiplier tube. Custom electronics allow us to determine the illuminated anode and hence the wavelength for each detected photon at high data rates. The photon arrival time relative to the exciting laser pulse is digitized by time-to-digital converters (TDCs). The information from each individual photon is also stamped with its absolute arrival time (time-stamped) to enable studies that make use of photon arrival time statistics. Thus, for each photon, the wavelength, the emission time relative to the laser pulse, and the absolute emission time are all recorded. Collection of many photons and histogramming of the data yields the correlated fluorescence spectrum and lifetime. The present dispersion system provides a spectral resolution of approximately 5 nm per anode element. The instrument response for measuring the photon emission time relative to the excitation laser pulse is about 150 ps. Enhancements currently in progress will also provide the capability for simultaneous polarization measurements.

Future Plans:

Single fluorophore studies of small ligand binding proteins.

We are working on several experiments to probe fluctuations in different properties of



specific local chemical environments within ligand binding proteins. One protein we are currently studying is streptavidin, a 53 kDa protein with an extremely strong binding affinity for its ligand, biotin. Biotin can bind in any of four equivalent deep pockets in the streptavidin molecule. The strong binding of biotin by streptavidin has numerous applications in biotechnology and is the basis of many affinity assay techniques. From bulk studies it is known that the fluorescence properties of many fluorophores, including Cy3 and tetramethylrhodamine (TMR), discussed below, change when they are closely bound to streptavidin through linkers to biotin.⁴

TMR is widely used for biological assays and single molecule studies due to its high quantum yield. When it is attached to streptavidin using biotin and a linker the dye is quenched to varying degrees depending on the linker. The quenching of TMR when it is attached to streptavidin using biotin and a linker is likely to be due to interaction with tryptophan residues in the biotin binding pocket.⁵ We are studying the time dependent fluctuations in the degree of quenching with various linkers to better understand the interaction between the protein and the dye. The first experiments use TMR-biotin, a commonly used label for streptavidin with a fairly long linker between the biotin and the dye. Preliminary results shown in Figure 2 illustrate fluctuations in the quenching that lead to changes in the fluorescence lifetime and an associated spectral shift.

Multiparameter spFRET

Single-molecule FRET is a powerful tool for studying conformational fluctuations in large molecules. By providing a measure of the distance between two fluorophores, FRET measurements can address questions such as whether fluctuations involve transitions between quasi-stable states or continuously sample a continuum of available configurations. Time-resolved FRET measurements can determine the rate of conformation changes between states and establish the times scales for various types of conformational changes.

There are many examples of the successful use of FRET to monitor single-molecule processes, but quantitative single-molecule FRET measurements are quite challenging due to the many factors that play a role in FRET efficiency. Our new apparatus is able to continuously record fluorophore spectra and lifetimes, which, along with separation, play an important role in the energy transfer efficiency in FRET. We are currently using protein and DNA spacer systems to develop quantitative FRET capabilities with our microscope. In preliminary experiments we have also time-resolved the FRET energy transfer process in single molecules on the subnanosecond time scale. Once fully developed these FRET methods will be applied to measure conformational fluctuations in the ligand-binding proteins that we are also studying using single fluorophores.

References:

1. Moerner, W.E. *J. Phys. Chem. B*, 2002, **106**, 910.
2. Xie, X.S. *J. Chem. Phys.*, 2002, **117**, 11204.
3. Luong, A.K.; Gradinaru, C.C.; Chandler, D.W.; and Hayden, C.C. *J. Phys. Chem. B*, **109**, 15691, 2005.
4. Gruber, H.; Hanh, C.D.; Kada, G.; Riener, C.K.; Harms, G.S.; Ahrer, W.; Dax, T.G.; and Knaus, H.-G. *Bioconj. Chem.*, 2000, **11**, 696.
5. Marmé, N.; Knemeyer, J.-P.; Sauer, M.; and Wolfrum, J. *Bioconj. Chem.*, 2003, **14**, 1133.

“Investigating atoms to aerosols with vacuum ultraviolet radiation”

Musahid Ahmed, Kevin R. Wilson and Stephen R. Leone
Chemical Dynamics Beamline
Lawrence Berkeley National Laboratory
University of California, Berkeley, CA 94720
mahmed@lbl.gov

The Chemical Dynamics Beamline at the Advanced Light Source (ALS), is a synchrotron user facility dedicated to state-of-the-art investigations in combustion dynamics, aerosol chemistry, nanoparticle physics, biomolecule energetics, spectroscopy, kinetics, and state-resolved chemical dynamics processes using tunable vacuum ultraviolet light for excitation or detection. The broad goals of the Chemical Dynamics Beamline are to perform high quality investigations in chemical physics and dynamics utilizing vacuum ultraviolet (VUV) light, while providing the user community with efficient access to the synchrotron and its sophisticated equipment, and at the same time fulfilling the missions and interests of the Department of Energy.

Aerosol Chemistry and Nanoparticle Physics -A rigorous understanding of the optical, electronic and chemical properties of nanoparticles is important for a broad range of fields including nanoscale electronics, materials science, as well as tropospheric, interstellar, and combustion chemistry. As such, there is a need to develop new molecularly incisive tools to probe nanoparticle properties in a size-specific way. Systematic studies using vacuum ultraviolet light (VUV) and soft x-ray radiation can contribute to the study of aerosol chemistry and nanoparticle physics in new and important ways. Therefore, in FY2004, a consortium of atmospheric scientists in collaboration with the chemical dynamics beamline group (CDG) formulated a joint proposal and received DOE funds to develop a new experimental platform to investigate aerosol chemistry and physics using VUV radiation. The experimental platform consists of a suite of commercial instruments to produce, size, and detect submicron aerosol particles, as well as ancillary reaction vessels needed to quantify heterogeneous particle phase chemistry. Central to this new effort is a novel nanoparticle endstation that was constructed by the CDG, to allow intense particle beams to be interrogated by VUV synchrotron radiation.¹ The main features of the apparatus are an aerodynamic lens system to generate focused particle beams and provisions to detect scattered photons, image photoelectrons and perform time of flight mass spectrometry on volatile species desorbed from aerosols² and nanoparticles. Below we detail some of these new results, which highlight both the progress to date and the unique capabilities of the Chemical Dynamics Beamline for nanoparticle research.

Light Scattering- Light scattering measurements of SiO₂ nanoparticles were conducted using VUV (7–20 eV) radiation. As a first test, spherical silica particles, chemically synthesized online, were studied. As predicted by Mie theory, these angular distributions show strong forward scattering. A careful comparison of scattered fluxes at visible and VUV wavelengths clearly show enhanced size sensitivity at VUV wavelengths.³ In a companion study, Eckart Rühl and coworkers (U. Würzburg, Germany) synthesized highly monodisperse (3–7% standard deviation), spherical SiO₂ nanoparticles using a colloidal chemistry technique. Modulations in the scattered light intensity as a function of scattering angle were observed and clearly distinguished from the strong forward scattering component observed in the chemically synthesized particles previously studied.⁴ The experimental results compared favorably with results from Mie scattering simulations for isolated particles. However, deviations from Mie simulations were observed for samples consisting of significant amounts of aggregates. In general, the present results indicate that the optical properties of free nanoparticles and their aggregates are sensitively probed by vacuum ultraviolet radiation.

Photoelectron Imaging of Nanoparticles- Velocity-map imaging (VMI) photoelectron spectroscopy combined with synchrotron radiation allows simultaneous measurement of angular and kinetic energy release from ionization events with 4 π steradian collection efficiency. The CDG applied VMI to free beams of nanoparticles for the first time. Detailed investigations were conducted on NaCl, KI, Au, and SiO₂ nanoparticles (50–500nm).

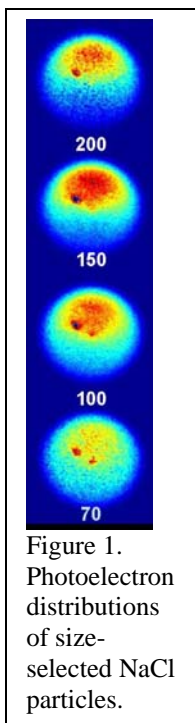


Figure 1. Photoelectron distributions of size-selected NaCl particles.

The kinetic energy release suggests that these ultra-fine particles exhibit, as expected for this size range, bulk-like electronic properties. However, a dramatic size-dependent asymmetry in the angular distributions of photoelectrons was observed for insulating nanoparticles, as shown for NaCl. Simply, photoelectrons are preferentially emitted from the side of the particle illuminated by the photon beam. While these particles are too large to exhibit quantum size effects, their dimensions are on the order of the photon penetration depth and electron inelastic mean free path. A simple model utilizing optical absorption and electron emission in NaCl is invoked to explain the asymmetry.

In contrast, gold nanoparticles (50–200nm) exhibit very different behavior. At all particles sizes studied thus far the photoelectron images are symmetric. To obtain a more rigorous quantitative explanation for the differences between gold and NaCl, we have initiated a collaboration with George Schatz (Northwestern). Schatz and coworkers have computed the internal electric field distribution explicitly using Mie theory in an effort to better understand the underlying physics of this interesting particle size-dependent asymmetry

The ionization energies of biological nanoparticles (glycine and phenylalanine-glycine-glycine) were determined using the VMI technique.⁵ X-ray powder diffraction studies on the glycine nanoparticles show that they are crystalline in nature and the reduced ionization energy when compared to gas phase results suggests that polarization energies play a role in the ionization process. A method was developed to quantify the molecular polarizability for glycine.

Finally, we expect to use the surface sensitivity of photoemission as another tool to probe heterogeneous particle phase chemistry. Initial studies have focused on examining photoemission from particles with core-shell morphologies. In particular, photoelectron images of thin films of anthracene (10–100nm) on ~100 nm NaCl, SiO₂ and Au seed particles have been measured.

Aerosol Chemistry- Additional studies are aimed at probing the reactivity of surface-bound polyaromatic hydrocarbon molecules with the ultimate goal to understand oxidative aging of soot particles in the troposphere. To accomplish this, binary nanometer-sized particles are made with monolayer coatings of anthracene on various inorganic (e.g. NaCl) and organic (stearic acid) seed particles. Upon reaction with ozone a variety of new particle-phase oxidation products are clearly identified by VUV single photon ionization mass spectrometry.⁶ Detailed studies of how the oxidation rate of anthracene depends on coating thickness and seed particle size are currently underway. Correlating changes in particle size with oxidation chemistry will also be used to better understand how chemistry influences particle morphology.

Photoionization of Biomolecules -With the aerosol apparatus developed at the beamline, a novel method is used to introduce fragile biomolecules into the gas phase via formation of aerosol nanoparticles, followed by thermal vaporization and detection by VUV photoionization mass spectrometry.⁷ The general strategy is to synthesize dry nanoparticles comprised of biomolecules that are then thermally vaporized in high vacuum. The resulting vapor, containing neutral biomolecules, can be “softly” ionized with tunable VUV synchrotron radiation producing nearly fragmentation-free mass spectra. To first demonstrate the general utility of this approach and to illustrate how internal energy affects single photon ionization mass spectra, the amino acids

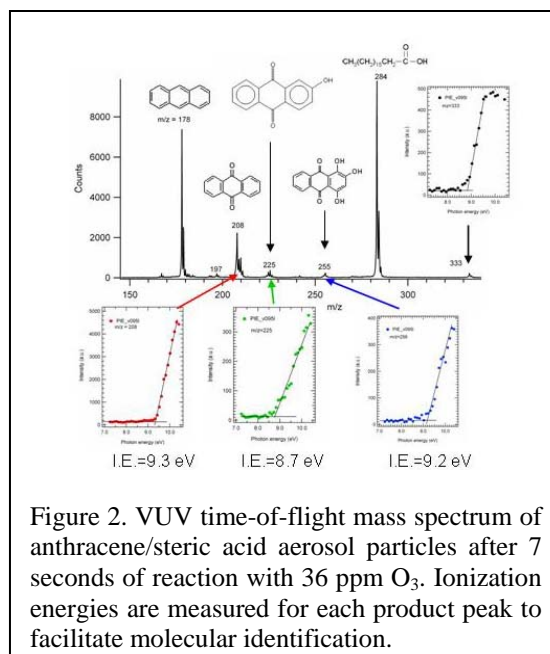


Figure 2. VUV time-of-flight mass spectrum of anthracene/stearic acid aerosol particles after 7 seconds of reaction with 36 ppm O₃. Ionization energies are measured for each product peak to facilitate molecular identification.

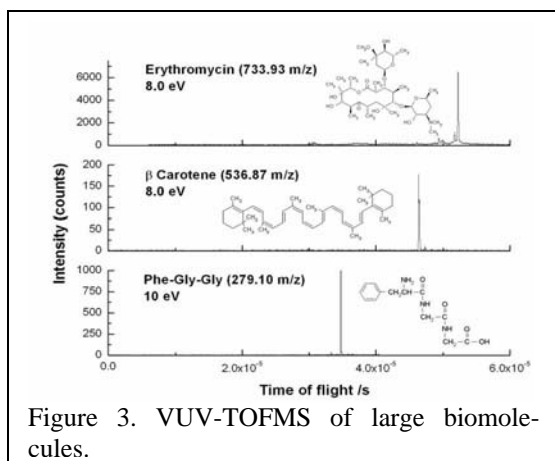


Figure 3. VUV-TOFMS of large biomolecules.

tryptophan and histidine⁸ were examined in detail. Erythromycin (733 amu) is the largest molecule that has been detected completely fragment free with this technique thus far. Coupling these measurements to electronic structure calculations will allow the unambiguous determination of adiabatic ionization energies and the structure of the resultant cation for these bio-molecules.

Photoionization of Water Clusters and Hydrated

Biomolecules- Studying the photoionization dynamics of water clusters allows for a window into understanding the properties of water from the gas phase to bulk. Exploratory studies using near-threshold VUV photoionization of water clusters were carried out. These are the first systematic studies

of the water cluster appearance energies (photoion threshold): the values exhibit a gradual decrease for small clusters ($n < 20$) and converge on a value of 10.6 ± 0.2 eV for bigger clusters. Photoelectron spectra of the water clusters strongly support the appearance energy values. Based on the appearance energy quantities, the dissociation energy and the proton affinity of neutral water clusters are evaluated.

Utilizing the same source, gas phase clusters of water with DNA bases (Guanine (G), Cytosine (C), Adenine (A) and Thymine (T)) are generated via thermal vaporization of the bases and expanding the resultant vapor in a continuous supersonic jet expansion of Ar seeded in water. Photoionization efficiency curves (PIE) are recorded for the DNA bases, dimers and the following water (W) clusters – G, GW_n ($n=1,2,3$), G_2 ; CW_n ($n=1-3$), C_2 ; A, AW_n ($n=1-4$) A_2 ; T, TW_n ($n=1-4$), T_2 . Analysis of this work is underway to understand the role of microhydration in the photoionization dynamics of DNA bases.

Laser Ablation and Desorption- The CDG group obtained the first direct PIE curves for small carbon clusters up to C_5 .⁹ Carbon clusters were created by laser ablation on graphite and subsequent supersonic jet cooling. The experimental results, complemented by ab initio calculations at the CASSCF level, allowed for the determination of ionization energies. In 2005-2006, Michael Duncan (U Georgia, Athens) with the CDG group measured the ionization energies of carbon clusters up to $n=18$, and Henry F. Schaefer's group (Georgia, Athens) is performing complementary theoretical calculations. Ralf Kaiser (U Hawaii) and the CDG, initiated a program to prepare free radicals and intermediate species by reaction of carbon clusters produced by laser ablation with hydrocarbons. Reactions with C_2H_2 allowed for the preparation of the C_3H radical in sufficient and stable quantities to determine its ionization onset with VUV-TOFMS. Joel Bowman (Emory) and Alex Mebel (Florida International U) are performing theoretical calculations to determine the structures of these radicals. Ricardo Metz (U Mass, Amherst) with the CDG, initiated a study of metal oxides, using the ablation apparatus that had been developed at the CDB. A mixture of metal oxides (e.g., Fe_3O_4) was pressed into a graphite rod and ablation was performed at kHz repetition rates with a Nd-YLF laser (527 nm). This new method allowed the IEs of FeO and CuO to be measured directly for the first time.¹⁰ Furthermore this ablation method has been coupled to photoelectron imaging, allowing more detailed information about the valence electronic structure of these important metal oxide materials.

Molecular nano-imaging- There is enormous interest in understanding how organic compounds influence the chemistry of nanoparticles – both inorganic and living. For example, the organic composition of nanometer-sized aerosol surfaces can play critical roles in both the radiative balance and chemistry of the troposphere. Organic molecules are also critical determinants in the structure and dynamics at boundaries of different cellular structures. Recently DOE has awarded funds to develop a novel national user facility, at the Chemical Dynamics Beamline, to perform chemical imaging on such surfaces using VUV photoionization mass spectrometry. The basic principle is to combine single photon ionization mass spectrometry with ion beam desorption for the direct detection of the neutrals via tunable VUV post-ionization. This technique, termed "molecular nano-imaging", has a theoretical spatial resolution of 10 nm and chemical specificity at the

molecular level. Traditional electron and optical-based imaging techniques generally lack sufficient chemical specificity to unravel the more complex systems prevalent in nature. Furthermore, many optical techniques do not scale well when reduced to nanometer dimensions. Imaging mass spectrometry, if the parent ion can be detected intact, is unique among microscopies in that labeling is not required because of high molecular specificity.

To fully exploit the chemical specificity of single photon ionization for mass spectral imaging, the fragmentation of the parent cation must be minimized. It is well known that the amount of fragmentation in a mass spectrum is extremely sensitive to the amount of internal energy within the parent ion or neutral molecule. "Proof-of-concept" experiments were undertaken with both photon (Nd-YLF laser, 527 nm, 1kHz) and ion (C_{60} ion gun, 5-20 kV, 10-14 kHz) beams to quantify these issues. The "bucky-ball" effort is a collaboration between beamline staff and Nick Winograd (Penn State). In both cases there was substantial enhancement of parent molecule signal with VUV post-ionization, and utilizing delayed extraction nearly fragment-free parent ions could be detected for certain molecules. These experiments were exploratory in nature and, while illuminating, require further analysis. However, in general, these experiments strongly suggest that tunable VUV photoionization mass spectrometry would be an ideal tool to map the chemical complexity of nano-scale aerosols and biological structures and will fit in very well with DOE missions to harness energy technologies for the future, bioremediation and the environmental impact of energy production.

References:

- ¹ J. Shu, K. R. Wilson, M. Ahmed, and S. R. Leone, "Coupling a versatile aerosol apparatus to a synchrotron: vacuum ultraviolet light scattering, photoelectron imaging, and fragment free mass spectrometry", *Rev. Sci. Instrum.* **77**, 043106 (2006)
- ² E. R. Mysak, K. R. Wilson, M. Jimenez-Cruz, M. Ahmed, and T. Baer. "Synchrotron Radiation Based Aerosol Time-of-Flight Mass Spectrometry for Organic Constituents," *Anal. Chem.* **77**, 5953 (2005)
- ³ J. Shu, K. R. Wilson, A. N. Arrowsmith, M. Ahmed, and S. R. Leone, "Light scattering of ultrafine silica particles by VUV synchrotron radiation," *Nano Lett.* **6**, 1009 (2005)
- ⁴ J. Shu, K. R. Wilson, M. Ahmed, S. R. Leone, C. E. Graf, and E. Ruhl, "Elastic light scattering from nanoparticles by monochromatic vacuum-ultraviolet radiation," *J. Chem. Phys.* **124**, 034707 (2006)
- ⁵ K. R. Wilson, D. S. Peterka, M. Jimenez-Cruz, S.R. Leone, and M. Ahmed. "VUV Photoelectron Imaging of Biological Nanoparticles – Ionization energy determination of nano-phase glycine and phenylalanine-glycine-glycine". *Phys. Chem. Chem. Phys.* **8**, 1884 (2006).
- ⁶ E. Gloaguen, E. R. Mysak, S. R. Leone, M. Ahmed, and K. R. Wilson "Investigating the chemical composition of mixed organic-inorganic particles by "soft" VUV photoionization: the reaction of ozone with anthracene on sodium chloride particles," *Int. J. Mass Spectrom.* (In press).
- ⁷ K. R. Wilson, M. Jimenez-Cruz, C. Nicolas, L. Belau, S. R. Leone, and M. Ahmed, "Thermal Vaporization of Biological Nanoparticles: Fragment-Free VUV Photoionization Mass Spectra of Tryptophan, Phenylalanine-Glycine-Glycine and β -Carotene," *J. Phys. Chem. A* **110**, 2106 (2006)
- ⁸ K. R. Wilson, L. Belau, C. Nicolas, M. Jimenez-Cruz, S. R. Leone, and M. Ahmed, "Direct determination of the ionization energy of histidine with VUV synchrotron radiation," *Int. J. Mass Spectrom.* **249-250**, 155, (2006)
- ⁹ C. Nicolas, J. Shu, D. S. Peterka, M. Hochlaf, L. Poisson, S. R. Leone, and M. Ahmed, "Vacuum ultraviolet photoionization of C_3 ," *J. Am. Chem. Soc.* **128**, 220 (2006)
- ¹⁰ R. B. Metz, C. Nicolas, M. Ahmed, and S. R. Leone, "Direct determination of the ionization energies of FeO and CuO with VUV radiation," *J. Chem. Phys.* **123**, 114313 (2005)

Spectroscopy of Organometallic Radicals

Michael D. Morse

Department of Chemistry

University of Utah

315 S. 1400 East, Room 2020

Salt Lake City, UT 84112-0850

morse@chem.utah.edu

I. Program Scope:

In this project, we seek to obtain fundamental physical information about unsaturated, highly reactive organometallic radicals containing open d subshell transition metal atoms. Gas phase electronic spectroscopy of jet-cooled transition metal molecules is used to obtain fundamental information about ground and excited electronic states of such species as the transition metal carbides and organometallic radicals such as CrC_2H , CrCH_3 , and NiCH_3 . High resolution infrared spectroscopy is applied to the unsaturated transition metal carbonyls, MCO , $\text{M}(\text{CO})_2$, $\text{M}(\text{CO})_3$, *etc.*

II. Recent Progress:

A. Optical spectroscopy of RuC , CrC_2H , CrCH_3 , and NiCH_3

During the past three years, we have carried out resonant two-photon ionization (R2PI) and dispersed fluorescence (DF) spectroscopic studies of the transition metal carbide, RuC ,¹ and of the polyatomic transition metal radicals CrC_2H , CrCH_3 , and NiCH_3 .² Our work on RuC has included rotationally resolved studies of the 0-0, 1-0, 2-0, 3-0, and 4-0 bands of the $[18.1]^1\Pi - X^1\Sigma^+$ system, which has allowed an RKR potential curve to be generated for the $[18.1]^1\Pi$ state. In addition, the $[21.4]0^+$, $[21.6]2$, and $[23.2]^3\Delta_3$ states have now been identified in RuC . Excited state lifetimes have been measured for all of these states, and rotationally resolved measurements of the line positions have been made, allowing bond lengths to be determined. Ruthenium carbide is now the best understood of all of the diatomic transition metal carbides, having 16 different electronic states (as defined by S , Λ , and Ω) identified and characterized. States that have been located and at least partially characterized include the ground $X^1\Sigma^+$ state, deriving from the $10\sigma^2 11\sigma^2 5\pi^4 2\delta^4$ configuration; all of the states ($^3\Delta_{3,2,1}$ and $^1\Delta_2$) deriving from the $10\sigma^2 11\sigma^2 5\pi^4 2\delta^3 12\sigma^1$ configuration; all of the states ($^1\Phi_3$, $^3\Phi_{4,3,2}$, $^1\Pi_1$, and $^3\Pi_{2,1,0^+,0^-}$) deriving from the $10\sigma^2 11\sigma^2 5\pi^4 2\delta^3 6\pi^1$ configuration; and the $^3\Delta_3$ state deriving from the $10\sigma^2 11\sigma^2 5\pi^4 2\delta^3 13\sigma^1$ configuration.

In other work, we have published the vibrationally resolved resonant two-photon ionization and dispersed fluorescence spectra of CrC_2H , CrCH_3 , and NiCH_3 .² These molecules are among the most complicated open d -subshell molecules yet known for which optical spectra have been obtained in the gas phase. The vibronically resolved spectra that have been recorded for CrC_2H and NiCH_3 have allowed metal-carbon vibrational frequencies and anharmonicities to be measured for these species in their excited states. For NiCH_3 , values of ω_e and $\omega_e x_e$ were also obtained for the ground state. For CrCH_3 and CrC_2H , values of $\Delta G_{1/2}$ for the Cr-C stretching vibration were also obtained for the ground state. Rotationally resolved scans over all three molecules have been accomplished, but these have not yet yielded to analysis. The NiCH_3 scans

show obvious perturbations, since the different vibrational levels of the upper state and the scans over the ^{58}Ni and ^{60}Ni species are all very different in appearance. In contrast, the rotationally resolved spectra of CrC_2H and CrCH_3 are a forest of lines. In the case of the ${}^6\Sigma^+ \leftarrow X^6\Sigma^+$ transition of CrC_2H (which has 54 rotational branches), we have recently been able to identify lines that belong to the P_1 , R_1 , R_2 , R_5 , R_{31} , R_{35} , R_{42} , and R_{62} branches. We are now experimenting with different numberings of these lines, and expect that we will be able to analyze and fit the spectrum.

Finally, during the collection of data on CrC_2H , we also recorded the spectrum of the minor isotopomer of chromium hydride, $^{50}\text{Cr}^1\text{H}$. We measured the excited state lifetime of this species, which is currently of considerable interest in astrophysics. This paper has now been published in the *Astrophysical Journal*.³

B. Infrared Spectroscopy of unsaturated transition metal carbonyls

We have completed the development of a slit-jet discharge source diode laser spectrometer for high-resolution investigations of unsaturated transition metal carbonyls. The device uses a slit orifice with a width of 200 μm and a length of 15 mm. A Teflon insulator separates the slit aperture from a pair of stainless steel discharge electrodes. During the operation of the pulsed valve, the discharge electrodes are biased to a negative potential, inducing a discharge in which electrons are accelerated into the slit channel, completing the circuit at the grounded slit nozzle body. Volatile organometallic molecules such as $\text{Cr}(\text{CO})_6$, $\text{Fe}(\text{CO})_5$, and $\text{Ni}(\text{CO})_4$ seeded in the argon carrier gas, are exposed to the discharge, producing fragment species such as CrCO , $\text{Cr}(\text{CO})_2$, $\text{Cr}(\text{CO})_3$, etc.

Following supersonic expansion into vacuum, the beam of molecular fragments is crossed with the output of a lead-salt diode laser that is multipassed across the length of the slit jet expansion (currently 15 times) using a Perry cell. The transmitted laser intensity is detected using a HgCdTe detector. In order to increase the detection efficiency and discriminate against precursor molecule absorptions and noise, the discharge is pulsed at 15 kHz and the preamplified signal is detected using a lock-in detector.

In addition to the main IR laser beam, partial reflections are used to record (1) fringes from a 0.048 cm^{-1} free spectral range germanium étalon, and (2) the spectrum of a reference gas, typically OCS , N_2O , or allene. These are used for absolute calibration of the instrument.

This system had been successfully tested using $\text{Fe}(\text{CO})_5$, and the CO stretching vibrations of FeCO and $\text{Fe}(\text{CO})_2$, which had previously been reported, were readily detected. Using $\text{Ni}(\text{CO})_4$, we have succeeded in recording the spectrum of the ν_1 mode (CO stretch) of $^{58}\text{NiCO}$ and $^{60}\text{NiCO}$. The fitted constants from our study provide band origins of 2010.692 89(34) and 2010.645 28(23) cm^{-1} for $^{58}\text{NiCO}$ and $^{60}\text{NiCO}$, respectively. Rotational constants and bond lengths determined from the spectra are consistent with values reported from the millimeter wave spectroscopic study that was published in 2004.

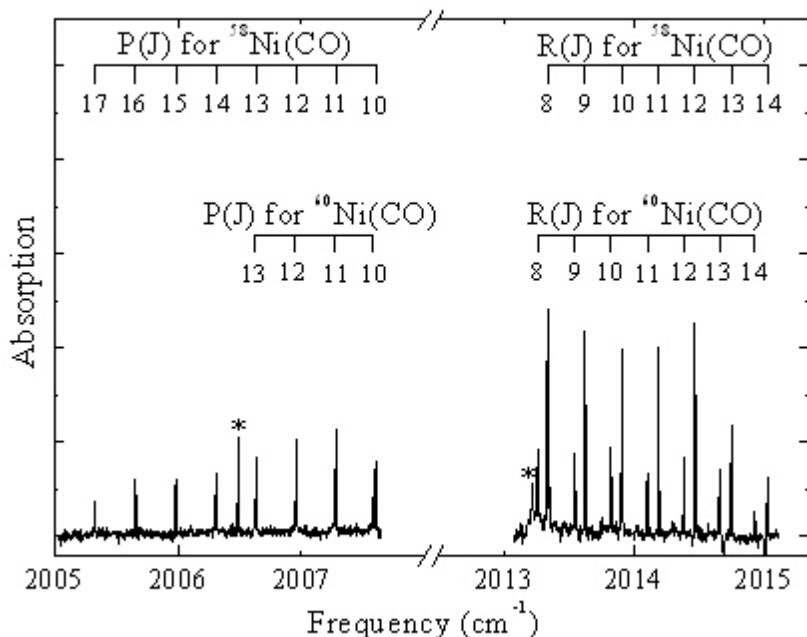


Figure 1. Rotationally resolved spectra of $^{58}\text{NiCO}$ and $^{60}\text{NiCO}$, in the CO stretching region.

In the course of collecting the NiCO spectrum, we also observed the spectrum of a molecule that depleted when the discharge was turned on. This was surprising, since the parent molecule, $\text{Ni}(\text{CO})_4$ has no known transitions in this region. After some investigation, the spectrum was determined to arise from the isotopically substituted species, $\text{Ni}(\text{CO})_3(^{13}\text{CO})$ and $\text{Ni}(\text{CO})_3(\text{C}^{18}\text{O})$, which constitute only 4.2 % and 0.08 % of the molecules in the sample, respectively. From the measured rotational constants, $B''(\text{Ni}(\text{CO})_3(^{13}\text{CO})) = 0.034736(2) \text{ cm}^{-1}$ and $B''(\text{Ni}(\text{CO})_3(\text{C}^{18}\text{O})) = 0.033764(4) \text{ cm}^{-1}$, the Ni-C and C-O bond lengths were determined to be $r_0(\text{Ni-C}) = 1.839(7) \text{ \AA}$ and $r_0(\text{C-O}) = 1.121(10) \text{ \AA}$.

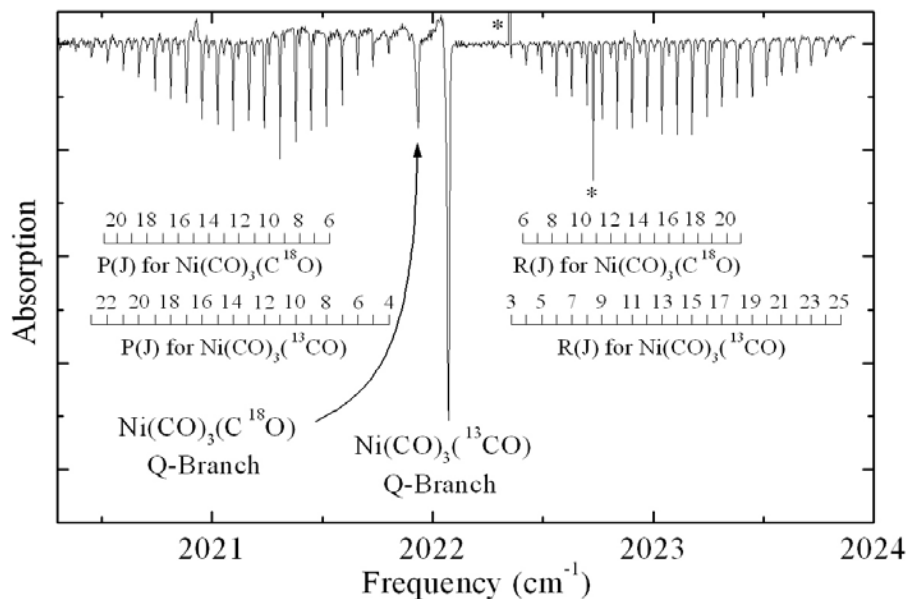


Figure 2. Rotationally resolved and assigned spectra of $\text{Ni}(\text{CO})_3(^{13}\text{CO})$ and $\text{Ni}(\text{CO})_3(\text{C}^{18}\text{O})$, in the CO stretching region.

III. Future Plans

A. R2PI and DF spectroscopy of transition metal carbides and radicals

Projects for the upcoming year include: (1) Assignment of the rotational lines in the ${}^6\Sigma^+ \leftarrow X^6\Sigma^+$ band system of CrCCH and fitting of the spectrum to extract the spectroscopic constants; (2) Analysis of the rotationally resolved spectrum of TiC, using dispersed fluorescence from single rovibronic levels to identify the lines; (3) Resolution of the rotational structure and analysis of a red band system of MoC; (4) A manuscript on the spin-forbidden $c^3\Sigma^+ \leftarrow X^1\Sigma^+$ system of YF will be written up and submitted for publication; (5) Attempts to record and analyze the spectra of several transition metal cyanides (or isocyanides) will be made. Species to be investigated will include CuCN, AgCN, AuCN, ScNC, and YNC (these latter two molecules are thought to be isocyanides, while the former are expected to be cyanides). When the spectrum of CrCCH is analyzed, we will attempt to record the spectrum of the isovalent molecule, CrCN.

B. IR spectroscopy of unsaturated transition metal carbonyls

We have been having difficulty finding spectra of other unsaturated transition metal carbonyls beyond FeCO, Fe(CO)₂, and NiCO. We have searched for spectra of CrCO, Cr(CO)₂, Ni(CO)₂, and Fe(CO)₃ without success. Attempts to modify the nozzle to allow the metal atom and CO to recombine more readily are being made, and it is hoped that these will result in the observation of spectra of these small molecules. In addition, we are attempting experiments in which H₂ is added to the carrier gas or is part of the precursor molecule (as in HMn(CO)₅, H₂Fe(CO)₄, and HCo(CO)₄) in order to obtain spectra of hydrogenated unsaturated species, such as HMnCO, HFeCO, and HCoCO. Other precursor molecules that will be employed include methyl compounds such as CH₃Mn(CO)₅ and CH₃Co(CO)₄. The aim of this work will be to establish the vibrational frequencies, rotational constants, geometries, bond lengths, and electronic symmetries of these parent molecules and their more interesting fragments.

IV. Publications from DOE Sponsored Research 2003-present:

1. N. F. Lindholm, D. A. Hales, L. A. Ober and M. D. Morse, "Optical spectroscopy of RuC: 18 000 - 24 000 cm⁻¹," J. Chem. Phys. **121**, 6855-60 (2004).
2. D. J. Brugh, R. S. DaBell and M. D. Morse, "Vibronic spectroscopy of unsaturated transition metal complexes: CrC₂H, CrCH₃, and NiCH₃," J. Chem. Phys. **121**, 12379-85 (2004).
3. S. Shin, D. J. Brugh, and M. D. Morse, "Radiative lifetime of the v=0,1 levels of the A⁶Σ⁺ state of CrH," Astrophys. J. **619**, 407-11, (2004).
4. Alonzo Martinez and Michael D. Morse, "Infrared Diode Laser Spectroscopy of Jet-Cooled NiCO, Ni(CO)₃(¹³CO), and Ni(CO)₃(C¹⁸O)," J. Chem. Phys. **124**, 124316/1 - 124316/8 (2006).

“Electronic Structure of Transition Metal Clusters, and Actinide Complexes, and Their Reactivities” October 2006

K. Balasubramanian

Dept of Mathematics, computer science and physics, California State University East Bay, Hayward CA; Chemistry and Material Science Directorate, Lawrence Livermore National Laboratory, University of California, Livermore, California 94550; Glenn T. Seaborg Center, Lawrence Berkeley National Laboratory, Berkeley, California 94720;

balu@csueastbay.edu

Program Scope

We work on two major areas: (1) computational chemistry and computational spectroscopy of transition metal clusters, carbides and complexes, (2) computational actinide chemistry of complexes of relevance to environmental management of high-level nuclear wastes. Many of our studies in transition metal area are driven by experimental works on gas-phase spectroscopy of transition metal compounds. Computational actinide chemistry has been an important area of interest for (1) interface with ongoing experimental works at LBNL, ORNL, (2) Educational outreach efforts in computational actinide chemistry as there is dearth of young actinide chemists. Computations of actinide complexes are also important to understanding of the complexes found in geochemical and biochemical environment and are thus critical to management of high-level nuclear wastes. Our studies are focused on the geometrical and electronic properties such as ionization potentials, electron affinities, and binding energies of transition metal species. Especially third and second row transition metal clusters transition metal carbides have been considered. Actinide complexes such as uranyl and plutonyl complexes are being studied in solution. These studies are made with relativistic complete active space multi-configuration self-consistent-field (CASSCF) followed by large-scale CI computations and relativistic CI (RCI) computations up to 60 million configurations.

Recent Progress

Results of our computational studies and comparison with experiment have been described extensively in publications¹⁻¹⁶, which contain details such as tables and figures. We have outlined here only the major highlights, in each of the categories. For this purpose, we have two major categories as described below.

Spectroscopic Properties of Transition Metal Species.

We have carried out systematic studies on the potential energy curves and spectroscopic constants of a number of second-row transition metal carbides such as MoC¹³, NbC¹⁰, ZrC¹⁴ and RuC¹. In addition in collaboration with experimental work, we have studied the gold dihydride², molecule. All of the second-row transition metal carbides are challenging due to the open-shell nature of the metal resulting in a number of low-lying electronic states for this molecule. We have carried out state-of-the-art complete active space multi-configuration self-consistent field followed by multireference configuration interaction methods in conjunction with relativistic effects. For MoC our computed transition energies to the 1³Δ and 4¹Δ states are 3430 and 8048 cm⁻¹ respectively, in fair agreement with the results obtained by Morse and coworkers [JCP 114, 2938, (2001)] namely, 4003 and 7834 cm⁻¹ respectively. The three band systems located at 18611, 20700 and 22520 cm⁻¹, observed by Morse et al. [JCP 109, 7851, (1998)] were attributed to the excited 11³Σ⁻, 14³Π, and 15¹Π states of MoC. Table I summarizes dipole moment trends.

Table I Dipole Moments of Some Second and Third row Transition Metal carbides.

TiC $8\sigma^1 9\sigma^1, ^3\Sigma^-$ 2.51 Debye	VC $8\sigma^2 1\delta^1, ^2\Delta$ 7.33 Debye	CrC $8\sigma^2 1\delta^2, ^3\Sigma^-$ 6.8 Debye	MnC	FeC $8\sigma^2 1\delta^3 9\sigma^1, ^3\Delta$ 2.36 Debye
ZrC $8\sigma^1 9\sigma^1, ^3\Sigma^-$ 3.23 Debye	NbC $8\sigma^2 1\delta^1, ^2\Delta$ 6.77 Debye	MoC $8\sigma^2 1\delta^2, ^3\Sigma^-$ 5.87 Debye	TcC	RuC $8\sigma^2 1\delta^4, ^1\Sigma^+$ 4.551 Debye

We have determined that the ground state of ZrC as $^3\Sigma^+$ although there are two low-lying $^1\Sigma^+$ states (below 5000 cm^{-1}) which strongly interact resulting in avoided crossings. The lowest $^1\Sigma^+$ state corresponds to a combination of $1\sigma^2 x\sigma^2 1\pi^4$ configurations whereas the second is an open shell singlet $1\sigma^2 2\sigma^1 3\sigma^1 1\pi^4$. Several avoided crossings were observed, for $^1\Pi$, $^3\Pi$, $^1\Delta$, $^3\Sigma^+$, and $^3\Delta$ states. We have identified $^3\Pi$ and $^1\Pi$ lying at 4367 and 5797 cm^{-1} respectively. The results are in good agreement with experimental findings of Rixon, Chowdhury and Merer [J. Mol. Spectrosc. 228, 554, (2004)], and indicate that the $^3\Pi$ - $^3\Sigma^+$, and $^1\Pi$ - $^1\Sigma^+$, bands located between 16000 - 19000 cm^{-1} are extremely complex due to near degeneracy of several $^1\Pi$ and $^3\Pi$.

Prof Lester Andrews carried out the matrix-isolation spectroscopy of AuH_2 molecule formed in solid hydrogen by reactions of excited gold atoms from laser ablation and irradiation after thermal evaporation. The X^2B_2 ground state of the AuH_2 molecule is separated by a 53 kcal/mol barrier from the $\text{Au}(^2D) + \text{H}_2$ decomposition products and it is 27 kcal/mole more stable than $\text{Au}(^2D) + \text{H}_2$. The bending modes of AuH_2 , AuHD , and AuD_2 have been observed at 638.1 , 570.6 , and 457.0 cm^{-1} . These frequencies and the lack of infrared intensity in the stretching modes are in agreement with the results of our calculations.

Electronic Structure of Actinide Complexes.

Our computational studies on actinide complexes were motivated by ongoing EXAFS studies of speciated complexes in geo and biochemical environments carried out by Prof Heino Nitsche's group at Berkeley, Dr. David Clark at Los Alamos and Dr. Gibson's work on small actinide molecules at ORNL. The hydrolysis reactions of uranyl, neptunyl and plutonyl complexes have received considerable attention due to their geochemical and biochemical importance but the results of free energies in solution and the mechanism of deprotonation have been topic of considerable uncertainty. We have computed deprotonating and migration of one water molecule from the first solvation shell to the second shell in $\text{UO}_2(\text{H}_2\text{O})_5^{2+}$, $\text{UO}_2(\text{H}_2\text{O})_5^{2+}\text{NpO}_2(\text{H}_2\text{O})_6^+$, and $\text{PuO}_2(\text{H}_2\text{O})_5^{2+}$ complexes. Our computed Gibbs free energy (7.27 kcal/m) in solution for the first time agrees with the experiment (7.1 kcal/m) while previous computations produced results in strong disagreement. Fig 1 below shows the mechanism of proton migration and hydroxide formation.

Transition state for the reaction $\text{UO}_2(\text{H}_2\text{O})_5^{2+} + \text{H}_2\text{O} \rightarrow \text{UO}_2(\text{H}_2\text{O})_4(\text{OH})^{2+} + \text{H}_3\text{O}^+$

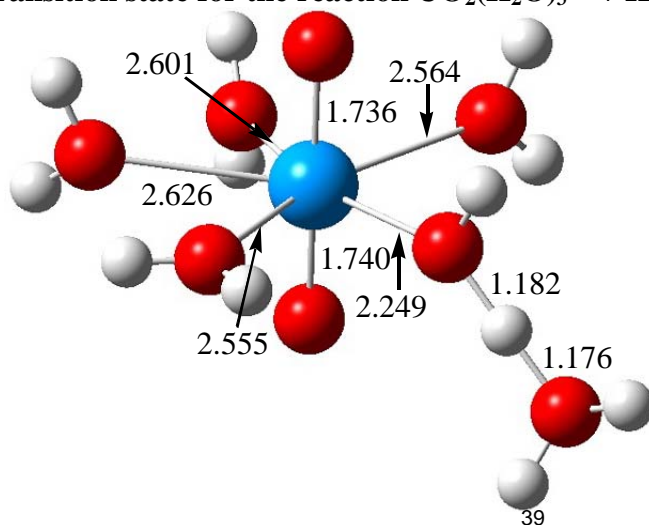
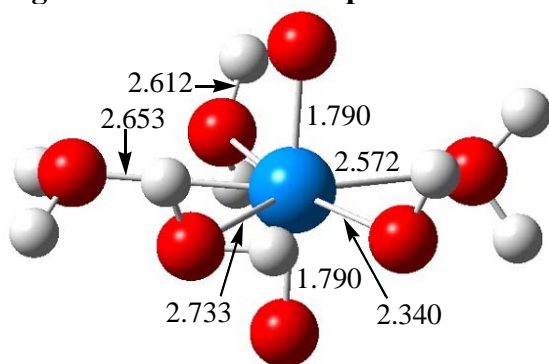


Figure below shows the optimized structure of $\text{NpO}_2(\text{H}_2\text{O})_4\text{OH}$ in aqueous solution.



We have studied the electronic and spectroscopic properties of plutonyl carbonate complexes of the types $\text{PuO}_2\text{CO}_3 \cdot n\text{H}_2\text{O}$, ($n=1,2$) and $\text{PuO}_2(\text{CO}_3)_3\text{Ca}_3$. Our computed equilibrium geometries and vibrational spectra of these species agree quite well with the EXAFS and Raman data available on related complexes. We have reported the results of *ab initio* quantum chemical computations on the plutonyl carbonate complex and its hydrated forms, viz., PuO_2CO_3 , $\text{PuO}_2\text{CO}_3 \cdot \text{H}_2\text{O}$ and $\text{PuO}_2\text{CO}_3 \cdot 2\text{H}_2\text{O}$. The results of our computations show that the computed geometries and vibrational frequencies are in reasonable agreement among these theoretical levels. Our computed geometries for the various interatomic distances at both MP2 and DFT levels agree quite well with the experimental EXAFS results of Clark et al. at Los Alamos in solution for the limiting Pu(VI) O_2 -carbonate complex. Our predicted equatorial carbonate vibrational mode frequency of 754 cm^{-1} at the MP2 level is consistent with the observed Raman band at 755 cm^{-1} in solution form of plutonyl carbonate complex..

Our computations on uranyl silicate complexes explained the observed contrasting pattern in the EXAFS spectra of Prof Nitsche and coworkers at Berkeley which showed two types of structures. With theoretical computations we were able to assign the origin of two different spectra to a bridge and atop type of complexes. We also studied the characteristics of $\text{UO}_2(\text{CO}_3)_2^{2-}$ and $\text{M}_2\text{UO}_2(\text{CO}_3)_2$ ($\text{M} = \text{Li}^+$, and Na^+) in solution using coupled cluster doubles (CCD). The uranyl carbonate complexes are known to form water-soluble metal salts. In order to understand the nature of metal binding with carbonate complexes, we have studied here the structure and bonding of $\text{UO}_2(\text{CO}_3)_2^{2-}$ and $\text{M}_2\text{UO}_2(\text{CO}_3)_2$ ($\text{M} = \text{Li}^+$, and Na^+). The gas-phase structure $\text{UO}_2(\text{CO}_3)_2^{2-}$ is a D_{2h} structure with the carbonates in the equatorial position and the uranyl forming the axial linear bonds.

Future Plan

We are studying the spectroscopic properties and potential energy curves of YC and YN. We have also been considering actinyl complexes of experimental importance in collaboration with Prof Nitsche. There are mind boggling questions concerning the nature of these species and the role of 5f versus 6d orbitals in bonding and how relativistic effects influence the structures of these species. There are many challenges as we attempt to study these species. Both relativistic effects including spin-orbit effects and electron correlation effects must be considered accurately. We have also been investigating actinide complexes of environmental importance and their salvation phenomena. We have been looking at methods to consider aqueous actinide complexes.

References to Publications of DOE-sponsored work in 2004-2006

1. R. Guo and K. Balasubramanian, "Spectroscopic Constants and Potential Energy Curves of Ruthenium Carbide: RuC ", *J. Chem. Phys.* **120**, 7418-7425(2004).
2. Lester Andrews, Xuefeng Wang, and K. Balasubramanian, "The Gold Dihydride Molecule, AuH_2 : Calculations of Structure, Stability and Frequencies, and the Infrared Spectrum in Solid Hydrogen", *J. Phys. Chem A.* **108**, 2936-2940 (2004).

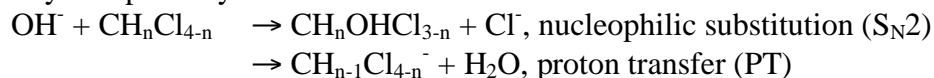
3. K. Balasubramanian, "Relativity and the Periodic Table", (D. Rouvray & R. B. King, editors), Periodic Table into the 21st Century, 2004
4. K. Balasubramanian, "Relativistic Double Group Spinor Representations of Non-rigid Molecules", *J. Chem. Phys.* **120**, 5524-5535(2004).
5. D. Majumdar and K. Balasubramanian, "Theoretical Study of the Electronic States of Nb₄, Nb₅ clusters and their anions (Nb₄⁻, Nb₅⁻), *J. Chem. Phys.* **121**, 4014-4032 (2004).
6. K. Balasubramanian, "Mathematical Basis of Periodicity in Atomic and Molecular Spectroscopy", Mathematics of the Periodic Table, Editors: R. B. King and D. H. Rouvray, Nova Press, NJ 2004
7. D. Chaudhuri and K. Balasubramanian, "Electronic Structure and Spectra of Plutonyl Complexes and their hydrated forms: PuO₂CO₃ and PuO₂CO₃.nH₂O (n=1,2)", *Chemical Physics Letters*, 399, 67-72 (2004)
8. D. Majumdar and K. Balasubramanian, "Theoretical studies on uranyl–silicate, uranyl–phosphate and uranyl–arsenate interactions in the model H₂UO₂SiO₄ · 3H₂O, HUO₂PO₄ · 3H₂O, and HUO₂AsO₄ · 3H₂O molecules", *Chemical Physics Letters*, **397**, 26-33 (2004).
9. D. Majumdar and K. Balasubramanian, "Theoretical studies on the electronic structures of UO₂(CO₃)₂²⁻ and its metal salts: M₂UO₂(CO₃)₂ (M = Li⁺, and Na⁺)", *Molecular Physics*, **103**, 931 – 938(2005)
10. P. A. Denis and K. Balasubramanian, "Spectroscopic Constants and Potential Energy Curves of low-lying electronic states of NbC", *J. Chem. Phys.* **123**, 054318 (2005) –Published online 9Aug 2005.
11. K. Balasubramanian, "Relativistic Effects in the Chemistry of very Heavy and super heavy Molecules", Lecture Series on Computer & Chemical sci. 4, 759-764 (2005) UCRL-JC-145416
12. Z. Cao and K. Balasubramanian, "Theoretical Studies of hydrated complexes of uranyl, neptunyl and plutonyl in aqueous solution: UO₂²⁺(H₂O)_n, NpO₂²⁺(H₂O)_n, and PuO₂²⁺(H₂O)_n", *J. Chem. Phys.* **123**, 114309-1 to 114309-12 (2005) UCRL-JRNL-221802
13. P. A. Denis and K. Balasubramanian, "Spectroscopic Constants and Potential Energy Curves of low-lying electronic states of MoC", *J. Chem. Phys.* 125, 024306-1, 024306-9 (2006) UCRL-JRNL-219159
14. P. A. Denis and K. Balasubramanian, "Spectroscopic Constants and Potential Energy Curves of low-lying electronic states of ZrC", *J. Chem. Phys.* **124**, 174312 (2006). UCRL-JRNL-218409
15. D. Chaudhuri and K. Balasubramanian, "Electronic Structure and Spectra of di and tri carbonate complexes of Plutonyl: PuO₂[CO₃]₂ and PuO₂[CO₃]₃Ca₃", *Chemical Physics Letters*, to be submitted
16. K. Balasubramanian and Z. Cao, "Fluxional Motions and internal rotational barriers of Water molecules bound to UO₂²⁺, NpO₂⁺, and PuO₂²⁺", *Chemical Physics Letters*, to be submitted

Molecular Theory & Modeling
Reactions of Ions and Radicals in Aqueous Systems

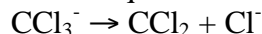
Bruce C. Garrett
Chemical Sciences Division
Pacific Northwest National Laboratory
902 Battelle Blvd.
Mail Stop K9-90
Richland, WA 99352
bruce.garrett@pnl.gov

The long-term objective of this project is to understand the factors that control the chemical reactivity of atomic and molecular species in aqueous environments. Chemical reactions in condensed phase environments play crucial roles in a wide variety of problems important to the Department of Energy (DOE), (e.g., corrosion in nuclear reactors promoted by reactive radical species such as OH, release of hydrogen from hydrogen storage materials, catalysis for efficient energy use, and contaminant degradation in the environment by natural and remedial processes). The need in all of these areas is to control chemical reactions to eliminate unwanted reactions and/or to produce desired products. The control of reactivity in these complex systems demands knowledge of the factors that control the chemical reactions and requires understanding how these factors can be manipulated to affect the reaction rates. The goals of this research are the development of theoretical methods for describing reactions in condensed phases (primary aqueous liquids) and their application to prototypical problems of interest to DOE.

Recent efforts have focused on understanding the mechanisms of two aqueous phase reactions – degradation of chloroform in basic aqueous solutions and the reaction of OH radicals with aqueous NaCl solutions to form Cl₂. Reactions of OH⁻ with chlorinated methane molecules can proceed by two pathways:



Our earlier studies of these reactions (Borisov et al. *JPCA* **105**, 7724, 2001) showed that the proton transfer pathway becomes energetically more favorable as the degree of chlorination increases. This result seems to support experimental studies (Hine and Dowell, *JACS* **76**, 2688, 1954), which concluded that the reaction with chloroform proceeds by the proton transfer pathway with subsequent reaction



The mechanism by which the diradical CCl₂ is further degraded was not determined in the experimental studies. A possible reaction of CCl₂ is insertion into a water molecule to form the chlorinated alcohol, CH(OH)Cl₂. The products from this 3-step PT pathway are identical to the products from the S_N2 reaction. We have used electronic structure calculations with variational transition state theory to understand the relative contributions of these two reaction pathways to the production of CH(OH)Cl₂ in the mechanism:





MP2/aug-cc-pVDZ calculations were carried out with solvent effects included by the polarizable continuum model (PCM). Variational transition state theory was used to calculate rate constants for activated processes, reactions (2)-(4). The association rate constant (k_A) was approximated by Conduction-Diffusion theory with the dissociation rate (k_D) determined by detailed balance. The reaction energetics are summarized in Figure 1. The S_N2 channel is calculated to have a much lower activation barrier relative to reactive complex 1 (RC1), i.e., 26.3 kcal/mol, in comparison to that for the proton transfer channel (the energy difference between TS3 and RC1), which is 36.3 kcal/mol. We are also using a hierarchical approach to evaluate the reaction energetics more accurately, ranging from highly accurate first principles calculations on model cluster systems to approximate treatment of solvation energies by QM/MM methods. Methods for including important dynamical effects of the solvent on the reaction kinetics are also being pursued.

Another focus of our research in the past couple of years has been on understanding the factors controlling radical reactions in aqueous systems. An important factor is the effect of the open-shell nature of the radical on the solvation structure around the radical, since solvation and solvent reorganization can play an important role in chemical reactivity. Towards this end, we studied OH radical interactions with water to understand how the unpaired orbital in OH can affect the interaction energy. For geometries with C_s symmetry, the two lowest electronic states have different symmetries (A' and A'') and their energies were calculated accurately using the CCSD(T)/aug-c-pVTZ level of theory. We performed calculations along scans for different intermolecular coordinates to systematically study the potential energy surfaces. The splitting between the two states is small, ranging from about 2.5 kcal/mol at the global minimum (where H_2O is the proton donor) to less than 0.5 kcal/mol at the minimum where OH is the proton donor. We also observed a crossing of the two states along one scan in which the geometries had C_1 symmetry.

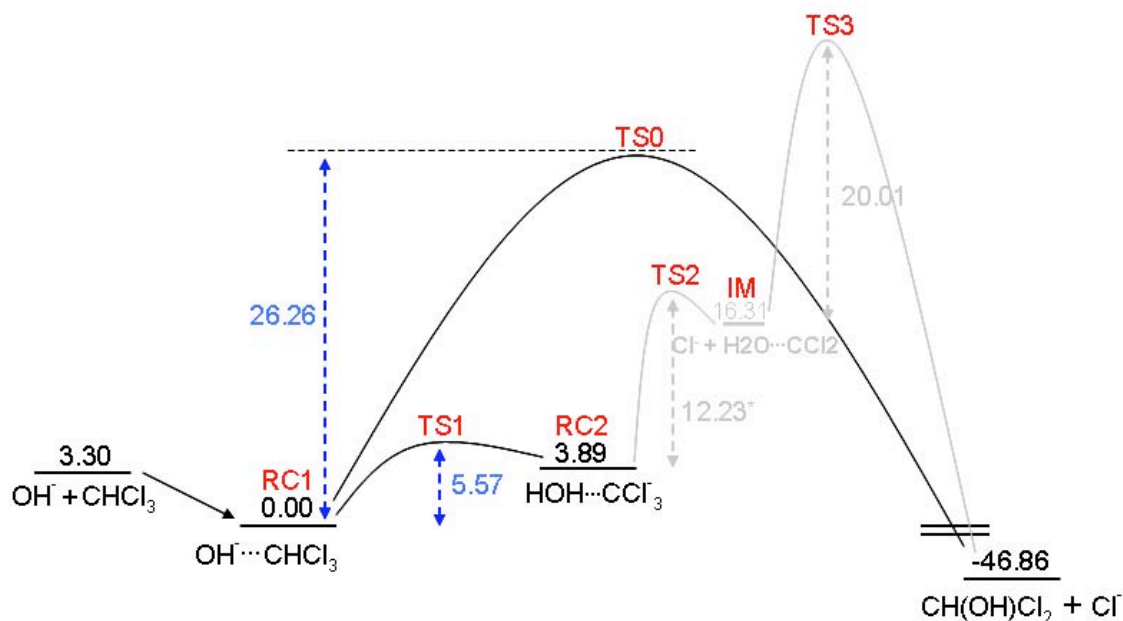


Figure 1: Schematic of the energetics for the $\text{OH}^- + \text{CHCl}_3 \rightarrow \text{CH}(\text{OH})\text{Cl}_2 + \text{Cl}^-$ reaction mechanism.

More recently, we employed CCSD(T)/aug-c-pVTZ calculations to decompose the binding energies of the $\text{OH}\cdot(\text{H}_2\text{O})_n$ ($n=2, 3$) complexes into their many-body contributions. We performed the energy decomposition with the scheme introduced by Hankins et al. [J. Chem. Phys. **53**, 4544 (1970)] and applied by Xantheas [J. Chem. Phys. **100**, 7523 (1994)] to water clusters. Geometries for the clusters were chosen to be the same as for the water clusters studied by Xantheas, with one of the hydrogen atoms removed from one of the water molecules (see Figure 2). We find that the 3-body contributions to total binding energies of these clusters are comparable to those seen for the water clusters. With basis set superposition error included, the 3-body contribution is about 17% in the $\text{OH}\cdot(\text{H}_2\text{O})_2$ cluster and about 24% in the $\text{OH}\cdot(\text{H}_2\text{O})_3$ cluster. The 4-body contribution is only 2% for the $\text{OH}\cdot(\text{H}_2\text{O})_3$ cluster, which is very similar to the value for the $(\text{H}_2\text{O})_4$ cluster. We are using these results to assess the accuracy of the newly developed hydroxide-water interaction potential where the water part is described by the Thole-type model (TTM) for larger OH – water clusters.

We have initiated studies of the reactions of OH radical with Cl^- ions in aqueous solutions to form Cl_2 . A possible mechanism begins with OH radical forming a stable complex with Cl^- . The complex can then interact with a second Cl^- ion to form OH^- and Cl_2^- . Charge transfer from Cl_2^- to OH radical then completes the process of forming Cl_2 . Preliminary studies indicate that the reaction of $\text{OH}\cdot\text{Cl}^-$ with Cl^- to form OH^- and Cl_2^- proceeds by an electronically nonadiabatic process. Future work will explore approaches to study the reaction dynamics of this process and determine if it is a feasible pathway for Cl_2 formation.

Collaborators on this project include M.-K. Tsai, G. K. Schenter, M. Dupuis, T. Iordanov, S. S. Xantheas, J. Li, S. Du, and J. Francisco. Battelle operates Pacific Northwest National Laboratory for the U. S. Department of Energy.

References to publications of DOE sponsored research (2004-present)

1. L. X. Dang and B. C. Garrett, "Molecular Mechanism of Water and Ammonia Uptake by the Liquid/Vapor Interface of Water," *Chemical Physics Letters* **385**, 309-313 (2004).
2. B. C. Garrett, "Ions at the Air/Water Interface," *Science* **303**, 1146-1147 (2004).
3. S. M. Kathmann, G. K. Schenter, and B. C. Garrett, "Multicomponent Dynamical Nucleation Theory and Sensitivity Analysis," *Journal of Chemical Physics* **120**, 9133-9141 (2004).
4. S. M. Kathmann, G. K. Schenter, and B. C. Garrett, "Dynamical Nucleation Theory: Understanding the Role of Aqueous Contaminants," in Proceedings of the 16th International Conference on Nucleation and Atmospheric Aerosols, edited by M. Kulmala and M. Kasahara (Kyoto University Press, 2004), p. 243-246.

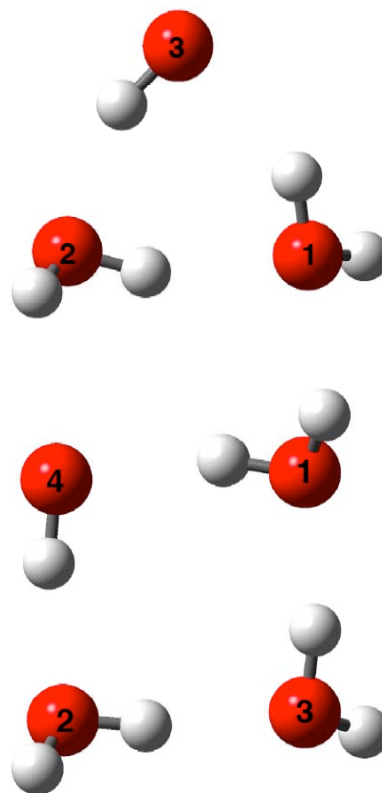


Figure 2. Geometries of $\text{OH}(\text{H}_2\text{O})_2$ (top) and $\text{OH}(\text{H}_2\text{O})_3$ (bottom) clusters used in many-body decomposition.

5. M. Roeselova, J. Vieceli, L. X. Dang, B. C. Garrett, and D. J. Tobias, "Hydroxyl Radical at the Air-Water Interface," *Journal of the American Chemical Society* **126**, 16308-16309 (2004).
6. B. C. Garrett, D. A. Dixon, D. M. Camaioni, D. M. Chipman, M. A. Johnson, C. D. Jonah, G. A. Kimmel, J. H. Miller, T. N. Rescigno, P. J. Rossky, S. S. Xantheas, S. D. Colson, A. H. Laufer, D. Ray, P. F. Barbara, D. M. Bartels, K. H. Becker, H. Bowen, S. E. Bradforth, I. Carmichael, J. V. Coe, L. R. Corrales, J. P. Cowin, M. Dupuis, K. B. Eisenthal, J. A. Franz, M. S. Gutowski, K. D. Jordan, B. D. Kay, J. A. LaVerne, S. V. Lymar, T. E. Madey, C. W. McCurdy, D. Meisel, S. Mukamel, A. R. Nilsson, T. M. Orlando, N. G. Petrik, S. M. Pimblott, J. R. Rustad, G. K. Schenter, S. J. Singer, A. Tokmakoff, L. S. Wang, C. Wittig, and T. S. Zwier, "Role of Water in Electron-Initiated Processes and Radical Chemistry: Issues and Scientific Advances," *Chemical Reviews* **105**, 355-389 (2005).
7. S. M. Kathmann, G. K. Schenter, and B. C. Garrett, "Ion-induced Nucleation: The Importance of Chemistry," *Physical Review Letters* **94**, 116104 (2005).
8. B. C. Garrett and D. G. Truhlar, "Variational Transition State Theory," in Theory and Applications of Computational Chemistry: The First 40 Years, edited by C. E. Dykstra, G. Frenking, K. S. Kim, and G. E. Scuseria (Elsevier, Amsterdam, 2005), p. 67-87.
9. T. D. Iordanov, G. K. Schenter, and B. C. Garrett, "Sensitivity analysis of thermodynamic properties of liquid water: A general approach to improve empirical potentials," *Journal of Physical Chemistry A* **110**, 762-771 (2006).
10. L. X. Dang, T. M. Chang, M. Roeselova, B. C. Garrett, and D. J. Tobias, "On NO_3^- - H_2O Interactions in Aqueous Solutions and at Interfaces," *Journal of Chemical Physics* **124** (2006).
11. B. C. Garrett, G. K. Schenter, and A. Morita, "Molecular Simulations of the Transport of Molecules Across the Liquid/Vapor Interface of Water," *Chemical Reviews* **106**, 1355-1374 (2006).
12. S. Du, J. S. Francisco, G. K. Schenter, T. D. Iordanov, B. C. Garrett, M. Dupuis, and J. Li, "The OH Radical - H_2O Molecular Interaction Potential," *Journal of Chemical Physics* **124**, 224318 (2006).
13. D. G. Truhlar and B. C. Garrett, "Variational Transition State Theory in the Treatment of Hydrogen Transfer Reactions," in Handbook of Hydrogen Transfer, edited by H. H. Limbach, J. T. Hynes, J. Klinman, and R. L. Schowen (VCH-Wiley, in press).
14. A. Fernandez-Ramos, B. A. Ellingson, B. C. Garrett, and D. G. Truhlar, "Variational Transition State Theory with Multidimensional Tunneling," in Reviews in Computational Chemistry, edited by K. B. Lipkowitz and D. B. Boyd (VCH Publishers, New York, in press).

Computational Studies of Radiolytic Species and Processes in Water

Daniel. M. Chipman, Chipman.1@nd.edu

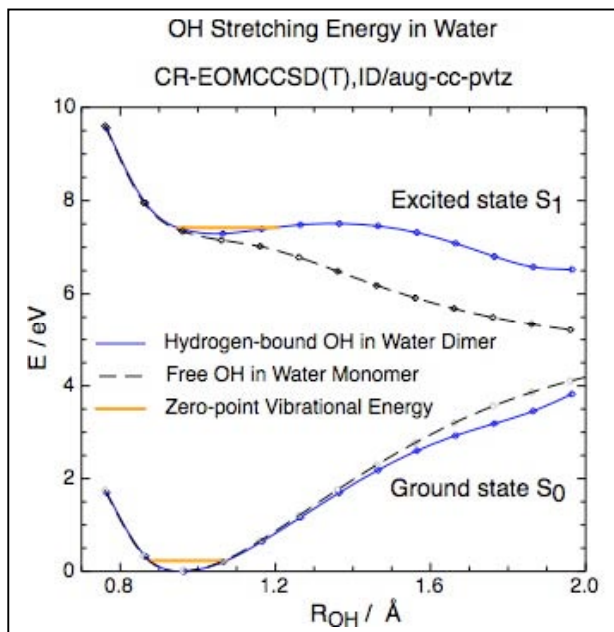
Radiation Laboratory, University of Notre Dame, Notre Dame, IN 46556

Program Scope

This program provides theoretical and computational support for experimental efforts in various group projects at the Notre Dame Radiation Laboratory that investigate water radiolysis. It particularly focuses on characterizing early events where aqueous radiolytic species are formed and transformed in the fs-ps time domain. The information from such studies is needed to provide initial conditions for Monte Carlo modeling of the subsequent inhomogeneous track chemistry and to understand how solvent influences the mechanisms of the various bimolecular reactions that ensue to produce final products.[7]

Recent Progress

We have found[5] in dimer, trimer, and tetrahedral pentamer water clusters that the lowest electronically excited state consistently develops a potential minimum near the Franck-Condon region in the stretching coordinate of an OH bond that participates in a hydrogen bond. This contrasts sharply with the strictly dissociative nature of this state in isolated water monomer. To learn more about this somewhat unexpected behavior, the water dimer has been examined in more detail[3] utilizing computational methods that are reliable even for large excursions from the equilibrium geometry. The excited potential minimum near the Franck-Condon region in the hydrogen-bound OH stretch coordinate of the dimer is found to be deep enough to support a quasibound vibrational state having lifetime long compared to the OH vibrational period. The constraint of an ice-like structure has also been relaxed, and it is found that a substantial fraction of excited dimers having liquid-like structures also support this quasibound vibrational state.



These findings give insight into the initial dynamics following electronic excitation of water, and provide support for the possible existence of exciton-like behavior at low energy that could furnish a mechanism for energy transport over substantial distances in ice and over short distances in liquid water.

Several advances have been made in an ongoing program to accurately yet efficiently include the effects of solvation on the electronic structure of a radiolytic solute by using an enhanced dielectric continuum model. Most such models used in practice dictate a cavity size prescription for which a nonnegligible fraction of the quantum-mechanically determined solute charge density penetrates outside the cavity into the dielectric region. Proper solution of the Poisson equation for the dielectric response in this situation leads to an often neglected volume polarization of the dielectric, in addition to the usually recognized surface polarization. We have developed a very efficient algorithm[1] to accurately compute this volume polarization dielectric effect.

Volume polarization of the dielectric is particularly important for solvation energies of charged solutes[1] and for solvation effects on second order properties. As an example of the latter we have shown a dramatic influence of volume polarization on the NMR shielding constants of acetonitrile, and also verified the utility of a simplified procedure developed to simulate the volume polarization effects in terms of an additional surface polarization.[8]

In hydrogen bonding solvents such as water the dielectric continuum model by itself is insufficient, because the interactions of a solute with nearby solvent molecules are significantly different than the long-range interactions with bulk solvent. This effect is particularly dramatic for a charged solute in water, and in this regard a simple means has been found to model the additional nondielectric hydrogen bonding effect on the solvation energy of an aqueous cation by empirically demonstrating that it correlates linearly with the normal electric field produced by the solute at the cavity surface.[2] Perhaps surprisingly, this correlation with the field is found to be significantly better than the analogous correlation with the solute electrostatic potential.

In order to investigate radiolytic systems, we are ultimately interested in developing a predictive capability for describing solvation effects on a solute that may have unpaired electron spin, may be highly distorted from its equilibrium geometry, and may be in an excited or ionized electronic state. Therefore, the number of empirically adjusted parameters in the solvation model must be kept to an absolute minimum, because appropriate experimental data is not usually available for calibration. For that reason, we define the dielectric cavity as an isodensity surface of the solute, which has only one parameter, namely the numerical value of the isodensity contour that governs the overall cavity size. After selecting that value, the isodensity criterion provides a cavity surface that automatically adapts itself to a naturally smooth shape dictated by the solute electronic structure. Computer code based on our original development in the Hondo electronic structure program has recently been implemented in the QChem[4] and Gamess programs to evaluate solvent dielectric contributions with an isodensity cavity around the solute, and to also provide for simulation or full evaluation of volume polarization effects.

The hydration structures and energetics of atomic oxygen anion, which is the conjugate base of OH radical, have been computationally characterized in clusters with up to five water molecules.[6] This provides insight into the hydration of $(\text{O}^-)(\text{H}_2\text{O})_n$ with comparison to the related proton-transferred family of $(\text{OH})(\text{OH})(\text{H}_2\text{O})_{n-1}$ structures. An exhaustive search yielded a total of 67 distinct local minimum geometries. For each cluster size n the lowest energy structure is always found in the $(\text{O}^-)(\text{H}_2\text{O})_n$ family, although with $n > 2$ there is considerable overlap in energy between other members of the $(\text{O}^-)(\text{H}_2\text{O})_n$ family with various members of the $(\text{OH})(\text{OH})(\text{H}_2\text{O})_{n-1}$ family. The hydrogen bonding arrangement tends to be nearly planar about the oxygen anion center in the lower energy members of the $(\text{O}^-)(\text{H}_2\text{O})_n$ family. This leaves the unpaired electron in an oxygen p -like orbital uninvolved in any hydrogen bond and so exposed for potential chemical interactions with other solutes. The hydrogen bonding arrangement tends to be substantially nonplanar about the anionic center that accepts hydrogen bonds in the $(\text{OH})(\text{OH})(\text{H}_2\text{O})_{n-1}$ family. Those OH bonds of water molecules or hydroxyl radicals that form hydrogen bonds to anionic centers are significantly stretched and anharmonic in comparison to those of equilibrium water molecules or OH radicals. The amount of the OH bond stretching is found to quantitatively correlate with the inverse of the distance to the other oxygen atom involved in the hydrogen bond.

Future Plans

Investigations into electronic excitation of water will be further pursued in several directions. An environment more representative of liquid water will be created both by including more solvent molecules in the explicitly treated cluster, either quantum mechanically or with effective fragment potentials, and by use of a dielectric continuum model for the remaining bulk solvent. The effects of additional degrees of geometric freedom and the various couplings among them will be examined to identify the most active coordinates necessary for inclusion in reduced dimensionality treatments of the excited potential energy surfaces. The scope of the studies will also be extended to examine the potential energy surfaces of additional low-lying excited states. Analogous investigations will be initiated to consider dissociative electron attachment processes that can occur through anionic Feshbach resonance states in water.

The dielectric continuum model we are developing to describe the influence of bulk solvent on the electronic structure of a radiolytic solute will be generalized to treat solute vertical excitation energies. Effects of volume polarization in the dielectric response are expected to be quite important there, because the solute cavity size is determined by the ground state charge density whereas the vertical excited state is generally more diffuse and so will penetrate even more outside the cavity. This generalization will require separation of the dielectric response into its fast optical and slow inertial components, which will each have its own distinct contribution from volume polarization.

BES Sponsored Publications in 2004-2006

D. M. Chipman, *New Formulation and Implementation for Volume Polarization in Dielectric Continuum Theory*, J. Chem. Phys. **2006**, *124*, 224111.

D. M. Chipman and F. Chen, *Cation Electric Field is Related to Hydration Energy*, J. Chem. Phys. **2006**, *124*, 144507.

D. M. Chipman, *Stretching of Hydrogen-Bonded OH in the Lowest Excited Electronic State of Water Dimer*, J. Chem. Phys. **2006**, *124*, 044305.

Y. Shao, L. F. Molnar, Y. Jung, J. Kussmann, C. Ochsenfeld, S. T. Brown, A. T.B. Gilbert, L. V. Slipchenko, S. V. Levchenko, D. P. O'Neill, R. A. DiStasio Jr, R. C. Lochan, T. Wang, G. J.O. Beran, N. A. Besley, J. M. Herbert, C. Y. Lin, T. Van Voorhis, S. H. Chien, A. Sodt, R. P. Steele, V. A. Rassolov, P. E. Maslen, P. P. Korambath, R. D. Adamson, B. Austin, J. Baker, E. F. C. Byrd, H. Dachsel, R. J. Doerksen, A. Dreuw, B. D. Dunietz, A. D. Dutoi, T. R. Furlani, S. R. Gwaltney, A. Heyden, S. Hirata, C.-P. Hsu, G. Kedziora, R. Z. Khalliulin, P. Klunzinger, A. M. Lee, M. S. Lee, W. Z. Liang, I. Lotan, N. Nair, B. Peters, E. I. Proynov, P. A. Pieniazek, Y. M. Rhee, J. Ritchie, E. Rosta, C. D. Sherrill, A. C. Simmonett, J. E. Subotnik, H. L. Woodcock III, W. Zhang, A. T. Bell, A. K. Chakraborty, D. M. Chipman, F. J. Keil, A. Warshel, W. J. Hehre, H. F. Schaefer III, J. Kong, A. I. Krylov, P. M. W. Gil, and M. Head-Gordon, *Advances in methods and algorithms in a modern quantum chemistry program package*, Phys. Chem. Chem. Phys. **2006**, *8*, 3172.

D. M. Chipman, *Excited Electronic States of Small Water Clusters*, J. Chem. Phys. **2005**, *122*, 044111.

D. M. Chipman and J. Bentley, *Structures and Energetics of Hydrated Oxygen Anion Clusters*, J. Phys. Chem. A **2005**, *109*, 7418.

B. C. Garrett, D. A. Dixon, D. M. Camaioni, D. M. Chipman, M. A. Johnson, C. D. Jonah, G. A. Kimmel, J. H. Miller, T. N. Rescigno, P. J. Rossky, S. S. Xantheas, S. D. Colson, A. H. Laufer, D. Ray, P. F. Barbara, D. M. Bartels, K. H. Becker, K. H. Bowen, Jr., S. E. Bradforth, I. Carmichael, J. V. Coe, L. R. Corrales, J. P. Cowin, M. Dupuis, K. B. Eisenthal, J. A. Franz, M. S. Gutowski, T. L. Head-Gordon, K. D. Jordan, S. M. Kathmann, B. D. Kay, J. A. LaVerne, S. V. Lymar, T. E. Madey, C. W. McCurdy, D. Meisel, S. Mukamel, A. R. Nilsson, T. M. Orlando, N. G. Petrik, S. M. Pimblott, E. Rohlfiing, J. R. Rustad, G. K. Schenter, S. J. Singer, A. Tokmakoff, L.-S. Wang, C. Wittig, and T. S. Zwier, *The Role of Water on Electron-Initiated Processes and Radical Chemistry: Issues and Scientific Advances*, Chem. Rev. **2005**, *105*, 335.

D. M. Chipman, *Simulation of Volume Polarization for the Influence of Solvation on Chemical Shielding*, Theor. Chem. Acc. **2004**, *111*, 61 (Tomasi honorary issue).

V. A. Rassolov and D. M. Chipman, *Alternative Fermi Contact Operators for EPR and NMR*, in "Calculation of NMR and EPR Parameters. Theory and Application." Ed. by M. Kaupp, M. Bühl, and V. G. Malkin (Wiley-VCH, Weinheim, 2004), pp. 493-504.

Molecular Theory & Modeling
Electronic Structure and Reactivity Studies in Aqueous Phase Chemistry

Michel Dupuis
Chemical Sciences Division
Pacific Northwest National Laboratory
902 Battelle Blvd.
Mail Stop K1-83
Richland, WA 99352
michel.dupuis@pnl.gov

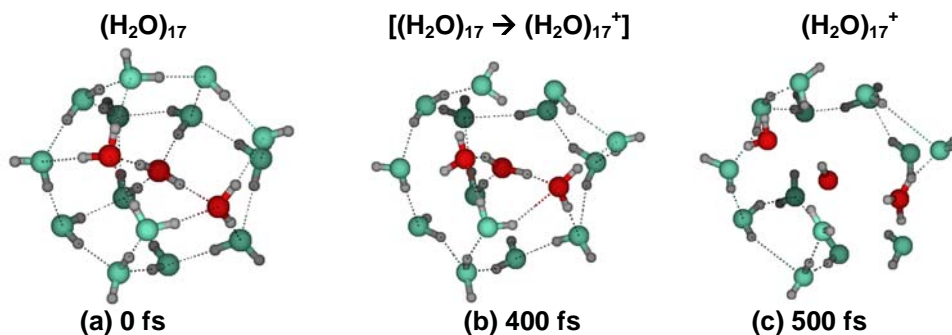
Summary.[#] We are interested in the theoretical characterization of molecular properties and reactivity of clusters and molecules, in particular in the condensed phase. One focus of our research involves the initial molecular processes that follow the primary energy deposition in radiolysis of water as observed in various applied technologies. We aim to characterize: i) the mechanisms and dynamics of the intrinsic reactions; ii) the effects of medium on the dynamics; iii) the mechanism of energy transfer within the solute and into the solvent; iv) the mechanism of (vibrational) energy transfer and/or secondary reactions in the locally-heated medium in the vicinity of the initial energy release. *Direct ab initio molecular dynamics* (MD) calculations are being carried out to investigate the ionization dynamics of the $(\text{H}_2\text{O})_{17}$ cluster which is the first water cluster that includes a four-fold coordinated water. The same MD methodology of direct *ab initio* MD method combined with quasi-classical initial conditions provides a powerful means to calculate vibrational spectra of clusters with account of anharmonicities and mode coupling. These effects are known to be particularly large in strongly interacting ion-water clusters. We continue to calculate spectra for several ion-water clusters, some of which are directly comparable to high resolution spectroscopic data that have recently become available.

Direct Dynamics Study of Chemical Reactions (*Dupuis with Furuhashi, JSPS, Tokyo*)

Motivation: We have undertaken a computational characterization of the primary processes induced by ionizing radiation of aqueous systems. We aimed to elucidate the initial reaction immediately following the ionization of $(\text{H}_2\text{O})_{17}$, to estimate the reaction time, and to quantify the vibrational energy transfer from the reactive subsystem to the medium.

Approach: Direct *ab initio* MD calculations at the RHF/3-21+G* level of the theory (that has been benchmarked to be of semi-quantitative accuracy) were carried out to investigate the ionization dynamics of the cluster $(\text{H}_2\text{O})_{17}$

which is the first water cluster that includes a four-fold coordinated water. Quasi-classical MD trajectories were calculated starting on the $(\text{H}_2\text{O})_{17}$ potential energy surface and switching to the $(\text{H}_2\text{O})_{17}^+$ energy



surface at a given ‘ionization’ time. It was observed that two neighboring water molecules to the ionized molecule interact strongly with the ionized molecule to form what we call a “reactive trimer (cluster)”. The other 14 water molecules constitute the “medium”.

Results: Within less than 50 fs after ionization a proton is observed to transfer from the ionized molecule to a neighboring molecule, and H_3O^+ and OH are formed. We characterize the distribution of vibrational energy before and after ionization by calculating the kinetic energy in the instantaneous intra-molecular vibrational internal

coordinates of the reactive cluster and of the “medium” cluster. Upon ionization it is observed that two “strongly” interacting water molecules move to closer contact the ionized water. One of the bonded OH acquires slower oscillations that ultimately end in one H⁺ atom being transferred to one of the two interacting water molecules within ~ 35 fs to form the hydronium ion and the OH radical. Following the proton transfer the hydronium ion and the third water molecule diffuse away from the OH radical. Upon ionization of (H₂O)₁₇, the total kinetic energy of the total 17-mer cluster increases. A kinetic energy increase is seen in all the low frequency inter-molecular modes of the “medium” 14-mer. These low-frequency modes act as the locally-heated bath. The increase in kinetic energy in the modes of the 14-mer is consistent with a reorganization of the “solvent” molecules upon creation of the ionized center to adopt a configuration more energetically favorable.

References to publications of DOE Chemical Physics sponsored research (2004-present)

1. T. Autrey, A. K. Brown, D. M. Camaioni, **M. Dupuis**, N. S. Foster, and A. Getty, “Thermochemistry of Aqueous Hydroxyl Radical from Advances in Photoacoustic Calorimetry and ab initio Continuum Solvation Theory”, *J. Am. Chem. Soc. (Communication)*, **126**, 3680 (2004).
2. **M. Dupuis** and M. Aida, “Vibrational Spectra from Quasiclassical Direct ab Initio Dynamics”, *Electronic Encyclopedia of Computational Chemistry*, Wiley & Sons, (2004).
3. M. Aida and **M. Dupuis**, “Fundamental Absorption Frequency from Quasi-classical Direct ab initio Molecular Dynamics: Diatomic Molecule”, *Chem. Phys. Lett.* 401, 170 (2005).
4. B. C. Garrett, D. A. Dixon, D. M. Camaioni, D. M. Chipman, M. A. Johnson, C. D. Jonah, G. A. Kimmel, J. H. Miller, T. N. Rescigno, P. J. Rossky, S. S. Xantheas, St. D. Colson, A. H. Laufer, D. Ray, P. F. Barbara, D. M. Bartels, K. H. Becker, K. H. Bowen, Jr., S. E. Bradforth, I. Carmichael, J. V. Coe, L. R. Corrales, J. P. Cowin, **M. Dupuis**, K. B. Eienthal, J. A. Franz, M. S. Gutowski, K. D. Jordan, B. D. Kay, J. A. LaVerne, S. V. Lyman, T. E. Madey, C. W. McCurdy, D. Meisel, S. Mukamel, A. R. Nilsson, T. M. Orlando, N. G. Petrik, S. M. Pimblott, J. R. Rustad, G. K. Schenter, S. J. Singer, A. Tokmakoff, L. S. Wang, C. Wittig, and T. S. Zwier, “The Role of Water on Electron-Initiated Processes and Radical Chemistry: Issues and Scientific Advances”, *Chem. Rev.* 105, 355 (2005).
5. J.D. Watts and **M. Dupuis**, “A Coupled-Cluster Analysis of the Photoelectron Spectrum of FeCl₃”, *Molec. Phys.* 103, 2223 (2005).
6. S. Hirata, M. Valiev, **M. Dupuis**, S.S. Xantheas, S. Sugiki, and H. Sekino, “Fast electron correlation methods for molecular clusters in the ground and excited states”. *Molec. Phys.* 103 2255 (2005).
7. M.Aida and **M. Dupuis**, “Fundamental Absorption Frequency from Quasi-classical Direct ab initio Molecular Dynamics: Diatomic Molecule”, *Chem. Phys. Lett.* 401, 170 (2005).
8. J.D. Watts and **M. Dupuis**, “A Coupled-Cluster Analysis of the Photoelectron Spectrum of FeCl₃”, *Molec. Phys.* 103, 2223 (2005).
9. M. Kolaski, H.M. Lee, C. Pak, **M. Dupuis**, and K.S. Kim, “Ab Initio Molecular Dynamics Simulations of an Excited State of X(H₂O)₃ (X=Cl, I) Complex”, *J. Phys. Chem. A* 109, 9419 (2005).
10. S. Du and J.S. Francisco, G.K. Schenter, T.D. Jordanov, B.C. Garrett, **M. Dupuis**, and J. Li, “The OH Radical-H₂O Molecular Interaction Potential”, *J. Chem. Phys.* 124, 224318 (2006).
11. A. Furuhashi, **M. Dupuis**, and K. Hirao, “Reactions associated with ionization in water: a direct ab initio dynamics study of ionization in (H₂O)₁₇”, *J. Chem. Phys.* 124, 164310 (2006).

This research was performed in part using the Molecular Science Computing Facility in the William R. Wiley Environmental Molecular Sciences Laboratory (EMSL) at the Pacific Northwest National Laboratory (PNNL). The EMSL is funded by DOE’s Office of Biological and Environmental Research. PNNL is operated by Battelle for DOE.

Molecular Theory & Modeling

Nucleation in Solution

Shawn M. Kathmann
Chemical Sciences Division
Pacific Northwest National Laboratory
902 Battelle Blvd.
Mail Stop K1-83
Richland, WA 99352
shawn.kathmann@pnl.gov

Program Scope

The focus of this project is to develop a fundamental understanding of the chemical physics governing crystallization in solution. DOE has underscored the importance of nucleation by stating, “Since most phase transitions involving nanostructured materials occur under conditions far from equilibrium, *the kinetic pathways available to these systems are numerous and not well understood. ... It will be important for making progress in the areas of synthesis and processing, therefore, to develop our understanding of nanochemistry and the broader general issues of nucleation and growth.*” Controlled crystallization is currently of great technological interest because crystal properties depend strongly on size, shape, and composition that differ significantly from either bulk or isolated molecules. The physical, electronic, and optical properties, in principle, can be “tuned” to create new crystals with desired characteristics. However, the desire of “materials by design” has been replaced by a “cook and look” approach simply because there are too many degrees of freedom in the relevant systems and appropriate molecular-level insight is needed to bridge the gap.

The physical reason why nucleation is so sensitive can be understood intuitively. Since the nucleation process involves many mechanistic steps (typically 10’s to 100’s), small changes in the thermodynamics and kinetics of each step can be amplified over the total number of steps required to reach the critical cluster – defined as the cluster at the top of the nucleation barrier. The sensitivity of nucleation to subtle variations in the interaction potentials, quantum nuclear degrees of freedom, etc., motivates the search for relative effects on nucleation in solution with and without various seeds (ions, impurities, contaminants, etc.).

Recent Progress

Crystallization (see Figure 1) is one of the most challenging problems in chemical physics. At a given temperature and pressure, saturation is defined as the concentration of the nucleating substance in equilibrium with the mother phase – when this concentration is achieved the chemical potentials of the solute in solution and the pure salt crystallites are equivalent. The driving force for salt crystallization in solution occurs when the actual solute concentration exceeds the solution solubility (sometimes referred to as supersaturation). Salts having large solubilities require higher salt concentrations to

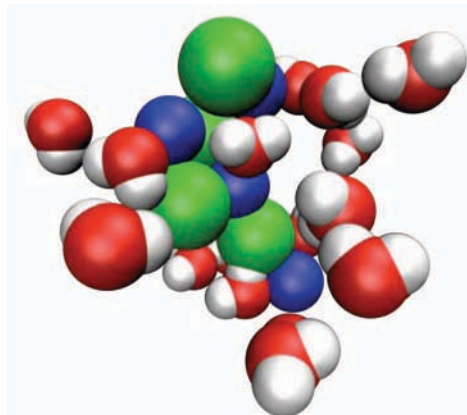


Figure 1. (NaCl)₄ salt in aqueous cluster.

crystallize than salts with lower solubilities. The relevant timescale for the nucleation event in solution is dictated by the potentials of mean force between the newly forming clusters and solvated ions. Nucleation is inherently a rare event and trying to observe it directly via molecular simulation at realistic conditions is computationally intractable at realistic conditions – the majority of time being spent searching irrelevant regions of the solution configuration space.

Recently, Dynamical Nucleation Theory (DNT) was developed as a molecular-level treatment of vapor-to-liquid nucleation kinetics based upon variational transition state theory to obtain rates and free energies for the underlying clustering reactions. DNT requires accurate interaction energies as well as statistical mechanical sampling of thermally relevant regions of cluster configuration space. The classical i -cluster Helmholtz free energy A_i is related to the partition function Q_{DNT} via

$$e^{-\beta A_i} = Q_{DNT} = \int d\mathbf{r}^i \exp[-\beta U(\mathbf{r}^i)] \chi(v) \quad (1)$$

where $\beta = 1/k_B T$, k_B is Boltzmann's constant, T is the temperature, $U(\mathbf{r}^i)$ is the interaction potential, and $\chi(v)$ is a characteristic function defining the relevant volume of configuration space, which we choose as a spherical constraining volume v whose origin is coincident with the i -cluster center-of-mass. The central result of DNT is that the evaporation rate constant for a molecule to escape the i -cluster is

$$\alpha_i = - \frac{1}{\sqrt{2\pi m k_B T}} \left. \frac{dA_i}{dr_{cut}} \right|_{r_{cut} = r^\ddagger} \quad (2)$$

where m is the mass of the monomer, r_{cut} is the radius of the constraining sphere, and r^\ddagger is the radius that minimizes the reactive flux. This shows that the variation of the cluster Helmholtz free energy is proportional to the rate constant for escape. Figure 2 shows an application of DNT to vapor-to-particle nucleation of water.

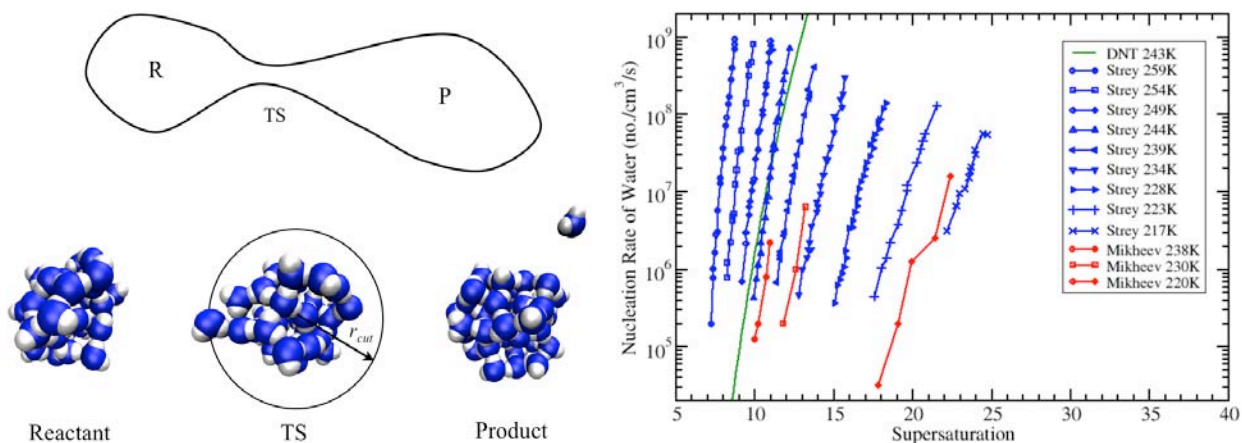


Figure 2. (Left) In DNT the Reactant is the i -cluster, the Transition State (TS) has one monomer on the dividing surface, and the Product is the $(i-1)$ -cluster plus a monomer at infinity. (Right) Comparison of DNT using the Dang-Chang polarizable water model at 243K to experimental measurements (Strey *et al.* and Mikheev *et al.*) for the homogeneous nucleation of water

Future Plans

Recently, we showed how various seed ions have a profound influence on the ion-induced nucleation of water from the vapor and how radically a molecular-level description departs from a Classical Nucleation Theory (CNT) continuum treatment. This work also addressed the century-old controversy concerning water's sign preference showing that the ion's chemical identity plays an essential role in addition to the sign in determining cluster thermodynamics.

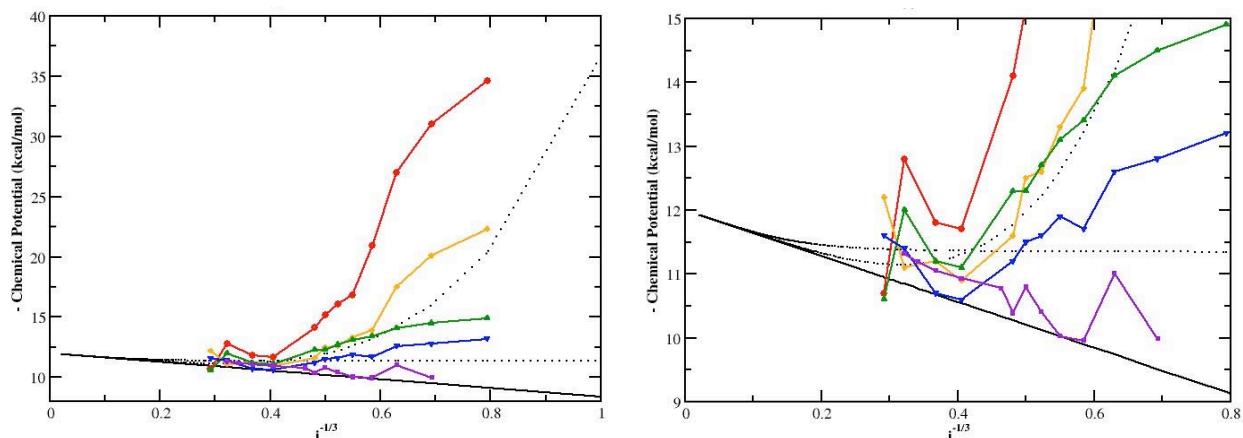


Figure 3. Size dependent chemical potentials of aqueous ionic clusters using ions of different size (2.35 Å and 4.40 Å) and sign (+/-): red (- and 2.35 Å), yellow (+ and 2.35 Å), green (- and 4.40 Å), blue (+ and 4.40 Å), purple (pure TIP4P water), upper dotted (CNT w/ion radius = 0.1 Å), lower dotted (CNT w/ion radius = 10 Å), solid black (CNT pure water).

We have also studied the influence of anharmonicity on the chemical potentials of $\text{Na}^+(\text{H}_2\text{O})_i$ and $\text{Cl}^-(\text{H}_2\text{O})_i$ clusters. Figure 4 shows good agreement between the full anharmonic Gibbs free energy differences (chemical potentials) compared to experiment at 298K. We also compare (see Figure 4) the chemical potentials using the Rigid-Rotor Harmonic Oscillator Approximation (RRHOA) to the full anharmonic results using 10's to 100's of millions of configurations. This comparison shows that using the RRHOA without quantifying its effect is unjustified.

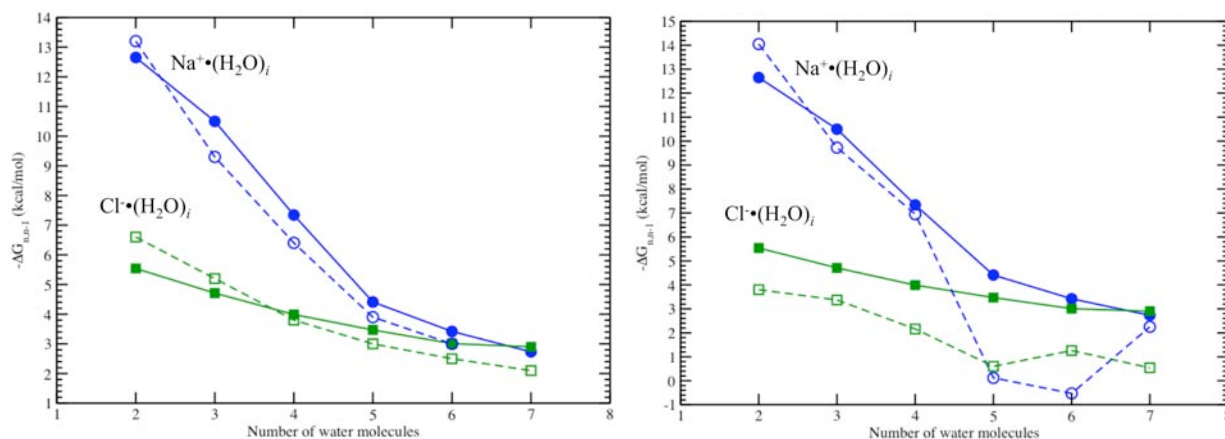


Figure 4. (Left) Anharmonic free energy differences (solid lines) compared to experiment (dashed lines) at 298K and (Right) anharmonic free energy differences (solid lines) compared to the RRHOA results (dashed lines) at 298K.

It is important to understand that we are referring to two different types of anharmonicity: (1) local anharmonicity of the vibrations for a given cluster configuration and (2) global anharmonicity resulting from sampling between the large number of configurations available within the relevant volume of configuration space. Additionally, using multiple minima in the RRHOA partition function (the so-called “superposition” approximation) still underestimates the full anharmonic free energy.

Nucleation of salt from concentrated solution presents several challenges not present in the dilute limit typically encountered in molecular simulations. A supersaturated solution generates clusters (or nuclei) of the new phase. These clusters can form homogeneously within the mother phase or heterogeneously on seeds, impurities, dust, or other irregularities that provide local regions of stability (e.g., defects, steps, edges, or other imperfections). To calculate the rates of salt cluster dissolution using DNT, simulations of the salt cluster thermodynamics must be performed. We are currently simulating aqueous salt clusters of various sizes to understand the free energy landscape as ions are added to the aqueous cluster – see Figure 1. We will present the size and concentration dependent thermodynamics for these aqueous salt clusters. Given that charge transfer effects may be important in dictating the difference between salts of AgCl versus NaCl, judicious electronic structure calculations are being performed.

Project Collaborators and Acknowledgements: G.K. Schenter, L.X. Dang, S.S. Xantheas, and B.C. Garrett. Battelle operates Pacific Northwest National Laboratory for the U. S. Department of Energy.

Publications of DOE Sponsored Research (2003-present)

1. “Thermochemistry and Kinetics of Evaporation and Condensation for Small Water Clusters” B.C. Garrett, S.M. Kathmann, and G.K. Schenter in *Water in Confining Geometries*, Eds. V. Buch and J.P. Devlin (2003 Springer-Verlag Berlin Heidelberg NewYork).
2. Multi-Component Dynamical Nucleation Theory And Sensitivity Analysis, S.M. Kathmann, G.K. Schenter, and B.C. Garrett, *J. Chem. Phys.*, **120**, 9133 (2004).
3. Dynamical Nucleation Theory: Understanding the Role of Aqueous Contaminants, S.M. Kathmann, G.K. Schenter, and B.C. Garrett, Proceedings of the 16th International Conference on Nucleation and Atmospheric Aerosols, Eds. M. Kasahara and M. Kulmala, (2004 Kyoto University Press).
4. Ion-Induced Nucleation: The Importance of Chemistry, S.M. Kathmann, G.K. Schenter, and B.C. Garrett, *Physical Review Letters*, **94**, 116104 (2005).
5. **Invited Article:** Understanding the Chemical Physics of Nucleation, S.M. Kathmann, A New Perspectives Issue: *Theoretical Chemistry Accounts*, **116**, 169-182, (2006).

New Ultrafast Techniques for Electron Radiolysis Studies

Principal Investigators: Robert A. Crowell*, David Gosztola and Ilya A. Shkrob

Radiation and Photochemistry Group, Chemistry Division, Argonne National Laboratory, Argonne, Illinois 60439; tel.: 630-252-8089; FAX: 630-252-9570; e-mail: Rob.Crowell@anl.gov

1. Program Scope

The Argonne Radiation and Photochemistry Group strives to study the fundamental interactions that arise from the interaction of ionizing radiation in the condensed phase and to make the connection between these basic events and chemical reactivity. Ultrafast ($<10^{-11}$ ps) physical processes play a pivotal role in all chemical reactions. Detailed knowledge of primary events such as energy (charge) transfer, thermalization, solvation and the chemistry of pre-thermalized species is essential in order to produce a complete picture of reactivity. Due to the lack of a suitable femtosecond source of ionizing radiation, experimental studies on the primary events in radiation induced chemical reactions are virtually nonexistent. It is the specific goal of this project to develop ultrafast electron pulse radiolysis techniques that can be used to study the fundamental processes associated with radiation induced chemical reactions. It is the ultimate goal of this project to provide such information so that we can gain a full understanding of radiation chemistry in the condensed phase. Achievement of this goal requires the implementation of ultrafast laser, radiolytic and x-ray spectroscopic techniques, techniques that currently do not collectively exist for this purpose. Recent advances in super-intense ultrashort laser technology have led to the ability to generate subpicosecond electron, proton and x-ray pulses *without* the use of a traditional electron accelerator. The objective of our current efforts is to develop a state-of-the-art table-top 15-20 TW terawatt laser system that will produce these types of radiation for chemical physics studies. Utilized in conjunction with our ultrafast laser system the electron pulses will provide unprecedented insight into many of the contemporary issues concerning the primary processes of radiation induced chemical reactions.

2. Progress Report

A laser wakefield accelerator (LWA) based upon a 15-20 TW laser system has been developed at Argonne's Terawatt Ultrafast High Field Facility (TUHFF). Details of the laser system have been described in previous CPIMS abstracts (see also ref. 17). More recently the LWA has been successful in the routine generation of subpicosecond electron pulses of energies in the MeV range and charges that are typically 2-3 nC. Details of the electron beam characterization can be found in the CPIMS abstract of David Gosztola. The most significant accomplishment of the past year has been the first ultrafast pulse radiolysis transient absorption (TA) measurements from the TUHFF LWA. The system has been specifically optimized for kinetic measurements in a pump-probe fashion. This requires averaging over many shots which necessitates stable, reliable generation of electron pulses.

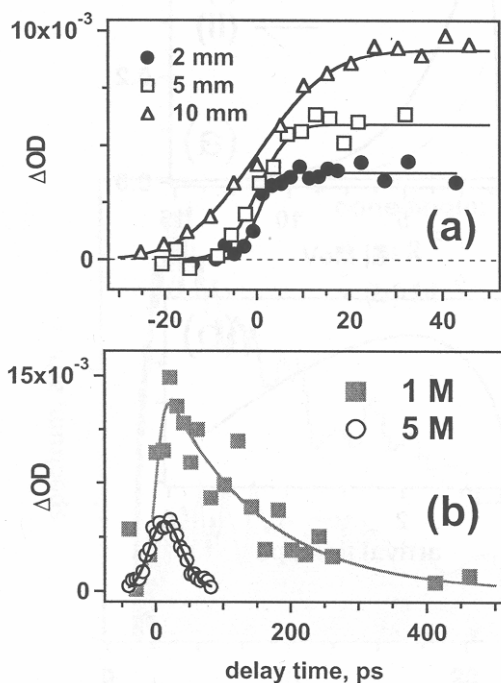


Figure 1(a) The rise of the transient absorbance (ΔOD) from hydrated electron in pulse radiolysis of water. (b) The decay kinetics of observed in pulse radiolysis of 1 and 5 mol dm^{-3} solutions of perchloric acid in water.

In order to assess the time resolution experimentally achievable using our system, we have studied the decay kinetics of hydrated electrons (e_{aq}^-) generated in pulse radiolysis of liquid water and concentrated perchloric acid solutions at 25 °C (Figure 1). Time resolution of a few picoseconds has been demonstrated. There are three factors that determine the rise time of the TA signal: (1) the formation time of the species and the time scale of their spectral evolution, (2) the pulse duration (and dispersion) of the electron beam at different points in the sample, and (3) the traveling time of the probe through the radiolytic zone. On the time scale of Figure 1(a), the formation of e_{aq}^- can be considered as instantaneous (although that is not necessarily correct for the TA signal, as explained above). Assuming that the pulse duration for the electrons emerging from the jet is comparable in the duration to the TW laser pulse, and knowing the electron spectrum, the dispersion of the arrival times for the electrons at the sample was estimated as 3–4 ps. Given the large diameter of the electron beam at the sample (which is commensurate with the sample thickness) one would expect that the

second factor determines the rise time of the TA signal observed. In principle, this rising part of the kinetics can be simulated from the calculated dose distribution (i.e., the distribution of e_{aq}^-) along the path of the probe beam. In reality, this distribution is not known exactly, and moreover it fluctuates from pulse to pulse. In order to make a comparison with other experimental systems the kinetics were fit by an error function which corresponds to a hypothetical experiment with a Gaussian pulse of electrons, infinitely thin sample and collinear beam geometry. The $1/e^2$ Gaussian times obtained from the data in this fashion are 17.9, 8.3, and 4.4 ps for 10, 5, and 2 mm cells, respectively. Thus the “pulse width” scales with the sample thickness, supporting the assumption of short electron pulse duration. Thus the best “pulse width” obtained was on the order of 4 ps. In principle, this width can be shortened further by the use of thinner samples, better shaping of the electron spectrum, and collinear detection.

We have also performed radiolysis of 1 and 5 mol dm^{-3} solutions of perchloric acid in a 10 mm optical path cell. Figure 6(b) shows the kinetics obtained. The fast decay is due to the reaction of e_{aq}^- with the hydronium (H_3O^+) ions in the solution (this reaction yields H atoms that do not absorb at 800 nm). The kinetics were fit to a single exponential convoluted with the error function. The obtained decay rates were 7.1×10^9 and $5.4 \times 10^{10} \text{ s}^{-1}$ in 1 and 5 mol dm^{-3} solutions, respectively. An intriguing feature of the 5 mol dm^{-3} kinetics shown in Figure 1(b) is the apparent broadening of the “pulse width.” This interesting behavior will be pursued in our subsequent studies.

3. Future Plans

The main focus of our current effort is directed towards using TUHFF to study the primary processes of radiation chemistry (see CPIMS abstract of Shkrob). Specifically, we are presently studying fast radical ion reactions. As multi-wavelength detection becomes available time resolved studies of spur thermalization and solvation will be pursued. Laser experiments in which water is biphotonically ionized using femtosecond pulses of ultraviolet light suggest that the local equilibrium between the cavity electron and water molecules around it is reached in < 1 ps, as judged from the evolution of the TA spectrum. Before this equilibrium is fully reached, the pre-thermalized electron occupies a distorted, loose cavity and exhibits a broad TA spectrum that is shifted to the red from the final one. As the electron thermalizes (with the characteristic time of ca. 200-300 fs) this TA spectrum continuously narrows and shifts to the blue; a similar shift can be observed for the thermalized electron when water is cooled from 100 to 0 °C. At 800 nm, the evolution of the TA signal is complete in 1.5 ps. The situation in pulse radiolysis is less clear, because the electrons are generated in spurs that thermalize with the water bulk on the picosecond time scale, as the heat generated in the excitation and ionization events diffuses away. The tremendous amount of energy that is deposited within the spur may result in the overall thermalization rate that is slower than that observed in photolysis.

Concurrent to pulse radiolysis technical developments that will lead to improved electron beam quality and detection sensitivity are being explored. These technical developments will bring the ultimate time resolution of the TUHFF LWA to well below a picosecond.

4. DOE Publications (2003 – present)

1. I. A. Shkrob, M. C. Sauer, Jr., R. Lian, R. A. Crowell, D. M. Bartels and S. E. Bradforth "Electron photodetachment from aqueous anions III. Dynamics of geminate pairs derived from photoexcitation of mono- and poly-valent anions," *J. Phys. Chem. A*, 110, 9071 (2006).
2. C. G. Elles, A. E. Jailaubekov, R. A. Crowell, S. E. Bradforth, "Excitation energy dependence of the mechanism for two-photon ionization of liquid H₂O and D₂O from 8.3 eV to 12.4 eV," *J. Chem. Phys.* 125, 044515 (2006)
3. D. A. Oulianov, R. A. Crowell, D. J. Gosztola, and Y. Li "Ultrafast time-resolved x-ray absorption spectroscopy of solvent-solute transient structures," *Nucl. Instr. and Meth. in Phys. Res. B*. 241, 82 (2005)
4. O. J. Korovyanko, R. C. Rey-de-Castro, C. G. Elles, R. A. Crowell, Y. Li "Optimization of a femtosecond Ti:sapphire amplifier using an acousto-optic programmable dispersive filter and a genetic algorithm," *Proc. of SPIE*, 6100, 183-188 (2006).
5. D. A. Oulianov, O. J. Korovyanko, R. A. Crowell, D. J. Gosztola, I. A. Shkrob, R. C. Rey-de-Castro, C. G. Elles, "Subpicosecond radiolysis by means of a terawatt laser wakefield accelerator," *Proc. of SPIE*, 601, 610126 (2006).

6. D. A. Oulianov, Yuelin Li, R. A. Crowell, I. A. Shkrob, D. J. Gosztola, O. Y. Korovyanko, and R. Rey-de-Castro "Femtosecond electron and x-ray source based on laser wakefield accelerator" Proc. of SPIE, 5920, 5920002-1 (2005)
7. R. A. Crowell, I. A. Shkrob, D. A. Oulianov, O. Korovyanko, D. J. Gosztola, Y. Li and R. Rey-Castro, "Motivation and development of ultrafast laser based accelerator techniques for chemical physics research," Nucl. Instr. and Meth. in Phys. Res. B , 241, 9 (2005).
8. M. C. Sauer Jr., I. A Shkrob, R. Lian, R. A. Crowell, D. M. Bartels, X. Chen, D. Suffren, and S. E. Bradforth, "Electron photo-detachment from aqueous anions. II. Ionic strength effect on geminate recombination dynamics and quantum yield for hydrated electron," J. Phys. Chem. A. 108, 10414 (2004).
9. R. Lian, R. A. Crowell, and I. A. Shkrob "Solvation of electrons generated by two 200nm photon ionization of liquid H₂O and D₂O," J. Phys. Chem. A. 109, 1510 (2005).
10. R. Lian, R. A. Crowell, I. A. Shkrob, D. M. Bartels, D. A. Oulianov, and D. J. Gosztola, "Recombination of Geminate (OH:e⁻) Pairs in Concentrated Alkaline Solutions: Lack of Evidence for Hydroxyl Radical Deprotonation," Chem. Phys. Lett. 389, 379 (2004).
11. M. C. Sauer Jr., I. A. Shkrob, and R. A. Crowell "Electron Photodetachment from Aqueous Anions. I. Quantum Yields for Generation of Hydrated Electron by 193 and 248nm Laser Photoexcitation of Sundry Inorganic Anions," J. Phys. Chem A, 108, 5490 (2004).
12. R. A. Crowell, R. Lian, I. A. Shkrob, J. Qian, D. A. Oulianov, and S. Pommeret, "Light-induced temperature jump causes power-dependent ultrafast kinetics of electrons generated in multiphoton ionization of liquid water," J. Phys. Chem. A 108, 9105 (2004).
13. R. Lian, D. A. Oulianov, I. A. Shkrob and R. A. Crowell, "Geminate recombination of electrons generated by above the gap (12.4eV) photoionization of liquid water," Chem. Phys. Lett., 398, 102.
14. R. Lian, R. A. Crowell, I. A. Shkrob, D. M. Bartels, X. Chen, and S. E. Bradforth, "Ultrafast Dynamics for the Electron Photodetachment of Aqueous Hydroxide," J. Chem. Phys. 120, 11712 (2004).
15. I. A. Shkrob, D. A. Oulianov, R. A. Crowell, and S. Pommeret "Frequency Domain single-shot (FDSS) ultrafast transient absorption spectroscopy" J. Appl. Phys. 96, 25 (2004).
16. R. A. Crowell, R. Lian, D. A. Oulianov, and I. A. Shkrob "Geminate recombination of the hydroxyl radicals generated from the 200nm photodissociation of hydrogen peroxide," Chem. Phys. Lett. 383, 481 (2004).
17. R. A. Crowell, D. J. Gosztola, I. A. Shkrob, D. Oulianov, C. D. Jonah, and T. Rajh "Ultrafast Processes in Radiation Chemistry," Radiat. Phys. Chem. 70, 501 (2004)
18. L. Zhao, R. Lian, I. A. Shkrob, R. A. Crowell, S. Pommeret, E. L. Chronister, A. D. Liu, and A. D. Trifunac,, "Ultrafast studies on the photophysics of matrix-isolated radical cations of polycyclic aromatic hydrocarbons," J. Phys. Chem. A 108, 25 (2004).

Surface Chemical Dynamics

M.G. White^a, N. Camillone III^a, and A.L. Harris^b

Brookhaven National Laboratory, Chemistry Department, Building 555, Upton, NY 11973
(mgwhite@bnl.gov, nicholas@bnl.gov, alexh@bnl.gov)

1. Program Scope

This program focuses on fundamental investigations of the dynamics, energetics and morphology-dependence of thermal and photoinduced reactions on bulk planar and nanoparticle surfaces that play key roles in energy-related catalysis and photocatalysis. Laser pump-probe methods are being used to investigate the dynamics of interfacial charge and energy transfer that leads to adsorbate reaction and/or desorption on metal and metal oxide surfaces. State- and energy-resolved measurements of the gas-phase products resulting from thermal and photoinduced reactions are used to infer the dynamics of product formation and desorption. Time-resolved correlation techniques are used to follow surface reactions in real time and infer the dynamics of adsorbate–substrate energy transfer and desorption. Extensions of this work include investigations of the size-dependence of photoinduced desorption and vibrational dynamics of small molecules on surfaces of supported metal nanoparticles. Complementary efforts use a new cluster ion beam apparatus for studying the structure, dynamics and reactivity of mass(size)-selected metal and metal compound nanoclusters in the gas-phase and deposited onto solid supports.

2. Recent Progress

Ultrafast Investigations of Desorption Dynamics. A primary focus of the direct time-domain investigation of physicochemical transformations at surfaces has been photoinduced cleavage of the molecule–surface bond.^{1,2} Femtosecond light pulses currently provide the only means for time-domain probing of surface chemical dynamics at molecularly-relevant timescales. However, the applicability of the results of such measurements to thermal chemical transformations can be questioned because short light pulses create conditions that are distinctly non-thermal. We have begun to address this issue by conducting a systematic test of the connection between fast photoinduced (Fig. 1) and slow thermal surface processes, examining the validity of the application of kinetics parameters derived from thermally-driven desorption (seconds timescale) to modeling the results of photoinduced desorption on femtosecond timescales. We have studied the desorption dynamics of CO and O₂ from Pd(111) using ~ 100 fs, 780 nm-wavelength pulses to provide a temporally well-defined excitation of the adsorbate–substrate complex. Our measurements of the photodesorption probability as a function of coverage show that the probability for desorption by femtosecond laser pulses can depend strongly on coverage and that the dependence is well understood in terms of the activated desorption rate used to describe thermal desorption (Fig. 2). To support this conclusion we have simulated the coverage-dependent desorption probabilities using two models: (i) a simplistic, “temperature-jump” model, where the adsorbate excitation is of the form of a square pulse and (ii) a detailed simulation based on the well-known two-temperature model.³ Overall, the nature of the observed coverage dependence is well predicted by models that use the thermal desorption activation energy derived from TPD experiments. That these models substantially reproduce the coverage dependence results represents the first systematic test of the hypotheses that: (i) the mechanism for molecule–surface bond cleavage in desorption induced by short optical pulses can be separated into two distinct steps, the electron-mediated photoexcitation of the adsorbate and the subsequent

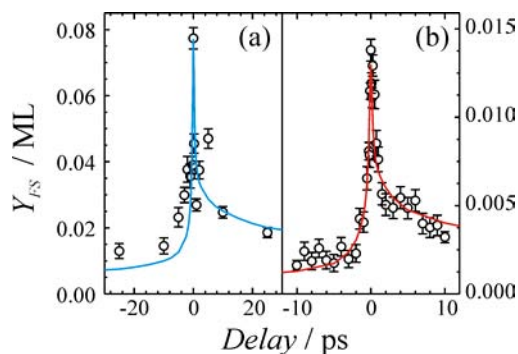


Figure 1. Two-pulse correlation measurements of the photodesorption of CO (a) and O₂ exhibiting dominant subpicosecond decay times consistent with fast electron-mediated processes. The solid lines are two-temperature model simulations incorporating temperature-dependent electronic frictional coupling.

desorption of the adsorbate, and (ii) that desorption occurs on the same potential energy surface following fast photoexcitation as it does in conventional thermal desorption.

Our simulations of ultrafast-pulse desorption have also led to new insight into electronic friction. We find that the electron-mediated adsorbate–substrate coupling strength is dependent on the temperature of the substrate electronic distribution (T_{el}). Though predicted theoretically by Brandbyge *et al.*,⁴ this dependence has been assumed negligible in earlier work.^{5–7} Recently Stépán *et al.*^{8,9} reported that a T_{el} -dependent friction was required to simulate their measurements of photoinduced surface diffusion. Our modeling has shown a similar result in the case of molecular desorption. Specifically, we find that a T_{el} -independent coupling constant that adequately models the photon-fluence dependence of the yield is incapable of reproducing the short temporal width observed in the two-pulse correlation (2PC) measurements. This is illustrated in Fig. 3, where only the model incorporating T_{el} -dependent friction reproduces the observed 2PC response. Our results indicate that the degree of coupling to adsorbate molecular resonances from the substrate Fermi sea increases as the population of electrons (holes) at energy levels further above (below) the Fermi level increases. This is consistent with the proposed hole-capture mechanism for the femtosecond-pulse photo-desorption of O_2 from Pd(111).¹⁰

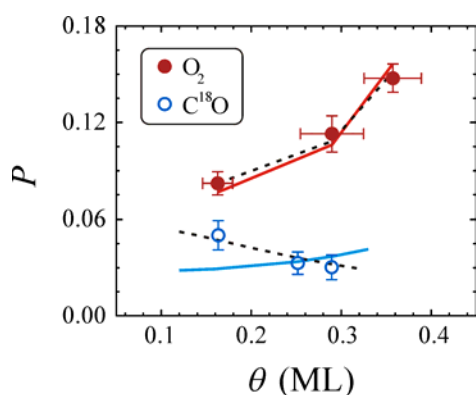


Figure 2. Coverage dependence of the photodesorption probability for O_2 and CO from Pd(111) (filled and open circles, respectively). The solid (dashed) line shows results of the electronic friction (temperature-jump) model.

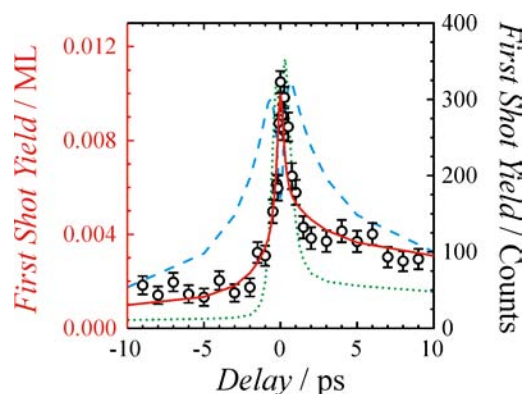


Figure 3. 2PC measurements of photoinduced desorption of O_2 from Pd(111) with best fits for three numerical models: two models with a T_{el} -independent friction (dashed and dotted lines) and one model with a T_{el} -dependent friction (solid line).

Structure and Reactivity of Transition Metal Compound Clusters. A recent approach to investigating the physical and chemical properties of metallic nanoclusters on solid supports involves the use of gas-phase cluster ion beams for depositing nanoclusters with precise control over particle size (mass) and surface coverage.^{11,12} Cluster deposition is particularly effective for investigations of small nanoclusters, 1–2 nm (< 200 atoms), where the geometric and electronic structure is evolving from molecular clusters to that of the extended solid (*e.g.*, semi-metal to metal transition). Furthermore, mass selection makes it possible to determine the stoichiometry of metallic compound clusters, *e.g.*, the metal-to-carbon ratio in a carbide cluster, prior to deposition. Current efforts involve the deposition of the $M_4S_6^+$ ($M = Mo, W$) on the Au(111) surface. A combined theoretical and experimental investigation of the gas-phase structure and reactivity of the $M_4S_6^+$ ($M = Mo, W$) “magic” cluster was carried out last year in which we proposed that the $M_4S_6^+$ structure is a compact cluster with the four metal atoms arranged in an internal tetrahedron surrounded by bridging S-atoms (near T_d symmetry). The choice of the Au(111) surface as the substrate was motivated by two factors: (i) the reconstructed $(22 \times \sqrt{3})$ -Au(111) “herringbone” surface is known to act as a template for cluster nucleation as recently demonstrated in our laboratory for Mo and MoC nanoparticles;¹³ and (ii) the atomic and electronic structure of the $Mo_4S_6/Au(111)$ system was the subject of a very recent theoretical DFT study by Gemming and Seifert.¹⁴ A key finding of the latter is that the Mo_4S_6 cluster remains intact and the geometry is only slightly distorted despite the substantial binding energy of the cluster to the Au(111) surface (4.1 eV). Using deposition energies of ≤ 0.25 eV/atom, Auger and x-ray photoelectron spectroscopy and temperature programmed desorption of CO indicate that the clusters deposit intact with the Mo atoms exposed and

available for adsorbate bonding. Initial deposition experiments under similar conditions have also been performed for the larger Mo_6S_8 and Mo_7S_{10} clusters. Comparisons of their CO TPD spectra show considerable shifts in CO binding (see Fig. 4) as expected from variations in the local electronic environment of the Mo-atoms in the different clusters. Parallel theoretical studies are also in progress in collaboration with Jose Rodriguez and Ping Liu (Chemistry Department, BNL) who are using DFT to investigate the electronic structure and CO binding energies for the $\text{Mo}_4\text{S}_6/\text{Au}(111)$ system.

Photoinduced Desorption and Reaction of O_2 on $\text{TiO}_2(110)$ Surfaces. We are currently investigating photoinduced reactions on single crystal $\text{TiO}_2(110)$ (rutile) surfaces with the goal of understanding the excitation and energy transfer processes that lead to surface reaction. Closely

connected with any photoinduced surface chemistry on TiO_2 is the interaction of O_2 with surface defects or vacancy sites at which an O^{2-} anion is missing. Adsorbed molecular oxygen is linked to the photooxidation activity of TiO_2 surfaces, however, fundamental questions remain as to the nature of the O_2 adsorption sites and the energy transfer processes that lead to desorption and reaction. Initial photochemistry experiments utilized a monochromatized HgXe-arc lamp source that can readily be tuned from below to above the TiO_2 band gap (~ 3.1 eV). We have measured the desorption kinetics for oxygen photodesorption, $h\nu + \text{O}_{2(\text{a})} \rightarrow \text{O}_{2(\text{g})}$, and CO photooxidation, $h\nu + \text{CO}_{(\text{a})} + \frac{1}{2} \text{O}_{2(\text{a})} \rightarrow \text{CO}_{2(\text{g})}$, for different surface treatments that are thought to lead to different surface structures and relative concentrations of surface and bulk defects.^{15,16} At low temperatures, the photodesorption yield curves versus time exhibit multiple decay rates which have been previously attributed to two different adsorbed O_2 species, α_1 - O_2 (“fast” decay) and α_2 - O_2 (“slow” decay).¹⁷ The latter are thought to be interconverted to a third state, β - O_2 , by heating the $\text{O}_2/\text{TiO}_2(110)$ surface from 200-400 K.¹⁸ The bonding characteristics of these photoactive O_2 species are not known, and the observed variation in desorption rates could reflect differences in O_2 adsorption site (bridge vs. five coordinated) and chemical binding, (O_2^- or O_2^{2-}) or unusual kinetics (*i.e.*, fractal behavior).¹⁹ Current experiments involve the use of laser pump-probe experiments in which photodesorbed O_2 will be detected by state-selective (2+1) REMPI or one-photon VUV ionization detection schemes which we have developed in this laboratory. Measurement of the final-state properties of desorbed O_2 has the potential to provide new insight into the desorption mechanism and distinguish desorption channels associated with chemically-distinct surface-bound O_2 species, *e.g.*, α - O_2 or β - O_2 .

3. Future Plans

Our planned work develops three interlinked themes: (i) the chemistry of supported nanoparticles and nanoclusters, (ii) the exploration of chemical dynamics on ultrafast timescales, and (iii) the photoinduced chemistry of molecular adsorbates. The investigations are motivated by the fundamental need to connect chemical reactivity to chemical dynamics in systems of relevance to catalytic processes — in particular metal and metal-compound nanoparticles and nanoclusters supported on oxide substrates. They are also motivated by fundamental questions of physical changes in the electronic and phonon structure of nanoparticles and their coupling to adsorbates and to the nonmetallic support that may alter dynamics associated with energy flow and reactive processes.

Ultrafast experiments investigating the dynamics of photoinduced desorption from nanoparticles will address development of a fundamental understanding of the changes in this simplest surface reaction (desorption) as the size of the metal substrate material is reduced from macroscopic (planar bulk surfaces)

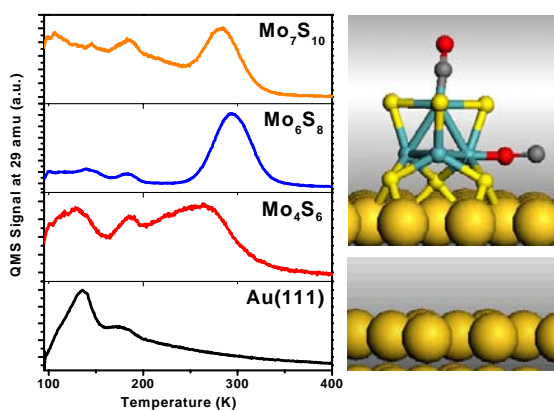


Figure 4: Left: Comparison of the CO thermal desorption spectra from a clean Au(111) single crystal surface and from surfaces prepared by depositing three different M_xS_y clusters on the Au(111) surface. Right: Calculated DFT structures for an ideal Au(111) surface (lower) and two CO molecules adsorbed onto the Mo_4S_6 cluster sitting in its lowest energy configuration.

to the nanoscale. Size-dependent chemical dynamics will also be the focus of experiments using our new cluster beam source to prepare a range of supported, size-selected nanoclusters for structure and reactivity studies. The latter will be complemented by ultrafast two-photon photoemission experiments to investigate the electronic structure and dynamics of the nanoclusters and molecular resonances involved in chemistry at their surfaces. In addition, time-resolved mid-IR surface spectroscopy experiments are planned to follow the dynamics of vibrational energy flow for adsorbates at nanoparticle surfaces and set the stage for investigations of chemical dynamics through ultrafast vibrational spectroscopy at surfaces.

On bulk metal surfaces we are planning further work to understand the relationship between thermal and photoinduced processes and the role of phonons in the desorption dynamics. We are also planning ultrafast studies of CO oxidation reaction dynamics on Pd. On metal oxide surfaces, we will work to resolve open questions regarding the identity of the surface binding sites and the bonding geometry of the various O₂ surface species on titania. We plan to employ velocity- and state-resolved measurements of species desorbed during photoexcitation to distinguish among the photoreaction channels in chemical systems that play central roles in photocatalysis on oxides.

Literature Cited

1. R.R. Cavanagh, D.S. King, J.C. Stephenson, T.F. Heinz, *J. Phys. Chem.*, **97**, 786 (1993) and references therein.
2. W. Ho, *J. Phys. Chem.*, **100**, 13050 (1996).
3. S.I. Anisimov, B.L. Kapeliovich, T.L. Perel'man, *Sov. Phys. JETP*, **39**, 375 (1974).
4. M. Brandbyge, P. Hedegård, T.F. Heinz, J.A. Misewich, D.M. Newns, *Phys. Rev. B*, **52**, 6042 (1995).
5. L.M. Struck, L.J. Richter, S.A. Buntin, R.R. Cavanagh, J.C. Stephenson, *Phys. Rev. Lett.*, **77**, 4576 (1996).
6. J.A. Misewich, A. Kalamarides, T.F. Heinz, M.M.T. Loy, *J. Chem. Phys.*, **100**, 736 (1994).
7. S. Funk, M. Bonn, D.N. Denzler, C. Hess, M. Wolf, G. Ertl, *J. Chem. Phys.*, **112**, 9888 (2000).
8. K. Stépán, J. Güdde, U. Höfer, *Phys. Rev. Lett.*, **94**, 236103 (2005).
9. K. Stépán, M. Dürr, J. Güdde, U. Höfer, *Surf. Sci.*, **593**, 54 (2005).
10. J.A. Misewich, S. Nakabayashi, P. Weigand, M. Wolf, T.F. Heinz, *Surf. Sci.*, **363**, 204 (1996).
11. U. Heiz, W.-D. Schneider, *J. Phys. D: Appl. Phys.*, **33**, R85 (2000).
12. M. Aizawa, L. Lee, S.L. Anderson, *J. Chem. Phys.*, **117**, 5001 (2002).
13. J.M. Horn, Z. Song, D.V. Potapenko, J. Hrbek, M.G. White, *J. Chem. Phys. B*, **109**, 44 (2005).
14. S. Gemming, G. Seifert, *Appl. Phys. A*, **82**, 175 (2005).
15. T.L. Thompson, J.T. Yates, *Topics in Catal.*, **35**, 197 (2005).
16. M. Li, W. Hebenstreit, U. Diebold, A.M. Tyryshkin, M.K. Bowman, G.G. Dunham, M.A. Henderson, *J. Phys. Chem. B*, **104**, 4944 (2004).
17. C.N. Rusu, J.T. Yates, *Langmuir*, **13**, 4311 (1997).
18. G. Lu, A. Linsebigler, J.T. Yates, *J. Chem. Phys.*, **102**, 4657 (1994).
19. T.L. Thompson, J.T. Yates, *J. Phys. Chem. B*, **110**, 7431 (2006).

DOE-Sponsored Research Publications (2003–2006)

1. J.M. Lightstone, H. Mann, M. Wu, P.M. Johnson, and M.G. White, "Gas-phase production of molybdenum carbide, nitride and sulfide clusters and nanocrystallites," *J. Phys. Chem. B*, **107**, 10359 (2003).
2. R.J. Beuhler and M.G. White, "State-resolved dynamics of oxygen atom recombination on polycrystalline Ag," *J. Chem. Phys.*, **120**, 2445 (2004)
3. J.M. Lightstone, M.J. Patterson and M.G. White, "Reactivity of the M₄S₆⁺ (M-Mo, W) cluster with CO and NH₃ in the gas-phase," *Chem. Phys. Lett.*, **413**, 429 (2005).
4. P. Liu, J.M. Lightstone, M.J. Patterson, J.A. Rodriguez, J.T. Muckerman and M.G. White, "Gas-phase interaction of thiophene with the Ti₈C₁₂⁺ and Ti₈C₁₂ met-car clusters," *J. Phys. Chem. B*, **110**, 7449 (2006).
5. J. M. Lightstone, M. J. Patterson, P. Liu, and M. G. White, "Gas-phase reactivity of the Ti₈C₁₂⁺ Met-car with triatomic sulfur-containing molecules: CS₂, SCO, and SO₂," *J. Phys. Chem. A*, **110**, 3505 (2006).
6. N. Camillone III, T. Pak, K. Adib, K.A. Khan, and R.M. Osgood, Jr., "Tuning molecule-surface interactions with nanometer-thick covalently-bound organic overlayers," *J. Phys. Chem. B*, **110**, 11334 (2006).

^a Principal Investigator; ^b Contributing Investigator

Experimental and Computational Studies of Ultrafast Electronic Relaxation and Charge Transfer in Molecular Systems of Importance to Chemistry

Edward C. Lim

Department of Chemistry & The Center for Laser and Optical Spectroscopy, The University of Akron,
319 Knight Chemical Laboratory, Akron, OH 44325-3601

elim@uakron.edu

Program Scope

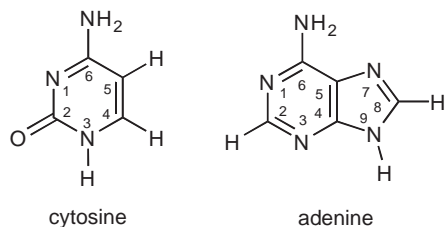
The primary objective of this project is to obtain a fundamental understanding of the mechanisms of ultrafast energy and charge transfers in photoexcited molecules of importance to Chemistry.

Traditionally, the photophysics of aromatic molecules is described in terms of $\pi\pi^*$ and $n\pi^*$ states that are assumed to be the only low-lying electronic states of relevance to electronic relaxation processes. Our recent work on fluorinated benzenes, coumarins, substituted benzonitriles and benzethynes, however, indicates that a biradical state of significant charge-transfer (CT) character (such as $\pi\sigma^*$ state) lies near or below the conventional excited states in a number of molecular systems. Because of the greatly different equilibrium geometry of a biradical state relative to $\pi\pi^*$ (and $n\pi^*$) states, the potential energy profile of the biradical state commonly crosses that of the initially prepared excited state (of $\pi\pi^*$ or $n\pi^*$ character) as well as the ground state, leading to an ultrafast radiationless decay (internal conversion) of the photoexcited molecules. During the past two years, our major research efforts have been directed toward the understanding of the origin of the ultrafast internal conversion in photoexcited nucleic acid bases and dialkylaminobenzonitriles, which have been topics of great interest during the past four decades.

Recent Progress

DNA Bases

The most striking photophysical property of the natural DNA bases is the femtosecond internal conversion that rapidly returns the photoexcited molecule to the ground state before chemical reaction in the excited state can cause UV photodamage. Equally intriguing is the effect simple chemical modifications have on internal conversion. In cytosine, for example, the ~ 720 fs excited-state lifetime of the unmodified base in water increases to ~ 88 ps by replacement of the C5 hydrogen, and to ~ 280 ps by acetylation of the amino group attached to the C4 carbon atom (see scheme for structures). In adenine, which is 6-aminopurine, the excited-state lifetime in water is about one ps, whereas 2-aminopurine has a nanosecond lifetime. Clearly, these are important observations that a successful model must be able to account for.



We have recently carried out CIS and CR-EOM-CCSD(T) calculations of the potential energy profiles of cytosine and its derivatives at optimized CIS geometries. The results indicate that the $S_1 \rightarrow S_0$ internal conversion occurs through a barrierless state switch from the initially excited $^1\pi\pi^*$ to a biradical state, which intersects the ground state at lower energy, Fig. 1. In the biradical state, the C5 and C6 hydrogen atoms are almost perpendicular to the average ring plane and displaced in opposite directions (see inset of Fig. 1). Replacement of the C5 hydrogen of cytosine by fluorine introduces an energy barrier for the $\pi\pi^* \rightarrow$ biradical state switch, whereas replacement of the C6 hydrogen by fluorine does not. The excited-state lifetimes of the two fluorinated cytosines are therefore expected to be vastly different. These predictions are borne out by experiment (~ 88 ps for 5-fluorocytosine and < 1 ps for 6-fluorocytosine). Replacement of one of the amino hydrogen atoms by an acetyl group (to yield N^4 -acetylcytosine) increases the energy barrier for the $^1\pi\pi^* \rightarrow$ biradical state switch even more (through the formation of an intramolecular C–H:O hydrogen bond), consistent with the greatly increased lifetime (~ 240 ps) of the molecule. Extension of these computational methodologies to uracil and thymine shows that the same biradical-mediated

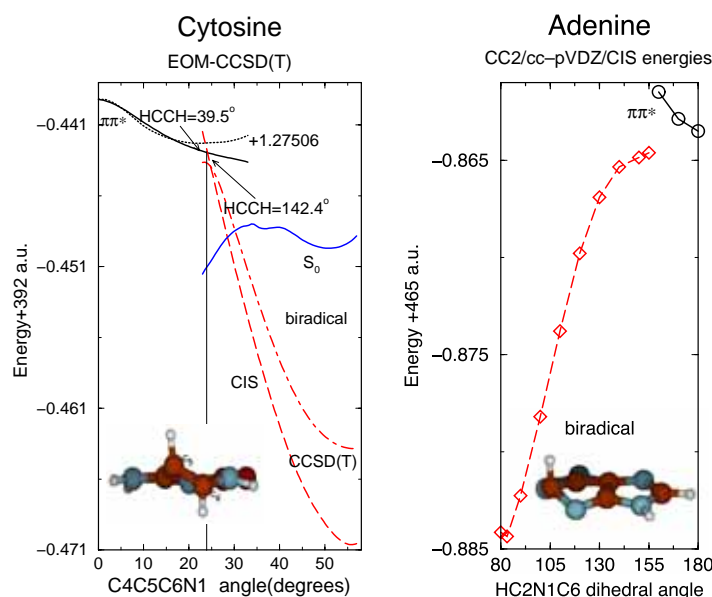


Figure 1.

state, which crosses both the $\pi\pi^*$ and the ground states, Fig. 1. The electronic structure of the biradical state is dominated by an electronic configuration in which one unpaired electron occupies a π^* orbital localized on the five-membered ring and the other occupies an orbital localized very strongly on a p-type C2 atomic orbital of the six-membered ring (see Fig. 1). The structure of the biradical state has a strongly puckered six-membered ring and the C2-H bond of adenine, or the C2-N bond of guanine, which is nearly perpendicular to the average ring plane, Fig. 1. Consistent with the predictions of the calculations, the measured $\pi\pi^*$ -state lifetime is extremely short (sub-picoseconds) in adenine and 9-methyladenine which have barrierless crossing to the biradical state, slightly longer in N,N-dimethyladenine (~ 3 ps), which has a small barrier for the $\pi\pi^* \rightarrow$ biradical state switch, and very long (nanoseconds) in 2-aminopurine, which has the biradical state substantially above the $\pi\pi^*$ state.

DMABN and Related Molecules

As the prototype of molecules that exhibit intramolecular charge transfer (ICT) in polar solvents, 4-dimethylamino-benzonitrile (DMABN) and related molecules have been of great interest for many years. In non-polar solvents, where no ICT reaction is observed, DMABN and several closely related aminobenzonitriles exhibit thermally activated internal conversion that occurs on a sub-picosecond time scale. In the gas phase (supersonic free jet), the aminobenzonitriles display an abrupt break-off (loss) of fluorescence for excitation at about 0.2 eV above the electronic origin of the S_1 state.

Our recently completed TDDFT/cc-pVDZ and CIS/cc-pVDZ calculations provide a rationale for the occurrence of the thermally activated internal conversion in non-polar solvents and the observation of the fluorescence break-off in the gas phase. The calculations show that a biradical state of $\pi\sigma^*$ configuration is of lower energy than the lowest-energy $\pi\pi^*$ state of L_b type, at their respective optimized geometries, Fig. 2. Because the vertical transition from the ground state of linear geometry to the bent $\pi\sigma^*$ state (with CCN angle of 120°) is Franck-Condon forbidden, direct excitation of the ground-state molecule to the $\pi\sigma^*$ state is not allowed, and the radiative transition from the $\pi\sigma^*$ state to the ground state is essentially dipole forbidden. At the optimized ground-state geometry, the vertical excitation energy of the dark $\pi\sigma^*$ state of DMABN or 4-aminobenzonitrile (ABN) is slightly greater than that of the $\pi\pi^*$ state, and the two states cross at CCN angle of about 150° . The energy barrier for the state crossing from the initially excited $\pi\pi^*$ state (L_b , also called LE, and higher-lying L_a) to the dark $\pi\sigma^*$ state is less than about 0.2 eV, which is in reasonable agreement with the observed activation energy for the thermally activated S_1 (L_b) $\rightarrow S_0$ internal conversion in alkane solvents and the threshold energy for the fluorescence break-off in the gas phase.

internal conversion applies to all of the pyrimidine bases. Interestingly, the calculations predict that the barrier height for the $\pi\pi^* \rightarrow$ biradical state switch is significantly smaller in 5-fluorouracil than in 5-fluorocytosine, such that the excited-state lifetime of the former should be very much shorter than that of the latter. This prediction is also consistent with experiment.

More recently, we have performed CC2, EOM-CCSD and CR-EOM-CCSD(T) calculations of the potential energy profiles of the purine bases, adenine and guanine, at optimized CIS geometries using the cc-pVDZ basis set. The results of this study indicate that the internal conversion of purine bases is also mediated by a biradical

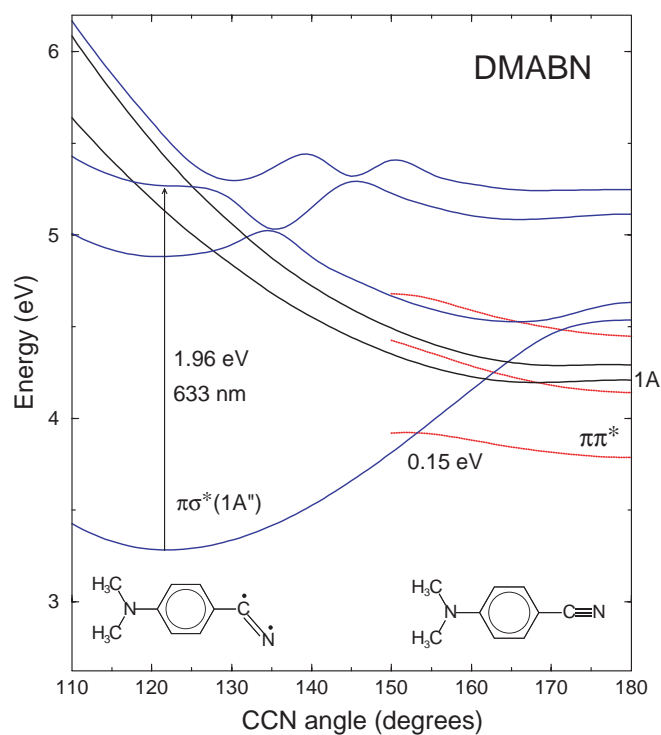


Figure 2.

is set to within the spectral region of the $\pi\sigma^* \leftarrow \pi\sigma^*$ absorption at 600 nm and a decrease in intensity when the probe wavelength is set to 460 nm, where the $\pi\pi^* \leftarrow \pi\pi^*$ absorption occurs. These results corroborate the existence of a low-lying $\pi\sigma^*$ state and the occurrence of an ultrafast (< 1 ps) state switch from the initially excited $\pi\pi^*$ state (L_b or L_a) to the $\pi\sigma^*$ state.

We have proposed that the highly polar $\pi\sigma^*$ state, with a large dipole moment, is the intermediate state of the sequential ICT reaction that takes the initially excited $\pi\pi^*$ state to the fully charge-separated ICT state of the molecule in polar solvents. Consistent with this proposal, we have found that the 4 ps rise time of the ICT-state absorption at 410 nm is identical to the decay time of the $\pi\sigma^*$ -state picosecond transient at 700 nm for DMABN in acetonitrile. This observation does not however rule out the conventional $LE \rightarrow$ ICT reaction mechanism, as rapid thermal equilibration between the $\pi\sigma^*$ and LE states would lead to an identical decay rates for the two states. Occurrence of a very rapid $LE-\pi\sigma^*$ equilibration is suggested by the decay rate of the LE fluorescence that is similar to the decay rate of the $\pi\sigma^*$ -state absorption.

Future Plans

The main focus of our work will be directed toward the detection and characterization of the dark intermediate states, using time-resolved vibrational spectroscopies (resonance Raman and IR). To clarify the mechanistic details of the ultrafast photoprocesses, we will carry out time-resolved studies of substituent effects (on electronic relaxations) for a number of other chemically modified DNA bases and aminobenzonitriles, and compare them with the predictions of the theoretical models. Extension of these studies to other classes of molecular systems, possessing low-lying $\pi\sigma^*$ /biradical states, is also planned.

Publication Listing DOE Support

1. T. Fujiwara and E. C. Lim, Binding Energies of the Neutral and Ionic Clusters of Naphthalene in Their Ground Electronic States, *J. Phys. Chem.*, **107**, 4381-4386 (2003).
2. T. Fujiwara, D. C. Moule, and E. C. Lim, A One-Photon Laser Induced Fluorescence and a Sequential Two-Photon Optical-Optical Double Resonance Excitation Study of the Vibrational Structure of the \tilde{B}^1A_1 ($\pi\pi^*$) State of Thiophosgene, *Cl₂SC*, *J. Chem. Phys.*, **119**, 7741-7748 (2003).

In the spectral range of 400-800 nm, our calculation on DMABN predicts only one intense excited-state absorption at about 700 nm, which is due to a $\pi\sigma^* \leftarrow \pi\sigma^*$ transition. The excited-state absorptions from the $\pi\pi^*$ state (L_b or L_a) are much weaker. The calculation also indicates that the $\pi\sigma^*$ state can be identified by the anomalous low frequency (~ 1460 cm^{-1}) of the CN stretch, relative to the corresponding vibrational frequencies (~ 2180 cm^{-1}) in the $\pi\pi^*$ and ground states. The greatly reduced CN stretch frequency of the $\pi\sigma^*$ state is due to the decrease in CN bond order (from three to two) that accompanies the $\pi \rightarrow \sigma^*$ excitation. Consistent with these predictions, DMABN, ABN, and 4-(diisopropylamino)-benzonitrile (DIABN) all display picosecond transient absorption at about 700 nm in non-polar and polar solvents, following the 267 nm or 305 nm excitation of the L_a state. Moreover, in DMABN, the Raman active 1467 cm^{-1} CN stretch, exhibits a large resonance enhancement when the probe (Raman excitation) wavelength

3. C. Gonzalez and E. C. Lim, Evaluation of the Hartree-Fock Dispersion (HFD) as Practical Tools for Probing Intramolecular Potentials of Small Aromatic Clusters: Comparison of the MP2 and HFD Intermolecular Potentials, *J. Phys. Chem. A*, **107**, 10105-10110 (2003).
4. T. Fujiwara, D. C. Moule, and E. C. Lim, Thiophosgene, A Molecule Tailor-Made for Testing Fundamental Theoretical Concepts of Radiationless Transitions: Intramolecular Dynamics of S_1 Cl_2CS , *J. Phys. Chem. A*, **107**, 10223-10227 (2003).
5. M. Z. Zgierski and E. C. Lim, Nature of the “Dark” State in Diphenylacetylene and Related Molecules: State Switch from the Linear $\pi\pi^*$ State to the Bent $\pi\sigma^*$ State, *Chem. Phys. Lett.*, **387**, 352-355. (2004).
6. T. Fujiwara, D. C. Moule, and E. C. Lim, Optical-Optical Double Resonance Probe of the Dark State of Thiophosgene in Supersonic Free Jet, *Chem. Phys. Lett.*, **389**, 165-170 (2004).
7. M. Z. Zgierski and E. C. Lim, On the Mechanism of Intramolecular Charge Transfer in para-Disubstituted Diphenylacetylenes Containing Electron-Donating and Electron-Accepting Groups: Role of $\pi\sigma^*$ State in Electron-Transfer Dynamics, *Chem. Phys. Lett.*, **393**, 143-149 (2004).
8. M. Z. Zgierski and E. C. Lim, The Role of $\pi\sigma^*$ State in Intramolecular Electron-Transfer Dynamics of 4-Dimethylaminobenzonitrile and Related Molecules, *J. Chem. Phys.*, **121**, 2462-2465 (2004).
9. D. C. Moule, T. Fujiwara, and E. C. Lim, Thiophosgene: A Tailor-Made Molecule for Photochemical and Photophysical Studies in *Advances in Photochemistry*, Vol. 28, D. C. Neckers, W.S. Jenks, and T. Wolff, Eds. (John Wiley & Sons, Inc., 2005), pp. 27-79.
10. M. Z. Zgierski and E. C. Lim, “Electronic and Vibrational Spectra of the Low-lying $\pi\sigma^*$ State of 4-Dimethylaminobenzonitrile: Comparison of Theoretical Predictions with Experiment”, *J. Chem. Phys.*, **122**, 111103-111106 (2005).
11. M. Z. Zgierski, T. Fujiwara and E. C. Lim, Photophysics of Aromatics Molecules with Low-lying $\pi\sigma^*$ States: Fluorinated Benzenes, *J. Chem. Phys.*, **122**, 144312-144318 (2005).
12. H. K. Kang, D. E. Kang, B. H. Boo, J. K. Lee and E. C. Lim, Existence of Intramolecular Triplet Excimer of Bis(9-fluorenyl)methane: Phosphorescence and Delayed Fluorescence Spectroscopic and *Ab Initio* Studies, *J. Phys. Chem. A*, **109**, 6799-6804 (2005).
13. T. Fujiwara, E. C. Lim, J. Kodet, R. H. Judge, and D. C. Moule, The Isotopic Dependence of Axes Switching in Thiophosgene Induced by $\tilde{A}^1A_2 (\pi\pi^*) \leftarrow X^1A_1$ Electronic Excitation, *J. Mol. Spec.*, **232**, 331-340 (2005).
14. R. Campos Ramos, T. Fujiwara, M. Z. Zgierski, and E. C. Lim, Photophysics of Aromatic Molecules with Low-Lying $\pi\sigma^*$ States: Excitation-Energy Dependence of Fluorescence in Jet-Cooled Aromatic Nitriles, *J. Phys. Chem. A* **109**, 7121-7126 (2005).
15. M. Z. Zgierski, S. Patchkovskii, and E. C. Lim, *Ab Initio* Study of a Biradical Radiationless Decay Channel of the Lowest Excited Electronic State of Cytosine and Its Derivatives, *J. Chem. Phys.*, **123**, 081101/1-081101/4 (2005).
16. M. Z. Zgierski, S. Patchkovskii, T. Fujiwara, and E. C. Lim, On the Origin of the Ultrafast Internal Conversion of Electronically Excited Pyrimidine Bases, *J. Phys Chem. A* **109**, 9384-9387 (2005).
17. B. H. Boo, D. E. Kan, H. K. Kang, M. Kwon, S. J. Yoo, J.-K. Lee, and E. L. Lim, Photodissociation of 2,2-Diphenylhexamethyltrisilane in a Supersonic Molecular Beam, *Chem. Phys. Lett.* **417**, 83-88 (2005).
18. T. Fujiwara, R. Campos Ramos, M. Z. Zgierski, and E. C. Lim, Geometries and Excited-State Dynamics of van der Waals Dimers and Higher Clusters of 1-Cyanonaphthalene, *J. Chem. Phys.*, **123**, 244306/1-244306/8 (2005).
19. T. Fujiwara, R. Campos Ramos, M. Z. Zgierski, and E. C. Lim, “Experimental and Theoretical Studies of the Conformational Structures of the Mixed Clusters of 1-Cyanonaphthalene with Water, *J. Chem. Phys.* **123**, 244307/1-244307/9 (2005).
20. T. Fujiwara, E. C. Lim, R. H. Judge, and D. C. Moule, “An Optical-Optical Double Resonance Probe of the Lowest Triplet State of Jet-Cooled Thiophosgene: Rovibronic Structures and Electronic Relaxation”, *J. Chem. Phys.* **124**, 124301/1-124301/12 (2006).

Rapid Bond-Breaking and Bond Making in Radical Ions

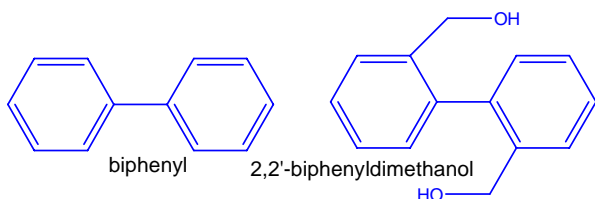
Principal Investigators: Andrew Cook, Sergei Lyman and John R. Miller,

jrmiller@bnl.gov Chemistry Department, Brookhaven National Laboratory

Scope: This program examines charged or radical species and develops tools to create and probe these species. Principal among these tools is the Laser Electron Accelerator Facility (LEAF) at Brookhaven that produces 7 ps electron pulses and detection systems. We encourage use of LEAF's present and planned capabilities by a broad range of scientists including members of this CPIMS meeting: See Facilities at <http://www.cfn.bnl.gov/default.asp> for a description.

A large effort is directed to understanding of electron transfer reactions relevant to of solar energy conversion, while other effort examines radiation chemistry that can be make electron pulse techniques more valuable to studies of charge transfer. The present abstract describes two types of bond-breaking reactions.

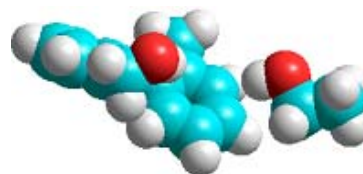
Proton Transfer to Radical Anions in Solution Because radical anions are powerful bases they are readily protonated to create neutral radicals. Weak proton donors like EtOH are known to protonate anions of many aromatic molecules to create cyclohexadienyl radicals with rates typically in the microsecond time region in neat EtOH. For biphenyl^{•-} the reported rate $1 \times 10^6 \text{ s}^{-1}$



is redetermined here to be $4.4 \times 10^5 \text{ s}^{-1}$ ($\tau=2.3 \mu\text{s}$). Addition of two MeOH substituents in 2,2'-biphenyldimethanol leads to the possibility of intramolecular proton transfer; indeed protonation now

occurs in 0.3 ns, more than a thousand times faster. The exceptional rate suggests a change of mechanism and the structure suggests the possibility of intramolecular protonation, in which an MeOH substituent donates a proton to the other ring. Deuterium substitution of the solvent or changing to an aprotic solvent instead point to fast proton transfer from the solvent, possibly in configurations like that illustrated at right.

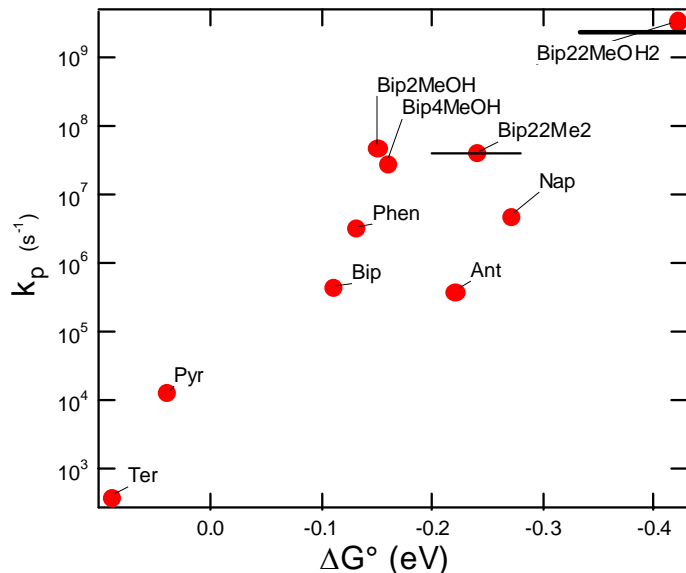
The fast rate is not due to intramolecular proton transfer, but to the more favorable free energy change for proton transfer to the anion of the biphenyl having two MeOH substituents. To reach this conclusion it was necessary to determine the appropriate thermodynamic information including the unknown, redox potential, $E^0(\text{Bip}(\text{MeOH})_2)$, which is probably unmeasurable with normal electrochemical techniques, and to learn that there is a free energy relation for these protonation rates. The free energy relation also required determination of the energies of the free radicals created by the



protonation reactions. Most of these are not known, and were computed by standard DFT methods.

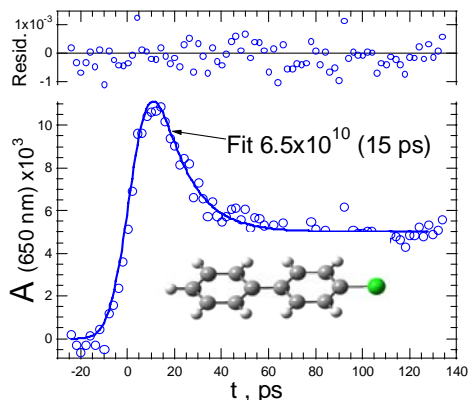
The observed relation rationalizes the six-decade range of proton transfer rate constants including the newly-measured protonation rates as well as rates from the literature where large variations were observed, but the reasons were not understood. Now these rates are understood to respond both to changes in energies of the anions (redox potentials) and to changes in the energies of the radical products.

Free energy relation for rate constants (pseudo first order) for protonation of radical anions in EtOH.

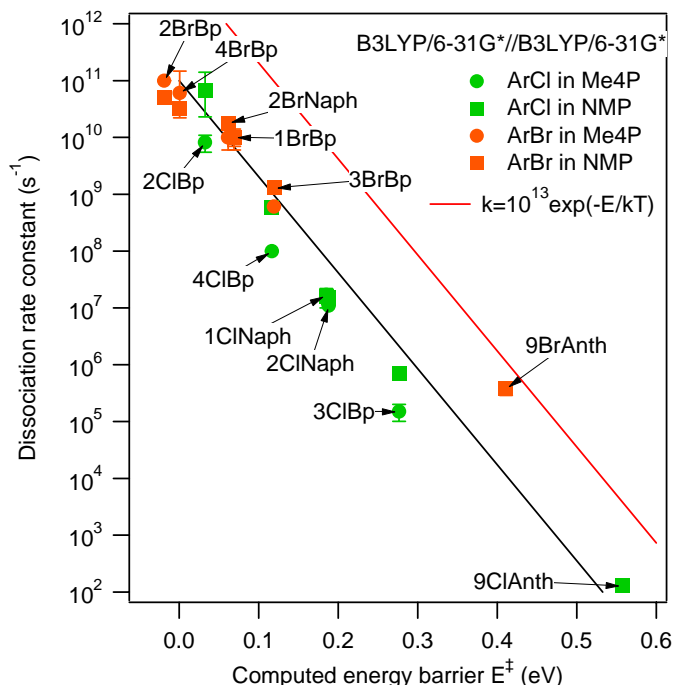


Dissociation of Aryl Halide Anions: Electronic Effects on Barriers

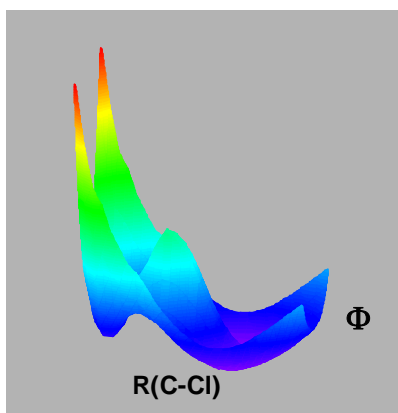
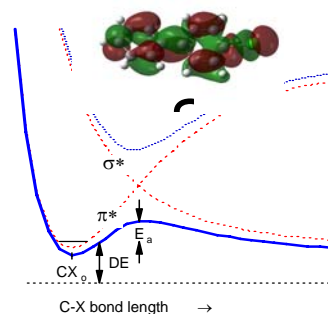
Charge transfer to organic molecules can result in scission of chemical bonds. An important class of such reactions is a one-electron reduction of organic halides in solution leading to dissociation of the carbon-halogen (C-X) bond to produce a carbon-centered radical and a halide anion. This reaction has been studied intensely



because it is a basic element of important chemical processes such as nucleophilic substitution reactions and Grignard reagent formation, but there has been little information on rates faster than 10^8 s^{-1} . Results shown at left illustrate transient absorption measurement at LEAF that obtains much shorter time



resolution. The results of such measurements on several molecules correlated well (shown above right) with computed energy barriers, although this series of fast dissociation reactions showed poor correlation with overall reaction energetics. Correlation with overall reaction energetics misses the important influence of *electronic effects* on the activation barriers for these fast reactions. These electronic effects lead to large reductions (shown right) in the adiabatic barriers compared to those for



crossings of the σ^* and π^* diabatic states. The reductions are large only if bonds bend to enable the necessary interactions, leading to conical intersections (left).

Earlier work had frequently framed the question of sequential vs. concerted reaction mechanisms. These experiments show that electron addition and bond scission occur in two distinct consecutive steps; as often occurs the idea of concerted reactions slips away as better time resolution becomes available. Further work on these reactions, if pursued, would attempt to illuminate the possibility of “concerted” reactions.

Future plans for experimental systems include: • Automated collection of spectra from visible through near IR, • A fast single-shot detection system for transient absorption described by Andrew Cook at this conference • Two types of pulse-pump-probe experiments that will combine excitation by electron and laser pulses • A wide range of continuous improvements to obtain improved stability, reliability and signal/noise ratios.

The experimental improvements will enable measurements of fast intramolecular electron transfer reactions. Essential here will be the single-shot experiment that will obtain high time resolution on custom-synthesized molecules not available in gram quantities. The same techniques will be applied to examination of charge transport in “molecular wires.”

Plans also include determination of geminate recombination following ionization in a variety of non-aqueous media, and energies of conjugated carboranes. The radiation chemistry of fluids useful for production of radical cations, such as CHCl_3 , is poorly understood and will be further investigated.

Publications 2003-2006

Faster Dissociation: Measured Rates and Computed Effects on Barriers in Aryl Halide Radical Anions

N. Takeda, P. V. Poliakov, A. R. Cook, and J. R. Miller
J. Am. Chem. Soc. 126, 4301-4309 (2004).

The LEAF Picosecond Pulse Radiolysis Facility at Brookhaven National Laboratory

J. F. Wishart, A. R. Cook and J. R. Miller
Rev. Sci. Inst. 75, 4359-4366 (2004).

Increased Yields of Radical Cations by Arene Addition to Irradiated 1,2-Dichloroethane

A. M. Funston and J. R. Miller
Radiat. Phys. Chem., 72, 601-611 (2005).

Benzene Radical Ion in Equilibrium with Solvated Electrons, R. A. Marasas, T. Iyoda, and J. R. Miller, *J. Phys. Chem. A* 107, 2033-2038 (2003).

Rate of ON-OO⁻ Bond Homolysis and the Gibbs Energy of Formation of Peroxynitrite, S. V. Lymar, G. A. Poskrebyshev, *J. Phys. Chem. A* 107, 7991-7996 (2003).

Hydroxyl Radical Formation by O-O Bond Homolysis in Peroxynitrous Acid

S. V. Lymar, R. F. Khairutdinov and J. K. Hurst, *Inorg. Chem.* 42, 5259-5266 (2003).

Spin-Forbidden Deprotonation of Aqueous Nitroxyl (HNO), V. Shafirovich and S. V. Lymar, *J. Am. Chem. Soc.* 125, 6547-6552 (2003).

Hyponitrite Radical, a Stable Adduct of Nitric Oxide and Nitroxyl

G. A. Poskrebyshev, V. Shafirovich, S. V. Lymar, *J. Am. Chem. Soc.* 126, 891-899 (2004).

Charge Transfer Through Terthiophene End-Capped Poly(arylene ethynylene)s

Funston, A. M.; Silverman, E. E.; Miller, J. R.; Schanze, K. S. *J. Phys. Chem. B* **2004**,

One-Electron Reduction of an "Extended Viologen" p-Phenylene-bis-4,4'-(1-aryl-2,6-diphenylpyridinium) Dication Funston, A.; Kirby, J. P.; Miller, J. R.; Pospíšil, L.; Fiedler, J.; Hromadová, M.; Gál, M.; Pecka, J.; Valásek, M.; Zawada, Z.; Rempala, P.; Michl, J. *J. Phys. Chem. B* **2005**, 109, 10862-10869.

Spectroscopy and Transport of the Triplet Exciton in a Terthiophene End-Capped Poly(phenylene ethynylene)

Funston, A. M.; Silverman, E. E.; Schanze, K. S.; Miller, J. R. *J. Phys. Chem. B.* **2006**; 110(36); 17736-17742.

Research Summaries
(by PI)

Model Catalysis by Size-Selected Cluster Deposition

Scott Anderson, Chemistry Department, University of Utah, 315 S. 1400 E. Rm. 2020, Salt Lake City, UT 84112. anderson@chem.utah.edu

Program scope: We are interested in understanding the effects of cluster size on physical and chemical properties of planar model catalysts prepared to depositing size-selected cluster ions on well defined substrates in ultra-high vacuum. Tool available include a variety of pulsed and temperature-programmed mass spectrometric techniques, x-ray photoelectron spectroscopy (XPS), Auger electron spectroscopy (AES), ion scattering (ISS), and infrared reflection absorption spectroscopy (IRAS). The goal is produce model catalysts that are well characterized, and where properties such as metal loading, substrate defect density, and metal cluster size can be varied independently, allowing us new insights into these very complex systems.

Recent Progress

During the past year, the focus of our DOE supported work has been on the gold/TiO₂ system, specifically on CO oxidation catalysis and adsorption behavior of water and its effects gold sintering behavior. In addition, we have made several instrumentation upgrades to facilitate the DOE-funded IRAS experiments, and to allow us to transfer samples to a unique single-electron tunneling instrument belonging to a colleague, and funded by AFOSR. We will be able to use this system for critical experiments on systems of interest to DOE as well.

1. Instrument upgrades

Our samples consist of a ~2.5 mm diameter spot of deposited clusters, supported on a ~1 cm² substrate. The small spot and low cluster coverage makes FT-IRAS unusually difficult. Our UHV system is designed so that sample preparation and characterization are carried out in a large UHV chamber, and the sample can be lowered through a triple seal into a small UHV chamber. This lower chamber serves as a load-lock, IRAS station, and high pressure cell. The initial design proved cumbersome, and in the past year we constructed a trapezoidal chamber that provides better optical access for IRAS, allows sample exchange without opening any conflat connections, and has interchangeable faceplates that can accommodate IRAS and the new UHV sample transfer hardware.

The sample transfer system is simply a small vacuum chamber that can be connected to the lower chamber on our end, and to a load/lock chamber on the microscope end, with gate valves that can be opened so that the sample can be transferred on the end of a home-made manipulator. In transit, the system is pumped by a getter pump, and holds in the low 10⁻¹⁰ Torr pressure range for hours.

2. Au_n/TiO₂.

At the end of 2005, completed a detailed study of CO oxidation on Au_n clusters deposited on rutile TiO₂(110), which found strong size effects and was able to show that the size dependence correlated strongly with the ability of the clusters to bind and activate molecular oxygen. The results are a nice demonstration of the information that can be extracted by a combination ion scattering, x-ray photoelectron spectroscopy (XPS) and mass spectrometry. We also published a separate study of agglomeration of Au deposited as Au⁺ upon annealing of the samples. One of the findings in these studies was that deposited Au_n clusters do not agglomerate significantly on the experimental time scale at room temperature. This result was later corroborated by STM experiments of Buratto and co-workers.¹ The exception is for gold atoms, which they, as well as STM researchers who deposit gold by thermal evaporation, find to agglomerate into large clusters at room temperature, but which our ion scattering results clearly show to be high dispersed. We tentatively attributed the difference between the experiments to the considerably faster time scale of our experiments. From the start of Au⁺ deposition to completion of an ion scattering characterization of dispersion, takes us approximately 5 minutes. I am told that the time scales in the STM experiment are longer – on the order of 30 - 120 minutes. In addition, our Au_n⁺ beam intensity is significantly higher than the fluxes used in the STM experiments, and slow delivery also tends to favor nucleation to a small density of large clusters.

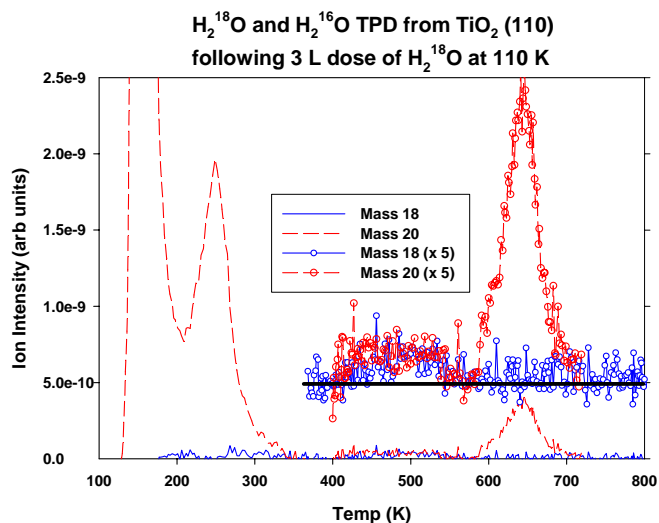
In November 2005, Besenbacher, Molina, Hammer and co-workers ("BMH")² reported a

reinterpretation of the Besenbacher group's seminal work on oxygen vacancies and mobility on rutile $\text{TiO}_2(110)$. One of the major changes was that water was found to bind very efficiently to oxygen vacancies on TiO_2 , mostly dissociating to generate a pair of hydroxyl sites. The process is rapid enough that they infer that the O-vacancy sites on the initially prepared TiO_2 surface are mostly converted to hydroxyl sites on the time scale needed for typical STM experiments. This result is important because theory indicates that Au atoms bind much more strongly to O-vacancy sites than to perfect TiO_2 , and indeed, we interpreted the stability of our deposited Au^+ to trapping at vacancies, based on a combination of XPS and ion scattering results. It may be that our experimental protocol was fast enough to avoid extensive hydroxylation of the vacancy sites, but this appears to be an important issue to resolve, as it is known that water significantly affects gold catalytic chemistry.

To do these experiments it was necessary to improve our vacuum quality. We currently have base pressure in the high 10^{-11} Torr range, and more importantly, water partial pressure in the 10^{-12} Torr range, with most of the background consisting of H_2 , He, and Ar. This low water partial pressure, together with our rapid deposition and analysis time scales, means that we can do experiments where the adventitious water dose is negligible, for comparison with experiments where deliberate water doses saturate sites on the surface.

To understand the ion scattering results, it is first necessary to review adsorption/desorption behavior for water on $\text{TiO}_2(110)$, which is summarized in the figure at right. Here we have prepared a clean, vacuum-annealed TiO_2 surface, then dosed it with H_2^{18}O at $T_{\text{surface}} \sim 110$ K, where the water all freezes on the surface. The data show signals for desorption of H_2^{18}O and H_2^{16}O as T_{surface} is ramped at 3 K/sec. The lowest temperature peak is condensed multilayer water, and the peak at 250 K corresponds to desorption of water in the monolayer directly bound to the TiO_2 surface. This behavior has been observed and discussed by previous authors, notably Henderson.³ The weak broad feature between 400 and 550 K was also observed by Henderson, and attributed to water desorbing from thermally induced defects on the surface. In Henderson's experiment, the surface was ^{18}O substituted and normal H_2O was used (the opposite of our experiment), with the result that essentially no ^{16}O - ^{18}O exchange was observed in the two low temperature peaks, but extensive exchange was observed for the broad "490 K" feature. We also see no exchange (i.e., no H_2^{16}O) for the two low temperature peaks, and we see ~40% exchange in the 490 K feature.

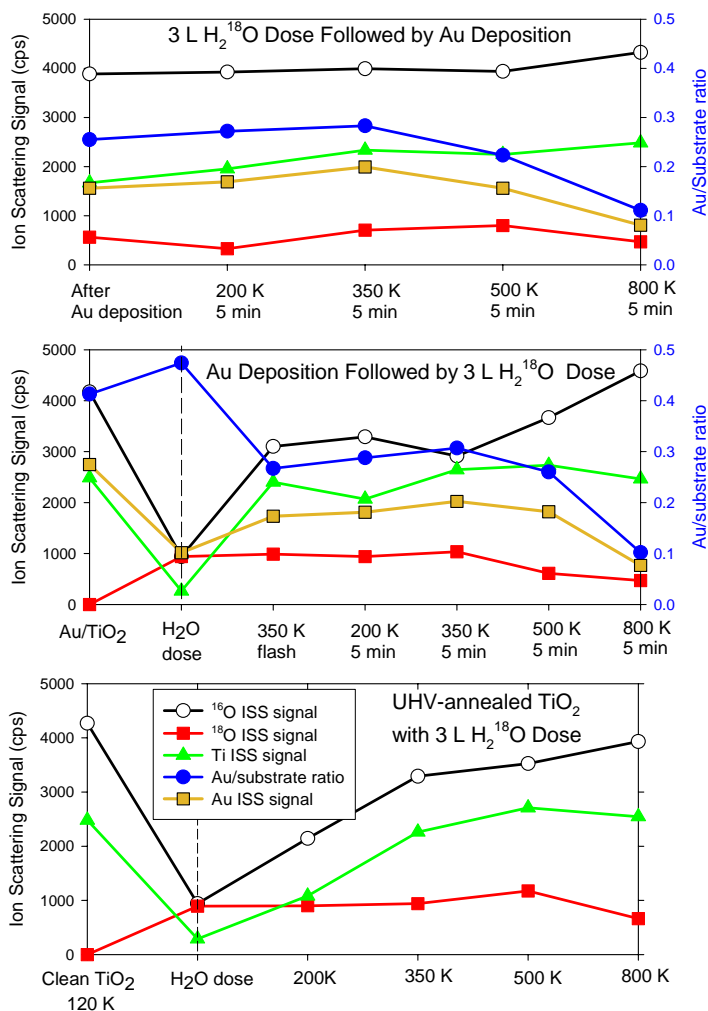
The more interesting observation is that there is a larger and sharper desorption feature for H_2^{18}O , at ~650 K. Previous TPD studies did not report results in this high temperature range. The surprising thing is not so much that the peak is there, but that there is almost no ^{18}O - ^{16}O exchange. We, of course, considered the possibility that this peak was an artifact of H_2^{18}O desorption from sample holder or manipulator surfaces, however, our differentially pumped TPD geometry makes such background peaks unlikely. Nonetheless, we did a number of control experiments, and the conclusion is that this really is mass 20 desorbing from $\text{TiO}_2(110)$, and mass 20 almost has to be H_2^{18}O . This conclusion is also consistent with ^{18}O - ^{16}O intensity ratios observed in the ion scattering results below. The implication is that there is a quite stable water binding site on UHV-annealed $\text{TiO}_2(110)$, where the system somehow preserves memory of which O atoms came from the water dose. Some suggestion of a state like this is found in the recent BMH paper², where they observe an adsorption site with two closely associated hydroxyls (A III 2OH) that persists even after flashing the surface to 600 K prior to STM imaging.



For the TiO_2 surface with 5% of a monolayer of Au deposited as Au^+ at $T_{\text{surface}} \sim 110\text{K}$, the TPD results are quite similar to those for clean TiO_2 , as expected from the small Au coverage. The main differences are that the features at $\sim 490\text{K}$ and $\sim 650\text{K}$ are both suppressed by a factor of ~ 2 , consistent with our assumption that Au binds at defect sites, presumably blocking water adsorption at low T_{surface} .

To characterize how water binds to the $\text{Au}/\text{TiO}_2(110)$ samples, and what effect this might have on agglomeration behavior of the gold, we carried out ion scattering (ISS) experiments, as shown in the figure to the right. The bottom frame shows results for Au-free vacuum-annealed $\text{TiO}_2(110)$. Note that ISS essentially shows the identity and concentrations of atoms in the top-most sample layer, however sensitivity is element specific, thus ISS is primarily useful in observing changes in surface layer concentrations as conditions are varied. For TiO_2 , the initial ISS shows ^{16}O and Ti only, as expected. After freezing $\sim 3\text{L}$ of H_2^{18}O on the surface, the ^{16}O and Ti signals are strongly attenuated by the overlayer of H_2^{18}O , and there is significant ^{18}O signal. (Unfortunately, ISS is not sensitive to H atoms). After 5 minutes annealing to 200K to desorb the multilayer water, there is $\sim 50\%$ recovery of the Ti and ^{16}O signals, indicating that the monolayer is not so close-packed as to completely block scattering from the underlying substrate. For annealing at 350K or higher, where monolayer water is also desorbed, the Ti signal is completely recovered, and the combination of ^{16}O and ^{18}O is close to the pre-dose ^{16}O level. Note that there is a significant decrease in ^{18}O signal upon annealing to 800K , consistent with the $\sim 650\text{K}$ mass 20 desorption feature shown in the TPD spectra above. The persistence of significant ^{18}O signal after 800K annealing indicates that there is some ^{18}O - ^{16}O exchange, presumably for water bound at defects, corresponding to the $\sim 490\text{K}$ TPD feature.

In the middle frame of the figure, 5% of a monolayer of Au was deposited as Au^+ at 110K , and an initial ISS was taken, showing Au, Ti, and ^{16}O signals. After the H_2^{18}O dose, the initial ISS signals are attenuated and there is an ^{18}O signal, much as in the clean TiO_2 experiment. After flashing for a few seconds to 350K to desorb multilayer and monolayer water, the Ti signal has recovered to nearly the pre-dose value, and the sum of the ^{18}O and ^{16}O signals are nearly equal to the pre-dose ^{16}O signal, as expected. The Au signal is still significantly attenuated however. Such attenuation could result either from agglomeration of Au during the flash to 350K , or to residual H_xO adsorbed on Au sites. In the former case, we would expect the Au signal to continue to decline as the sample is annealed to successively higher temperatures leading to additional agglomeration, whereas the actual Au signal continues to increase slowly for T_{anneal} up to 350K , and declines only at higher temperatures. This result suggests that for temperatures below $\sim 350\text{K}$, the main effect is desorption of H_xO from gold sites, and agglomeration sets in only at higher



temperatures, as proposed in our original study of Au sintering on TiO₂(110). In that study, we proposed that Au atoms bound to oxygen vacancy defects were thermally stable up to room temperature.

The obvious question is whether pre-filling the vacancies with hydroxyls from a water dose would block Au adsorption at those sites. The top frame shows results for TiO₂ that was exposed to 3 L of H₂¹⁸O, then flashed to 350 K to desorb multilayer and monolayer water prior to 5% ML Au⁺ deposition. This pre-treatment should leave H_xO bound to the defect states that are also the strongest sites for Au adsorption. Note that for annealing up to 350K, there is little change in the Au signal or Au/substrate ratio, but that at higher T_{anneal}, the gold signal decreases. The final state after 800 K annealing is quite similar for the samples where water was dosed before and after Au deposition. The main difference is at T_{anneal} = 500K, where there is significantly more Au agglomeration (decrease in Au signal) for the water-predosed sample, suggesting that water did block Au adsorption into the most stable binding sites.

Future Plans

Work will proceed along two fronts during the coming year. We plan to examine CO oxidation on larger Au clusters on TiO₂ and examine effects of water adsorption. We will also begin work on two new systems: Pd_n/Alumina and Pd_n/Au. The improved IRAS sensitivity will allow us to characterize adsorbates more completely in those systems, as well as reactivity and adsorption/desorption properties.

Citations

- ¹ X. Tong, L. Benz, P. Kemper, H. Metiu, M. T. Bowers, and S. K. Buratto, *J. Am. Chem. Soc.* **127**, 13516 (2005).
- ² S. Wendt, R. Schaub, J. Matthiesen, E. K. Vestergaard, E. Wahlstrom, M. D. Rasmussen, P. Thostrup, L. M. Molina, E. Lægsgaard, I. Stensgaard, B. Hammer, and F. Besenbacher, *Surf. Sci.* **598**, 226–245 (2005).
- ³ M. A. Henderson, *Langmuir* **12** (21), 5093 (1996).

DOE-Funded Publications Since 2003

"Deposition dynamics and chemical properties of size-selected Ir clusters on TiO₂", Masato Aizawa, Sungsik Lee, and Scott L. Anderson, *Surf. Sci.* 542 (2003) 253-75
"CO oxidation on Au_n/TiO₂ catalysts produced by size-selected cluster deposition" Sungsik Lee, Chaoyang Fan, Tianpin Wu, and Scott L. Anderson, *JACS* (comm) 126 (2004) 5682-3.
"Agglomeration, Support Effects, and CO Adsorption on Au/TiO₂ (110) Prepared by Ion Beam Deposition" Sungsik Lee, Chaoyang Fan, Tianpin Wu, and Scott L. Anderson, *Surf. Sci.* 578 (2005) 5-19
"Agglomeration, Sputtering, and Carbon Monoxide Adsorption Behavior for Au/Al₂O₃ Prepared by Au_n⁺ Deposition on Al₂O₃/NiAl(110)", Sungsik Lee, Chaoyang Fan, Tianpin Wu, and Scott L. Anderson, *J. Phys. Chem. B* 109 (2005) 11340-11347
"Cluster size effects on CO oxidation activity, adsorbate affinity, and temporal behavior of model Au_n/TiO₂ catalysts", Sungsik Lee, Chaoyang Fan, Tianpin Wu, and Scott L. Anderson, *J. Chem. Phys.* 123 (2005) 124710 13 pages.

THERMOCHEMISTRY AND REACTIVITY OF TRANSITION METAL CLUSTERS AND THEIR OXIDES

P. B. Armentrout

315 S. 1400 E. Rm 2020, Department of Chemistry, University of Utah,
Salt Lake City, UT 84112; armentrout@chem.utah.edu

Program Scope

The objectives of this project are to obtain quantitative information regarding the thermodynamic properties of transition metal clusters, their binding energies to various ligands, and their reactivities. Using a guided ion beam tandem mass spectrometer, we examine the reactions of size-specific transition metal cluster ions with simple molecules and measure the absolute cross sections as a function of kinetic energy for each reaction.

Since 2003, our DOE sponsored work has included studies of the kinetic energy dependences of the size-specific chemistry of Co_n^+ ($n = 2 - 16$) cluster ions reacting with D_2 ,¹ of Ni_n^+ ($n = 2 - 18$) and Co_n^+ ($n = 2 - 20$) reacting with O_2 ,^{2,3} and of Fe_n^+ ($n = 1 - 19$) cluster ions reacting with N_2 .⁴ Further, we have extended our studies to reactions with more complex molecules, specifically, the size-specific reactions of Fe_n^+ ($n = 2 - 15$) with ammonia (ND_3),⁵ and Ni_n^+ ($n = 2 - 16$) with methane (CD_4).⁶ An invited review of our recent work that emphasizes the relationship to bulk phase properties was also published.⁷ The latter point is illustrated in Figure 1 for the example of cobalt clusters bound to hydrogen and oxygen where it is clear that bulk phase bond dissociation energies (BDEs) are approached for modest-sized clusters. Comparable behavior has been observed for V, Cr, Fe, and Ni clusters bound to D and O atoms.

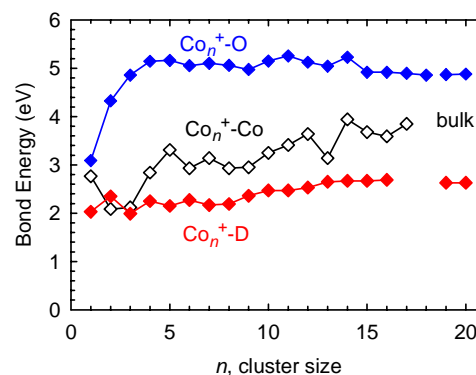


Figure 1. BDEs of D, Co, and O to Co_n^+ as a function of cluster size. Lines labeled bulk indicate the BDEs of H and O atoms to Co films.

Recent Progress

Reactions of Clusters with D_2 . We have now studied V_n^+ ($n = 2 - 13$),⁸ Cr_n^+ ($n = 2 - 14$),⁹ Fe_n^+ ($n = 2 - 15$),¹⁰ Co_n^+ ($n = 2 - 16$),¹ and Ni_n^+ ($n = 2 - 16$)¹¹ cluster ions reacting with D_2 . For all four metal systems, the only products observed are M_nD^+ and M_nD_2^+ . The failure to observe M_mD^+ and M_mD_2^+ products where $m < n$ indicates that the M_nD^+ and M_nD_2^+ products dissociate exclusively by D and D_2 loss, consistent with the thermochemistry derived in this work.

In the Co system, all clusters that form Co_nD_2^+ , $n = 4, 5, \geq 9$, do so in barrierless exothermic processes except for $n = 9$. Comparison of the thermal rates of reaction for cobalt clusters finds that they approach the collision limit for large clusters ($n \geq 11$) and parallel but are somewhat faster than the rates observed for neutral cobalt clusters.

Using methods developed over the past decade,¹² we analyze the kinetic energy dependence of the endothermic cross sections in order to determine threshold energies for these

there are usually two independent routes to measure BDEs for each cluster to D, C, CD, and CD₂, e.g., $D_0(\text{Ni}_6^+-\text{D})$ can be measured in the primary reaction of Ni_6^+ or the secondary reaction of Ni_7^+ . We find that the values obtained from the primary and secondary processes are in good agreement with one another for D (which also agrees with the results from reactions with D₂), C, and CD. For the CD₂ ligand, however, we find that the BDEs obtained from the primary reaction are generally low compared with those from the secondary reaction, which is evidence that there are barriers in excess of the endothermicity of the initial dehydrogenation reaction. For larger clusters, evidence suggests that the barrier lies in the initial dissociative chemisorption step.

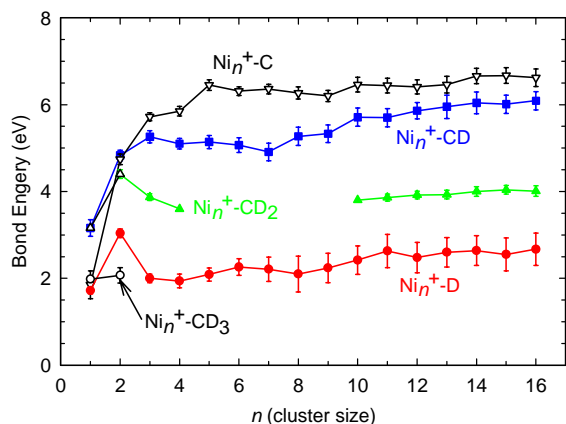


Figure 4. BDEs of D, C, CD, CD₂, and CD₃ to Ni_n^+ vs. cluster size.

Figure 4 shows the final BDEs determined in the nickel study.⁶ We find that the values vary somewhat for small clusters but rapidly reach a relatively constant value with increasing cluster size. The magnitudes of these bonds are consistent with simple bond order considerations, namely, D (and CD₃) form one covalent bond, CD₂ forms two, and CD and C form three. Given the results of Figure 1, it seems reasonable that our experimental BDEs for larger clusters should provide reasonable estimates for heats of adsorption to surfaces. As little experimental information is available for *molecular* species binding to surfaces, the thermochemistry derived here for clusters bound to C, CD, and CD₂ provides some of the first experimental thermodynamic information on such molecular species.

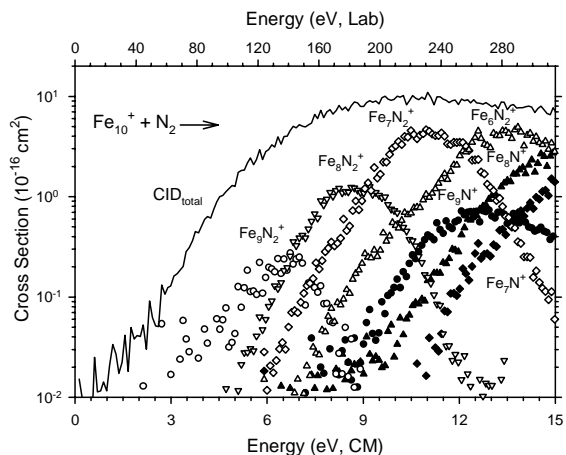


Figure 5. Reaction of Fe_{10}^+ with N_2 showing cross sections for dinitride (open symbols), mononitride (closed symbols), and the total CID products (solid line).

Reactions of Iron Clusters with N₂. This study⁴ is designed to provide insight into the rate-limiting step in the Haber process, which uses a promoted iron catalyst to manufacture ammonia from N₂ and H₂ at high pressures and temperatures. Despite the very strong N₂ bond energy of 9.76 eV, activation of this molecule on iron cluster cations, Fe_n^+ ($n = 1 - 19$), is observed, as illustrated in Figure 5. Both Fe_mN_2^+ and Fe_mN^+ product ions, where $m \leq n$, are observed and the former can be identified as a dinitride species. An energetic barrier for N₂ activation of about 0.48 eV is obtained for the largest clusters. Fe_n^+-N and Fe_n^+-2N bond energies as a function of cluster size are derived from threshold analysis of the kinetic-energy dependences of the endothermic reactions.

These experimental values are somewhat smaller than bulk phase values, although this is potentially because the activation barriers for N₂ activation have been underestimated in the surface work, as previously suggested by Benziger.¹⁸

Future Plans

Experimental work has been completed on the reactions of Co_n^+ with N_2 and CD_4 . These systems are designed to allow us to examine the periodic trends in the thermochemistry and reaction mechanisms for activation of dinitrogen and methane. We have also initiated studies of oxygenated iron clusters, Fe_nO_m^+ , which might mimic the chemistry of metal oxide surfaces. A broad range of stoichiometries have been produced although larger clusters tend to form clusters containing nearly equal numbers of iron and oxygen atoms. Initially, our studies are focusing on characterizing the thermodynamic stabilities of these clusters by examining their dissociation behavior in collisions with Xe. Some 30 different iron oxide cluster cations (with $n = 1 - 10$) have been examined and the kinetic energy dependent cross sections are being analyzed to obtain both oxygen and iron bond energies for these clusters. We intend to then examine the possibility that specific oxidation states of the iron clusters might induce efficient oxidation of species like methane.

Publications resulting from DOE sponsored research in 2003 – present (1 – 7) and References

1. F. Liu and P. B. Armentrout, *J. Chem. Phys.* **122**, 194320-1-12 (2005).
2. D. Vardhan, R. Liyanage, and P. B. Armentrout, *J. Chem. Phys.* **119**, 4166 (2003).
3. F. Liu, F.-X. Li, P. B. Armentrout, *J. Chem. Phys.* **123**, 064304-1-15 (2005).
4. L. Tan, F. Liu, P. B. Armentrout, *J. Chem. Phys.* **124**, 084302-1-14 (2006).
5. R. Liyanage, J. B. Griffin, and P. B. Armentrout, *J. Chem. Phys.* **119**, 8979 (2003).
6. F. Liu, X.-G. Zhang, R. Liyanage, and P. B. Armentrout, *J. Chem. Phys.* **121**, 10976 (2004).
7. P. B. Armentrout, *Eur. J. Mass Spectrom.* **9**, 531 (2003).
8. R. Liyanage, J. Conceição, and P. B. Armentrout, *P. B. J. Chem. Phys.* **116**, 936 (2002).
9. J. Conceição, R. Liyanage, and P. B. Armentrout, *Chem. Phys.* **262**, 115 (2000).
10. J. Conceição, S. K. Loh, L. Lian, and P. B. Armentrout, *J. Chem. Phys.* **104**, 3976 (1996).
11. F. Liu, R. Liyanage, and P. B. Armentrout, *J. Chem. Phys.* **117**, 132 (2002).
12. P. B. Armentrout, *Advances in Gas Phase Ion Chemistry*, Vol. 1; N. G. Adams and L. M. Babcock, Eds.; JAI: Greenwich, 1992; pp. 83-119.
13. K. Christmann, *Surf. Sci. Report*, **9**, 1 (1988). M. E. Bridge, C. M. Comrie, and R. M. Lambert, *J. Catal.* **58**, 28 (1979). K. H. Ernst, E. Schwarz, and K. Christmann, *J. Chem. Phys.* **101**, 5388 (1994).
14. J. Xu, M. T. Rodgers, J. B. Griffin, and P. B. Armentrout, *J. Chem. Phys.* **108**, 9339 (1998).
15. J. B. Griffin and P. B. Armentrout, *J. Chem. Phys.* **108**, 8062 (1998).
16. J. B. Griffin and P. B. Armentrout, *J. Chem. Phys.* **106**, 4448 (1997).
17. R. Liyanage, X.-G. Zhang, and P. B. Armentrout, *J. Chem. Phys.* **115**, 9747 (2001).
18. J. B. Benziger, in *Metal-Surface Reaction Energetics*, edited by E. Shustorovich (VCH, New York, 1991), pp. 53–107.

Role of Solvent: Reactions in Supercritical Fluids

David M. Bartels and Daniel M. Chipman
Notre Dame Radiation Laboratory, Notre Dame, IN 46556
e-mail: bartels.5@nd.edu; chipman.1@nd.edu

Program definition

For a number of years this project has pursued the use of radiolysis as a tool in the investigation of solvent effects in chemical reactions. A theoretical and computational component is currently being incorporated that will support the analysis and interpretation of experimental results. The project has now evolved toward the particular study of solvent effects on reaction rates in supercritical (sc-)fluids. Even more specifically, radical reactions in supercritical water are targeted because of interest to use sc-water as a coolant in future (GEN-IV) nuclear power plants. This has proven very fruitful from the basic science standpoint, as virtually any reaction we investigate exhibits behavior best characterized as “weird”.

An anthropomorphic way to think about near-critical phenomena, is that the fluid is trying to decide whether it is a liquid or a gas. The cohesive forces between molecules that tend to form a liquid are just being balanced by the thermal entropic forces that cause vaporization. The result, on a microscopic scale, is the highly dynamic formation and dissipation of clusters and larger aggregates. The fluid is extremely heterogeneous on the microscopic scale. A solute in a supercritical fluid can be classified as either attractive or repulsive, depending on the potential between the solute and solvent. If the solute-solvent potential is more attractive than the solvent-solvent potential, the solute will tend to form the nucleus of a cluster. When the solute-solvent potential is repulsive, one might expect the solute to remain in a void in the fluid as the solvent molecules cluster together. Extremely large partial molal volumes are known for hydrophobic molecules in near-critical water, indicating an effective phase separation. Such variations in local density around the solute will have implications for various spectroscopies and for reaction rates.

Our purpose in this work is to determine free radical reaction rates in supercritical fluids to develop an understanding of the important solvent effects. Among these will be the effect of local density enhancements (or depletions) on the solvation of reactants and transition states, potential of mean force in the relative diffusion (caging effects), and possible nonequilibrium energy and momentum transfer issues. Relatively few studies of free radical reactions have been carried out under supercritical conditions. We do not propose to extensively review the literature on this subject: an issue of Chemical Reviews [Chemical Reviews, 99, (1999)] contains several useful reviews of work up to 1999.

The ultimate goal of our study is the development of a predictive capability for free radical reaction rates, even in the complex microheterogeneous critical regime. No such capability now exists. The calculation of transition state geometries for free radical reactions by ab initio methods in the gas phase is still not completely reliable, though very good progress has been made. The calculation of condensed phase transition states is a much more difficult task because of the large number of configurations that must be considered, and the perturbation of the reaction energetics by the solvent.

The immediate goal of this work is to determine representative free radical reaction rates in sc-fluid and develop an understanding of the important variables to guide development and use of predictive tools. Electron beam radiolysis of water (and other fluids) is an excellent

experimental tool with which to address these questions. The primary free radicals generated by radiolysis of water, $(e^-)_{aq}$, OH, and H, are respectively ionic, dipolar, and hydrophobic in nature. Their recombination and scavenging reactions can be expected to highlight the effects of clustering (i.e. local density enhancements) and solvent microheterogeneity both in terms of relative diffusion and in terms of static or dynamic solvent effects on the reaction rates. We already have transient absorption data for several of these species that highlights interesting and unexpected reaction rate behavior. A major thrust of the next several years will be to push time-resolved EPR detection of H atoms in sc-water. The Chemically Induced Dynamic Electron Polarization (CIDEP) generated in H atom recombination reactions provides another unique probe of the cage dynamics and potential of mean force. How different will be the potential of mean force between H atoms and between $(e^-)_{aq}$ and H? How easily will H atoms penetrate into water clusters?

Recent Progress

Much of our progress in this year has been in writing-up and understanding experiments that were carried out in previous years. One very interesting study concerned the absorption edge of liquid water, up to supercritical temperatures. The edge shifts to the red by ca. 0.6 eV on going from room temperature to 400°C, at 250bar pressure. The room temperature spectrum is blue-shifted by ca. 0.8eV with respect to the gas phase, so we expected by decreasing the density at 400°C that we would shift another 0.2 eV toward the red. Instead, the edge shifts slightly toward the blue when we change density from 0.3g/cc down to 0.05g/cc ! This must be due to a line-narrowing effect, but we do not know its origin. Since we have only recorded the edge down to 190nm, it is clear we need to build a short-path cell for supercritical water studies to further investigate this effect.

Major progress was made in understanding free radical reactions in high temperature sub-critical water. We found that both for reaction $H + O_2 \rightarrow HO_2$ and reaction $2 OH \rightarrow H_2O_2$, the rates are nearly diffusion limited at room temperature, but above 200°C the rate constants become nearly independent of temperature. Comparison with the gas phase reactions show the rates in water are almost identical to the gas phase “high pressure limit”, where there is always a third body present. This represents a breakdown of the “caging effect” in water because diffusion is fast at elevated temperature. If water does not significantly perturb the OH radical potential, it means we can readily make theory-based predictions for reactions like $H + OH \rightarrow H_2O$, which have not yet been measured in solution.

In the process of measuring the OH recombination reaction, it was necessary to study and quantify the UV absorption spectrum. The main band in water at 230nm is not present in the gas phase, and its origin is controversial. By increasing the temperature to 350°C it becomes clear that the 230nm band has decreased in intensity by a factor of two, and a weak band at 310nm has appeared. This is where OH absorbs in the gas phase, and we interpret the absorption in water as “free” OH, while the 230nm band must be hydrogen bonded OH. It implies that by 350°C, over half of the OH radicals are NOT hydrogen bonded to water.

In ab initio studies, progress has been made that now allows for reliable computation of the two major contributions to the very large hydration energies of charged solutes. One large contribution is due to long range interactions with bulk solvent molecules, which can be satisfactorily described with dielectric continuum theory provided that volume polarization effects arising from quantum mechanical penetration of solute charge outside its cavity is properly taken into account. A new formulation has been implemented to allow accurate yet

facile computation of this contribution, and computer code for such calculations based on an isodensity cavity surface has been installed in widely distributed electronic structure program packages. The other main contribution is due to strong short-range hydrogen bonding interactions with first-shell water molecules. For cations this contribution has been demonstrated to correlate linearly with the electric field produced by the solute, in a manner that is analogous to the correlation previously demonstrated for anionic solutes while still maintaining the same basic cavity prescription.

Future Plans

Immediate plans are to continue the optical transient absorption measurements of OH radical and hydrated electron reaction rates. Calculations are in progress to characterize the nature of the OH absorption at 250nm in water, with a view toward understanding why this absorption seems to disappear in supercritical water. In the case of OH reactions, the transient absorption experiments will be complemented by measurements of product yields to infer reaction rates by competition. A most important target is the reaction $H_2 + OH$ in supercritical water. Mechanisms of prototypical radiolytic reactions in aqueous solution such as $H + OH \rightarrow H_2O$, $H_2 + OH \rightarrow H + H_2O$, $H_2 + O^- \rightarrow H + OH^-$, $OH + OH \rightarrow H_2O_2$ and $OH + OH^- \rightarrow O^- + H_2O$, as well as the OH/O⁻ equilibrium, will be characterized by ab initio methods as initial steps toward the ultimate goal of understanding their unusual temperature dependences.

A major new effort will involve direct EPR measurements of free radicals in supercritical water. The primary target of this experiment is the hydrogen atom. The hydrogen atom is the prototypical free radical, and its reactions in condensed phase are naturally a subject of great theoretical interest. Moreover, extensive isotope effect information can be generated by comparison of D atom and muonium atom reactions. H (and D) atoms are readily generated in acidic water by electron beam radiolysis. Time-resolved EPR is found to be a convenient and specific technique for H atom detection. The large hyperfine coupling of H or D atoms make their signals unambiguous. Virtually always, time-resolved H atom signals are found to be polarized by Chemically Induced Dynamic Electron Polarization (CIDEP) in the radical recombination reactions.

The most exciting aspect of EPR detection of H and D atoms in sc-water is the potential to measure CIDEP in the H+H and D+D recombination reactions. One can calculate an average polarization enhancement per diffusional encounter, from a stochastic Liouville equation description of the combined spin and spatial diffusion. The enhancements depend upon the time-integrated spin exchange between the radicals of a pair during a diffusive encounter, and the degree of singlet triplet mixing (proportional to the difference in Larmor frequencies of the two radicals). Because spin exchange is typically very short-ranged and singlet-triplet mixing is slow, the phenomenon is sensitive to re-encounters and the full diffusional dynamics. Polarization enhancements have been calculated for the simple case of spherical radicals freely diffusing in a continuum. H atoms in liquid water may come close to this idealization, but quantitative measurements on this system have never been successfully carried out even at room temperature. Diffusion is never fully free, and forces between the radicals will affect the size of the polarization enhancements. The size of polarization generated in these encounters can readily be estimated via the stochastic Liouville equation, assuming some relative diffusion governed by a potential of mean force. Will the mean force of the solvent in sc-water effectively keep H atoms apart or hold them together? How sensitive will the CIDEP be to solvent density? Will the H + H recombination remain in the diffusion limit or become "third-body" limited?

Publications, 2004-2006

- Marin T.W.; Takahashi K.; Bartels D.M. *J. Chem. Phys. accepted for publication*. Temperature and density dependence of the light and heavy water ultraviolet absorption edge.
- Chipman D.M. (2006). *J. Chem. Phys.* 124, 224111/1-10. New formulation and implementation for volume polarization in dielectric continuum theory.
- Chipman D.M.; Chen F. (2006). *J. Chem. Phys.* 124, 144507/1-5. Cation electric field is related to hydration energy.
- Shao Y.; Molnar L.F.; Jung Y.; Kussmann J.; Ochsenfeld C.; Brown S.T.; Gilbert A.T.B.; Slipchenko L.V.; Levchenko S. V.; O'Neill D. P.; DiStasio Jr. R.A.; Lochan R. C.; Wang T.; Beran G.J.O.; Besley N.A.; Herbert J.M.; Lin C.Y.; Van Voorhis T.; Chien S.H.; Sodt A.; Steele R. P.; Rassolov V.A.; Maslen P.E.; Korambath P.P.; Adamson R.D.; Austin B.; Baker J.; Byrd E.F.C.; Dachsel H.; Doerksen R.J.; Dreuw A.; Dunietz B.D.; Dutoi A.D.; Furlani T.R.; Gwaltney S.R.; Heyden A.; Hirata S.; Hsu C.-P.; Kedziora G.; Khalliulin R.Z.; Klunzinger P.; Lee A.M.; Lee M.S.; Liang W.Z.; Lotan I.; Nair N.; Peters B.; Proynov E.I.; Pieniazek P.A.; Rhee Y.M.; Ritchie J.; Rosta E.; Sherrill C.D.; Simmonett A.C.; Subotnik J.E.; Woodcock III H.E.; Zhang W.; Bell A.T.; Chakraborty A.K.; Chipman D.M.; Keil F.J.; Warshel A.; Hehre W.J.; Schaefer III H.F.; Kong J.; Krylov A.I.; Gil P.M.W.; Head-Gordon M. (2006). *Phys. Chem. Chem. Phys.* 8, 3172-3191. Advances in methods and algorithms in a modern quantum chemistry program package.
- Bartels D.M.; Takahashi K.; Cline J.A.; Marin T.W.; Jonah C.D. (2005). *J. Phys. Chem. A* 109, 1299-307. Pulse radiolysis of supercritical water III. Spectrum and thermodynamics of the hydrated electron.
- Chipman D.M.; Bentley J. (2005). *J. Phys. Chem. A* 109, 7418-28. Structures and energetics of hydrated oxygen anion clusters.
- Garrett B.C.; Dixon D.A.; Camaioni D.M.; Chipman D.M.; Johnson M.A.; Jonah C.D.; Kimmel G.A.; Miller J.H.; Rescigno T.N.; Rossky P.J.; Xantheas S.S.; Colson S.D.; Laufer A.H.; Ray D.; Barbara P.F.; Bartels D.M.; Becker K.H.; Bowen H.; Bradforth S.E.; Carmichael I.; Coe J.V.; Corrales L.R.; Cowin J.P.; Dupuis M.; Eisenthal K.B.; Franz J.A.; Gutowski M.S.; Jordan K.D.; Kay B.D.; LaVerne J.A.; Lymar S.V.; Madey T.E.; McCurdy C.W.; Meisel D.; Mukamel S.; Nilsson A.R.; Orlando T.M.; Petrik N.G.; Pimblott S.M.; Rustad J.R.; Schenter G.K.; Singer S.J.; Tokmakoff A.; Wang L.S.; Wittig C.; Zwiernik T.S. (2005). *Chem. Rev.* 105, 355-89. Role of water in electron-initiated processes and radical chemistry: Issues and scientific advances
- Marin T.W.; Jonah C.D.; Bartels D.M. (2005). *J. Phys. Chem. A*, 109, 1843-8. Reaction of hydrogen atoms with hydroxide ions in high-temperature and pressure water.
- Mezyk S.P.; Bartels D.M. (2005). *J. Phys. Chem. A* 109, 11823-7. Rate constant and activation energy measurement for the reaction of atomic hydrogen with thiocyanate and azide in aqueous solution.
- Lian R.; Crowell R.A.; Shkrob I.A.; Bartels D.M.; Oulianov D.A.; Gosztola D. (2004). *Chem. Phys. Lett.* 389, 379-84. Recombination of geminate (OH, e(aq)(-)) pairs in concentrated alkaline solutions: lack of evidence for hydroxyl radical deprotonation.
- Chipman D.M. (2004). *Theor. Chem. Acc.* 111, 61-65. Simulation of Volume Polarization for the Influence of Solvation on Chemical Shielding.
- Marin T.W.; Bartels D.M.; Jonah C.D. (2004). *Ind. Eng. Chem. Res.* 43, 1888-9. Evaluation of silica-coated tubing for the measurement of hydrogen peroxide in hot water.
- Mezyk S.P.; Cooper W.J.; Madden K.P.; Bartels D.M. (2004). *Environ. Sci. Technol.* 38, 3161-7. Free radical destruction of N-nitrosodimethylamine in water.
- Mezyk S.P.; Jones J.; Cooper W.J.; Tobien T.; Nickelsen M.G.; Adams J.W.; O'Shea K.E.; Bartels D.M.; Wishart J.F.; Tornatore P.M.; Newman K.S.; Gregoire K.; Weidman D.J. (2004). *Environ. Sci. Tech.* 38, 3994-4001. Radiation chemistry of methyl tert-butyl ether in aqueous solution.

Clusters: Unraveling Fundamental Oxygen Transfer Reaction Mechanisms Effected by Heterogeneous Catalysts

A. W. Castleman, Jr.
Pennsylvania State University
Departments of Chemistry and Physics
104 Chemistry Building
University Park, PA 16802
awc@psu.edu

Program Scope:

Catalysts are of significant importance to maintaining the economic competitiveness of the nation. They play a crucial role in reducing the energy requirements and increasing the activity and selectivity of industrially and environmentally relevant reactions as well as processes involved in energy production and storage. Developing an understanding of the basic principles that govern catalytic reactions is necessary to allow the directed design of catalysts with improved activity and selectivity. Historically, research in heterogeneous catalysis has involved the empirical observation of catalytic processes and has only in recent years evolved to include sensitive surface science techniques. Our program, utilizing gas phase metal oxide cluster ions, is designed to elucidate specific aspects of the basic principles needed to understand the nature of catalytic active sites responsible for oxygen transfer reactions involving transition metal oxide and noble metal catalysts. These studies serve to shed light on the molecular level mechanisms involved in these reactions.

Recently, there has been a significant increase in the use of gas phase clusters to model industrially and environmentally significant reactions occurring at the surface of heterogeneous metal oxide catalysts. Gas phase cluster studies provide a valuable complementary method for probing the catalytic active sites responsible for selected classes of reactions. Our continuing program is designed to investigate the role of ionic charge state, oxidation state, structure, stoichiometry, and elemental composition on the efficiency of oxygen transfer reactions. These studies of gas phase clusters allow the investigation of complicated catalytic reactions at the nanoscale and avoid common problems associated with surface science techniques, such as effects which arise due to various methods of catalyst preparation. Through these studies, information useful to understanding the molecular level mechanisms of catalytic reactions is being obtained. Such understanding may be used to guide the production of customized catalysts with improved selectivity and turn over rates.

Recent Progress:

Throughout the recent grant period, we have continued our efforts aimed at unraveling the molecular level details of oxygen transfer reactions. After completing a detailed analysis of the kinetics of the oxidation of ethylene by vanadium oxide clusters, we commenced a new comprehensive study of CO reactions in the presence of transition metal and noble metal oxide clusters. These studies were directed towards unraveling the fundamental steps of carbon monoxide oxidation, a reaction of substantial importance to environmental pollution abatement. Our recent efforts have revealed some new and significant findings regarding the oxidation of carbon monoxide in the presence of gold oxide and iron oxide clusters. Furthermore, we have obtained additional insight into the mechanistic details of these reactions through collaboration with the theoretical groups of Professor Vlasta Bonačić-Koutecký at the Humboldt University in Berlin and Professor Shiv N. Khanna at the Virginia Commonwealth University in Richmond, Virginia.

Our recent experiments, in combination with theoretical calculations, have revealed relationships between the structures of gold dimer and trimer oxide anion clusters and how they react with CO. Our unique experiments explored the reactivity of gold oxide anion clusters containing oxygen in both the atomic and molecular form. In combination with theoretical calculations we were able to discern that, in contrast to current thought, the presence of a peripheral oxygen atom on the gold anion cluster is necessary but not always sufficient to effect the oxidation of CO. We determined that it is a synergistic effect between the presence of a peripheral oxygen atom and

surmountable reaction barriers that dictates the favorability of the oxidation reaction. To our knowledge, this fact has not previously been revealed and is of fundamental value in tailoring the design of more efficient and selective catalysts.

The systematic study of gold dimer and trimer oxide anions also revealed that when an electron acceptor group such as an O atom or an O₂ subunit is present on the cluster, CO cannot be oxidized by the transfer of a bridging oxygen atom. This is due to the fact that the electron acceptor group increases the charge difference between the gold atom and the bridging O atom, resulting in a stronger, more ionic bond. This stronger binding of the bridging O atom to Au prevents it from reacting with CO. In addition, findings from our recent work demonstrate that molecular O₂ groups bound to gold dimer and trimer anion clusters are not sufficiently activated to oxidize CO. Theoretical calculations predict that only under conditions where cooperative effects exist due to the presence of multiple CO molecules can oxidation by an O₂ subunit occur.

The influence of size on the reactivity of gold oxide anion clusters with CO was also made apparent by our recent findings. With the addition of a single gold atom, it was observed that the dominant reaction channel changed from CO oxidation to CO association or replacement of an O₂ group by CO. Studies of larger gold oxide anions, Au_nO_m⁻ (n ≥ 4) also revealed that the number of O atoms present on the cluster directly determines how many CO molecules can be adsorbed. Gold oxide anions containing an odd number of oxygen atoms were observed to bind multiple CO atoms. In contrast, clusters with an even number of oxygen atoms were not observed to have multiple CO molecules attached. These results clearly demonstrate that, for the interaction of Au_xO_y⁻ clusters with CO, each atom counts towards determining the reactivity.

Our joint experimental and theoretical findings, furthermore, enabled us to propose a general reaction mechanism describing CO oxidation in the presence of active gold oxide anion clusters. This mechanism involves the initial formation of a complex with a weakly bound CO molecule. This complex formation is followed by charge transfer from the cluster to CO, resulting in a species containing a CO₂ subunit. This complex fragments by either rotation of the CO group or by bond rearrangement involving the simultaneous cleavage of the Au-O bond and formation of a Au-C bond. Final emanation of the CO₂ product is accompanied by charge transfer back to Au. The mechanistic insight gained from our studies shows, in detail, how gold cluster anions transfer oxygen to CO, thereby neutralizing this harmful atmospheric pollutant.

Studies have been undertaken to determine the influence of ionic charge state on oxidation reaction mechanisms. Recent experiments on the reactivity of gold oxide cations with CO using a guided ion beam mass spectrometer have revealed dominant products of the form Au_nO_m(CO)_x⁺. These species have been identified to be the products of either a CO association reaction, replacement of atomic or molecular oxygen with carbon monoxide, or the oxidation of CO without subsequent dissociation of the CO₂ product from the cluster. For the anions, we did not observe products containing both CO and oxygen for the monomer or dimer species. However, with those anionic clusters containing three or more gold atoms, species of the form Au_nO_m(CO)_x⁻ began to emerge. Through density functional calculations performed for the dimer and trimer anion clusters, a relationship between the energy of the lowest unoccupied molecular orbital (LUMO) of the gold oxide anion species and the binding energy of CO to the cluster was revealed. Such a relationship may also be relevant for CO adsorption on gold oxide cation clusters and calculations are currently underway to address this possibility. In addition to reactions producing Au_nO_m(CO)_x⁺ species, cluster cations containing four gold atoms also revealed an oxygen atom transfer pathway. In each of these cases, however, the CO oxidation product was a weak reaction channel dominated by the more intense Au_nO_m(CO)_x⁺ products. Several gold oxide cation species also exhibited loss of a gold atom upon reaction with CO. This indicates that, for certain species, the CO association channel may be exothermic enough to induce fragmentation of the gold oxide cation cluster. Through discussions with our theoretical collaborators in Berlin we are currently working to unravel the reaction mechanisms responsible for the various products observed in our recent experiments. Insight into the energetics of these reaction pathways and the strength of CO binding to Au_nO_m⁺ clusters will provide information relevant to the conditions necessary to effect CO oxidation at cationic gold sites in heterogeneous catalysts. This recent work, in combination with our previous results for gold oxide anions, reveals how ionic charge state influences the selectivity of different reaction channels for gold oxide clusters.

Stimulated by recent theoretical findings regarding the catalytic activity of iron oxide clusters for CO oxidation, we have also undertaken a systematic study of the reactivity of Fe_xO_y^{+/-} clusters with CO. In

comparison with gold, iron is a much more affordable and readily available material. Iron oxides, therefore, are a much more economical catalyst for effecting this environmentally important reaction. Mass selected experiments using a guided ion beam mass spectrometer reveal that CO oxidation is the dominant reaction pathway for most iron oxide anion clusters. Small iron oxide anion clusters containing one or two iron atoms exhibit loss of atomic and molecular oxygen with no CO association products. Beginning at the iron trimer series, small intensities of $\text{Fe}_x\text{O}_y(\text{CO})^-$ are observed. In addition, for certain Fe_xO_y^- clusters the reaction with CO produced products with one less iron atom, indicating that fragmentation of the parent cluster was taking place. In contrast to the anion clusters, only four of the cationic species were observed to oxidize CO. For most of the cationic iron oxide clusters a CO attachment product was observed having a stoichiometry of $\text{Fe}_x\text{O}_{y-1}(\text{CO})^+$. To provide structural information, collision induced dissociation (CID) experiments were performed on the iron oxide clusters using an inert collision gas (Xe). The fragmentation products reveal different cluster building blocks depending on charge state. We are currently engaged in discussions with our theoretical collaborators in Richmond to investigate the role of charge state and the strength of oxygen binding on the reactivity of these iron oxide clusters with CO. These studies, therefore, in addition to providing experimental confirmation of an important theoretical prediction, provide detailed insight into the influence of stoichiometry and ionic charge state on the catalytic activity of iron oxides.

Encouraged by our results for $\text{Fe}_x\text{O}_y^{+/-}$ clusters, we have also started preliminary studies of the reactivity of additional late 3d transition metal oxide clusters with CO. Moving across the periodic table we are systematically investigating cobalt oxide, nickel oxide, and copper oxide clusters. It will be valuable to study the effect of additional d electrons and changes in electron affinity on the reactivity of late 3d transition metals with CO. Similar to our previous studies, we are probing the influence of stoichiometry, ionic charge and oxidation state, and size using the guided ion beam mass spectrometer. CID studies provide insight into the elementary structural building blocks of these species and theoretical input will aid in providing a thorough description of the behavior of late 3d transition metals oxide clusters in the presence of CO.

To build upon our recent work on single metal oxide clusters, we recently began studies using a newly designed dual rod laser vaporization source coupled to our guided ion beam instrument. This source enables us to study the reactivity of bimetallic metal oxide clusters. Preliminary experiments employing this new capability have been directed towards investigating the reactivity of small gold/silver oxide anions and cations with CO. Our results indicate different reaction channels depending on charge state and degree of oxidation of the AuAg subunit. The studies also enable a determination of the role of local charge density in the effectiveness of the oxidation reaction. Through comparison of this recent data with results for pure gold oxide and silver oxide clusters we are testing the effect of the presence of two metals with different electronegativity on the reactivity with CO. These results will provide insight into how centers of electron deficiency and enhancement impact the reactivity of noble metal oxides.

Future Studies:

To further understand the molecular level mechanisms involved in heterogeneous catalysis, we plan to investigate the effects of elements used as catalyst support materials and as dopants on the oxidation of CO and simple hydrocarbons such as butane and butene by gas phase clusters. Subsequently, related studies of the chemistry of nitrogen oxides and SO_2 will be undertaken. These efforts will allow us to continue exploring the effect of electronegativity and charge density on the reactions of binary metal oxide clusters. With regard to catalyst support materials, we plan to study the reactivity of $\text{Au}_n\text{M}_x\text{O}_y^{+/-}$ ($\text{M} = \text{Mg}, \text{Si}, \text{Al}$) clusters. Magnesium oxide, silicon oxide, and aluminum oxide are common catalyst support materials that are used in a variety of industrial chemical processes. For these experiments, we will employ the guided ion beam mass spectrometer to study the reactivity of mass selected cluster ion species as well as structural aspects through collision induced dissociation. These studies will commence with investigation of the reactivity of $\text{M}_x\text{O}_y^{+/-}$ ($\text{M} = \text{Mg}, \text{Si}, \text{Al}$) clusters to ascertain the inherent reactivity of clusters made up of support materials in the absence of catalyst materials. A detailed study of the reactions of bimetallic oxide cluster ions comprised of gold and other elements with varying stoichiometry and electronegativity will then be conducted to discern the effect of the interaction between the catalyst and support material. The influence of dopants such as K and Na which are commonly incorporated into

heterogeneous catalysts will also be investigated through studies of bimetallic metal oxide clusters containing these elements.

We also plan to continue our collaboration with the theoretical groups of Professor Vlasta Bonačić-Koutecký and Professor Shiv N. Khanna in order to gain further insight into the energetics and reaction mechanisms that are involved in the oxidation reactions. The information gained from the combined experimental and theoretical studies will provide valuable insight into the fundamental molecular level mechanisms occurring during catalytic oxygen transfer reactions and the physical and chemical factors that influence these processes.

Publications Resulting from this Grant:

538. "Cluster Dynamics: Influences of Solvation and Aggregation," Q. Zhong and A. W. Castleman, Jr., *Quantum Phenomena in Clusters and Nanostructures* (S. N. Khanna and A. W. Castleman, Jr., Eds.) Springer: Berlin, Heidelberg, New York, Hong Kong, London, Milan, Paris, Tokyo, (2003).
544. "Comparison of Methyl and Hydroxyl Protons Generated in a Coulomb Explosion Event: Application of a Time-of-Flight Gating Technique to Methanol Clusters," E. S. Wisniewski and A. W. Castleman, Jr., special issue of *Int. J. Mass Spectrom.* devoted to Gaseous Ion Thermochemistry and Solvation **227**, 577 (2003).
551. " $V_2O_5^+$ Reactions with C_2H_4 and C_2H_6 : Theoretical Considerations of Experimental Findings," D. R. Justes, A. W. Castleman, Jr., R. Mitrić, and V. Bonačić-Koutecký, *Eur. Phys. J. D* **24**, 331 (2003).
559. "Photodissociation of Sulfur Dioxide: The \tilde{E} State Revisited," K. L. Knappenberger and A. W. Castleman, Jr., *J. Phys. Chem. A*, **108**, 9-14 (2004).
560. "Probing the Dynamics of Ionization Processes in Clusters", A. W. Castleman, Jr. and T. E. Dermota, *Latest Advances in Atomic Cluster Collisions* (A. Solov'yov and J.-P. Connerade, Eds.) World Scientific: Singapore, New Jersey, London, 253-269 (2004).
561. "Ultrafast dynamics in cluster systems", T. E. Dermota, Q. Zhong, and A. W. Castleman, Jr., *Chemical Reviews*, **104**, 1861-1886 (2004)
563. "Reactivity of Atomic Gold Anions Toward Oxygen and the Oxidation of CO: Experiment and Theory," M. L. Kimble, A. W. Castleman, Jr., R. Mitrić, C. Bürgel, and V. Bonačić-Koutecký, *J. Am. Chem. Soc.*, **126**, 2526-2535 (2004).
564. "Probing the Oxidation of Carbon Monoxide Utilizing Au_n^- ," M. L. Kimble and A. W. Castleman, Jr., *Proceedings of Gold 2003: New Industrial Applications for Gold Conference* Vancouver, Canada, September 28 – October 1, 2003.
565. "Gas phase Studies of Au_n^+ for the Oxidation of Carbon Monoxide," M. L. Kimble and A. W. Castleman, Jr., Special Issue of the *Int. J. Mass Spectrom.*, in Honor of Professor Tilmann D. Märk. **233**, 99-101 (2004).
568. "Reactions of Vanadium and Niobium Oxides with Methanol," D. R. Justes, N. A. Moore, and A.W. Castleman, Jr., *J. Phys. Chem. B*, **108**, 3855-3862 (2004).
570. "Elucidating Mechanistic Details of Catalytic Reactions Utilizing Gas Phase Clusters," M. L. Kimble, D. R. Justes, N. A. Moore, and A. W. Castleman, Jr., *Clusters and Nano-Assemblies: Physical and Biological Systems* (P. Jena, S. N. Khanna, B. K. Rao, Eds.) World Scientific: Singapore, New Jersey, London, 127-134 (2005).
572. "The Influence of Cluster Formation on the Photodissociation of Sulfur Dioxide: Excitation to the E State", K. L. Knappenberger, Jr., and A. W. Castleman, Jr., *J. Chem. Phys.*, **121**, 3540-3549 (2004).
573. "A Kinetic Analysis of the Reaction between $(V_2O_5)_{n=1,2}^+$ and Ethylene," N. A. Moore, R. Mitrić, D. R. Justes, V. Bonačić-Koutecký, and A. W. Castleman, Jr., *J. Phys. Chem. B*, **110**, 3015 (2006)
586. "Clusters: A bridge between disciplines," A. W. Castleman, Jr., Puru Jena, *Proc. Nat. Acad. Sci.* **103**, 10552 (2006)
588. "Interactions of CO with $Au_nO_m^-$ ($n \geq 4$)", M. L. Kimble, A. W. Castleman, Jr., C. Bürgel, R. Mitrić, and V. Bonačić-Koutecký, *Int. J. Mass. Spec.* **254**, 163 (2006).
592. "Clusters: A bridge across the disciplines of physics and chemistry," Puru Jena, A. W. Castleman, Jr., *Proc. Nat. Acad. Sci.* **103**, 10560 (2006)
593. "Clusters: A bridge across the disciplines of environment, materials science, and biology," A. W. Castleman, Jr., Puru Jena, *Proc. Nat. Acad. Sci.* **103**, 10554 (2006)

An Exploration of Catalytic Chemistry on Au/Ni(111)

Professor S. T. Ceyer
Department of Chemistry
Massachusetts Institute of Technology
Cambridge, MA 02139
stceyer@mit.edu

Project Scope

This project explores the breadth of catalytic chemistry that can be effected on a Au/Ni(111) surface alloy. A Au/Ni(111) surface alloy is a Ni(111) surface on which 10-30% of the Ni atoms are replaced at random positions by Au atoms. That is, the vapor deposition of a small amount of Au onto Ni single crystals does not result in an epitaxial Au overlayer or the condensation of the Au into droplets. Instead, it results in a strongly bound surface alloy. Gold atoms at coverages less than 0.3 ML replace Ni atoms on a Ni(111) surface, even though Au is immiscible in bulk Ni. The two dimensional structure of the clean Ni surface is preserved. This alloy is found to stabilize an adsorbed peroxo-like O₂ species that is shown to be the critical reactant in the low temperature catalytic oxidation of CO and that is suspected to be the critical reactant in other oxidation reactions. These investigations may reveal a new, practically important catalyst for catalytic converters and for the production of some widely used chemicals.

Recent Progress

We discovered that the Au/Ni(111) surface alloy, with Au coverages up to 0.3 ML, efficiently catalyzes the oxidation of CO at 70 K.

Saturation coverage of molecular O₂ is adsorbed on the 0.24 ML Au/Ni surface alloy at 77 K. The dominant feature, at 865 cm⁻¹, of the vibrational spectrum of the oxygen layer, as measured by high resolution electron energy loss spectroscopy, is assigned to the vibration of the O=O bond of molecular oxygen adsorbed on the alloy with its bond axis largely parallel to the surface. Molecular oxygen so adsorbed is characterized as a peroxo (O₂⁻²) or superoxo (O₂⁻¹) species. Shoulders at about 950 cm⁻¹ and 790 cm⁻¹ indicate the presence of both peroxo or superoxo species at multiple sites.

The feature at 865 cm⁻¹ and its shoulders disappear after heating this layer to 150 K while two features at 580 and 435 cm⁻¹, attributed to atomically adsorbed O, grow in. The feature at 580 cm⁻¹ is the same frequency as observed for O atoms bound to Ni(111) while a lower frequency feature, at 435 cm⁻¹, is attributed to O atoms bound to Ni atoms that are adjacent to the Au atoms. Note that there is no evidence for atomically bound O

at 77 K. Therefore, O₂ adsorption on the Au/Ni(111) surface alloy at 77 K is solely molecular. In contrast, O₂ dissociatively adsorbs on Ni(111) at 8 K, while it adsorbs neither molecularly nor dissociatively on Au(111) at or above 100 K.

When a beam of thermal energy CO is directed at the O₂ covered Au/Ni(111) surface alloy held at 70 K, gas phase CO₂ is immediately produced. A control experiment demonstrates that no CO₂ is produced when the CO beam impinges on the crystal mount. Clearly, CO reacts with molecularly adsorbed O₂ on this alloy at 70 K.

After exposure of the O₂-covered surface alloy at 70 K to CO, two C=O stretch vibrational modes are observed at 2170 and 2110 cm⁻¹, along with the Au/Ni-CO stretch mode at 435 cm⁻¹. The O=O mode at 865 cm⁻¹ is much reduced in intensity, while the shoulder at 790 cm⁻¹ has maintained its intensity. The decrease in intensity of the 865 cm⁻¹ feature is interpreted to mean that some of the molecularly adsorbed O₂ has reacted with CO to form gas phase CO₂. The product remaining from this reaction is an O atom adsorbed to Au, as evidenced by the appearance of a new feature at 660 cm⁻¹. The molecularly adsorbed O₂ that gives rise to the feature at 790 cm⁻¹ does not react with CO.

This alloy surface covered with CO and some molecularly adsorbed O₂ is heated at 2 K/s while the partial pressures at masses 44 and 28 are monitored. Rapid production and desorption of CO₂ is clearly observed between 105-120 K, along with CO desorption. Production of CO₂ in this temperature range occurs at the same temperature at which O₂ dissociates. This observation suggests that CO₂ formation occurs between a CO and a "hot" O atom that has not yet equilibrated with the surface after bond dissociation. From 120 K to about 250 K, CO₂ is slowly produced by reaction of the adsorbed O atoms represented by the mode at 660 cm⁻¹ and by the adsorbed O atoms that did not react immediately as a hot O atom upon O₂ dissociation between 105-120 K. No O₂ is observed to desorb.

These results demonstrate that Au/Ni(111) catalyzes the oxidation of CO at low temperature. Clearly, substitution of a small number of Ni atoms on the Ni(111) surface by Au atoms has dramatically changed the Ni chemistry. The oxidation of CO on Ni has never been observed under UHV laboratory conditions, presumably because both the oxygen atom and CO are too strongly bound, and hence the barrier to their reaction is too large. Introduction of gold into the Ni lattice serves to weaken the bonds between oxygen and CO so as to allow the reaction to proceed. These results also imply that nanosize Au clusters are not a necessary requirement for low temperature CO oxidation in general. Rather, interaction of the Au atoms around the perimeter of the Au nanocluster with the transition metal of the oxide support likely provides the active sites that stabilize the adsorption of molecular O₂ that is necessary for the oxidation of CO.

Future Plans

A major thrust of this project is to explore the range of reactivity of the O₂ species molecularly adsorbed on the Au/Ni(111) surface alloy. The hypothesis is that our newly observed molecular O₂ adsorbate is the crucial reactant in two oxidation reactions to be studied: the direct synthesis of H₂O₂ from H₂ and O₂ and the epoxidation of propylene to form propylene oxide. In addition, it is planned to investigate whether the Au/Ni surface alloy is also active for the reduction of NO by CO. It is possible that a molecularly adsorbed NO species with a bond order approaching one is the active species in the NO reduction reaction at low temperature on the Au/Ni(111) surface alloy.

Publication

Catalyzed CO Oxidation at 70 K on an Extended Au/Ni Surface Alloy

D. L. Lahr and S. T. Ceyer

J. Am. Chem. Soc. **128**, 1800 (2006)

Ph.D. Thesis

Molecular Oxygen Adsorbates at a Au/Ni(111) Surface Alloy and Their Role in Catalytic CO Oxidation at 70 – 250 K

D. L. Lahr - June, 2006 – Massachusetts Institute of Technology

Theory of Dynamics in Complex Systems

David Chandler

Chemical Sciences Division
Lawrence Berkeley National Laboratory
And
Department of Chemistry
University of California, Berkeley
Berkeley, California 94720

My group's DOE sponsored research is devoted to developing and applying theoretical treatments of complex systems, especially in the near future, for understanding fuel-generating processes in liquids, solid and their interfaces, and for understanding non-equilibrium methods of assembling advanced materials.

Several studies of super-cooled liquids and glasses have recently been completed. To treat the phenomena exhibited by such materials, my coworkers and I have considered models based upon a coarse grained picture of space and time, for which Refs. [1] and [2] are illustrative. We have shown that these models can be used to interpret thermal properties, such as the precipitous growth of relaxation times as temperature is lowered towards a glass transition, and we have uncovered an unsuspected crossover, where the relaxation of a glass former evolves from hierarchical dynamics at low temperatures to diffusive dynamics yet lower temperatures. We have shown how this crossover is manifested experimentally [3]. This particular manifestation focuses on so-called "decoupling," where viscosity growth, for example, is not proportional to a diffusion constant inverse. We have also succeeded at explaining decoupling and demonstrated its connection to distributions of exchange and persistence processes in glass forming materials [4].

Decoupling is a fluctuation effect, and when such effects are present, one expects the presence of growing length scales as with a phase transition, and also non-linear response. In our work, we have demonstrated that growing length scales are found in $d+1$ dimensions, where d is the physical dimension, and 1 refers to time [5, 6]. Dynamical arrest of glass formers is an order-disorder phenomenon in space-time, namely an entropy crisis in trajectory space. Others before us have ventured the view that the dynamical arrest of glass formers is related to an entropy crisis. This view has in the past suffered from inconsistencies. It had before been suggested that this collective phenomenon would occur in state space. By showing it occurs in trajectory space, we have avoided the inconsistencies of prior treatments.

We have also recently completed our nascent studies of virus capsid assemblies [7]. Nature's ability to engineer the fabrication of these nano-scale objects is truly remarkable. We have created a class of mesoscopic models obeying Newtonian dynamics that can exhibit assembly, used transition path sampling to examine the assembly, and mapped out ranges of conditions over which kinetically trapped glassy

configurations are avoided and self-assembly occurs. The capsid formation is a phase transition in space-time. Unlike nucleation of an equilibrium phase, a process we have also recently studied with transition path sampling [8], nucleation in capsid assembly is a clustering of trajectories in trajectory space. Future work on this topic will explore this class of order-disorder phenomena, as the understanding we hope to reach should provide guidance to experimentalists carrying nano-structure assembly.

Other projects ongoing in our group and supported by DOE involve studies of general course graining methods. With a large simulation study facilitated by NERSC super computers to study molecular dynamics of systems in excess of 100,000 atoms, we have demonstrated that a greatly simplified field of binary numbers provides a sufficient description of solvent when the dynamics of that solvent, such as its evaporation, drives the formation long-lived metastable structures. We have also begun developing models that will enable our planned work studying electrolysis of water at electrode surfaces.

References:

1. Pan, A.C, J.P. Garrahan and D. Chandler. " Heterogeneity and growing length scales in the dynamics of kinetically constrained lattice gases in two dimensions," *Phys. Rev. E.* **72**, 041106 (2005).
2. Chandler, D., J.P. Garrahan, R.L. Jack, L. Maibaum and A.C. Pan, "Length scale dependence of dynamic four-point susceptibilities in glass formers," *cond-mat/0605084*, accepted by *Phys. Rev. E.*, (2006).
3. Pan, A.C., J.P. Garrahan and D. Chandler, "Decoupling of self-diffusion and structural relaxation during a fragile-to-strong cross-over in a kinetically constrained lattice gas" *ChemPhysChem* **6** 1783-1785 (2005).
4. Jung, Y.J., J.P. Garrahan and D. Chandler, "Dynamical exchanges in facilitated models of super cooled liquids", *J Chem. Phys.* **123**, 084509 (2005).
5. Merolle, M., J.P. Garrahan and D. Chandler, "Space-time thermodynamics of the glass transition", *PNAS* **102**, 10837-10840, (2005).
6. Jack, R.L, J.P. Garrahan and D. Chandler, "Spacetime thermodynamics and subsystem observables in a kinetically constrained model of glassy systems," *cond-mat/0604068*, submitted to *J. Chem. Phys.* (2006).
7. Hagan, M.F. and D. Chandler, " Dynamic pathways for viral capsid assembly," *Biophys. J.* **91**, 42-54 (2006).
8. Pan, A.C, T.J. Rappl, D. Chandler, and N.P. Balsara, "Neutron scattering and Monte Carlo determination of the variation of the critical nucleus size with quench depth," *J. Phys. Chem. B* **110**, 3692-3696 (2006).

Center for Radiation Chemistry Research: Excited States of Benzoquinone Radical Anion, New Ultrafast Single-Shot Detection at LEAF, and Non-Exponential Charge Capture.

Principle Investigators: Andrew R. Cook, John R. Miller

Chemistry Department, Brookhaven National Laboratory
Bldg. 555, Upton NY 11973
acook@bnl.gov

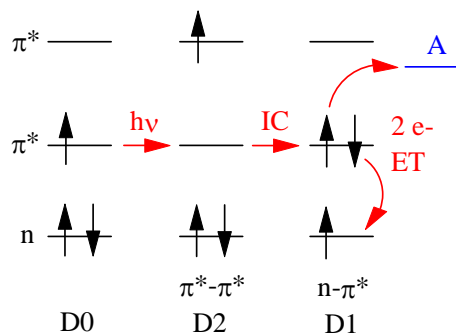
Program Scope:

This program examines charged and radical species in solution and develops tools to create and probe such species. Principal among these tools is the Laser Electron Accelerator Facility (LEAF) at Brookhaven that produces 7 ps electron pulses and associated detection systems. Pulse radiolysis is often the most convenient and sometimes the only method to rapidly produce and study isolated radical species. This poster will present recent results in understanding some novel excited states in quinone radical anions, an exciting new detection technique that will open the door to new avenues of research at BNL, and a first application of that new technique. Additional efforts in our lab are separately described in summaries by Sergei Lyamar, Jim Wishart, and John Miller.

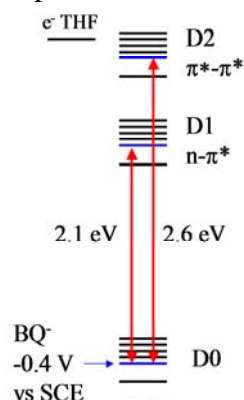
Recent Progress:

1. Excited States of Benzoquinone Radical Anion

One facet of this program focuses on identifying of radical anions and cations whose excited states could be useful for driving electron transfer reactions. The lowest excited state of *p*-benzoquinone radical anion ($BQ^{\bullet-}$) was of particular interest due to its large excited state energy and an exceptionally long lifetime of 60 ns. However, previous bimolecular experiments showed no evidence for electron transfer where reactions with other solutes were energetically favorable. While this may simply be due to rapid back transfer of electrons in the encounter complex, the other fascinating possibility is that $BQ^{\bullet-}$ is somehow electron-transfer inert, unable to participate in rapid electron-transfer reactions. A source for such possible inhibitions are the 2-electron processes that occur in $BQ^{\bullet-}$ shown in the figure to the right. Photoexcitation of the ground D_0 state at 460 nm of the allowed π^* - π^* transition forms the second excited doublet state, D_2 , which rapidly relaxes to the optically forbidden n - π^* D_1 state through an orbital change of 2 electrons. Electron transfer either out of or into the D_1 state will also require a 2-electron change. If electron transfer to/from D_1 is inhibited, then it is likely that electron capture directly into the D_1 state would be similarly inhibited, since it would require the same 2-electron change.



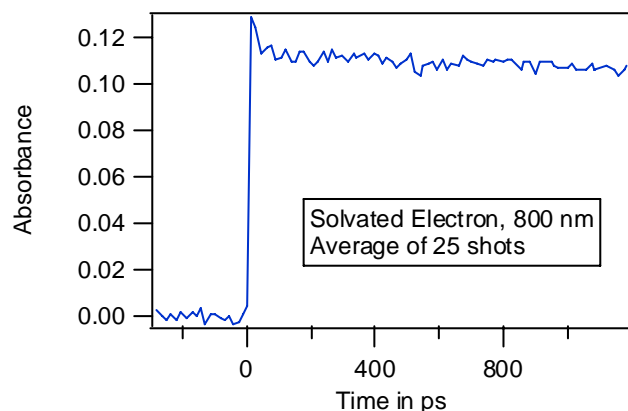
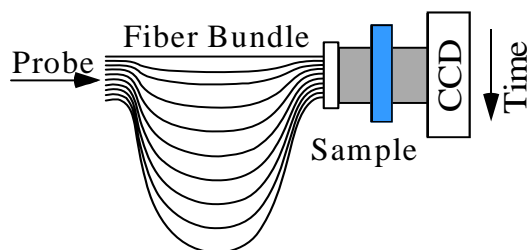
It was to test this second hypothesis that current experiments were focused. Electron capture in solvents like tetrahydrofuran and isooctane rapidly and preferentially forms excited states of $BQ^{\bullet-}$, which is expected since the energy of the solvated electron is estimated to be ~ 260 mV higher than the D2 state where no special 2-electron changes are needed. The situation changes however as alkyl-groups are added to BQ making the reduction potential more negative, as can be seen in the scheme to the left. The blue lines are the energies of the $BQ^{\bullet-}$ states, while the black lines are those of the substituted quinones assuming the excited state energies remain unchanged. Electron capture rates in THF have been measured and compared with literature rates. It is clear from this comparison that electron capture into the upper, D2, state is the best fit to the data. In fact, even for a quinone such as duroquinone where capture into the D2 state is estimated to be uphill by 80 mV, the D2 state is preferred over the energetically favorable D1 state. This large inhibition for electron capture into the lowest excited state is due to the 2-electron changes required, and is most likely what was responsible for the lack of observed bimolecular electron transfer in earlier experiments.



2. New Ultrafast Single-shot Detection at LEAF

While pulse radiolysis brings special benefits to investigation of electron transfer, its application to intramolecular electron transfer is usually limited to times longer than 0.1 ns. This limitation occurs because valuable donor-spacer-acceptor molecules cannot be subjected to the thousands of pulses needed to collect transients with the pulse-probe system. To bring these experiments to such molecules and also to examine viscous or solid samples such as ionic liquids that cannot be flowed, an ultrafast single-shot transient absorption detection system has been developed. UFSS methods also eliminate certain types of noise, greatly reduce data-collection times compared to classical delay line sampling techniques, and minimize waste.

For work in our laboratory, we have constructed an UFSS experiment using optical fiber bundles shown schematically to the right. This apparatus uses a prototype bundle of 100 fibers of different length, with an average of 15 ps of delay fiber-to-fiber providing a data over a time window of 1.5 ns in a single laser shot. A 100 fs laser probe pulse is directed into the end of the bundle, an imaged



successively in the sample, where it is collinearly overlapped with either (or both) an electron pulse or laser excitation pulse, and onto a signal CCD camera. Each image collected thus contains 100 different spots, each of which has information at a different time relative to the electron pulse. The measured risetime of the system is 1.6 ps at 800 nm, which was shown to be improvable to 0.5 ps with

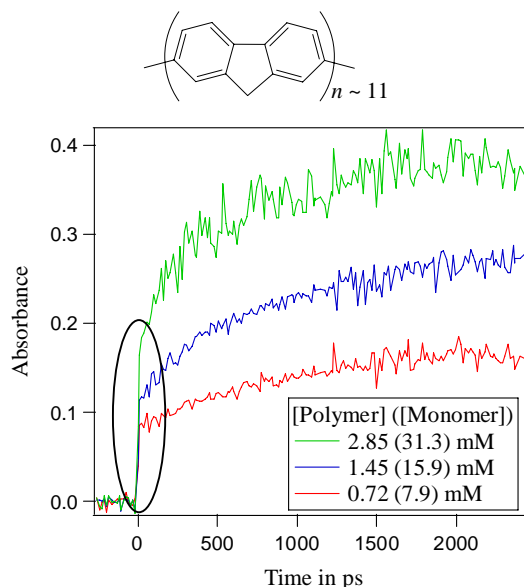
fiber chirp precompensation. Sample data collected in a pulse radiolysis experiment with a 2 mm cell of an aqueous solution containing 20% methanol and 0.1 M NaOH is shown above. The rise of the solvated electron absorption is clearly seen, with a rise time limited by the 10 ps electron pulse. This data was collected with an average of 25 electron pulses. Similar data collected with standard variably delayed pump-probe spectroscopy would have required $10^3 - 10^4$ shots! Probes with different colors have been accomplished with an OPA and simple refocusing. This new detection system has tremendous potential to enable new science in our lab, and the first application is described below.

3. Non-Exponential Charge Capture and Transport in Molecular Wires

It is well known that diffusion-controlled reactions of transiently produced species are characterized by transient terms in the Smoluchowski equation at early times. While typically unobserved for small molecules, such effects become important for long, relatively immobile molecules, providing a unique opportunity to probe such transient terms in the diffusion equation since their timescale can extend well into the nanosecond regime. These effects are known to depend on shape of the molecules, and are the subject of a recent theory by Traytak. Relevant not only to such basic physical chemistry questions, understanding and modeling these complicated kinetics and the corresponding yields of charges captured is important to work in our group involving charge motion in polymeric molecular wire materials. Good knowledge of charge capture kinetics is important to this project in order to separate them from charge transfer processes that may occur on comparable timescales in wires with additional electron or hole sinks attached to their ends.

Polyfluorene molecules with an average of 11 fluorene units or 92 Å in length were studied using the new fiber-UFSS experiment described above. The figure to the right shows charge capture kinetics for three different concentrations of polymer in THF at 580 nm where the anion of the molecule absorbs strongly. Such data with 10 ps time resolution would not have been collectable with standard sampling pulse-probe techniques due to limited quantities of sample. There are 2 main features of this data. First is the large rise that occurs within the time resolution of the experiment. About 20 % of this step is due to absorption of solvated electrons. While another part of the step was found to be due to rapidly formed excited states, a significant part was found to be due to wire anions formed on timescales faster than diffusion.

Given the very low concentration of molecules, capture of highly mobile presolvated or “dry” electrons cannot account for this component. Rather, it seems likely that due to the large volume of these molecules a sufficient number of electrons are formed within a reaction distance, R_{ij} , of the wires and react before diffusion occurs. The second main feature of this data is the slower rise, which can be modeled together with the solvated electron disappearance after accounting for the fast rise. This component contains the diffusional part of electron capture. As expected,



the kinetics are not adequately modeled by a single exponential capture rate, but were well described by two exponentials used as an approximation to the full Smoluchowski diffusion equation, where the reaction distance is an effective one described by the Traytak theory. While more experiments are needed to provide a quantitative test of this model, a few observations can be made. First, the data appears to show more capture at short times than is predicted by the model. Second, the Traytak model predicts a larger effective reaction distance than the data supports. The discrepancy might be explained by capture occurring at less than diffusion controlled rates, or possibly due errors in the literature value of the diffusion coefficient. Despite uncertainties with the model however, present efforts do provide a sufficiently good description of the data to support future efforts in measuring charge transport in similar wires with endcaps.

Future Plans:

- Confirmation of electron capture inhibition into the lowest excited state of $BQ^{\bullet*}$ will be sought with conductivity detected experiments using mixtures of ISO and TMS to smoothly vary V_0 around the π^* - π^* excited state of BQ^{\bullet} . Can the magnitude of the inhibition be determined?
- Significant noise reduction in fiber-UFSS experiments is expected to be possible and will be pursued. This will be combined with modified imaging optics to extend the achromatic range and minimize refocusing.
- Electron and hole capture will be studied in a variety of different length oligo-fluorenes and polythiophenes, and compared to the theory by Traytak to see if a consistent set of physically reasonable parameters can be determined. Can the model be used to accurately predict kinetics for arbitrary wire lengths?
- Apply the description of capture kinetics to systems with endcapped wires. Can we observe charge transfer rates to the ends of these molecules?

DOE Supported Publications (2003-2006):

Unimolecular dissociation of aryl halide radical anions in organic solvents studied by pulse radiolysis, N. Takeda, P. P. Poliakov, A. R. Cook, J. R. Miller, *Abstr. Pap. Am. Chem. Soc.*, **226**, U319-U319 (2003)

Faster Dissociation: Measured Rates and Computed Effects on Barriers in Aryl Halide Radical Anions, Takeda, N.; Poliakov, P. V.; Cook, A. R.; Miller, J. R. *J. Am. Chem. Soc.*, **2004**, *126*, 4301-4309.

The LEAF Picosecond Pulse Radiolysis Facility at Brookhaven National Laboratory, Wishart, J. F.; Cook, A. R.; Miller, J. R. *Rev. Sci. Inst.* **2004**, *75*, 4359-4366.

Chemical Kinetics and Dynamics at Interfaces

Solvation/Fluidity on the Nanoscale, and in the Environment

James P. Cowin, Fundamental Sciences Division
Pacific Northwest National Laboratory
P.O. Box 999, Mail Stop K8-88, Richland, Washington 99352
jp.cowin@pnl.gov

Program Scope

Interfaces have a unique chemistry, unlike that of any bulk phase. This is true even for liquid interfaces, where one might have (incorrectly) pre-supposed that a liquid's lack of rigidity might strongly suppress perturbations due to the interface. Ice interfaces also tend to have adherent liquid brine films in nature, and even pure ice has surface regions with sufficient disorder (for a monolayer or two) to resemble liquids. This program explores interfacial effects including changes in fluidity and transport, and solvation. The applicability of the knowledge gained extends reactions and transport across two-phase systems (like microemulsions), electrochemical systems, and in many situations where a fluid is present in molecular-scale amounts... such as in cell membranes, enzymes and ion channels, or at environmental interfaces at normal humidities, such as the surfaces of atmospheric or soil particles. We explore these systems with several unusual methods. These include re-creating liquid-liquid interfaces using molecular beam epitaxy, and use of a molecular soft landing ion source. We also explore fundamental properties of bulk ice, that relate to such issues as proton transport, amorphous ice properties, and even the effect of ice in formation of planets.

Recent Progress (2005-2006)

Dissociation of Water on Pt(111), Buried Under Ice [1] (Yigal Lilach, Martin J. Iedema, James P. Cowin)

Adsorbed water, well studied on metallic surfaces, is largely thought to not dissociate on Pt(111). As illustrated in Figure 1, as long as ΔH_{ads} is several kT 's smaller than the activation energy required for dissociation E_a , the molecules will desorb rather than dissociate. How could one manipulate this, to induce water to dissociate on Pt? Either by: 1) Increasing the kinetic barrier to desorption till it is bigger than E_a (i.e. the bricks in Figure 1) (this keeps the molecules on the surface at temperatures above their "usual" desorption temperature) 2) Changing in the energy levels of the reactants or products. We showed that growing thick layers of ice on Pt(111) does both, and leads to extensive dissociation in the first layer of water. Careful, 3-step temperature programmed desorption (TPD) and work function measurements show that water dissociates on Pt(111) for T as low as 151K [1][2].

D or O pre-adsorbed on Pt(111) are well known to react with water to form D_3O^+ or OD. TPD's (at 1k/sec) of ~ 2 ML D_2O adsorbed on clean Pt, and Pt pre-dosed with D (~ 0.7 ML from ~ 30 L at 150K) and O (0.1ML), are shown in Fig. 2a, and closely resemble published TPD. On clean Pt the first-ML TPD peaks at 172K, the second-ML peak is at about 145K. Water adsorption with pre-adsorbed D shifts the first-ML peak upward 2K. Adsorption on O/Pt creates a new adsorption state, desorbing at ~ 200 K.

Multilayer ice TPD's usually tell little about the layers closest to the Pt, as the 0-order kinetics of the

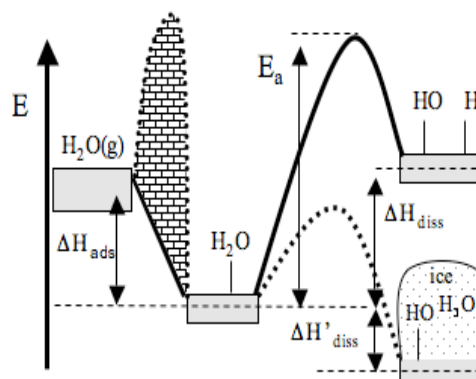


Figure 1: First monolayer water dissociation energies diagram. Adding ice on top of the first ML blocks its desorption kinetics (i.e. the brick wall). The dissociation kinetic barrier E_a and ΔH_{diss} are both shown as preventing dissociation until altered by the ice layers (lower right).

overlying ice completely obscures TPD information from the last monolayers –the "buried water". We made this observable by: 1) Careful isothermal desorption (Fig. 2 inset) of the thick ice film at T low enough to prevent desorption of the last 1-2ML of water at the Pt surface (and any ionic-stabilized water). 2) Drop T to stop the desorption. 3) Do a normal TPD of the remaining water. Figure 2b shows the results. The subsequent "normal" TPD (at 1k/sec) of the buried D₂O film shows the expected first ML peak at ~170K, but reduced in size). The TPD is dominated by two new peaks, one at 200K and a second peak at ~185K. Such peaks were never reported before in the literature for pure water films. The combined area under these two new peaks is roughly double that of a full ML of water (the 170K peak seen in Figure 2a). We attribute these peaks to the recombination of ~1ML of dissociated water. Buried water TPD of H₂O is also shown in

Fig. 2b, and are similar to D₂O, only shifted down by ~6K.

To investigate if these new binding states could be due to trace O₂ contaminating the multilayer water, we carefully heated to 225K, to just desorb all the water but not O. Any surface O will remain and will be evident in its effects on the TPD of subsequently deposited water, creating a 200K TPD peak. Figure 2c shows no noticeable O contamination of the Pt. Compare this to when we created a buried water layer starting on top of an O-pre-dosed Pt surface (~0.1 ML O in Figure 2c). This indicates that the O contamination is normally ≤ 0.01 ML. Similar experiments for pre-adsorbed H excluded trace H contamination. Confirming the water dissociation were large changes in work function (see Proton Segregation section and [2]) seen for $T_{\text{growth}} \geq 151$ K (for thick H₂O films) or 162K (for thick D₂O films). Water dissociation at the Pt surface leads to a small fraction of the hydronium ions being trapped at the vacuum-ice interface. These are carried upward during the ice growth.

Theory has suggested partial dissociation for even 1 ML of water on Pt(111): Feibelman via density functional theory [3][4], Jacob et al. [5], and Meng [6]. Much theory predicts no dissociation, e.g. ref. [7]. Prior experiments only indirectly hinted at dissociation. Hopefully this new work will promote new theory and experiments for multilayer water.

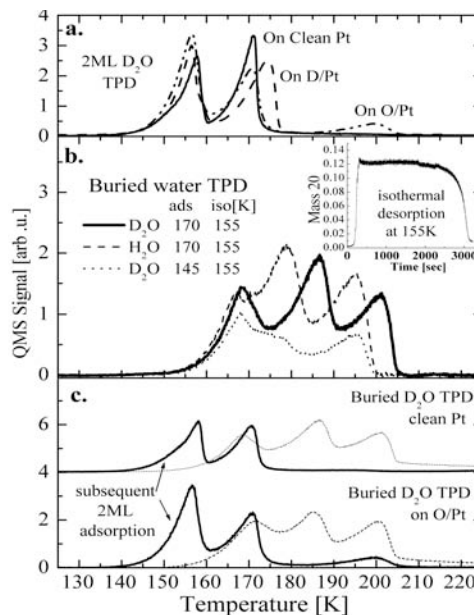


Figure 2: a) TPD of 2ML D₂O on Pt clean and pre-dosed with ~0.7ML D or ~0.1ML O. b) Buried water TPD. Insert: isothermal desorption of 150ML D₂O. c) Probing for residual O: Buried D₂O TPD to 225K ($T_{\text{growth}}=170$ K, $T_{\text{isothermal}}=155$ K) on clean Pt (dotted) and O/Pt (dashed), followed by re-dosing with D₂O (solid).

Proton Segregation at Ice Interfaces [2] (Yigal Lilach, Martin J. Iedema, James P. Cowin)

Hydronium segregates to the surface of H₂O (D₂O) ice films grown on Pt(111) above 151K (158K). This is observed as a voltage that develops across the films, utilizing work function measurements. The dependence of this voltage on the film thickness is explained by a simple equilibrium model. This model suggests ΔG of ~ -0.1 eV for the movement of ions toward the ice-vacuum interface from the bulk ice. The experiments were performed in a UHV chamber, equipped with a quadrupole mass spectrometer (QMS) for temperature programmed desorption (TPD). Water (H₂O or D₂O) was dosed by a very-flat-intensity-distribution-profile large tube doser, for layers 100 to 1000's of monolayers thick with deposition rate of up to 300ML/sec. Work function changes, $\Delta\Phi$, (including any voltage across the water film = V_{film}) were measured during the TPD by a Kelvin probe. The clean Pt surface is used as the reference state, with $\Delta\Phi=0$ for it. If we refer to any work function change that is inherent to things happening at or very near the Pt-ice (or ice-vacuum) interface as $\Delta\Phi_{\text{int}}$, then $\Delta\Phi = \Delta\Phi_{\text{int}} - V_{\text{film}}$. Usually $|V_{\text{film}}|$ is much larger than $|\Delta\Phi_{\text{int}}|$ so we report $-\Delta\Phi = -\Delta\Phi_{\text{int}} + V_{\text{film}}$, often $\approx V_{\text{film}}$.

Figure 3A shows $-\Delta\Phi$ for 3000 ML H₂O ice films, grown via the tube doser at T_{growth} between 140-

178K at about 400 ML/s. After growth, the gas-source is removed, and the temperature dropped to about 80 K. Then as the films are slowly heated (0.2K/sec) changes in $-\Delta\Phi$ of the sample are measured. The drop in $-\Delta\Phi$ above 200 K happens when the multilayer water desorbs, and the clean Pt is recovered. The dashed line shows the signal of mass 18 in the QMS, from which the coverage can be accurately obtained [8]. For T_{growth} at 150K, the story is nearly the same, and is similarly for deuterated ice, seen in Fig.3b, except shifted to slightly higher temperatures. Looking again at Fig 3a, for H_2O ice, something qualitatively different happens at $T_{\text{growth}} = 151$ K, just one K higher than the previous curve: the film starts with a positive voltage. This positive initial voltage gets much larger as T_{growth} increases, reaching around 9V. The D_2O films have a slightly higher threshold temperature, 157K.

Figure 4 shows the coverage dependence of film voltages for D_2O films grown at 165K, 170K and 180K. For consistency, the voltages presented in this figure are all measured at 170K. The voltage dependence is initially linear with coverage, then it reaches a saturation value at a coverage of several thousands of monolayers. This, and other evidence, (not shown) indicate that this voltage originates from charges on top of and within the ice films, that originally came from the Pt-ice interface. We found that a simple model fits the data well. Hydronium from the dissociation of water at the Pt-ice interface, at a concentration of q , had a small probability (~ 1 to $10\% = f_0$) of being found at the ice-vacuum interface, in some sort of equilibrium, for the very first part of the ice growth, say up to about 30 ML. As the films get thicker, these hydroniums (~ 0.01 ML) at the ice-vacuum interface become trapped there, in a local minimum. As the film grows, most of these ions will stay on top of the ice film. But a small fraction ($f_1 \approx .02\%$) are lost for each new monolayer of ice, to become trapped in the bulk ice.

This creates a film voltage V that goes as film thickness L (in ML) as:

$$V(L) = \left(\frac{q \cdot f_0 \cdot h_{\text{ML}}}{\epsilon \cdot \epsilon_0 \cdot f_1} \right) \cdot \left(1 - e^{-Lf_1/h_{\text{ML}}} \right)$$

where h_{ML} is the thickness a single monolayer of water, ϵ_0 is the vacuum permittivity, and ϵ is dielectric constant of water ice. Figure 4 shows that this fits the data very well. For D_2O h_{ML}/f_1 increases from 800 ± 100 ML at 165K to 6000 ± 2000 ML at 180K (confidence level of 0.95). This means that the tendency of the ions to segregate to the ice-vacuum interface increases with temperature. The amount of charge lifted from the Pt-ice interface (qf_0) is found to decrease from 2% of a monolayer ($1 \text{ ML} = 1.5 \times 10^{15} \text{ atoms/cm}^2$) at 165K to 0.5% of a monolayer at 180K.

Since $\Delta G = -RT \ln K$, the free energy for the charge segregation to the vacuum ice interface, compared to being stranded in the bulk ice can be estimated from this model. With the simplest of assumptions, the ΔG values are -0.09eV , -0.11eV and -0.14eV for 165K, 170K and 180K respectively. The model, while simplistic, should produce feasible thermodynamic information if it is valid. From the dependence of ΔG on the temperature, ΔH and ΔS can be calculated to be 0.35eV and 0.0027eV/K . This suggests that the reaction of an ion moving from a layer below the surface to the surface is endothermic by 0.35eV , which is a value which very close to the energy of a single hydrogen bond. The value of the entropy change means there are

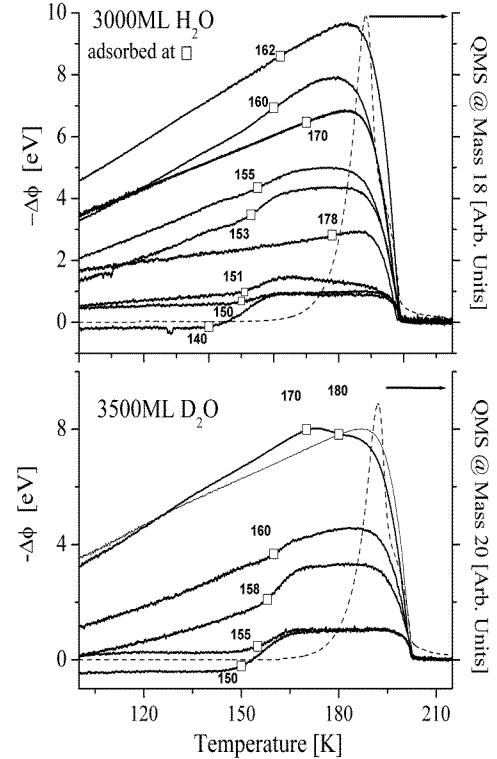


Figure 3. a) $-\Delta\Phi$ after adsorbing 3000 ML of H_2O on Pt(111) at the indicated temperature, cooling the sample to 80K and then reheating at a constant rate of 0.2K/sec. The QMS desorption signal is indicated as a dashed line. b) The same effect is reproduced in D_2O films.

more degrees of freedom for the ion on the surface, which drives the reaction forward. This is fundamentally a reasonable idea, however the value of ΔS is much too big.

With some additional assumptions we can repeat the extraction of thermodynamic constants obtain an equilibrium constants, this time for the free energy of moving a hydronium from the Pt-ice interface to the ice-vacuum interface. This analysis results in $\Delta H = -0.18 \text{ eV}$ and $\Delta S = -0.0014 \text{ eV/K}$. This exothermic value for the reaction adsorbed hydronium \rightarrow solvated hydronium is remarkably close to the value -0.1 eV estimated from a Born-Haber cycle [9]. The paper, in preparation, will look at these thermodynamic estimates more thoroughly than we can present here, and now.

Future Plans

We are adding FTIR this fall, to probe the surface and bulk species in our films. We have already added low energy secondary ion mass spectrometry (15 to 150 eV Cs ions). Together these will tell us a great deal about the identity and location of ions on and within the films. It will also answer many questions we have about the nature of the dissociated water created for the thick ice films. We will be able to understand the solvation effects on ion dissociation and transport much better, because of these new measurements. We also hope to better understand in bulk ice the motion of hydronium and L and D defects.

References

- [1] Y Lilach, MJ Iedema, JP Cowin, "Dissociation of Water on Pt(111), Buried Under Ice" submitted 2006 to Phys. Rev Lett.
- [2] Y. Lilach, M.J. Iedema, J.P. Cowin, (in prep).
- [3] P.J. Feibelman, Phys. Rev. Lett. 91 (2003) 59601.
- [4] P.J. Feibelman, Science 295, (2002) 99.
- [5] T. Jacob, W.A. Goddard, J. Am. Chem. Soc. (2004) 9360.
- [6] S. Meng, Surf. Sci. 575 (2005) 300.
- [7] H Ogasawara, B Brena, D Nordlund, M Nyberg, A Pelmenschikov, LG Pettersson, A Nilsson, Phys. Rev. Lett. 89 (2002) 276102.
- [8] MJ Iedema, MJ Dresser, DL Doering, JB Rowland, WP Hess, AA Tsekouras, JP Cowin, J. Phys. Chem. B 102 (1998) 9203.
- [9] N. Kizhakevariam, E. M. Stuve, Surf, Sci. 275 (1992) 223.

Other recent papers supported fully or partially by this BES program:

- Bell, R, HF Wang, K Wu, MJ Iedema, JP Cowin, "Nanometer-Resolved Interfacial Fluidity." *J. Amer. Chem. Soc.* 125: 5176-5185
- Bell, R, HF Wang, MJ Iedema, JP Cowin, Sculpting Nanoscale Liquid Interfaces, in "ACS Symposium Series 861: Mesoscale Phenomena in Fluid Systems" ed. F. Case and P. Alexandridis, Amer. Chem. Soc. , Chapter 12, pp. 191-203
- Gallagher, MC, MS Fyfield , LA Bumm, JP Cowin, SA Joyce; Structure of Ultrathin MgO films on Mo(001), Thin Solid Films 445, 96
- Krueger, BJ, VH Grassian, MJ Iedema, JP Cowin, A Laskin "Probing Heterogeneous Chemistry of Individual Atmospheric Particles Using Scanning Electron Microscopy and Energy Dispersive X-ray Analysis." *Anal. Chem.*, 75: 5170-5179 .
- Laskin, A, DJ Gaspar, WH. Wang, SW Hunt, JP Cowin, SD Colson, BJ Finlayson-Pitts "Reactions at Interfaces As a Source of Sulfate Formation in Sea-Salt Particles." *Science*, 301: 340-344 .
- Wang, HF, RC Bell, MJ Iedema, AA Tsekouras, JP Cowin, "Sticky Ice Grains Aid Planet Formation", *Astrophys. J.* 620, 1027 (2005).

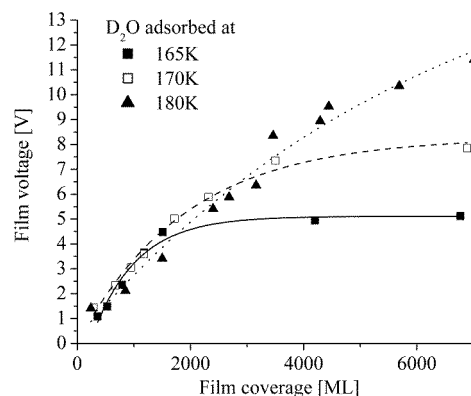


Figure 4. The voltage of films of varying thicknesses grown at the indicated temperatures. Each point is the voltage taken from a curve as in Figure 1, at 170K. The curves are the best fits to $a(1-e^{-L/b})$.

Computational Studies of Liquid Interfaces

Liem X. Dang

Chemical Sciences Division

Pacific Northwest National Laboratory

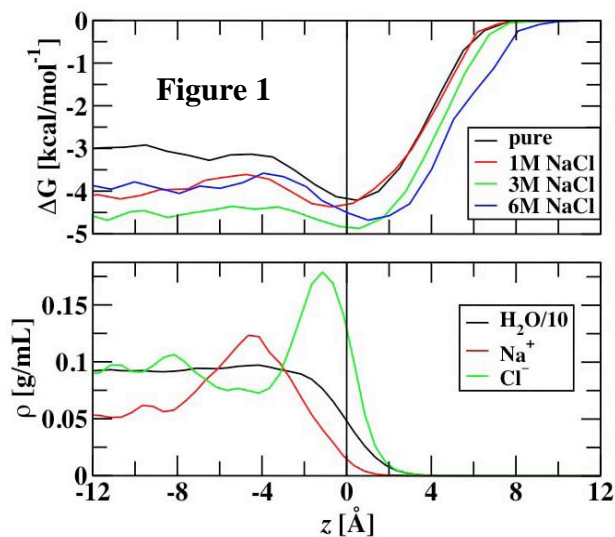
902 Battelle Blvd., Mail Stop K1-83

Richland, WA 99352

liem.dang@pnl.gov

Summary. The adsorption and distribution of ions at aqueous liquid interfaces are fundamental processes encountered in a wide range of chemical and biological systems. In particular, the manner in which solvent molecules solvate ions is relevant to problems in chemical and physical processes. For example, solvation of ions affects chemical reactions at interfaces and the distribution of ions and/or counter-ions influences the structure and stability of large molecules and membranes. The focus of research on this project is the characterization of solvation processes at aqueous liquid interfaces using molecular dynamics (MD) computer simulation techniques. We develop fundamental, molecular-scale information about the interactions of ions and molecules in solvent phases and across aqueous liquid interfaces. We focus special effort on understanding the precise mechanism and dynamics of the transfer process, and on learning the role of many-body effects on the transfer mechanism of solutes across the aqueous liquid interface. We use MD simulations to compute surface potentials, potentials of mean force for dilute solutions and density profiles in concentrated solutions. In addition, research on chemical separation science involves the development of methods and potential models for use in the simulation of crown ether molecules mediating ion transport across water-organic liquid interfaces. Results of this research further our understanding of ion transport across liquid-liquid interfaces, which in turn, provides basic knowledge needed to address DOE's environmental restoration issues.

Computational Observation of Enhanced Solvation of the Hydroxyl Radical with Increased NaCl Concentration. The goal of the current study is to determine the free energy profile of a hydroxyl radical across the air-water interface of NaCl aqueous salt solutions and determine if

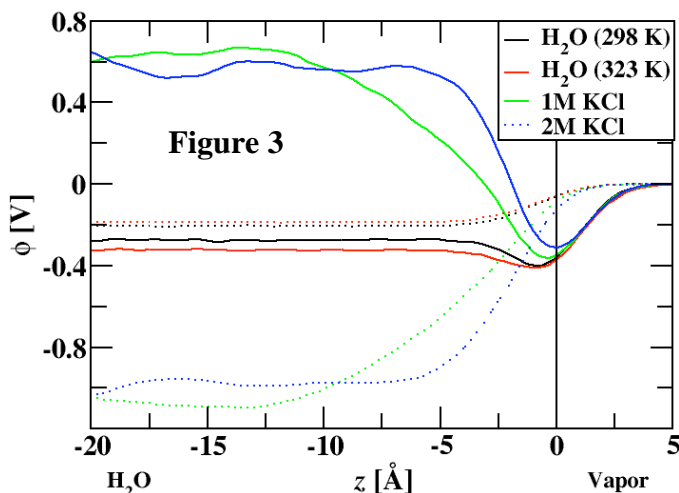
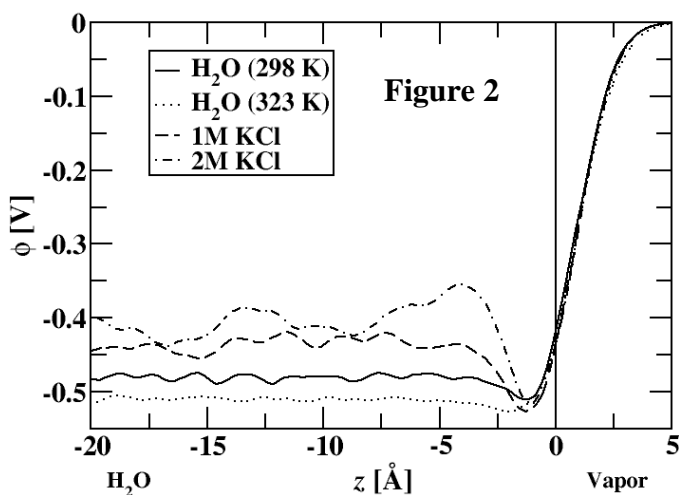


salt concentration has a significant effect on solvation. To the best of our knowledge, the present work is the first application of the potential of mean force (PMF) approach to the evaluation of the effects of salt concentration on the uptake process of pollutant solutes by the air-water interface. The utilization of the PMF technique allows for the quantification of the effect of salt concentration on the free energy minima magnitudes and positions, and for the determination of overall aqueous free energies, which can often be compared with experiment. The PMF profiles are given in Figure 1, where zero represents the Gibbs dividing surface of water. Figure 1 shows the

potential of mean force for hydroxyl radical (top) approaching the aqueous phase from the gas phase (right of figure). Specific density profiles for the 3M NaCl system are shown at the bottom of Figure 1 where the presented H₂O density is a tenth of its actual density. The estimated uncertainties were 0.1 and 0.2 kcal/mol at the interface and bulk, respectively. Near the Gibbs dividing surface, there is a difference between the free energy minimums of 3M (4.87 kcal/mol) and P (4.13 kcal/mol) of 0.74 kcal/mol. In the bulk, this difference is larger, with 3M and P having aqueous free energies of -4.5 and -3.2 kcal/mol, respectively, leading to a difference of 1.3 kcal/mol, nearly double the difference at the interface. Our results provided evidence for an increased uptake of OH radicals in the 3M simulations compared to pure water. We also observed that the free energy minimum at the interface is far less pronounced in the 3M case, the OH radicals are less likely to be present at the interface. This could have an interesting consequence that, despite the higher concentration of OH radicals in the droplet, the surface reactivity might be lower.

Simulated Surface Potentials at the Vapor-Water Interface for the KCl Aqueous Electrolyte Solution.

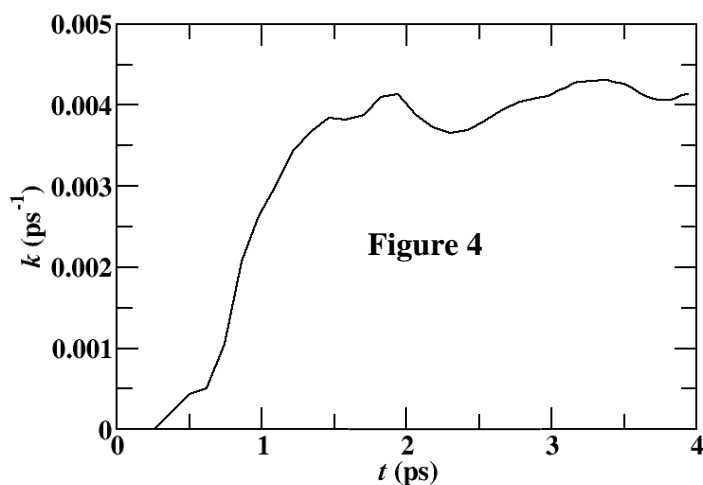
The interfaces between an aqueous solution and its vapor have been widely studied due to their importance for biological, environmental, and atmospheric chemistry. The measurement of surface potential has long been a technique to determine the interfacial



water orientation and ion distribution at vapor-liquid interfaces. The surface potential is defined as the difference in electrical potential between a neutral aqueous liquid and its coexisting vapor phase. The direct experimental determination of the surface potential remains a challenge. For instance, the surface potential across the interface between a vapor and neat water is a point of contention, with surface potential measurements not always agreeing on sign. However, the facts that the surface potential increases with the addition of alkali halide salts, and that it decreases with increased temperature for pure water, are currently accepted. The total electric potential as a function of position for all systems studied are given in Figure 2, and the decomposition of the surface potentials into contributions from static charges and induced dipoles at 298 K for pure water, 1M KCl, and 2M KCl are given in Figure 3. The value obtained in the current study for water (-480 mV) is consistent with that of a previous study of the surface potential

of the Dang-Chang water, and the most recent values calculated for the non-polarizable TIP4P and SPC/E water models. The static charge distribution is essentially the measurement of the average angle between the water C_{2v} molecular axis and the z-axis as a function of the z coordinate. The negative surface potential clearly indicates the presence of a preferred orientational order of water molecules near the interface. Specifically, as a water molecule approaches the interface, the probability for its hydrogen atoms to point *away* from the water center of mass increases.

Hydroxyl Radical Transfer Rate from Interface to Bulk by Transition Path Sampling. The transition path sampling technique was utilized to determine the rate of transfer of the hydroxyl radical from the water interface to the bulk and analyze its transition state. Polarizable potentials were used to model the interactions between the hydroxyl radical and the Dang-Chang water force field. To calculate the rate, a total of 37250 trajectories of 4 ps in length, connecting states where the hydroxyl radical was at the interface with cases when it is in the bulk, were performed. Figure 4 gives the value determined for the rate as a function of time, converging to $0.004 \pm 0.0005 \text{ ps}^{-1}$. The rate was also calculated from transition state theory from the free energy profile calculated from the potential of mean force technique, giving a value of 0.015 ps^{-1} . This



corresponds to a transmission coefficient of 0.2, compared to a value of 0.15 ± 0.05 for the transfer of a model solute across a model liquid-liquid interface, showing good agreement. Analysis of 100 transition states harvested from the transition path trajectories was performed. It was found that while an interfacial hydroxyl radical was most likely to have its hydrogen pointing towards the water bulk, cases where its hydrogen pointed away were more likely to result in a transfer into the bulk. Also, a hydroxyl radical in the transition state

had on average fewer water oxygens in its first solvation shell than on average when near the interface. This was despite similar first oxygen-hydrogen peak heights for both hydroxyl radical and water oxygen and hydrogen combinations, i.e. a donating hydrogen bond from a water and a donating hydrogen bond from a hydroxyl radical resulted in a similar donating hydrogen-accepting oxygen radical structure. The likelihood is that hydroxyl radicals at the transition state had broader oxygen-hydrogen-oxygen angular distributions for their hydrogen bonds with water, leading to weaker hydrogen bonds.

Collaborators on this project include Tsun-Mei Chang, Collin Wick, Bruce C. Garrett, Gregory Schenter, John Fulton, Matina Roeselova, Pavel Jungwirth and Douglas J. Tobias (UC, Irvine).

References to publications of DOE sponsored research (2003-present)

1. L. X. Dang, "Solvation of the Hydronium Ion at the Water Liquid/Vapor Interface," *Journal of Chemical Physics* **119**, 6351 (2003).
2. T. M. Chang and L. X. Dang, "On Rotational Dynamics of an NH_4^+ Ion in Water," *Journal of Chemical Physics* **118**, 8813 (2003).
3. L. X. Dang and T. M. Chang, "Many-Body Interactions in Liquid Methanol and its Liquid/Vapor Interface: A Molecular Dynamics Study," *Journal of Chemical Physics* **119**, 9851 (2003).
4. L. X. Dang, G. K. Schenter and J. L. Fulton "EXAFS Spectra of Dilute Solutions of Ca^{2+} and Sr^{2+} in Water and Methanol," *Journal Phys. Chem.* **B 107**, 14119 (2003).
5. L. X. Dang and B. C. Garrett. "Molecular Mechanism of Water and Ammonia Uptake by the Liquid/Vapor Interface of Water" *Chemical Physics Letters* **385**, 309 (2004).
6. L. X. Dang, "Ions at the Liquid/Vapor Interface of Methanol" *Journal of Physical Chemistry A* **108**, 9014 (2004). **Featured on Journal Cover**
7. M. Roeselova, J. S. Vieceli, L. X. Dang, B. C. Garrett and D. J. Tobias "Hydroxyl radical at the air-water interface" *Journal of American Chemical Society* **126**, 16308 (2004).
8. T.-M. Chang and L. X. Dang "Liquid/Vapor Interface of Methanol-Water Mixtures: A Molecular Dynamics Study" *Journal of Physical Chemistry B* **109**, 5759 (2005).
9. M. M., T. Frigato, L. Levering, H. C. Allen, D. J. Tobias, L. X. Dang and P. Jungwirth "A Unified Molecular Picture Of The Surfaces Of Aqueous Acid, Base, And Salt Solutions" *Journal of Physical Chemistry B* **109**, 7617 (2005). **Featured on Journal Cover.**
10. Wick CD, **Dang LX** "Investigating Pressure Effects On Structural and Dynamical Properties of Liquid Methanol with Many-Body Interactions" *Journal of Chemical Physics* **123** (18): Art. No. 184503 Nov 8 2005.
11. Vieceli J, Roeselova M, Potter N, et al. "Molecular Dynamics Simulations of Atmospheric Oxidants at the Air-Water Interface: Solvation and Accommodation of OH and O_3 " *Journal of Physical Chemistry B* **109** (33): 15876-15892 AUG 25 2005.
12. Wick CD and **Dang LX** "Diffusion at The Liquid-Vapor Interface of an Aqueous Ionic Solution Utilizing a Dual Simulation Technique" *Journal of Physical Chemistry B* **109** (32): 15574-15579 AUG 18 2005.
13. Chang TM and **Dang LX** "Liquid-Vapor Interface of Methanol-Water Mixtures: A Molecular Dynamics Study" *Journal of Physical Chemistry B* **109** (12): 5759-5765 Mar 31 2005.
14. V. -A. Glezakou, Y. C. Chen, J. L. Fulton, G. K. Schenter and **L. X. Dang** "Electronic Structure, Statistical Mechanical Simulations, and EXAFS Spectroscopy of Aqueous Potassium" *THEORETICAL CHEMISTRY ACCOUNTS* **115** (2-3): 86-99 MAR 2006. **Invited article**
15. **L. X. Dang** and T. M. Chang, "Recent Advances in Molecular Simulations of Ion Solvation at Liquid Interfaces" *CHEMICAL REVIEWS* **106** (4): 1305-1322 APR 2006. **Featured on Journal Cover**
16. Wick CD, **Dang LX** and Jungwirth P. "Simulated Surface Potentials at the Vapor-Water Interface for the KCl Aqueous Electrolyte Solution" *Journal of Chemical Physics* **125** (2): Art. No. 024706 Jul 14 2006.

17. Wick CD and **Dang LX** “Computational Observation of Enhanced Solvation of the Hydroxyl Radical with Increased NaCl Concentration” *Journal of Physical Chemistry B* 110 (18): 8917-8920 May 11 2006. **Featured on Journal Cover**
18. Oliver Höfft, Andriy Borodin, Uwe Kahnert, Volker Kempter, **Liem X. Dang**, and Pavel Jungwirth “Surface Segregation of Dissolved Salt Ions” *Journal of Physical Chemistry B* 110 (24): 11971-11976 Jun 22 2006. **Featured on Journal Cover**
19. Wick CD and **Dang LX** “Distribution, Structure, and Dynamics of Cesium and Iodide Ions at the H₂O-CCl₄ and H₂O-Vapor Interfaces” *Journal of Physical Chemistry B* 110 (13): 6824-6831 APR 6 2006.
20. **Dang LX**, Chang TM, Roeselova M, et al. “On NO₃⁻-H₂O Interactions in Aqueous Solutions and at Interfaces” *Journal of Chemical Physics* 124 (6): Art. No. 066101 FEB 14 2006.

Infrared Spectroscopy of Transition Metal-Molecular Interactions in the Gas Phase

DE-FG02-96ER14658

Michael A. Duncan

Department of Chemistry, University of Georgia, Athens, GA 30602-2556

maduncan@uga.edu

Program Scope

The focus of our research program is the study of gas phase metal clusters to evaluate their potential as models for the fundamental interactions present on heterogeneous catalytic surfaces. These clusters are molecular sized aggregates of metals or metal compounds (oxides, carbides). We focus specifically on the bonding exhibited by "physisorption" on cluster surfaces. Complexes containing one or more metal atoms bound to small molecules provide the models for physisorption. Infrared spectroscopy in various forms is employed to measure the vibrational spectroscopy of the metal clusters themselves and, in particular, the spectra of physisorbed molecules. These studies investigate the nature of the metal-adsorbate interaction and how it varies with metal composition and cluster size. The vibrational frequencies measured are compared with the predictions of theory to reveal the electronic state and geometric structure of the system. Ionic clusters are studied with mass-selected infrared photodissociation spectroscopy. Experimental measurements are supplemented with calculations using density functional theory (DFT).

Recent Progress

The main focus of our work over the last two years has been infrared spectroscopy of mass-selected cation-molecular complexes, e.g., $\text{Ni}^+(\text{C}_2\text{H}_2)_n$, $\text{Ni}^+(\text{H}_2\text{O})_n$, $\text{Nb}^+(\text{N}_2)_n$ and $\text{M}^+(\text{CO})_n$. These species are produced by laser vaporization in a pulsed-nozzle cluster source, mass-selected with a specially designed reflectron time-of-flight mass spectrometer and studied with infrared photodissociation spectroscopy using an IR optical parametric oscillator laser system (IR-OPO; wavelength coverage: 2000-4500 cm^{-1}). We have studied the infrared spectroscopy of various transition metal ions in complexes with the ligands indicated. In each system, we examine the shift in the frequency for selected vibrational modes in the adsorbate molecule that occur upon binding to the metal. The number and frequencies of IR-active modes in multi-ligand complexes reveals the structures of these systems, while sudden changes in vibrational spectra or IR dissociation yields are used to determine the coordination number for the metal ion in these complexes. In some systems, new vibrational bands are found beginning at a certain complex size that correspond to intra-cluster reaction products. In small complexes with strong bonding, we use the method of "rare gas tagging" with argon or neon to enhance dissociation yields. In all of these systems, we employ a close interaction with theory to investigate the details of the metal-molecular interactions that best explain the spectroscopy data obtained. We perform our own density functional theory (DFT) or MP2 calculations (using Gaussian 03W) and when higher level methods are required (e.g., CCSD),

we collaborate with local theorists (P.v.R. Schleyer, H.F. Schaefer). Our infrared data on these transition metal ion-molecule complexes are the first available, and they provides many examples of unanticipated structural and dynamic information.

$M^+(C_2H_2)_n$ clusters have been studied for the metals vanadium, iron, cobalt, copper and nickel in the region of the symmetric and asymmetric stretching modes of acetylene. Although the symmetric stretch is not IR active for the isolated molecule, distortion of the ligand in these complexes induces IR activity for this mode. The C-H stretches in these systems are shifted to the red by 30-50 cm^{-1} from the corresponding modes in the isolated acetylene molecule, consistent with predictions for π -complexes. However, the magnitude of the red-shift is different for the different metals, consistent with the relative amounts of sigma donation and π -back bonding. Fe^+ , Co^+ and Ni^+ all form π -complexes with acetylene, while V^+ forms a three-membered ring metallacycle. Multiple acetylene complexes have been studied for Ni^+ and Co^+ . Coordination numbers are established as four acetylenes for nickel and three for cobalt. New vibrational bands emerge that are shifted even further to the red, but these are only seen after the coordination is exceeded by one ligand. These bands are assigned to the presence of either 1) a cyclobutadiene ligand that results from an intracluster cyclization reaction or 2) an unusual C-H hydrogen bonding configuration.

$M^+(H_2O)_n$ complexes and those tagged with argon have been studied for iron, nickel, vanadium, cobalt, copper and zinc complexes. In the vanadium system, partial rotationally resolved spectra have been obtained. In the iron system, complexes with one or two water molecules (argon tagged) exhibit isomeric structures for both argon and water binding sites. Nickel complexes have been studied for up to 30 water molecules, providing a detailed probe of the dynamics of solvation. Hydrogen bonded structures appear for the first time at a cluster size of $n=4-5$, and the free-OH symmetric stretch disappears at $n=8$ indicating that most external water molecules are bound within a hydrogen bonding network after this size. The IR signature that we have recently identified for clathrate structures in protonated water clusters, $H^+(H_2O)_n$, is a single peak for the free-OH asymmetric stretch, but this signature is not found for the $Ni^+(H_2O)_n$ complexes. Systematic trends in the magnitude of the shifts for the O-H stretches in these systems are under investigation.

$M^+(N_2)_n$ complexes have been studied in the N-N stretch region for Fe^+ , V^+ and Nb^+ complexes. Again, binding to metal makes this mode IR active even though it is forbidden in the isolated molecule. Theory shows that most metals prefer end-on binding configurations, but some (e.g., cobalt) prefer to bind side-on as in a π -complex. The N-N stretch is red shifted for these metals compared to this frequency for the free nitrogen molecule, in much the same way that carbonyl stretches also shift to the red. $M^+(N_2)_4$ complexes for both of these metals are found to have a square-planar structure. However, the most stable coordination for both metals occurs in a complex with six ligands. In Nb^+ , addition of the fifth ligand induces a spin change on the metal ion from quintet to triplet, and this spin state persists in the larger complexes.

$M^+(CO)_n$ complexes are analogous to conventional complexes in inorganic chemistry. However, we are able to make these systems without the complicating influences of solvent or counter ions. The C-O stretch in most transition metal complexes shifts strongly to the red from free CO, and this vibration falls below 2000 cm^{-1} . This lies outside the tuning range of our OPO lasers in their most efficient configuration. To circumvent this initial difficulty, we have examined so-called non-classical carbonyl complexes of gold, silver and platinum. $M^+(CO)_n$ complexes for these systems have been studied, and they exhibit the expected blue-shift of the carbonyl stretch

relative to free CO. The size dependence of these resonances provides insight into the structures of these complexes.

Future Plans

Future plans for this work include the extension of these IR spectroscopy studies to more ligands, to complexes with multiple metal atoms and to a more extended region of the IR spectrum. In the vanadium-water system, we have already measured spectra in the water bending mode region for complexes containing up to 15 metal atoms, using a free electron laser. This work establishes the feasibility of studies on larger metal systems. We want to study more reactive metals with hydrocarbons such as ethylene or methane that might produce carbenes, vinylidene or ethylidyne species. These systems should exhibit characteristic IR spectra, and will allow us to make better contact with IR spectroscopy on metal surfaces. Studies of carbon monoxide have been limited so far because the tuning range of our present laser system only extends down to 2000 cm^{-1} . However, new crystals have just become available (silver-gallium-selenide) to extend the range of OPO systems like ours down to the $1000\text{-}2000\text{ cm}^{-1}$ range. We recently obtained one of these crystals, which will allow us to study ligands like CO and to probe other adsorbate molecules in additional vibrational modes (C-C stretch of acetylene, water bending mode, etc.).

In all of these studies, we have focused on the qualitative effects of metal-adsorbate interactions and trends for different transition metals interacting with the same ligand. Our collaboration with theory has revealed that density functional theory has serious limitations for these metal-ligand complexes that were not previously recognized. This is particularly evident in metals such as vanadium and iron, where two spin states of the metal lie at low energy. DFT has difficulty identifying the correct relative energies of these spin states. Further examinations of this issue are planned, as it has significant consequences for the applications of DFT.

Publications (2003-2006) for this Project

1. M.A. Duncan, "Infrared Spectroscopy to Probe Structure and Dynamics in Metal Ion-Molecule Complexes," *Intl. Rev. Phys. Chem.* **22**, 407 (2003).
2. N.R. Walker, G.A. Grieves, R.S. Walters and M.A. Duncan, "The Metal Coordination in $\text{Ni}^+(\text{CO}_2)_n$ and $\text{NiO}_2^+(\text{CO}_2)_m$ Complexes," *Chem. Phys. Lett.* **380**, 230 (2003).
3. R.S. Walters, N.R. Walker, D. Pillai and M.A. Duncan, "Infrared Spectroscopy of $\text{V}^+(\text{H}_2\text{O})$ and $\text{V}^+(\text{D}_2\text{O})$ Complexes: Ligand Deformation and an Incipient Reaction," *J. Chem. Phys.* **119**, 10471 (2003).
4. N.R. Walker, R.S. Walters and M.A. Duncan, "Infrared Photodissociation Spectroscopy of $\text{V}^+(\text{CO}_2)_n$ and $\text{V}^+(\text{CO}_2)_n\text{Ar}$ Complexes," *J. Chem. Phys.* **120**, 10037 (2004).
5. T.D. Jaeger, A. Fielicke, G. von Helden, G. Meijer and M.A. Duncan, "Infrared Spectroscopy of Water Adsorption on Vanadium Cluster Cations (V_x^+ ; $x=3\text{-}15$)," *Chem. Phys. Lett.* **392**, 409 (2004).

6. R.S. Walters and M.A. Duncan, "Infrared Spectroscopy of Solvation and Isomers in $\text{Fe}^+(\text{H}_2\text{O})_{1,2}\text{Ar}_m$ Complexes," *Austr. J. Chem.* **57**, 1145 (2004).
7. N.R. Walker, G.A. Grieves, R.S. Walters and M.A. Duncan, "Growth Dynamics and Intracluster Reactions in $\text{Ni}^+(\text{CO}_2)_n$ Complexes via Infrared Spectroscopy," *J. Chem. Phys.* **121**, 10498 (2004).
8. R.S. Walters, P.v.R. Schleyer, C. Corminboeuf and M.A. Duncan, "Structural Trends in Transition Metal Cation-Acetylene Complexes Revealed Through the C-H Stretch Fundamentals," *J. Am. Chem. Soc.* **127**, 1100 (2005).
9. T.D. Jaeger and M.A. Duncan, "Infrared Photodissociation Spectroscopy of $\text{Ni}^+(\text{benzene})_x$ Complexes," *J. Phys. Chem. A* **109**, 3311 (2005).
10. E.D. Pillai, T.D. Jaeger and M.A. Duncan, "Infrared spectroscopy and density functional theory of small $\text{V}^+(\text{N}_2)_n$ clusters," *J. Phys. Chem. A* **109**, 3521 (2005).
11. R.S. Walters, E.D. Pillai and M.A. Duncan, "Solvation Processes in $\text{Ni}^+(\text{H}_2\text{O})_n$ Complexes Revealed by Infrared Photodissociation Spectroscopy," *J. Am. Chem. Soc.* **127**, 16599 (2005).
12. R.S. Walters, E.D. Pillai, P.v.R. Schleyer and M.A. Duncan, "Vibrational spectroscopy of $\text{Ni}^+(\text{C}_2\text{H}_2)_n$ ($n=1-4$) complexes," *J. Am. Chem. Soc.* **127**, 17030 (2005).
13. N.R. Walker, R.S. Walters and M.A. Duncan, "Frontiers in the Infrared Spectroscopy of Gas Phase Metal Ion Complexes," *New J. Chem.* **29**, 1495 (2005).
14. V. Kasalova, W.D. Allen, H.F. Schaefer, E.D. Pillai and M.A. Duncan, "Model systems for probing metal cation hydration: The $\text{V}^+(\text{H}_2\text{O})$ and $\text{ArV}^+(\text{H}_2\text{O})$ complexes," *J. Chem. Phys.*, submitted.
15. E.D. Pillai, T.D. Jaeger and M.A. Duncan, "Infrared Spectroscopy of $\text{Nb}^+(\text{N}_2)_n$ Complexes: Coordination, Structures and Spin States" *J. Am. Chem. Soc.*, submitted.

Photochemistry at Interfaces

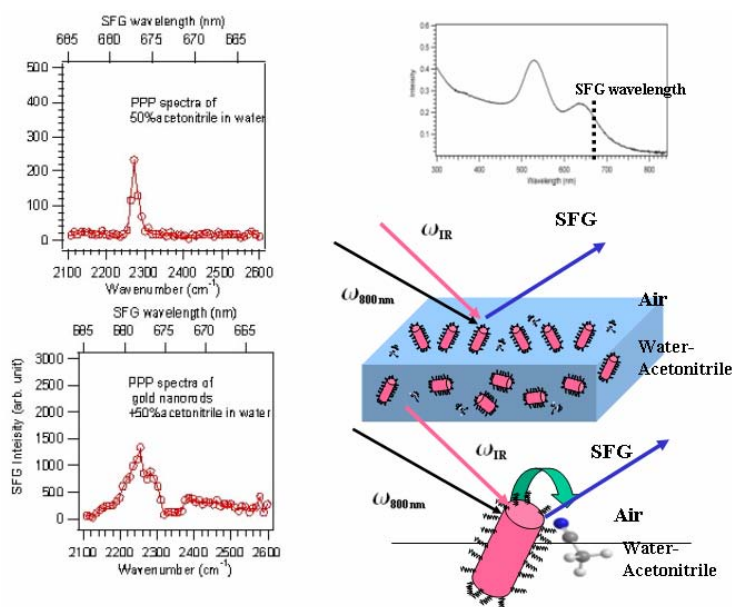
Kenneth B. Eisenthal
Department of Chemistry
Columbia University
New York, NY 10027
eisenth@chem.columbia.edu

A. Charging of Aqueous/Single Crystal α -TiO₂ Interface

In order to develop chemical models capable of predicting surface charging at aqueous/solid oxide interfaces it is necessary to relate protonation reactions to surface structure. To achieve this we have used an SHG method developed in our laboratory that relates the amplitude of the SHG signal to the electrostatic potential at the interface. In past work we investigated aqueous/Al₂O₃ single crystal interface. In the work reported here we have extended these studies to the aqueous/TiO₂ 110 single crystal interfaces. We have made good progress towards our goal of connecting the SHG experimental results with theory by collaborating with three theoreticians who modeled the protonation reactions at the aqueous/TiO₂ 110 single crystal interface. They used a revised Multi Site Complexation model of surface oxygen protonation using ab initio calculations of relaxed Ti-O bond lengths for a hydrated 110 TiO₂ surface. To compare experiment with theory we used the quantity generally used to characterize aqueous/solid oxide interfaces, namely the point of zero charge, i.e. the pH at which the net surface charge is zero. The SHG experiments yielded the value of 4.8 ± 0.3 and theory 4.76. Although this agreement is impressive further experimental and theoretical work on other single crystal oxide surfaces are needed to test what appears to be a promising model of charging at aqueous/solid oxide interfaces.

B. Second Order Nonlinear Optical Studies of Gold Nanorods

A linear optical measurement of the spectrum of Au nanorods in solution detects dipolar surface plasmons but offers no information about other plasmon resonances. With SHG and SFG however, multipolar (quadrupole, magnetic dipole) plasmon resonances appear in the SHG and SFG spectra of the Au nanorods. We have preliminary results on SHG scattering from 52nm \times 20nm Au nanorods at the air/water interface and in bulk water, with more complete results on the SFG scattering at the air/acetonitrile-water solution interface. We overlapped a femtosecond 120 fs IR pulse and a 3 ps visible pulse in space and tune at the interface.



We selected the acetonitrile-water solution as the bulk liquid because we have SFG measurements of the $-\text{C}\equiv\text{N}$ vibration at the air/acetonitrile-water interface, and we want to compare the effects of the Au nanorods on the SFG signal. We tuned the frequency of the IR light to be resonant with the $-\text{C}\equiv\text{N}$ vibrational frequency. By then tuning the visible light to a frequency that brings the sum frequency $\omega_{SF} = \omega_{VIS} + \omega_{IR}$ into resonance with a surface plasmon of the Au nanorods we could determine if there was any resonant enhancement of the SFG signal due to coupling of the SFG and a Au nanorod plasmon. The figure above shows the experimental arrangement and the sum frequency signal in the presence and absence of the nanorods for the PPP polarization combination, where the first letter gives the polarization of the sum frequency, second the visible and the third the IR. The five fold enhancement gives the minimum plasmon enhancement because the surface concentration of Au nanorods is low, which means that most of the surface acetonitrile molecules are not near a nanorod. A better experiment would be to look for resonance with vibrations of the capping molecules that are attached to the nanorods. We have not been able to carry out this experiment because the temperature and humidity fluctuations this summer have made the lasers unstable. We are trying to get Columbia to do something about this.

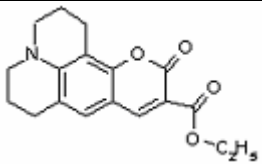
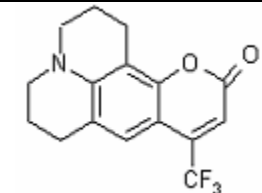
C. Solvation Dynamics at a Liquid/Liquid Interface

The response of polar solvent molecules to a sudden charge redistribution in the solute following excitation has an “instantaneous” electronic polarizability response, which is followed by the slower orientational and rotational motions of the solvent molecules. There have been considerable efforts to understand the role of these solvent motions in chemical reactions, particularly charge transfer reactions, i.e. electron and proton transfer. Just as solvation dynamics in bulk liquids are important in bulk chemical reaction dynamics, it is relevant to chemistry at liquid interfaces as well. Using a femtosecond pump-SHG probe method we have studied solvation dynamics at air/water, charged surfactant air/water, silica/acetonitrile, and silica/butanol interfaces. The solvation dynamics were found to be slower at the water interfaces than in bulk water, but faster at the silica interfaces than in the bulk liquids. We have extended our studies of interfacial solvation to include solvation dynamics at a liquid/liquid interface. These experiments are the first measurements of solvation dynamics at a liquid/liquid interface. The probe molecules were the coumarin dyes, C314 and C153, at N,N'-dimethylaniline/aqueous interfaces. The average solvation time at the air/water interface for C314 was found to be slower, 900 ± 150 fs than at the DMA/aqueous interface, 360 ± 60 fs. The solvation time of C153 at the DMA/aqueous interface was found to be the same as C314; its value is 370 ± 70 fs. In bulk water the values for similar coumarins are 600-900fs. The solvation dynamics at the DMA/aqueous interfaces reported here are directly relevant to electron transfer dynamics at these interfaces.

D. Electron Transfer at the N,N'-dimethylaniline/aqueous Interface

In earlier studies we carried out the first time resolved electron transfer at an organic liquid/aqueous interface. DMA was selected as the organic liquid in contact with water because the ground state DMA can serve as the electron donor to the excited state coumarin acceptor. As a consequence the translational motions needed to bring the donor and acceptor to a reaction distance is no longer a factor in the electron transfer dynamics. This approach is similar to our earlier work on electron transfer in bulk DMA. On photoexcitation of C314 at the DMA/aqueous interface we observed electron transfer from an interfacial ground state donor, molecule, DMA, to an excited state coumarin 314. We also observed the back electron transfer from the C314 radical anion to the DMA radical cation. We now report on our studies of a different coumarin, C153, selected because we can compare its electron transfer dynamics at the DMA/aqueous interface with results in bulk DMA obtained by other researchers. The table gives our measured values and provides a comparison of C153 at the interface vs. bulk DMA. From these data we conclude that C314 and C153 have the same electron transfer dynamics. The small differences in their dipole moments and hyperpolarizabilities and interfacial spectral shifts clearly do not affect the dynamics. Our finding, given in part C, established that their solvation dynamics are the same, which together with their having the same reduction potentials, are consistent with the electron transfer

dynamics being the same for these coumarins. We note that the electron transfer reaction of C153 at the DMA/aqueous interface is faster than in bulk DMA. We have calculated the redox potentials at the interface using bulk values and the Nitzan solvation correction to obtain the interface value. The interface electron transfer is favored over the bulk dynamics by 350 mV for the redox contribution including ion pair stabilization. The reorganization energy is surmised to be smaller at the interface than in bulk DMA based on measurements of interface polarity, estimated by spectral shifts at the interface with respect to bulk DMA. This also points to faster dynamics at the interface. We plan to compare these results with several theoretical treatments of electron transfer at liquid/liquid interfaces based on the Marcus model.

		DMA/H ₂ O interface			Bulk DMA	E _{red}
		τ_{solv}	τ_{ET}	τ_{BET}	$\tau_{\text{ET}}^{\text{a}}$	
	C314	360±60 fs	14±2 ps	183±5 ps	-	-1.721 eV
	C153	370±70 fs	11±3 ps	173±3 ps	3.4 ps (0.3) 25 ps (0.7) Avg 18 ps	-1.731 eV

a) results of studies by other research groups

Future Plans

We plan to enhance our capabilities to investigate ultrafast chemical and physical phenomena at liquid interfaces by setting up a femtosecond pump-vibrational sum frequency generation (VSFG) probe as a complement to our current pump SHG probe set up. It is our intent to apply time resolved VSFG to investigate the dynamics of interfacial molecules in their excited electronic states. The objectives are to determine the various radiationless pathways by which a range of excited state molecules in various liquid interfacial environments decay by photophysical and photochemical mechanisms. VSFG is a vibrational spectroscopy, which consequently has the valuable characteristic of being sensitive to the structure of the molecule and its interactions with its environment. SHG is an electronic spectroscopy and therefore it is more challenging to detect structural changes and the small spectral shifts relative to the widths of electronic states. With the ultrafast VSFG capability we will be able to measure the vibrational spectra of excited state molecules in their singlet and triplet states and the transient chemical species that they produce. The excited state vibrational spectra yields information on the excited state potential energy surfaces, e.g. force constants, specific intermolecular interactions, e.g. the possible breaking of hydrogen bonds, and the formation of isomeric structures. Knowledge of the individual spectra is of particular value in that it can be used to differentiate the various chemical species at the interface and their evolution in time.

References.

- Eissenthal, Kenneth B. **Nonlinear spectroscopy of aqueous interfaces** *Abstracts of Papers*, 232nd ACS National Meeting, San Francisco, CA, United States, Sept.10-14, 2006(2006)
- Nguyen, Kim T.; Shang, Xiaoming; Eissenthal, Kenneth B. **Molecular Rotation at Negatively Charged Surfactant/Aqueous Interfaces** *J. Phys. Chem. ACS ASAP*
- Eissenthal, Kenneth B. **Second harmonic spectroscopy of aqueous nano- and microparticle interfaces** *Chem. Rev.* (2006), 106(4), 1462-1477

- Eisenthal, Kenneth B. **Aqueous/nano-microparticle interfaces.** *Abstracts of Papers, 231st ACS National Meeting*, Atlanta, GA, United States, March 26-30, 2006 (2006)
- Eisenthal, Kenneth B. **Equilibrium and ultrafast dynamics at liquid interfaces** *Abstracts of Papers, 231st ACS National Meeting*, Atlanta, GA, United States, March 26-30, 2006 (2006)
- Wong, Paula; Liu, Jian; Subir, Mahamud; Eisenthal, Kenneth B. **Effect of gramicidin A on ion transport across liposome membrane** *Abstracts of Papers, 231st ACS National Meeting*, Atlanta, GA, United States, March 26-30, 2006 (2006)
- McArthur, Eric A.; Eisenthal, Kenneth B. **Ultrafast Excited-State Electron Transfer at an Organic Liquid/Aqueous Interface** *J. Am. Chem. Soc.*(2006), 128(4), 1068-1069
- Rao, Yi; Comstock, Matthew; Eisenthal, Kenneth B. **Absolute Orientation of Molecules at Interfaces** *J. Phys. Chem. B* (2006), 110(4), 1727-1732
- Fitts, Jeffrey P.; Machesky, Michael L.; Wesolowski, David J.; Shang, Xiaoming; Kubicki, James D.; Flynn, George W.; Heinz, Tony F.; Eisenthal, Kenneth B. **Second-harmonic generation and theoretical studies of protonation at the water/ α -TiO₂(110) interface** *Chem. Phys. Lett.* (2005), 411(4-6), 399-403
- Eisenthal, Kenneth B. **Molecules at Aqueous Interfaces.** *Abstracts, 37th Middle Atlantic Regional Meeting of the American Chemical Society, New Brunswick, NJ, United States, May 22-25, 2005*(2005)
- Fitts, Jeffrey P.; Shang, Xiaoming; Flynn, George W.; Heinz, Tony F.; Eisenthal, Kenneth B. **Electrostatic Surface Charge at Aqueous/ α -Al₂O₃ Single-Crystal Interfaces as Probed by Optical Second-Harmonic Generation.** *J. Phys. Chem. B* (2005), 109(16), 7981-7986
- Fitts, Jeffrey P.; Shang, Xiaoming; Machesky, Michael L.; Wesolowski, David J.; Kubicki, James D.; Flynn, George W.; Heinz, Tony F.; Eisenthal, Kenneth B. **Charging behavior at single crystal oxide/water interfaces determined by optical second harmonic generation spectroscopy** *Abstracts of Papers, 229th ACS National Meeting, San Diego, CA, United States March 13-17, 2005* (2005)
- Eisenthal, Kenneth B. **Laser studies of nanoparticle-water interface** *Abstracts of Papers, 229th ACS National Meeting, San Diego, CA, United States March 13-17, 2005* (2005)
- Liu, Jian; Shang, Xiaoming; Pompano, Rebecca; Eisenthal, Kenneth B. **Antibiotic assisted molecular ion transport across a membrane in real time.** *Faraday Discuss.*(2005), 129, 291-299
- Garrett, Bruce C. et al. **Role of water in electron-initiated processes and radical chemistry: issues and scientific advances.** *Chem. Rev.* (2005), 105(1), 355-389
- Benderskii, Alexander V.; Henzie, Joel; Basu, Saonli; Shang, Xiaoming; Eisenthal Kenneth B. **Femtosecond Aqueous Solvation at a Positively Charged Surfactant/water Interface** *J. Phys. Chem. B* (2004), 108(37), 14017-14024
- Eisenthal, Kenneth B.; Xiaoming, Shang; David, Zimdars; Kim, Nguyen; Jian, Liu; Rachel, Pompano. **Molecular dynamics at aqueous interfaces.** *Abstracts of Papers, 228th ACS National Meeting, Philadelphia, PA, United States August 22-26, 2004* (2004)
- Pompano, Rebecca R.; Liu, Jian; Shang, Xiaoming; Eisenthal, Kenneth B. **Laser study of antibiotic assisted molecular-ion transport through lipid bilayers in real time.** *Abstracts of Papers, 227th ACS National Meeting, Anaheim, CA, United States March 28-April 1, 2004*
- Eisenthal, Kenneth B. **Molecules at the liquid interfaces** *Abstracts of Papers, 226th ACS National Meeting, New York, NY, United States Sept.7-11, 2003* (2003)
- Eisenthal, Kenneth B.; Benderskii, Alexander V.; Shang, Xiaoming. **Solvation and rotation dynamics at liquid interfaces** *Abstracts of Papers, 225th ACS National Meeting, New Orleans, LA, United States March 23-27, 2003* (2003)
- McArthur, Eric; Shang, Xiaoming; Eisenthal Kenneth B. **Design and construction of surface second harmonic spectrometer and its application in investigation biological systems** *Abstracts of Papers, 225th ACS National Meeting, New Orleans, LA, United States March 23-27, 2003* (2003)

Interfacial Oxidation of Complex Organic Molecules

G. Barney Ellison — (Grant DE-FG02-93ER14364)

We are building a new experiment to study the oxidation of surfactants coating water droplets. Our instrument is designed to produce a stream of organic aerosols, size-select them and inject them into an atmospheric flow tube where they will be dosed with OH radicals. The resultant oxidized particles will be analyzed with a novel aerosol mass spectrometer.

The device we are fabricating will: a) produce a stream of 1 μm organic aerosols in a flow tube with a VOAG, b) oxidize them with OH/O₂ radicals, and c) to analyze these particles with a novel aerosol mass spectrometer. The organic aerosols will be coated with the ammonium salt of an alcanoic acid such as lauric acid, CH₃(CH₂)₁₀CO₂⁻NH₄⁺. We will use a VOAG to produce a stream of particles of a constant, nominal diam. of 1 μm . A 1 μm organic aerosol contains roughly 10¹⁰ waters in the core and carries about 10⁷ surfactant CH₃(CH₂)₁₀CO₂⁻ ions. The heat of vaporization of water is 40.7 kJ mol⁻¹; therefore it takes roughly 1 nJ to vaporize a 1 μm drop. Our device will use a 10 nsec OPO IR source to dissociate these aqueous droplets. The LaserVision OPO is pumped by a YAG laser and delivers 10 mJ of 2.94 μm (3400 cm⁻¹) radiation focused to a 1 mm spot. The imaginary part of the refractive index of water provides the absorption coefficient and a 1 μm droplet will absorb 6 nJ of the 10 mJ pulse. There are no organic vibrational modes that are resonant with the 3400 cm⁻¹ radiation; all of the 6 nJ will be absorbed by the water core of the particle. The surfactant-coated droplet will completely dissociate and release the carboxylates for analysis by a quadrupole mass filter.

We are fabricating a drift region following the laser/aerosol dissociation region. The drift cell will operate at about 100 Td and it will gently dissociate the RCO₂⁻(water clusters)_n. Photodissociation of a 1 μm droplet in will release 10⁷ ions and a gentle extraction lens (200 V cm⁻¹) will collect the resultant RCO₂⁻ ions into a quadrupole mass filter.

My student Luis Cuadra-Rodriguez has spend several months visiting EMSL at the Pacific Northwest National Laboratories. He has been working in

Dr. A. Zelenyuk's laboratory and has been experimenting with different ways to generate organic aerosols.

The work of Cuadra-Rodriguez and Zelenyuk have focused on the mechanisms of water loss from micron-sized particles. Because of the extremely high particle transmission efficiency of aerodynamic lens inlets, they are widely use in aerosol mass spectrometers. One of the consequences of transporting particles from high ambient pressure into the vacuum is that it is accompanied by a rapid drop in relative humidity (RH). Since many atmospheric particles exist in the form of hygroscopic water droplets, a drop in RH may result in a significant loss of water and even a change in phase. How much water is lost in these inlets is presently unknown. Since water loss can affect particle size, transmission efficiency, ionization probability, and mass spectrum, it is imperative to provide definitive experimental data that can serve to guide the field to a reasonable and uniform sampling approach. In this study, we present the results of a number of highly resolved measurements, conducted under well-defined conditions, of water evaporation from a range of particles, during their transport through an aerodynamic lens inlet. We conclude that the only sure way to avoid ambiguities during measurements of aerodynamic diameter in instruments that utilize low-pressure aerodynamic lens inlets is to dry the particles prior to sampling. This work is described¹ by a paper; further results will be reported² at the American Geophysical Union meeting in Dec. 2006.

¹ Alla Zelenyuk, Dan Imre, and Luis A. Cuadra-Rodriguez, "Evaporation of Water from Particles in the Aerodynamic Lens Inlet: An Experimental Study", *Anal. Chem.* (in press, 2006).

² Luis A. Cuadra-Rodriguez, Alla Zelenyuk, Dan Imre, and G. Barney Ellison, "The Effect Of Organic Surfactants On The Properties Of Common Hygroscopic Particles: Effective Densities, Reactivity And Water Evaporation Of Surfactant Coated Particles," Abstract submitted to AGU (Dec. 2006).

Modeling of Cooperative Phenomena in Surface Reaction Processes

Jim Evans

Ames Laboratory – USDOE and Department of Mathematics,
Iowa State University, Ames, IA 50011

evans@ameslab.gov

PROGRAM SCOPE:

This component of the Chemical Physics Program at Ames Laboratory focuses on the modeling of **heterogeneous catalysis and semiconductor surface phenomena**. This effort integrates *electronic structure analysis, non-equilibrium statistical mechanics, and multi-scale modeling*. The electronic structure component includes development and application in Mark Gordon's group of QM/MM methods (specifically a Surface Integrated Molecular Orbital - Molecular Mechanics approach) to treat adsorption and reaction phenomena on semiconductor surfaces. DFT-VASP analysis by Da-Jiang Liu of chemisorption and reaction energetics on metal surfaces is also utilized. The *non-equilibrium statistical mechanics and multi-scale modeling studies* of surface phenomena by Liu and Evans include Kinetic Monte Carlo (KMC) simulation of atomistic models and coarse-grained continuum formulations. One aspect of this effort relates to heterogeneous catalysis on metal surfaces, where we consider both reactions on extended single crystal surfaces (including connecting atomistic to mesoscale behavior) as well as nanoscale catalyst systems (exploring the role of fluctuations). Another aspect focuses on reaction processes on semiconductor surfaces (including etching and oxidation).

RECENT PROGRESS:

HETEROGENEOUS CATALYSIS ON METAL SURFACES

(i) Atomistic modeling of CO-oxidation on unreconstructed metal(100) surfaces. We have developed realistic atomistic multi-site lattice-gas models and associated efficient KMC simulation algorithms to describe CO-oxidation on unreconstructed metal(100) surfaces under low-pressure conditions [1-3,12]. Essential requirements for realistic modeling include: multiple adsorption sites with distinct binding energies at least for CO; precise determination of adspecies interactions which control ordering in the mixed adlayer; incorporation of rapid surface mobility of CO, and lower but significant mobility of O; realistic description of adsorption-desorption kinetics and of Langmuir-Hinshelwood reaction kinetics. Energetic parameters are determined with guidance from DFT analysis, but typically with some refinement in order to recover key aspects of experimental observations for constituent single-adspecies systems. The initial application was for CO+O/Pd(100) analyzing, e.g., bistability; temperature-programmed reaction kinetics, and ordering in the mixed reactant adlayer. Recent work focused on CO+O/Rh(100) where DFT fails to predict relative binding energies for CO at various sites.

(ii) Multiscale simulation of mesoscale patterns in surface reactions: chemical diffusion in mixed reactant adlayers. We have developed an equation-free Heterogeneous Multiscale Method --- Heterogeneous-Coupled-Lattice-Gas (HCLG) simulation [3,6,14] --- which has successfully connected a realistic description local ordering and reaction kinetics at the atomic level (as described above) to mesoscale pattern formation and front propagation (on the scale of microns). The latter length scale is controlled by rapid diffusion of adspecies such as CO.

Consequently, HCLG requires as input a precise analysis of the chemical diffusivity of such adspecies in interacting mixed reactant adlayers. Thus, we have recently developed and implemented a general algorithm to obtain both thermodynamic and kinetic components of diffusion coefficients in such mixed adlayers [14].

(iii) Fluctuation-induced transitions and sharp fronts in nanoscale reaction systems: Studies of CO-oxidation on metal Field Emitter Tips (FET's) provide a powerful tool for in-situ real-time investigation of fluctuation effects and spatial front formation in nanoscale reaction systems [15]. Previously, we have characterized fluctuation-induced transitions in such bistable systems using simplified lattice-gas models, and also characterized non-equilibrium critical phenomena near cusp points in the bifurcation diagram. Recently, we have applied realistic atomistic modeling to provide a more sophisticated description of such behavior. For higher pressures or lower temperatures, we find non-mean-field-type fluctuation-induced transitions and atomically sharp reaction fronts associated with reactant phase separation [15].

SEMICONDUCTOR SURFACE CHEMISTRY AND SURFACE SCIENCE

(i) Morphological evolution during etching and oxidation of vicinal Si(100). Exposure of vicinal Si(100) to oxygen at ~600C produces step recession due to etching ($\text{Si} + \text{O}(\text{ads}) \rightarrow \text{SiO}(\text{gas}) + \text{vacancy}$) in competition with surface oxide formation ($\text{Si} + 2\text{O}(\text{ads}) \rightarrow \text{SiO}_2$). Vacancies diffuse to and erode steps, whereas oxide islands mask etching of the underlying Si and pin receding steps [8,10]. Our initial atomistic lattice-gas modeling integrated insight from QM/MM analysis in the Gordon group on adsorption dynamics and reaction energetics. The modeling [8,10] recovered the observed dramatic bending of meandering S_B steps around pinning sites, and the snap-off of stiffer S_A steps. Numerous other aspects of behavior were explored including the nature of etch pit nucleation, and mixed-mode pit nucleation and step flow on alternating terraces. Recent work has begun to implement phase-field modeling of surface morphology coupled with appropriate reaction kinetics. This will provide a powerful and versatile toll to analyze reaction phenomena on large length scales and for a broader regime of experimental control parameters (e.g., surface temperature).

(ii) Nucleation of atomic rows of Ga on Si(100). Previously, we implemented atomistic modeling to describe homogeneous nucleation of single-atom-wide metal rows during deposition of Ga on Si(100), in particular explaining the observed unusual row length distribution [9]. Our recent studies considered the effect of heterogeneous nucleation at C-defects [13].

OTHER TOPICS: CATALYSIS IN MESOPOROUS SYSTEMS, ETC.

Our initial studies of catalysis in mesoporous systems focused on developing models to analyze the kinetics of polymerization (e.g., of PPB) within mesoporous silica (MCM-41) which has been functionalized with internal catalysts sites (e.g., Cu^{2+}). We have adopted a stochastic atomistic lattice-gas modeling strategy elucidating the interplay between anomalous diffusive transport of reactant monomers within the mesopore, the distribution of catalytic sites within the pore, and the resulting polymerization kinetics and product polymer chain length distribution.

Other general statistical mechanical studies focus on non-equilibrium phase transitions in cooperative far-from-equilibrium systems (modeling non-linear reaction systems, and population dynamics in biosystems). The goal is to advance understanding of these phenomena to a level comparable to that for equilibrium systems.

FUTURE PLANS:

HETEROGENEOUS CATALYSIS ON METAL SURFACES

(i) CO-oxidation and NO-reduction reactions on metal surfaces of Rh, Pd, etc. We will develop further realistic atomistic models for catalytic reactions on various extended single-crystal metal (111) and (100) surfaces. In addition, such models will be applied to elucidate reaction behavior in nanoscale systems (e.g., on the nanofacets of FET's and supported clusters). Efforts will begin to explore higher-pressure catalysis and associated oxide formation processes. Models will incorporate input from electronic structure studies, and we will analyze reaction behavior primarily utilizing KMC simulation.

(ii) Multiscale modeling of pattern formation in surface reactions. We will continue to develop multiscale algorithms as part of our HCLG approach (including implementation of parallel KMC simulation and efficient algorithms for on-the-fly analysis of chemical diffusion). Most other heterogeneous multiscale methods assume local equilibration, a feature which is often not satisfied in surface reaction systems with long-range ordering of the adlayer. We will pursue specialized approaches to more efficiently treat such systems.

(iii) Experimental Collaborations: adlayer dynamics (STM) and the role of steps (LEEM). We plan to explore surface phenomena related to ordering and dynamics in mixed adlayers on metal surfaces probed by in-situ STM by the Salmeron group. We will also explore the role of steps in reactions, particularly involving NO dissociation. Our goal here is to develop models which couple reaction kinetics to step dynamics, and which allow description of behavior observed with in-situ LEEM by the Imbihl group.

SEMICONDUCTOR SURFACE CHEMISTRY AND SURFACE SCIENCE

Our modeling of etching and other reactions on vicinal Si(100) will focus developing coarse-grained phase-field type formulations to describe morphology on a larger scale than atomistic modeling. This latter approach is potentially highly versatile, allowing efficient integration of various models for the surface chemistry with a computationally efficient framework to describe complex surface morphologies. QM/MM will be applied to provide precise and detailed information on key energetics as input to such modeling. Processes of interest will include etching by oxygen and oxidation, etching via halogens, sputtering, and film growth via CVD.

OTHER TOPICS: CATALYSIS IN MESOPOROUS SYSTEMS, ETC.

We will pursue investigations of the stochastic atomistic model for polymerization kinetics in mesoporous systems, implementing refinements to capture features of existing and planned experiments. Some guidance on the specification of polymer diffusivity may derive from solid-state NMR studies using pulsed field gradient (PFG) methods. Further effort will focus on the "extrusion regime", which is of particular interest for future experimental studies, e.g., ring-opening polymerization of lactide. We aim to model the occurrence of "kinetic phase-transitions" in product output with varying control parameters, such as entropic or other driving forces for extrusion, the distribution of catalytic sites, and control of reactant input (including chiral selectivity) via gatekeepers which could induce diffusion offsets for different reactants.

Analysis will continue of non-equilibrium phase transitions in a variety of stochastic models with application to poisoning in catalytic systems, and cooperative behavior in biosystems.

PUBLICATIONS SUPPORTED BY USDOE FOR 2004-: (*indicates partial SciDAC support)

- [1] *Lattice-Gas Modeling of CO Adlayers on Pd(100)*, D.-J. Liu, J. Chem. Phys. **121**, 4352 (2004), 6pp.
- [2] *Lattice-Gas Modeling of the Formation and Ordering of Oxygen Adlayers on Pd(100)*, D.-J. Liu and J.W. Evans, Surface Science **563**, 13-26 (2004).
- [3] *From Atomic Scale Reactant Ordering to Mesoscale Reaction Front Propagation: CO Oxidation on Pd(100)*, D.-J. Liu and J.W. Evans, Phys. Rev. B **70**, 193408 (2004), 4pp.
- [4] *Crossover between Mean-Field and Ising Critical Behavior in a Lattice-Gas Reaction-Diffusion Model*, D.-J. Liu, N. Pavlenko and J.W. Evans, J. Stat. Phys., **114**, 101-114 (2004).
- [5] *Atomistic Modeling of Morphological Evolution during Simultaneous Etching and Oxidation of Si(100)*, M. Albao, D.-J. Liu, C. H. Choi, M.S. Gordon and J.W. Evans, Surf. Sci. **555**, 51-67 (2004).*
- [6] *Connecting-the-Length-Scales from Atomistic Ordering to Mesoscale Spatial Patterns in Surface Reactions: HCLG Algorithm*, D.-J. Liu and J.W. Evans, SIAM Multiscale Model. **4**, 424-446 (2005)*
- [7] *Kinetic Monte Carlo Simulation of Non-Equilibrium Lattice-Gas Models: Basic and Refined Algorithms applied to Surface Adsorption Processes*, J.W. Evans, Handbook Materials Modeling A, S. Yip, Ed. (Springer, Berlin, 2005), Ch.5.12.*
- [8] *Competitive Etching and Oxidation of Vicinal Si(100) Surfaces*, M.A. Albao, D.-J. Liu, C.H. Choi, M.S. Gordon and J.W. Evans, MRS Proc. **859E**, JJ3.6 (2005), 6pp.*
- [9] *Monotonically Decreasing Size Distributions for One-Dimensional Ga Rows on Si(100)*, M.A. Albao, M.M.R Evans, J. Nogami, D. Zorn, M.S. Gordon and J.W. Evans, Phys. Rev. B **71**, 071523 (2005), 8pp.*
- [10] *Simultaneous Etching and Oxidation of Vicinal Si(100) Surfaces: Atomistic Lattice-Gas Modeling of Morphological Evolution*, M.A. Albao, D.-J. Liu, M.S. Gordon and J.W. Evans, Phys. Rev. B. **72**, 195420 (2005), 12pp.
- [11] *Morphological Evolution during Epitaxial Thin Film Growth: Formation of 2D Islands and 3D Mounds*, J.W. Evans, P.A. Thiel and M.C. Bartelt, Surface Science Reports, **61**, 1-128 (2006).
- [12] *Atomistic Lattice-Gas Modeling of CO-oxidation on Pd(100): Temperature-Programmed Spectroscopy and Steady-State Behavior*, D.-J. Liu and J.W. Evans, J. Chem. Phys. **124**, 154705 (2006), 13pp.
- [13] *Reply to Comment: Monotonically Decreasing Size Distributions for Ga Rows on Si(100)*, M.A. Albao, M.M.R Evans, J. Nogami, D. Zorn, M.S. Gordon and J.W. Evans, Phys. Rev. B **74**, 037402 (2006), 3pp.*
- [14] *Chemical Diffusion in Mixed CO+O Adlayers and Reaction Front Propagation in CO-oxidation on Pd(100)*, D.-J. Liu and J.W. Evans, J. Chem. Phys. **125**, in press (2006), 8pp.*
- [15] *Fronts and Fluctuations in a Tailored Model for CO-oxidation on Unreconstructed Metal(100) Surfaces*, D.-J. Liu and J.W. Evans, J. Phys.: Cond. Matt., to appear (2007). Special issue: *Chemical Kinetics beyond the Textbook: Fluctuations, Many-Particle Effects, and Anomalous Dynamics*, K. Lindenberg, G. Oshanin, M. Tachiya, ed.s.

Liquid and Chemical Dynamics in Nanoscopic Environments (DE-FG03-84ER13251)

Michael D. Fayer
Department of Chemistry, Stanford University, Stanford, CA 94305
fayer@stanford.edu

Liquids and water in particular, are the medium for a vast amount of chemistry ranging from biology to geology. In many systems, water does not exist in its bulk form, but rather in nanoscopic environments in which the water is contained in compartments of one nanometer to a few tens of nanometers in size. In such nanometer environments, the structure and dynamics of water (and other liquids) will be influenced both by confinement and interfacial effects. Important processes, such as chemical reactions and proton transfer, depend on the dynamics of the solvent. This program is addressing the fundamental and technologically important issues of the nature and dynamics of nanoscopic water and how chemical processes, particularly proton transfer, are influenced by nanoscopic environments.

Recently we have made extensive progress in achieving the goals briefly outline above. We are examining the dynamics of water in reverse micelles using ultrafast infrared pump-probe and vibrational echo experiments. We have also obtained the first measurements of the dynamics of water in Nafion membranes used in fuel cells with IR pump-probe experiments. We have obtained important new results on proton dynamics in bulk water and nanoscopic water in reverse micelles through the study of a photoacid using ultrafast UV/Vis methods. The observations and comparison to the direct measurements on nanoscopic water are revealing how confinement on a nanometer length scale influences proton transfer dynamics. In addition, for the first time we have been able to place a photoacid in the nanoscopic pores of Nafion membranes and study the proton transfer dynamics in the membranes. We have also used UV/Vis techniques to study photoinduced electron transfer and geminate recombination in liquids.

Nanosopic Water Dynamics

Reverse micelles have been used in many different applications, from nanoparticle synthesis to enzymatic reactions. The unique chemical nanostructures that are formed when surfactant molecules are mixed with small amounts of water and a nonpolar phase are suitable for bringing hydrophobic and hydrophilic components together at the surfactant interface. We are using reverse micelles as a model system to explore the dynamics of water in confinement. Aerosol OT (AOT) reverse micelles have been studied for decades since they readily form monodispersed spherical nanopools of water. AOT contains an anionic head group with Na^+ counter ions. The size of AOT reverse micelles is readily tunable by adjusting the relative concentrations of water to surfactant in the ternary system. The ratio of these concentrations is given by w_0 ($= [\text{H}_2\text{O}]/[\text{surfactant}]$). We have investigated a comprehensive distribution of reverse micelles ($w_0 = 2 - 60$) using FT-IR absorption spectroscopy, ultrafast infrared vibrational pump-probe, and vibrational echo spectroscopies to elucidate the dynamics of water in confinement.

The OD stretch mode of isotopically mixed water (~5% HOD in H_2O) is used as the experimental probe of water dynamics. Isotopic dilution is essential to keep sample optical densities low (~0.3) and prevent vibrational excitation transport. As the reverse micelle size decreases (i.e. w_0 decreases), the absorption spectra of OD hydroxyl stretch shifts to higher frequency. This indicates that the hydrogen bond network is affected in these systems because the hydroxyl stretch frequency is sensitive to its environment. The featureless absorption spectra do not readily reveal the dynamics of water in reverse micelles because different dephasing mechanisms and timescales are convoluted in the linear absorption line shape.

Pump-probe spectroscopy has the capability of determining the lifetime of a vibrational transition, which can be important because many chemical processes are vibrationally mediated and are affected by how quickly energy is dissipated into the surroundings. The vibrational lifetime of bulk water is observed to be 1.7 ps. The lifetimes are observed to increase with decreasing reverse micelle size. $w_0 = 60$ (28 nm): $T_1 = 1.8$ ps; $w_0 = 40$ (18 nm): $T_1 = 1.7$ ps; $w_0 = 20$ (7 nm): $T_1 = 2.1$ ps; $w_0 = 10$ (4 nm): $T_1 = 2.7$ ps; $w_0 = 5$ (2.6 nm): $T_1 = 4.4$ ps; $w_0 = 2$ (1.7 nm): $T_1 = 5.2$ ps, where the numbers in parenthesis are the water nanopool diameters. Measuring the pump-probe decays at two different polarizations, parallel and perpendicular to the pump pulse, permits the determination of the orientational relaxation of water molecules. Figure 1 displays decays of the orientational anisotropy induced by the polarized pump pulse. Within a few picoseconds water molecules present in the bulk form have sampled most of the

orientational configuration space (decay time 2.6 ps). These motions are dramatically reduced in the smallest reverse micelles; the anisotropies decay in tens of picoseconds. Simple diffusion models of the orientational relaxation cannot capture the complex dynamics that are observed in the small reverse micelles.

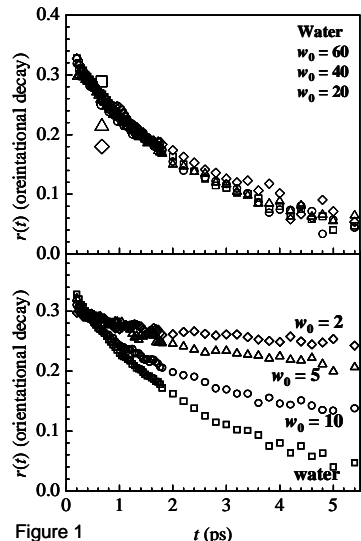


Figure 1

In particular, the orientational anisotropies of the small reverse micelles studied ($w_0 = 10, 5$ and 2) require a bi-exponential functional form to fit the data. We have described the dynamics using a restricted orientational diffusion model ('wobbling in a cone'). This model requires that the water molecules diffuse within a restricted cone of semiangle θ which is followed by full orientational relaxation. The model extracts the diffusion constants for motion in the conical volume as well as motion sampling the sphere of all possible orientations. The two diffusion constants are observed to decrease with decreasing reverse micelle size indicating that all diffusive timescales are affected by confinement in an AOT reverse micelle.

Vibrational echo spectroscopy has the capability of unraveling all contributions to the broadening of a spectroscopic transition. The dynamics and environmental heterogeneity contribute to a great extent in the broadening of the hydroxyl stretch absorption line shape. Spectral diffusion, which reflects how quickly molecules sample all available environments, can be measured using the vibrational echo pulse sequence. The hydroxyl stretch mode is ideally suited to probe fluctuations in the

hydrogen bond network since it is strongly coupled to it.

A convenient way to display the multidimensional data obtained in the vibrational echo experiment is to depict the peak position of the frequency resolved echo trace as a function of T_w (time between second and third pulses). This is shown in figure 2. It is evident that there are essentially two relevant timescales that cause the dephasing of the water molecules in all samples. The fast dynamics are similar in all reverse micelles but the longer spectral diffusion timescale is dramatically affected. It changes from ~ 1.5 ps for bulk water to 15 ps for the $w_0 = 2$ reverse micelles. The fast dynamics are interpreted as local hydrogen bond fluctuations while the longer timescale is attributed to the collective evolution of the hydrogen bond network which involves the making and breaking of hydrogen bonds. This process slows down by an order of magnitude and is consistent with the restricted motion that was observed in the orientational anisotropy data.

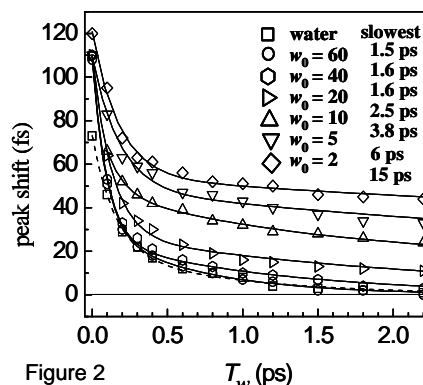


Figure 2

All of the data consistently reveal that dramatic departures from bulk like water occur for reverse micelles smaller than $w_0 = 20$. This defines a length scale for the perturbation of water dynamics since $w_0 = 20$ has a radius of ~ 3.5 nm. Water molecules more than a few of nanometers away from a highly charged interface cannot be dynamically distinguished from water molecules in the bulk. The role of the interface in the dynamics of water is currently under investigation. It is important to determine what types of nanoscopic environments will most strongly influence the dynamics. The nanoscopic water dynamics may be correlated with photoinduced reaction dynamics to determine the role of a nanoscopic environment in chemical processes.

To further study the effects of confinement in a technologically important system, recent experiments have focused on water confined in the pores and channels of the polymer electrolyte membrane, Nafion. The Nafion membrane conducts protons from the anode to the cathode in a fuel cell by way of water molecules absorbed within the membrane. The mechanism of proton conduction is not well understood but it depends critically on the degree of hydration and, therefore, on the dynamical characteristics of the water within the membrane. Nafion is the industry standard fuel cell membrane due to its resilience and high proton conductivity. Much research in fuel cell membranes has focused on creating even more effective alternatives to Nafion and in order to do this, a detailed understanding of the dynamics of water inside the membrane is important. Pump-probe experiments on the dynamics of water in a Nafion membrane not only provide interesting information about the behavior of confined water but also have applications in the design of future fuel cell membranes. In our initial measurements, some of which is published, we have looked at the OD hydroxyl stretch spectrum as well as the vibrational

lifetime and orientational relaxation as a function of hydration (water content). Like reverse micelles, we see dramatic changes as the water content is decreased in all three observables. The hydroxyl spectrum shifts to the blue and its structure changes. The vibrational lifetimes become longer and the orientational relaxation becomes much longer. These experiments are providing the details of the microscopic nature of water in Nafion membranes.

Proton Transfer in Nanoconfinement

In the last several decades there has been a growing interest in how the processes in water change under nanoconfinement. The motivation for study of processes under nanoconfinement becomes clear when one considers how commonly nanometer sized droplets act as a medium for aqueous chemical reactions in biology and important catalytic reactions. Our studies in AOT reverse micelles have shown that the dynamics of water dramatically slow as the size of the water pool is decreased. The goal of this project is to quantitatively understand how these altered properties of water can effect chemical reactions, such as proton transfer reactions, which are ubiquitous in chemical and biological processes. Proton transfer requires a global rearrangement of the water hydrogen bonded network. Therefore, we should expect the different environment of nanoconfined water to dramatically change the nature of a proton transfer reaction relative to the bulk aqueous environment.

Excited state proton transfer (ESPT) has proven to be one of the most useful approaches for studying the dynamics of proton transfer to a solvent. It has long been known that for various classes of aromatic molecules the pK_a in an electronically excited state can decrease relative to the ground state by 7 units or more. Using this property, combined with an ultrafast excitation, the progress of a proton transfer process to the solvent can be followed. 8-hydroxypyrene-1,3,6-trisulfonate (HPTS or pyranine) has been one of the most useful photoacids for studying ESPT.

By measuring the ultrafast UV/Vis pump-probe spectrum of HPTS in reverse micelles we can see how changing the micelle radius affects the dynamics of deprotonation. Pumping the system with an intense ultrafast pulse at 400 nm, we can measure the spectral dynamics of the protonated species. By selection the Depending probe wavelength we can observe either the photoproduct grow in as the acid dissociates (425 nm) or the decay of the reactant (550 nm).

The dynamic for HPTS show three distinct time components. The first accounts for the solvation dynamics of water and happens on a timescale of about 800 fs, which agrees with solvation times measured for similar molecules in water. The next component occurs on a timescale of 3 ps and is

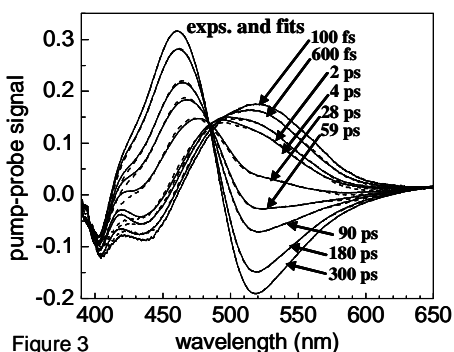


Figure 3

modeled as due to an initial deprotonation step. The second step accounts for full deprotonation and is a much longer process with a characteristic time of around 90 ps. The following mechanism to account for these dynamics was first proposed by Eigen and Weller in 1964 has recently been supported by theoretical models of proton transfer. Figure 3 displays the full spectrum as a function of time (solid curves) for HPTS in water. There are also theoretical fits (dashed curves) that are essentially indistinguishable from the data. The unprecedented quality of the data makes detailed analysis possible. Similar data is obtained for HPTS in the reverse micelles. The trends with micelle size are shown in figure 4. The largest micelles are essentially the same as bulk water except for a long time asymptotic value which is distinct in finite volume. Major differences between bulk water and the confined environment appear for the smaller reverse micelles. The changes begin in the range of sized at which the experiments performed directly on water show substantial differences in hydrogen bond dynamics. For the first time we have been able to put HPTS in Nafion membranes to obtain microscopic details of proton transfer in these fuel cell membranes.

The largest micelles are essentially the same as bulk water except for a long time asymptotic value which is distinct in finite volume. Major differences between bulk water and the confined environment appear for the smaller reverse micelles. The changes begin in the range of sized at which the experiments performed directly on water show substantial differences in hydrogen bond dynamics. For the first time we have been able to put HPTS in Nafion membranes to obtain microscopic details of proton transfer in these fuel cell membranes.

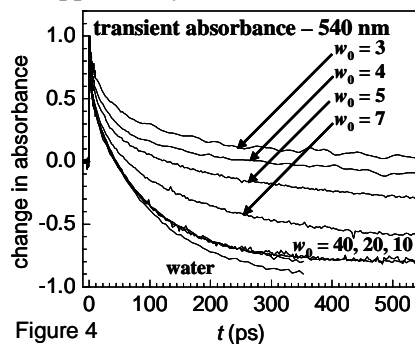


Figure 4

We are continuing all aspects of the work briefly described above. We are examining non-ionic head group reverse micelles to understand the role of the interface on the dynamics of confined water. We are extending our studies of water in Nafion and other confined systems. We are improving the

vibrational echo experiments to full phase sensitive 2D heterodyne detected spectroscopy which provides greater detail. We are continuing the studies of proton transfer, particularly in Nafion and other confined systems.

Publication from DOE Sponsored Research 2003 – present

1. “Orientational Relaxation and Vibrational Excitation Transfer in Methanol - Carbon Tetrachloride Solutions,” K. J. Gaffney, I. R. Piletic, and M. D. Fayer, *J. Chem. Phys.*, **118**, 2270-2278 (2003).
2. “Structural Dynamics of Hydrogen Bonded Methanol Oligomers: Vibrational Transient Hole Burning Studies of Spectral Diffusion,” I. R. Piletic, K. J. Gaffney, and M. D. Fayer, *J. Chem. Phys.* **119**, 423-434 (2003).
3. “Ultrafast Heterodyne Detected Infrared Multidimensional Vibrational Stimulated Echo Studies of Hydrogen Bond Dynamics,” John B. Asbury, Tobias Steinel, C. Stromberg, K. J. Gaffney, I. R. Piletic, Alexi Goun, and M. D. Fayer, *Chem. Phys. Lett.* **374**, 362-371 (2003).
4. “Hydrogen Bond Dynamics Probed with Ultrafast Infrared Heterodyne Detected Multidimensional Vibrational Stimulated Echoes,” John B. Asbury, Tobias Steinel, C. Stromberg, K. J. Gaffney, I. R. Piletic, Alexi Goun, and M. D. Fayer, *Phys. Rev. Lett.* **91**, 237402-1 – 237402-4 (2003).
5. “Hydrogen Bond Breaking Probed with Multidimensional Stimulated Vibrational Echo Correlation Spectroscopy,” John B. Asbury, Tobias Steinel, C. Stromberg, K. J. Gaffney, I. R. Piletic, and M. D. Fayer, *J. Chem. Phys.* **119**, 12981-12997 (2003).
6. “Hydrogen Bond Networks: Structure and Evolution After Hydrogen Bond Breaking,” John B. Asbury, Tobias Steinel, and M. D. Fayer, *J. Physical Chemistry B* **108**, 6544-6554 (2004).
7. “Vibrational Echo Correlation Spectroscopy Probes of Hydrogen Bond Dynamics in Water and Methanol,” John B. Asbury, Tobias Steinel, and M. D. Fayer, *J. Lumin.* **107**, 271-286 (2004).
8. “Photoinduced Electron Transfer and Geminate Recombination for Photoexcited Acceptors in a Pure Donor Solvent,” V. O. Saik, A. A. Goun and M. D. Fayer, *J. Chem. Phys.* **120**, 9601-9611 (2004).
9. “Photoinduced Intermolecular Electron Transfer in Liquid Solutions,” V. O. Saik, A. A. Goun, J. Nanda, Koichiro Shirota, H. L. Tavernier, and M. D. Fayer, *J. Phys. Chem.* **108**, 6696-6703 (2004).
10. “Photoinduced Electron Transfer in the Head Group Region of Sodium Dodecyl Sulfate Micelles,” J. Nanda, P. K. Behera, H. L. Tavernier and M. D. Fayer, *J. Lumin.* **115**, 138-146 (2005).
11. “Dynamics of Water Confined on a Nanometer Length Scale in Reverse Micelles: Ultrafast Infrared Vibrational Echo Spectroscopy,” Howe-Siang Tan, Ivan R. Piletic, Ruth E. Riter, Nancy E. Levinger and M. D. Fayer, *Phys. Rev. Lett.* **94**, 057405(4) (2005).
12. “Orientational Dynamics of Water Confined on a Nanometer Length Scale in Reverse Micelles,” Howe-Siang Tan, Ivan R. Piletic, and M. D. Fayer, *J. Chem. Phys.* **122**, 174501(9) (2005).
13. “The Dynamics of Nanoscopic Water: Vibrational Echo and IR Pump-probe Studies of Reverse Micelles,” Ivan R. Piletic, Howe-Siang Tan and M. D. Fayer, *J. Phys. Chem. B* **109**, 21273-21284 (2005).
14. “Polarization Selective Spectroscopy Experiments: Methodology and Pitfalls,” Howe-Siang Tan, Ivan R. Piletic and M. D. Fayer, *J.O.S.A. B* **22**, 2009-2017 (2005).
15. “Photoinduced Electron Transfer and Geminate Recombination in Liquids on Short Time Scales: Experiments and Theory,” Alexei Goun, Ksenija Glusac, and M. D. Fayer, *J. Chem. Phys.* **124**, 084504(11) (2006).
16. “Testing the Core/Shell Model of Nanoconfined Water in Reverse Micelles Using Linear and Nonlinear IR Spectroscopy,” Ivan R. Piletic, David E. Moilanen, D. B. Spry, and Nancy E. Levinger, M. D. Fayer, *J. Phys. Chem. A* **110**, 4985-4999 (2006).
17. “Photoinduced Electron Transfer and Geminate Recombination in the Group Head Region of Micelles,” Ksenija Glusac, Alexei Goun, and M. D. Fayer, *J. Chem. Phys.* accepted (2006).
18. “What Non-linear IR Experiments Can Tell You About Water That the IR Spectrum Can’t,” Ivan R. Piletic, David E. Moilanen, Nancy E. Levinger, Michael D. Fayer, *J. Am. Chem. Soc.* accepted (2006).
19. “Tracking Water’s Response to Structural Changes in Nafion Membranes,” David E. Moilanen, Ivan R. Piletic, and M. D. Fayer, *J. Phys. Chem. A* **110**, 9084-9088 (2006).
20. “Vibrational Echo and Pump-Probe Spectroscopic Studies of the Dynamics of Water Molecules Confined to Nanoscopic Dimensions,” Ivan R. Piletic, Howe Siang Tan, David E. Moilanen, Ben Spry, and M. D. Fayer, *Femtochemistry VII: Fundamental Ultrafast Processes in Chemistry, Physics, and Biology*; Castleman, A. W., Jr., Kimble, M. L., Eds.; Elsevier: Amsterdam, 195-203 (2006).

Program Title: Electronic Structure Theory: Surface Chemistry, Solvent Effects, and Catalysis

Principal Investigator: Mark S. Gordon, Ames Laboratory, 201 Spedding Hall, Iowa State University, Ames, IA 50011; mark@si.fi.ameslab.gov

Program Scope: This research effort focuses on the exploration of clusters and how clusters relate to condensed phase issues, such as surface science (including surface functionalization and degradation, heterogeneous catalysis, surface growth, surface diffusion), intermolecular forces (including solvent effects on chemical reactions, as well as liquid-liquid and liquid surface phenomena), molecular wires, and new theory and code developments to support and enhance these applications. The surface science effort is part of an ongoing collaboration with the group of Jim Evans. The interface of electronic structure theory with non-equilibrium statistical mechanics at the mesoscale is a particularly powerful combination. All electronic structure theory developments are implemented into the GAMESS (General Atomic and Molecular Electronic Structure Theory) suite of programs.

Recent Progress:

Theory and Code Development. Several new highly parallel electronic structure codes have been developed under the auspices of the SciDAC program. These include closed second order perturbation theory (MP2) energies and gradients¹, unrestricted open shell MP2 energies and gradients^{1,9}, restricted open shell MP2 energies and gradients¹⁹, Full configuration interaction (Full CI) energies², multi-configurational SCF analytic Hessians²⁰, and analytic closed shell Hessian²⁶. An important part of this effort has been new improvements in the Distributed Data Interface (DDI)^{5,7} in GAMESS¹³ that enables the successful parallelism. A particularly exciting new feature in GAMESS is the fragment molecular orbital (FMO) method⁷. The FMO method facilitates accurate computations of very large molecular systems (e.g., tens of thousands of atoms) with very high accuracy by a clever method of dealing with small fragments of the whole, one or two at a time. Because each fragment can be computed essentially independently, the method is very amenable to a high degree of parallelism. Also as part of the SciDAC effort, new advances have been made in the effective fragment potential (EFP) method, a very sophisticated method for treating intermolecular forces without the use of fitted parameters.²⁵ Because many of the clusters of interest to us involve transition metals and other heavier elements, considerable effort has been devoted to developing^{3,6} and applying^{11,22} new methods for treating relativistic effects, such a spin-orbit coupling. A very popular approach for adding non-dynamic correlation to MCSCF calculations is multi-reference second order perturbation theory (MRMP2). Because not all such methods are fully size-consistent, we performed a careful study to show which methods are, and are not, size consistent, and why¹².

Applications. Several studies of clusters have been completed that are related to the Si(100) surface and phenomena that occur on this surface. An earlier study of the molecular and electronic structure of SiC₃ and Si₂C₂ was followed up by a definitive study of the former molecule²¹. Likewise, an initial study of small silicon-oxygen

clusters that employed lower levels of theory (density functional theory and MP2)⁴ was followed by a much broader study based on more reliable coupled cluster methods¹⁷. The latter study was more definitive and unearthed several previously unknown species. Electronic structure calculations for the study of the Si(100) surface can be accomplished using the embedded cluster model SIMOMM (Surface Integrated Molecular Orbital Molecular Mechanics) method developed by us. The advantage of SIMOMM is that the MM part of the calculation is computationally inexpensive, so a large MM regions can be used to represent the bulk. This method was used to study the adsorption of acetylene on the Si(100) surface¹⁰ and etching of the Si(100) surface^{8,18}. The latter work is an excellent example of using the insight gained from electronic structure theory as input into large-scale kinetic Monte Carlo (KMC) simulations. A long-term combined electronic structure-KMC effort in the study of the adsorption, diffusion, and growth of Group III metals (Al, Ga, In) onto the Si(100) surface was initiated by a study of Ga on Si(100)^{14,24}. Because there is considerable interest in the solvation of small ions, a systematic study was performed on adding water molecules to F⁻ and Cl⁻, using MP2, Hartree-Fock, and the EFP method¹⁵. All three methods agree that small clusters have the ion on the surface of the water cluster, but that interior ions are the lowest energy species once the number of waters increases to about 12 (F⁻) or 18 (Cl⁻). The CEEIS (Correlation Energy Extrapolation by Intrinsic Scaling) method developed by Bytautas and Ruedenberg was applied to the complete potential energy curve of F₂, leading to sub-cm⁻¹ accuracy for all vibrational frequencies and the discovery of at least one new vibrational energy level²³. Finally, a very exciting new theory-experiment collaboration has been initiated to study 3-D heterogeneous catalysis in SiO pores. This effort involves the groups of Lin, Pruski, Angelici, and Sadow, as well as the Evans group.

Future Plans:

Theory and Code Development. In order to expand the feasible size of the QM region in SIMOMM, a parallel ORMAS code will be developed. ORMAS (Occupation Restricted Multiple Active Spaces), like FMO, facilitates a subdivision of an MCSCF active space and therefore greatly increases the size of an MCSCF calculation that is feasible. As part of the 3-D catalysis effort, we plan to interface the EFP method with the MM part of SIMOMM, so that solvent effects on the catalysis process can be studied. This will have broader implications, because an EFP-MM interface will allow GAMESS users to study a wide variety of interfacial chemistry. The SIMOMM method itself will be extended to be applicable to the silica and alumina surfaces that are important to the catalysis effort. The EFP method will be extended to treat open shell species (e.g., OH) and gradients for the EFP interface with the QM region will be developed further and implemented into GAMESS. In order to enhance our ability to study excited state chemistry in the presence of a solvent, interfaces between EFP and a series of excited state QM methods will be developed and implemented.

Applications. Our effort in surface science, often in collaboration with the Evans, Lin, and Pruski groups, will focus on phenomena that occur on the Si(100) surface, and on the silica, alumina, and doped silica surfaces of importance to the 3-D catalysis effort. Previous calculations on the oxygen-based etching of Si(100) predicted some barrier heights that seemed to be too high, based on the KMC predictions. It is not clear at this

point whether the root cause is the electronic structure theory, the KMC model, or misinterpretation of the experiments. To address the first issue, we will revisit the electronic structure calculations with much larger basis sets and higher levels of theory. We will also address some new issues related to etching, including oxygen diffusion on the surface and etching by other species, such as Cl. Studies of Group III elements on the Si(100) surface will continue with both Al and Ga, employing the parallel ORMAS method to expand the size of the QM cluster. Calculations related to the 3-D heterogeneous catalysis project have been initiated and will continue. The potential energy surface for the catalyzed Henry (nitroaldol) reaction will be completed. Several “preparatory” calculations on the species that are present on the silica surface, and the interactions among these, will be completed. These gas phase calculations will provide us with a baseline against which the SIMOMM calculations on the silica surface can be compared. Several calculations that involve water are planned or have been initiated, all using the EFP method. These include a systematic cluster-based analysis of the solvation of NaOH, including the ionization potential of Na and the electron affinity of Cl, as a function of the number of waters present, and a systematic study of the origin of the dipole moment enhancement in liquid water

References:

1. C. M. Aikens, S. P. Webb, R. Bell, G.D. Fletcher, M.W. Schmidt, and M.S. Gordon, “A derivation of the frozen-orbital unrestricted open shell and restricted closed shell MP2 analytic gradient expressions”, *Theor. Chem. Accts.*, **110**, 233 (2003).
2. Z. Gan, Y. Alexeev, R.A. Kendall, and M.S. Gordon, “The Parallel Implementation of a Full CI Program”, *J. Chem. Phys.*, **119**, 47 (2003).
3. D.G. Fedorov, S. Koseki, M.W. Schmidt and M.S. Gordon, “Spin-orbit coupling in Molecules: Chemistry beyond the adiabatic approximation”, *Int. Revs. Phys. Chem.*, **22**, 551 (2003).
4. W.C. Lu, C.Z. Wang, V. Nguyen, M.W. Schmidt, M.S. Gordon and K.M. Ho, “Structures and Fragmentation of Small Silicon Oxide Clusters by *ab initio* Calculations, *J. Phys. Chem.*, **A107**, 6936 (2003).
5. R.M. Olson, M.W. Schmidt, M.S. Gordon, and A.P. Rendell, “Enabling the Efficient Use of SMP Clusters: The GAMESS/DDI Model”, *Proc. Supercomputing*, **2003**
6. D. Fedorov, M.W. Schmidt, S. Koseki, and M.S. Gordon, “Spin-Orbit Coupling and Applications to Chemistry”, “Recent Advances in Relativistic Molecular Theory”, Vol. 5, K. Hirao and Y. Ishikawa, Eds., World Scientific, Singapore, pp. 107-136, 2004.
7. D.G. Fedorov, R.M. Olson, K. Kitaura, M.S. Gordon, and S. Koseki, “A new hierarchical parallelization scheme: Generalized distributed data interface (GDDI), and an application to the fragment molecular orbital method (FMO)”, *J. Comp. Chem.*, **25**, 872 (2004).
8. M.A. Albao, D.-J. Liu, C.H. Choi, M.S. Gordon, and J.W. Evans, “Atomistic Modeling of Morphological Evolution Due to Competition Between Oxidation and Etching of Si(100)”, *Surface Science*, **555**, 51 (2004).
9. C.M. Aikens and M.S. Gordon, “Parallel Unrestricted MP2 Analytic Gradients using the Distributed Data Interface”, *J. Phys. Chem.*, **108**, 3103 (2004).
10. J.M. Rintelman and M.S. Gordon, “Adsorption of Acetylene on Si(100)-(2x1)”, *J. Phys. Chem.*, **108**, 7820 (2004).

11. S. Koseki, Y. Ishihara, D.G. Fedorov, M.W. Schmidt and M.S. Gordon, "Dissociation Potential Curves of Low-Lying States in Transition Metals. II. Hydrides of Groups 3 and 5", *J. Phys. Chem.*, **108**, 4707 (2004).
12. J.M. Rintelman, I. Adamovic, S. Varganov, and M.S. Gordon, "Multi-Reference Second-Order Perturbation Theory: How Size Consistent is 'Almost Size Consistent'?", *J. Chem. Phys.*, **122**, 044105 (2005).
13. M.S. Gordon and M.W. Schmidt, "Advances in Electronic Structure Theory: GAMESS a Decade Later", *Theory and Applications of Computational Chemistry*, Ch. 41, C. E. Dykstra, G. Frenking, K.S. Kim, G.E. Scuseria, Eds., Elsevier, 2005.
14. M.A. Albao, M.M.R. Evans, J. Nogami, D. Zorn, M.S. Gordon, and J.W. Evans, "Monotonically decreasing size distributions for one-dimensional Ga Rows on Si(100)", *Phys. Rev. B*, **72**, 035426 (2005).
15. D.D. Kemp and M.S. Gordon, "Theoretical Study of the Solvation of Fluorine and Chlorine Anions by Water", *J. Phys. Chem* **A109**, 7688 (2005). [**13th most downloaded paper july-sept 2005**]
16. Marvin A. Albao, Da-Jiang Liu, Cheol H. Choi, Mark S. Gordon, and J. W. Evans, "Competitive Etching and Oxidation of Vicinal Si(100) Surfaces", *MRS Proceedings Vol. 859E* (2005) JJ3.6
17. P.V. Avramov, I. Adamovic, K.-M. Ho, C.Z. Wang, W.C. Lu, and M.S. Gordon, "Potential Energy Surfaces of Si_mO_n Cluster Formation and Isomerization", *J. Phys. Chem.*, **A109**, 6294 (2005).
18. M. Albao, D.-J. Liu, M.S. Gordon, and J.W. Evans, "Simultaneous Etching and Oxidation of Vicinal Si(100) Surfaces: Atomistic Lattice-Gas Modeling of Morphological Evolution", *Phys. Rev. B*, **72**, 195420 (2005).
19. C.M. Aikens and M.S. Gordon, "Scalable Implementation Of Analytic Gradients For Second-Order Z-Averaged Perturbation Theory Using The Distributed Data Interface", *J. Chem. Phys.*, **124**, 014107 (2006).
20. T.J. Dudley, R.M. Olson, M.W. Schmidt, and M.S. Gordon, "Parallel Coupled Perturbed CASSCF Equations and Analytic CASSCF Second Derivatives", *J. Comp. Chem.*, in press.
21. J.M. Rintelman, M.S. Gordon, G.D. Fletcher, and J. Ivanic, "Reinvestigation of SiC₃ with multireference perturbation theory", *J. Chem. Phys.*, **124**, 034303 (2006).
22. S. Koseki, T. Matsushita, and M.S. Gordon, "Dissociation Potential Curves of Low-Lying States in Transition Metal Hydrides. III. Hydrides of Groups 6 and 7", *J. Phys. Chem*, **A110**, 2560 (2006).
23. L. Bytautas, N. Matsunaga, T. Nagata, M.S. Gordon, and K. Ruedenberg, "Full *ab initio* determination of the potential energy curve and the vibrational energy spectrum of the fluorine molecule to wavenumber accuracy by a new quantum chemical method", *Phys. Rev. Lett.*, submitted.
24. M.R. Albao, M.M.R. Evans, J. Nogami, D. Zorn, M.S. Gordon, and J.W. Evans, Reply to 'Comment on "Monotonically decreasing size distributions for one-dimensional Ga rows on Si(100)"', *Phys. Rev. B*, **74**, 1 (2006).
25. H. Li and M.S. Gordon, "Gradients of the Polarization Energy in the Effective Fragment Potential Method", *J. Chem. Phys.*, submitted.
26. Y. Alexeev, M.W. Schmidt, T.L. Windus, M.S. Gordon, "A Parallel Distributed Data CPHF Algorithm for Analytic Hessians", *J. Comp. Chem.*, submitted.

COMPUTATIONAL NANOPHOTONICS: MODELING OPTICAL INTERACTIONS AND TRANSPORT IN TAILORED NANOSYSTEM ARCHITECTURES

Stephen K. Gray (gray@tcg.anl.gov),¹ Julius Jellinek (jellinek@anl.gov),¹
George C. Schatz (schatz@chem.northwestern.edu),² Mark A. Ratner
(ratner@chem.northwestern.edu),² Mark I. Stockman (mstockman@gsu.edu),³ Koblar A.
Jackson (jackson@phy.cmich.edu),⁴ Serdar Ogut (ogut@uic.edu)⁵

¹Chemistry Division, Argonne National Laboratory, Argonne, IL 60439; ²Department of Chemistry, Northwestern University, Evanston, IL 60208; ³Department of Physics and Astronomy, Georgia State University, Atlanta, GA 30303; ⁴Department of Physics, Central Michigan University, Mt. Pleasant, MI 48859; ⁵Department of Physics, University of Illinois at Chicago, Chicago, IL 60607

PROGRAM SCOPE

Computational methods are used to study light interactions with nanosystems. Metal nanoparticles (MNPs) and nanoscale holes in metal films are of particular interest. Microscopic studies of electronic, structural and optical properties, and continuum-level electrodynamic studies are involved. A goal is to learn how to confine and manipulate electromagnetic energy on the nanoscale. A wide range of methods is needed, and another goal is to develop a suite of nanophotonics simulation tools. We also work with applied mathematicians and computer scientists in developing algorithms and software with high-performance capabilities.

At a microscopic level, we must understand the mechanisms underlying the assembly of atoms into clusters and clusters into larger systems. Understanding these mechanisms and the parameters they depend on is essential for designing cluster-based architectures with desired nanophotonics properties. Atomic-level mechanisms are ultimately defined by interatomic interactions. Accurate, efficient descriptions of these interactions are sought in order to uncover correct mechanisms. This work also provides optical information, e.g. static and dynamic polarizabilities, for the estimation of size-dependent dielectric properties relevant to our electrodynamic work.

Numerical solutions of Maxwell's equations, assuming certain dielectric properties, are used to model light interacting with various nanosystems. The solutions allow us to develop an understanding of physical phenomena such as surface plasmons (SPs). SPs are collective electronic excitations near the surfaces of metallic structures. The intensity and localization of SPs make them relevant to chemical and biological sensing, nanoscale optics and optoelectronics.

RECENT PROGRESS

Microscopic Studies of Electronic, Structural and Optical Properties: The development of accurate, computationally efficient semiempirical many-body potentials for metals is crucial for predictive large-scale dynamical simulations of assembly of nanosystems relevant to nanophotonics. One central issue is the best choice of the set of fitting properties ("defining set") from a given manifold of known (e.g., measured) properties. Different metals are, in general, characterized by different defining sets. Some metals (e.g., Au) possess more than one defining set. We find that our fitting procedure is robust in that even in this latter case it defines the values of the adjustable parameters uniquely. Extending our earlier work on Ni and Ag MNPs, and in collaboration with M. J. Lopez, we used our new Au potential to perform extensive simulations of structural forms of Au particles with up to ~ 2000 atoms (~ 4.4 nm). The size-evolution of the preferred structural motif(s) we find is different from that suggested by earlier studies. This evolution is characterized by competition between icosahedral (I_h) and decahedral (D_h) structures. This competition has, in fact, been observed experimentally in gas phase and deposited Au MNPs of 3-18 nm in sizes [K. Koya *et al.*, *Phys. Rev. Lett.* **92**, 115507 (2004)]. We also constructed a

new potential for Al using bulk and dimer properties and are applying it to determine structural and thermal properties of Al MNPs.

As a paradigm of a supported nanophotonic system, we studied the (101) face of alpha-quartz doped with Ag (one Ag atom per surface of a unit cell). Three cuts of this surface, which expose different O and/or Si atoms, were explored. State-of-the-art density functional theory (DFT) computations were used to characterize the pristine surfaces as well as the various Ag bonding arrangements on them, including their binding energies and charge-transfer characteristics. We found that the energetically preferred arrangements correspond to insertion of the Ag atoms into the Si-O rings formed by the pristine surfaces. An interesting insertion mechanism is the one that is accompanied by the rings opening up and joining to form helices that run along the quartz surface. Data obtained in this work will be used as input for construction of accurate, efficient variable-charge and polarizable force fields for large-scale dynamical simulations of assembly of photonic nanoarchitectures on supports.

We carried out DFT explorations of structural, electronic and optical properties of metal and semiconductor clusters of relevance to nanophotonics. The most systematic and complete to date study of Ag_n , $n = 9-20$, [28], drawing upon a large database of structures obtained in our earlier work [29], revealed that, contrary to results based on empirical potentials, Ag_n clusters do not follow an icosahedral growth pattern. Instead, the lowest-energy conformations of Ag_n are double-layered, platelet-like structures for $n = 9-16$, and they become near-spherical, compact arrangements for $n \geq 17$. Signatures of this size-induced structural/shape transition are found in the cohesive energy, relative stability, and dipole polarizability of the clusters. The IPs and the HOMO-LUMO gaps computed for the most stable conformations are in good agreement with measured data, corroborating the correctness of the predicted structures. Interestingly, the most stable conformations of Ag_n are the same as those of Cu_n over the size range $n = 9-20$, and the size-evolution of both closely resembles that of Na_n . This means that the d -electrons play only a minor role in defining the structural characteristics of Ag_n and Cu_n clusters.

DFT was also used to study the structural forms and electronic properties of anionic Si_n^- , $n = 20-45$ [30], and neutral As_n , $n \leq 28$, identifying new energetically competitive isomers and general structural motifs [31]. Computed spectra of electron binding energies were compared with measured photoelectron spectra (PES). We found that the PES measured for Si_{27}^- clearly reflects the prolate-to-near-spherical shape transition in Si_n^- at $n = 27$. We extended our earlier comparative study of hollow cage vs space-filling structures of Au_n , $n=32, 38, 44, 50, 56$ [7], to their dipole moments and polarizabilities [32]. These characteristics not only carry the fingerprints of the two classes of structures, but show opposite trends in their size-evolution in these classes.

Static and time-dependent DFT (TDDFT) were used to explore isomer-specificity of the dipole polarizabilities and optical absorption spectra of small Ag_n , $n=1-8$, and Au_n , $n = 1-3$, clusters [33] (cf. also [12]). Both show clear isomer-dependence, and it is the spectra computed for the most stable structures that agree with the measured data best. The analysis reveals the important role of the d electrons in the optical transitions: 1) They screen the s electrons, which results in reduction of the associated oscillator strengths, and 2) They contribute directly to the transitions even at low energies. Both effects are stronger in Au_n , which is a consequence of the closer proximity and, consequently, higher degree of hybridization of the s and d levels in Au than in Ag.

We also explored the optical properties of Si_n , $n = 20-28$ [34], revealing that prolate and compact structures of these clusters have distinctly different spectra. The positions and intensities of the lines and their overall size-evolution can be explained remarkably well within the *classical* Mie theory, which was originally developed to characterize light absorption by MNPs.

Comparison with experimental data for Si_{21} shows that it is the spectrum of the prolate isomer (which is 0.5 eV more stable than its compact counterpart) that is in accord with experiment.

A new methodological development was our formulation of a general scheme for partitioning the total dipole moment and polarizability of an n -atom system into site-specific (e.g., atomic) contributions. [35]. It is based on partitioning the space into nonoverlapping “site” (e.g., “atomic”) volumes. Site-specific contributions are further partitioned into dipole (dielectric-type) and charge transfer (metallic-type) components. We used this scheme to obtain insight into the response of Si_n clusters to an external electric field. We found: 1) The response is indeed strongly site-specific – surface atoms possess considerably larger polarizabilities than interior atoms; 2) The contribution of the charge transfer components to the total polarizability increases with cluster size; 3) The anisotropy of the cluster shape affects its polarizability. Prolate clusters, for example, respond stronger to fields along the prolate axis than to fields perpendicular to it. We will apply the new scheme to a variety of systems to gain a more fundamental understanding of their material-, size-, structure-, and charge-state-dependent properties, including photonic ones.

Electrodynamics Studies: The electromagnetic fields that result when light interacts with nanostructures are predicted with rigorous computational methods such as the discrete dipole approximation (DDA) and the finite-difference time-domain (FDTD) method, as well as with methods appropriate to particular situations such as the quasistatic method.

DDA has been applied to triangular prisms, cubes and other anisotropic MNP structures. Previously, we worked with the Mirkin group to study Au triangular prisms that they have synthesized, leading to the first observation of quadrupole resonance effects for this particle shape [13]. We also characterized the properties of higher multipole resonances [14]. Recently we studied pyramid-shaped Au MNPs that the Odom group has fabricated. These are relatively large MNPs, so there are complex multipolar excitations, but the calculated results are in good qualitative agreement with experiment. A unique contribution was the characterization of the wave vector dependence of the SP resonance wavelength of one of the quadrupolar resonances, which is something that has not been done before for localized SP resonances.

The FDTD method was used to study the interaction of light with holes in metal films, including the contrast between SP excitation in particles vs holes, and the influence of SP excitation on the transmission of light through the holes. For isolated holes [38] we demonstrated SP enhanced transmission. However the enhancement effects from these studies are quite modest ($< 10\%$). Larger enhancements (400%) are obtained if each hole is surrounded by circular grooves, or is in an array with the appropriate spacing. We also characterized field enhancement factors, $g^2 = |\mathbf{E}|^2/|\mathbf{E}_0|^2$ [39], which for isolated holes are similar in size to those for a sphere, $g^2 \sim 10^2$. For holes surrounded by optimal grooves, the enhancement is larger ($g^2 \sim 10^3$). Since surface enhanced Raman scattering (SERS) is enhanced by g^4 , the large field enhancement values are such that nonresonant SERS measurements should be possible.

Other FDTD work involved calculations of the near-field patterns of hole arrays to affirm the unique sensitivity of a newly proposed near-field optical spectroscopy (NSOM) method [39, 40], and a study of ellipsoidal cross section shaped nanowires of relevance to SERS [41], and a study of light interactions with nanoscale slits in metals [21]. This latter study showed, remarkably, that voids in metallic structures can be used to transport and bend light with remarkable efficiency, a result of relevance to the development of dense, all-optical, nanoscale circuitry.

The final set of electrodynamic studies we discuss involve the use of quasistatic method codes, which are appropriate to small particle sizes compared to the applied wavelength.

We predicted that an efficient nanolens, which is a self-similar aggregate of a few MNPs, in an active medium of semiconductor quantum dots is an efficient spaser [22]. We also developed a

theory of second-harmonic generation by a nanolens [23]. The second harmonic local fields form a very sharp nanofocus between the smallest MNPs where these fields are enhanced by more than two orders of magnitude. This effect can be used for diagnostics and nanosensors. We recently investigated this class of phenomena to predict and describe giant fluctuations of local SH fields in random nanostructures [24].

We modeled two-pulse coherent control of electron photoemission in a complex random metallic nanosystem, as well as a specially designed V-shaped nanoantenna. showing one can localize the ultrafast optical fields with spatial resolution down to 2 nm [25]. In the nanoantenna, it is possible to control on a nanometric scale the position of the photoemission hot spot.

Finally, we described the interaction of ultrashort infrared laser pulses with clusters and dielectrics. Rapid ionization occurs on a sub-laser wavelength scale below the conventional breakdown threshold. It starts with the formation of nanodroplets of plasma that grow like forest fires, without any need for heating of the electrons promoted to the conduction band. This effect is very important for the physics of laser damage of semiconductors and dielectrics by a moderate-intensity radiation. This research has recently been extended to include some effects of the nanostructured plasmas generated in the process of the photoinduced damage (modification) of the solids [26].

FUTURE PLANS

Our effort directed at construction of more accurate, efficient semiempirical potentials for MNPs and particle-support systems will be expanded to include Cu, Pt, and Pd. In addition to pure particles, we will also consider bimetallic ones. The new potentials will be used in large-scale dynamical simulations of cluster-based nanoassembly. The assembly mechanisms will be studied as a function of cluster size and composition, as well as the characteristics of the supports. As a means of achieving assembly of nanostructures with desired photonic properties, we will study the role of patterning of the supports. An important aspect will be exploration of the thermal stability of the assembled nanosystems.

We will continue DFT explorations of structural, electronic and optical properties of metal and semiconductor clusters. Emphasis will be on the size-evolution of properties, and the studies will be extended to clusters of larger sizes. Among the central issues will be isomer-specificity of the dielectric and optical features. In addition to the neutral clusters, we will explore their anionic and cationic counterparts. For some metals, such as Cu and Ag, we expect the charged clusters to exhibit size-driven shape transitions similar to those found in their neutral counterparts, albeit at different sizes consistent with the electron shell-filling model. We will take advantage of the fact that for anionic clusters measured size-resolved PES are available. We will use these PES as benchmarks for evaluation of our computed isomer-specific spectra of electron binding energies and, consequently, the validity of the predicted structures. Bimetallic clusters will also be considered. We will study the effects of doping of a pure cluster by one or more atoms of another element as a means of altering (possibly even tuning) its dielectric and optical properties. The systems for which we will explore optical properties include pure and hydrogen-passivated Si nanospheres.

Further development and application of our site-specific polarizability methodology will occur. It will provide a unifying tool in the analyses of different size-driven properties and phenomena and a means of understanding possible correlations and couplings between them. For example, we will apply it to analyze the size-driven changes in dielectric and optical properties, on the one hand, and the size-induced transition to metallicity, on the other, as well as the possible connection between the two. We will extend the formulation to include heterosystems and systems with defects and will apply the extended approach to analyze bimetallic clusters, nanosystems with defects and voids, and the effects of different surface terminations. Our

methodological work will also include further analysis of the GW-Bethe-Salpeter approach and its comparative evaluation vs TDDFT in collaboration with J. R. Chelikowsky.

The ultimate goal of these studies is to obtain a fundamental understanding of the finite-size aspects of the dielectric and optical properties of nanosystems and the dependence of these properties on size, structure, and composition. This understanding will lead to formulation of physical models for efficient evaluation and analysis of photonic characteristics over a broad range of sizes and connection with the electrostatics description of the bulk limit.

Our electrostatics work will involve continued work on the MNP and hole/metal film systems, as well as an increased focus on the coupling of these systems to nonlinear materials and microscopic features.

We will continue working on hole arrays and related structures in metallic thin films. In particular, the complex near-fields and transmission spectra that we have previously been able to understand with the aid of our FDTD calculations for simple hole arrays [15, 17], makes such structures good candidates to be highly sensitive biological and chemical sensors. With this in mind, and in collaboration with the Odom and Rogers experimental groups, we will investigate the fundamental properties of more structured hole array systems.

A new FDTD code will be developed that uses hexagonal grid elements, which will have superior convergence properties compared to square grid codes. We will use it to characterize hard problems, such as particles with sharp points and very large ($> 1 \mu\text{m}$) structures. We will work with our mathematics and computer science collaborators on the development of a 3D, adaptive mesh refinement (AMR), FDTD code. This work will build on the 2D AMR-FDTD code [44]. We also will develop 2D and 3D finite-element-based codes, to complement the FDTD ones.

We will study the coupling of plasmonic systems to nonlinear materials and molecular systems. The near fields and optical properties that arise from introduction of a Kerr nonlinear material between two MNPs will be studied with the FDTD method. A combined nanophotonics/molecular electronics problem, involving MNP electrodes linked by molecular wire will be modeled. Finally, we will develop and apply methods in which electrostatics is combined with quantum chemistry to model enhanced infrared, Raman and nonlinear optical processes, as well as to connect more directly with the microscopic components of our program.

PUBLICATIONS OF DOE SPONSORED RESEARCH (2004-2006)

1. Unraveling the shape transformation in silicon clusters, K. A. Jackson, M. Horoi, I. Chaudhuri, Th. Frauenheim and A. A. Shvartsburg, *Phys. Rev. Lett.* **83**, 013401 (1-4) (2004).
2. Surface plasmons at single nanoholes in Au-films, L. Yin, V. K. Vlasko-Vlasov, A. Rydh, J. Pearson, U. Welp, S.-H. Chang, S. K. Gray, G. C. Schatz, D. E. Brown, and C. W. Kimball, *Appl. Phys. Lett.* **85**, 467-469 (2004).
3. Dipolar emitters at nanoscale proximity of metal surfaces: Giant enhancement of relaxation, I. A. Larkin, M. I. Stockman, M. Achermann, and V. I. Klimov, *Phys. Rev. B* **69**, 121403(R) (1-4) (2004).
4. Coherent control of nanoscale localization of ultrafast optical excitation in nanosystems, M. I. Stockman, D. J. Bergman, and T. Kobayashi, *Phys. Rev. B* **69**, 054202 (1-10) (2004).
5. Plasmon hybridization in nanoparticle dimers, P. Nordlander, C. Oubre, E. Prodan, K. Li, and M. I. Stockman, *Nano Letters* **4**, 899-903 (2004).
6. Nanofocusing of optical energy in tapered plasmonic waveguides, M. I. Stockman, *Phys. Rev. Lett.* **93**, 137404 (1-4) (2004).
7. Hollow cages versus space-filling structures for medium-Sized gold clusters: The spherical aromaticity of the Au₅₀ cage, J. Wang, J. Jellinek, J. Zhao, Z. Chen, R. B. King and P. v. R. Schleyer, *J. Phys. Chem. A*, **109**, 9265-9269 (2005).

8. Stuffed fullerene structures for medium-sized silicon clusters, J. Zhao, J. Wang, J. Jellinek, S. Yoo, and X. C. Zeng, *Eur. Phys. J. D* **34**, 35-37 (2005).
9. First-principles investigations of the polarizability of small and intermediate-sized Cu clusters, M. Yang and K. Jackson, *J. Chem. Phys.* **122**, 184317 (2005).
10. Statistical evaluation of the big bang search algorithm, K.A. Jackson, M. Horoi, I. Chaudhuri, Th. Frauenheim, and A. A. Shvartsburg, *Comp. Mater. Sci.* **35**, 232-237 (2005).
11. Shape, polarizability and metallicity in Si clusters, K. A. Jackson, I. Chaudhuri, M. Yang, and Th. Frauenheim, *Phys. Rev. A* **71**, 033205 (1-6) (2005).
12. Size dependence of static polarizabilities and optical absorption spectra of Ag_n (n = 2 – 8) clusters from first principles, J. C. Idrobo, S. Ogut, and J. Jellinek, *Phys. Rev. B* **72**, 085445 (1-8) (2005).
13. Observation of the quadrupole plasmon mode for a colloidal solution of gold nanoprisms, J. E. Millstone, S. Park, K. L. Shuford, L. Qin, G. C. Schatz and C. A. Mirkin, *J. Am. Chem. Soc.* **127**, 5312-5313 (2005).
14. Multipolar Excitation in Triangular Nanoprisms, K. L. Shuford, M. A. Ratner and G. C. Schatz, *J. Chem. Phys.* **123**, 114713 (1-9) (2005).
15. Surface plasmon generation and light transmission by isolated nanoholes and arrays of nanoholes in thin metal films, S.-H. Chang, S. K. Gray and G. C. Schatz, *Optics Express* **13**, 3150-3165 (2005).
16. Electrodynamics simulations of surface plasmon behavior in metallic nanostructures, S. K. Gray, T.-W. Lee, S.-H. Chang and G. C. Schatz, *Proc. SPIE Int. Soc. Opt. Eng.* **5927**, 96 (2005).
17. Surface plasmon standing waves in large-area subwavelength hole arrays, E.-S. Kwak, J. Henzie, S.-H. Chang, S. K. Gray, G. C. Schatz, and T. W. Odom, *Nano Lett.*, **5**, 1963-1967 (2005).
18. Near-field photochemical imaging of noble metal nanostructures, C. Hubert, A. Rumyantsev, G. Lerondel, J. Grand, S. Kostcheev, L. Billot, A. Vial, R. Bachelot, P. Royer, S.-H. Chang, S. K. Gray, G. P. Wiederrecht, and G. C. Schatz, *Nano Lett.* **5**, 615-619 (2005).
19. Controlled spatiotemporal excitation of metal nanoparticles with chirped optical pulses, T.-W. Lee and S. K. Gray, *Phys. Rev. B*, **71**, 035423 (1-9) (2005).
20. Regenerated surface plasmon polaritons, T.-W. Lee and S. K. Gray, *Appl. Phys. Lett.* **86**, 141105 (1-3) (2005).
21. Subwavelength light bending by metal slits, T. W. Lee and S. K. Gray, *Optics Express*, **13**, 9652-9659 (2005).
22. Surface plasmon amplification by stimulated emission in nanolenses, K. Li, Xiangting Li, M. I. Stockman, and D. J. Bergman, *Phys. Rev. B* **71**, 115409 (1-4) (2005).
23. Enhanced second harmonic generation in a self-similar chain of metal nanospheres, K. Li, M. I. Stockman, and D. J. Bergman, *Phys. Rev. B* **72**, 153401(1-4) (2005).
24. Giant fluctuations of second harmonic generation on nanostructured surfaces, M. I. Stockman, *Chem. Phys.* (invited paper) **318**, 156-162 (2005).
25. Nanolocalized nonlinear electron photoemission under coherent control, M. I. Stockman and P. Hewageegana, *Nano Lett.* **5**, 2325-2329 (2005).
26. Hole-assisted energy deposition in dielectrics and clusters in the multiphoton regime, L. N. Gaier, M. Lein, M. I. Stockman, G. L. Yudin, P. B. Corkum, M. Y. Ivanov, and P. L. Knight, *J. Mod. Optics* **52**, 1019-1030 (2005).
27. Imperfect perfect lens, I. A. Larkin and M. I. Stockman, *Nano Lett.* **5**, 339-343 (2005).
28. First-principles study of intermediate size silver clusters: Shape evolution and its impact on cluster properties, M. Yang, K. A. Jackson, and J. Jellinek, *J. Chem. Phys.*, *in press* (2006).
29. Structure and shape variations in intermediate size copper clusters, M. L. Yang, K. A. Jackson, C. Koehler, T. Frauenheim, and J. Jellinek, *J. Chem. Phys.* **124**, 024308 (1-6) (2006).

30. Structural evolution of anionic silicon clusters Si_N ($20 \leq N \leq 45$), J. Bai, L.-F. Cui, J. Wang, S. Yoo, X. Li, J. Jellinek, C. Koehler, T. Frauenheim, L.-S. Wang, and X. C. Zeng, *J. Phys. Chem. A* **110**, 908-912 (2006).
31. Density-functional study of small and medium-sized As_n clusters up to $n = 28$, J. Zhao, X. Zhou, X. Chen, J. Wang, and J. Jellinek, *Phys. Rev. B* **73**, 115418 (1-10) (2006).
32. Dipole polarizabilities of medium-sized gold clusters, J. Wang, M. Yang, J. Jellinek, and G. Wang, *Phys. Rev. A* **74**, 023202 (1-5) (2006).
33. Structural, electronic, and optical properties of noble metal clusters from first principles, S. Ogut, J. C. Idrobo, J. Jellinek, and J. Wang, *J. Clust. Sci.*, *in press* (2006).
34. First principles absorption spectra of medium-sized Si clusters: Time-dependent local density approximation versus predictions from Mie theory, J. C. Idrobo, M. Yang, K. A. Jackson and S. Ogut, *Phys. Rev. B*, *in press* (2006).
35. Site-specific polarizabilities: Probing the atomic response of silicon clusters to an external electric field, K. Jackson, M. Yang, and J. Jellinek, in *Lecture Series in Computer and Computational Sciences*, Vol. 4, G. Maroulis and T. Simos, Eds., VSP, Leiden, *in press* (2006).
36. Multiple plasmon resonances in gold nanorods, E. K. Payne, K. L. Shuford, S. Park, G. C. Schatz and C. A. Mirkin, *J. Phys. Chem. B* **110**, 2150-2154 (2006).
37. Manipulating the optical properties of pyramidal nanoparticle arrays, J. Henzie, K. L. Shuford, E.-S. Kwak, G. C. Schatz and T. W. Odom, *J. Phys. Chem. B* **110**, 14028-14031 (2006).
38. Finite-difference time-domain studies of light transmission through nanohole structures, K. L. Shuford, Mark A. Ratner, S. K. Gray and G. C. Schatz, *Appl. Phys. B* **84**, 11-18 (2006).
39. Electric field enhancement and light transmission in cylindrical nanoholes, K. L. Shuford, M. A. Ratner, S. K. Gray, and G. C. Schatz, *J. Comp. Theor. Nanoscience*, *in press* (2006).
40. Apertureless scanning near-field optical microscopy: a comparison between homodyne and heterodyne approaches, L. Gomez, R. Bachelot, A. Bouhelier, G. P. Wiederrecht, S.-H. Chang, S. K. Gray, G. Lerondel, F. Hua, S. Jeon, J. A. Rogers, M. E. Castro, S. Blaize, I. Stephanon, and P. Royer, *J. Opt. Soc. Am. B* **23**, 823-833 (2006).
41. Error signal artifact in apertureless scanning near-field optical microscopy, L. Billot, M. Lamy de la Chapelle, D. Barchiesi, S.-H. Chang, S. K. Gray, J.A. Rogers, A. Bouhelier, P.-M. Adam, J.-L. Bijeon, G. P. Wiederrecht, R. Bachelot, and P. Royer, *Appl. Phys. Lett.* **89**, 023105 (1-3) (2006).
42. A computational study of the interaction of light with silver nanowires of different eccentricity, J. M. Oliva and S. K. Gray, *Chem. Phys. Lett.* **427**, 383-389 (2006).
43. Fourier spectral simulations and Gegenbauer reconstructions for electromagnetic waves in the presence of a metal nanoparticle, M. S. Min, T.-W. Lee, P. F. Fischer, and S. K. Gray, *J. Comp. Phys.* **213**, 730-747 (2006).
44. Multigrid FDTD with Chombo, Z. Meglicki, S. K. Gray, and B. Norris, *Comp. Phys. Comm.*, *in press* (2006).

Acknowledgment: Work at Argonne National Laboratory was supported by the U.S. Department of Energy, Office of Basic Energy Sciences, Division of Chemical Sciences, Geosciences, and Biosciences under DOE Contract No. W-31-109-ENG-38.

Dynamics of Electrons at Interfaces on Ultrafast Timescales

Charles B. Harris, P.I.
Chemical Sciences Division,
Lawrence Berkeley National Lab
1 Cyclotron Road, Mail Stop Latimer,
Berkeley, CA 94720
CBHarris@lbl.gov

Program scope

This is a comprehensive program to study the properties of electrons at molecule/metal interfaces on the femtosecond timescale and the nanometer lengthscale. We examine a broad variety of systems (examples include atomic adsorbates, polymer oligomers, and model solvents) and phenomena (electron solvation and localization, the band structure of interfaces, and the electronic coupling of adsorbates to a metal substrate) with both experiment and theory.

Our primary experimental technique is angle-resolved two-photon photoemission (2PPE). Briefly, a femtosecond laser pulse excites electrons from the valence band of a Ag(111) substrate to the interface with an adsorbed molecular film (typically 1–3 monolayers thick). Some delay time later, Δt , a second laser pulse photoemits the electron, sending it to a time-of-flight detector. From the kinetic energy of the electron and the photon energy of the probe pulse, we can deduce the binding energy of the electronic state. The wavelength dependence of the photoemission spectrum tells whether the state is initially occupied, unoccupied, or a final state resonance.

This technique also gives us access to a wealth of information about the electron's dynamics. The kinetics of population decay and dynamical energy shifts (two-dimensional electron solvation) are determined with < 35 meV energy resolution and ~ 100 fs time resolution. An additional experimental degree of freedom is the angle between the surface normal and the detector. Only electrons with a specific amount of momentum parallel to the surface will reach the detector. The energy versus parallel momentum (the dispersion) gives the effective mass of the electron, m^* . For localized electrons ($m^* \gg 1$) the amplitude of the signal versus parallel momentum can give an estimate of the spatial extent of localization in two dimensions.

Two-photon photoemission accesses both electronic states of the molecular film, such as the highest occupied molecular orbital (HOMO) and the lowest unoccupied molecular orbital (LUMO), as well as states intrinsic to the surface. Image-potential states (IPS) are an important example of the latter. The IPS electrons are bound a few angstroms from the metal surface, making them sensitive probes of the electronic structure and dynamics of monolayer adsorbate films. Any changes in IPS energies directly reflect the behavior of the thin film itself. Additionally, interactions with surface disorder or with the dynamic motions of adsorbates can localize the electron in the plane of the surface.

Recent progress

Intraband relaxation : Intraband relaxation of delocalized IPS electrons is omnipresent in 2PPE. The kinetics of population decay as a function of parallel momentum show that electrons quickly relax to the bottom of the IPS band in many different adsorbate systems. Nevertheless, the process is not well understood. The simplest organizing principle to understand these many observations is friction, and this concept explains complications that arose in previous analyses as direct consequences of the fluctuation-dissipation theorem. We have developed a theory based on Smoluchowski's equation for overdamped harmonic motion to de-

scribe the motion of electrons down an IPS band. This theory has a coefficient of friction as its only free parameter, and we find that the friction extracted from the model is equivalent to the friction one would expect for that due to electron-electron scattering between the IPS electron and the electrons in the substrate. Further work is underway to examine the friction as a function of thin film material in an effort to see if it may be tuned by, for example, attempting to decouple the IPS electron from the substrate. Finally, these methods will be extended to further elucidate the mechanism of electron localization, which may be concomitant with intraband relaxation or even provide a channel for it.

C₆₀/Ag(111) : In addition to probing image potential states, 2PPE can be used to study electronic states of molecular films. Because this technique is a two-photon process, we can examine both initially occupied (HOMO) and initially unoccupied (LUMO) states. Furthermore, through the use of angle-resolved spectra, we can directly measure the effective masses of these states when they are incorporated into electronic bands in a thin film. These band masses are important quantities in modelling electronic transport, and techniques that can extract them for both occupied and unoccupied states are few and far between. In the case of *C₆₀/Ag(111)*, we have experimentally determined the effective masses of the HOMO, LUMO, LUMO+1, and LUMO+2-derived bands. These results were then examined from a theoretical standpoint through the use of both quantum chemical calculations and group theory (Figure 1). Further work will focus on exploring the differences between excitonic and anionic transport in this and related systems.

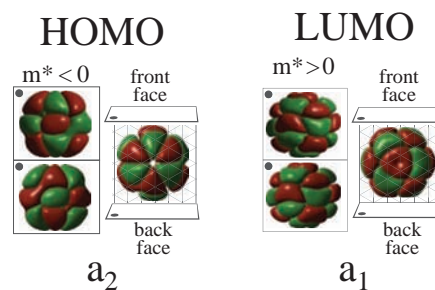


Figure 1: The *C₆₀* orbitals may be studied both through direct calculation of their wavefunctions or by the use of group theory. Shown are one of the five degenerate orbitals of the HOMO and one of the three degenerate orbitals of the LUMO. The HOMO state has a_2 symmetry on the surface and a negative effective mass, whereas the LUMO state has a_1 symmetry on the surface and a positive effective mass.

Photoconductivity of organic semiconductors : Photoconductivity in organic semiconductors has garnered considerable research attention in the search for sustainable energy sources. In particular, the factors for consideration in optimizing these devices, which include the efficiency of photogeneration and the carrier dynamics at an interface, merit a close investigation of the physical chemistry at the interface. Using 2PPE, we have probed the dynamics of excitons and free charge carriers at the interface of *Ag(111)* and PTCDA, a widely-studied planar aromatic hydrocarbon. By varying the morphology of the surface, we can examine the role of crystallinity or structural disorder in affecting the carrier dynamics at an interface. The time scale of typical photoconduction measurements range from pico- to micro-seconds, whereas our experimental set-up allows us to measure the ultrafast, femtosecond electronic response. We also use 2PPE to understand the mechanisms of optical excitation at an interface, including intramolecular or metal-to-molecule processes, and the subsequent effects of layer thickness. Moreover, our angular-resolution enables us to measure the effective masses of these carriers, and determine the delocalized or localized nature of the charges as well as the extent to which crystallinity and temperature affects these parameters.

Continuing and Future work

DMSO/Ag(111) : Our solvation results for nitriles can be extended by comparing them with DMSO. Acetonitrile and DMSO have very similar dipole moments and dielectric constants, yet they behave very differently as electrochemical solvents. Two-photon photoemission results of one monolayer of *DMSO/Ag(111)* show that the DMSO monolayer does not solvate the IPS electrons, but the multilayer solvates a great deal

and dynamically localizes the electrons. This is an important contrast to nitriles, which solvate and localize IPS electrons at all coverages. This is a direct, molecular scale probe of the contrasting differential capacitance of these two molecules as measured in electrochemistry.

Biphasic thin films : One area in which we plan to extend our investigations is to develop further comparisons between the systems we currently study and systems of more relevance to electrochemistry. Many electrochemical processes, however, take place in mixed environments, and so we are beginning to explore the behavior of electrons in multi-component thin films. The electron dynamics in these films are not necessarily related to any one of the components. For example, thin films containing a 1:1 mixture of meta- and para-xylene display electron localization dynamics different from those of either of the pure molecules on their own, and it is not yet entirely clear why this is the case. We have also recently started studying mixed systems of water and small organic molecules. Small amounts of water impurities have been seen to affect electron localization, and in some instances we have observed features with increased lifetimes at these interfaces. A full exploration of these systems should greatly aid in making further connections between the properties of individual electrons at interfaces and the behavior of large numbers of electrons in electrochemical cells or devices.

Inter- and intra-band relaxation : Our current model of intraband relaxation could be made more robust by adding an interband relaxation term as a source or sink for electron population dynamics. We are investigating effects of an interband electron sink, such as into a localized state, on the kinetics of intraband population decay. Various models for an electron sink have been proposed, and simulations are underway to characterize the optimal sink shape, energy gap, etc. In addition, the theory is bolstered by a series of 2PPE experiments on organic molecules which exhibit a slowly rising localized state and obvious dynamics of intraband relaxation.

Thiophene polymers and copper phthalocyanine : Interfacial dynamics coupled with a heterogeneous thin film should elucidate the role of interfacial energy levels and barrier heights on charge dynamics. While the need to match energy levels to facilitate charge transfer at an interface is well-known, we plan on using 2PPE to follow the dynamics for a series of heterojunctions to study the effects of surface heterogeneity on a fixed energy level. This should hopefully elucidate the processes of charge transfer at an interface with respect to photogeneration in an organic heterojunction.

Articles supported by DOE funding 2003–2006

- [1] S. T. Shipman, S. Garrett-Roe, P. Szymanski, A. Yang, M. L. Strader, and C. B. Harris. “Determination of band curvatures by angle-resolved two-photon photoemission in thin films of C-60 on Ag(111).” *J. Phys. Chem. B*, **110**, 20 (2005).
- [2] S. Garrett-Roe, S. T. Shipman, P. Szymanski, M. L. Strader, A. Yang, and C. B. Harris. “Ultrafast electron dynamics at metal interfaces: Intraband relaxation of image state electrons as friction.” *J. Phys. Chem. B*, **109**, 43 (2005).
- [3] P. Szymanski, S. Garrett-Roe, and C. B. Harris. “Time- and angle-resolved two-photon photoemission studies of electron localization and solvation at interfaces.” *Prog. Surf. Sci.*, **78**, 1 (2005).
- [4] I. Bezel, K. J. Gaffney, S. Garrett-Roe, S. H. Liu, A. D. Miller, P. Szymanski, and C. B. Harris. “Measurement and dynamics of the spatial distribution of an electron localized at a metal–dielectric interface.” *J. Chem. Phys.*, **120**, 845 (2004).

- [5] C. B. Harris, P. Szymanski, S. Garrett-Roe, A. D. Miller, K. J. Gaffney, S. H. Liu, and I. Bezel. "Electron solvation and localization at interfaces." In "Proc. SPIE," volume 5223, pages 159–168 (2003).
- [6] P. T. Snee, S. Garrett-Roe, and C. B. Harris. "Dynamics of an excess electron at metal/polar interfaces." *J. Phys. Chem. B*, **107**, 13608 (2003).

Catalysis at Metal Surfaces Studied by Non-Equilibrium and STM Methods

Ian Harrison

Department of Chemistry, University of Virginia

Charlottesville, VA 22904-4319

harrison@virginia.edu

This research program aims to employ non-equilibrium techniques to investigate the nature of the transition states for activated dissociative chemisorption of small molecules on catalytic metal surfaces. Two separate approaches/ideas are under investigation. In the first, we posit that dissociative chemisorption reactions on metal surfaces are primarily surface mediated electron transfer reactions for many hard-to-activate small molecules. Accordingly, the lowest lying affinity levels of these adsorbates, which are accessible by surface photochemistry and scanning tunneling microscopy (STM), will play a key electronic structure role in determining barrier heights for dissociative chemisorption. Electron transfer excitation into these adsorbate affinity levels followed by image potential acceleration towards the surface and rapid quenching may leave the adsorbate in the “transition state region” of the ground state potential relevant to thermal catalysis from where desorption and/or dissociation may ultimately occur. Using a low temperature scanning tunneling microscope (STM) we have been investigating the thermal, electron, & photon induced chemistry of CH_3Br ,¹ CO_2 , and CH_4 on $\text{Pt}(111)$.² In our second approach towards probing surface transition states, we will dose hot gas-phase molecules on to a cold surface and measure dissociative sticking coefficients macroscopically^{3,4} via Auger electron spectroscopy (AES) or microscopically by imaging chemisorbed fragments via low T_s STM. A local hot spot, microcanonical unimolecular rate theory (MURT) model of gas-surface reactivity^{5,6,7} will be used to extract transition state characteristics for dissociative chemisorption. The MURT model has proven useful for understanding, analyzing, and predicting the dynamics of activated dissociative chemisorption for systems ranging in size from H_2 on $\text{Cu}(111)$ ⁸ to C_2H_6 on $\text{Pt}(111)$,⁴ even for quantum state resolved dynamics.^{8,9} An important long-range goal of our research is to microscopically characterize the different transition states for dissociative chemisorption occurring at metal terrace sites as compared to step sites – a goal of long-standing interest to the catalysis and electronic structure theory communities.¹⁰

A Ph.D. thesis was completed that examined the ordering behavior and photochemistry of several small molecules on $\text{Pt}(111)$. Fig. 1 shows STM and RAIRS evidence for the formation of a well-ordered (6 x 3) monolayer of CH_3Br on $\text{Pt}(111)$ in which all the molecules are oriented along the surface normal, and top sites and 3-fold hollow sites are populated in equal measure.¹ The self-assembly kinetics for this monolayer of rod-like dipolar molecules (1.8 Debye) were surprisingly slow. Consequently, it seems likely that many earlier investigations of adsorbed methyl halides conducted at temperatures under 100 K were examining non-equilibrium molecular configurations. The CH_3 photofragment angular distribution from the 193 nm photoinduced dissociative electron attachment (DEA) to CH_3Br within the annealed and oriented monolayer varied as $\cos^2\theta$. The relatively broad angular distribution indicates that the CH_3 photofragments are subject to orientation changing dynamics as they escape from the oriented monolayer. Ordered monolayers of CO_2 and CH_4 monolayers were observed by STM. Methyl radicals produced by 193 nm irradiation of adsorbed CH_4 were also visualized by STM. Several manuscripts are being written up based on these studies.

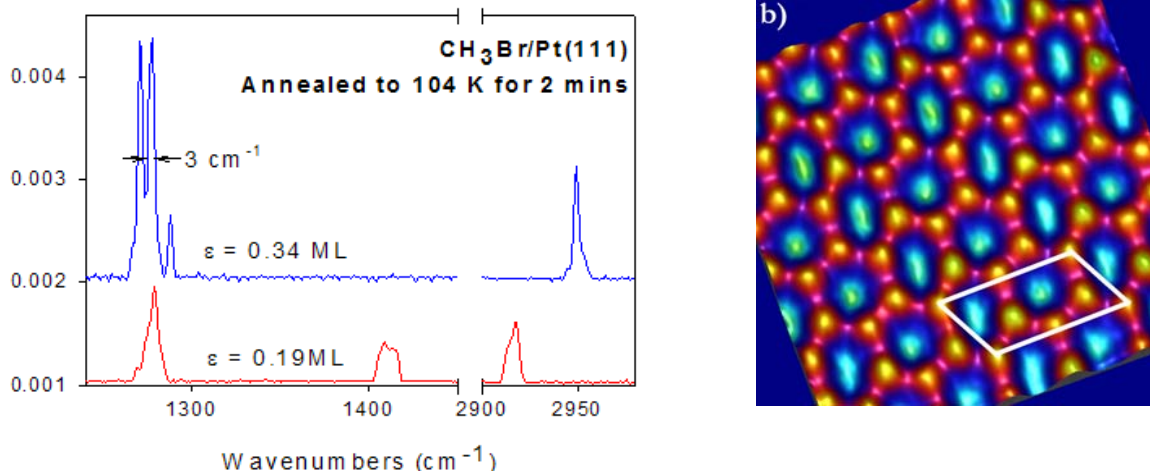


Fig. 1 (a) RAIRS spectra of a well-annealed CH_3Br submonolayer and monolayer. The absence of the ν_5 mode near 1410 cm^{-1} in the ordered monolayer spectrum requires that all molecules within the monolayer are oriented along the surface normal, unlike their behavior in submonolayers. (b) STM image of the annealed (6×3) CH_3Br monolayer rendered in 3D [$40\text{ \AA} \times 40\text{ \AA}$; $T_s = 30\text{ K}$, $I = 10\text{ pA}$ and $V_B = -10\text{ mV}$].¹

Achieving a molecular-level understanding of activated dissociative chemisorption is important because it is a reactive step that oftentimes rate limits important petrochemical processes, such as the steam reforming of methane on Ni catalysts¹¹ that yields the industrial supply of H_2 and synthesis gas. Figure 2(a) shows MURT predictions for thermal dissociative sticking coefficients of CH_4 on low index single crystal metal surfaces based on prior extraction of transition state parameters from analysis of supersonic molecular beam experiments. Surface metal atoms on supported nanoscale metal catalysts are found to be less reactive towards CH_4 than those on flat single crystal metal surfaces. This is a surprising finding because methane reforming is structure sensitive¹¹ and the nanoscale catalysts expose step and high index planes that are thought to be particularly reactive. It may be that some of the surface atoms on the nanocatalysts become poisoned or are tempered by a build-up of carbon under high working pressures such that their *macroscopically* averaged reactivity does not accurately characterize reactivity at their most active sites. We are working towards using low T_s STM in conjunction with effusive molecular beam measurements to *microscopically* characterize the transition states at terraces and at step edges on single crystal surfaces. Figure 2(b) shows that it is possible to extract macroscopically averaged CH_4 dissociative transition state characteristics for single crystal surfaces based on variable $S(T_g, T_s)$ sticking coefficient measurements using a heated effusive gas doser, AES of chemisorbed C, and 3-parameter MURT analysis.³ Electronic structure theory¹² and a CH_4 supersonic molecular beam experiment on $\text{Pt}(553)$ ¹³ suggest that $\text{Pt}(111)$ step sites have a CH_4 dissociation threshold energy, E_0 , some 30 kJ/mol lower than on $\text{Pt}(111)$ terraces. We have designed and are currently assembling a differentially pumped, heated effusive molecular beamline to impinge CH_4 on to a $\text{Pt}(111)$ surface held at $T_s = 80\text{ K}$ and image the CH_3 dissociation products left behind by STM. By locally measuring $S(T_g, T_s \sim 80\text{ K})$ as a function of T_g in combination with MURT analysis we hope to directly characterize the transition states at steps and terraces. Figure 3 provides MURT simulations of possible experimental outcomes with $\Delta E_0 = 30\text{ kJ/mol}$ between terraces and steps.

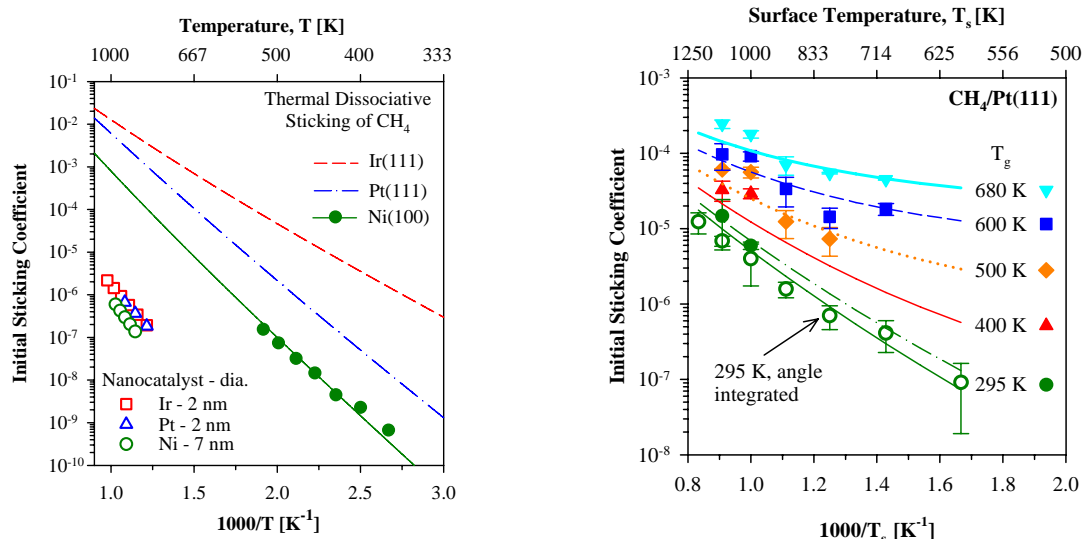


Fig. 2 (a) Thermal dissociative sticking coefficients for CH_4 on supported metal nanocatalysts and single crystal metal surfaces are compared [points are experimental data,^{11, 14-16} lines are MURT predictions^{3, 9, 17}]. (b) MURT predictions (lines) of dissociative sticking coefficients $S(T_g, T_s)$ for CH_4 impinging on Pt(111) for several gas temperatures of an effusive CH_4 molecular beam are compared to experiment (points).³ The MURT transition state parameters used are ($E_0 = 49$ kJ/mol, $\nu_D = 335$ cm^{-1} , $s = 2$).

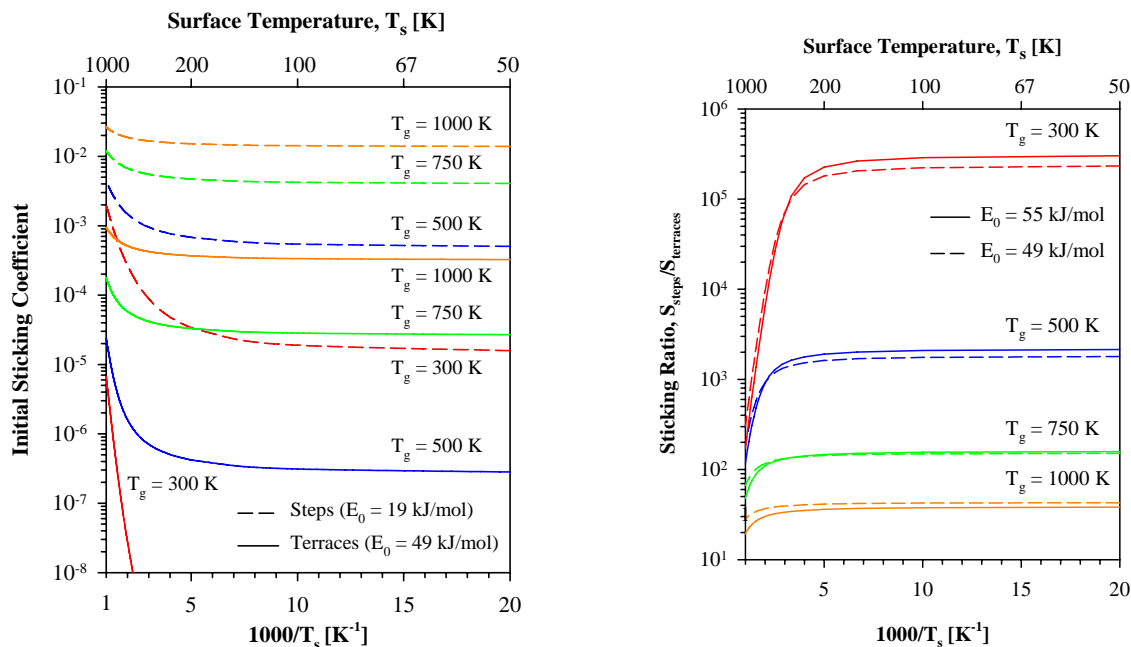


Fig. 3 (a) MURT predictions of $S(T_g, T_s)$ for dissociative chemisorption of CH_4 on Pt(111) terraces and steps for several gas temperatures of an effusive CH_4 beam. The simulations assume that only the reaction threshold energy, E_0 , differs at the steps. Surface temperatures above ~ 80 K should keep the surface free of physisorbed CH_4 during effusive beam dosing (i.e., $\tau_d(T_s = 80$ K) $< 10^{-3}$ s) and so STM imaging of CH_3 dissociation fragments near steps or terraces could fix local $S(T_g, T_s)$ values. (b) Ratio of $S(T_g, T_s)$ values for steps versus terraces based on two reasonable MURT parameter sets (i.e., terrace $E_0 = 52 \pm 3$ kJ/mol; steps 30 kJ/mol less).

DOE Publications since 2003: none

References:

- ¹ T. C. Schwendemann, I. Samanta, T. Kunstmann and I. Harrison, "CH₃Br Structures on Pt(111): Ferroelectric Self Assembly of Dipolar and Weakly Adsorbed Molecules," *J. Phys. Chem. B* submitted (2006).
- ² T. C. Schwendemann, "Atomic Scale Investigations of the Thermal and Electron Induced Chemistry of Small Molecules on Pt(111) as Revealed by Scanning Tunneling Microscopy," Ph.D. Thesis, University of Virginia (2005).
- ³ K. M. DeWitt, L. Valadez, H. L. Abbott, K. W. Kolasinski and I. Harrison, "Using effusive molecular beams and microcanonical unimolecular rate theory to characterize CH₄ dissociation on Pt(111)," *J. Phys. Chem. B* **110**, 6705-6713 (2006).
- ⁴ K. M. DeWitt, L. Valadez, H. L. Abbott, K. W. Kolasinski and I. Harrison, "Effusive molecular beam study of C₂H₆ dissociation on Pt(111)," *J. Phys. Chem. B* **110**, 6714-6720 (2006).
- ⁵ A. Bukoski, D. Blumling and I. Harrison, "Microcanonical unimolecular rate theory at surfaces. I. Dissociative chemisorption of methane on Pt(111)," *J. Chem. Phys.* **118**, 843-871 (2003).
- ⁶ H. L. Abbott, A. Bukoski and I. Harrison, "Microcanonical unimolecular rate theory at surfaces. II. Vibrational state resolved dissociative chemisorption of methane on Ni(100)," *J. Chem. Phys.* **121**, 3792-3810 (2004).
- ⁷ A. Bukoski, H. L. Abbott and I. Harrison, "Microcanonical unimolecular rate theory at surfaces. III. Thermal dissociative chemisorption of methane on Pt(111) and detailed balance," *J. Chem. Phys.* **123**, 094707 (2005).
- ⁸ H. L. Abbott and I. Harrison, "Seven-dimensional microcanonical treatment of hydrogen dissociation dynamics on Cu(111): Clarifying the essential role of surface phonons," *J. Chem. Phys.* **125**, 024704 (2006).
- ⁹ H. L. Abbott, A. Bukoski, D. F. Kavulak and I. Harrison, "Dissociative chemisorption of methane on Ni(100): Threshold energy from CH₄ (2v₃) eigenstate-resolved sticking measurements," *J. Chem. Phys.* **119**, 6407-6410 (2003).
- ¹⁰ F. Abild-Pedersen, O. Lytken, J. Engbaek, G. Nielsen, I. Chorkendorff and J. K. Norskov, "Methane activation on Ni(111): Effects of poisons and step defects," *Surf. Sci.* **590**, 127 (2005).
- ¹¹ J. M. Wei and E. Iglesia, "Isotopic and kinetic assessment of the mechanism of reactions of CH₄ with CO₂ or H₂O to form synthesis gas and carbon on nickel catalysts," *J. Catal.* **224**, 370-383 (2004).
- ¹² Z. P. Liu and P. Hu, "General rules for predicting where a catalytic reaction should occur on metal surfaces: A density functional theory study of C-H and C-O bond breaking/making on flat, stepped, and kinked metal surfaces," *J. Am. Chem. Soc.* **125**, 1958-1967 (2003).
- ¹³ A. T. Gee, B. E. Hayden, C. Mormiche, A. W. Kleyn and B. Riedmuller, "The dynamics of the dissociative adsorption of methane on Pt(533)," *J. Chem. Phys.* **118**, 3334-3341 (2003).
- ¹⁴ J. M. Wei and E. Iglesia, "Isotopic and kinetic assessment of the mechanism of methane reforming and decomposition reactions on supported iridium catalysts," *Phys Chem Chem Phys* **6**, 3754-3759 (2004).
- ¹⁵ J. M. Wei and E. Iglesia, "Mechanism and site requirements for activation and chemical conversion of methane on supported Pt clusters and turnover rate comparisons among noble metals," *J. Phys. Chem. B* **108**, 4094-4103 (2004).
- ¹⁶ B. O. Nielsen, A. C. Luntz, P. M. Holmblad and I. Chorkendorff, "Activated Dissociative Chemisorption of Methane on Ni(100) - a Direct Mechanism under Thermal Conditions," *Catal. Lett.* **32**, 15-30 (1995).
- ¹⁷ H. L. Abbott and I. Harrison, "Dissociative chemisorption and energy transfer for methane on Ir(111)," *J. Phys. Chem. B* **109**, 10371-10380 (2005).

ELECTRONIC STRUCTURE AND OPTICAL RESPONSE OF NANOSTRUCTURES

Martin Head-Gordon (mhg@cchem.berkeley.edu)¹,
Steven G. Louie (sglouie@berkeley.edu)²,
Lin-Wang Wang (lwwang@lbl.gov)³,
Emily A. Carter (eac@princeton.edu)⁴,
James R. Chelikowsky (jrc@ices.utexas.edu)⁵,

¹*Department of Chemistry, University of California, and Chemical Sciences Division, Lawrence Berkeley National Laboratory, Berkeley, CA 94720;* ²*Department of Physics, University of California, and Materials Sciences Division, Lawrence Berkeley National Laboratory, Berkeley, CA 94720;* ³*Computational Research Division, Lawrence Berkeley National Laboratory, Berkeley, CA 94720;* ⁴*Department of Mechanical & Aerospace Engineering, Princeton University, Princeton, NJ 08544;* ⁵*Departments of Physics and Chemical Engineering, Institute for Computational Engineering and Sciences, University of Texas, Austin, TX 78712*

1. Scope of Project.

There has been much progress in the synthesis, characterization and theoretical studies of various nanostructures such as nanotubes, nanocrystals, atomic wires, organic and biological nanostructures, and molecular junctions. However, there remain immense challenges to obtain a basic understanding of the properties of these structures and their interactions with external probes to realize their potential for applications. Some exciting frontiers in nanoscience include molecular electronics, nanoscale opto-electronic devices, nanomechanics (nanomotors), light harvesting and emitting nanostructures. The ground and electronic excited properties of the nanostructures and how they are coupled to the external stimulations/probes are crucial issues.

Since nanostructures are neither at the molecular nor the bulk limits, the calculations of their electronic and optical properties are subject to severe computational bottlenecks. The present program therefore focuses on the electronic structure theory and modeling of nanostructures, including their electronic excited-state and optical properties, with applications to topics of current interest. We are attacking the rate-determining steps in these approaches in collaboration with a team of applied mathematicians, led by Juan Meza, Head of LBNL's High Performance Computing Research Department.

2. Summary of Recent Progress.

As this is a large multi-investigator program, space precludes us summarizing all projects that are underway. Below, we highlight a selection of recent accomplishments. See also Emily Carter's separate abstract for additional detail and references on work led by her group on new embedding methods, and their application to the Kondo effect for Co on Cu surfaces.

Optical response of nanotubes: Excitonic, electron-phonon coupling, and finite temperature effects. We are investigating the optical properties of nanotubes employing accurate first-principles methods (DFT and the GW-BSE approach). We developed a formalism and carried out ab initio calculations on the radiative lifetime of excitons in single-walled carbon nanotubes (SWCNTS) [16]. We found that the radiative lifetime at room temperature, including

both momentum conservation and finite temperature effects, is ~ 10 ns, in agreement experiment. In another study, we calculated the electron-phonon coupling of electronic states in carbon nanotubes and found in general a monotonic decrease in excitation energy with increasing temperature. Furthermore, we determined a competing effect due to thermal expansion, which can dominate over the electron-phonon coupling [17]. These results explain conflicting shifts in excitation energy observed experimentally between carbon nanotubes suspended in air and those in bundles or coated with surfactant. We have also developed an insightful group theory analysis of the selection rules for exciton excitations in carbon nanotubes in one- and two-photon absorption.[19] Finally, we found that self-energy and electron-hole interaction effects are even more important in the optical response of boron nitride nanotubes, which exhibit stronger excitonic binding energies than CNTs of similar diameter and more complex behaviors.[18]

Spintronic Materials and the role of “self-purification” in semiconductor nanocrystals. [24] Dilute magnetic semiconductors (DMS) have an introduced magnetic impurity, and exhibit unique magnetic, magneto-optical, and magneto-electrical effects. They hold the promise of using electron spin, in addition to charge, for creating a new class of “spintronic” semiconductor devices with unprecedented functionality. We expect that nano-crystalline DMS should exhibit intriguing magnetic properties, which are different from those of the bulk, because quantum confinement is known to enhance spin-spin interactions. A key issue in these systems is the role of “self-purification”, which occurs when a defect (such as an impurity atom) migrates to the surface of the nanocrystal, leaving the interior defect free. It is enhanced in the nano-regime as a defect atom need only diffuse a few bond lengths to reach the surface. We determined the relative heats of formation for defects in nanocrystals as a function of size, finding that the heat of formation of defects for magnetic impurities becomes less favorable as the size of the nanocrystal decreases. This “thermodynamic” measure reinforces the likelihood that nanocrystals will be susceptible to self-purification processes.

Scaled opposite spin electron correlation energy for large systems. [10,12,20] We want to make the proven electron correlation methods of molecular quantum chemistry applicable to nanoscale systems. We have shown that the simplest useful many body method is the opposite spin second order many body correlation energy. It is both computationally less expensive, and more accurate than standard second order perturbation theory. In addition to a fast conventional implementation, we have also developed a low-scaling implementation that exploits spatial locality. We have applied this new method to compute the binding energy of fullerene to tetraphenylporphyrin, giving the first many-body prediction. The result is a binding energy of about 30 kcal/mol, in contrast to conventional DFT, which predicts the complex to be unbound, as a consequence of neglect of dispersion interactions.

Local coupled cluster theory with smooth potential energy surfaces. [13,14,23] To make accurate infinite order many body methods feasible for nanoscale systems requires a partitioning that treats weak correlations by lowest order perturbation theory, and strong correlations to infinite order. Previous attempts to do this have shown promising computational speedups, but have failed to give potential energy surfaces that are smooth with respect to nuclear displacements (due to discontinuous changes as to which correlations are weak versus strong as nuclear coordinates are displaced). We have designed the first partitioning that yields mathematically smooth potential energy surfaces, by modifying the matrix elements describing

electron correlation with a “bump function” that takes them to zero smoothly and rapidly. We have just reported the first viable implementation of this very exciting new approach.

Exact scattering state calculation using planewave pseudopotential Hamiltonian for quantum transport. [4] We have developed an efficient new method to calculate the elastic quantum transport using auxiliary periodic boundary conditions. This method allows the use of conventional ground state *ab initio* programs and has a similar computational cost as a ground state calculation. We have extended our initial model that used approximate evanescent states in the electrodes, with a systematic approach to calculate the complex band structures for the electrodes with the planewave nonlocal pseudopotential formalism. Using these exact evanescent states, we get exact scattering state solutions for any energy and incoming electrode states.

Screened exchange density functional calculations of alloys and d-states. [5,26,27] We have compared the screened exchange local density approximation (sX-LDA) method against GW and variational quantum Monte Carlo results for the nonlocal potentials, exchange-correlation holes, self-energy terms and exchange correlation energies. This provides guidance for future improvements to sX-LDA. We have also applied sX-LDA to a variety of problems where largely only LDA results were previously available. This includes the band structure of calcium hexaborides (confirming that it is a semiconductor), and the band gap bowing of the semiconductor alloys (LDA and sX-LDA gave very similar bowing parameters although the band gap slope as a function of the alloy concentration can be very different), and d-states.

3. Summary of Research Plans.

- New low-scaling algorithms for the GW-BSE methodology.
- Development of an opposite-spin many-body approach to excited states.
- Exciton-phonon coupling to simulate ultrafast photo-excited dynamics in finite temperature and/or resonant spectroscopy of nanostructures, with emphasis on CNTs.
- Study carbon nanotubes of different diameters and chiralities, and wide bandgap BN nanotubes for which we expect even more dominant excitonic effects.
- Algorithmic improvements and forces for the smooth local coupled cluster method.
- Joint development of new eigensolvers for electronic structure calculations.
- Improvements to the sX-LDA approach based on our recent benchmark tests

4. Partial list of publications from DOE Sponsored Work, 2005-present.

[1] J. B. Neaton, K. H. Khoo, C. D. Spataru, and S. G. Louie, “Electron Transport and Optical Properties of Carbon Nanostructures from First Principles,” *Computer Phys. Comm.* **169**, 1 (2005).

[2] R.B. Capaz, C.D. Spataru, P. Tangney, M.L. Cohen, and S.G. Louie, “Temperature Dependence of the Band Gap of Semiconducting Carbon Nanotubes,” *Phys. Rev. Lett.* **94**, 036801 (2005).

[3] R.B. Capaz, C.D. Spataru, P. Tangney, M.L. Cohen, and S.G. Louie, “Temperature and hydrostatic pressure effects on the band gap of semiconducting carbon nanotubes,” 27th Conference on the Physics of Semiconductors, *AIP Conference Proceedings* **772**, 1047 (2005).

[4] L.W. Wang, “Elastic quantum transport calculations using auxiliary periodic boundary conditions”, *Phys. Rev. B* **72**, 45417(2005).

- [5] B. Lee, L.W. Wang, "Electronic structure of calcium hexaborides", *Appl. Phys. Lett.* **87**, 262509 (2005).
- [6] X. Huang, A. Makmal, J. R. Chelikowsky, and L. Kronik: "Size dependent spintronic properties of dilute magnetic semiconductor nanocrystals," *Phys. Rev. Lett.* **94**, 236801 (2005).
- [7] X. Huang, Eric Lindgren and J.R. Chelikowsky: "Surface passivation method for semiconductor nanostructures," *Phys. Rev. B* **71**, 165328 (2005).
- [8] C. Bekas, Y. Saad, M.L. Tiago and J.R. Chelikowsky: "Computing charge densities with partially reorthogonalized Lanczos," *Comp. Phys. Comm.* **171**, 175 (2005).
- [9] J.E. Subotnik and M. Head-Gordon, "A localized basis that allows fast and accurate second order Moller-Plesset calculations", *J. Chem. Phys.* **122**, 034109 (2005) (9 pages).
- [10] Y. Jung, A. Sodt, P.M.W. Gill and M. Head-Gordon, "Auxiliary basis expansions for large-scale electronic structure calculations", *Proc. Nat. Acad. USA* **102**, 6692-6697 (2005).
- [11] P.M.W. Gill, A.T.B. Gilbert, S.W. Taylor, G. Friesecke, and M. Head-Gordon, "Decay behavior of least-squares expansion coefficients", *J. Chem. Phys.* **123**, 061101 (2005)
- [12] R.C. Lochan, Y. Jung, and M. Head-Gordon, "Scaled opposite spin second order Moller-Plesset theory with improved physical description of long-range dispersion interactions", *J. Phys. Chem. A* **109**, 7598-7605 (2005).
- [13] J.E. Subotnik and M. Head-Gordon, "A local correlation model that yields intrinsically smooth potential energy surfaces", *J. Chem. Phys.* **123**, 064108 (2005).
- [14] J.E. Subotnik, A.D. Dutoi, and M. Head-Gordon, "Fast localized orthonormal virtual orbitals which depend smoothly on nuclear coordinates", *J. Chem. Phys.* **123**, 114108 (2005) (9 pages).
- [15] M. Lopez del Puerto, M.L. Tiago, I. Vasiliev & J.R.Chelikowsky: "Real space calculations of the ground & excited state properties of the water molecule," *Phys. Rev. A* **72**, 052504 (2005).
- [16] C.D. Spataru, S. Ismail-Beigi, R.B. Capaz, and S.G. Louie, "Theory and ab initio calculation of radiative lifetime of excitons in semiconducting carbon nanotubes," *Phys. Rev. Lett.* **95**, 247402 (2005).
- [17] S.B. Cronin, Y. Yin, A.Walsh, R.B. Capaz, A. Stolyarov, P. Tangney, M. L. Cohen, S.G. Louie, A.K. Swan, M.S. Unlu, B.B. Goldberg, and M. Tinkham, "Temperature dependence of the optical transition energies of carbon nanotubes: the role of electron-phonon coupling and thermal expansion," *Phys. Rev. Lett.* **96**, 127403 (2006)
- [18] C.H. Park, C.D. Spataru, and S.G. Louie, "Excitons and many-electron effects in the optical response of single-walled boron nitride carbon nanotubes," *Phys. Rev. Lett.* **96**, 126105 (2006).
- [19] E.B. Barros, R.B. Capaz, A. Jorio, G.G. Samsonidze, A.G. Souza Filho, S. Ismail-Beigi, C.D. Spataru, S.G. Louie, G. Dresselhaus, M.S. Dresselhaus, "Selection rules for one- and two-photon absorption by excitons in carbon nanotubes," *Phys. Rev. B* **73**, 241406(R) (2006).
- [20] Y. Jung and M. Head-Gordon, "A fast correlated electronic structure method for computing interaction energies of large van der Waals complexes applied to the fullerene-porphyrin dimer", *Phys. Chem. Chem. Phys.* **8**, 2831-2840 (2006).
- [21] Y.M. Rhee, R.A. DiStasio Jr., R.C. Lochan, and M. Head-Gordon, "Analytical gradient of restricted second order Møller-Plesset correlation energy with the resolution of the identity approximation, applied to the TCNE dimer anion complex", *Chem. Phys. Lett.* **426**, 197-203 (2006).
- [22] R. Steele, R.A. Distasio Jr., Y. Shao, J. Kong & M. Head-Gordon, "Dual basis second order Møller-Plesset theory: a reduced cost reference for correlation calculations", *J. Chem. Phys.* **125**, 074108 (2006).
- [23] J.E. Subotnik, A. Sodt, and M. Head-Gordon, "A near linear-scaling smooth local coupled cluster algorithm for electronic structure", *J. Chem. Phys.* **125**, 074108 (2006)
- [24] G. Dalpian and J.R. Chelikowsky: "Self-Purification in Semiconductor Nanocrystals," *Phys. Rev. Lett.* **96**, 226802 (2006).
- [25] M. Lopez del Puerto, M.L. Tiago, J.R. Chelikowsky: "Excitonic effects and optical properties of passivated CdSe clusters," *Phys. Rev. Lett.* **97**, 096401 (2006).
- [26] B. Lee, L.W. Wang, "Electronic structure of zinc-blende $\text{Al}_x\text{Ga}_{1-x}\text{N}$: screened-exchange study", *Phys. Rev. B* **73**, 153309 (2006).
- [27] B. Lee, L.W. Wang, "Band gap bowing & electron localization of GaInN ", *J. Appl. Phys.* (in press).

Chemical Kinetics and Dynamics at Interfaces

Laser induced reactions in solids and at surfaces

Wayne P. Hess (PI), Kenneth M. Beck, and Alan G. Joly

Chemical Sciences Division
Pacific Northwest National Laboratory
P.O. Box 999, Mail Stop K8-88,
Richland, WA 99352, USA
wayne.hess@pnl.gov

Additional collaborators on these projects include AL Shluger, PV Sushko, P Perozzo, JT Dickinson, K Tanimura, G Xiong, and M Henyk

Program Scope

Electronic excitation of solid surfaces and bulk materials induces chemical and physical changes relevant to the fields of solar energy conversion, photocatalysis, and radiation chemistry. Irradiation by UV, or higher energy photons, produces energetic species such as core holes and free electrons, that relax to form electron-hole pairs, excitons, and other transient species capable of driving surface and bulk reactions. These less energetic secondary products induce the transformations commonly regarded as radiation damage. Photo-stimulated desorption, of atoms or molecules, provides a direct window into these important processes and is particularly indicative of electronic excited state dynamics. The interaction between light and nanoscale oxide materials is fundamentally important in catalysis, microelectronics, sensor technology, and materials processing. Excited state chemistry in solids is inherently complex and greater understanding is gained using a combined experiment/theory approach. We collaborate with leading solid-state theorists who use *ab initio* calculation to model laser desorption and photoemission experiments. The experiments are designed specifically to test hypothetical models and theoretical predictions resulting from the calculations.

We have developed laser techniques to induce selective solid-state chemistry using tunable femtosecond and nanosecond lasers to excite wide-gap materials under highly controlled conditions. We use a variety of optical spectroscopies to characterize chemically reactive surface sites of nanocube samples grown by chemical vapor deposition or highly disperse thin films grown by reactive ballistic deposition (RBD) techniques. Experimentally, we monitor particle emission using quantum-state specific laser ionization and probe surface chemical transformations using surface sensitive techniques such as x-ray photoelectron spectroscopy. We have demonstrated that laser control of desorbed products and quantum states is possible by judicious choice of laser wavelength, pulse duration, and delay between femtosecond pulses. To date we have explored mainly incoherent or passive control strategies using single pulses and pulse pairs. Our main goal is to verify our hypothetical models rather than pursuit of laser control as an end in itself.

Recent Progress and Future Direction

Our laboratory studies are based on surface science and laser excitation and probe techniques. We interrogate desorbed atoms or molecules from ionic crystals using resonance enhanced multiphoton ionization and time-of-flight mass spectrometry. In single-pulse experiments, photon

energies are chosen to excite specific surface structural features that lead to particular desorption reactions. The photon energy selective approach takes advantage of energetic differences between surface and bulk exciton states and probes the surface exciton directly. Application of this approach to controlling the yield and state distributions of desorbed species requires detailed knowledge of the atomic structure, optical properties, and electronic structure within a developing surface exciton desorption model. To date we have thoroughly demonstrated surface-selective excitation and reaction on alkali halides. However, the technological applications of alkali halides are limited compared to oxide materials. Oxides serve as dielectrics in microelectronics and form the basis for exotic semi- and super-conducting materials. Although the electronic structure of oxides differs considerably from alkali halides, it now appears possible to generalize the exciton model for laser surface reactions to these interesting new materials.

Our model indicates that it is possible to excite the surface over the bulk of ionic oxide crystals using tunable excitation and thus induce controllable surface specific reactions. For MgO and CaO the energies required to generate bulk excitons are 7.7 and 6.8 eV, respectively. However, UV diffuse reflectance spectra of high surface area materials reveal optical absorptions at significantly lower energies. On MgO nanocubes with pronounced corner and edge features two emission bands at 3.4 and 3.3 eV result from the excitation of 4-coordinated surface O_{4C}^{2-} anions in edges at 5.4 eV and of regular oxygen-terminated corners at 4.6 eV, respectively. We have confirmed that surface excitons can be directly excited in both CVD and RBD MgO thin films at oxygen- and magnesium-terminated corners with 4.6 eV radiation (Beck et al., 2006). These results indicate that site-selective excitation is possible for low-coordinated surface sites and that with further development, nano-scale surface sculpting may be achievable.

In the particular case of CaO CVD-grown nanocubes, emission spectra were recorded with excitation energies between 5.2 and 3.7 eV. In fact, 3.7 eV corresponds to the minimum excitation energy that is associated with significant photoluminescence emission. For the entire excitation energy range, there is only one emission band with a maximum at 3.0 eV detectable, the shape of which is also excitation energy independent. The associated excitation spectrum reveals one asymmetric curve, which suggests that more than one excitation process contributes to the photoluminescence emission at 3.0 eV. The higher energy optical absorption spectrum can be decomposed into two constituents at 4.2 and 4.7 eV. BaO is an intriguing extension of our oxide studies because not only are transition energies shifted toward visible wavelengths but the bonding is more covalent than for either MgO or CaO. We will selectively excite CVD and RBD grown samples of alkaline earth oxides using nanosecond UV pulses generated by broadly tunable OPO laser sources and probe desorbed atoms using laser ionization techniques.

We ask the question “Can an oxide surface exciton or a combination of excitons lead to controllable desorption and hence specific surface modification?” If exciton based desorption can be generalized to oxides then selective excitation of surface excitons could lead to controllable surface sculpting, on an atomic scale, for many important materials. The O-atom velocity and kinetic energy profiles for 4.7 eV photo-excitation have been obtained indicating that surface excitons can possibly combine leading to hyperthermal O-atom desorption. The O-atom KE distribution is clearly hyperthermal indicating that a surface exciton mechanism could likely be responsible.

While exciton-based desorption is plausible for MgO, we note that the higher valence may require a bi- or tri-exciton mechanism. The details of this mechanism need to be delineated and confirmed by demonstrating laser control of the various desorption processes. We have recently observed hyperthermal neutral Mg-atom desorption. This is quite a novel result as Mg-atom desorption requires that two electron transfer to a corner site Mg^{2+} ion in a very short time and

then desorb prior to relaxation. The hyperthermal distribution indicates that the exciton model is extendable now to metal atom desorption processes – a previously unknown mechanism. Future plans include femtosecond pulse-pair photo-emission electron microscopy to probe dynamics of oxide nanostructures on surfaces.

Our excitation techniques are site specific as it is possible to selectively excite terrace, step, or corner surface sites. Therefore, we have explored various sample preparation techniques that produce high concentrations of low-coordinated surface sites such as 4-coordinated steps and 3-coordinated corner or kink sites. In particular, we have employed reactive ballistic deposition (a technique developed in Bruce Kay's lab) to grow very high surface area MgO thin films. These films have been thoroughly characterized using XPS, SEM, TEM, and XRD techniques. Similarly, we have also studied laser desorption of MgO nano-powders grown by a chemical vapor deposition technique. The nano-powders show cubic structure and edge lengths ranging between 3 and 10 nm (through TEM analysis). Both sample types provide unique insight into site-selective exciton-based desorption processes and are the focus of ongoing work. We plan to grow and study several other oxide surfaces in the near term including CaO, BaO, ZrO₂, and TiO₂.

References to publications of DOE BES sponsored research (2003 to present)

1. "Photon stimulated desorption from KI: Laser control of I-atom velocity distributions." M Henyk, AG Joly, KM Beck, and WP Hess, *Surf. Sci.* **528**, 219 (2003).
2. "Synergistic effects of exposure of surfaces of ionic crystals to radiation and water." JT Dickinson, KH Nwe, WP Hess, and SC Langford, *Appl. Surf. Sci.* **208**, 2 (2003).
3. "Surface excitons detected by atomic desorption." AG Joly, KM Beck, M Henyk, WP Hess, PV Sushko, and AL Shluger, *Surf. Sci.* **544**, L683 (2003).
4. "The origin of temperature-dependent yield of Frenkel-pairs generated by valence excitation in NaCl." K Tanimura and WP Hess, *Phys. Rev. B*, **69**, 155102 (2004).
5. "Laser control of product electronic state: desorption from alkali halides." KM Beck, AG Joly, N Dupuis, P Perozzo, W Hess, P Sushko, and A Shluger, *J. Chem. Phys.* **120**, 2456 (2004).
6. "Determination of surface exciton energies by velocity resolved atomic desorption." WP Hess, AG Joly, KM Beck, PV Sushko, and AL Shluger, *Surf. Sci.* **564**, 62 (2004).
7. "Interaction of wide band gap single crystals with 248 nm excimer laser irradiation: laser induced near-surface absorption in single crystal NaCl." K H Nwe, S C Langford, WP Hess, and JT Dickinson, *J. Appl. Phys.* **97**, 043501 (2005).
8. "Interaction of wide band gap single crystals with 248 nm excimer laser irradiation: The effect of water vapor and temperature on laser desorption of neutral atoms from sodium chloride." KH Nwe, SC Langford, WP Hess, and JT Dickinson, *J. Appl. Phys.* **97**, 043502 (2005).
9. "A mechanism of photo-induced desorption of oxygen atoms from MgO nano-crystals." PE Trevisanutto, PV Sushko, AL Shluger, KM Beck, M Henyk, A.G. Joly, and W.P. Hess. *Surf. Sci.* **593**, 210 (2005).

- 10) "Laser control of desorption through selective surface excitation." WP Hess, AG Joly, KM Beck, M Henyk, PV Sushko, PE Trevisanutto, and AL Shluger, *J. Phys. Chem.* **109**, Feature Article (2005).
- 11) "Surface electronic properties and site-specific laser desorption processes of highly structured nanoporous MgO thin films." M Henyk, KM Beck, MH Engelhard, AG Joly, WP Hess, and JT Dickinson, *Surf. Sci.* **593**, 242 (2005).
- 12) "Introduction to Photoelectron Emission Microscopy: Principles and Applications." G Xiong, AG Joly, WP Hess, M. Cai, and JT Dickinson, *J. Chin. Elec. Microsc. Soc.* **25**, 16 (2006).
- 13) "Carrier Dynamics in α -Fe₂O₃ Thin-films and Single Crystals Probed by Femtosecond Transient Absorption and Reflectivity." AG Joly, JR Williams, SA Chambers, G Xiong, WP Hess, and DM Laman, *J. Appl. Phys.* **99**, 1 (2006).
- 14) "In-situ photoemission electron microscopy study of thermally-induced martensitic transformation in CuZnAl shape memory alloy." G Xiong, AG Joly, KM Beck, WP Hess, M Cai, SC Langford, and JT Dickinson, *Appl. Phys. Lett.* **88**, 091910 (2006).
- 15) "Site-specific laser modification of MgO nano-clusters: Towards atomic scale surface structuring." KM Beck, M Henyk, C Wang, PE Trevisanutto, PV Sushko, WP Hess, and AL Shluger, *Phys. Rev. B* **74**, 045404 (2006).
- 16) "Two-hole localization mechanism for electronic bond rupture of surface atoms by laser-induced valence excitation of semiconductors." K Tanimura, E Inami, J Kanasaki, and WP Hess *Phys. Rev. B* **74**, 035337 (2006).
- 17) "Excited carrier dynamics of α -Cr₂O₃/ α -Fe₂O₃ core-shell nanostructures." G Xiong, AG Joly, WP Hess, G Holtom, CM Wang, DE McCready, and KM Beck, *J. Phys Chem. B* **110**, 16937 (2006).
- 18) "Probing electron transfer dynamics at MgO surfaces by Mg-atom desorption." A.G. Joly, M Henyk, KM Beck, PE Trevisanutto, PV Sushko, WP Hess, and AL Shluger, *J. Phys. Chem. B Lett.* (accepted).
- 19) "Laser-induced oxygen vacancy formation and diffusion on TiO₂ (110) surfaces probed by photoemission electron microscopy." G. Xiong, AG Joly, KM Beck, WP Hess, *Phys. Stat. Sol. (c)* (accepted).
- 20) "Excitation-density dependent carrier dynamics on the Si(001)-(2x1) surface." T Ichibayashi, S Tanaka, K Tanimura, and WP Hess, *Phys. Rev. B* (accepted).

Optical Spectroscopy at the Spatial Limit

Wilson Ho

Department of Physics & Astronomy and Department of Chemistry
University of California, Irvine
Irvine, CA 92697-4575 USA

wilsonho@uci.edu

Program Scope:

This project is concerned with the experimental challenge of reaching single molecule sensitivity with sub-molecular spatial resolution in optical spectroscopy and photochemistry. These experiments would lead to an understanding of the inner machinery of single molecules that are not possible with other approaches. Results from these studies will provide the scientific basis for understanding the properties, processes, and phenomena in chemical and physical systems at the nanoscale. The experiments rely on the combination of the unique properties of lasers and scanning tunneling microscopes (STM).

Recent Progress:

Nanoscale electrostatics plays a determining role in the operation of nanoscale electron transport devices. In particular, electrostatic interaction between the conduction channel and nearby charge traps has been shown to lead to a variety of different effects, such as random telegraph noise and hysteretic behavior in the current-voltage characteristics. However, in the current literature, the real-space studies of these effects have been lacking, so that the exact nature of these charge traps, as well as the relation between their locations and their effect on the conduction channel could not be determined directly. In paper [Ref. 1], the imaging and spectroscopic capabilities of the scanning tunneling microscope are used to visualize the effect of charging of local impurity levels on charge transport in C_{60} monolayer crystals. The impurities were introduced by depositing individual Ag atoms on the C_{60} monolayer, which resulted in formation of Ag- C_{60} charge-transfer complexes in the monolayer. Differential conductance spectroscopy shows that charging of these impurities affects the conduction through C_{60} molecules located around the impurities. This effect is used to observe the electrostatic interaction of a pair of charged impurities. Charging of one impurity charge trap is found to shift the energy levels of the other, an analogue of the field-effect action. The interaction between two charged traps serves as a general model for impurity-conduction channel electrostatic interaction and provides experimental evidence on the role of the impurity field-effect action in charge transport at the nanoscale.

The combination of optical excitation with ultrahigh spatial resolution has been long sought after owing to its substantial scientific and technological interests. To date, techniques available to achieve the high spatial resolution with laser illumination are limited by diffraction to about half of the optical wavelength. Although the introduction of near-field scanning optical microscopes (NSOM), either aperture-based or tip-enhanced (also called apertureless), has

successfully extended the spatial resolution beyond the diffraction limit, resolution below 1 nm still remains elusive. In principle, the coupling of photons to the tunneling process in a scanning tunneling microscope (STM) would yield high spatial, spectral and temporal sensitivity. In Publication [Ref. 2], we report atomic scale spatial resolution in the coupling of visible photons to a single molecule in the junction of the STM. For the first demonstration, we present photo-induced electron transfer to a single magnesium porphine (MgP) molecule adsorbed on an ultrathin oxide grown on a metallic substrate [5 \AA Al_2O_3 grown on $\text{NiAl}(110)$] in a STM junction at 10 K. We show that the electron transfer probability is confined spatially to the molecule, exhibits variations in different parts of the molecule, and depends on the photon energy and flux as well as the tip-molecule distance. These results allow us to deduce the mechanism as involving resonant tunneling of a photoexcited electron to the molecule. The demonstrated ability of coupling photons to the tunneling electrons leads to new opportunities to explore molecular dynamics with simultaneous spatial, spectral, and temporal resolutions. In Fig. 1 below, a schematic of the novel mechanism behind the achievement of atomic scale photon coupling is illustrated.

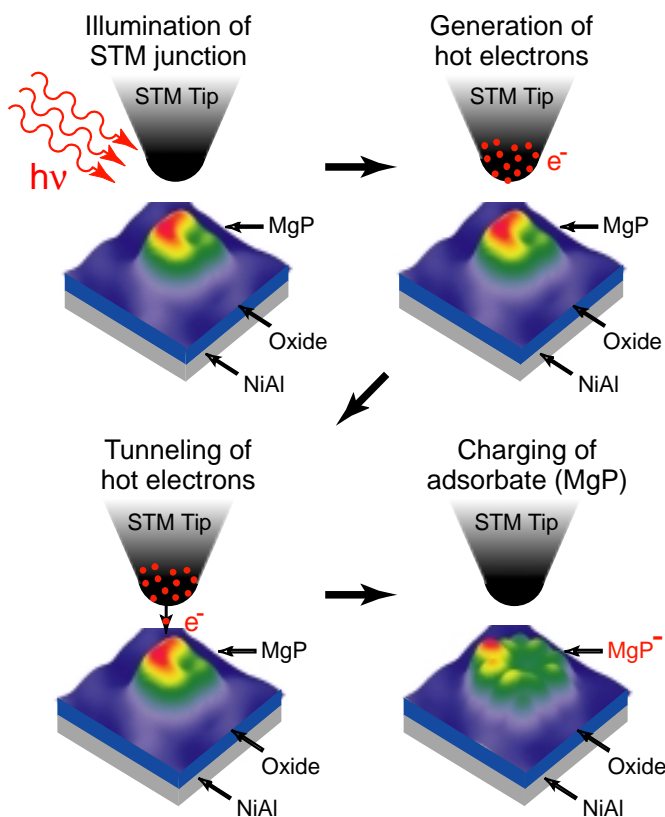


Fig. 1: Sequential steps for photo-induced transfer of an electron to a single molecule of magnesium porphine adsorbed on a 5 \AA thick Al_2O_3 grown on $\text{NiAl}(110)$ substrate. To enable the experiment, the power of the laser is stabilized to 0.1% to avoid temperature drifts and fluctuations. The laser generates hot electrons in the tip. The excited electrons tunnel more efficiently due to the lower barrier. The negatively charged molecule (MgP^-) is stabilized on the oxide surface. The atomic scale resolution is inherent in the mechanism of photo-induced tunneling, resonant in this case with the molecular orbital state.

The experiment measures the probability of photo-induced electron transfer to a particular point inside the single molecule. The point of tunneling can be precisely controlled by positioning the last atom on the tip over a chosen point of the molecule. The atomic scale resolution of photo-induced effect was demonstrated by measuring the photo-induced electron transfer probability as a function of position inside the single molecule. The results from such measurements are shown in Fig. 2.

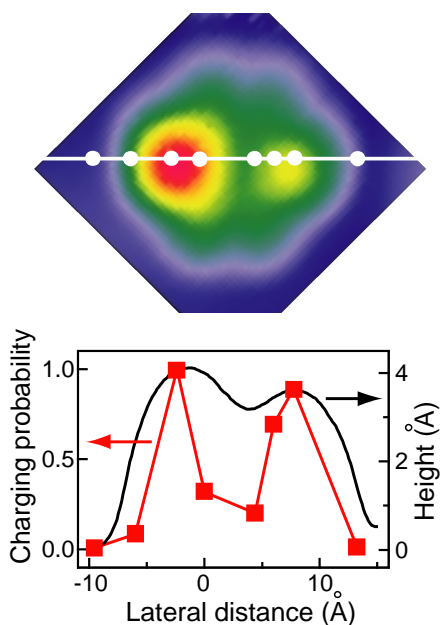


Fig. 2: Spatial dependence of electron transfer inside a single magnesium porphine molecule. A STM image of the molecule is shown on the top. The white dots show the positions inside the molecule where the photo-induced electron transfer probability was measured. These probabilities are plotted below, showing large spatial variations that correlate with the electronic structure of the molecule, consistent with the mechanism of photo-induced mechanism resonant with the molecular electronic state.

Publication [Ref. 2] demonstrates the feasibility of single-molecule experiments that combine the high spatial resolution of scanning tunneling microscopy (STM) with optical methods of excitation and detection. On the one hand, this combination allows one to cross-correlate the optical properties of individual molecules with their adsorption configuration and vibrational and electronic spectra obtained using STM. On the other hand, tunneling-induced photon emission and laser-induced tunneling allow one to observe completely new phenomena where electron transport couples to photons: single-molecule electroluminescence, photo-assisted tunneling. This opens an exciting possibility of controlling the electron tunneling with femtosecond laser pulses, which could allow probing the internal molecular dynamics simultaneously with femtosecond temporal and Ångstrom-spatial resolutions.

Future Plans:

The focus of the research will be on the coupling of lasers to the STM and to the determination of the conditions for achieving optical effects with sub-molecular resolution. How can sub-molecular processes be induced by photons with near-IR, visible, and near-UV wavelengths? During this grant period, we have succeeded in observing photo-induced electron transfer to a single molecule with atomic scale resolution. This observation depends on several factors: 1. stable STM, 2. stable laser power, 3. appropriately chosen system for first demonstration. These initial results open up new opportunities that we will explore in the coming year. Several experiments are in progress. First, the present experiments are extended to excitation with femtosecond lasers to explore atomic scale nonlinear optical effects inside a single molecule. Irradiation with two femtosecond pulse trains with variable delays between them can lead to the first demonstration of simultaneous spatial and temporal experiment. Second, the feasibility of laser induced fluorescence from single molecules is being explored, to probe the fluorescence as a function of position within the single molecule. Such demonstration will lead to new opportunities to explore molecular dynamics inside single molecules.

References to Publications of DOE Sponsored Research (2003-present):

- [1] G.V. Nazin, X.H. Qiu, and W. Ho, “Charging and Interaction of Individual Impurities in a Monolayer Organic Crystal”, *Phys. Rev. Lett.* **95**, 166103-1-4 (2005).
- [2] S.W. Wu, N. Ogawa, and W. Ho, “Atomic Scale Coupling of Photons to Single-Molecule Junction”, *Science* **312**, 1362-1365 (2006).

THEORY OF THE REACTION DYNAMICS OF SMALL MOLECULES ON METAL SURFACES

Bret E. Jackson

Department of Chemistry
701 LGRT
University of Massachusetts
Amherst, MA 01003
jackson@chem.umass.edu

Program Scope

Our objective is to develop realistic theoretical models for molecule-metal interactions important in catalysis and other surface processes. The dissociative adsorption of diatomics on metals, Eley-Rideal and Langmuir-Hinshelwood reactions, recombinative desorption and sticking on surfaces are all of interest. To help elucidate the UHV-molecular beam experiments that study these processes, we examine how they depend upon the nature of the molecule-metal interaction, and experimental variables such as substrate temperature, beam energy, angle of impact, and the internal states of the molecules. Electronic structure methods based on Density Functional Theory (DFT) are used to compute the molecule-metal interaction potentials. Both time-dependent quantum scattering techniques and quasi-classical methods are used to examine the reaction dynamics. Some effort is directed towards developing improved quantum scattering methods that can adequately describe reactions on surfaces, as well as include the effects of temperature (lattice vibration) in quantum dynamical studies.

Recent Progress

We have continued our studies of Eley-Rideal (ER) and hot atom reactions. In an ER reaction, a gas-phase particle combines directly with another particle adsorbed onto a substrate. These reactions are often very exothermic. Extensive studies of the reactions of H atom beams with H-covered metal surfaces demonstrated that the cross sections for his ER reaction are small, on the order of $0.1 - 0.2 \text{ \AA}^2$, even though this is a strongly exothermic and barrier-less reaction. Studies of the reaction dynamics showed why the cross section is small, and showed that the incident H atoms prefer to trap onto the surface without reacting, even at relatively high H atom coverages. These trapped “hot” atoms initially have 2 or more eV of excess energy, and are highly mobile on the surface for several 100’s of fs. If they react with an adsorbate before dissipating this excess energy into the substrate, the molecular hydrogen formed can be highly excited, as in a more direct ER process. Our dynamical and kinetic models for ER and HA reactions are in excellent agreement with experiment, and demonstrate that these hot atom (HA) reactions dominate molecular hydrogen formation on metal surfaces. A textbook chapter summarizing these DOE-funded ER and HA studies appeared in “The Chemical Physics of Solid Surfaces” [2].

We have concluded our studies of the $\text{H(g)} + \text{Cl/Au(111)}$ reaction, which have been motivated primarily by two detailed experimental studies of this system. These experiments observe strong H atom trapping and a thermal Langmuir-Hinshelwood channel for HCl formation, as well as ER and HA channels. One of our findings is that the ER reaction cross section is much larger than for $\text{H(g)} + \text{H/metal}$ reactions, roughly $1 - 2 \text{ \AA}^2$. This is due to a steering mechanism [1], and arises from the relatively large distance of the adsorbed Cl above the metal. The incoming H atom is strongly attracted to both the Cl and

the metal, but it encounters the layer of adsorbed Cl atoms first, and steers towards them. Thus there is no competition between ER reaction and trapping of the H atom onto the surface. There are also some interesting variations of ER reactivity with the Cl vibrational state, and an exchange pathway is observed (for the first time), in which the H remains bound while the Cl desorbs. More than two years have been spent using quasi-classical trajectories to study this reaction for the case of large Cl coverages, and with dissipation of the trapped hot atoms' energy into the lattice [6]. The ER and HA reaction pathways for HCl formation are a bit more complicated than for molecular Hydrogen formation. We find that HA reactions dominate the formation of HCl. We also find that there must be significant energy loss into the substrate excitations, from either the trapped hot H atoms, or the excited product HCl, in order to agree with experiment.

In an earlier study of H atom recombination on Ni(100), we allowed the lattice atoms to move, which required that we construct a potential energy surface based upon the instantaneous positions of the lattice atoms and the adsorbates. We avoided the usual problems associated with pairwise potentials by using a potential based upon ideas from embedded atom and effective medium theory, but instead of using the isolated atom electron densities, we fit the one and two-body terms to reproduce the results of our high-level electronic structure calculations. More recently we have used the part of this potential describing the Ni-Ni interactions to study the sputtering of Ni surfaces by Ar beams, in order to further test the utility of these potentials [4]. We find that this form for the potential very accurately describes the energy required to severely distort the lattice or to remove one or more Ni atoms from the lattice. Agreement of sputtering yields and threshold energies with experiments is greatly improved over earlier models.

We continued our studies of H-graphite interactions. These reactions are believed to play an important role in the formation of molecular Hydrogen on graphitic dust grains in interstellar space, as well as in the etching of the graphite walls of fusion reactors. Using electronic structure methods, we demonstrated that an H atom could chemisorb onto a graphite terrace carbon, with the bonding C atom puckering out of the surface plane by several tenths of an Å. We computed the potential energy surface for the ER reaction of an incident H atom with this chemisorbed H atom, and suggested that the reaction cross sections should be very large – on the order of 10 \AA^2 . Motivated by our studies, the group of Küppers (Bayreuth) demonstrated experimentally that H could indeed chemisorb, and that the lattice did pucker. Our computed adsorbate vibrational frequencies and (recombinative) thermal desorption temperatures were found to be in excellent agreement with experiment. Küppers and co-workers then measured the cross sections for the $\text{H(g)} + \text{D/graphite}$ ER reaction to form HD(g) , and again, theory and experiment were in excellent agreement. We demonstrated that the H_2 formed in these ER reactions should be very highly excited, vibrationally. It has been suggested that vibrationally excited H_2 might be responsible for some of the unique chemistry that occurs in interstellar clouds.

More recently, both our efforts and the efforts of the experimental groups have been focused on graphite edges. Real graphite surfaces are rough in the sense that a sizable fraction of the exposed carbon atoms can be on the edges of graphite planes, as opposed to the terraces. We have performed total energy electronic structure calculations to examine how H atoms react with edge vs terrace carbons. We found that the hydrogenation of an edge carbon proceeded with no barrier, and that the barrier for addition of a second hydrogen to the edge carbons was small [3]. These studies of graphite are also relevant to a sizable body of work examining molecular hydrogen adsorption in and on nano-crystalline graphite. We have examined how molecular hydrogen can chemisorb onto such structures, and have found two low energy pathways where H_2 dissociatively adsorbs over one or two edge carbons, resulting in a doubly-hydrogenated edge carbon, or two neighboring singly-

hydrogenated edge carbons, respectively [3]. The doubly-hydrogenated structure gives rise to a peak that has been observed (but not explained) in the radial distribution functions extracted from neutron scattering studies of graphitic nano-structures exposed to H₂. We have demonstrated that the vapor pressure of H₂ in equilibrium with these hydrogenated structures is too small to be useful for hydrogen storage, due to the strength of the bonds.

The experiments of the Küppers group have shown that the sticking probabilities of H on the graphite terrace are large, roughly 0.4. Given the significant lattice distortion required for chemisorption, this is surprising. We used electronic structure methods to map out the H-graphite interaction as a function of the position of the bonding carbon, and found a barrier to chemisorption of about 0.2 eV, in excellent agreement with recent experiments. A potential energy surface for trapping and sticking was constructed, and a low-dimensional collinear quantum study of the trapping process was implemented [5]. We found that the bonding carbon reconstructs in about 50 fs. Our results suggested that sticking proceeds via a trapping resonance, which relaxes by dissipating energy into the substrate over a ps or so. More recently we computed the full three-dimensional potential, and used classical mechanics to compute the sticking cross sections [7], which are on the order of 0.1 Å² at energies not too far above the barrier. However, when averaged over the experimental incident energy distribution, the computed sticking probabilities were only around 0.05. The proposed mechanism involving a trapping resonance was confirmed. While an improved model that included a fully dynamical graphite lattice did not significantly increase the sticking, we have since come to understand the discrepancy between experiment and theory (ms in preparation). Using DFT, we have found that the graphite lattice can undergo extensive reconstruction when additional H atoms are chemisorbed in the vicinity of an adsorbed H. The binding energies, and the barriers to chemisorption, can vary dramatically from site to site. Our work suggests that while the initial (true zero coverage) sticking may indeed be small, the addition of subsequent H atoms, in specific locations relative to the initial adsorbates, may happen with a large probability. This has now been confirmed by two sets of experiments. The Küppers group has now measured sticking down to (true) zero coverage, finding probabilities of around 0.1. They observe that sticking increases as coverage increases. This group and another have also observed pair formation, via STM, where H atoms are observed to cluster together on the surface, due to these preferred binding sites.

We have long been interested in the dissociative adsorption of methane on metals, and have computed barriers to methane dissociation on the Ni(100) surface. A problem that is not well understood is how and why methane reactivity varies with the temperature of the metal. To explore this we have examined how these barriers change due to lattice distortion. We have found that when a Ni atom puckers out of the plane of the surface, the barrier to dissociation over this Ni atom decreases. Three dimensional quantum scattering calculations were implemented, which allowed for the motion of the metal lattice atom over which the reaction occurs. It was found that the lattice had time to reconstruct during the reaction, even at collision energies of an eV or so. The net result is that the reactivity was significantly larger than for the static lattice case. We compared our results to the standard recoil model, used for many years to explain the effects of thermal lattice motion on dissociative adsorption. For this model, the lattice recoils into the surface during the collision, leading to a lower reactivity. We clearly demonstrated that when a lattice reconstruction in the presence of the adsorbate is possible, the physics is completely different from what has long been assumed.

Future Plans

We expect to make much progress this coming year on the problem of methane dissociation on metals. We have demonstrated that lattice motion can significantly modify the barrier to methane dissociation on Ni(100). Our work also clearly shows that the standard model for including lattice motion in these problems, in which the barrier simply moves back and forth with the vibrating metal atom, are incorrect. We are currently using DFT to construct potential energy surfaces for methane dissociation on Ni(111) and Pt(111) that explicitly includes the position of the metal atom. The dissociation probability as a function of incident energy, surface temperature, and molecular vibrational state will be computed for Ni(100), Ni(111) and Pt(111) using our 5 degree-of-freedom quantum model. We will then analyze the wealth of experimental data that exists for these systems. Specifically, we hope to understand the role played by lattice motion and reconstruction in this important reaction. Standard models have suggested that thermal effects should be more significant on Ni than Pt, due to the smaller mass, but this is not what has been observed. Perhaps the existence of lattice reconstruction can explain this discrepancy. We intend to also examine this behavior on the step and defect sites of these Ni and Pt surfaces. It is likely that the magnitudes of the thermal fluctuations and any reconstructions are larger at these defect sites than on the terraces.

References

- [1]. J. Quattrucci, B. Jackson, and D. Lemoine "Eley-Rideal reactions of H atoms with Cl adsorbed on Au(111): Quantum and quasiclassical studies, *J. Chem. Phys.* 118, 2357-2366 (2003).
- [2]. B. Jackson, "Eley-Rideal and hot atom reactions between H atoms on metal and graphite surfaces," in "The Chemical Physics of Solid Surfaces," vol. 11, D. P. Woodruff, ed., pp 51-77, Elsevier Science B. V. (2003).
- [3]. X. Sha and B. Jackson, "The Location of Adsorbed Hydrogen in Graphite Nanostructures," *J. Am. Chem. Soc.* 126, 13095-13099 (2004).
- [4]. Z. B. Guvenc, R. Hippler and B. Jackson, "Bombardment of Ni(100) surface with low-energy argons: molecular dynamics simulations, *Thin Solid Films* 474, 346-357 (2005).
- [5]. X. Sha, B. Jackson, D. Lemoine and B. Lepetit, "Quantum studies of H Atom Trapping on a graphite surface," *J. Chem. Phys.* 122, 014709, 1-8 (2005).
- [6]. J. Quattrucci and B. Jackson, "Quasi-classical study of Eley-Rideal and Hot Atom reactions of H atoms with Cl adsorbed on a Au(111) surface, *J. Chem. Phys.* 122, 074705, 1-13 (2005).
- [7]. J. Kerwin, X. Sha and B. Jackson, " Classical studies of H atom trapping on a graphite surface," *J. Phys. Chem. B* (in press, 2006).

Understanding the Electron-water Interaction at the Molecular Level: Integrating Theory and Experiment in the Cluster Regime: DE-FG02-06ER15800

Program Manager: Dr. Gregory Fiechtner

K. D. Jordan (jordan@pitt.edu), Dept. of Chemistry, University of Pittsburgh, Pittsburgh, PA 15260
and M. A. Johnson (mark.johnson@yale.edu), Dept. of Chemistry, Yale University, New Haven, CT 06520

We continue to concentrate on uncovering the molecule-level rearrangements that mediate excess electron accommodation by water. In the bulk, this process yields a “hydrated electron”, or e_{aq}^- , that is an intrinsic intermediate in radiation-damaged biological systems as well as in the spontaneous degradation of aqueous waste associated with the processing of radioactive material.⁶ Our emphasis is to establish how structural aspects of the local electron binding site control both the binding energy of the excess electron as well as its relaxation dynamics by studying the $(H_2O)_n^-$ cluster anions as model systems.

One of the emerging questions regards the nature of the three isomeric classes displayed by the $(H_2O)_n^-$ clusters that are grouped according their electron binding energies (denoted I, II and III in decreasing order of vertical electron detachment energy (VDE)). A major discovery from our program has been the identification of the binding site in the highest binding isomer (I) in the smaller ($n = 3 - 6$) clusters, where the excess electron is preferentially attached to a particular water molecule that is tethered to the network with a double H-bond acceptor (AA) motif as indicated in the inset in Fig. 1.⁷ The AA water molecule orients both its H-atoms directly into the electron cloud, an arrangement that yields a unique, red-shifted spectral signature band in the intramolecular bending region. In a detailed study of the hexamer anion isomers, we also established that the more weakly binding isomer (class II) does not display this motif,⁴ so that, in the small size regime, differences in the *local* binding arrangement are primarily responsible for the different overall electron binding energies. In the past year, we have extended this work to explore whether the AA binding motif persists in the larger type I clusters, as well as to establish the spectra corresponding to an ion ensemble with a well-defined temperature.

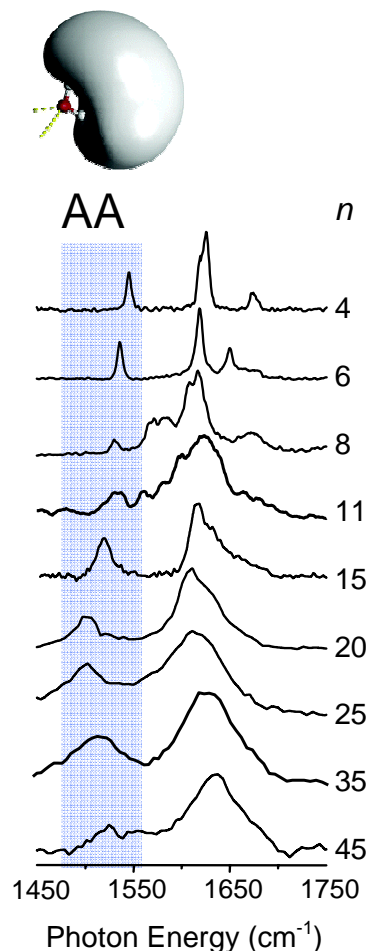


Fig. 1. Vibrational spectra of the $(H_2O)_n^-$ clusters in the HOH bending region. Spectra from $n = 4 - 11$ were obtained via argon predissociation, while the higher clusters were obtained via multiphoton dissociation at the free electron laser (FELIX) in the Netherlands. The spectral signature of the AA binding motif (highlighted) is present in all clusters studied.

A. *Evolution of the AA binding site in larger clusters: Bending spectra via Ar tagging and multiphoton dissociation of 20 K $(\text{H}_2\text{O})_n^-$ ions at FELIX.*

At Yale, we carried out a study of the $(\text{H}_2\text{O})_n^- \cdot \text{Ar}$ clusters in the intramolecular bending region, which indicated that the AA motif is still present in the binding site up to $n = 24$.¹ We also engaged in a collaborative effort with Prof. Daniel Neumark (Berkeley) and Dr. Knut Asmis (Fritz Haber Institute, Berlin) to survey the spectra of $(\text{H}_2\text{O})_n^-$ ions cooled in a multipole RF trap to a well-defined temperature (20K). In this case, spectra in the intramolecular bending region were obtained in a multiphoton dissociation mode using the free electron laser (FELIX) in the Netherlands. The results of this effort are combined in Fig. 1, and the signature AA band is clearly evident up to $n = 45$, the highest cluster size studied. This is significant because recent studies of the ultrafast decay dynamics of the electronically excited states of these clusters indicate that their internal conversion (IC) rates smoothly extrapolate to that of the bulk e_{aq}^- . This, in turn, establishes that one can now implement microscopic, molecular level simulations to understand the origin of the very fast IC rates in the context of a concrete (that is, spectroscopically characterized) local binding environment.

B. *Experimental determination of the site-specific interactions of intramolecular vibrations with the excess electron by analysis of “Fano” lineshapes.*

Our structural characterization of the small clusters provides an excellent opportunity to unravel the detailed coupling strengths of *particular* water molecules within the network to the excess electron attached to the AA water molecule. Here we capitalized on the fact that the higher energy OH stretch vibrations lie above the VDE in the $n = 3 - 5$ clusters, while the OD stretches lie below the VDE. Thus, we can first establish the vibrational level pattern using vibrational predissociation of the $(\text{D}_2\text{O})_n^-$ systems, and then use this information to follow how these transitions are distorted when they become embedded in the electron continuum in the $(\text{H}_2\text{O})_n^-$ isotopomer. Application of this approach to the tetramer is shown in Fig. 2, where it is clear that the most red-shifted bands, which arise from the OH stretching vibrations of the AA water molecule, are much more distorted than the higher energy band associated with the dangling OH stretching vibrations on the AD waters. Analysis of this pattern reveals that the autodetachment lifetimes of the symmetric (AA_s), asymmetric (AA_{as}) and free OH stretch vibrations of $(\text{H}_2\text{O})_4^-$ are 80, 200 and 520 fs, respectively. Note that the relaxation time of the AA symmetric stretching vibration is close to the relaxation time of the electronically excited state of

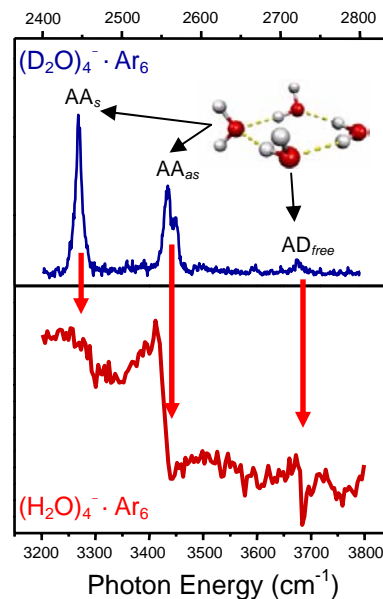


Fig. 2. Sharp vibrational resonances in the low energy OD stretching region of the $(\text{D}_2\text{O})_4^-$ complex reveal the pattern of vibrational band origins strongly distorted by rapid autodetachment in the higher energy OH stretching bands of $(\text{H}_2\text{O})_4^-$. AA and AD labels indicate the H-bonding environment according to the number of acceptor (A) and donor (D) bonds.

the larger $(\text{H}_2\text{O})_n^-$ clusters (~ 100 fs). Most recently, we have extended our study of the coupling of vibrationally excited states to the autodetachment continuum to include the intramolecular bending modes, which required working with the very weak binding trimer anion. Interestingly, the bending motion of the AA water molecule is *not* particularly strongly coupled to the excess electron with an autodetachment lifetime of about 600 fs.

C. *Isolating the spectra of type II clusters using isomer-photosensitive population modulation.*

An important unresolved aspect of the anionic water clusters is whether the excess electron is sequestered on the inside or resides on the surface, and to what extent this solvation morphology is related to the isomer classes.

For example, Neumark and co-workers have advanced the hypothesis that the primary difference between the type I and II forms at larger ($n > 40$) sizes is that they correspond to interior and surface states, respectively. As discussed in section A, however, we have already established that the AA motif is common to the type I isomers in this size regime, and that at $n = 6$, type II does not display the AA signature band in the bending region. We are therefore engaging a set of experiments designed to recover the bending spectra of isomer II at large sizes. In such an experiment, we first use a powerful infrared laser to photodeplete the contribution of isomer II from an ensemble that contains both I and II, and then we scan the vibrational spectrum of the resulting ion packet. By comparing the spectra before and after photodepletion of II, the contribution of II can be extracted by spectral subtraction. The first results from the application of this scheme to the $n = 7$ and 8 species are very promising, as illustrated in Fig. 3. This strategy has allowed us to establish that, in both cases, the type II clusters again do not display the AA local binding motif.

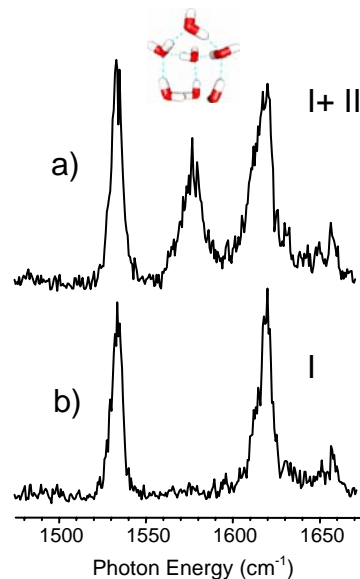


Fig. 3. Infrared spectra of the $(\text{H}_2\text{O})_7^- \cdot \text{Ar}_4$ species a) before, and b) after photodepletion of the isomer II species with a preceding off-resonant laser.

D. *Application of the Drude model to probe new electron binding motifs in larger, three dimensional networks.*

Interpretation of the spectral patterns displayed by the $(\text{H}_2\text{O})_n^-$ isomers in the context of structures required development and implementation of computation methods that can handle the high-order effects at play in these intrinsically diffuse electron distributions. The Pittsburgh portion of the team has applied a model employing quantum Drude oscillators to describe dispersion-like interactions between the excess electron and the water molecules to examine the electron binding motifs in $(\text{H}_2\text{O})_n^-$ clusters and to characterize the $(\text{H}_2\text{O})_6^-$ cluster at finite temperature.¹⁵ These studies have

revealed the existence of a new binding motif, illustrated in Fig. 4, in which the excess electron is bound primarily by the dispersion/polarization contribution (as opposed to the long range electric dipole moment evident in the observed structures like that of the tetramer ion shown in the inset in Fig. 2). These calculations have also revealed that the $(\text{H}_2\text{O})_6^-$ cluster has several isomers that weakly bind the excess electron and yet are more stable than the observed AA species.

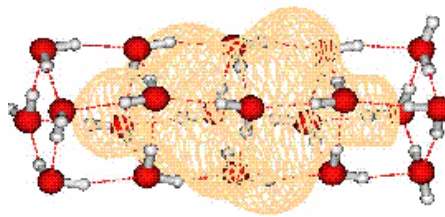


Fig. 4. Example of a cluster for which binding of the excess electron is dominated by polarization and dispersion

References for papers published under DOE support

1. "Infrared spectroscopy of water cluster anions, $(\text{H}_2\text{O})_{n=3-24}^-$ in the HOH bending region: Persistence of the double H-bond acceptor (AA) water molecule in the excess electron binding site of the class I isomers," J. R. Roscioli, N. I. Hammer and M. A. Johnson, *J. Phys. Chem. A*, **110**, 517-7520, 2006.
2. "Vibrational predissociation spectroscopy of the $(\text{H}_2\text{O})_{6-21}^-$ clusters in the OH stretching region: Evolution of the excess electron-binding signature into the intermediate cluster size regime," N. I. Hammer, J. R. Roscioli, J. C. Bopp, J. M. Headrick and M. A. Johnson, *J. Chem. Phys.*, **123**, 244311, 2005.
3. "Infrared spectrum and structural assignment of the water trimer anion," N. I. Hammer, J. R. Roscioli, M. A. Johnson, E. M. Myshakin and K. D. Jordan, *J. Phys. Chem. A*, **109**, 11526-11530, 2005.
4. "Identification of two distinct electron binding motifs in the anionic water clusters: A vibrational spectroscopic study of the $(\text{H}_2\text{O})_6^-$ isomers," N. I. Hammer, J. R. Roscioli and M. A. Johnson, *J. Phys. Chem. A*, **109**, 7896-7901, 2005.
5. "An infrared investigation of the $(\text{CO}_2)_n^-$ clusters: Core ion switching from both the ion and solvent perspectives," J-W. Shin, N.I. Hammer, M. A. Johnson, H. Schneider, A. Glob and J. M. Weber, *J. Phys. Chem. A*, **109**, 3146-3152, 2005.
6. "Role of water in electron-initiated processes and radical chemistry: Issues and scientific advances," Bruce C. Garrett *et al.*, *Chem. Rev.*, **105**, 355-390, 2005.
7. "How do small water clusters bind an excess electron?" N. I. Hammer, J-W. Shin, J. M. Headrick, E. G. Diken, J. R. Roscioli, G. H. Weddle and M. A. Johnson, *Science*, **306**, 675-679, 2004.
8. "Infrared signature of structures associated with the $\text{H}^+ \cdot (\text{H}_2\text{O})_n$, $n = 6-27$, clusters," J-W. Shin, N. I. Hammer, E. G. Diken, M. A. Johnson, R. S. Walters, T. D. Jaeger, M. A. Duncan, R. A. Christie and K. D. Jordan, *Science*, **304**, 1137-1140, 2004.
9. "The vibrational spectrum of the neutral $(\text{H}_2\text{O})_6$ precursor to the "magic" $(\text{H}_2\text{O})_6^-$ cluster anion by argon-mediated, population-modulated electron attachment spectroscopy," E. G. Diken, W. H. Robertson and M. A. Johnson, *J. Phys. Chem. A*, **108**, 64-68, 2004.
10. "Large anharmonic effects in the infrared spectra of the symmetrical $\text{CH}_3\text{NO}_2^- \cdot (\text{H}_2\text{O})$ and $\text{CH}_3\text{CO}_2^- \cdot (\text{H}_2\text{O})$ complexes," E.M. Myshakin, K.D. Jordan, E.L. Sibert III and M. A. Johnson, *J. Chem. Phys.*, **119**, 10138-10145, 2003.
11. "Spectroscopic determination of the OH^- solvation shell in the $\text{OH}^- \cdot (\text{H}_2\text{O})_n$ clusters," W. H. Robertson, E. G. Diken, E. A. Price, J-W. Shin and M. A. Johnson, *Science*, **299**, 1367-1372, 2003.
12. "Molecular aspects of halide ion hydration: The cluster approach," W. H. Robertson and M. A. Johnson, *Annual Review of Physical Chemistry*, **54**, 173-213, 2003.
13. "Dominant structural motifs of $\text{NO}^- \cdot (\text{H}_2\text{O})_n$ complexes: Infrared spectroscopic and *ab initio* studies," K. M. Myshakin, W. H. Robertson, G. H. Weddle, K. D. Jordan and M. A. Johnson, *J. Chem. Phys.*, **118**, 4945-4953, 2003.
14. "Electron Binding Motifs of $(\text{H}_2\text{O})^-$ Clusters," T. Sommerfeld and K. D. Jordan, *J. Am. Chem. Soc.*, **128**, 5828-5833, 2006.
15. "Low-lying Isomers and Finite Temperature of $(\text{H}_2\text{O})_6^-$," T. Sommerfeld, S. D. Gardner, A. DeFusco, and K. D. Jordan, *J. Chem. Phys.*, *in press*

Chemical Kinetics and Dynamics at Interfaces

Structure and Reactivity of Ices, Oxides, and Amorphous Materials

Bruce D. Kay (PI), R. Scott Smith, and Zdenek Dohnalek

Chemical Sciences Division
Pacific Northwest National Laboratory
P.O. Box 999, Mail Stop K8-88
Richland, Washington 99352
bruce.kay@pnl.gov

Additional collaborators on these projects include P. Ayotte, C. T. Campbell, J. L. Daschbach, H. Jonsson, J. Kim, G. A. Kimmel, N. G. Petrik, G. K. Schenter, and T. Zubkov

Program Scope

The objective of this program is to examine physiochemical phenomena occurring at the surface and within the bulk of ices, oxides, and amorphous materials. The microscopic details of physisorption, chemisorption, and reactivity of these materials are important to unravel the kinetics and dynamic mechanisms involved in heterogeneous (i.e., gas/liquid) processes. This fundamental research is relevant to solvation and liquid solutions, glasses and deeply supercooled liquids, heterogeneous catalysis, environmental chemistry, and astrochemistry. Our research provides a quantitative understanding of elementary kinetic processes in these complex systems. For example, the reactivity and solvation of polar molecules on ice surfaces play an important role in complicated reaction processes that occur in the environment. These same molecular processes are germane to understanding dissolution, precipitation, and crystallization kinetics in multiphase, multicomponent, complex systems. Amorphous solid water (ASW) is of special importance for many reasons, including the open question over its applicability as a model for liquid water, and fundamental interest in the properties of glassy materials. In addition to the properties of ASW itself, understanding the intermolecular interactions between ASW and an adsorbate is important in such diverse areas as solvation in aqueous solutions, cryobiology, and desorption phenomena in cometary and interstellar ices. Metal oxides are often used as catalysts or as supports for catalysts, making the interaction of adsorbates with their surfaces of much interest. Additionally, oxide interfaces are important in the subsurface environment; specifically, molecular-level interactions at mineral surfaces are responsible for the transport and reactivity of subsurface contaminants. Thus, detailed molecular-level studies are germane to DOE programs in environmental restoration, waste processing, and contaminant fate and transport.

Our approach is to use molecular beams to synthesize “chemically tailored” nanoscale films as model systems to study ices, amorphous materials, supercooled liquids, and metal oxides. In addition to their utility as a synthetic tool, molecular beams are ideally suited for investigating the heterogeneous chemical properties of these novel films. Modulated molecular beam techniques enable us to determine the adsorption, diffusion, sequestration, reaction, and desorption kinetics in real-time. In support of the experimental studies, kinetic modeling and Monte Carlo simulation techniques are used to analyze and interpret the experimental data.

Recent Progress and Future Directions

Understanding the Sticking Probability of Water Molecules on Ice The adsorption of molecules on surfaces is an important step in many processes, including crystal growth, catalysis, and atmospheric aerosol and cloud formation. In order for a molecule not to be reflected during a collision it needs to lose the energy associated with the component of momentum normal to the surface. Based on this it is expected that the adsorption probability decreases with increasing normal momentum for systems that do not have an activation barrier to adsorption. Hence, for a fixed kinetic energy the sticking probability decreases as the incoming direction of the molecule is moved away from the surface normal. This behavior, termed “normal energy scaling”, is frequently observed for the adsorption of molecules on smooth metal surfaces. When the surface is highly corrugated, that is, when there is a large variation of

the potential energy as the incident molecule is moved along the surface, the conversion between parallel and perpendicular components of the momentum occurs readily and the sticking probability then scales with the total incident kinetic energy. Most systems exhibit adsorption behavior somewhere between normal and total energy scaling.

The adsorption of water on ice is unusual in this regard in that sticking coefficient is found to scale well with only the incident momentum component *along* the surface. That is, molecules with the same velocity along the surface but with quite different velocity normal to the surface exhibit the same sticking probability. The explanation for this behavior appears to be a strong variation of the molecule–surface interaction energy as the molecule rotates, leading to scattering into the vapor phase if the molecule does not have enough time to adjust its orientation into an attractive configuration as it moves along the surface. Classical scattering calculations employing the empirical TIP4P water potential semi-quantitatively reproduce the experimental molecular beam results. This intriguing behavior arises from the strong orientational dependence of hydrogen bonding in water and may be characteristic of hydrogen-bonded systems in general. Other hydrogen-bonded systems will be explored in future studies.

Crystalline Ice Growth on Pt(111) and Pd(111): Observation of a Hydrophobic water Monolayer In collaboration with Greg Kimmel and Nikolay Petrik we have investigated the growth of crystalline ice (CI) and ASW films on Pt(111) and Pd(111) using rare gas physisorption. It is well-known that the water monolayer wets both of these metals and it was widely-believed that these substrates were good templates for the epitaxial growth of crystalline ice films. Our studies confirm that the water monolayer wets both substrates at all temperatures investigated (20-155 K) and that ASW films deposited below ~125 K also wet the water monolayer. Surprisingly, crystalline ice films grown at higher temperatures ($T > 135$ K) do not wet the water monolayer! Furthermore, the wetting ASW films dewet exposing the underlying water monolayer as they transform to CI upon heating. These findings demonstrate that the water monolayer on both Pt(111) and Pd(111) is *hydrophobic* with respect to the growth of CI.

The structure of the water monolayer on these metals is key to understanding the observed *hydrophobicity*. For both Pt(111) and Pd(111) recent experiments and theory indicate that all water molecules in the first monolayer interact significantly with the metal substrate. The water molecules form a nearly-planar, hexagonal array with each molecule hydrogen-bonded to three other water molecules in the array. In this array half the water molecules bind to the underlying metal through the oxygen lone pair and the other half have a hydrogen atom point toward the metal. Therefore, each water molecule in the monolayer forms four bonds, leaving no dangling OH groups or lone pair electrons protruding into the vacuum. Since this fully-coordinated water monolayer has no additional attachment points it is *hydrophobic* to additional water growth. Future experiment will employ these techniques in combination with FTIR to explore water adsorption and film growth on a variety of other metal and metal-oxide substrates.

Methane Adsorption, Dissociation and Reaction on Pd nanoparticles on MgO (100) Heterogeneous catalysts consisting of transition metal nanoparticles dispersed on oxide supports are pervasive in modern industrial applications, such as oil refining, organic synthesis, and reduction of greenhouse gas or other emissions. Understanding the effect that the nanometer scale confinement of matter has on catalytic properties is a current scientific challenge, since it is clear that late transition metal particles below 6 nm in diameter can often have very different chemical and catalytic reactivity (normalized to metal surface area) than larger particles of the same material. This may be due to the fact that a large fraction of the particle's surface metal atoms are in sites with coordination numbers much lower than on larger particles, or special electronic effects. Oxide-supported Pd nanoparticles are used to catalyze low-temperature methane combustion to reduce NO_x emissions inherent to normal air combustion. The reaction depends critically on the dissociation of methane molecules at the Pd surface.

We studied the dissociative adsorption of methane on size controlled Pd particles grown on MgO(100). A combination of molecular beam scattering and surface analytical techniques were employed to directly probe the fraction of methane molecules that dissociate at the Pd surface as a function of the molecular beam energy and incident angle. Control measurements on the Pd(111) surface confirmed “normal energy scaling” for the methane dissociative sticking probability consistent with an activation barrier

normal to the surface. In contrast, sticking measurements on supported Pd particles (~3 nm wide) with the methane beam directed normal to the MgO(100) surface results in a large fraction of the methane/Pd collisions occurring on regions of the particles where the beam direction is far from the local particle surface normal, resulting in a lower sticking probability. It is important to decouple this effect from the measured sticking probabilities in order to compare the intrinsic reactivity of the Pd particles with Pd(111). By carefully considering the expected equilibrium particle shape and obtaining the area fraction of the particles experimentally, we can make a quantitative comparison between sticking on the particles and sticking on the (111) surface. We find that the intrinsic reactivity of the surfaces of small Pd particles (~3 nm) for methane compared to Pd(111) is at most two times larger. We emphasize the importance of having a good knowledge of particle structure before attempting such a molecular beam study of nanoparticle reactivity. This type of correction has not been applied previously, but should be broadly applicable to molecular beam studies of particle reactivity, so that the actual activity of the particles can be probed and compared to flat metal surfaces. Clearly this topic is a fertile area for future research.

Cryogenic CO₂ Formation on Oxidized Gold Clusters Synthesized via Reactive Layer Assisted Deposition The catalytic chemistry of gold is a topic of great current interest. Specifically, supported gold clusters have been shown to catalyze the oxidation of CO to CO₂ at low temperature. It is believed that the rate-limiting step in this reaction is the dissociative chemisorption of molecular oxygen. Recent studies by Mullins and colleagues employing an atomic oxygen beam to oxidize gold have shown that CO₂ formation can occur at temperatures as low as 65 K. The formation of oxidized gold is the key to this reactivity.

In previous work we developed a new method for synthesizing metal oxide (MgO) nanostructures which has subsequently been termed Reactive Layer Assisted Deposition (RLAD). In the RLAD technique, a beam of metal atoms is deposited onto multilayers of condensed oxygen. In the present study, gas-phase Au atoms are deposited onto a multilayer film of molecular oxygen. Heating the film resulted in the formation of oxidized gold clusters confirmed using a combination of X-ray photoelectron spectroscopy and temperature programmed desorption (TPD). The reactivity of the oxidized clusters with CO was studied using a combination of molecular beam scattering techniques and TPD. These studies show that the oxidized gold clusters readily react with CO to produce CO₂ at temperatures as low as 35 K. At temperatures between 180 and 300 K, the isothermal oxidation reaction runs to completion, resulting in a clean gold surface. The initial CO₂ production rate decreases with increasing temperature due to a kinetic competition between CO desorption and reaction. These results clearly show that deposition of atomic, charge neutral gold onto a multilayer of O₂ at 22 K forms chemisorbed atomic oxygen. Future studies will examine the structure and chemical reactivity of a variety of novel metal and metal-oxide nanostructures using these techniques.

References to Publications of DOE sponsored Research (CY 2003- present)

1. "The deposition angle-dependent density of amorphous solid water films", Z. Dohnalek, G. A. Kimmel, P. Ayotte, R. S. Smith and B. D. Kay, *Journal of Chemical Physics*, **118**, 364, (2003)
2. "Molecular Beam Studies of Nanoscale Films of Amorphous Solid Water" .R. S. Smith, Z. Dohnalek, G. A. Kimmel, G. Teeter, P. Ayotte, J. Daschbach and B. D. Kay. In *Water in Confining Geometries*; V. Buch and J. P. Devlin, Eds.; Springer, pp 337, (2003).
3. "Temperature independent physisorption kinetics and adsorbate layer compression for Ar adsorbed on Pt(111)", G. A. Kimmel, M. Persson, Z. Dohnalek and B. D. Kay, *Journal of Chemical Physics*, **119**, 6776, (2003).
4. "Adsorption, desorption, and clustering of H₂O on Pt(111)", J. L. Daschbach, B. M. Peden, R. S. Smith and B. D. Kay, *Journal of Chemical Physics*, **120**, 1516, (2004).

5. "Helium diffusion through H₂O and D₂O amorphous ice: Observation of a lattice inverse isotope effect", J. L. Daschbach, G. K. Schenter, P. Ayotte, R. S. Smith and B. D. Kay, *Physical Review Letters*, **92**, 198306, (2004).
6. "Reactive growth of nanoscale MgO films by Mg atom deposition onto O₂ multilayers", J. Kim, Z. Dohnalek, J. M. White and B. D. Kay, *Journal of Physical Chemistry B*, **108**, 11666, (2004).
7. "Role of water in electron-initiated processes and radical chemistry: Issues and scientific advances", B. C. Garrett, et al. *Chemical Reviews*, **105**, 355, (2005)
8. "Influence of surface morphology on D₂ desorption kinetics from amorphous solid water", L. Hornekaer, A. Baurichter, V. V. Petrunin, A. C. Luntz, B. D. Kay and A. Al-Halabi, *Journal of Chemical Physics*, **122**, 124701, (2005).
9. "n-Alkanes on MgO(100). I. Coverage-dependent desorption kinetics of n-butane", S. L. Tait, Z. Dohnalek, C. T. Campbell and B. D. Kay, *Journal of Chemical Physics*, **122**, 164707, (2005).
10. "n-Alkanes on MgO(100). II. Chain length dependence of kinetic desorption parameters for small n-alkanes", S. L. Tait, Z. Dohnalek, C. T. Campbell and B. D. Kay, *Journal of Chemical Physics*, **122**, 164708, (2005).
11. "Structural characterization of nanoporous Pd films grown via ballistic deposition", J. Kim, Z. Dohnalek and B. D. Kay, *Surface Science*, **586**, 137, (2005).
12. "Adsorption and Desorption of HCl on Pt(111)", JL Daschbach, J Kim, P Ayotte, RS Smith and BD Kay, *Journal of Physical Chemistry B*, **109**, 15506, (2005).
13. "Water Adsorption, Desorption and Clustering on FeO(111)" J. L. Daschbach, Z. Dohnálek, S-R. Liu, R. S. Smith, and B. D. Kay, *Journal of Physical Chemistry B* **109**, 10362, (2005).
14. "Methane Adsorption and Dissociation and Oxygen Adsorption and Reaction with CO on Pd Nanoparticles on MgO(100) and on Pd(111)", S. L. Tait, Z. Dohnálek, C. T. Campbell, B. D. Kay," *Surface Science* **591**, 90, (2005)
15. "Crystalline Ice Growth on Pt(111): Observation of a Hydrophobic Water Monolayer" G. A. Kimmel, N. G. Petrik, Z. Dohnálek, and B. D. Kay , *Physical Review Letters* **95**, 166102, (2005).
16. "What Determines the Sticking Probability of Water Molecules on Ice?", E.R. Batista, P. Ayotte, A. Bilic, B.D. Kay, and H. Jonsson, *Physical Review Letters* **95**, 223201, (2005).
17. "Cryogenic CO₂ Formation on Oxidized Gold Clusters Synthesized via Reactive Layer Assisted Deposition" J. Kim, Z. Dohnálek, and B. D. Kay, *Journal of The American Chemical Society Communication*, **127**, 14592, (2005).
18. "The Effect of Incident Collision Energy on the Phase and Crystallization Kinetics of Vapor Deposited Water Films" R. S. Smith, T. Zubkov, and B. D. Kay, *Journal of Chemical Physics*, **124**, 114710, (2006)
19. "Layer-by-layer Growth of Thin Amorphous Solid Water Films on Pt(111) and Pd(111)", G. A. Kimmel, N. G. Petrik, Z. Dohnálek, and B. D. Kay ", *Journal of Chemical Physics*, **125**, 044713, (2006)
20. "Growth of Epitaxial Thin Pd(111) Films on Pt(111) and Oxygen Terminated FeO(111) Surfaces" Z. Dohnálek, J. Kim, and B. D. Kay, , *Surface Science* (in press 2006)

Chemical Kinetics and Dynamics at Interfaces

Non-Thermal Reactions at Surfaces and Interfaces

Greg A. Kimmel (PI) and Nikolay G. Petrik

Fundamental Science Directorate

Pacific Northwest National Laboratory

P.O. Box 999, Mail Stop K8-88

Richland, WA 99352

gregory.kimmel@pnl.gov

Program Scope

The objective of this program is to investigate non-thermal reactions at surfaces and interfaces using ultra-high vacuum, surface science techniques. The fundamental mechanisms of radiation damage to molecules in the condensed phase are of considerable interest to a number of scientific fields ranging from radiation biology to astrophysics. In nuclear reactor design, waste processing, radiation therapy, and many other situations, the non-thermal reactions in aqueous systems are of particular interest. Since the interaction of high-energy radiation (gamma-rays, alpha particles, etc.) with water produces copious amounts of low-energy secondary electrons, the subsequent reactions of these low-energy electrons are particularly important. The general mechanisms of electron-driven processes in homogeneous, dilute aqueous systems have been characterized in research over the last several decades. More recently, the structure of condensed water and its interactions with electrons, photons, and ions have been extensively studied and a variety of non-thermal reaction mechanisms identified. However, the complexity of the electron-driven processes, which occur over multiple length and time scales, has made it difficult to develop a detailed molecular-level understanding of the relevant physical and chemical processes.

We are focusing on low-energy, electron-stimulated reactions in thin water films. Our approach is to use a molecular beam dosing system to create precisely controlled thin films of amorphous solid water (ASW) and crystalline ice (CI). Using isotopically layered films of D₂O, H₂¹⁶O and H₂¹⁸O allows us to explore the spatial relationship between where the incident electrons deposit energy and where the electron-stimulated reactions subsequently occur within the films. Furthermore, working with thin films allows us to explore the role of the substrate in the various electron-stimulated reactions.

Recent Progress:

Structure of Crystalline Ice and Amorphous Solid Water Films on Pt(111) and Pd(111)

In collaboration with Bruce Kay and Zdenek Dohnálek, we have investigated the growth of crystalline ice and ASW films on Pt(111) and Pd(111) using rare gas physisorption. The water monolayer wets both substrates at all temperatures investigated (20-155 K). At low temperatures ($T \leq 120$ K), additional water layers kinetically wet the water monolayer. However, crystalline ice films grown at higher temperatures ($T > 135$ K) do not wet the monolayer. The results are consistent with recent theory and experiments suggesting that the molecules in the water monolayer form a surface with no dangling OH bonds or lone pair electrons, giving rise to a *hydrophobic water monolayer* on Pt(111) and Pd(111).

Since the van der Waals interaction of a rare gas atom with a metal surface is a sensitive function of the distance between them, the TPD spectra of rare gas atoms can be used to assess the height of a desorbing atom above a metal surface. Since the desorption of 1 ML of Kr (or Ar, N₂, etc) from bare Pt (or Pd) and 1, 2 or multilayers of water can be readily distinguished, this same approach can also be used to determine the height distribution of a thin water film grown on a metal substrate.

Figure 1 shows the fraction of a Pt(111) substrate that is not covered by any water, F_0 , and that portion covered by only one layer of water, F_1 , as a function of the water coverage, θ . Since water wets Pt(111), F_0 decreases linearly from 1 to 0 as θ increases from 0 to 1 ML (fig. 1A).

FI versus θ depends on the growth conditions. For temperatures below ~ 120 K which results in the growth of ASW films, the second (and third) layers of water wet the water monolayer and FI decreases linearly as θ increases from 1 to 2 ML (fig. 1A, open triangles).

In contrast to low temperature ASW growth, CI films grown at higher temperatures, where the water mobility is higher, are dramatically different. For $\theta > 1$ ML, the CI films do not wet the water monolayer on Pt(111). The inset of Fig. 1B shows the Kr TPD spectra for ~ 1 ML of Kr on various coverages of water ranging from 1 ML to 50 ML grown at 152 K. For CI films, the WI peak is readily distinguished from the Kr desorbing from the multilayer ice crystallites, CI (inset). The WI TPD peak indicative of Pt covered with only one layer of water does not completely disappear even for total water coverages as high as ~ 45 ML.

CI films grown at other temperatures (140-155 K) also do not wet the water monolayer. The coverage at which the WI TPD peak disappears depends on the growth temperature and flux: At higher growth temperatures or lower fluxes, higher total water coverages are required to completely cover the water monolayer. The fraction of the surface covered by only one monolayer of water, FI , highlights the different grow mode for CI for $\theta > 1$ ML: At 152 K, FI decreases over a much longer length scale, not vanishing until $\theta \sim 50$ ML (Fig. 1B, triangles).

Recent experimental and theoretical results indicate for water films for $\theta \leq 1$ on Pt(111) and Pd(111) all the molecules in the first layer interact significantly with the metal substrate: Half the molecules bind to the surface through the oxygen lone pair, half have a hydrogen atom pointing toward the metal, and all the molecules form hydrogen bonds to 3 neighboring water molecules. Therefore, each molecule in the monolayer forms four bonds, leaving no dangling OH bonds or lone pair electrons protruding into the vacuum. Heuristically, the water monolayer described above is expected to be *hydrophobic* with a *low surface free energy* owing to its fully-coordinated bonding configuration, in agreement with our observations.

Electron-Stimulated Production of O_2 in Thin Amorphous Solid Water Films

We have investigated the low-energy, electron-stimulated production of molecular oxygen from pure amorphous solid water (ASW) films and ASW films co-dosed with H_2O_2 . The O_2 yield is dose-dependent, indicating that precursors are involved in the O_2 production. For temperatures below ~ 80 K, the O_2 yield at steady state is relatively low and nearly independent of temperature. At higher temperatures, the yield increases rapidly. The O_2 yield is enhanced from H_2O_2 -dosed water films, but the experiments show that H_2O_2 is not the final precursor in the reactions leading to O_2 . Instead, a stable precursor for O_2 is produced through a multi-step reaction sequence probably involving the reaction of OH radicals to produce H_2O_2 and then HO_2 . We have developed a kinetic model which qualitatively accounts for the observations.

At all temperatures, the O_2 ESD signal is initially approximately zero and then increases until reaching a steady state value. Since the initial O_2 ESD yield is zero, increases with electron dose, and promptly recovers after an interruption of the electron irradiation, the O_2 is produced from a stable precursor which accumulates in the film with increasing electron dose. However, the dose dependence of the ESD yield at lower temperatures suggests that the O_2 precursor is not produced directly by a non-

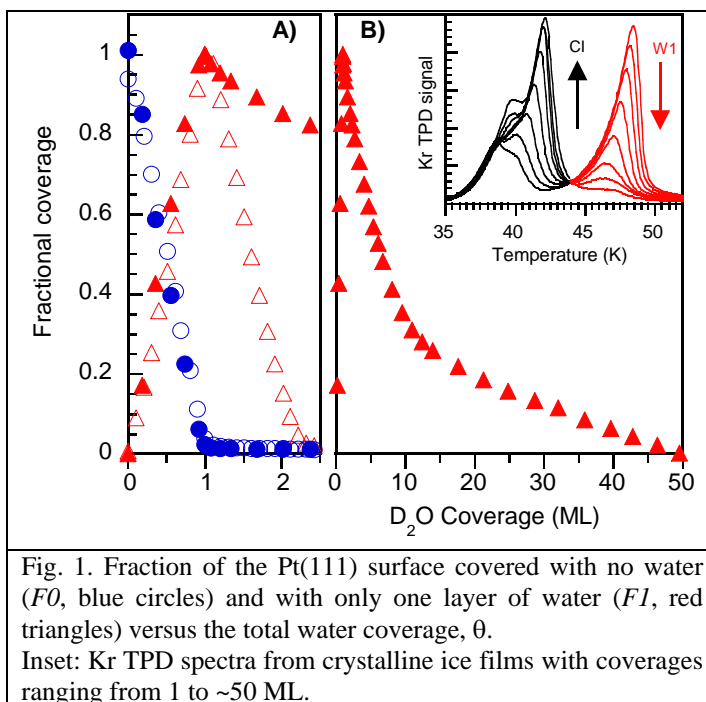


Fig. 1. Fraction of the Pt(111) surface covered with no water ($F0$, blue circles) and with only one layer of water (FI , red triangles) versus the total water coverage, θ . Inset: Kr TPD spectra from crystalline ice films with coverages ranging from 1 to ~ 50 ML.

thermal reaction, but is itself the product of a reaction (or reactions) between some other precursors. To test H_2O_2 as a possible precursor, we investigated the O_2 ESD from water films dosed with H_2O_2 . Compared to neat H_2O films, a significant enhancement of O_2 ESD for the H_2O_2 -dosed samples is observed suggesting H_2O_2 is a precursor to O_2 . However, the experiments indicate that H_2O_2 is not the *final* precursor. In particular, the O_2 ESD signal from H_2O_2 -dosed films is initially zero and increases as $\sim(1-e^{-\alpha t})$ at early times for all temperatures, indicating that further reactions that produce HO_2 , are required prior to the electron-stimulated production of O_2 .

Based on the experiments, we developed a kinetic model of the O_2 ESD in which OH is produced by the dissociation of electronically excited water molecules at the vacuum interface. The OH radicals then react to produce H_2O_2 and HO_2 . The O_2 results from an electron-stimulated reaction involving the HO_2 . The model qualitatively reproduces the results for both neat H_2O and H_2O_2 -dosed films.

Electron-stimulated production of molecular oxygen in ASW on Pt(111): Precursor transport through the hydrogen bonding network

The low-energy, electron-stimulated production of molecular oxygen from thin ASW films adsorbed on Pt(111) is investigated. For ASW coverages less than ~ 60 monolayers (ML), the O_2 ESD yield depends on coverage in a manner that is very similar to the H_2 ESD yield: Both have a pronounced maximum at ~ 20 ML due to reactions at the Pt/water interface. Independent of the ASW film thickness, the final reactions leading to O_2 occur at or near the ASW/vacuum interface. However for ASW coverages less than ~ 40 ML, reactions at the ASW/Pt interface contribute to the O_2 production at the ASW/vacuum interface presumably via the generation of OH radicals near the Pt substrate. The OH segregates to the vacuum interface where it contributes to the reactions at that interface. The electron-stimulated migration of precursors to the vacuum interface occurs via transport through the hydrogen bond network of the ASW *without motion of the oxygen atoms*.

The coverage dependence of the O_2 ESD indicates that there is a coupling between the reactions at the Pt interface and the O_2 ESD for films with coverages less than ~ 40 ML. However, experiments with isotopically labeled films show that the *final* reaction of the sequence that leads to O_2 occurs predominantly at or near the vacuum interface. Thus, one or more of the initial steps in the reaction sequence occurs at the Pt interface with the reaction intermediates subsequently migrating through the hydrogen bond network of the film to the vacuum interface. Diffusion of species, such as L- and D-defects, and H_3O^+ and OH^- , via proton hopping and molecular rotations is well known. The important point is that these species move through the ice *without* any motion of the oxygen atoms to new lattice sites within the ice. In the present case, since OH is believed to be the first reaction intermediate in the production of O_2 , OH (or HO_2) is a likely candidate for a migrating species.

Since hydrogen peroxide is readily dissociated by energetic electrons into two OH's, isotopically labeled H_2O_2 can be used to test for electron-stimulated transport of OH precursors. The O_2 ESD signals

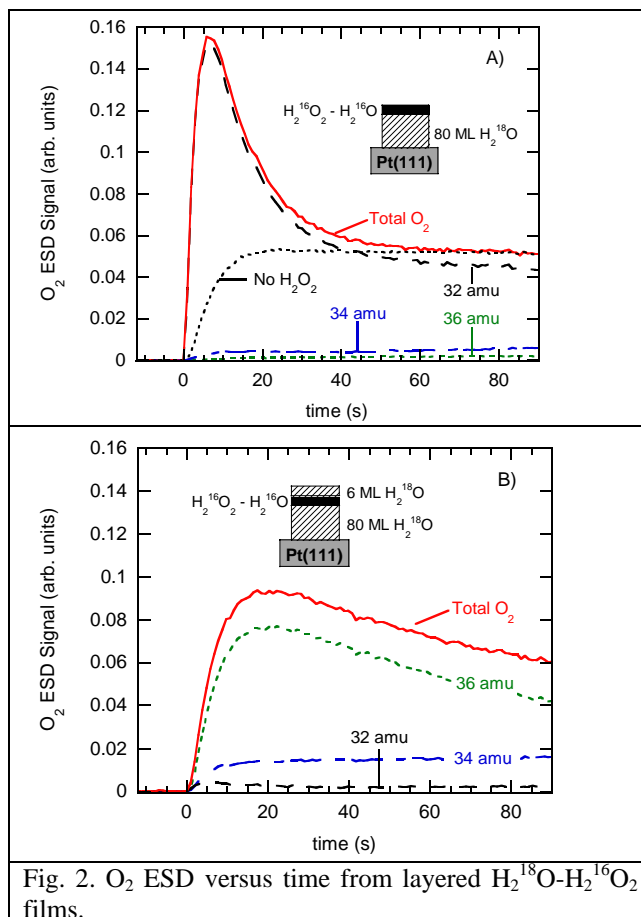


Fig. 2. O_2 ESD versus time from layered $\text{H}_2^{18}\text{O}-\text{H}_2^{16}\text{O}_2$ films.

versus time for $^{16}\text{O}_2$, $^{16}\text{O}^{18}\text{O}$, and $^{18}\text{O}_2$ from an 80 ML film of H_2^{18}O capped with ~ 7 ML of $\text{H}_2^{16}\text{O}_2\text{-H}_2^{16}\text{O}$ are shown in Fig. 2a. The films were dosed and irradiated at 100 K. The total O_2 ESD yield is defined as the sum of the three components. Also shown for comparison is the $^{18}\text{O}_2$ ESD signal versus time from an 80 ML film of pure H_2^{18}O . The prominent maximum in the O_2 ESD at early time in the hydrogen peroxide pre-dosed films arises because the initial concentration of precursors exceeds the steady state concentration. When the $\text{H}_2^{16}\text{O}_2$ layer is not capped with any H_2^{18}O , the $^{16}\text{O}_2$ ESD signal (Fig. 2a, dashed line) is dominant showing that most of the O_2 is produced in the $\text{H}_2^{16}\text{O}_2\text{-H}_2^{16}\text{O}$ layer *at the vacuum interface*. When the $\text{H}_2^{16}\text{O}_2\text{-H}_2^{16}\text{O}$ is subsequently capped with 6 ML of H_2^{18}O , the O_2 ESD signal still has a peak due to the pre-dosed H_2O_2 (Fig. 2b). However, in this case the extra O_2 ESD signal is *primarily in the $^{18}\text{O}_2$ channel* showing it is made at the vacuum interface (Fig. 2b, dotted line) while *the $^{16}\text{O}_2$ ESD signal is relatively small*. This result clearly shows that the oxygen atoms *initially* associated with the O_2 precursors (i.e. the $\text{H}_2^{16}\text{O}_2$) do not migrate to the vacuum interface, but the precursors nonetheless enhance the O_2 ESD at the vacuum interface.

Future Directions:

Important questions remain concerning the factors that determine the structure of thin water films on various substrates. We plan to investigate the structure of thin water films on non-metal surfaces, such as oxides, and on metals where the first layer of water does not wet the substrate. For the non-thermal reactions in water films, we will use FTIR spectroscopy to characterize the electron-stimulated reaction products and precursors. The mechanisms of the non-thermal precursor migration through ASW films need to be further explored. We will also investigate the non-thermal reactions at lower electron energies (i.e. closer to the ionization threshold for water). Finally, we plan to investigate the lifetimes of excited states in ASW and CI using pump-probe fluorescence measurements.

References to publications of DOE sponsored research (FY 2003 – present)

1. Z. Dohnálek, Greg A. Kimmel, Patrick Ayotte, R. Scott Smith, and Bruce D. Kay, "The deposition angle-dependent density of amorphous solid water films," *J. Chem. Phys.* **118**, 364 (2003).
2. Nikolay G. Petrik and Greg A. Kimmel, "Electron-Stimulated Reactions at the Interfaces of Amorphous Solid Water Films Driven by Long-Range Energy Transfer from the Bulk," *Phys. Rev. Lett.*, **90**, 166102 (2003).
3. Greg A. Kimmel, Mats Persson, Z. Dohnálek, and Bruce D. Kay, "Temperature independent physisorption kinetics and adsorbate layer compression for Ar adsorbed on Pt(111)," *J. Chem. Phys.* **119**, 6776 (2003).
4. R. S. Smith, Z. Dohnálek, G.A. Kimmel, G. Teeter, P. Ayotte, J. Daschbach and B. D. Kay, "Molecular Beam Studies of Nanoscale Films of Amorphous Solid Water." in *Water in Confining Geometries*. V. Buch and J. P. Devlin, Springer. p. 337 (2003).
5. Nikolay G. Petrik and Greg A. Kimmel, "Electron-stimulated reactions in thin D_2O films on Pt(111) mediated by electron trapping," *J. Chem. Phys.* **121**, 3727 (2004).
6. Nikolay G. Petrik and Greg A. Kimmel, "Electron-stimulated production of molecular hydrogen at the interfaces of amorphous solid water films on Pt(111)," *J. Chem. Phys.* **121**, 3736 (2004).
7. Nikolay G. Petrik and Greg A. Kimmel, "Electron-stimulated sputtering of thin amorphous solid water films on Pt(111)," *J. Chem. Phys.* **123**, 054702 (2005).
8. Bruce C. Garrett, et al., "Role of Water in Electron-Initiated Processes and Radical Chemistry: Issues and Scientific Advances," *Chem. Rev.* **105**, 355 (2005).
9. Greg A. Kimmel, Nikolay G. Petrik, Zdenek Dohnálek and Bruce D. Kay, "Crystalline ice growth on Pt(111): Observation of a hydrophobic water monolayer," *Phys. Rev. Lett.* **95** (2005) 166102.
10. Nikolay G. Petrik, Alexander Kavetsky and Greg A. Kimmel, "Electron-Stimulated Production of Molecular Oxygen in Amorphous Solid Water," *J. Phys. Chem. B.* **110**, 2723 (2006).
11. Greg A. Kimmel, Nikolay G. Petrik, Zdenek Dohnálek and Bruce D. Kay, "Layer-by-layer growth of thin amorphous solid water films on Pt(111) and Pd(111)," *J. Chem. Phys.* **125**, 044713 (2006).
12. Nikolay G. Petrik, Alexander Kavetsky and Greg A. Kimmel, "Electron-stimulated production of molecular oxygen in amorphous solid water on Pt(111): Precursor transport through the hydrogen bonding network," *J. Chem. Phys.* **accepted** (2006).

Single-Molecule Kinetics and Dynamics in the Condensed Phase and at Interfaces

Time Resolved Single-Molecule Chemical Imaging Studies of Interfacial Electron Transfer

H. Peter Lu

Bowling Green State University

Department of Chemistry and Center for Photochemical Sciences

Bowling Green, OH 43403

hplu@bgsu.edu

Program Scope

Our research is focused on the use of single-molecule high spatial and temporal resolved techniques to understand molecular dynamics in condensed phase and at interfaces. Single-molecule approaches are unique for heterogeneous and complex systems because the static and dynamic inhomogeneities can be identified, characterized, and/or removed by studying one molecule at a time. Single-molecule spectroscopy reveals statistical distributions correlated with microscopic parameters and their fluctuations, which are often hidden in ensemble-averaged measurements. Single molecules (and molecular complexes) are observed in real time as they traverse a range of energy states, and the effect of this ever-changing "system configuration" on chemical reactions and other dynamical processes can be mapped. We selected two system classes for our molecular dynamics research: 1) electron transfer reactions on solid surfaces (interfaces) related to solar energy conversions and 2) reactions and dynamics in proteins and protein complexes. Understanding the complex interfacial electron transfer dynamics is crucial for developing dye-sensitized solar energy conversion and photo-catalysis technique, and it is particularly powerful to study such heterogeneous systems by site-specific spectroscopy at single-molecule sensitivity and nanoscale specificity. The selection of biomolecules in studying condensed-phase chemical dynamics reflects both relevance and advantages. The proteins have been engineered by years of evolution to perform dynamics (large-scale conformational motion, cooperativity, selective chemistry, etc.) that are both relevant to molecular interaction and reaction dynamics in condensed phase and interfaces. Many of them have been studied at length by other methods at the ensemble level providing a sound basis for interpretation of new data that are not obtainable in ensemble-averaged experiments. Comparison the single-molecule experimental results with theoretical modeling and computational simulations have been demonstrated to be informative and productive. In our research, we have been developing and applying single-molecule photon stamping spectroscopy, time-resolved single-molecule anisotropy, single-molecule fluctuation and fluorescence resonance energy transfer (FRET) spectroscopy, near-field and atomic force microscopy-enhanced confocal imaging microscopes, and surface enhanced Raman spectroscopy to the study of interfacial electron transfer dynamics and single-protein conformation and reaction dynamics.

Recent Progress and Future Plans

Single-Molecule Interfacial Electron Transfer Dynamics Reveals Intermittent Reaction Dynamics-beyond the Conventional Kinetics Scope. Interfacial electron transfer (ET) plays an important role in many chemical processes. Specifically, interfacial ET in TiO₂-based systems is critical to solar energy technology, catalysis, and waste water treatments. However, the microscopic mechanism of interfacial ET is not well understood with regard to atomic surface structure, molecular structure, bonding, orientation, and molecular motion. We have applied single-molecule spectroscopy to single-molecule studies of

photo-sensitized interfacial ET processes in Coumarin 343-TiO₂ nanoparticle (NP) and Cresyl Violet-TiO₂ NP systems, using time-correlated single photon counting coupled with scanning confocal fluorescence microscopy. Fluorescence intensity trajectories of individual dye molecules adsorbed on TiO₂ NP surface showed fluorescence fluctuations and blinking, with time constants distributed from milliseconds to seconds. The fluorescence fluctuation dynamics were found to be inhomogeneous from molecule to molecule and from time to time, showing significant static and dynamic disorders in the interfacial ET reaction dynamics. We attribute fluorescence fluctuations to the interfacial ET reaction rate fluctuations in competing with the nanosecond excited-state relaxation of the dye molecules, associating redox reactivity intermittency with the fluctuations of molecule-TiO₂ electronic and vibronic coupling. Intermittent interfacial ET dynamics of individual molecules could be characteristic of a surface chemical reaction strongly involved with and regulated by molecule-surface interactions. The intermittent interfacial reaction dynamics that likely occur among single molecules in other interfacial and surface chemical processes can typically be observed by single-molecule studies, but not by conventional ensemble-averaged experiments. To decipher the underlying mechanism of the intermittent interfacial electron transfer dynamics, we plan to study porphyrin interfacial electron transfer on single crystal TiO₂ surfaces by using ps and fs pump-probe ultrafast single-molecule spectroscopy. Our study will focus on understanding the interfacial electron transfer dynamics at specific crystal sites (kinks, planes, lattices, and corners) with high-spatially and temporally resolved topographic/spectroscopic characterization at individual molecule basis.

Correlated AFM-Raman Spectroscopy and Imaging Studies of Inhomogeneous Vibrational Reorganization Energy Barriers of Interfacial Electron Transfer. To identify and characterize inhomogeneous interfacial chemical reaction dynamics, it is highly advantageous to obtain both topographic and vibrational spectroscopic characterization of surfaces and interfacial systems. For example, the site-to-site variations in the geometries and interactions at the molecule-TiO₂ interface result in an inhomogeneous distribution of electron transfer rates that can be effectively evaluated with vibrational-mode resolved near-field AFM-Raman analysis. In recent years, there have been tremendous advances in applying SERS to study nanoparticles and nanostructures at a single-molecule basis. Applying near-field AFM-Raman spectroscopy and analysis at single TiO₂ nanoparticle level, we have found that for alizarin/TiO₂ interfacial electron transfer systems, the vibrational reorganization energy barriers of interfacial electron transfer are inhomogeneous at nanometer scale. We determined that (1) the total vibrational reorganization energy was inhomogeneous from site to site; (2) the alizarin/TiO₂ bridging normal modes were the primary contributor to the total vibrational reorganization energy and its inhomogeneity; (3) the mode-specific analyses indicated that the energy distributions were inhomogeneous for bridging normal modes and less inhomogeneous or homogeneous for nonbridging normal modes, especially for modes far away from the alizarin-TiO₂ coupling hydroxyl modes; and (4) the vibrational reorganization energy inhomogeneity was closely associated with the local environmental heterogeneity of the alizarin/TiO₂ interface. It is most likely that the vibrational reorganization energy inhomogeneities contributed to the inhomogeneous dynamics of the interfacial electron transfer processes.

In the future, we will further investigate single-molecule electronic coupling, electron transfer driving force, and back electron transfer dynamics in order to characterize the molecular-level origins of the inhomogeneous and complex interfacial electron transfer dynamics in the solar energy conversion system. However, there is a significant technical challenge. To date, there is no single experimental technique capable of imaging the interfacial electron transfer processes with both high-spatial and short-time resolution. We will further develop our new approach that combines three complementary techniques: single-molecule time-resolved fluorescence spectroscopy, single-particle Raman spectroscopy, and scanning tunneling microscopy and spectroscopy to address this technical need. An understanding of the fundamental interfacial electron transfer processes will be important for developing efficient light harvesting systems and broadly applicable to problems in interface chemistry and physics. Our

experimental measurements will focus on electron transfer involving individual molecules, dimers, and small clusters of adsorbed molecules, on TiO₂ surfaces, under ambient conditions. The adsorbed molecules will be selected porphyrin and perylene derivatives. The substrates will consist of single-crystal and thin film rutile and anatase. AFM metal-tip and STM imaging will be performed on identical sites to extract dynamical data at a molecular spatial resolution. Using this approach, correlated information on the adsorption-site structure, molecular orientation, electronic structure, and single-molecule interfacial electron transfer dynamics will be obtained for the forward and backward electron transfer reactions.

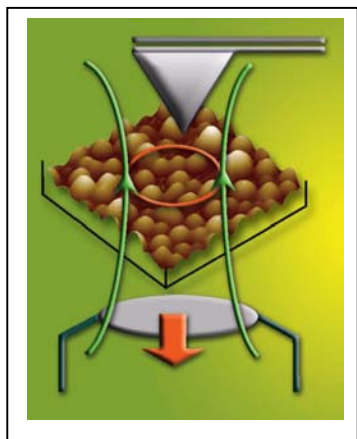


Figure 1. Schematic of STM or atomic force microscopy (AFM) metal tip enhanced SERS spectroscopy and imaging of interfacial electron transfer in dye-TiO₂ nanoparticle systems. The method combines metallic-tip scanning (either Au-coated AFM or STM metallic tips) with Raman imaging microscopy. The Au coated tip generates high local electric field enhancement under laser illumination, which provides a strong near-field Raman excitation at a specific nanoparticle or local site under the Au-AFM/STM tip. The SERS enhancement only exists when the tip is on top of the measurement site within a nanometer range, facilitating high spatial resolution.

Single-Molecule Antibunching Spectroscopy Studies of Back Electron Transfer by Probing the Ground State Recovering Dynamics of the Dye Molecules. Back electron transfer defines the efficiency of the solar energy conversion to electricity in dye-sensitization systems. It is a high challenge to probe the single-molecule back electron transfer dynamics when the dye molecule is non-fluorescent at its oxidized state after a forward electron transfer from the dye to the conduction band of TiO₂ semiconductor. We have demonstrated, for the first time, a measurement of single-molecule back electron transfer dynamics by single-molecule antibunching spectroscopy. The photon-antibunching is a fundamental quantum behavior that an individual molecule as a single quantum system can not simultaneously emit two photons. The correlation time of the photon antibunching reflects the dye molecule ground state recovering time; in this case, the ground state recovering time is predominately associated with the back electron transfer time. We have demonstrated the use of photon antibunching to measure reverse dynamics of the metal-to-ligand charge transfer (MLCT) of a ruthenium complex molecule. Using photon antibunching measurements under laser excitation, non-classical photon statistics, and excitation power dependent measurements, we were able to selectively measure the single-molecule MLCT state lifetime (i.e. back charge transfer time). We will apply this new technical approach to study back electron transfer dynamics in dye-TiO₂ systems, focusing on understanding the excess electron scattering dynamics in the bulk and at the interfaces of TiO₂ crystals. Electron surface-trapping states involving with back electron transfer will also be characterized by both the single-molecule spectroscopy and AFM-Raman spectroscopy.

References to publications of DOE sponsored research (FY2004–present)

1. Ruchuan Liu, Dehong Hu, Xin Tan, and H. Peter Lu, "Revealing Two-State Protein-Protein Interactions of Calmodulin by Single-Molecule Spectroscopy," *J. Am. Chem. Soc.* **128**, 10034-10042 (2006).

2. Jin Wang, Qiang Lu, and H. Peter Lu, "Single-Molecule Dynamics Reveals Cooperative Binding-Folding in Protein Recognition," *PLoS Computational Biology*, **2**, 842-852 (2006).
3. Dehong Hu and H. Peter Lu, "Single molecule electron transfer process of ruthenium complexes," *Proc. SPIE* Vol. **6092**, 609207 (2006).
4. Duohai Pan, Nick Klymyshyn, Dehong Hu, and H. Peter Lu, "Tip-enhanced near-field Raman spectroscopy probing single dye-sensitized TiO₂ nanoparticles," *Appl. Phys. Lett.*, **88**, 093121(2006).
5. Duohai Pan, Dehong Hu, and H. Peter Lu, "Probing Inhomogeneous Vibrational Reorganization Energy Barriers of Interfacial Electron Transfer," *J. Phys. Chem. B*, **109**, 16390-16395 (2005).
6. Dehong Hu and H. Peter Lu, "Single-Molecule Triplet-State Photon Antibunching at Room Temperature," *J. Phys. Chem. B*, **109**, 9861-9864 (2005).
7. H. Peter Lu, invited review article, "Probing Single-Molecule Protein Conformational Dynamics," *Acc. Chem. Res.* **38**, 557-565 (2005).
8. H. Peter Lu, "Single-Molecule Study of Protein-Protein and Protein-DNA Interaction Dynamics," an invited book chapter in *Protein-Ligand Interactions*, edited by Uli Nienhaus, The Humana Press Inc., 2005.
9. H. Peter Lu, invited review article, "Site-Specific Raman Spectroscopy and Chemical Dynamics of Nanoscale Interstitial Systems," *J. Physics: Condensed Matter*, **17**, R333-R355 (2005).
10. V. Biju, Miodrag Micic, Dehong Hu, and H. Peter Lu, "Intermittent Single-Molecule Interfacial Electron Transfer Dynamics," *J. Am. Chem. Soc.* **126**, 9374-9381 (2004).
11. Xin Tan, Dehong Hu, Thomas C. Squier, and H. Peter Lu, "Probing Nanosecond Protein Motions of Calmodulin by Single-Molecule Fluorescence Anisotropy," *Applied Phys. Lett.*, **85**, 2420-2422 (2004).
12. Miodrag Micic, Dehong Hu, Greg Newton, Margie Romine, H. Peter Lu, "Correlated Atomic Force Microscopy and Fluorescence Lifetime Imaging of Live Bacterial Cells," *Surface and Colloid B*, **34**, 205-212 (2004).
13. H. Peter Lu, invited review, "Single-molecule spectroscopy studies of conformational change dynamics in enzymatic reactions," a special issue of *Curr Pharm Biotech* (The way down from single genes, and proteins to single molecules.), **5**, 261-269 (2004).
14. Dehong Hu, H. Peter Lu, "Single Molecule Implanting of T4 Lysozyme on Bacterial Cell Surface: Towards Study Single Molecule Enzymatic Reaction in Living Cells," *Biophys. J.*, **87**, 656-661 (2004).
15. D. Hu, M. Micic, N. Klymyshyn, Y. D. Suh, H. Peter Lu, "Correlated topographic and spectroscopic imaging by combined atomic force microscopy and optical microscopy," *J. Luminescence*, **107**, 4-12 (2004).
16. G. Harms, G. Orr, H. Peter Lu, "Probing ion channel conformational dynamics using simultaneous single-molecule ultrafast spectroscopy and patch-clamp electric recording," *Appl. Phys. Lett.*, **84**, 1792-1794 (2004).
17. Xin Tan, Perihan Nalbant, Alexei Touthkine, Dehong Hu, Erich R. Vorpagel, Klaus M. Hahn, and H Peter Lu, "Single-Molecule Study of Protein-Protein Interaction Dynamics in a Cell Signaling System," *J. Phys. Chem. B.*, **108**, 737 (2004).
18. Miodrag Micic, Nicholas Klymyshyn, H. Peter Lu, "Finite Element Method Simulations of the Near-Field Enhancement at the vicinity of Fractal Rough Metallic Surfaces," *J. Phys. Chem. B.*, **108**, 2939 (2004).

Reactivity of Nitrogen Oxides, Oxoacids, and Oxoanions in Aqueous Solution

Sergei V. Lyamar

Chemistry Department, Brookhaven National Laboratory, Upton, NY 11973-500

e-mail: lyamar@bnl.gov

Program Scope

The title compounds are involved in environmental problems, such as acid rain, global warming, ozone depletion, and urban smog. Nitrogen-oxygen intermediates are also central to the radiation-induced reactions that occur within highly radioactive nuclear waste; even more important and diverse are the biological roles of nitrogen oxides.

The inorganic chemistry of nitrogen includes a large number of metastable compounds and is not sufficiently understood, especially for the nitrogen in low positive oxidation states, whose chemistry is of the greatest current interest. For instance, the nearest redox neighbors of NO and the simplest nitrogen(+1) species are nitroxyl (H-N=O) and its conjugate NO⁻ anion. Experiment-based suggestions that nitroxyl can be produced *en route* to NO, is itself a major player in cellular metabolism, can be used for therapeutic intervention, and is a precursor to cytotoxic peroxyxynitrite, ONOO⁻, have engendered strong interest in the chemistry of HNO/NO⁻. Until recently, however, important aspects of the nitroxyl aqueous chemistry have been largely misunderstood. Although numerous important reactions of nitroxyl have been proposed, none of them was directly observed and little quantitative information exists on the reactivity of nitroxyl and its adducts. Among the latter, the most prominent is peroxyxynitrite (ONOO⁻), an isomeric form of nitrate and a major player in atmospheric chemistry, the chemistry of Hanfor nuclear wastes, and in human disease.¹

Despite a large body of research, there is no consensus concerning the fundamental properties of this species. This is definitely an area where there is a clear need for accurate elucidation of the prospective reactions in terms of their rates and mechanisms, and the radiation chemistry techniques can furnish the necessary experimental data.

Progress

Recently, we²⁻⁵ have begun a reevaluation of the thermodynamics and reactivity of nitroxyl and have concluded that: (i) NO⁻ has a triplet ground state, whereas the ground state of HNO is a singlet (Fig. 1), and (ii) ¹HNO is a much weaker acid, $pK_a(^1\text{HNO}/^3\text{NO}^-) \approx 11.4$, than it was widely accepted previously (pK_a of 4.7^{6,7}). In nearly all reported cases invoking nitroxyl as an intermediate, the rate-determining step was its generation, which allows little insight into properties and reactivity. In

contrast, we have used laser flash photolysis of trioxodinitrate (HN₂O₃⁻/N₂O₃²⁻) and pulse radiolysis of aqueous NO to rapidly generate the nitroxyl species and to investigate their reactivity.

A *spin-forbidden proton-transfer* reaction $^1\text{HNO} + \text{OH}^- \rightarrow ^3\text{NO}^- + \text{H}_2\text{O}$ has been investigated (Fig. 2).³ Spin-forbidden bond breaking/making reactions are rare in chemistry and

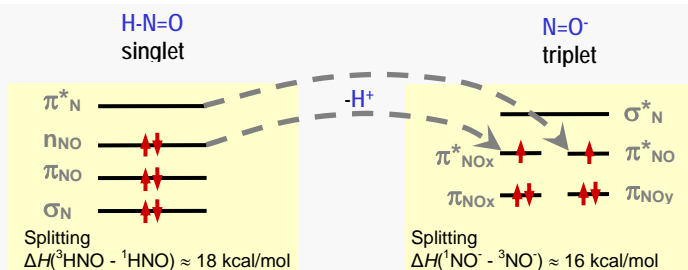


Fig. 1. Top MO structure for ground-state HNO and NO⁻. A proton removal from HNO transforms the π and π^* orbitals into a degenerate pair, giving rise to triplet NO⁻.

nitroxyl presents an opportunity to explore the effect of spin prohibition on the reaction mechanisms. The kinetic isotope effect and activation parameters are found to be: $k_{\text{H}}/k_{\text{D}} = 3.1$, $\log(A, \text{M}^{-1} \text{s}^{-1}) = 10.0$ and $E_a = 7.2 \text{ kcal/mol}$ for H⁺ transfer, and $\log(A, \text{M}^{-1} \text{s}^{-1}) = 10.4$ and $E_a = 8.4$

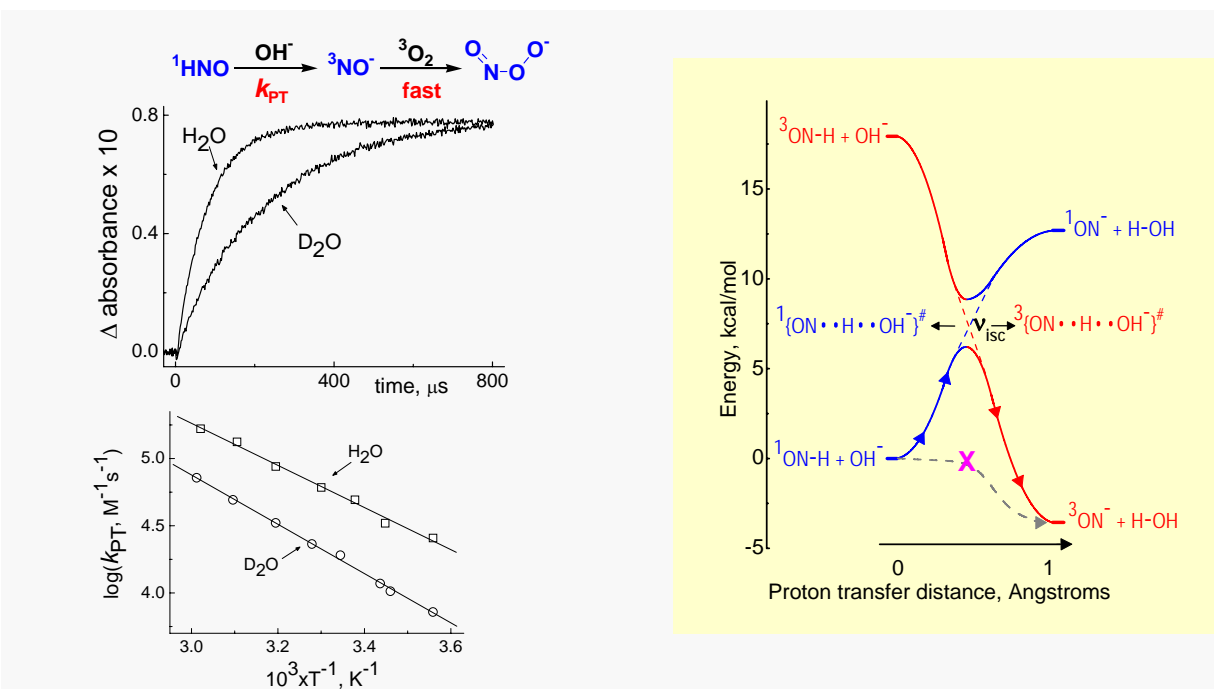
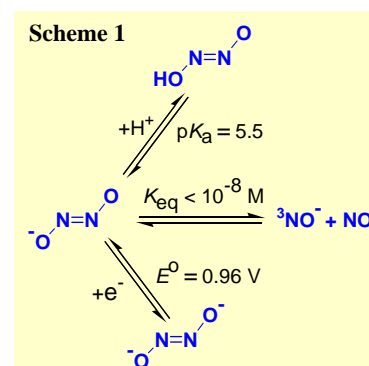


Fig. 2. Left: due to the lack of optical absorption by both ^1HNO and $^3\text{NO}^-$, their protolytic equilibration with OH^- could not be monitored directly, but could be measured in near UV using the rapid formation of peroxynitrite. Both the kinetic isotope effect and temperature dependence reveal that the reaction energetics, not intersystem crossing, controls the rate. Right: because of spin restrictions the reaction cannot take a barrierless path; instead the system must “climb” along the singlet energy surface to its intersection with the triplet term, where a very facile spin change occurs.

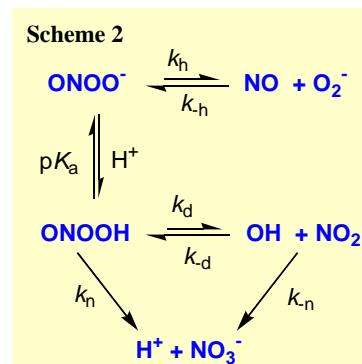
kcal/mol for D^+ transfer. These data show that the nuclear reorganization requirements arising from the spin prohibition necessitate significant activation before spin change can take place, but the spin change itself occurs extremely rapidly, $v_{\text{isc}} \sim 10^{11} \text{ s}^{-1}$. Such a facile intersystem crossing is explained by the involvement of $^1(n, n) \rightarrow ^3(n, \pi^*)$ change in the reactant-like transition state (Fig. 1) that is typically rapid due to large spin-orbit coupling. The major conclusion of this first mechanistic study of a spin-forbidden acid base reaction in water is that a synergy between the spin prohibition and the reaction energetics creates an intersystem enthalpy barrier and is solely responsible for slowness of this reaction; the spin prohibition alone plays a minor role.

The hyponitrite radicals (N_2O_2^- and HN_2O_2), the adducts of NO and nitroxyl, have been produced by oxidation of hyponitrite with OH^- , N_3^- , or SO_4^{2-} in the NO-free solutions and all major properties of N_2O_2^- and HN_2O_2 have been revised (Scheme 1).⁴ The N_2O_2^- radical exhibits an absorption spectrum that differs drastically from those reported,^{6,7} suggesting the radical misassignment in prior work. Both N_2O_2^- and HN_2O_2 are shown to be over 3 orders of magnitude more stable to elimination of NO than suggested previously. The data combined with *ab initio* calculations show that the radicals are both strongly oxidizing, $E^0(\text{N}_2\text{O}_2^-/\text{N}_2\text{O}_2^{2-}) = 0.96$ and $E^0(\text{HN}_2\text{O}_2, \text{H}^+/\text{H}_2\text{N}_2\text{O}_2) = 1.75$ V, and moderately reducing, $E^0(2\text{NO}/\text{N}_2\text{O}_2^-) = -0.38$ and $E^0(2\text{NO}, \text{H}^+/\text{HN}_2\text{O}_2) = -0.06$ V, vs NHE. These properties make the hyponitrite radical an important intermediate in the aqueous redox chemistry of NO.

Energetics and bond homolyses of peroxynitrite and its acid (ONOO^- and ONOOH), have been investigated^{8,9} to resolve major disputes in the literature concerning the reactivity of these species.



The equilibrium constant $K_h = 3.6 \times 10^{-12}$ M for the dissociation of the ON-OO⁻ bond is determined from the k_h and k_{-h} rate measurements (Scheme 2), which yield $\Delta_f G^0(\text{ONOO}^-) = 16.4 \pm 0.3$ and $\Delta_f G^0(\text{ONOOH}) = 7.36 \pm 0.36$ kcal/mol for the formation free energies. These data and the measurements of (i) the decomposition rate and product yields over wide range of peroxyxynitrite concentrations, (ii) the volume of activation, and (iii) complex patterns of inhibition of O₂ formation by radical scavengers are shown to be quantitatively in accord with a reaction model wherein ONOOH reactions are initiated by O-O bond homolysis, but exclude a proposed model that does not involve formation of radical intermediates.^{10,11}



Future Plans

Today, the reactions of ³NO⁻ with O₂ and ¹HNO/³NO⁻ with NO (progress section) remain the only two nitroxyl reactions measured directly despite the expectations of the rich chemistry based on the properties of nitroxyl, which is simultaneously a Lewis acid and base, a hydrogen atom donor, and a redox agent. This chemistry will be explored along with the properties and reactivity of the most consequential adducts of nitroxyl.

Spin-forbidden bond breaking/making reactions involving nitroxyl will be investigated. The first is protonation of ³NO⁻ by Brønsted acids; reactions of this type could appreciably modulate nitroxyl reactivity in buffered environments. The second spin-forbidden reaction of interest is the addition of ³O₂ to ¹HNO, which could directly lead to peroxyxynitrite, ONOO⁻, and is potentially very significant because it replaces mildly reducing HNO by strongly oxidizing ONOO⁻. Direct time-resolved measurements will be done at submolar concentrations of O₂ with a high pressure system that is under construction.

Pathways and energetics of NO reduction will be investigated with the purposes to develop new methods of generating nitroxyl and to establish its thermochemistry. With respect to the former, reduction of NO by the CO₂⁻ radical is of special interest, as it may provide a convenient method for producing nitroxyl species with radiolysis over a broad range of pH. Although the reduction potentials for NO and pK_a for HNO are germane to our model of nitroxyl reactivity, all present estimates for these quantities involve significant assumptions spreading a range of ~0.1 V and ~4 pK_a units.^{2,12-14} We will attempt determination of nitroxyl thermochemistry by measuring its redox equilibria.

Recombination reaction ¹HNO + ¹HNO will be investigated. This reaction is believed to directly generate N₂O + H₂O,^{15,16} which we conjecture is unlikely for such a complex change because the H-atom positions in the (HNO)₂ adduct are improper for water elimination. A hyponitrite-like, possibly very long-lived, intermediate (perhaps *cis*-hyponitrite) must be involved. Because this reaction is universally used as a reference in competition experiments,¹⁷⁻¹⁹ the properties of possible intermediates need to be identified.

Properties and reactivity of nitroxyl adducts with NO and NO₂⁻ will be investigated. We have found that the NO adduct, the hyponitrite radical (N₂O₂⁻), is rapidly and practically irreversibly formed from ¹HNO/³NO⁻ in NO-containing environments⁵ and should be both strongly oxidizing and moderately reducing,⁴ which makes it a major player in the nitroxyl-related chemistry. However, nothing is known about N₂O₂⁻ reactivity and the most important prospective reactions will be explored.

Thermal decomposition of trioxodinitrate (N₂O₃²⁻) is by far the most widely used source of nitroxyl in a very large body of published work. Redox potentials for N₂O₃²⁻ are unknown, but we expect it to be readily oxidizable. However, possible redox reactions of HN₂O₃⁻/N₂O₃²⁻ are, with

rare exceptions, ignored. We will investigate the one-electron oxidation mechanism and possible formation and properties of the N_2O_3^- radical, which has been implicated in various reactions. One-electron reduction of $\text{HN}_2\text{O}_3^-/\text{N}_2\text{O}_3^{2-}$ that may provide a convenient alternative pathway to the hyponitrite radical will also be explored.

Collaborators on this project include Drs. V. Shafirovich (NYU) and J. K. Hurst (WSU); past contribution from Dr. G. A. Poskrebyshev is acknowledged.

References (DOE sponsored publications in 2003-present are marked)

- (1) Lymar, S. V. In *McGraw-Hill Yearbook of Science and Technology 2002*; McGraw-Hill: NY, 2002, pp 263-266.
- (2) Shafirovich, V.; Lymar, S. V. *Proc. Natl. Acad. Sci. USA* **2002**, *99*, 7340-7345.
- (3*) Shafirovich, V.; Lymar, S. V. "Spin-Forbidden Deprotonation of Aqueous Nitroxyl (HNO)," *J. Am. Chem. Soc.* **2003**, *125*, 6547-6552.
- (4*) Poskrebyshev, G. A.; Shafirovich, V.; Lymar, S. V. "Hyponitrite Radical, A Stable Adduct of Nitric Oxide and Nitroxyl," *J. Am. Chem. Soc.* **2004**, *126*, 891-899.
- (5*) Lymar, S. V.; Shafirovich, V.; Poskrebyshev, G. A. "One-Electron Reduction of Aqueous Nitric Oxide: A Mechanistic Revision," *Inorg. Chem.* **2005**, *44*, 5212-5221.
- (6) Grätzel, M.; Taniguchi, S.; Henglein, A. *Ber. Bunsen-Ges. Phys. Chem.* **1970**, *74*, 1003-1010.
- (7) Seddon, W. A.; Fletcher, J. W.; Sopchyshyn, F. C. *Can. J. Chem.* **1973**, *51*, 1123-1130.
- (8*) Lymar, S. V.; Khairutdinov, R. F.; Hurst, J. K. "Hydroxyl Radical Formation by O-O Bond Homolysis in Peroxynitrous Acid," *Inorg. Chem.* **2003**, *42*, 5259-5266.
- (9*) Lymar, S. V.; Poskrebyshev, G. A. "Rate of ON-OO⁻ Bond Homolysis and the Gibbs Energy of Formation of Peroxynitrite," *J. Phys. Chem. A* **2003**, *107*, 7991-7996.
- (10) Kissner, R.; Koppenol, W. H. *J. Am. Chem. Soc.* **2002**, *124*, 234-239.
- (11) Maurer, P.; Thomas, C. F.; Kissner, R.; Ruegger, H.; Greter, O.; Rothlisberger, U.; Koppenol, W. H. *J. Phys. Chem. A* **2003**, *107*, 1763-1769.
- (12) Dutton, A. S.; Fukuto, J. M.; Houk, K. N. *Inorg. Chem.* **2005**, *44*, 7687-7688.
- (13) Dutton, A. S.; Fukuto, J. M.; Houk, K. N. *Inorg. Chem.* **2005**, *44*, 4024-4028.
- (14) Tossell, J. A. *Geochim. Cosmochim. Acta* **2005**, *69*, 5647-5658.
- (15) Bonner, F. T.; Hughes, M. N. *Comments Inorg. Chem.* **1988**, *7*, 215-234.
- (16) Bazyliniski, D. A.; Hollocher, T. C. *Inorg. Chem.* **1985**, *24*, 4285-4288.
- (17) Liochev, S. I.; Fridovich, I. *Free Radic. Biol. Med.* **2003**, *34*, 1399-1404.
- (18) Miranda, K. M.; Paolucci, N.; Katori, T.; Thomas, D. D.; Ford, E.; Bartberger, M. D.; Espey, M. G.; Kass, D. A.; Feelisch, M.; Fukuto, J. M.; Wink, D. A. *Proc. Natl. Acad. Sci. USA* **2003**, *100*, 9196-9201.
- (19) Sulc, F.; Immoos, C. E.; Pervitsky, D.; Farmer, P. J. *J. Am. Chem. Soc.* **2004**, *126*, 1096-1101.
- (20*) Garrett, B. C.; Dixon, D. A.; Camaioni, et al. "Role of Water in Electron-Initiated Processes and Radical Chemistry: Issues and Scientific Advances," *Chem. Rev.*, **2005**, *105*, 355-390.

METALLIC NANOPARTICLES UNDER IRRADIATION

Dan Meisel

The Radiation Laboratory, University of Notre Dame
Notre Dame, IN 46556 dani@nd.edu

Program Scope

This program explores the processes that are initiated by the absorption of ionizing radiation in multi-phase systems of metallic particles of nano-scale dimensions dispersed in aqueous solutions. In these systems the energy may be absorbed by both phases and thus, energy and charge carriers may be exchanged between the two phases. Furthermore, the interface between the phases provides a medium for reactions of short-lived intermediates that can change their fate. Quantification of these processes, determining the extent of charge transfer among the phases and measuring the effect of the interfaces on the rate of the reactions of the radicals generated in each phase is the goal of this program. These effects are of interest both as a matter of fundamental interest and as a primary factor in a large number of technological applications in energy production and utilization. Metal-aqueous interfaces are common in nuclear reactors or in environmental remediation schemes; they are of major concern in managing nuclear materials and can be used in radiotherapy. Metal-water interfaces are of catalytic utility in essentially all schemes for H₂ production from water but we propose that may also contribute to preferential localization of radiation damage in a desired tissue.

The fate of ionization products in the aqueous phase is well documented. Recent studies also provide information on the fate of charge carriers generated by ionizing radiation in insulator (e.g., SiO₂, ZrO₂) and semiconductor (e.g., TiO₂) nanoparticles.^(1,2) However, very little information is available on the processes that follow ionization in metals. Survival of electron-hole pairs in metals is expected to be short-lived and of low yield because of the high density of free carriers in the material that would lead to annihilation of the excess charge. Nonetheless, if the particles are small there is finite probability that they will reach the interface. If that is indeed the case and their transfer to the aqueous phase can be demonstrated, then, perhaps they might be used to funnel radiation damage to a pre-determined target, for example a malignant cell.

Recent Progress

Demonstration of exchange of charge carriers between metallic nanoparticles and aqueous solutions is a formidable task. The specific absorption of ionizing radiation in the MeV's-energy range by matter is proportional to its electron density, and thus, the energy is preferentially absorbed by the solid particles. For example, for Au or Pt, of density ~20 g cm⁻³, the energy absorbed by an atom in the particle is ~20 times higher than by a molecule of water. As discussed in last year's report, many currently evolving methodologies can specifically bind biomolecules to the metallic interface, which allows *a-priori* selection of the identity of the targeted species at the particle interface. Our recently determined cross-sections of adsorbed molecules and radical at the surface of particles allow us to measure the efficiency of charge capture at the particle surface.⁽¹⁾ We also followed recently developed synthetic procedures to generate silver particles of pre-determined sizes and, significantly, free of any foreign organic material at the interface. This synthesis utilized the reaction of H₂ with the metal oxide, Ag₂O in

this case, to produce the metal and water. We have shown that the surface potential at the interface is negative (~ 30 meV, pH dependent, point of zero charge at pH ~ 7) and thus, hydroxide ions, partially complexed to residual unreduced silver ions at the surface are providing the zeta potential to maintain the particles dispersion. Density function calculations show that complexation at the surface of the metallic particle stabilizes significantly the hydroxide ions, essentially independent of the presence of small amounts of unreduced ions of the metals. Nonetheless, we have shown experimentally that 4-5% of the silver ions remain unreduced, but the majority remains in the bulk of the solution not at the surface. The later affect the spectroscopy of the particle via its effect on the charge density in the particle, but as importantly, is responsible for the unusually hydrophilic surface of the particle that resembles an oxide-hydroxide surface. Because of this uncommon stability, large concentrations of the particles (tenths of mole per liter) could be obtained in solution (Figure 1).

The particles prepared by the method described above were tested for their effect on yields from the radiolysis of aqueous dispersions at a broad range of concentrations. As can be seen in Figure 1, catalytic hydrogen production is obtained from all reducing radical already at low catalyst concentrations and this yield remain constant to the

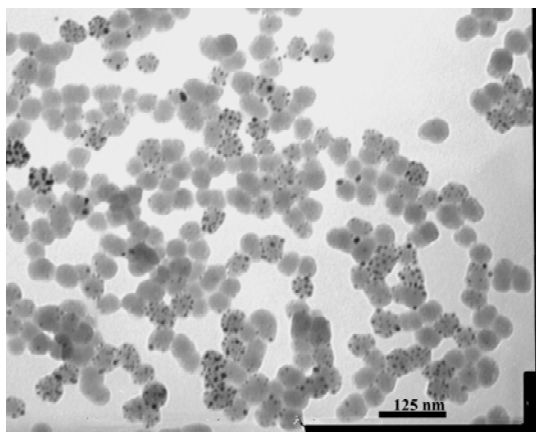


Figure 2: TEM micrographs of 6 nm Ag particles on 45 nm silica particles. Note cooperative attachment of the silver

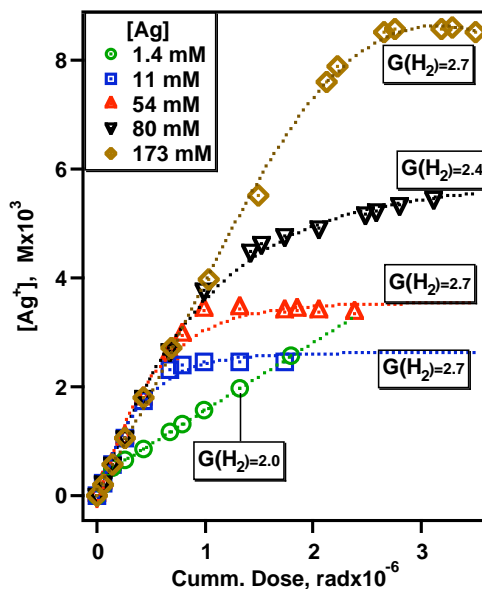


Figure 1: Concentration of silver ions and yield of H_2 at increasing concentrations of 30 nm Ag particles. $[Ag^+]$ was measured via the missing H_2 yield. Limiting H_2 yields are shown in the figure at various Ag particle concentrations. Containing 0.1 M of each, 2-propanol and acetone.

highest $[Ag]$ tested. Little is to be gained by increasing the catalyst concentration, even though the rate of the hydrogen evolution reaction increases by the same amount. On the other hand, even at this high metal concentration the fraction of energy absorbed by the metal is too small to provide any information on the fate of carriers produced in the particle. For comparison, gold particles of larger particles ($r \geq 500$ nm) do not allow carriers escape even when more than 50% of the energy is absorbed by the particles. The mounting difficulties with the large concentrations of metallic particles required to demonstrate the effects we seek lead us to propose the new directions described in the Proposed Plans section.

In a parallel effort we studied the effect of solid supports on the reactions of metallic particles on radiolysis products. We deposited metallic particles on silica particles using bridging

molecules ($\text{NH}_2\text{-(CH}_2\text{)}_3\text{-Si(OCH}_3\text{)}_4$) to overcome the mismatch between the hydrophobic metallic and the hydrophilic silica surfaces. While this attachment is straightforward, we notice that the presence of silver islands enhances further adsorption of particles (Figure 2). In these particles the new silica-metallic interface provides another pathway for carriers to cross between the phases. In particular we wonder about the effect of holes that are known to accumulate in the oxide as the electrons escape into the aqueous phase, directly or via the metallic islands. Our results indicate that the yield of hydrogen significantly decreases as the silica concentrations increase but it is unclear yet if this is a result of holes accumulation in the silica or destruction of radicals at the silica-water interface, which is commonly considered to be inert. Dose and dose rate effects on the yields are currently examined in order to resolve this point.

Future Plans

The difficulties associated with the high metallic particle concentrations, alluded to above, lead us to propose a different strategy to test the potential of targeting radiation damage using nanoparticles. We will measure the yield of water radiolysis as we scan the energy of the radiation near the core-electron edges of the metal (e.g., ~25 keV for silver). Depending on the fate of carriers the yields should depend on photon energy in a rather narrow energy range. In a parallel effort we are now preparing, together with our collaborators at the Weizmann Institute, Israel, multilayered nanotubes that we believe may offer opportunities for vectorial unidirectional charge transfer processes.

Publications Sponsored by this DOE Program, 2004-2006

- (1) B. H. Milosavljevic and D. Meisel, "Kinetic and Thermodynamic Aspects of Adsorption on Silica Nanoparticles. A Pulse Radiolysis Study", *J. Phys. Chem. B*, 108, 1827-30 (2004).
- (2) B. H. Milosavljevic, S. M. Pimblott and D. Meisel, "Yields And Migration Distances of Reducing Equivalents in the Radiolysis Of Silica Nanoparticles", *J. Phys. Chem. B* 108, 6996-7001, (2004).
- (3) Dan Meisel, "Basics of Radiation Chemistry in the Real World: Nanoparticles in Aqueous Suspensions", Proceedings of the International Atomic Energy Agency Workshop on "Advances in Radiation Chemistry of Polymers", IAEA Press, Vienna, ISSN 1011-4289, ISBN 92-0-112504-6, pp. 5-14 (2004).
- (4) P. V. Kamat, K. G. Thomas, S. Barazzouk, G. Girishkumar, K. Vinodgopal and D. Meisel "Self-Assembled Linear Bundles of Carbon Nanotubes and Their Alignment in a DC-Field", *J. Am. Chem. Soc.*, 126, 10757-62 (2004).
- (5) K. Vinodgopal, Mehul Haria, Dan Meisel, Prashant Kamat, "Fullerene-Based Carbon Nanostructures for Methanol Oxidation", *Nano Letters*, 4, 415-8 (2004).
- (6) Dan Meisel, "Radiation Effects on Nanoparticles", Proceedings of the International Atomic Energy Agency Panel on "Emerging Applications of Radiation in Nanotechnology," IAEA Press, Vienna, ISSN 1011-4289, ISBN 92-0-100605-5, pp. 130-41 (2005).
- (7) Bruce C. Garrett, et al., "The Role of Water in Electron-Initiated Processes and Radical Chemistry: Issues and Scientific Advances", *Chem. Rev.* 105, 355-90, 2005.
- (8) D. Lahiri, B. A. Bunker, B. Mishra, Z. Zhang, D. Meisel, C. M. Doudna, M. F. Bertino, F. D. Blum, A. T. Tokuhira, S. Chattopadhyay, T. Shibata, J. Terry, "Bimetallic Pt-Ag And Pd-Ag Nanoparticles", *J. App. Phys.* 97, 094304-12 (2005).
- (9) Dan Meisel, "Radiation Effects in Nanoparticles", Proceedings of the International Atomic Energy Agency meeting on "Emerging Applications of Radiation in Nanotechnology," IAEA Press, Vienna, ISSN 1011-4289, ISBN 92-0-100605-5, pp. 130-41 (2005).
- (10) G. Merga, B. H. Milosavljevic, D. Meisel, "Radiolytic Yields in Aqueous Suspensions of Gold Particles", *J. Phys. Chem. B* 110, 5403-8 (2006).

LASER DYNAMIC STUDIES OF PHOTOREACTIONS ON SINGLE-CRYSTAL AND NANOSTRUCTURED SURFACES

Richard Osgood, Center for Integrated Science and Engineering, Columbia University, New York, NY 10027, Osgood@columbia.edu

Program Scope or Definition:

The scope of our current research program is to examine the photon-initiated reaction mechanisms, half-collision dynamics, and other optically induced dynamics effects, which occur for adsorbates on well-characterized, semiconductor or metal-oxide surfaces. Our recent work in this program has yielded several new research findings regarding the basic chemical dynamics of surface photofragmentation.

The goal of the current program has been to develop a thorough understanding of the dynamics of surface photoreactions using UHV-prepared model molecular-adsorbate/*nanostuctured* surface systems. The research questions in our evolving program are as follows: What are the mechanisms for reactions on nanostructured surfaces? For substrate-electron transfer reactions, how do substrate ligands modify the chemistry? What new resonant-excitation physics are introduced by elementary excitations on a nanoobject surface? *In particular, the research plan of this program is to extend our understanding of the photodynamics of molecular adsorbates by concluding our studies of heterogeneous photoelectron transfer using well characterized thiolate spacer layers; examining fragmentation on nanostructured metal-oxide surfaces, including those with complex reconstruction and nanofaceted surfaces; and investigating dynamical processes on nanoobjects, including in-situ-deposited metal clusters and vapor-grown metal-oxide nanowires.* Our primary dynamics probe is measurement of the kinetic energy and internal energies of the desorbed photofragments using time-of-flight (TOF) mass-spectroscopy and resonance-enhanced multiphoton ionization (REMPI) in conjunction with a pulsed tunable UV- or visible-laser system. Important components of this research involve collaboration or close consultation with the Surface Dynamics Group in the Chemistry Department at Brookhaven National Laboratory and the use of instrumentation at BNL's two major user facilities, the Center for Functional Nanomaterials and the National Synchrotron Light Source. The project will also use variable-temperature STM imaging to investigate surface-bound reactions and appropriate E&M and chemical computational tools.

Recent Progress:

Photochemistry Using Nanoscale Thiolate Spacer Layers (Project Completion)

Our particular motivation for this work was to use self-assembled thiol layers for "spacer layers," intervening, either actively or passively, between the surface of a solid and the electron-transfer region at or near its surface. Nanoscale spacer layers can range from simple noble gases to SAMs of functionalized long-chain organothiols. Often it is important that the molecules comprising the spacer layer be covalently bound to the substrate surface because, for single-molecule-thick spacer layers, more loosely bound species, e.g., noble-gas atoms, cannot prevent percolation of more strongly bound, e.g., dipolar molecules, to the substrate surface. In all cases, it is important to understand molecular interactions at the surfaces of the spacer layers to perform and interpret the experiments involving them.

In the experiments, completed this last year we used a model system consisting of layers formed by *in-vacuo* deposition of the two shortest alkyl disulfides for use as spacer layers of differing thickness, allowing studies of MeBr adsorption and electron-transfer reactions atop organic thin films at a controlled distance from the underlying GaAs substrate. As a result we performed our experiments at the short-chain limit, using spacer-layer

molecules containing one and two carbon atoms, where we expect the changes in molecule-surface interactions to be the most significant. With regards to molecular order, we found that the MeBr-adsorption growth modes are markedly modified from those on the bare surface and that as the distance between the GaAs surface and the MeBr increases, the activation energy of desorption for the MeBr, at low coverages, decreases, indicating a decrease in the strength of the surface-adsorbate interaction. Furthermore, as the surface-adsorbate interaction strength decreases, the *relative* strength of the adsorbate-adsorbate lateral interactions was enhanced. This was most dramatically seen for MeBr adsorption atop the spacer layer formed by Et₂S₂ chemisorption, in which case desorption of MeBr molecules adsorbed directly atop the spacer layer occurs at *lower* temperature than that of multilayer MeBr. Electron transfer photochemistry was carried out on these layers and this showed that in fact electron-transfer dropped off as the thiolate-layer thickness increased via use of longer chain molecules. These electron-transfer experiments have been described in a major review article cited below.

Surface Dynamics on and Formation and Characterization of Metal-Oxide Nanoobjects

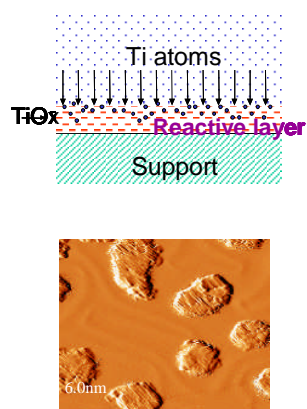


Fig. 1: TiO₂ nanoparticles formed by RLAD on a single-crystal Au substrate: top, schematic of process; bottom, SEM of particles on the same substrate

A major-goal of the current program is to carry out surface dynamics on free-standing metal-oxide nanocrystals. The most common method of preparation of these objects is via either colloidal or metal-nanodot catalyzed growth (this second approach was examined in the previous year). A second approach, which we have now examined in much more detail is to use TiO₂ nanoparticles, that are prepared by reactive-layer-assisted deposition (RLAD). In this approach Ti atoms are initially deposited on a multilayer of H₂O (or NO₂) and subsequently grown on a Au(111) substrate at temperature of >100 K. Our initial work characterized the chemical, structural and electronic properties of these oxide nanoparticles using XPS, STM and STS. This work was done collaboratively with Jan Hrbek at Brookhaven National Laboratory. Our experiments showed that ~1nm diameter TiO₂ particles, formed with an H₂O reactive layer, could be obtained after raising the substrate temperature to 300K; see Fig. 1.

Similar results were obtained when a NO₂ reactive layer was used. Since this method for preparing well-defined TiO₂ nanoparticles is UHV compatible and produces particles with no terminating ligands, it can be used in molecular-level studies of reaction dynamics of photocatalytic processes on TiO₂ nanoparticle surfaces. Our work during this year in this project examined first additional characterization of the particle growth – particularly its extension to Ti-nitride materials.

- *STM Studies at Columbia University*

STM is an excellent tool, with which to study the formation, and eventually reactivity, of nanoparticles of metal oxides such as TiO₂, since it can be used to examine both the atomic structure, order, and composition of nanoparticles after their formation. In addition as part of the characterization of nanoparticles, it is also important to examine the thermal reactivity of an ensemble of particles using *in situ* TPD. Our initial plan for this area was to do our STM work in collaboration with the BNL Nanocenter. Thus our STM research was first carried

out by Dr. Zhen Song, and in collaboration with Jan Hrbek at BNL. We have since obtained our own STM and begun experimentation at Columbia. We are planning further upgrades in the measurement capability in the near future. Figure 2 shows two STM pictures, which illustrate the initial stages of our work. We attach several recent STM pictures to illustrate our initial work.

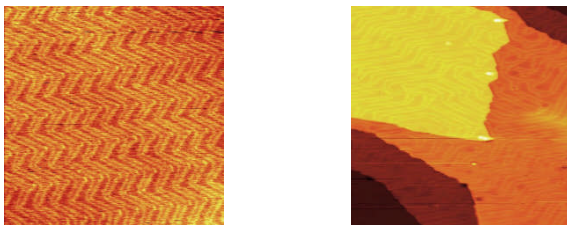


Fig. 2: Two STM pictures showing a well prepared Au surface. Left panel shows Au herringbone reconstruction and the right stepped domains on same

• *Photochemical Dynamics Studies on Well Characterized*

Nanoparticles: More recently we have begun an investigation of the dynamics of

the UV photochemistry of these particles as well. Currently we are implementing fabrication and mounting of a Ti-deposition source into our UHV chamber, which is equipped with time of flight (TOF) mass spectrometry, TPD, AES, and LEED instruments. We will follow the preparation developed by our group to prepare the TiO₂ nanoparticles, that is, the nanoparticles will be grown under UHV conditions utilizing RLAD method. The major advantage of investigating characteristics of nanoparticles in this UHV system is its capability of probing the energetics of light-induced surface reactions via the TOF method.

Plasmonic Photochemistry

In nanooptical chemistry, surface plasmon polaritons (SPP) have recently attracted much interest, including work in the DOE surface reaction dynamics community. SPPs are *p*-polarized strongly localized surface waves that form at metal/dielectrics interfaces. Because of their spatial optical-field localization, SPPs play an important role in metallic nanoobject physics and chemistry. Because of its resonant response and strong field confinement, the electromagnetic field of localized or propagating SPP modes is greatly enhanced as compared to the excitation field. As a result, the excitation of SPPs at metal nanoparticles or surface defects on a metal/dielectric interface represents an efficient interface-selective method for probing of chemical processes and as an interesting approach for enhanced surface photoreactions

In the past we have examined optically excited local plasmon-enhanced surface chemistry and its use in driving the growth of specific nanostructures by a resonant feedback process. Recently we have begun to examine the use of propagating plasmonic waves to drive surface reactions and to probe surface features. Our interest is in both linear and nonlinear processes. Both have been examined in our recent paper. This connection, is of interest to understand whether a propagating plasmon waves could interact with a surface feature to produce SHG radiation. Such interactions could form the basis for a new approach for high-resolution imaging of surface features or investigation of structural properties of colloids. In fact, however, there have been no theoretical and limited studies investigating scattered SHG by propagating SPPs. With these points in mind, we have analyzed the process of the SH generated during scattering of an SPP, which is propagating on a flat metal/dielectric interface, by one-dimensional metallic nanostructures, such as linear ridges (protuberances) or grooves (indentations). We have used a formulation based on the reduced Rayleigh equations, to first determine the total electromagnetic field at the fundamental frequency (FF). Subsequently, we have computed the induced nonlinear surface polarization density at the SH and use it to compute the dominant multipoles in a series expansion. We then use these multipoles to calculate the electromagnetic field and its spectral distribution at the SH. Our formalism has a wide applicability, as it can be used to study metallic nanostructures of arbitrary shape and can

describe metals whose dielectric constant is described by a Drude or Lorentz model, that is, most metals with good optical properties. Our results clearly show that the properties of the emitted SH are highly sensitive to the material and geometrical characteristics of the metallic surface or metal/dielectric interface, through the surface susceptibility $\chi_s^{(2)}$ and surface profile function $f(x_1)$.

Future Plans

Our future research efforts will be focused on the formation of TiO₂ nanoparticles supported on single-crystal surfaces utilizing RLAD under well defined ultra-high vacuum conditions with the ultimate goal of understanding and controlling laser-induced surface processes on these nanoparticles. As an initial project, we plan to investigate photoreaction dynamics of methyl bromide adsorbed on TiO₂/Au nanoparticles surfaces using time-of-flight and quadrupole mass spectrometry. We wish to compare TOF signatures of species desorbing from TiO₂ nanoparticles to those ejected from single-crystal surfaces. Also, we intend to examine the effect of nanoparticle size on bond-cleavage mechanism and on photochemical characteristics of nanoparticles. In addition, we will examine the formation chemistry of nanoparticles using RLAD in order to understand and control conditions for obtaining monophase nanoparticles. Finally we will begin to examine use of plasmonic resonances to enhance reactions on metallic nanoparticles supported on oxides thin films.

Recent DOE-Sponsored Publications

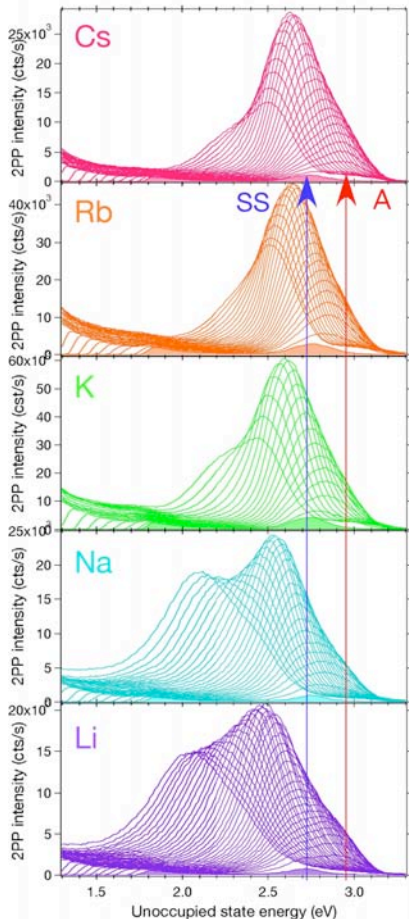
1. K. Adib, G.G. Totir, J.P. Fitts, G.W. Flynn, S.A. Joyce and R.M. Osgood, Jr., "Chemistry of CCl₄ on Fe₃O₄(111)-(2x2) Surfaces in the Presence of Adsorbed D₂O." *Surf. Sci.* **537**, 191 (2003).
2. Z. Zhu, A. Srivastava, and R.M. Osgood, Jr., "Reactions of Organosulfur Compounds with Si(100)," *J. Phys. Chem. B* **107**, 13939 (2003).
3. A. Srivastava and R.M. Osgood, Jr., "State-Resolved Dynamics of 248 nm Methyl-Iodide Fragmentation on GaAs(110)." *J. Chem. Phys.* **119**, 10298 (2003).
4. K.T. Rim, J.P. Fitts, T. Muller, K. Adib, N. Camillone III, R.M. Osgood, Jr., S.A. Joyce and G.W. Flynn, "CCl₄ Chemistry on the Reduced Selvege of a α -Fe₂O₃(0001) Surface: A Scanning Tunneling Microscopy Study." *Surf. Sci.* **541**, 59 (2003).
5. K.T. Rim, T. Muller, J.P. Fitts, K. Adib, N. Camillone III, R.M. Osgood, Jr., E.R. Batista, R.A. Friesner, B.J. Berne, S.A. Joyce, and G.W. Flynn, "An STM Study of Competitive Surface Reactions in the Dissociative Chemisorption of CCl₄ on Iron Oxide Surfaces," *Surf. Sci.* **524**, 113 (2003).
6. G. G. Totir, Y. Le and R. M. Osgood, Jr., "Photoinduced-Reaction Dynamics of Halogenated Alkanes on Iron-Oxide Surfaces: CH₃I on Fe₃O₄(111)-(2x2)," *J. Phys. Chem. B* **109**, 8452 (2005).
7. Z. Zhu, T. Andelman, M. Yin, T-L. Chen, S.N. Ehrlich, S.P. O'Brien, R.M. Osgood, Jr., "Synchrotron X-ray Scattering of ZnO Nanorods: Periodic Ordering and Lattice Size," *J. Mater. Res.* **21**, 1033 (2005).
8. Z. M. Zhu, T. Chen, Y. Gu, J. Warren and R. M. Osgood, Jr., "Zinc-oxide Nanowires Grown by Vapor-Phase Transport Using Selected Metal Catalysts: A Comparative Study," *Chem. Mats.* **17**, 4227 (2005).
9. Z. Song, J. Hrbek, R.M. Osgood, Jr., "Formation of TiO₂ Nanoparticles by Reactive-Layer-Assisted Deposition and Characterization By XPS and STM," *Nano. Letts.* **5**, 1357(2005).
10. G.Y. Le, G.G. Totir, G.W. Flynn, and R.M. Osgood, Jr., "Chloromethane Surface Chemistry on Fe₃O₄(111)-(2x2): A Thermal Desorption Spectroscopy Comparison of CCl₄, CBr₂Cl₂, and CH₂Cl₂," *Surf. Sci.* **600**, 665 (2006).
11. N. Camillone III, T.R. Pak, K. Adib, R.M. Osgood, Jr., "Tuning Molecule-Surface Interactions with Sub-Nanometer-Thick Covalently-Bound Organic Monolayers." *J. Phys. Chem B* (2006).
12. R.M. Osgood, Jr., "Photoreaction Dynamics of Molecular Adsorbates on Semiconductor and Oxide Surfaces." Accepted by *Chemical Reviews* (2006).
13. Lina Cao, N. C. Panoiu, and R. M. Osgood, Jr., "Surface Second-Harmonic Generation from Surface Plasmon Waves Scattered by Metallic Nanostructures." Submitted to *Nano Lett.*

Optical manipulation of ultrafast electron and nuclear motion on metal surfaces

Hrvoje Petek (petek@pitt.edu)
Department of Physics and Astronomy
University of Pittsburgh
Pittsburgh, PA 15269

Since the pioneering work of Langmuir on electron emission from metals, alkali atom overlayers on metal surfaces have been central to development of theories of chemisorption.¹⁻⁴ Our research goal is to study dynamics of alkali atoms on noble metal surfaces in response to excitation by a near UV light. The surface desorption dynamics are initiated by the photoinduced charge transfer from the metal substrate to the chemisorbed alkali atoms. Transforming the ionized alkali atoms in the ground state into a neutral excited state turns on the repulsive forces initiating the alkali atom photodesorption.⁵ To be able to interpret the dynamical studies, it is important to characterize the electronic structure of chemisorbed alkali atoms. Our activities have focused on two main subjects: 1) the theoretical calculation of the unoccupied electronic structure of alkali atoms; and 2) the search for the p_x and p_y symmetry unoccupied states. In this report we mainly focus on the electronic structure calculations.

Our experimental observations that motivated the theoretical study are summarized in Figs. 1 and 2. Previously, we have performed a survey two-photon photoemission



(2PP) spectra of the ns state for all the available alkali atoms Li-Cs on Cu(111) surface. The survey has also been partially completed for Ag(111) surface, where we obtained similar results. Figure 1 shows 2PP spectra of different alkali atoms chemisorbed on Cu(111) surface for a series of exposures resulting in sub-monolayer coverages ($0 < \theta < 0.1$ ML). At zero coverage, the only sharp feature in the 2PP spectra is the intrinsic occupied Shockley surface state (SS) at -0.39 eV relative to E_F . Upon adsorption of alkali atoms, a new state labeled A appears in 2PP spectra at a final energy that is just above SS for all alkali atoms. The state A is the unoccupied alkali atom state, which surprisingly appears at nearly identical binding energy with respect to the vacuum level of approximately -1.95 eV for each alkali atom independent of the principal quantum number n . Increasing the alkali atom coverage reduces the work function Φ , and along with it, the energy of A and to a lesser extent that of SS. Because A is stabilized in energy faster than SS, changing the coverage tunes the separation between A and SS into resonance with the

Figure 1. Details of 2PP spectra of the $SS \rightarrow A$ resonance as a function of alkali atom coverage for Li-Cs that show the alkali atom DOS, which is independent of the principle quantum number n .

laser, resulting in the enhancement of the 2PP intensity in Fig. 1.⁵ After extracting the energy of A in the pre-resonant, resonant, and post-resonant regions, where the peak assignment is unambiguous, in Fig. 2 we plot of the ns state energy vs. the work function shift $\Delta\Phi$. In addition to the nearly identical binding energy in the low coverage limit for all alkali atoms on both surfaces, the alkali atom resonance shifts to a lower energy with an identical $\Delta\Phi^{3/2}$ dependence.

The n independent energy is surprising because the ionization potential of isolated alkali atoms differs by ~ 1.5 eV between Cs and Li. Yet, when the alkali atoms are brought to the surface, their energy is independent of their free-atom properties. This suggests that there is a compensating correlation between the ionization potential (IP) of alkali atoms and the chemisorption distance, which suppresses the element-specific differences. Similar results for Ag(111) surfaces suggest that this could be a universal feature of the alkali atom chemisorption. To understand the origin for the similarity in the electronic structure for the alkali atom group, which represents one of the simplest chemisorption systems, we performed theoretical calculations on electronic and surface structures of alkali atoms on Cu(111) and Ag(111).

According to the Gurney model, the chemisorption of alkali atoms occurs through the configuration interaction of the valance ns state of the alkali atoms with the continuum of states in the metal.^{2-4, 6} As alkali atoms are brought to the proximity of a metal surface, their highest occupied ns states are perturbed through Coulomb interaction with electrons in the metal.

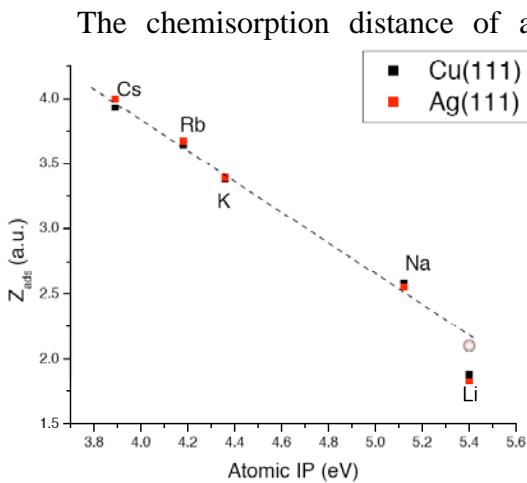


Figure 3. The inverse correlation between the chemisorption distance and the IP of isolated alkali atoms.

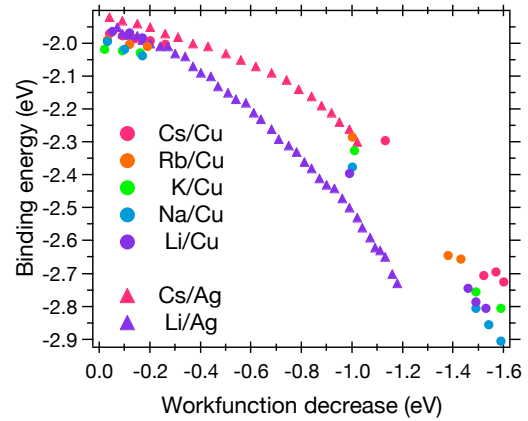


Figure 2. The binding energy of alkali atom resonance for different coverages of alkali atoms on Cu(111) and Ag(111) surfaces plotted against the work function change. Li/Ag(111) data are affected by diffusion of Li into the substrate.

The chemisorption distance of alkali atoms, which defines the energy of the unoccupied states observed in the experiment, was calculated by the plane-wave pseudo-potential density functional theory (DFT). Since the properties of alkali atom surfaces depend on the coverage, calculations were performed for the 2×2 , 4×4 , and 7×7 structures. The high coverage surfaces had shorter bond lengths, and exhibited considerable rumpling of the substrate. For the 7×7 structure we surmised that the chemisorption bond lengths have converged to their low coverage limit, and the rumpling is minimized. The chemisorption bond lengths for the 7×7 structure of alkali atoms on Cu(111) are shown in Table I, along with the experimental bond lengths from high

coverage experimental studies. On the Cu surface, the calculations show that small alkali atoms (Li and Na) favor the hollow sites, while the large ones (Rb and Cs) prefer the on top position. The two sites were equally favored for K on Cu(111). The agreement between experiment and theory is good considering the coverage difference between experiment and theory, and the strong rumpling of the surfaces.

Table I. The calculated chemisorption bond lengths and binding energies of alkali atoms on Cu(111).

	7 x 7 (Å)	Experimental	Binding energy (eV)
Li (hollow)	2.111	2.08/2.15 (LEED) [1]	-2.04
Na (hollow)	2.480		-2.21
K(top)	2.915	3.05± 0.02 (SEXAFS) [2]	-2.20
Rb(top)	3.045	3.07 (X-ray) [3]	-2.19
Cs(top)	3.196	3.01± 0.05 (LEED) [4]	-2.12

With the chemisorption distances determined, we plot in Fig. 3 the alkali atom distances from the image plane with respect to the free atom IP. As we surmised, there is an autocorrelation between the IP and the chemisorption distance of alkali atoms. The ns state of the smallest alkali atom (Li) at the shortest chemisorption distance has to be destabilized by the largest amount to compensate for its highest IP. The DFT bond lengths give a near-linear correlation. However, Li deviates most severely from the trend, because DFT underestimates its chemisorption length. This can be attributed to its high charge/radius ratio, which creates a large gradient in the charge density. We confirmed the failure of DFT by calculating the bond length for the Li dimer. The circles in Fig. 3 give the expected bond lengths for Li from a linear extrapolation from other alkali atoms.

Having obtained the chemisorption distance, we calculated the unoccupied state energy as a function of alkali atoms-surface distance using the wave packet propagation method of Borisov et al.^{7,8} According to this model, the potential experienced by the ns electron of the alkali atom can be described by the following contributions:

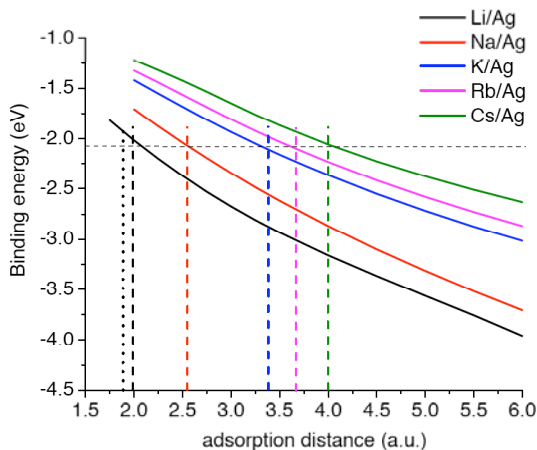


Figure 4. The calculated binding energy of the ns resonance as a function of adsorption distance. The dashed lines indicate the DFT adsorption distances.

$$V_{ns} = V_{\text{surf}} + V_{\Delta\text{surf}} + V_{\text{core}} + V_{\text{opt}}, \quad [1]$$

where, V_{surf} and $V_{\Delta\text{surf}}$ describe the surface potential and its modification by the presence of alkali atom, V_{core} describes the interaction of the valence ns electron with the alkali atom ionic core, and V_{opt} is included to satisfy the boundary conditions. The energy of the ns state, which is established at large distance by aligning the work function Φ of the metal with the IP of the free atom, increases on account of the Coulomb repulsion with the screening charge in the metal. Assuming that the electron and nuclear motions can be separated, the ionic alkali atom core creates a negative image charge at the metal surface, which repels the

ns electron with the $1/2Z$ dependence. The electron, however, is stabilized by the surface image potential, which asymptotically has the $-1/4Z$ dependence. As an alkali atom is brought to a surface, its *ns* state is destabilized with respect to the Fermi level E_F . Figure 4 shows the energy of the unoccupied resonance as a function of distance from the Ag surface (similar results are obtained for Cu(111)), with the DFT chemisorption distances indicated by the dashed lines. For Li The dotted line is calculated with the PBE and the dashed line with B3LYP functionals. We also expect that the difference between Li and other alkali atoms may reflect more covalent nature of the atom surface bond.

We can derive qualitatively similar alkali atom binding energies by assuming the asymptotic Coulomb potentials for the electron-image charge repulsion and the asymptotic surface attraction. From these leading terms (see above), the binding energy is approximately given by $E_0 = IP - 1/4Z$. This simple expression gives nearly quantitative binding energies in a range of -2.21 to -2.39 for $n > 2$. For Li, the binding energy is only -2.01 eV because of afore discussed problem in the DFT bond length. Thus, the linear Z correlation in Fig. 3 has the origin in electrostatic forces acting on the *ns* electron, which in the Z range of interest can be approximated by a Taylor expansion of the expression for E_0 . The experimental and theoretical results presented above provide for the first time a quantitative understanding of the alkali atom chemisorption on metals.

References

- ¹ I. Langmuir, Phys. Rev. **43**, 224 (1933).
- ² R. W. Gurney, Phys. Rev. **47**, 479 (1935).
- ³ J. W. Gadzuk, Phys. Rev. B **1**, 2110 (1970).
- ⁴ J. P. Muscat and D. M. Newns, Prog. Surf. Sci. **9**, 1 (1978).
- ⁵ H. Petek and S. Ogawa, Annu. Rev. Phys. Chem. **53**, 507 (2002).
- ⁶ P. Nordlander and J. C. Tully, Phys. Rev. B **42**, 5564 (1990).
- ⁷ A. G. Borisov, A. K. Kazansky, and J. P. Gauyacq, Surf. Sci. **430**, 165 (1999).
- ⁸ A. G. Borisov, J. P. Gauyacq, A. K. Kazansky, et al., Phys. Rev. Lett. **86**, 488 (2001).

Collaborations: We (Dr. Jin Zhao) have performed the theoretical study of alkali atom chemisorption in collaboration with Prof. P. Echenique, Prof. E. Chulkov, and Dr. Daniel Garcia-Portal of Donostia International Physics Center, San Sebastian, Spain, and Dr. Andrei Borisov, of CNRS, France. The calculations were performed at the Environmental Molecular Sciences Laboratory, a national scientific user facility sponsored by the DOE Office of Biological and Environmental Research and located at Pacific Northwest National Laboratory.

Publications: A joint experimental/theoretical study of the alkali atom chemisorption and electronic structure is in preparation.

Funds: There will be no unexpanded funds at the end of the funding period.

X-ray Spectroscopy of Volatile Liquids and their Surfaces

Richard J. Saykally
Department of Chemistry
University of California
Berkeley, CA 94720-1460
saykally@berkeley.edu

and

Chemical Sciences Division
Lawrence Berkeley National Laboratory

Program Scope or Definition

The goal of this project is to explore and develop novel methodologies for probing the nature of volatile liquids and solutions and their surfaces, employing combinations of liquid microjet technology, with synchrotron X-ray and Raman spectroscopies.

Recent Progress

Utilizing the intense monochromatic soft X-Rays available at the LBNL Advanced Light Source (ALS), and employing liquid microjets for convenient temperature and composition control, we have carried out a systematic study of the perturbative effect of a variety of inorganic salts on the unoccupied water orbitals which are a sensitive probe of the local solvation environment. We conclude that monovalent cations have a very small effect on the local electronic structure, whereas simple anions are strongly perturbative[5]. Moreover, these anions exhibit markedly ion-specific perturbations, while the multivalent cations all produce the same effects. Divalent cations[12] exhibit ion-specific perturbations, however, and we attribute these (as well as the ion-specific anion perturbations) to a combination of electric field effects on and charge transfer with the first solvent shell molecules, as deduced via comparisons with density functional theory calculations. We also identified a strong blue-shift in the k-edge spectrum of the hydronium ion, relative to that of water, probably due to the tighter electron binding[11].

Much debate has followed the publication of a study of the local structure of liquid water by X-ray spectroscopy by Nilsson and coworkers [*Science* **304**, 995 (2004)], wherein it was claimed that room temperature liquid water comprises 2-coordinate rings and chains of hydrogen bonded molecules, rather than the widely accepted locally tetrahedral network. We found that our own studies of the X-ray absorption spectra of normal and supercooled water made via total electron yield (TEY) detection could be interpreted quite nicely in terms of the traditional model[3,6], and we have presented detailed arguments showing that the theoretical methods used by Nilsson et al. To interpret their spectra are too approximate to support their dramatic proposals for a revised structure of liquid water[13]. We have found that Raman spectroscopy of liquid microjets provides a useful complement to our XAS studies. Building on our recent investigation of the temperature-dependent Raman spectrum of water, wherein we found that a histogram of the electric field distribution along the OH bonds computed from a Monte Carlo simulation accurately represents the observed spectra[8], we have proceeded to study ionic solutions by this combined experimental/theoretical approach as a means of ascertaining the

local environments around aqueous ions. We again find that the E-field histograms faithfully reproduce the T-dependent Raman spectra, and make it possible to deduce a detailed new molecular picture of how simple ions are solvated in water [paper to be submitted soon].

Liquid microjet technology affords the opportunity to study the details of water evaporation, free from the obfuscating effects of condensation that have plagued previous studies. Studying small (diameter < 5 μm) jets with Raman thermometry, we find compelling evidence for a significant energetic barrier to evaporation, in contrast to most current models[10,14].

Using Liquid microjets to avoid the problem of radiation damage to fragile solutes, we have measured the pH-dependent NEXAFS spectra of several amino acids, including glycine, proline, lysine, and the dipeptide diglycine[4,9]. We find that the nitrogen terminus of primary amino acids is sterically shielded at high pH, and exists in an “acceptor-only” state, wherein neither amine proton is involved in hydrogen bonding to the surrounding solvent. The diglycine study characterized a similar behavior in this first study of the peptide bond hydration.

We have recently addressed the long standing controversy over whether continuum or a multi-component (“intact” or “broken bond,” etc.) models best describe the hydrogen bond interactions in liquid water. The temperature dependence of water’s Raman spectrum has long been considered to be among the strongest evidence for a multi-component distribution. However, we have shown, using a combined experimental and theoretical approach, that many of the features of the Raman spectrum considered to be hallmarks of a multi-state system, including the asymmetric band profile, the isosbestic (temperature invariant) point, and van’t Hoff behavior, actually result from a continuous distribution[5]. This work complements our study of the structure of pure liquids by X-ray absorption spectroscopy that has been ongoing. We have published a joint theory/experiment study of liquid methanol that characterized the nature of H-bonded domains[6,7].

Future Plans

In forthcoming scheduled runs at the Berkeley ALS, we plan to focus on the following problems:

1. Complete the study of ionic perturbation of local water structure, such that the entire Hofmeister series is ultimately addressed. We seek a comprehensive picture of the effects of both cations and anions on the local structure of water.
2. Raman spectroscopy measurements will also be performed on these systems, the data from which provide complementary insights and aid in the theoretical modeling. We will further develop the use of E-field distributions from simulations to interpret the spectra.
3. Extend our studies of amino acid hydration vs. pH to include all natural amino acids. Use the same approach to study hydration of the peptide bonds in small polypeptides, nucleotide bases, nucleosides, and nucleotides.
4. Measure NEXAFS spectra for pure liquid water, alcohols, and hydrocarbons, seeking to

achieve deep supercooling via controlled evaporation. In conjunction with theoretical modeling, we will seek a coherent description of the liquid structure and bonding in these systems.

5. We will continue to explore and compare ion and electron detection of NEXAFS spectra, seeking to reproduce earlier measurements of surface phenomena obtained with ion detection. Thus far, we have not been able to reproduce the original measurements with our newly-designed X-ray spectrometer.
6. We plan to continue our exploration of the evaporation of liquid water by Raman thermometry, seeking to ascertain the effects of salts on the evaporation process.

References (DOE supported papers 2003-present)

1. K.R. Wilson, B.S. Rude, J. Smith, C.D. Cappa, D.T. Co, R.D. Schaller, M. Larsson, T. Catalano, and R.J. Saykally, "Investigation of volatile liquid surfaces by synchrotron x-ray spectroscopy of liquid microjets," *Review of Scientific Instruments* **75**, 725-736 (2004). LBNL-56347
2. C.D. Cappa, K.R. Wilson, B.M. Messer, R.J. Saykally, and R.C. Cohen, "Optical cavity resonances in water micro-droplets: Implications for shortwave cloud forcing," *Geophysical Research Letters* **31**, L10205 (2004). LBNL-56357
3. J.D. Smith, C.D. Cappa, K.R. Wilson, B.M. Messer, R.C. Cohen, and R.J. Saykally, "Energetics of Hydrogen Bond Network Rearrangements in Liquid Water," *Science* **306**, 851-853 (2004). LBNL-56349
4. B.M. Messer, C.D. Cappa, J.D. Smith, K.R. Wilson, M.K. Gilles, R.C. Cohen, and R.J. Saykally, "pH Dependence of the Electronic Structure of Glycine," *J. Phys. Chem. B* **109**, 5375-5382 (2005). LBNL-56348
*Cover Article.
5. C.D. Cappa, J.D. Smith, K.R. Wilson, B.M. Messer, M.K. Gilles, R.C. Cohen, and R.J. Saykally, "Effects of Alkali Metal Halide Salts on the Hydrogen Bond Network of Liquid Water," *J. Phys. Chem. B* **109**, 7046-7052 (2005). LBNL-56812*Cover Article.
6. J.D. Smith, C.D. Cappa, B.M. Messer, R.C. Cohen and R.J. Saykally, Response to Comment on "Energetics of Hydrogen Bond Network Rearrangements in Liquid Water," *Science* **308**, 793b (2005). LBNL-57117
7. K.R. Wilson, M. Cavalleri, B.S. Rude, R.D. Schaller, T. Catalano, A. Nilsson, L.G.M. Pettersson, and R.J. Saykally, "X-ray Absorption Spectroscopy of Liquid Methanol Microjets: Bulk Electronic Structure and Hydrogen Bonding Network," *J. Phys. Chem. B* **109**, 10194-10203 (2005). LBNL-56350
*Cover Article.
8. J.D. Smith, C.D. Cappa, K.R. Wilson, R.C. Cohen, P.L. Geissler, and R.J. Saykally, "Unified description of temperature-dependent hydrogen-bond rearrangements in liquid water," *PNAS* **102**, 14171-14174 (2005). LBNL-58789
9. B.M. Messer, C.D. Cappa, J.D. Smith, W.S. Drisdell, C.P. Schwartz, R.C. Cohen, R.J. Saykally, "Local Hydration Environments of Amino Acids and Dipeptides Studied by X-

- ray Spectroscopy of Liquid Microjets,” *J. Phys. Chem. B* **109**, 21640-21646 (2005). LBNL-59184
10. C.D. Cappa, W. Drisdell, J.D. Smith, R.J. Saykally, and R.C. Cohen, “Isotope Fractionation of Water During Evaporation Without Condensation,” *J. Phys. Chem. B* **109**, 24391-24400 (2005). LBNL-59505
 11. C.D. Cappa, J.D. Smith, B.M. Messer, R.C. Cohen, and R.J. Saykally, “The Electronic Structure of the Hydrated Proton: A Comparative X-ray Absorption Study of Aqueous HCl and NaCl Solutions,” *J. Phys. Chem. B* **110**, 1166-1171 (2006). LBNL-59504
 12. C.D. Cappa, J.D. Smith, B.M. Messer, R.C. Cohen, and R.J. Saykally, “Effects of Cations on the Hydrogen Bond Network of Liquid Water: New Results from X-ray Absorption Spectroscopy of Liquid Microjets,” *J. Phys. Chem. B* **110**, 5301-5309 (2006). LBNL-59955
 13. J.D. Smith, C.D. Cappa, B.M. Messer, W.S. Drisdell, R.C. Cohen, and R.J. Saykally, “Probing the Local Structure of Liquid Water by X-ray Absorption Spectroscopy,” *J. Phys. Chem. B* (ASAP Article 8/19/2006). – C.B. Harris special issue.
 14. J.D. Smith, C.D. Cappa, W.S. Drisdell, R.C. Cohen, and R.J. Saykally, “Raman Thermometry Measurements of Free Evaporation from Liquid Water Droplets,” *JACS* (ASAP Article 9/12/2006).

Molecular Theory & Modeling

Development of Statistical Mechanical Techniques for Complex Condensed-Phase Systems

Gregory K. Schenter
Chemical Sciences Division
Pacific Northwest National Laboratory
902 Battelle Blvd.
Mail Stop K1-83
Richland, WA 99352
greg.schenter@pnl.gov

Program Scope

The long-term objective of this project is to advance the understanding of the relation between detailed descriptions of molecular interactions and the prediction and characterization of macroscopic collective properties. To do this, we seek to better understand the relation between the form and representation of intermolecular interaction potentials and simulation techniques required for statistical mechanical determination of properties of interest. Molecular simulation has the promise to provide insight and predictive capability of complex physical and chemical processes in condensed phases and interfaces. For example, the transport and reactivity of species in aqueous solutions, at designed surfaces, in clusters and in nanostructured materials play significant roles in a wide variety of problems important to the Department of Energy.

We start from the premise that a detailed understanding of the intermolecular interactions of a small collection of molecules, through appropriate modeling and statistical analysis, will enable us to understand the collective behavior and response of a macroscopic system, thus allowing us to predict and characterize thermodynamic, kinetic, material, and electrical properties. Our goal is to improve understanding at the molecular level in order to address increasingly more complex systems ranging from homogeneous bulk systems to multiple phase or inhomogeneous ones, to systems with external constraints or forces. Accomplishing this goal requires understanding and characterization of the limitations and uncertainties in the results, thereby improving confidence in the ability to predict behavior as systems become more complex.

Recent Progress

In developing interaction potentials, we have recently focused on the relation between accurate *ab initio* electronic structure calculations of aqueous ion clusters, extended x-ray absorption fine structure (EXAFS) measurements and empirical potentials used in molecular simulation. We concentrated on understanding the first peak of the ion-water radial distribution function for Ca^{2+} , K^+ and Cl^- in water. (See Figure 1.) We employ the rigid-body polarizable water model of Dang and Chang to describe the water-water intermolecular interaction.

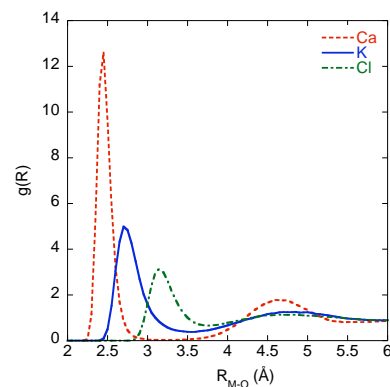


Figure 1. Comparison of Ion-Water Radial distribution functions from simulation at 300K.

This model recovers the structure and thermodynamic properties of the bulk and the liquid/vapor interface of water. Ion-water potential parameters were obtained to recover bulk properties such as solvation enthalpies. How do these models describe the local solvation structure determined from EXAFS measurement? What about the properties of clusters? To further test our empirical parameterization, we considered the enthalpy of formation of the clusters. In Figure 2, we compare the enthalpy of formation for $K^+(H_2O)_n$ clusters, and in Figure 3, for $Cl^-(H_2O)_n$ clusters.

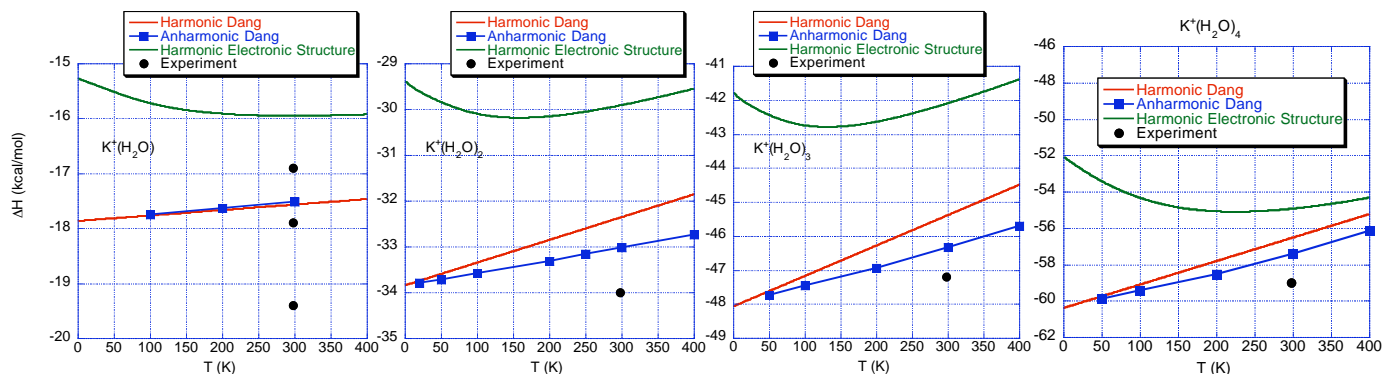


Figure 2. $K^+(H_2O)_n$ cluster enthalpy of formation, comparing anharmonic to harmonic analysis using an empirical potential (Dang), harmonic electronic structure (aug-cc-pVDZ/MP2), and a compilation of experimental measurements (Keese and Castleman, *J. Phys. Chem. Ref. Data*, **15**, 1011 (1986)).

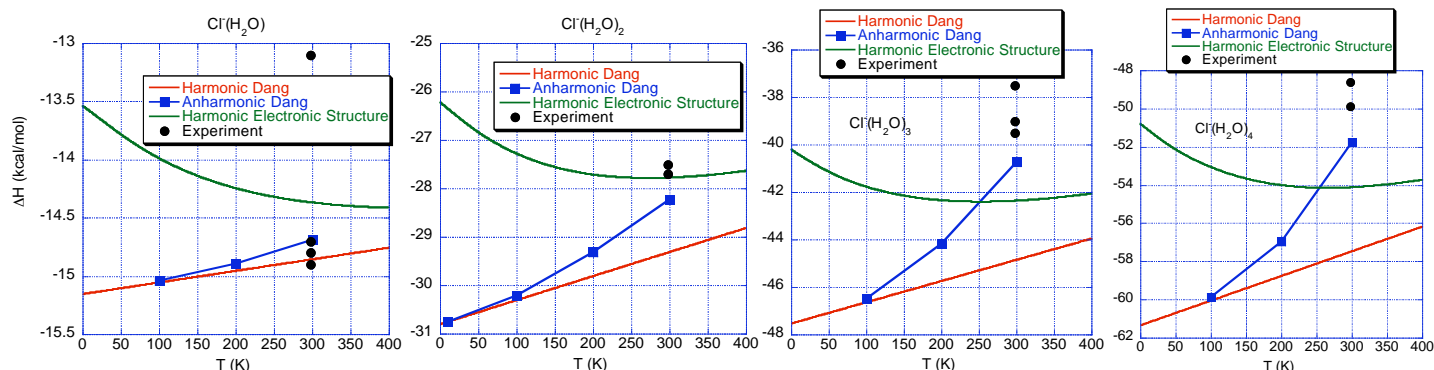


Figure 3. $Cl^-(H_2O)_n$ cluster enthalpy of formation, comparing anharmonic to harmonic analysis using an empirical potential (Dang), harmonic electronic structure (aug-cc-pVDZ/MP2), and a compilation of experimental measurements (Keese and Castleman, *J. Phys. Chem. Ref. Data*, **15**, 1011 (1986)).

From this analysis we find that as the clusters get larger it is important to consider anharmonicity for the empirical potentials to be consistent with experimental measurement. The width of this first peak of the radial distribution function, the Debye-Waller factor (DWF), obtained from simulation using the empirical potential was found to have significant deviations from values obtained from analysis of EXAFS measurements. To understand this, we found the DWF to be correlated to the symmetric and antisymmetric normal modes of small, symmetric, ion-water clusters. ($M^q(H_2O)_n$ for $n=1-6$) We found a universal relation between the harmonic cluster DWF and the M-O distance. Using converged electronic structure information from the cluster system we successfully corrected the deficiencies in the empirical potentials to recover values for the DWF that were consistent with experimental measurement. For Ca^{2+} , the empirical potential value for the DWF is $\sigma_{MD}^2 = 0.0066 \text{ \AA}^2$, the electronic structure corrected value, $\sigma_{ES-MD}^2 = 0.0107 \text{ \AA}^2$, while the experimentally measured value is $\sigma_{EXAFS}^2 = 0.0115 \text{ \AA}^2$. For K^+ ,

$\sigma_{MD}^2 = 0.0221 \text{ \AA}^2$, $\sigma_{ES-MD}^2 = 0.0276 \text{ \AA}^2$, and $\sigma_{EXAFS}^2 = 0.0293 \text{ \AA}^2$. For Cl^- , $\sigma_{MD}^2 = 0.0334 \text{ \AA}^2$, $\sigma_{ES-MD}^2 = 0.0271 \text{ \AA}^2$, and $\sigma_{EXAFS}^2 = 0.0290 \text{ \AA}^2$.

Future Plans

In future studies we will refine our description of ion-solvent interaction in the low concentration limit as we explore the relation between *ab initio* electronic structure calculations of clusters and EXAFS measurement, seeking consistency between the approaches. In the next stage of development we will consider the influence of molecular interaction between ion-pairs. Our challenge is to be able to account for changes in features in EXAFS measurement as a function of solute concentration. Initial simulations of the concentration dependence of HCl EXAFS will allow us to better characterize $\text{H}_3\text{O}^+ \text{Cl}^-$ ion pairing in aqueous solution. Can this interaction be effectively described using an empirical potential? In future studies we will concentrate on CaCl_2 and AgCl solutions as electronic structure calculations and experimental EXAFS measurements are being performed.

In an effort to develop more robust representations of intermolecular interaction, we continue to explore the use of semiempirical self-consistent field (SCF) methods. Neglect of differential diatomic overlap (NDDO) methods that include such parameterizations as MNDO, AM1, and PM3, have the ability to treat the formation and breaking of chemical bonds, but have been found to poorly describe hydrogen bonding and weak electrostatic complexes. In contrast, most empirical potentials are not able to describe bond-breaking and formation, but have the ability to add missing elements of hydrogen bonding using classical electrostatic interactions. We continue to develop a method that combines aspects of both NDDO-based SCF techniques and classical descriptions of polarization to describe the diffuse nature of the electronic wavefunction in a self-consistent manner. We have developed the self-consistent polarization NDDO (SCP-NDDO) theory with the additional description of molecular dispersion developed as a second-order perturbation theory expression. Initial efforts using this approach have allowed us to parameterize the model to reproduce the accurate MP2/CBS estimates of small water cluster binding energies of Xantheas *et al*, as well as the intramolecular frequency shifts as a function of cluster size. Initial steps have been made to parameterize protonated and hydroxide water clusters. Future efforts will extend the parameterization to aqueous solvation of more complex ions.

We will continue to explore the relation between information obtained from electronic structure calculations corresponding to the Born-Oppenheimer surface and effective potentials to be used in classical mechanical simulation. To do this it is necessary to investigate the role of quantum statistical mechanical effects and understand the sensitivity of empirical potentials to the parameters that define them. This involves merging the efforts of recent Refs. 14, 15 and 18.

Collaborators on this project include B. C. Garrett, S. M. Kathmann, S. S. Xantheas, and L. X. Dang, V.-A. Glezakou, John Fulton, Yongsheng Chen, T. D. Jordanov and D. T. Chang. Battelle operates Pacific Northwest National Laboratory for the U. S. Department of Energy.

References to publications of DOE sponsored research (2003-present)

1. B. C. Garrett, S. M. Kathmann, and G. K. Schenter, "Thermochemistry and Kinetics of Small Water Clusters," in "Water in Confining Geometries", edited by V. Buch and J. P. Devlin, (Springer-Verlag, New York, 2003) p. 25.

2. Y. D. Suh, G. K. Schenter, L. Zhu, and H. P. Lu, "Probing nanoscale surface enhanced Raman-scattering fluctuation dynamics using correlated AFM and confocal ultramicroscopy," *Ultramicroscopy* **97**, 89 (2003).
3. L. Zhu, G. K. Schenter, M. Micic, Y. D. Suh, N. Klymyshyn, and H. P. Lu, "Nanosurface-enhanced Raman scattering fluctuation dynamics," in *Proceedings of SPIE*, 4962, "Manipulation and Analysis of Biomolecules, Cells, and Tissues," edited by D. V. Nicolau, J. Enderlein, R. C. Leif, and D. L. Farkas, (SPIE, Bellingham, WA, 2003) p. 70.
4. G. K. Schenter, B. C. Garrett, and D. G. Truhlar, "Generalized transition state theory in terms of the potential of mean force," *J. Chem. Phys.* **119**, 5828 (2003).
5. M. Dupuis, G. K. Schenter, B. C. Garrett, and E. E. Arcia, "Potentials of mean force with ab initio mixed Hamiltonian models of solvation," *J. Molec. Struct. (THEOCHEM)* **632**, 173 (2003).
6. L. X. Dang, G. K. Schenter, and J. L. Fulton, "EXAFS Spectra of the Dilute Solutions of Ca^{2+} and Sr^{2+} in Water and Methanol," *J. Phys. Chem. B* **107**, 14119 (2003).
7. M. P. Hodges, R. J. Wheatley, G. K. Schenter, and A. H. Harvey, "Intermolecular potential and second virial coefficient of the water-hydrogen complex," *J. Chem. Phys.* **120**, 710 (2004).
8. S. M. Kathmann, G. K. Schenter, and B. C. Garrett, "Multicomponent dynamical nucleation theory and sensitivity analysis," *J. Chem. Phys.* **120**, 9133 (2004).
9. J. L. Daschbach, G. K. Schenter, P. Ayotte, R. S. Smith, and B. D. Kay, "Helium diffusion through H_2O and D_2O amorphous ice: Observation of a lattice inverse isotope effect," *Phys. Rev. Lett.* **92**, 198306 (2004).
10. S. M. Kathmann, G. K. Schenter, and B. C. Garrett, "Dynamical Nucleation Theory: Understanding the Role of Aqueous Contaminants," in *Proceedings of the 16th International Conference on Nucleation and Atmospheric Aerosols*, edited by M. Kulmala and M. Kasahara (Kyoto University Press, 2004), p. 243.
11. S. M. Kathmann, G. K. Schenter, and B. C. Garrett, "Ion-Induced Nucleation: The Importance of Chemistry," *Phys. Rev. Lett.* **94**, 116104 (2005).
12. B. C. Garrett, D. A. Dixon, et al "The Role of Water on Electron-Initiated Processes and Radical Chemistry: Issues and Scientific Advances," *Chem. Rev.* **105**, 355 (2005).
13. V. -A. Glezakou, Y. C. Chen, J. L. Fulton, G. K. Schenter and L. X. Dang "Electronic Structure, Statistical Mechanical Simulations, and EXAFS Spectroscopy of Aqueous Potassium" *Theoret. Chem. Acc.* **115**, 86 (2006).
14. T. D. Iordanov, G. K. Schenter, and B. C. Garrett, "Sensitivity Analysis of Thermodynamics Properties of Liquid Water: A General Approach to Improve Empirical Potentials," *J. Phys. Chem. A* **110**, 762 (2006).
15. C. D. Wick and G. K. Schenter, "Critical Comparison of Classical and Quantum Mechanical Treatments of the Phase Equilibria of Water," *J. Chem. Phys.* **124**, 114505 (2006).
16. B. C. Garrett, G. K. Schenter, and A. Morita, "Molecular Simulations of the Transport of Molecules across the Liquid/Vapor Interface of Water," *Chem. Rev.* **106**, 1355 (2006).
17. S. Du, J. S. Francisco, G. K. Schenter, T. D. Iordanov, B. C. Garrett, M. Dupuis, and J. Li, "The OH radical – H_2O molecular interaction potential," *J. Chem. Phys.* **124**, 224318 (2006).
18. G. S. Fanourgakis, G. K. Schenter, and S. S. Xantheas, "A Quantitative Account of Quantum Effects in Liquid Water," *J. Chem. Phys.*, in press (Oct 14, 2006).

Reactive Intermediates in High Energy Chemistry.

Principal Investigators: Ilya A. Shkrob,^{*} Robert A. Crowell, and David Gosztola

Radiation and Photochemistry Group, Chemistry Division, Argonne National Laboratory, Argonne, Illinois 60439; tel.: 630-2529516; FAX: 630-2529570; e-mail: shkrob@anl.gov

1. Program Scope.

We aim to (i) study localization, thermalization, and reactions of short-lived reaction intermediates (such as electrons and holes) generated by ionization, electron detachment, and other energetic processes in aqueous systems and molecular liquids and solids and (ii) characterize the structure and dynamics of self-trapped charges (e.g., excess electrons) in such media. Our main approach is using short laser and electron pulses to study the dynamics subsequent to the energetic events. Other methods include nanosecond pulse radiolysis and laser photolysis and time-resolved conductivity and magnetic resonance. The use of fast and slow techniques, combined use of short-pulse lasers and particle accelerators, addressing both the kinetic and structural aspects of the chemistry, and advanced theoretical modeling are the constituents of our multifaceted approach. Our ability to pursue such comprehensive studies is aided by a newly completed, operational 10 TW table-top laser system capable of generating subpicosecond electron pulses (T^3 system). Chemical dynamics in radiolytic spurs can be studied on the picosecond time scale with this setup (the first account of such studies can be found on <http://arxiv.org/abs/physics/0608106>). Our effort is currently focused on further development of this T^3 system into a universal tool for pulse radiolysis and pursuing groundbreaking pulse-probe ultrafast experiments on aqueous systems, including practically-important concentrated solutions. Despite this overriding focus, we vigorously pursue the research on the reactive intermediates generated both in radiolysis and laser photolysis, as summarized below.

2. Progress report.

The studies completed during the previous two years were reviewed in the 2004 and 2005 CPIMS report. In FY 2006, our ultrafast laser studies on aqueous systems addressed (1) the energy dependence of ionization of liquid water, (2) H-OH dissociation and ionization that follows 2-photon excitation of water, and (3) a detailed study of charge transfer to solvent (CTTS) reactions involving polyvalent anions (carried out in collaboration with S. E. Bradforth of USC). We also studied electron attachment/detachment to polynitriles (in the context of our electron encapsulation program) and examined in much detail, theoretically, electron solvation in water, using a combination of mixed quantum classical molecular dynamics (MD) and density functional theory (DFT) and *ab initio* approaches (in collaboration with B. J. Schwartz of UCLA). Some of these studies are summarized below.

2.1. Excitation-energy dependence and mechanism for 2-photon ionization of liquid water

Laser excitation provides an opportunity to explore the ionization mechanism of liquid water. A defining aspect of our study is the ability to tune the excitation energy over a wide range (8-12 eV), and observe its effect on the dynamics of hydrated electron, e^- , generated in the ionization.

Connecting our results with the electronic structure of liquid water reveals details about the nature of the excited states and the ionization mechanism. Transient absorption spectroscopy was used to study geminate recombination kinetics of e^- . Modeling the kinetics of the electron reveals its average ejection length and thus provides insight into the ionization mechanism. This length increases monotonically from 0.9 nm at 8.3 eV to 4 nm at 12.4 eV, with the increase taking place most rapidly above 9.5 eV. We connect our results with recent advances in the understanding of the electronic structure of liquid water, interpreting it as a gradual switchover between several ionization mechanisms. The isotope dependence of the electron thermalization provides additional information about the mechanisms. The electron ejection length has a similar energy dependence for D_2O , but is consistently shorter than in H_2O by 0.3 nm across the entire range of excitation energies studied. We suggest that autoionization plays a major role throughout this range, but the amount of nuclear reorganization of the excited states involved decreases monotonically as the energy increases towards 11 eV, at which the direct process becomes prevalent. However, even at 12.4 eV (which is well above the optical gap of water) the ionization is not fully dominated by this direct process. Surprisingly, the isotope effect on the electron thermalization is opposite to that observed in radiolysis, at all photon energies. The cause of this discrepancy remains unclear. Our result suggests that electron thermalization in radiolytic spurs is qualitatively different from isolated pairs generated by laser photoionization. Theorists, take note!

2.2. Water ionization vs. dissociation in low-energy (8.3 eV) 2-photon excitation of water.

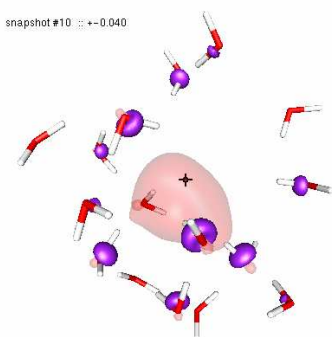
Following the dynamics of OH radicals (that absorb in the UV), in addition to hydrated electrons (that absorb in the near IR), provides a glimpse of the complex dynamics following 2-photon excitation by revealing the branching between ionization and H-OH bond dissociation. We find that the two processes occur with equal probability for an excitation energy of 9.3 eV, while the dissociation channel prevails for 8.3 eV excitation. At the lower energy, we observed the geminate recombination kinetics of the hydroxyl, and determined that the initial H...OH separation is > 0.6 nm, which is in agreement with recent MD simulations of dissociating H_2O in amorphous ice. Without doubt, this photodissociation yields *hot* H atoms with excessive kinetic energy; we find no evidence for caging of the resulting geminate radical pairs (contrary to aqueous H_2O_2 photodissociation that was also studied in our laboratory). The competition among ionization and dissociation channels reveals important details about the dynamics in the excited electronic states of liquid water, and how the liquid environment changes the behavior of those states relative to the gas phase (which is currently at the center of much attention). H-bonding effects have a strong influence on the excited state dynamics in the liquid, and our experiments provide an important experimental benchmark for comparison with theoretical results.

2.3. Electron encapsulation and electron trapping by polynitriles

Is it possible to design a supramolecular cage (a macrocycle dispersed in a solvent/matrix with low electron affinity) that would “solvate” the excess electron in the same fashion in which several solvent molecules do that co-operatively in polar liquids? Such an “encapsulated electron” would be very helpful for structural and dynamics studies of electron solvation and might be useful for molecular and nano- electronics (as the encapsulated electrons would be the smallest charged “molecular capacitors”). Two general strategies have been pursued: electron localization using polar groups arranged (i) inside or (ii) outside of the cage. The second

approach is more convenient from the synthetic standpoint, but it is limited to polynitriles. We demonstrated, both experimentally and theoretically, that this second approach faces a problem: instead of dipole binding, the electron attaches to the nitrile groups forming molecular anions with bent C-C-N fragments. Since the energy cost of this bending is high, for dinitrile anions in *n*-hexane the binding energies are extremely low (setting the absolute record for endothermicity of electron attachment) and for mononitriles, these binding energies are lower still, and the entropy of electron attachment is anomalously small. DFT modeling suggests that the mononitrile molecules substitute for the solvent molecules at the electron cavity, “solvating” the electron by their methyl groups. Such “solvated electrons” actually resemble more closely multimer radical anions in which the electron density is shared (mainly) between C 2*p* orbitals in the solute/solvent molecules, instead of existing as cavity electrons. The way in which the excess electron density is shared by such solvent molecules is similar to the way in which this sharing occurs in large polynitrile anions, such as octacyanocyclododecane⁻. Our study thus reveals *limitations of the concept of “solvated electron” for organic liquids: it might be impossible to draw a clear line between such species and a certain class of radical anions*. It also demonstrates the feasibility of electron encapsulation. A specific design for such a trap that is based on calix[4]cyclohexanol is discussed in <http://arxiv.org/abs/physics/0607089>. It is shown by DFT modeling, that one of the conformations of this macrocycle forms the optimum trap for the electron. The resulting “encapsulated electron” strikingly resembles the solvated electron in alcohols and water. We are currently testing these and other predictions of the theory.

2.3. Multielectron modeling of hydrated electron.



Historically, the models for solvated electron treated this species as a single quantum particle in a fluctuating classical potential, “a particle in a box,” without providing justification for such a treatment. The limitations of this approach have long been recognized, and our theoretical studies seek to overcome these by providing a consistent multielectron model. This task is important for radiation chemistry as the excess electrons play the central role in (e.g., aqueous) chemistry, and current level of understanding their structure and dynamics is not entirely satisfactory. Without understanding the structure of the thermalized species, it is difficult to understand thermalization/solvation process. DFT

and *ab initio* methods were used to rationalize magnetic spin parameters of electron trapped in alkaline glasses, as observed using EPR and Electron Spin Echo Envelope Modulation (ESEEM) spectroscopies. Water cluster anions ($n < 24$) that localize the electron internally were examined. EPR parameters of these anions were defined mainly by the cavity size and the coordination number; the water molecules in the second solvation shell were shown to play a minor role. An idealized model of hydrated electron, e^- (attributed to L. Kevan) in which six OH groups arranged in an octahedral pattern provided the closest match to the experimental parameters. The salient feature of these models is the significant transfer (10-20%) of spin density into the frontal O 2*p* orbitals of water molecules (see the figure above). Spin bond polarization involving these oxygen orbitals accounts for small, negative hyperfine coupling constants for protons in the OH groups that form the electron cavity. For more detail, see <http://arxiv.org/abs/physics/0607228>. In a follow-up study, adiabatic mixed quantum-classical (MQC) molecular dynamics (MD)

simulations were used to generate hundreds of snapshots of the e^- in water along the 80 ps trajectory. Cluster anions (that included two complete solvation shells) centered on the cavity were extracted and embedded in a 20 Å x 20 Å x 20 Å matrix of fractional point charges representing the rest of the solvent. DFT and single-excitation configuration interaction (CIS) methods were then applied to these embedded clusters. The results of these calculations were used to examine the structure of the singly occupied and the lower unoccupied molecular orbitals, the electronic and vibrational density of states, the UV-VIS-near IR absorption spectra, the hyperfine coupling (hfc) tensors, and the IR-Raman spectra of e^- . The calculated hfc tensors were used to compute EPR and ESEEM spectra that compared very favorably to the experimental ones. The calculated vibrational spectra of the hydrated electron are consistent with the downshifted bending and stretching modes recently observed in resonance Raman experiments. The hybrid model also accounts for 190-nm absorption band in addition to the VIS/near-IR absorption bands. We also showed how the MQC-CIS model rationalizes extremely rapid (< 200 fs) loss of polarized signal in transient hole burning (THB) experiments -- that cannot explained by the current MQC models. Thus, our study suggests that to explain several important experimentally observed properties of the hydrated electron, many-electron effects *must* be included. Nevertheless, the ensemble-averaged radial wavefunctions and energetics in our hybrid model are close to the *s*- and *p*-like states obtained in one-electron models. Thus, one-electron models can provide reasonable approximation to the multielectron picture of e^- for some applications, despite their flaws.

3. Future plans.

We have already began picosecond pulse radiolysis studies of liquid water using the T3 source and we will focus our entire effort on such studies next year, diversifying into several classes of molecular liquids and solids. Other priorities are the studies of photoionization in aqueous and nonaqueous liquids, electron encapsulation and structural characterization of excess electrons, and structural studies of CTTS systems and solvation using time-resolved x-ray absorption.

Recent journal publications (2005-2006 only).

- (1) C. G. Elles, A. E. Jailaubekov, R. A. Crowell, and S. E. Bradforth, *Excitation-energy dependence of the mechanism for two-photon ionization of liquid H₂O and D₂O from 8.3 to 12.4 eV*, J. Chem. Phys. **125** (2006) 044515
- (2) I. A. Shkrob, *Ammoniated electron as a solvent stabilized multimer radical anion*, J. Phys. Chem. A **110** (2006) 3967.
- (3) I. A. Shkrob and M. C. Sauer, Jr., *Towards electron encapsulation. Polynitrile approach*, J. Phys. Chem. A **110** (2006) 8126
- (4) R. Lian, D. A. Oulianov, R. A. Crowell, I. A. Shkrob, X. Chen, and S. E. Bradforth, *Electron Photodetachment from Aqueous Anions. III. Dynamics of Geminate Pairs Derived from Photoexcitation of Mono- and Poly- valent Anions*, J. Phys. Chem. A **110** (2006) 9071.
- (5) I. A. Shkrob and M. C. Sauer, Jr., *Electron Trapping by Polar Molecules in Alkane Liquids: Cluster Chemistry in Dilute Solution*, J. Phys. Chem. A **109** (2005) 5754.
- (6) I. A. Shkrob and M. C. Sauer, Jr., *Photo-Stimulated Electron Detrapping and the Two-State Model for Electron Transport in Nonpolar Liquids*; J. Chem. Phys. **122** (2005) 134503
- (7) R. Lian, R. A. Crowell, and I. A. Shkrob, *Solvation and thermalization of electrons generated by above the gap (12.4 eV) two-photon ionization of liquid H₂O and D₂O*, J. Phys. Chem. A. **109** (2005) 1510

Generation, Detection and Characterization of Gas-Phase Transition Metal
Containing Molecules

Timothy C. Steimle

Department of Chemistry and Biochemistry

Arizona State University

Tempe, Arizona 85287-1604

E-mail: tsteimle@asu.edu

I. Program Scope

The objective is to identify transient, transition metal containing, molecules and produce highly quantitative information that elucidates bonding mechanism and can be used to evaluate the predictability of electronic structure calculations. Experimental determination of permanent electric dipole moments, μ_E , magnetic dipole moments, μ_B , and magnetic hyperfine interactions are the focus because these properties are highly sensitive to the nature of the chemically relevant valence electrons. Dipole moments are particularly useful because they are the most fundamental electrostatic property and enter into the description of numerous phenomena. The number of unpaired valence electrons, which correlates with the reactivity of these molecules, is readily extracted from the magnetic dipole moment.

Two experimental approaches for determining μ_E , μ_B and hyperfine parameters are being pursued: high resolution (near the natural linewidth limit) visible electronic spectroscopy using laser induced fluorescence (LIF) detection, and mid-infrared high-resolution direct absorption in the O-H, C-H and N-H fundamental stretching spectral region (3.0 μ m-3.6 μ m). Small magnetic (Zeeman) and electric (Stark) field induced shifts in the very high resolution spectra are analyzed to produce experimental values for μ_B and μ_E , respectively. The transition metal containing radical molecules are produced in the reaction of laser ablated metals with a mixture of supersonic expanding gaseous reagents. The molecules are produced with an internal temperature of typically 10 K to minimize spectral congestion.

II. Recent Progress

A. Cobalt fluoride, CoF (Publ. #6)

Cobalt complexes of the general form (salen)CoX (salen= *N,N'*-bis(salicylidene)-1,2-diaminoalkane; X=halide) are highly active catalysts for copolymerization of propylene oxide and CO₂ and cyclohexene oxide and CO₂. Variation of the halide produces large changes in the catalytic activity. Prediction of the observed changes, which are electronic and not steric in nature, requires highly accurate theoretical methods which are currently impractical for complexes such as (salen)CoX. Simple cobalt mono-halides, CoX, are excellent prototypes for investigating the predictive power of such methods, since their molecular properties can be measured with good accuracy. There are no high-level electronic structure predictions for the nature of the ground and low-lying states of any cobalt monohalide. To date, the properties of CoF, the subject of the present investigation, have been interpreted assuming that there is an analogy with CoH. Both molecules have an inverted $^3\Phi$ ground state and a low-lying $^3\Delta$ state. Assuming it behaves like CoH, CoF in the $X^3\Phi_1$ state should have a two open-shell configuration:

$$\dots(3d\sigma)^2(3d\delta)^3(3d\pi)^3 \rightarrow {}^3\Phi, {}^3\Delta, {}^3\Pi \text{ and } {}^3\Sigma^- \quad (1)$$

Chemical intuition (i.e. the greater electronegativity of F compared to H), suggests that the bonding is dominated by ionic interactions for CoF but not for CoH. Simple electrostatic arguments, coupled with the ideas of stabilization due to F^- to Co^+ back donation, suggest that the Φ_i ground state of CoF should arise primarily from the four open-shell configuration:

$$\dots(3d\sigma)^1(3d\delta)^3(3d\pi)^3(4s/4p,\sigma)^1 \rightarrow {}^{3,5}\Phi, {}^{3,5}\Delta, {}^{3,5}\Pi \text{ and } {}^{3,5}\Sigma^- \quad (2)$$

In this project we: a) generated the first molecular beam of CoF, b) recorded the visible high resolution laser induced fluorescence spectrum, and c) analyzed the ^{59}Co ($I=7/2$) and ^{19}F ($I=1/2$) magnetic hyperfine interaction in the $[18.8]{}^3\Phi_I$ and $X{}^3\Phi_I$ states. It was clearly shown that the assumed analogy between CoH and CoF is incorrect and that the four open-shell configuration (Eq. 2), and not the two open-shell configuration (Eq. 1), is the dominant configuration.

B. Hyperfine interaction and dipole moment of RhO

Rhodium is an important component in both heterogeneous and homogeneous catalysis. The catalysis of CO and H_2 oxidation on solid rhodium (A.B. Mhadeshwar and D.G. Vlachos, *J. Catalysis*, **234** 46-63 (2005)) is an example of the former, and direct C-H bond activation using rhodium complexes (Yanagisawa et al *JACS* **128**, 11748 (2006)) is an example of the latter. The cost of rhodium has prohibited its large scale use. An understanding of the unusual catalytic activity of rhodium-clusters and rhodium containing molecules will guide efforts to a synthesis of less expensive alternatives. The nature of the catalytic activity can be garnered from electronic structure calculations. The methodologies used to calculate the properties of rhodium-clusters and rhodium containing molecules are best accessed by a comparison of the experimentally measured electric dipole moment, μ_E , with predicted values. In this study we determined μ_E for the $X^4\Sigma_{3/2}^-$ [15.8] ${}^2\Pi_{1/2}$ and [16.0] ${}^2\Pi_{1/2}$ states of RhO and the magnetic hyperfine parameters for $^{103}Rh(I=1/2)$ for these three states. This is the first determination of μ_E for any rhodium containing molecule (e.g. RhO). The field-free spectroscopy of RhO has been partially characterized by others (R.F. Heuff, et al *J. Mol. Spectrosc.*, **231**, 99(2005).

Table 1. DFT predictions^a and measured ^{103}Rh values of b_F and μ_E for RhO ($X^4\Sigma^-$)

Functional	Basis set	b_F (cm^{-1})	$ \mu $ (Debye)
B3LYP	LanL2DZ	-1.11×10^{-7}	4.107
	LanL2DZ	-1.31×10^{-7}	3.878
	3-21G	-0.0041	3.322
	DGDZVP	-0.0052	3.987
ROB3LYP	LanL2DZ	-1.83×10^{-7}	3.900
	3-21G	-0.0048	3.327
	DGDZVP	-0.0058	4.049
Experiment (This Work)		-0.00698(32)	3.81(2)

^aStevens et al *Chem. Phys. Lett.* 421, 281-286 (2006).

Prompted by our preliminary report at the CPIMS2005 meeting, Ian Carmichael (Radiation Laboratory Notre Dame) performed Density Functional Theory (DFT) predictions of b_F and μ_E for ground state RhX (X=C,N,F, P and Cl) (Stevens et al, Chem. Phys. Lett. 421, 281-286 (2006)) molecules. Our experimental results for RhO ($X^4\Sigma^-$) are compared with the DFT predictions in Table 1. The B3LYP functional with the DGDZVP basis gives the best simultaneous agreement for b_F and μ_E .

C. Relativistic effects: Uranium Monoxide, (UO) (submitted for publication)

This project was done in collaboration with Prof. M. Heaven at Emory University. All experimental work was performed at Arizona State University. Like the late transition metal-containing systems, the diatomic oxides and halides of the lanthanides have many low-lying electronic states due to the presence of open f and d orbitals on the metal. This situation poses a challenge for *ab initio* calculations which require high-level relativistic methods to obtain meaningful results. Simple ligand field theory (LFT) models may provide an alternative avenue for understanding the complex electronic structures of these molecules. As a means of testing the applicability of LFT to heavy metal containing systems, the permanent electric dipole moments, μ , and magnetic g -factors for uranium monoxide, UO, have been determined from analyses of optical Stark and Zeeman spectra recorded at a spectral resolution that approaches the natural linewidth limit. Numerous branch features in the previously characterized (0,0) [18.403]5-X(1)4 and (0,0) [18.404]5-X(1)4 electronic transitions were recorded in the presence of tunable static electric (Stark effect) or magnetic (Zeeman effect) fields. The lines exhibited unusually large Zeeman tuning effects. A ligand field model and an *ab initio* electronic structure calculation (R. Tyagi Ph.D. Thesis, The Ohio State University-Private (2005)) were used to interpret the ground state properties. The results indicate that the low energy electronic states of UO are sufficiently ionic for the meaningful application of ligand field theory models.

D. Search for new Rh-containing molecules

Our initial search for new rhodium containing molecules, has been fruitful. Examples of LIF spectra are given in Figure 1.

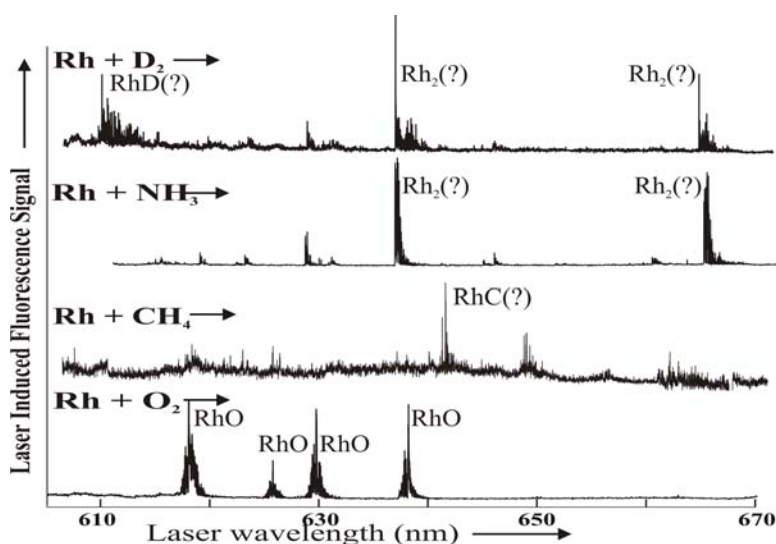


Figure 1. Survey spectral scans in the 605-670 nm range of the products of laser ablated rhodium with D_2 , NH_3 , CH_4 and O_2 . The electronic transitions are detected using LIF. Numerous new Rh-containing molecules are evident. High-resolution recordings of the observed systems are proposed.

E. Development of Difference Frequency (DF) laser system for mid-IR

This system incorporates two recent technological advances that greatly facilitate DFG: a) the traditional Ar⁺ laser is replaced by a powerful, compact, and low-noise, single frequency, cw, diode-pumped Nd:YAG laser, and b) the mixing media is a periodically polled lithium niobate (PPLN) crystal. The periodic-polling facilitates phase matching eliminating the need for accurate temperature control. The light source is now fully operational.

III. Future Plans

A. Optical Stark spectroscopy of Rhodium Containing Molecules

Identification of the carriers of the spectra in Figure 1 and those that appear in other regions of the visible spectrum will be the immediate objective. The identification will be based upon the analysis of the dispersed LIF spectra, which will give ground state vibrational information, and reactions with isotopic substituted reagents.

B. Improving the sensitivity of the Mid-IR spectrometer

Not too surprisingly, our initial attempts to detect simple absorption in the free-jet expansion have not been successful. The spectrometer is being modified to include a multi-pass cell and frequency modulation schemes to improve the sensitivity.

C. Unexpended funds

There will be no unexpended funds at the end of the funding period.

Publications of DOE sponsored research - 2003-present:

1. "The permanent electric dipole moments of ruthenium monocarbide, RuC" T.C. Steimle, W. Virgo and J. M. Brown, J. Chem. Phys. **118**, 2620-2625 (2003)
2. "The permanent electric dipole moments and magnetic hyperfine interactions of ruthenium mononitride, RuN. Timothy C. Steimle and Wilton Virgo, J. Chem. Phys. **119**, 12965 (2003).
3. "The permanent electric dipole moments of Ruthenium Monocarbide in the ³Π and ³Δ states" Wilton L. Virgo, Timothy C. Steimle, Laura E. Aucoin and J.M. Brown, Chem. Phys. Lett. **391**,75-80, (2004).
4. "The permanent electric dipole moments of WN and ReN and nuclear quadrupole interaction in ReN" Timothy C. Steimle and Wilton Virgo, J. Chem. Phys. **121** 12411 (2004).
5. "The permanent electric dipole moment and hyperfine interaction in Ruthenium Monofluoride, RuF." Timothy C. Steimle, Wilton L. Virgo and Tongmei Ma, J. Chem. Phys. **124**, 024309-7 (2006).
6. "High Resolution Laser Induced Fluorescence Spectroscopy of the [18.8] ³Φ_i – X ³Φ_i (0,0) Band of Cobalt Monofluoride" Timothy C. Steimle, Tongmei Ma, Allan G. Adam, William D. Hamilton and Anthony J. Merer, J. Chem. Phys. **125**, 6 064302-1-064302-9 (2006)

Computational Nanophotonics: Model Optical Interactions and Transport in Tailored Nanosystem Architectures

DOE Grant DE-FG02-03ER15486

PI: Mark Stockman

Department of Physics and Astronomy, Georgia State University, Atlanta, GA
30303

E-mail: mstockman@gsu.edu, URL: <http://www.phy-astr.gsu.edu/stockman>

Report for the Period of 08/2004 – 09/2006

Program Scope

The program is directed toward development of new computational approaches to photoprocesses in nanostructures whose geometry and composition are tailored to obtain desirable optical responses. The emphasis of this specific program is on the development of computational methods and prediction and computational theory of new phenomena of optical energy transfer and transformation on the extreme nanoscale (down to a few nanometers).

1 Recent Progress

1.1 SPASER: Effect, and Prospective Devices [1, 2]

We have earlier introduced a novel concept of SPASER (Surface Plasmon Amplification by Stimulated Emission of Radiation) [3]. Spaser is predicted to generate ultrashort (10-100 fs) ultraintense (optical electric field $\sim 10^8$ V/cm or greater) pulses of local optical fields at nanoscale. When realized experimentally spaser may completely change the nanooptics.

Recently, we have shown theoretically that the efficient nanolens, which is a self-similar aggregate of a few metal nanosphere, in an active medium of semiconductor quantum dots is an efficient spaser [2]. This spaser possesses a sharp hot spot of local fields in its nanofocus between the minimum-radius nanospheres.

To carry out this work, we have developed a computational code that uses central-multipole expansion and can find quasistatic plasmonic eigenmodes in an arbitrary aggregate of metal nanospheres. To describe the sharp nanofocus, we have to use up to 40 multipoles per nanosphere. Our method has been used also in the research on the hybridization of the plasmonic eigenmodes in clusters of nanospheres [4].

Another related recent development has been an experiment by a group of Dr. Eng of Technical University of Dresden (Germany) where the principles of spaser have been confirmed [5].

1.2 Nanofocusing of Optical Energy in Tapered Plasmonic Waveguides [6, 7]

We have predicted theoretically that surface plasmon polaritons propagating toward the tip of a tapered plasmonic waveguide are slowed down and asymptotically stopped when they tend to the tip. This phenomenon causes accumulation of energy and giant local fields at the tip. There are various prospective applications of this proposed effect in nanooptics and nanotechnology. Because there is transfer from micro- to nanoscale of not only energy, but also coherence (phase), these results allow for full coherent control on the nanoscale.

These computations have been performed on the basis if a semianalytical method based on WKB approximation. The effects that are missing in these computations are back-scattering of surface plasmon polaritons and the three-dimensional scattering due to the finite degree of the grading of the waveguide. These effects can only be taken into account based on numerical methods. There are two perspective such methods that we are considering: finite-difference time domain and the mode-overlap discretization. The

latter method approximates propagation through a graded waveguide by the propagation through a uniform segment with the mode-matching to the next segment. It is commonly used in microwave waveguide engineering; it is simple and efficient but neglects the three-dimensional scattering. However, for the case of a dielectric waveguide in the thick metal, there is no three-dimensional scattering, so the mode-overlap discretization method is especially well suited.

1.3 Coherent Control of Ultrafast Energy Localization on Nanoscale [8, 9]

Our research has significantly focused on the problem of controlling localization of the energy of ultrafast (femtosecond) optical excitation on the nanoscale. We have proposed and theoretically developed a general approach to solving this fundamental problem [8, 10-14]. It is difficult to overestimate possible applications of this effect, including nano-chip computing, nanomodification (nanolithography), and ultrafast nano-sensing.

Recently, we have shown [9] that using two-pulse (interferometric) coherent control in a complex random nanosystem it is possible to localize the ultrafast optical fields with spatial resolution of down to 2 nm. In specially designed V-shape nanoantennas, it is possible to move the “hot spot” of plasmonic excitation to a given nanometric hot spot along a 30 nm extension of this nanoantenna [9].

Following our pioneering work, there has recently been an explosion of activity on both theoretical [15-18] and experimental [19-22] investigations of the ultrafast coherent control on the nanoscale. This field will rapidly grow into one of the most important in the nanoscience with application to the nanoscale computations, sensing, spectroscopy, etc. It will require our increased attention to stay at the forefront. We are currently investigating a new computational method to define the limit of the coherent control on the nanoscale, which is based on the back-propagation (time-reversal) principles.

1.4 Efficient Nanolens [2, 23-25]

As an efficient nanolens, we have proposed a self-similar linear chain of several metal nanospheres with progressively decreasing sizes and separations [26]. The proposed system can be used for nano-optical detection, Raman characterization, nonlinear spectroscopy, nano-manipulation of single molecules or nanoparticles, and other applications. Recently, we have shown [2] that this nanolens surrounded by an active medium of nanocrystal quantum dots can be an efficient spaser. Another development has been a theory of the second-harmonic generation in an efficient nanolens (a linear self-similar aggregate of a few metal nanospheres) [24]. The second harmonic local fields form a very sharp nanofocus between the smallest spheres where these fields are enhanced by more than two orders of magnitude. This effect can be used for diagnostics and nanosensors. Recently we have computationally found the enhancement coefficient of the Surface Enhanced Raman Scattering (SERS) and have shown that it is considerably different from commonly used fourth power of the field enhancement [25].

1.5 Second Harmonic Generation on Nanostructured Surfaces [27]

This research resulted from an international collaboration with the group of Prof. Joseph Zyss (France). [27-29]. Based on the spectral-expansion Green's function theory, we theoretically describe the topography, polarization, and spatial-coherence properties of the second-harmonic (SH) local fields at rough metal surfaces. We have recently investigated this class of phenomena to predict and describe giant fluctuations of local SH fields in random nanostructures [27].

1.6 Strong Field Effects in Nanostructures: Forest Fire Mechanism of Dielectric Breakdown [30, 31]

This research is a result of an extensive international collaboration (UK, Germany, Canada, and the USA). We have described the interaction of ultrashort infrared laser pulses with clusters and dielectrics. Rapid ionization occurs on a sub-laser wavelength scale below the conventional breakdown threshold. It starts with the formation of nanodroplets of plasma that grow like forest fires, without any need for heating of the electrons promoted to the conduction band. This effect is very important for the physics of laser damage of semiconductors and dielectrics by a moderate-intensity radiation. This research has recently been extended to include some effects of the nanostructured plasmas generated in the process of the photoinduced damage (modification) of the solids [30, 31].

1.7 Nanoplasmonics at Metal Surface: Enhanced Relaxation and Superlensing [32, 33]

We have considered a nanoscale dipolar emitter (quantum dot, atom, fluorescent molecule, or rare earth ion) in a nanometer proximity to a flat metal surface. There is strong interaction of this emitter with unscreened metal electrons in the surface nanolayer that causes enhanced relaxation due to surface plasmon excitation and Landau damping. For the system considered, conventional theory based on metal as continuous dielectric fails both qualitatively and quantitatively.

In a recent development [33], we have considered a principal limitations on the spatial resolution on the nanoscale of the “Perfect Lens” introduced by Pendry, also known as the superlens. In the conventional, local electrodynamics, the superlens builds a 3d image in the near zone without principal limitations on the spatial resolution. We have shown that there is a principal limitation on this resolution, ~ 5 nm in practical terms, which originates from the spatial dispersion and Landau damping of dielectric responses of the interacting electron fluid in metals.

1.8 Theory of SERS [25, 34]

We have revisited theory of one of the most important phenomena in nanoplasmonics, Surface Enhanced Raman Scattering [25, 34]. This theory shows that the predicted levels of enhancement in the red spectral region are still several orders of magnitude less than the enhancement factors $\sim 10^{13} - 10^{14}$ observed experimentally. The difference may be due to the effects not taken into account by the theory: self-similar enhancement [26] or chemical enhancement [35].

1.9 Excitation of Surface Plasmon Polaritons (SPPs) by Free Electron Impact [36]

We have provided theoretical support and interpretation for the experimental investigation of the SPP generation by free-electron impact. This effect can be used as a basis of a novel method to visualize eigenmodes of plasmonic nanosystem by exciting them with an electron microscope beam.

2 Publications Resulting from the Grant

The major articles published by our group during this Report (2004-2006) period are indicated by bold typeface at the corresponding headings above.

References

1. D. J. Bergman and M. I. Stockman, *Can We Make a Nanoscopic Laser?*, Laser Phys **14**, 409-411 (2004).
2. K. Li, X. Li, M. I. Stockman, and D. J. Bergman, *Surface Plasmon Amplification by Stimulated Emission in Nanolenses*, Phys. Rev. B **71**, 115409-1-4 (2005).
3. D. J. Bergman and M. I. Stockman, *Surface Plasmon Amplification by Stimulated Emission of Radiation: Quantum Generation of Coherent Surface Plasmons in Nanosystems*, Phys. Rev. Lett. **90**, 027402-1-4 (2003).
4. P. Nordlander, C. Oubre, E. Prodan, K. Li, and M. I. Stockman, *Plasmon Hybridization in Nanoparticle Dimers*, Nano Lett. **4**, 899-903 (2004).
5. J. Seidel, S. Grafstroem, and L. Eng, *Stimulated Emission of Surface Plasmons at the Interface between a Silver Film and an Optically Pumped Dye Solution*, Phys. Rev. Lett. **94**, 177401-1-4 (2005).
6. M. I. Stockman, in *Plasmonics: Metallic Nanostructures and Their Optical Properties II*, edited by N. J. Halas and T. R. Huser, *Delivering Energy to Nanoscale: Rapid Adiabatic Transformation, Concentration, and Stopping of Radiation in Nano-Optics* (SPIE, Denver, Colorado, 2004), Vol. 5512, p. 38-49.
7. M. I. Stockman, *Nanofocusing of Optical Energy in Tapered Plasmonic Waveguides*, Phys. Rev. Lett. **93**, 137404-1-4 (2004).
8. M. I. Stockman, D. J. Bergman, and T. Kobayashi, *Coherent Control of Nanoscale Localization of Ultrafast Optical Excitation in Nanosystems*, Phys. Rev. B **69**, 054202-10 (2004).
9. M. I. Stockman and P. Hewageegana, *Nanocalibrated Nonlinear Electron Photoemission under Coherent Control*, Nano Lett. **5**, 2325-2329 (2005).
10. M. I. Stockman, S. V. Faleev, and D. J. Bergman, *Coherent Control of Femtosecond Energy Localization in Nanosystems*, Phys. Rev. Lett. **88**, 67402-1-4 (2002).
11. M. I. Stockman, S. V. Faleev, and D. J. Bergman, *Coherently Controlled Femtosecond Energy Localization on Nanoscale*, Appl. Phys. B **74**, S63-S67 (2002).
12. M. I. Stockman, S. V. Faleev, and D. J. Bergman, *Coherently-Controlled Femtosecond Energy Localization on Nanoscale*, Appl. Phys. B **74**, 63-67 (2002).

13. M. I. Stockman, D. J. Bergman, and T. Kobayashi, in Proceedings of SPIE: Plasmonics: Metallic Nanostructures and Their Optical Properties, edited by N. J. Halas, *Coherent Control of Ultrafast Nanoscale Localization of Optical Excitation Energy* (SPIE, San Diego, California, 2003), Vol. 5221, p. 182-196.
14. M. I. Stockman, S. V. Faleev, and D. J. Bergman, in Ultrafast Phenomena XIII, *Coherently-Controlled Femtosecond Energy Localization on Nanoscale* (Springer, Berlin, Heidelberg, New York, 2003).
15. M. Sukharev and T. Seideman, *Phase and Polarization Control as a Route to Plasmonic Nanodevices*, Nano Lett. **6**, 715-719 (2006).
16. M. Sukharev and T. Seideman, *Coherent Control Approaches to Light Guidance in the Nanoscale*, J. Chem. Phys. **124**, - (2006).
17. T. Brixner, F. J. G. d. Abajo, J. Schneider, C. Spindler, and W. Pfeiffer, *Ultrafast Adaptive Optical near-Field Control*, Phys. Rev. B **73**, 125437 (2006).
18. T. Brixner, F. J. G. d. Abajo, J. Schneider, and W. Pfeiffer, *Nanoscopic Ultrafast Space-Time-Resolved Spectroscopy*, Phys. Rev. Lett. **95**, 093901 (2005).
19. A. Kubo, K. Onda, H. Petek, Z. Sun, Y. S. Jung, and H. K. Kim, *Femtosecond Imaging of Surface Plasmon Dynamics in a Nanostructured Silver Film*, Nano Lett. **5**, 1123-1127 (2005).
20. A. Kubo, K. Onda, H. Petek, Z. Sun, Y. S. Jung, and H. K. Kim, in Ultrafast Phenomena XIV, edited by T. Kobayashi, T. Okada, T. Kobayashi, K. A. Nelson and S. D. Silvestri, *Imaging of Localized Silver Plasmon Dynamics with Sub-Fs Time and Nano-Meter Spatial Resolution* (Springer, Niigata, Japan, 2004), Vol. 79, p. 645-649.
21. P. v. d. Walle, L. Kuipers, and J. L. Herek, in Ultrafast Phenomena XV, *Coherent Control of Light in Metal Nanostructures* (Pacific Grove, California, 2006), p. Paper TuD3.
22. M. Bauer, D. Bayer, T. Brixner, F. J. G. d. Abajo, W. Pfeiffer, M. Rohmer, C. Spindler, and F. Steeb, in Ultrafast Phenomena XV, *Adaptive Control of Nanoscopic Photoelectron Emission* (Pacific Grove, California, 2006), p. Paper ThB3.
23. M. I. Stockman, K. Li, X. Li, and D. J. Bergman, in Plasmonics: Metallic Nanostructures and Their Optical Properties II, edited by N. J. Halas and T. R. Huser, *An Efficient Nanolens: Self-Similar Chain of Metal Nanospheres* (SPIE, 2004), Vol. 5512, p. 87-99.
24. K. Li, M. I. Stockman, and D. J. Bergman, *Enhanced Second Harmonic Generation in a Self-Similar Chain of Metal Nanospheres*, Phys. Rev. B **72**, 153401-1-4 (2005).
25. K. Li, M. I. Stockman, and D. J. Bergman, *Li, Stockman, and Bergman Reply to Comment on "Self-Similar Chain of Metal Nanospheres as an Efficient Nanolens"*, Phys. Rev. Lett. **97**, 079702 (2006).
26. K. Li, M. I. Stockman, and D. J. Bergman, *Self-Similar Chain of Metal Nanospheres as an Efficient Nanolens*, Phys. Rev. Lett. **91**, 227402-1-4 (2003).
27. M. I. Stockman, *Giant Fluctuations of Second Harmonic Generation on Nanostructured Surfaces*, Chem. Phys. **318**, 156-162 (2005).
28. M. I. Stockman, D. J. Bergman, C. Anceau, S. Brasselet, and J. Zyss, *Enhanced Second-Harmonic Generation by Metal Surfaces with Nanoscale Roughness: Nanoscale Dephasing, Depolarization, and Correlations*, Phys. Rev. Lett. **92**, 057402-1-4 (2004).
29. M. I. Stockman, D. J. Bergman, C. Anceau, S. Brasselet, and J. Zyss, in Complex Mediums V: Light and Complexity, edited by M. W. McCall and G. Dewar, *Enhanced Second Harmonic Generation by Nanorough Surfaces: Nanoscale Depolarization, Dephasing, Correlations, and Giant Fluctuations* (SPIE, 2004), Vol. 5508.
30. L. N. Gaier, M. Lein, M. I. Stockman, P. L. Knight, P. B. Corkum, M. Y. Ivanov, and G. L. Yudin, *Ultrafast Multiphoton Forest Fires and Fractals in Clusters and Dielectrics*, J. Phys. B: At. Mol. Opt. Phys. **37**, L57-L67 (2004).
31. L. N. Gaier, M. Lein, M. I. Stockman, G. L. Yudin, P. B. Corkum, M. Y. Ivanov, and P. L. Knight, *Hole-Assisted Energy Deposition in Dielectrics and Clusters in the Multiphoton Regime*, J Mod Optic **52**, 1019-1030 (2005).
32. I. A. Larkin, M. I. Stockman, M. Achermann, and V. I. Klimov, *Dipolar Emitters at Nanoscale Proximity of Metal Surfaces: Giant Enhancement of Relaxation in Microscopic Theory*, Phys. Rev. B **69**, 121403(R)-1-4 (2004).
33. I. A. Larkin and M. I. Stockman, *Imperfect Perfect Lens*, Nano Lett. **5**, 339-343 (2005).
34. M. I. Stockman, in Springer Series Topics in Applied Physics, edited by K. Kneipp, M. Moskovits and H. Kneipp, *Surface Enhanced Raman Scattering – Physics and Applications* (Springer-Verlag, Heidelberg New York Tokyo, 2006).
35. J. Jiang, K. Bosnick, M. Maillard, and L. Brus, *Single Molecule Raman Spectroscopy at the Junctions of Large Ag Nanocrystals*, J. Phys. Chem. B **107**, 9964-9972 (2003).
36. M. V. Bashevov, F. Jonsson, A. V. Krasavin, N. I. Zheludev, Y. Chen, and M. I. Stockman, *Generation of Traveling Surface Plasmon Waves by Free-Electron Impact*, Nano Lett. **6**, 1113-1115 (2006).

Understanding Nanoscale Confinement Effects in Solvent-Driven Chemical Reactions

Ward H. Thompson

Department of Chemistry, University of Kansas, Lawrence, KS 66045

Email: *wthompson@ku.edu*

Program Scope

It is now possible to synthesize nanostructured porous materials with a tremendous variety of properties including sol-gels, zeolites, organic and inorganic supramolecular assemblies, reverse micelles, vesicles, and even proteins. The interest in these materials derives from their potential for carrying out useful chemistry (*e.g.*, as microporous and mesoporous catalysts with critical specificity, fuel cell electrodes and membranes, molecular sieves, and chemical sensors) and for understanding the chemistry in similar systems found in nature. Despite the advances in synthetic techniques, our understanding of chemistry in solvents confined in nanoscale cavities and pores is still relatively limited. Ultimately, one would like to design nanostructured materials adapted for specific chemical purposes, *e.g.*, catalysis or sensing, by controlling the cavity/pore size, geometry, and surface chemistry. To develop guidelines for this design, we must first understand how the characteristics of the confining framework affect the chemistry. Thus, the overarching question addressed by our work is *How does a chemical reaction occur differently in a nano-confined solvent than in a bulk solvent?*

Solvent-driven reactions, typically those involving charge transfer, should be most affected by confinement of the solvent. The limited number of solvent molecules, geometric constraints of the nanoscale confinement, and solvent-wall interactions can have dramatic effects on both the reaction energetics and dynamics. A fundamental understanding of such solvent-driven reactions in nano-confined solvents will impact many areas of chemistry and biology. The diversity among nanoscale cavities and pores (*e.g.*, in their size, shape, flexibility, and interactions with the solvent and/or reactants) makes it difficult to translate studies of one system into predictions for another. Thus, we are focusing on developing a unified understanding of reaction dynamics in the diverse set of confinement frameworks, including nanoscale pores of varying surface chemistry.

Recent Progress

Proton Transfer. A model intramolecular phenol-amine proton transfer system in a CH₃Cl solvent confined in a smooth, hydrophobic spherical cavity has been investigated. Monte Carlo and mixed quantum-classical molecular dynamics (MD) simulations have been used to investigate reaction complex position distributions, free energy curves, and proton transfer reaction dynamics for a reaction system described by a two-state valence bond model.

The key result of our Monte Carlo simulations¹ in spherical, hydrophobic nanocavities was that the reaction coordinate must involve motion of the reaction complex from near the cavity wall to the interior (analogous to previous time-dependent fluorescence results²). This was confirmed by mixed quantum-classical MD simulations in which the proton is treated quantum mechanically while all the other coordinates are described classically. Specifically, we used vibrationally adiabatic simulations (based on nonequilibrium trajectories initiated as reactants) to obtain a first-order look at the rate constants and reaction mechanism.³ We determined the effects of cavity size and O-N hydrogen bond distance on the reaction free energy, forward rate constant, and mechanism (two stepwise and one concerted pathway were observed). The results could be explained based on the solvent polarity dependence on both cavity size and position in the cavity as well as barriers to diffusion due to solvent layering.

Model Silica Pores. One of the most critical characteristics of confining frameworks is the

surface chemical functionality. We have developed a method for generating atomistic models of roughly cylindrical pores in amorphous silica using a repulsive resist.⁵ The pores are generated by annealing and then cooling molten SiO₂ around a set of repulsive “beads” that define the pore (this approach can thus be applied to any shape pore or cavity). This generates physically reasonable, yet easily tunable, silica pore surfaces. Specifically, it allows us to generate pore surfaces that can be readily functionalized so that surface-specific chemistry can be investigated. That is, with the bare surface prepared, we designate sites where chemistry is likely to take place on the surface. First, we define the surface region, *e.g.*, based on a distance from the pore center. Second, these reactive sites are determined by a Si-O distance parameter. Between the surface penetration and Si-O distance cutoff, we have two freely adjustable parameters with which to control the surface composition. Hydrophilic (–O-H terminated) and hydrophobic (–O-CH₃, –O-CH₂-CH₃, or –O-C(CH₃)₃ terminated) pores can be generated with this approach.

Conformational Equilibria and the Two-State Model. A key picture that has emerged in fundamental studies of nanoconfined liquids is the two-state model, which assumes that confined molecules can be divided into two classes: those near the interface with the confining framework and those away from the interface, in the “interior.” Further, the properties of the liquid in the interior region are assumed to be identical or similar to that of the bulk liquid, while the properties of the interfacial liquid are strongly modified. This approach has been used to describe equilibrium and dynamical properties including conformational equilibria, reactivity, collective and individual reorientational dynamics, and solvation dynamics. However, the physical picture underlying the two-state model, where it can be truly powerful, is difficult to probe experimentally⁷ and has not been well-tested by simulation.

We have used the silica pore models described above to test the two-state model for conformational equilibria. Specifically, we have used MD simulations to investigate the *trans-gauche* equilibrium of ethylene glycol (EG) confined in roughly cylindrical (radius ~ 12 Å), hydroxyl-terminated silica pores.⁶ (The conformational equilibria in nanoconfined solvents⁸ has significant implications for the design of catalysts, and their potential for selectivity, based on such nanostructured materials.) These simulations were motivated by previous work of Luo and Jonas who measured the EG conformational equilibrium in sol-gel pores of different sizes (31.4 to 68.5 Å in diameter) and surface functionality (hydrophilic and hydrophobic).⁹ They found that F_t , the fraction of *trans* conformers, which is $\sim 0.36 \pm 0.10$ in bulk EG,¹⁰ increases as the pore size decreases in hydrophilic sol-gels. Interestingly, F_t does not change with pore size in hydrophobic-terminated pores. We have been able to understand the different trends in hydrophilic- and hydrophobic-terminated pores and have further probed the applicability of the two-state model in hydroxyl-terminated pores by examining the equilibrium in the “interior” and “surface” populations. Our results include: **1)** We simulated 11 different hydrophilic pores – the F_t for these are shown in Fig. 1 – and observed significant heterogeneity. We found that results from a single amorphous silica pore should be interpreted with great care and the conclusions accompanied by a *caveat*. **2)** Generally speaking, the two-state model is not supported by our results. In the vast majority of pores (9 of 11) the

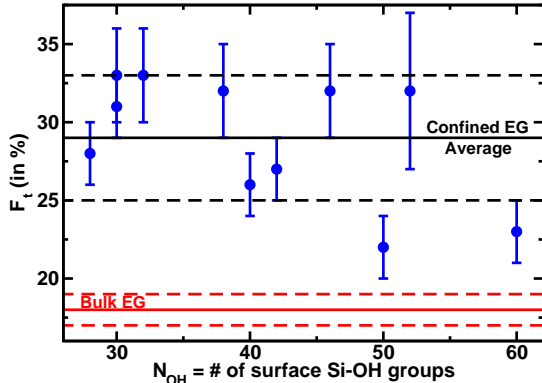


Figure 1: Fraction of *trans* conformer, F_t , versus N_{OH} for nanoconfined EG in 11 simulated pores (symbols). (Dashed lines indicate error bars.)

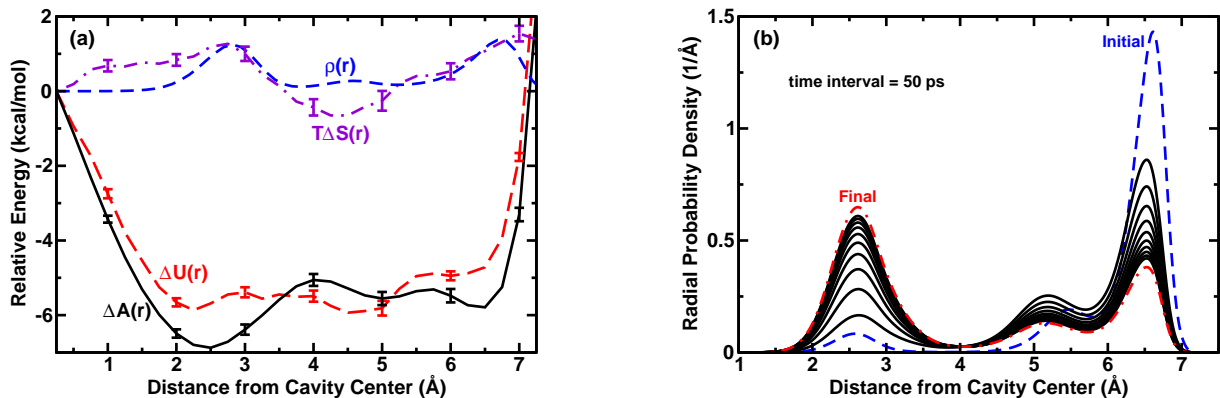


Figure 2: (a) The relative free energy ΔA , internal energy, ΔU , and entropic contribution $T\Delta S$ are plotted as a function of dye molecule position along with the solvent density, $\rho(r)$. (b) The time-dependent dye molecule position distribution from the Smoluchowski equation is shown.

F_t for surface and interior populations are the same within error bars and the F_t for the interior population is distinctly different than that for the bulk EG (see Fig. 1).

Time-Dependent Fluorescence. We have previously used simulations of time-dependent fluorescence to provide insight into the equilibrium and dynamical behavior of charge transfer systems in nanoconfined solvents. We are extending this work to elucidate 1) entropic effects, 2) the applicability of Fokker-Planck-type descriptions, and 3) the validity of linear response theory. Specifically, we are calculating entropic and internal energy contributions to the free energy of a model dye molecule dissolved in nanoconfined solvents (CH_3I , CH_3CN , CH_3OH , and H_2O). Results for an excited state molecule in CH_3I solvent ($\rho = 2.052 \text{ g/cm}^3$) confined in a 10 \AA spherical, hydrophobic cavity are shown as a function of position in Fig. 2(a). From this data it can be seen that the global minimum in the free energy is different than that for the internal energy, indicating that entropic effects play an important role. The radial solvent density is also plotted in Fig. 2(a) for comparison; it appears that (not unexpectedly) there is a correlation between the solvent density, $\rho(r)$, and $T\Delta S(r)$ and we are further investigating this.

Equilibrium and nonequilibrium MD simulations can be powerful tools for investigating chemistry in nanoconfined solvents. Yet they can also be demanding, particularly when solute behavior is of interest (*e.g.*, a chemical reaction complex or dye molecule). To address this issue and provide further insight into the behavior of nanoconfined solvents, we are investigating the applicability of Fokker-Planck-type descriptions of solute dynamics. Specifically, we are modeling the time-dependent fluorescence using a Smoluchowski equation. The results of a preliminary Smoluchowski simulation are shown in Fig. 2(b); the results show the change in the dye molecule distribution of positions with time after excitation (based on the calculated free energies in CH_3I , $\rho = 2.052 \text{ g/cm}^3$, $R_{\text{cav}} = 10 \text{ \AA}$; see Fig. 2(a)). These will be validated against nonequilibrium MD simulations and should assist in the development of reaction rate theories.

Linear response theory is widely applied to describe dynamics in liquids and has been quite successful. However, there are questions about its applicability near interfaces and in nanoconfined solvents. We have tested linear response theory in the latter case by comparing it to nonequilibrium MD simulations for the time-dependent fluorescence of a model dye molecule in a spherical, hydrophobic nanocavity. We have found that linear response theory can have shortcomings in these systems and should be applied with caution.

Future Plans

We are currently working on four extensions of our work on proton transfer reactions in nanoconfined solvents. 1) We are carrying out nonadiabatic mixed quantum-classical dynamics to examine the role of tunneling. 2) We are simulating the vibrational spectrum of the reaction complex in a nanoconfined solvent, which is a potentially important experimental probe. 3) We are developing, based on *ab initio* calculations, new valence bond models for intra- and intermolecular proton transfer systems that are experimentally accessible. 4) We are examining the proton transfer reaction in silica pores with varying surface chemistry.

We also plan other extensions related to both proton transfer and more general phenomena in nanoconfined solvents. We will investigate Fokker-Planck-type descriptions of charge transfer reactions in nanoconfined solvents which could provide significant insight into the effect of confining framework properties on reaction equilibria and dynamics. Further, we will determine entropic contributions to the free energy surfaces of proton transfer reactions and examine the surface chemistry dependence using the silica pore models we have developed.

References

- [1] †S. Li and W.H. Thompson, *J. Phys. Chem. B* **109**, 4941-4946 (2005). "Proton Transfer in Nano-confined Polar Solvents. I. Free Energies and Solute Position "
- [2] †W.H. Thompson, *J. Chem. Phys.* **120**, 8125-8133 (2004). "Simulations of Time-Dependent Fluorescence in Nano-Confined Solvents"
- [3] †W.H. Thompson, *J. Phys. Chem. B* **109**, 18201-18208 (2005). "Proton Transfer in Nano-confined Polar Solvents. II. Adiabatic Proton Transfer Dynamics"
- [4] †S. Li and W.H. Thompson, *Chem. Phys. Lett.* **405**, 304-309 (2005). "How Accurate is Time-Independent Perturbation Theory for Calculating Frequency Shifts of Diatomic Molecules in Rare Gas Fluids?"
- [5] †T.S. Gulmen and W.H. Thompson, "Model Silica Pores with Controllable Surface Chemistry for Molecular Dynamics Simulations" in *Dynamics in Small Confining Systems VIII*, edited by J.T. Fourkas, P. Levitz, R. Overney, M. Urbakh (Mater. Res. Soc. Symp. Proc. **899E**, Warrendale, PA, 2005), 0899-N06-05.
- [6] †T.S. Gulmen and W.H. Thompson, *Langmuir* (submitted). "A Test of the Two-State Model of Nanoconfined Solvents: The Conformational Equilibrium of Ethylene Glycol in Silica Pores."
- [7] I.R. Piletic, D.E. Moilanen, D.B. Spry, N.E. Levinger, and M.D. Fayer, *J. Phys. Chem. A* **110**, 4985-4999 (2006).
- [8] †J.A. Gomez, A.K. Tucker, T.D. Shepherd, and W.H. Thompson, *J. Phys. Chem. B* **109**, 17479-17487 (2005). "Conformational Free Energies of 1,2-Dichloroethane in Nanoconfined Methanol"
- [9] R.-S. Luo and J. Jonas, *J. Raman. Spectrosc.* **32**, 975-978 (2001).
- [10] M. Schwartz, *Spectrochim. Acta* **33A**, 1025-1032 (1977).
- [11] †J.A. Gomez and W.H. Thompson, *J. Phys. Chem. B* **108**, 20144 - 20154 (2004). "Monte Carlo Simulations of Absorption and Fluorescence Spectra in Ellipsoidal Nanocavities"
- [12] †S. Li, T.D. Shepherd, and W.H. Thompson, *J. Phys. Chem. A* **108**, 7347-7355 (2004). "Simulations of the Vibrational Relaxation of a Model Diatomic Molecule in a Nano-confined Polar Solvent"

†DOE-sponsored publication.

Structural Dynamics in Complex Liquids Studied with Multidimensional Vibrational Spectroscopy

Andrei Tokmakoff

Department of Chemistry, Massachusetts Institute of Technology, Cambridge, MA 02139

E-mail: tokmakof@MIT.edu

Our work on complex liquids has focused on characterizing the structural fluctuations and rearrangements of water's hydrogen bonding network in order to understand how these dynamics influence aqueous reactivity. Water's complexity is due to its ability to form four hydrogen bonds with its neighbors, resulting in a local tetrahedral environment that is remarkably structured for the liquid phase. The time averaged structure of water's hydrogen bonding network can readily explain many of water's anomalies, such as the lower density of ice as compared to liquid water and water's high boiling point as compared to similarly sized liquids. However, aqueous reactivity is most influenced by the fluctuations and distortions about water's time averaged structure. Water's ability to rapidly solvate nascent charge results from extremely fast intermolecular fluctuations which are the motions responsible for restructuring the liquid upon a change in electrostatic charge. Likewise, many theories of the anomalous diffusion of excess protons in liquid water have implicated the breaking and making of hydrogen bonds as a necessary step in the mechanism of transfer.

We use ultrafast infrared spectroscopy of the OH stretch of HOD in D₂O to resolve the structural rearrangements of water's hydrogen bonding network. Infrared spectroscopy of the OH stretch is an ideal technique because of its structural sensitivity. The OH stretch lineshape is significantly broadened due to its interaction with its hydrogen bonded neighbors. Strong hydrogen bonds result in a weakening of the OH force constant and therefore a red shift in frequency while weak or broken configurations appear blue shifted as compared to band center. Conceptually our experiments aim to correlate the OH stretch frequency with the hydrogen bonded environment and then watch the time dependence of this frequency in order to report on the exchange of hydrogen bonding structures.

Previously we have shown how vibrational echo peak shift spectroscopy and polarization-selective pump-probe measurements could be used to observe the intermolecular dynamics of the hydrogen bonded pair. These measurements found that local intermolecular fluctuations on a sub 200 fs timescale, in particular the underdamped motion of the hydrogen bond and the hindered rotations or librations of individual OH dipoles, preceded the many molecule, collective reorganization of the liquid that occurred on a 1 ps timescale. Such measurements, while providing the average time in between hydrogen bond switching events (i.e. ~1 ps), provided no information on the mechanism of switching because these measurements integrated over all hydrogen bonding environments.

Our recent work has focused on using two-dimensional infrared (2D IR) spectroscopy to fully characterize the vibrational dynamics of the OH stretch of HOD in D₂O. Time-dependent evolution of the 2D IR lineshape serves as a spectroscopic observable that tracks how different hydrogen bonding environments interconvert while changes in spectral intensity result from vibrational relaxation and molecular reorientation of the OH dipole. High fidelity acquisition of 2D lineshapes is essential in order to harvest information on hydrogen bond dynamics. Over the past year we have developed new methods to ensure high quality lineshapes. Essential to non-distorted Fourier transforms is accurate knowledge of the time delays between excitation pulses. We have demonstrated a HeNe-based calibration procedure to obtain $\lambda/60$ accuracy of time delays and implemented balanced spectral interferometry to increase the signal to noise ratio by a factor of four.

For waiting times up to the vibrational lifetime of 700 fs, changes in the 2D lineshape reflect the spectral evolution of OH oscillators induced by hydrogen bond dynamics. We have developed a number of metrics that exploit the sensitivity of rephasing pathways to frequency correlation to quantify the time dependence of these lineshapes. Simple approximations to the nonlinear response functions show that these measures can be formally related to the frequency correlation function. The frequency dynamics, characterized through the 2D lineshape analysis metrics, show a rapid 60 fs decay, an underdamped oscillation on a 130 fs timescale induced by hydrogen bond stretching, and a long time decay constant of 1.4 ps. 2D surfaces for waiting times larger than 700 fs are dominated by the effects of vibrational relaxation and the thermalization of this excess energy by the solvent bath.

Asymmetries in the 2D lineshapes and frequency dependence of the 2D lineshape metrics arise from qualitatively different spectral relaxation of molecules on the red and blue sides of the lineshape. MD simulations and empirical observations show that it is most reasonable to attribute these regions of the spectra to hydrogen bonded (HB) and non-hydrogen bonded (NHB) oscillators, respectively. The 2D lineshape metrics that we have developed allow us to track the exchange of HB and NHB oscillators. We find that NHB oscillators rapidly return to HB frequencies on the timescale of librational motions in water. HB oscillators are observed undergoing underdamped oscillations about the hydrogen bond preceding activated barrier crossing that accompanies the switching of hydrogen bonding partners. Our experimental results indicate that hydrogen bond switching is a concerted process in which the NHB state appears only fleetingly as a transition state along the hydrogen bond switching coordinate or as a large distortion about a hydrogen bond.

The fact that hydrogen bond switching is a concerted motion implies that an appropriate reaction coordinate for describing the exchange of hydrogen bonding partners must involve the collective motion of no less than three water molecules. We are currently using MD simulations of the switching even to test a number of multibody coordinates that would effectively characterize the free energy surface, barrier, and transition state configuration for hydrogen bond switching. We have shown that the switching free energy surface probed by our experiments is well described by a bifurcation coordinate that

describes distance and/or angular changes in configuration between the hydrogen bond donor and the initial and final acceptor molecules.

In a new direction, we are currently performing experiments aimed to examine proton transport in liquid water. Upon the addition of strong deuterated acid to a dilute solution of HOD in D₂O, the OH absorption intensity decreases in intensity and broadens to lower frequency. This red shifted absorption is attributed to the formation of Eigen cations, a central H₃O⁺ ion hydrogen bonded to three neighboring water molecules. Likewise, a strong continuous absorption that appears from low frequency up to the OH absorption band has been assigned to the formation of Zundel species, a proton symmetrically shared between two water molecules. Experiments that probe the dynamics of these bands and the exchange between them will provide insight into the fluctuations that drive proton transport in liquid water. Similar experiments on concentrated alkaline solutions are also underway which examine charge defect transport in water.

In the arena of technological developments, we have recently demonstrated the ability to acquire optical and infrared two-dimensional spectra in a single laser interaction. Single shot 2D spectroscopy will be important for the study of non-equilibrium processes and irreversible chemical reactions. The method is a double resonance pump-probe experiment in which a frequency dispersed pump beam is overlapped with a broadband cylindrically focused probe beam. Following the sample the probe is frequency dispersed in the direction perpendicular to the pump dispersion axis. The probe is imaged onto a CCD detector and differential transmission changes are measured. The image encodes the observed spectral changes as a function of pump and probe frequency. Detection of mid-IR 2D spectra is made possible by upconverting the mid-IR probe image into the visible with sum frequency generation.

DOE Supported Publications (2003-2006)

1. "Coherent 2D IR Spectroscopy: Molecular structure and dynamics in solution," M. Khalil, N. Demirdöven and A. Tokmakoff, *J. Phys. Chem. A*, **107** (2003) 5258.
2. "Ultrafast hydrogen bond dynamics in the infrared spectroscopy of water," C. J. Fecko, J. D. Eaves, J. J. Loparo, A. Tokmakoff and P. G. Geissler, *Science*, **301** (2003) 1698.
3. "Dynamics of hydrogen bonds in water: Vibrational echoes and two-dimensional infrared spectroscopy," C. J. Fecko, J. D. Eaves, J. J. Loparo, S. T. Roberts, A. Tokmakoff and P. L. Geissler, in *Ultrafast Phenomena XIV*, ed. by T. Kobayashi, T. Okada, T. Kobayashi, K. A. Nelson, S. DeSilvestri (Springer-Verlag, Berlin).
4. "A unified analysis of ultrafast vibrational and orientational dynamics of HOD in D₂O," J. J. Loparo, C. J. Fecko, J. D. Eaves, S. T. Roberts and A. Tokmakoff, in *Ultrafast Phenomena XIV*, ed. by T. Kobayashi, T. Okada, T. Kobayashi, K. A. Nelson, S. DeSilvestri (Springer-Verlag, Berlin).
5. "Solvation dynamics of N-methylacetamide in D₂O, CDCl₃ and DMSO-d₆," M. F. DeCamp, L. P. DeFlores, J. M. McCracken, and A. Tokmakoff, in *Ultrafast*

- Phenomena XIV*, ed. by T. Kobayashi, T. Okada, T. Kobayashi, K. A. Nelson, S. DeSilvestri (Springer-Verlag, Berlin, 2005).
6. "Reorientational and configurational fluctuations in water observed on molecular length scales," J. J. Loparo, C. J. Fecko, J. D. Eaves, S. T. Roberts and A. Tokmakoff, *Physical Review B*, **70** (2004) 180201.
 7. "Generation of 45 femtosecond pulses at 3 μm with a KNbO_3 optical parametric amplifier," C. J. Fecko, J. J. Loparo and A. Tokmakoff, *Opt. Commun.*, **241** (2004) 521.
 8. "Local hydrogen bonding dynamics and collective reorganization in water: Ultrafast IR spectroscopy of HOD/D₂O," Christopher J. Fecko, Joseph J. Loparo, Sean T. Roberts and Andrei Tokmakoff, *Journal of Chemical Physics*, **122** (2005) 054506.
 9. "Amide I vibrational dynamics of N-methylacetamide in polar solvents: The role of electrostatic interactions," Matthew F. DeCamp, Lauren DeFlores, Justine M. McCracken, Andrei Tokmakoff, Kijeong Kwac, and Minhaeng Cho, *Journal of Physical Chemistry B*, **109** (2005) 11016.
 10. "Upconversion multichannel infrared spectrometer," Matthew F. DeCamp and Andrei Tokmakoff, *Optics Letters*, **30** (2005) 1818.
 11. "Electric field fluctuations drive vibrational dephasing in water," Joel D. Eaves, Andrei Tokmakoff, and Phillip L. Geissler, *J. Phys. Chem. B*, **109** (2005) 9424.
 12. "Polarizable molecules in the vibrational spectroscopy of water," E. Harder, J.D. Eaves, A. Tokmakoff and B.J. Berne, *Proc. Nat'l. Acad. Sci., USA*, **102** (2005) 11611.
 13. "Hydrogen bonds in liquid water are broken only fleetingly," J. D. Eaves, J. J. Loparo, C. J. Fecko, S. T. Roberts, A. Tokmakoff and P. L. Geissler, *Proc. Nat'l. Acad. Sci., USA*, **102** (2005) 13019.
 14. "A study of phonon-assisted exciton relaxation dynamics for a (6,5) enriched DNA-wrapped single walled carbon nanotubes sample," S. G. Chou, M. F. DeCamp, J. Jiang, Ge. G. Samsonidze, E. B. Barros, F. Plentz, A. Jorio, M. Zheng, G. B. Onoa, E. D. Semke, A. Tokmakoff, R. Saito, G. Dresselhaus, M. S. Dresselhaus, *Physical Review B*, **72** (2005) 195415.
 15. "Single-shot two-dimensional spectrometer," Matthew F. DeCamp and Andrei Tokmakoff, *Optics Letters*, **31** (2006) 113.
 16. "Spectral signatures of heterogeneous protein ensembles revealed by MD simulations of 2DIR spectra," Ziad Ganim and Andrei Tokmakoff, *Biophysical Journal*, in press.
 17. "Characterization of spectral diffusion from two-dimensional line shapes," S.T. Roberts, J.J. Loparo, and A. Tokmakoff, *J. Chem. Phys.*, **125** (2006) 084502.

The Role of Electronic Excitations on Chemical Reaction Dynamics at Metal, Semiconductor and Nanoparticle Surfaces

John C. Tully

Department of Chemistry, Yale University, P. O. Box 208107,

New Haven, CT, 06520-8107 USA

john.tully@yale.edu

Program Scope

Achieving enhanced control of the rates and molecular pathways of chemical reactions at the surfaces of metals, semiconductors and nanoparticles will have impact in many fields of science and engineering, including heterogeneous catalysis, photocatalysis, materials processing, corrosion, solar energy conversion and nanoscience. However, our current atomic-level understanding of chemical reactions at surfaces is incomplete and flawed. Conventional theories of chemical dynamics are based on the Born-Oppenheimer separation of electronic and nuclear motion. Even when describing dynamics at metal surfaces where it has long been recognized that the Born-Oppenheimer approximation is not valid, the conventional approach is still used, perhaps patched up by introducing friction to account for electron-hole pair excitations or curve crossings to account for electron transfer. There is growing experimental evidence that this is not adequate. We are examining the influence of electronic transitions on chemical reaction dynamics at metal and semiconductor surfaces. Our program includes the development of new theoretical and computational methods for nonadiabatic dynamics at surfaces, as well as the application of these methods to specific chemical systems of experimental attention. Our objective is not only to advance our ability to simulate experiments quantitatively, but also to construct the theoretical framework for understanding the underlying factors that govern molecular motion at surfaces and to aid in the conception of new experiments that most directly probe the critical issues.

Recent Progress

We have made progress on several fronts. The first of these is an improved ab initio calculation of the potential energy surfaces and nonadiabatic couplings that govern the interaction of the NO molecule with the Au(111) surface. Our prior effort using finite gold clusters revealed interesting features about the extent of charge flow onto the NO molecule as a function of atomic positions. However, it produced a binding energy far too high to be of quantitative use. We have now carried out extensive calculations of the ground state energy and molecular charge as a function of atomic positions, using the plane wave density functional code VASP. The resulting binding energy of about 20 kJ/mole produces NO trapping probabilities in reasonable accord with experiment, in contrast to results using the previously calculated binding energy of 57 kJ/mole. The partial charge on the NO molecule as computed by VASP also appears more reliable than the cluster results, at least at large molecule-surface separations where we can estimate the correct behavior.

We have also made progress in constructing a “diabatic” 2x2 Hamiltonian matrix from the ab initio results, required in order for us to examine dynamics beyond the adiabatic (ground state) approximation. The diagonal elements of the 2x2 matrix are the diabatic neutral and ionic potential energy surfaces. These are coupled by an off-diagonal potential surface such that the ground state becomes a mixture of ionic and neutral configurations; i.e., the lower energy root of the 2x2 Hamiltonian matrix. In order to uniquely define the 2x2 symmetric matrix, we need three independent pieces of information at each nuclear configuration. Previously we computed only two, the ground state energy and the Lowdin or Bader charge on the NO molecule, which we assign to be the square of the coefficient of the ionic configuration in the ground state. We supplied the missing piece of information by prescribing a form for the off-diagonal coupling, a simple exponential function of the distance of the molecule from the surface. This latter feature introduced worrisome uncertainty. We have now formulated and executed a more rigorous method for extracting the diabatic neutral and negative ion energies by computing the shift in the ab initio ground state energy upon application of a small electric field. This provides us with an ab initio determination of the missing third piece of information. Once we satisfactorily fit the diabatic Hamiltonian elements to manageable analytical forms, we will begin to explore the role of transient negative ion formation on inelastic scattering of NO from gold, with direct reference to the ongoing experiments of Wodtke and coworkers.

A third accomplishment over the last year is the development and testing of a new theory of dynamics at metal surfaces, submitted to *Physical Review*. At metal surfaces nonadiabatic behavior is the rule rather than the exception. Electron-hole pair transitions, charge transfer and hot-electron-induced motion can be dominant pathways for energy flow. Recent experiments have demonstrated that molecular vibrational energy and reaction exothermicity can produce highly excited electrons, even resulting in electron emission. Current theories of dynamics with electronic transitions – Ehrenfest, surface-hopping and electronic friction – all have limitations and inaccuracies. The latter has been very valuable in incorporating transfer of energy to conduction electrons in molecular dynamics simulations. Ab initio calculation of the friction tensors has proved feasible and apparently accurate in many situations. However, the electronic friction formalism is based on a weak coupling approximation, a consequence of which is that large amounts of energy can be dissipated only through multiple low-energy electron excitations. Recent experiments by the Wodtke and Somorjai groups demonstrate dramatically that individual electrons in the metal can receive as much as 2 eV or more of excitation. This cannot be described by an electronic friction. Our new approach does not assume weak coupling, and can be applied even to cases where a sudden electron jump between adsorbate and surface may occur. (Electronic friction relies on gradual changes in the electron distribution.) We invoke a Markov (no memory) approximation that allows trajectories to branch, as with surface hopping, but is much more practical to apply to this application. The Markov approximation, in this implementation, is accurate in the wide band limit; i.e., in cases where the lifetime-induced width of the adsorbate negative ion state is narrow compared to the width of the metallic conduction band. This is usually, although not always, true for chemical reactions at metal surfaces. When the wide band limit is valid, our approach takes advantage of the presence of the continuum to greatly simplify the electronic equations of motion. In addition, our method correctly

calculates distributions of observables, rather than simply the averages yielded by Ehrenfest dynamics. Initial tests against accurate fully quantum mechanical one-dimensional benchmarks are very promising. The method should have direct applicability to electron transfer at metal and semiconductor surfaces, and we plan to extend it to apply to chemical reactions at surfaces.

A final accomplishment is a qualitative analysis of the mechanism of electron ejection upon scattering of highly vibrationally excited NO from a cesiated gold surface, as observed by Wodtke and coworkers. Starting with the Markov, wide-band formalism described above, we have made a number of further simplifications to allow us to obtain a simple estimate of the vibrational relaxation pathways and branching ratios of final states, as well as the distribution of excited conduction electron energies. We find that the Franck-Condon overlaps between vibrational states on the neutral and anionic NO diabats play a crucial role in determining vibrational relaxation. In addition, our mechanism explicitly includes the direct creation of energetic electron-hole pairs in the metal. Using interaction parameters estimated from experiment, we calculate vibrational energy distributions and electron emission probabilities that are in quite reasonable accord with the measurements of the Wodtke group. This analysis was crude, but the agreement with experiment is a very encouraging sign that our theoretical strategy is on the right track. This work has been accepted for publication in the *Journal of Chemical Physics* (see reference below).

Future Plans

The goals of our research program include both specific aspects of the NO-Au system and more general investigations of nonadiabatic behavior at surfaces. With regard to the former, we plan to address NO-Au in the following stages:

1. Complete the plane wave DFT calculations (using the VASP code) of the NO-gold interaction, with and without an applied electric field.
2. Re-parameterize the 2x2 matrix representation to fit the improved *ab initio* data using the electric field data to provide off-diagonal couplings.
3. Carry out adiabatic molecular dynamics simulations to assess the importance of nonadiabatic transitions.
4. Carry out surface hopping dynamics on the 2x2 diabatic Hamiltonian.
5. Carry out Markov diabatic dynamics simulations as described above to introduce electronic excitations explicitly.
6. Through analysis of the results of application of this hierarchy of theoretical methods, draw conclusions about the importance and nature of nonadiabatic electronic transitions both in the NO-Au system and more generally.

While the NO-Au system is a valuable starting point, our goal is to develop the theoretical tools required to describe the dynamics of a wide variety of nonadiabatic molecule-surface processes. We propose to further develop the nonadiabatic dynamics approach described above. We will also work toward developing improved *ab initio* methods for computing the energies and widths of lifetime-broadened electronic states, through extension of “constrained density functional theory”. These are the properties that determine the rate and extent of electron transfer as a molecule approaches the surface.

We will carry out *ab initio* calculations of energies, charge distributions and level widths as input to constructing valence-bond type Hamiltonians for a number of chemical systems beyond NO-Au. One system of immediate interest is the CO oxidation reaction on platinum. Somorjai and coworkers have recently carried out a series of experiments demonstrating that this exothermic chemical reaction can produce excited electrons with energies corresponding to a significant fraction of the energy released in the reaction. They examined the CO oxidation reaction on a thin film of platinum grown on a semiconductor substrate, and observed a sizeable chemicurrent in the semiconductor. Since the Schottky barrier between the metal and the substrate exceeds 1 eV in this case, electrons must be excited with at least this amount of energy. We have begun conversations with Somorjai to pursue this intriguing direction. Another class of systems to be pursued is the interaction of oxygen atoms and oxygen molecules with metal and semiconductor surfaces. Both the oxygen atom and molecule are ground state triplets with low-lying singlets, and both accept an electron when approaching a metal surface, so there may be several mechanisms of nonadiabaticity in play. For example, in gas phase reactions of the oxygen molecule, the ground $O_2(^3\Sigma_g^-)$ state is generally much less reactive than the excited $O_2(^1\Delta_g)$ of the oxygen molecule. As the reactants approach, the potential energy surfaces that correlate asymptotically with $O_2(^3\Sigma_g^-)$ and $O_2(^1\Delta_g)$ usually cross each other. However, because they correspond to different total spin and because spin-orbit coupling is weak, there is a negligible probability of a transition; the dynamics can be assumed to evolve on a single potential energy surface. At a metal surface, however, as the O_2 molecule reaches the crossing point, a near-resonant 2-electron exchange can convert the molecule from the triplet to the singlet; spin-orbit or magnetic interactions are not required. This is related to the “Kondo effect” that is of current interest in the condensed matter theory community. This argument suggests that the triplet ground state of oxygen may have nearly the same reactivity as the excited singlet state at metal surfaces. However, for the one case studied experimentally, dissociation of O_2 on Al(111), this does not appear to be the case; $O_2(^3\Sigma_g^-)$ has a small reaction probability in spite of a low reaction barrier on the ground state surface. Addressing this type of process properly by theory is an important challenge; it is likely that these considerations will require us to re-evaluate many chemical reaction pathways involving radical reactants or intermediates on metal surfaces. In addition, similar behavior can be expected for above band gap excited state dynamics at semiconductor surfaces. Finally, chemistry at the surfaces of metallic or semiconductor nanoparticles may display new features resulting from the discretization of the valence and conduction bands due to finite size.

References

1. “Vibrational Relaxation of NO on Au(111) via Electron-Hole Pair Generation”, Neil Shenvi, Sharani Roy, Priya Parandekar, and John C. Tully, *J. Chem. Phys.*, in press.

Chemical Kinetics and Dynamics at Interfaces

*Gas Phase Investigation of Condensed Phase Phenomena*¹

Lai-Sheng Wang (PI)

Department of Physics, Washington State University, 2710 University Drive, Richland, WA, 99354 and the Chemical Sciences Division, Pacific Northwest National Laboratory, P.O. Box 999, MS K8-88, Richland, WA 99352. E-mail: ls.wang@pnl.gov

Program Scope

This program is aimed at obtaining a microscopic understanding of environmental materials and solution chemistry in the gas phase using a variety of cluster models. Our primary experimental technique is photoelectron spectroscopy (PES) coupled with electrospray ionization (ESI), which is used to produce solvated clusters from solution samples. Experiment and ab initio calculations are combined to:

- obtain a molecular-level understanding of the solvation of complex anions (both singly and multiply charged) important in condensed phases
- understand the molecular processes and initial steps of dissolution of salt molecules by polar solvents
- probe the structure and dynamics of solutions and air/solution interfaces

Complexes anions, in particular multiply charged anions, are ubiquitous in nature, often found in solutions and solids. However, few complex anions have been studied in the gas phase due to the difficulty in generating them and their intrinsic instability as a result of strong intramolecular Coulomb repulsion in the case of multiply charged anions. Microscopic information on the solvation and stabilization of these anions is important for the understanding of solution chemistry and properties of inorganic materials or atmospheric aerosols involving these species. Gas phase studies with controlled solvent numbers and molecular specificity are ideal to provide such microscopic information. We have developed a new experimental technique to investigate multiply charged anions and solvated species directly from solution samples and probe their electronic structures, intramolecular Coulomb repulsion, stability, and energetics using electrospray and PES. A central theme of this research program lies at obtaining a fundamental understanding of environmental materials and solution chemistry. These are important to waste storage, subsurface and atmospheric contaminant transport, and other primary DOE missions.

Recent Progress (2004-2006)

Interior and Interfacial Aqueous Solvation of Benzene Dicarboxylate Dianions: Aqueous solvation of benzene dicarboxylate dianions (BCD^{2-}) was studied by means of PES and molecular dynamics simulations. Photoelectron spectra of hydrated ortho-, and para- BCD^{2-} with up to 25 water molecules were obtained. An even-odd effect was observed for the *p*- BCD^{2-} system as a result of the alternate solvation of the two negative charges. However, the high polarizability of the benzene ring makes the two carboxylate groups interact with each other in *p*- BCD^{2-} , suppressing the strength of this even-odd effect compared with the linear dicarboxylate dianions linked by an aliphatic chain. No even-odd effect was observed for the *o*- BCD^{2-} system, because each solvent molecule can interact with the two carboxylate groups at the same time due to their proximity. For large solvated clusters, the spectral features of the solute decreased while the solvent features became dominant, suggesting that both *o*- and *p*- BCD^{2-} are situated in the center of the solvated clusters. Molecular dynamics simulations with both non-polarizable and polarizable force fields confirmed that all three isomers (*o*-, *m*-, and *p*- BCD^{2-}) solvate

¹ Collaborators on these projects include X. B. Wang, H. K. Woo, and P. Jungwirth.

in the aqueous bulk. However, upon methylation the hydrophobic forces overwhelm electrostatic interactions and, as a result, the calculations predict that the tetra-methyl *o*-BCD²⁻ is located at the water surface with the carboxylate groups anchored in the liquid and the methylated benzene ring tilted away from the aqueous phase.

Observation of Weak C-H...O Hydrogen-Bonding by Unactivated Alkanes: Weak C-H...O hydrogen bonding has been recognized to play a major role in biological molecular structures and functions. Using the newly developed low-temperature PES apparatus we studied the C-H...O hydrogen bonding between unactivated alkanes and the carboxylate functional group. We observed that gaseous linear carboxylates, CH₃(CH₂)_nCO₂⁻, assume folded structures at low temperatures due to weak C-H...O hydrogen bonding between the terminal CH₃ and CO₂⁻ groups for $n \geq 5$. Temperature-dependent studies showed that the folding transition depends on both the temperature and the aliphatic chain length. Theoretical calculations revealed that for $n = 3-8$, the folded conformations are more stable than the linear structures, but C-H...O hydrogen bonding only forms for species with $n \geq 5$ due to steric constraint in the smaller species. One C-H...O hydrogen bond is formed in the $n = 5$ and 6 species, whereas two C-H...O hydrogen bonds are formed for $n = 7$ and 8. Comparison of the photoelectron spectral shifts for the folded relative to the linear conformations yielded lower limits for the strength of the C-H...O hydrogen bonds in CH₃(CH₂)_nCO₂⁻, ranging from 1.2 kcal/mol for $n = 5$ to 4.4 kcal/mol for $n = 8$.

Temperature-Dependent Photoelectron Spectroscopy of Methyl-Benzoate Anions and the Observation of Steric Effect in ortho-Methyl-Benzoate: Temperature-dependent photoelectron spectra of benzoate anion (C₆H₅CO₂⁻) and its three methyl-substituted isomers (*o*-, *m*-, *p*-CH₃C₆H₄CO₂⁻) have been obtained using a newly developed low-temperature PES apparatus that features an electrospray source and a cryogenically controlled ion trap. Detachment channels due to removing electrons from the carboxylate group and benzene ring π electrons were distinctly observed. Well-resolved vibrational structures were obtained in the lower binding energy region due to the OCO bending modes, except for *o*-CH₃C₆H₄CO₂⁻, which yielded broad spectra even at the lowest ion trap temperature (18 K). Theoretical calculations revealed a large geometry change in the OCO angles between the anion and neutral ground states, consistent with the broad ground state bands observed for all species. A strong steric effect was observed between the carboxylate and the methyl group in *o*-CH₃C₆H₄CO₂⁻, such that the -CO₂⁻ group is pushed out of the plane of the benzene ring by $\sim 25^\circ$ and its internal rotational barrier is significantly reduced. The low rotational barrier in *o*-CH₃C₆H₄CO₂⁻, which makes it very difficult to be cooled vibrationally, and the strong coupling between the OCO bending and CO₂ torsional modes yielded the broad PES spectra for this isomer. It is shown that there is *no* C-H...O hydrogen bond in *o*-CH₃C₆H₄CO₂⁻ and the interaction between the carboxylate and methyl groups in this anion is found to be repulsive in nature.

Probing the Low-Barrier Hydrogen Bond in Hydrogen Maleate in the Gas Phase: Photoelectron spectra of maleic and fumaric acid monoanions (*cis*-/*trans*-HO₂CCH=CHCO₂⁻) were obtained at low temperatures to investigate the strength of the low-barrier hydrogen bond in hydrogen maleate. Vibrational structure was observed for *trans*-HO₂CCH=CHCO₂⁻ due to the OCO bending modes; however *cis*-HO₂CCH=CHCO₂⁻ yielded a broad and featureless spectrum. The electron binding energy of *cis*-HO₂CCH=CHCO₂⁻ is about 1 eV blue-shifted relative to *trans*-HCO₂CH=CHCO₂⁻ due to the formation of a strong intramolecular hydrogen bond in the *cis*-isomer. Theoretical calculations (CCSD(T)/aug-cc-pVTZ and B3LYP/aug-cc-pVTZ) were carried out to estimate the strength of the intramolecular hydrogen bond in *cis*-HO₂CCH=CHCO₂⁻. Combining experimental and theoretical calculations, the intramolecular hydrogen bond strength in hydrogen maleate is estimated to be 21.5 ± 2.0 kcal/mol.

Low-Temperature PES of Aliphatic Dicarboxylate Monoanions, HO₂C(CH₂)_nCO₂⁻ ($n = 1 - 10$) - Hydrogen Bond Induced Cyclization and Strain Energies: Photoelectron spectra of singly-charged dicarboxylate anions HO₂C(CH₂)_nCO₂⁻ ($n = 1 - 10$) were obtained at two different temperatures (300 and

70 K). The electron binding energies of these species were observed to be much higher than the singly-charged monocarboxylate anions, suggesting the singly-charged dicarboxylate anions are cyclic due to strong intramolecular hydrogen bonding between the terminal $-\text{CO}_2\text{H}$ and $-\text{CO}_2^-$ groups. The measured electron binding energies were observed to depend on the chain length, reflecting the different $-\text{CO}_2\text{H}\cdots\text{O}_2\text{C}-$ hydrogen bonding strength as a result of strain in the cyclic conformation. A minimum binding energy was found at $n = 5$, indicating that its intramolecular hydrogen bond is the weakest. At 70 K, all spectra are blue-shifted relative to the room temperature spectra with the maximum binding energy shift occurring at $n = 5$. These observations suggest that the cyclic conformation of $\text{HO}_2\text{C}(\text{CH}_2)_5\text{CO}_2^-$ (a ten-membered ring) is the most strained among the ten anions. The present study shows that the $-\text{CO}_2\text{H}\cdots\text{O}_2\text{C}-$ hydrogen bonding strength is different among the ten anions and it is very sensitive to the strain in the cyclic conformations.

Future Plans

The main thrust of our BES program will continue to focus on cluster model studies of condensed phase phenomena in the gas phase. The experimental capabilities developed provide us with opportunities to examine fundamental chemical physics issues in complex anion solvation and solution chemistry. While we continue our work on the molecular processes of solvation of complex anions, the following outline a few themes for the Chemical Physics Program for the immediate and near future.

Confirmation Change vs. Temperature: the Effect of Entropy: The low-temperature electrospray PES apparatus recently completed in our laboratory has significantly expanded our capability and flexibility to study solvated species in the gas phase. In the past year, we have studied the effects of temperature and hydrogen bonding on the conformations of a series of organic anions containing the carboxylate functional groups. In the near future, we plan to reexamine the microsolvation of dicarboxylate dianions, which has been investigated previously using our room temperature apparatus. We observed an interesting phenomenon of solvent-induced conformation change, that is, the linear dicarboxylate dianions become folded at certain solvent number due to strong cooperative water-water hydrogen bonding. Although the previous experiment was done at room temperature, the real temperature of the cluster was unknown. However, theoretical calculations indicate that the folding transition is not only dependent on the solvent number, but also on the cluster temperature due to the effect of entropy. In our new apparatus, the ion trap temperature can be controlled and varied from 17 to 400 K. Systematic studies of the folding conformation change as a function of temperature will be performed and compared with MD simulations.

Probing the Initial Steps of Dissolution: Detailed knowledge of how polar molecules are dissolved in a solvent is essential to understanding the chemistry taking place in salt solutions and the fate and transport of environmental pollutants. Solvated clusters of simple polar molecules have been used as molecular models to probe the initial steps of dissolution. Divalent anions provide convenient systems for our PES experiments because of the negative charge in ion pairs of the form A^+B^{2-} , for example, NaSO_4^- . We plan to produce solvated species in the form of $\text{A}^+\text{B}^{2-}(\text{H}_2\text{O})_n$ as a function of solvent number. We anticipate that the photoelectron spectral evolution should reflect the solvation state of $\text{A}^+\text{B}^{2-}(\text{H}_2\text{O})_n$ and should provide experimental information on the molecular details of the initial dissolution steps of the A^+B^{2-} ion pair.

Gas Phase Studies of Free and Solvated Oligonucleotides: The ionization of nucleotides plays very important roles in the chemistry of DNA. Induced by electrophiles or ionizing radiation, the electron deficient site (hole) on the nucleotide and its migration directly leads to DNA damages. In most cases, the initial oxidation site or the electron-loss center ultimately moves via the DNA π stack to end up at a guanine base, resulting in a guanine cation. This is attributed to the low ionization potential of guanine relative to the other DNA bases. Thus the electronic structure of nucleotides and their ionization properties are essential for understanding the mechanism of DNA damages. Gas phase PES studies probe

the intrinsic electronic properties of the nucleotides and provide important experimental data to compare with and verify theoretical methods. We have already studied nucleotide anions in the gas phase and observed that nucleotides with guanine bases possess low ionization potentials, consistent with the fact that guanine is most susceptible to oxidation to give the guanine cation in DNA damages. We plan to study the gas phase formation of the Watson-Crick base pairs, as well as solvent and counter-ion stabilization on the structure and energetics of DNA nucleotides in the gas phase.

References to Publications of DOE Sponsored Research (FY 2004-2006)

1. "Solvent-Mediated Folding of A Doubly Charged Anion" (X. Yang, Y. J. Fu, X. B. Wang, P. Slavicek, M. Mucha, P. Jungwirth, and L. S. Wang), *J. Am. Chem. Soc.* **126**, 876-883 (2004).
2. "Solvation of the Azide Anion (N_3^-) in Water Clusters and Aqueous Interfaces: A Combined Investigation by Photoelectron Spectroscopy, Density Functional Calculations, and Molecular Dynamics Simulations" (X. Yang, B. Kiran, X. B. Wang, L. S. Wang, M. Mucha, and P. Jungwirth), *J. Phys. Chem. A* **108**, 7820-7826 (2004).
3. "Bulk vs. Interfacial Aqueous Solvation of Dicarboxylate Dianions" (B. Minofar, M. Mucha, P. Jungwirth, X. Yang, Y. J. Fu, X. B. Wang, and L. S. Wang), *J. Am. Chem. Soc.* **126**, 11691 (2004).
4. "Direct Experimental Observation of the Low Ionization Potentials of Guanine in Free Oligonucleotides Using Photoelectron Spectroscopy" (X. Yang, X. B. Wang, E. R. Vorpapel, and L. S. Wang), *Proc. Natl. Acad. Sci. (USA)* **101**, 17588-17592 (2004).
5. "The Role of Water on Electron-Initiated Processes and Radical Chemistry: Issues and Scientific Advances" (B. C. Garrett, *et al.*), *Chem. Rev.* **105**, 355-389 (2005).
6. "Interior and Interfacial Aqueous Solvation of Benzene Dicarboxylate Dianions and Their Methylated Analogues: A Combined Molecular Dynamics and Photoelectron Spectroscopy Study" (B. Minofar, L. Vrbka, M. Mucha, P. Jungwirth, X. Yang, X. B. Wang, F. J. Fu, and L. S. Wang), *J. Phys. Chem. A* **109**, 5042-5049 (2005).
7. "Observation of Weak C-H...O Hydrogen-Bonding by Unactivated Alkanes" (X. B. Wang, H. K. Woo, B. Kiran, and L. S. Wang), *Angew. Chem. Int. Ed.* **44**, 4968-4972 (2005).
8. "Vibrational Cooling in A Cold Ion Trap: Vibrationally Resolved Photoelectron Spectroscopy of Cold C_{60}^- Anions" (X. B. Wang, H. K. Woo, and L. S. Wang), *J. Chem. Phys.* **123**, 051106 (2005).
9. "Probing the Low-Barrier Hydrogen Bond in Hydrogen Maleate in the Gas Phase: A Photoelectron Spectroscopy and *Ab initio* Study" (H. K. Woo, X. B. Wang, L. S. Wang, and K. C. Lau), *J. Phys. Chem. A* **109**, 10633-10637 (2005).
10. "Temperatures Dependent Photoelectron Spectroscopy of Methyl-Benzoate Anions: Observation of Steric Effect in *Ortho*-Methyl-Benzoate" (H. K. Woo, X. B. Wang, B. Kiran, and L. S. Wang), *J. Phys. Chem. A* **109**, 11395-11400 (2005).
11. "Determination of the Electron Affinity of the Acetyloxyl Radical (CH_3COO) by Low Temperature Anion Photoelectron Spectroscopy and *ab initio* Calculations" (X. B. Wang, H. K. Woo, L. S. Wang, B. Minofar, and P. Jungwirth), *J. Phys. Chem. A* **110**, 5047-5050 (2006).
12. "Low-Temperature Photoelectron Spectroscopy of Aliphatic Dicarboxylate Monoanions, $HO_2C(CH_2)_nCO_2^-$ ($n = 1 - 10$): Hydrogen Bond Induced Cyclization and Strain Energies" (H. K. Woo, X. B. Wang, K. C. Lau, and L. S. Wang), *J. Phys. Chem. A* **110**, 7801-7805 (2006).
13. "First Steps Towards Dissolution of $NaSO_4^-$ by Water" (X. B. Wang, H. K. Woo, B. Jagoda-Cwiklik, P. Jungwirth, and L. S. Wang), *Phys. Chem. Chem. Phys.*, in press.

Ionic Liquids: Radiation Chemistry, Solvation Dynamics and Reactivity Patterns

James F. Wishart

Chemistry Department, Brookhaven National Laboratory, Upton, NY 11973-5000

wishart@bnl.gov

Program Definition

Ionic liquids (ILs) are a rapidly expanding family of condensed-phase media with important applications in energy production, nuclear fuel and waste processing, improving the efficiency and safety of industrial chemical processes, and pollution prevention. ILs are nonvolatile, noncombustible, highly conductive, recyclable and capable of dissolving a wide variety of materials. They are finding new uses in chemical synthesis, catalysis, separations chemistry, electrochemistry and other areas. Ionic liquids have dramatically different properties compared to conventional molecular solvents, and they provide a new and unusual environment to test our theoretical understanding of charge transfer and other reactions. We are interested in how IL properties influence physical and dynamical processes that determine the stability and lifetimes of reactive intermediates and thereby affect the courses of chemical reactions and product distributions.

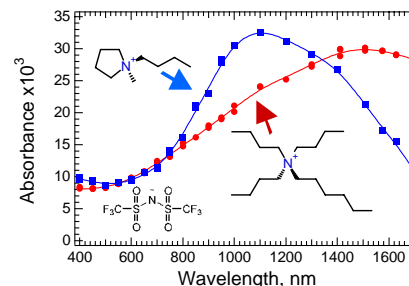
Successful use of ionic liquids in radiation-filled environments, where their safety advantages could be significant, requires an understanding of ionic liquid radiation chemistry. For example, characterizing the primary steps of IL radiolysis will reveal radiolytic degradation pathways and suggest ways to prevent them or mitigate their effects on the properties of the material. An understanding of ionic liquid radiation chemistry will also facilitate pulse radiolysis studies of general chemical reactivity in ILs, which will aid in the development of applications listed above. Very early in our radiolysis studies it became evident that slow solvation dynamics of the excess electron in ILs (which vary over a wide viscosity range) increases the importance of pre-solvated electron reactivity and consequently alters product distributions. Parallel studies of IL solvation phenomena using coumarin-153 dynamic Stokes shifts and polarization anisotropy decay rates are done to compare with electron solvation studies and to evaluate the influence of ILs on charge transport processes.

Methods. Picosecond pulse radiolysis studies at BNL's Laser-Electron Accelerator Facility (LEAF) are used to identify reactive species in ionic liquids and measure their solvation and reaction rates. IL solvation and rotational dynamics are measured by TCSPC and fluorescence upconversion measurements in the laboratory of E. W. Castner at Rutgers Univ. Diffusion rates are obtained by PGSE NMR in S. Greenbaum's lab at Hunter College, CUNY. We and our collaborators (R. Engel (Queens College, CUNY) and S. Lall-Ramnarine, (Queensborough CC, CUNY)) develop and characterize new ionic liquids specifically designed for our radiolysis and solvation dynamics studies. Professor Mark Kobrak of CUNY Brooklyn College performs molecular dynamics simulations of solvation processes. A collaboration with M. Dietz and coworkers at ANL is centered around the properties and radiolytic behavior of ionic liquids for nuclear separations.

Recent Progress

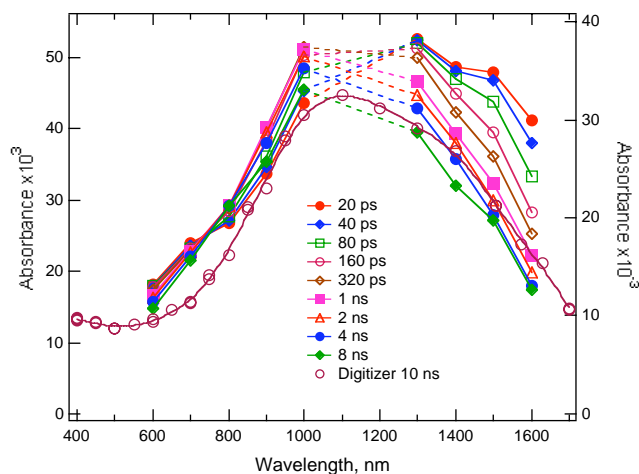
Solvated Electrons. Experiments performed at LEAF demonstrated for the first time that radiolysis of $[R_4N][NTf_2]$, $[R_4N][N(CN)_2]$, and $[R_4P][N(CN)_2]$ ionic liquids produces solvated electrons that absorb over a broad range in the near infrared and persisting for hundreds of nanoseconds [1,3,5]. The e_{solv}^- spectra of NTf_2^- salts of the *N*-methyl,*N*-butylpyrrolidinium (P_{14}^+) and hexyltributylammonium ($HxBu_3N^+$) cations are shown at right. (Each spectrum is representative of four examples of liquids with similar structures.) The differences in band shape and position indicate different distributions of electron solvation cavity sizes and shapes as a function of cation structure, the nature of which may be revealed by future MD simulations.

Pre-solvated electron reactivity and solvation dynamics in ILs. In the course of kinetic measurements described below it was found that relatively low scavenger concentrations substantially reduced the initial yield of solvated electrons [1]. Direct scavenging of pre-solvated ("dry") electrons competes effectively with the slower



electron solvation processes in ionic liquids. For example, a pyrene concentration of only 63 mM reduces the solvated electron yield to 37% of the scavenger-free value. This finding has major implications for processing of radioactive materials, where seemingly innocuous quantities of solutes may scavenge electrons very effectively. Conversely, dry electron scavenging facilitates the use of pulse radiolysis in electron transfer studies by providing a way to circumvent diffusion-limited precursor formation rates. Measurements of excess electron solvation processes and emission dynamics (Stokes shift and polarization anisotropy decay) of solvatochromic coumarin-153 show that the reorganization dynamics of ionic liquids occur on much longer timescales (nanoseconds) than in conventional polar solvents (picoseconds). The slow solvation dynamics would also be expected to significantly alter transition state dynamics and provide a potential means to control product distribution. This becomes particularly important for transition states with a very different polarity from the reactants and/or products.

To look at electron solvation with higher time resolution, we used low-viscosity pyrrolidinium salts and developed novel ionic liquids with even lower melting points and viscosities, based on ether-substituted pyrrolidinium cations [5]. These liquids have RT viscosities low enough (65-95 cP) to flow through the picosecond pulse-probe transient absorption system at LEAF, which requires sample exchange to avoid cumulative radiation effects. Consequently, the electron solvation process was directly observed in three ILs by monitoring the decay of pre-solvated electrons at multiple wavelengths (to yield a solvated electron spectrum similar to the blue curve above). In *N*-methyl,*N*-butyl-pyrrolidinium NTf₂⁻ the electron solvation lifetime $\langle\tau_{\text{solv}}\rangle$ is 260 ps, while $\langle\tau_{\text{solv}}\rangle$ obtained from coumarin 153 Stokes shift measurements is 220 ps.



Even slower solvation processes were observed in pulse radiolysis studies of ionic liquids containing ether-, alcohol- and alkyl-functionalized quaternary ammonium dications $(\text{CH}_3)_2(\text{R})\text{N}^+(\text{CH}_2)_n\text{N}^+(\text{R})(\text{CH}_3)_2$ (NTf₂⁻)₂, where R = (CH₂)₃OH, (CH₂)₂OCH₂CH₃, or (CH₂)₃CH₃ and n = 3–8. Spectra on nanosecond timescales revealed that solvation of the excess electron is particularly slow in the case of the alcohol-derivatized ionic liquids. The blue shift of the electron spectrum to the customary 650 nm peak takes 25-40 nanoseconds at RT (viscosities ~4500-6800 cP). Comparison with the ~1 ns electron solvation time observed in similarly viscous 1,2,6-trihydroxyhexane (2500 cP) reveals the hindering effect of the ionic liquid lattice on hydroxypropyl side chain reorientation [4].

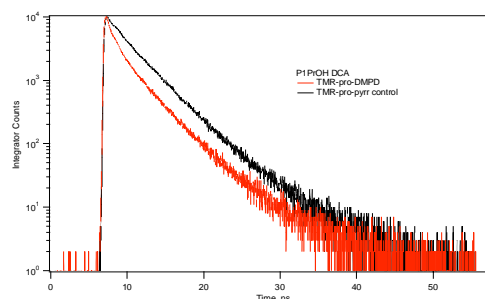
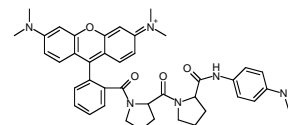
Reaction rates. Electron reactions with several aromatic acceptors, acids, and oxygen were measured in (MeBu₃N⁺)(NTf₂⁻). Rate constants for solvated electron capture by benzophenone, pyrene and phenanthrene were on the order of $1.6 \times 10^8 \text{ M}^{-1} \text{ s}^{-1}$, typically 100 times slower than observed in conventional polar solvents [1]. The reactions of hydrogen atoms with several of the same reactants were measured in the same ionic liquid. H-atoms react very rapidly with pyrene and phenanthrene ($\sim 3 \times 10^9 \text{ L mol}^{-1} \text{ s}^{-1}$) to form H-adduct radicals [2]. The H-atom rate constants are similar to the values measured or estimated for the same reactions in aqueous solutions. The H-atom reactions with the aromatic hydrocarbons must be diffusion-controlled, but are faster than diffusion-controlled reactions for solvated electrons in the same ionic liquid.

The results indicate that the diffusion rate for the solvated electron in ionic liquids can be significantly lower than those of small neutral molecules or radicals such as the H-atom, in contrast to the situation in molecular solvents. These results support the contention that the diffusion constants of charged and neutral reactants differ considerably in ionic liquids, which could lead to a means of controlling reactivity and transport phenomena through rational selection of ionic liquid properties.

Radiolysis of borated ionic liquids. In 2001 a group from Los Alamos calculated that processing plutonium in boron-containing ionic liquids could substantially reduce the risk of nuclear criticality accidents. Understanding the reactions that radiation induces within ionic liquids is vitally important to their applications in this area. Consequently we have investigated the radiation chemistry of ionic liquids prepared from carborane (CB⁻) and

bis(oxalato)borate (BOB⁻) anions. Experiments in liquids derived from the CB₁₁H₆Br₆⁻ and BOB⁻ anions and studies of the same anions diluted in NTf₂⁻ ionic liquids indicate the major radiation stability concern may be the reaction of the solvated electron with the CB and BOB anions, a problem that could be addressed by including imidazolium or pyridinium cations in the ionic liquid mixtures.

Charge transport in ionic liquids. Rates of intramolecular electron transfer (IET) reactions of peptide-bridged donor-acceptor systems tetramethylrhodamine-(proline)_n-dimethylphenylenediamine, (n = 1, 2) were measured in four ionic liquids, providing an opportunity to compare IET processes in ionic liquids and in molecular solvents (e.g., water, methanol, CH₃CN, CH₂Cl₂). Pyrrolidinium cations of different hydrophilicity were combined with triflylamide (NTf₂⁻) and dicyanamide (DCA⁻) anions. The IET process in question was the reductive quenching of the fluorescent TMR cation excited state by DMPD, measured by TCSPC detection of TMR emission. IET in the ionic liquids was found to be slower than in molecular solvents. While IET reactions for n = 2 prolines in the triflylamide liquids showed a single slow exponential decay, TCSPC profiles in the dicyanamide liquids showed double exponential decays indicating fast and slow electron transfer processes, the faster one suggesting a specific anion effect that will be studied by using a wider range of ionic liquid anions in future work. (In collaboration with S. S. Isied and E. W. Castner, Rutgers University.)



Future Plans

Electron solvation and reactivity. The validity of proposed pre-solvated electron scavenging mechanisms will be tested by exploring the competition between the electron solvation and electron capture processes in ionic liquids. Electron solvation dynamics in several families of low-viscosity ILs will be measured by pulse-probe radiolysis. Subsequently, scavengers will be added to measure the kinetics of pre-solvated electron capture. It is well known from work in molecular solvents that many scavengers, for example SeO₄²⁻, have widely different reactivity profiles towards pre-solvated and solvated electrons. By quantitative measurement of the scavenging profiles of many reactants, we hope to explain such conundrums mechanistically.

Many ionic liquids with slow electron solvation rates are too viscous to be flowed for pulse-probe experiments. Detailed studies of electron solvation in these ILs will be possible upon installation of the “ultrafast single-shot” detection system at LEAF. In the meantime, C-153 solvation dynamics studies will serve as proxies for the electron results to aid the study of pre-solvated electron scavenging mechanisms as measured by “time-zero” radiolytic product yields.

Charge transport in ionic liquids. Pulse radiolysis will be used to study how ionic liquids affect charge-transport reactions related to solar energy photoconversion systems, where their characteristics may prove valuable. IL-based photoelectrochemical cells have already been reported. Focus areas will be the combined effects of ionic solvation and slow solvent relaxation on the energy landscape of charge transport, including specific counterion effects depending on the ionic liquid, and the influence of the lattice-like structure of ionic liquids on the distance dependence of electron transport reactions.

Non-classical diffusion in ionic liquids. Ionic liquids contain considerable void space due to the poor packing that makes them liquids instead of solids. The combination of voids and the ionic lattice result in unusual diffusion rate trends reported in the literature. Kinetic and high-pressure pulsed-gradient spin echo NMR studies of diffusion rates of charged and neutral species will examine how ionic liquids modulate diffusion as a function of size and charge.

Publications on ionic liquids

1. *Spectrum and Reactivity of the Solvated Electron in the Ionic Liquid Methyltributylammonium Bis(trifluoromethylsulfonyl)imide* J. F. Wishart and P. Neta *J. Phys. Chem. B* **107**, 7261-7267 (2003).

2. *Pulse Radiolysis Study of the Reactions of Hydrogen Atoms in the Ionic Liquid Methyltributylammonium Bis(trifluoromethylsulfonyl)imide* J. Grodkowski, P. Neta and J. F. Wishart *J. Phys. Chem. A*, **107**, 9794-9799 (2003).
3. *Radiation Chemistry of Ionic Liquids: Reactivity of Primary Species* J. F. Wishart in "Ionic Liquids as Green Solvents: Progress and Prospects" Rogers, R. D. and Seddon, K. R., Eds.; *ACS Symp. Ser.* **856**, Ch. 31, pp. 381-396, American Chemical Society, Washington, DC, 2003.
4. *Effects of Functional Group Substitution on Electron Spectra and Solvation Dynamics in a Family of Ionic Liquids* J. F. Wishart, S. I. Lall-Ramnarine, R. Raju, A. Scumpia, S. Bellevue, R. Ragbir, and R. Engel *Radiat. Phys. Chem.* **72**, 99-104 (2005).
5. *Dynamics of Fast Reactions in Ionic Liquids* A. M. Funston and J. F. Wishart in "Ionic Liquids IIIA: Fundamentals, Progress, Challenges and Opportunities" Rogers, R. D. and Seddon, K. R., Eds.; *ACS Symp. Ser.* **901**, Ch. 8, American Chemical Society, Washington, DC, 2005. (ISBN 0-84123-893-6).
6. *Ultrafast Dynamics of Pyrrolidinium Cation Ionic Liquids* H. Shirota, A. M. Funston, J. F. Wishart, E. W. Castner, Jr. *J. Chem. Phys.* **122**, 184512 (2005), selected for the *Virtual Journal of Ultrafast Science* (6/05).
7. *Radiation Chemistry of Ionic Liquids* J. F. Wishart, A. M. Funston, and T. Szreder in "Molten Salts XIV, Proceedings of the 2004 Joint International Meeting of the Electrochemical Society, Honolulu, HI, 2004", R. A. Mantz and P. Trulove, Eds. The Electrochemical Society, Inc., Pennington, NJ, in press.

Publications on other subjects

8. *Reactions of Charged Species in Supercritical Xenon as Studied by Pulse Radiolysis* R. A. Holroyd, J. F. Wishart, M. Nishikawa, and K. Itoh *J. Phys. Chem. B* **107**, 7281-7287 (2003).
9. *Do Main Chain Hydrogen Bonds Create Dominant Electron Transfer Pathways? An Investigation in Designed Proteins* Y. Zheng, M. A. Case, J. F. Wishart, and G. L. McLendon *J. Phys. Chem. B* **107**, 7288-7292 (2003).
10. *Radiation Chemistry of Methyl-tert-Butyl Ether (MTBE) in Aqueous Solution* S. P. Mezyk, J. Jones, W. J. Cooper, T. Tobien, M. G. Nickelsen, J. W. Adams, K. E. O'Shea, D. M. Bartels, J. F. Wishart, P. M. Tornatore, K. S. Newman, K. Gregoire, and D. J. Weidman *Envir. Sci. Tech.*, **38**, 3994-4001 (2004).
11. *Long-Range Electron Transfer across Peptide Bridges: the Transition from Electron Superexchange to Hopping* R. Abdel Malak, Z. Gao, J. F. Wishart, and S. S. Isied, *J. Am. Chem. Soc.* **126**, 13888-13889 (2004).
12. *Convergence of Spectroscopic and Kinetic Electron Transfer Parameters for Mixed-Valence Binuclear Dipyridylamide Ruthenium Ammine Complexes* A. J. Distefano, J. F. Wishart, and S. S. Isied *Coord. Chem. Rev.*, **249**, 507-516 (2005).
13. *The LEAF Picosecond Pulse Radiolysis Facility at Brookhaven National Laboratory* J. F. Wishart, A. R. Cook, and J. R. Miller *Rev. Sci. Inst.* **75**, 4359-4366 (2004), selected for the *Virtual Journal of Ultrafast Science* (12/04).
14. *Search for the 3-body Photodisintegration of Be* D. E. Alburger, R. E. Chrien, R. J. Sutter, and J. F. Wishart, *Phys. Rev. C* **70**, 064611 (2004).
15. *Radiolysis with RF Photoinjectors: Supercritical Xenon Chemistry* J. F. Wishart in "Femtosecond Beam Science" Uesaka, M., Ed.; Imperial College Press, London, 2005, pp. 351-356. (ISBN 1-86094-343-8).
16. *Reactivity of Acid Generators for Chemically Amplified Resists with Low-Energy Electrons* A. Nakano, T. Kozawa, S. Tagawa, T. Szreder, J. F. Wishart, T. Kai and T. Shimokawa *Jpn. J. Appl. Phys.*, **45**, L197-L200 (2006).

Electronically non-adiabatic interactions at the gas-solid interface

Alec M. Wodtke, Department of Chemistry and Biochemistry, University of California, Santa Barbara, California, 93106 and Daniel J. Auerbach Hitachi San Jose Research Center, 650 Harry Road, San Jose, California, 95120-6099

We have designed, commissioned, and begun using an advanced molecular beam surface scattering apparatus, with much improved capability over our past instrument. Using this instrument, we are able to observe vibrationally inelastic scattering of HCl($v=0 \rightarrow 1$) in collisions with a Au(111) surface under conditions where the vibrational excitation probability is as low as 10^{-6} , an unprecedented level of sensitivity. We have obtained comprehensive scattering data including angular and rotational distributions at 6 surface temperatures and 4 incidence energies of translation (24 collision conditions). At low surface temperatures, vibrational excitation of HCl molecules ($v=0 \rightarrow 1$) has been observed when HCl molecular beams at energies of 0.59 eV to 1.37 eV are scattered from a Au (111) surface at low surface temperature ($T_s = 273\text{K}$). The vibrational excitation probability depends strongly on incidence kinetic energy, E_i , exhibiting a threshold near $\sim E_i = 0.57$ eV. We measured the absolute vibrational excitation probability which varies from $10^{-6} \sim 10^{-5}$ over this energy range, 1-2 orders of magnitude higher than the thermal equilibrium expectation value. The magnitude

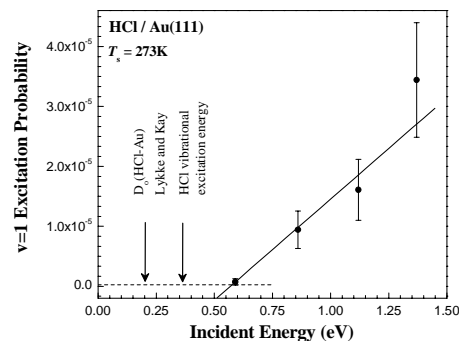


Figure 1: Mechanical T-V excitation at low surface temperature: Incidence energy dependence of vibrational excitation probability of HCl ($v=0 \rightarrow 1$) from Au(111) at 273K surface temperature. The dash line at 2.5×10^{-7} is the thermal expectation value. Also shown is the orientation averaged binding energy of HCl to Au(111) derived K.R. Lykke, B.D. Kay: *J. Chem. Phys.* 92 (1990) 2614. and the HCl vibrational ($v=0 \rightarrow 1$) excitation energy. The dashed horizontal line indicates the thermal expectation value.

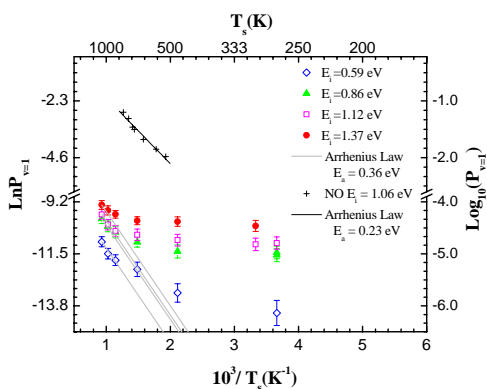


Figure 2 Transition from mechanical (T-V) to electronically non-adiabatic vibrational excitation with increasing surface temperature: Vibrational excitation probability vs. Surface temperature for several values of the incidence energy. Comparison to NO data is also shown (See Rettner et al., *Phys. Rev. Lett.*, (1985) 55 1904). The Arrhenius like dependence is expected for hot electron hole pair induced vibrational excitation. The slope of the Arrhenius like plot is given by the $v=0,1$ energy gap (0.23 eV for NO and 0.36 eV for HCl).

of the excitation probability, the near specular angular distributions of the scattered $v=1$ molecules and the dramatic narrowing of the angular distribution near threshold are all consistent with a direct translation to vibration (T-V) mechanical energy transfer mechanism.

We observe a change in scattering mechanism at elevated surface temperature. Here, the characteristic pseudo Arrhenius dependence on T_s is seen. See Fig. 2. We interpret this as a transition from a mechanical to an electronically non-adiabatic mechanism. This data set is a remarkable benchmark for theory as both mechanical and electronically non-adiabatic dynamics must be handled on an even footing.

This work also demonstrates how the magnitude of electronically non-adiabatic coupling to molecular vibration may be quantitatively compared between different molecule/surface scattering systems. Figure 2 shows the comparison of the present data to the previous work for NO scattering from Ag(111). The non-adiabatic coupling is $\sim 10^3$ higher for NO/Ag in comparison to HCl/Au. Theoretical studies of measurements such as these may help us to obtain a predictive understanding of non-adiabatic influences for molecules at metal surfaces.

Molecular Theory & Modeling
Structural and thermodynamic properties of liquid water and ice

Sotiris S. Xantheas
 Chemical Sciences Division
 Pacific Northwest National Laboratory
 902 Battelle Blvd.
 Mail Stop K1-83
 Richland, WA 99352
sotiris.xantheas@pnl.gov

The objective of this research effort is to provide accurate structural and thermodynamic properties of the various phases of water. We rely on the use of a recently developed interaction potential for water, which was parameterized from highly accurate electronic structure calculations for small water clusters. The adopted approach of describing “one-molecule-at-a-time” allows for the proper description of the intermolecular interactions between water molecules as they interact in small clusters at the microscopic level as well as in larger collections like the liquid and ice at the macroscopic level.

The model is based on the physically correct *non-linear* character of the monomer dipole moment surface (DMS), which is incorporated within the Thole-type, polarizable, flexible (TTM2.1-F, revision 2.1) interaction potential. This attribution has been used in order to describe the fact that the dipole derivative with respect to the elongation of the intramolecular OH bond does not lie along the nuclear displacement vector. Our scheme is based on the use of geometry-dependent charges which, for each monomer conformation, are adjusted in order to reproduce the monomer DMS. Simulations under periodic boundary conditions (PBC) of several supercells consisting of up to 288 molecules of water used to sample the proton disorder in the ice Ih lattice yield an average value of $\vartheta_{HOH}(I_h) = 108.4^\circ \pm 0.2^\circ$ for the minimized structures ($T=0$ K) and $108.1^\circ \pm 2.8^\circ$ at $T=100$ K (see Figure 1). Analogous simulations for liquid water predict an average value of $\vartheta_{HOH}(liquid) = 106.3^\circ \pm 4.9^\circ$ at $T=300$ K. The corresponding results with the non-linear (based on fixed charges) DMS exhibiting a decrease in the bend angle are also shown. The TTM2.1-F potential is therefore the *only* classical potential, which, starting from the gas phase value for the bend angle (104.52°), reproduces its experimentally observed *increase* in the ice Ih lattice and in liquid water. In contrast, *all* other classical potentials, which are based on the use of fixed (non-geometry

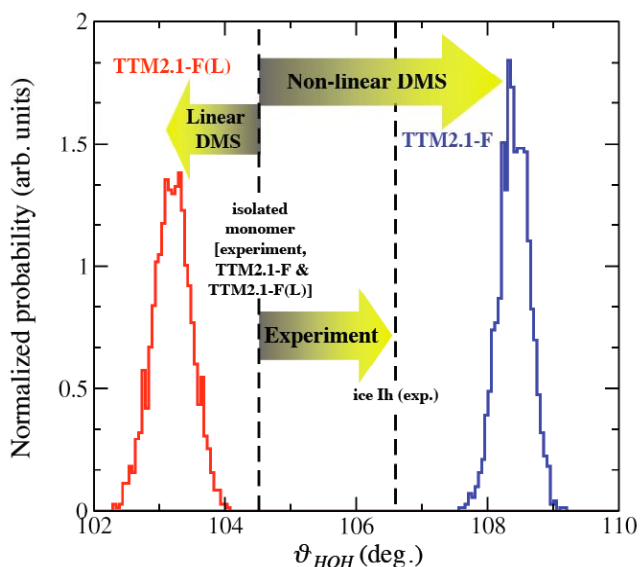


Figure 1. Normalized probability distribution of monomer bend angles in the optimized ($T=0$ K) ice Ih lattice with the TTM2.1-F (non-linear DMS, geometry dependent charges) and TTM2.1-F(L) (linear DMS, constant charges) potentials. Experimental values for the monomer and the average in the ice lattice are also indicated.

dependent) charges, predict a *decrease* of the monomer bend angle in ice Ih and in liquid water with respect to the gas phase monomer value.

The increase of the monomer bend angle in the liquid and in ice can therefore be attributed to the intramolecular charge transfer within the monomer arising from the change in the internal geometry due to the intermolecular interaction. This otherwise subtle effect, amounting to the shift of just 0.005-0.008 e from the hydrogen towards the oxygen atom in the ice Ih lattice, has a dramatic consequence on the monomer's internal geometry.

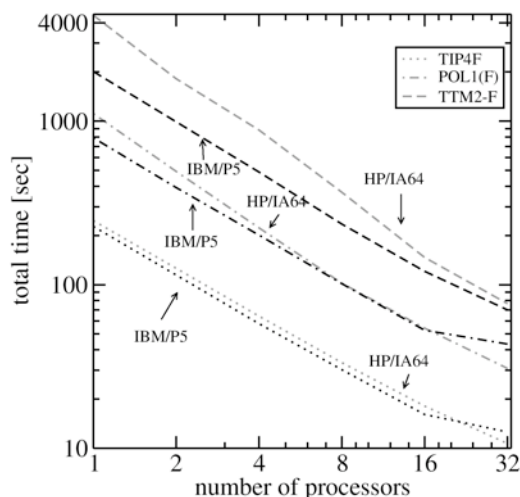


Figure 2. Time to solution for 1,000 MD steps in a system with 512 water molecules under periodic boundary conditions on the HP/IA64 and IBM/P5 platforms on 1-32 processors.

performance for simulations of liquid water with a polarizable potential under PBC.

The fact that the TTM2.1-F potential is parametrized to high-level electronic structure calculations (i.e to the Born-Oppenheimer PES) requires the explicit account of zero-point effects in order to obtain the macroscopic properties of the systems under study. We report converged quantum statistical mechanical simulations of liquid water with the TTM2.1-F interaction potential. Centroid molecular Dynamics (CMD) simulations of total length of 600 ps with a 0.05 fs time step for a periodic unit cell of 256 molecules with up to 32 replicas (beads) per atom suggest that the quantum effects contribute 1.01 ± 0.02 kcal/mol to the enthalpy of formation for

Classical molecular dynamics simulations with the new potential were performed following an efficient parallelization scheme under PBC based on Ewald's scheme for handling the long-range electrostatic and induction interactions. The algorithm is designed for systems containing several thousands of polarizable sites in the simulation box. Its performance, on both shared and distributed memory architectures, is shown in Figure 2 for the TTM2.1-F and another 2 commonly used interaction potentials; one flexible, polarizable (DC-F), the other flexible, pairwise-additive (TIP4F). As a result of the efficient calculation of the induced dipole moments, a superlinear scaling with the number of the processors is observed. To the best of our knowledge, these are the first reported results of parallel scaling and

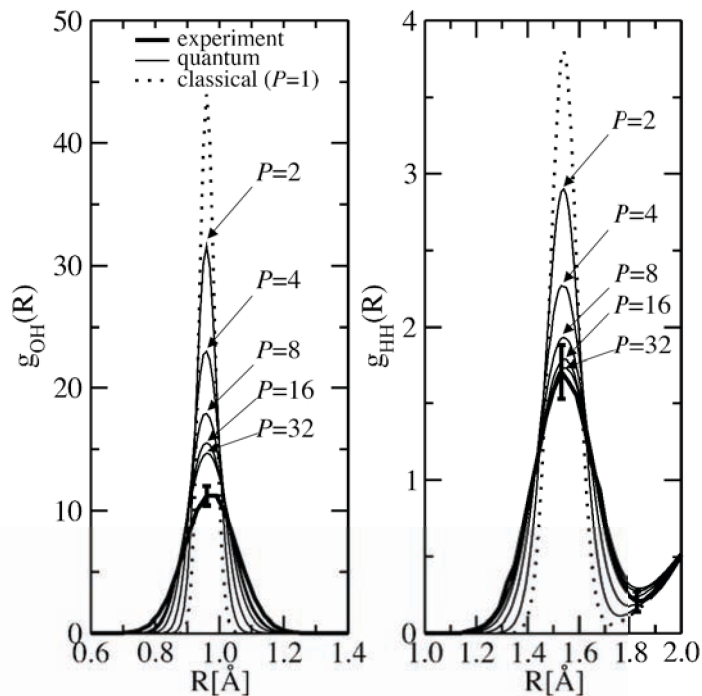


Figure 3. Convergence of the intramolecular O-H and H-H RDFs with the number of beads, P for liquid water at $T=298.15$ K. The classical ($P=1$) and the experimental RDFs are also indicated.

liquid water at 298K. They furthermore demonstrate, for the first time, a quantitative agreement with experiment for the heights and broadening of the intramolecular OH and HH peaks in the radial distribution functions (see Figure 3). The corresponding heat of vaporization for the liquid is 11.25 ± 0.02 kcal/mol ($P=32$ beads), just 0.74 kcal/mol higher than the experimental value of 10.51 kcal/mol. We attribute this difference to the following factors: (i) inaccuracies in the representation of the underlying (D_e) potential energy surface, (ii) convergence of the quantum statistical simulations with P and (iii) inaccuracies in the estimation of zero-point energy arising from errors in the hydrogen bonded frequencies. The first is associated with an error of ~ 0.2 kcal/mol whereas the second one is < 0.1 kcal/mol. The third factor is associated with the largest error contributing an estimated 0.4 kcal/mol to the enthalpy. We are currently exploring ways to reduce those errors.

Future plans include the extension of the quantum simulations for different thermodynamic states of liquid water, the examination of the various phases of ice as well as the consequence of quantum effects on the transport properties and the infrared spectra of liquid water.

Acknowledgements: This research was performed in part using the computational resources in the Molecular Science Computing Facility (MCSF) in the William R. Wiley Environmental Molecular Sciences Laboratory. Battelle operates Pacific Northwest National Laboratory for the US Department of Energy.

Collaborators on this project include G. S. Fanourgakis, G. K. Schenter (PNNL, Chemical Sciences Division), V. Tipparaju, J. Nieplocha (PNNL, Computational Sciences and Mathematics Division) and P. J. Rossky (Univ. of Texas at Austin)

References to publications of DOE sponsored research (2004-present)

1. S. S. Xantheas, E. Aprà, "The binding energies of the D_{2d} and S_4 water octamer isomers: High-level electronic structure and empirical potential results", *Journal of Chemical Physics* **120**, 823 (2004)
2. J. M. Bowman, S. S. Xantheas, "Morphing of *ab initio*-based interaction potentials to spectroscopic accuracy: Application to $\text{Cl}(\text{H}_2\text{O})$ ", *Pure and Applied Chemistry* **76**, 29 (2004)
3. C. J. Burnham and S. S. Xantheas, "On the importance of zero-point effects in molecular level classical simulations of water", *Journal of Molecular Liquids* **110**, 177 (2004)
4. S. S. Xantheas, "Intermolecular Interactions and Cooperative Effects from Electronic Structure Calculations: An Effective Means for Developing Interaction Potentials for Condensed Phase Simulations" in *Novel Approaches to the Structure and Dynamics of Liquids: Experiments, Theories and Simulations*, NATO Science Series II: Mathematics, Physics and Chemistry vol. 133 J. Samios and V. A. Durov (Eds.), pp. 1-15, Kluwer Academic Publishers, Dordrecht, The Netherlands (2004)
5. G. S. Fanourgakis, E. Aprà and S. S. Xantheas, "High-level *ab-initio* calculations for the four low-lying families of minima of $(\text{H}_2\text{O})_{20}$: I. Estimates of MP2/CBS binding energies and comparison with empirical potentials", *Journal of Chemical Physics* **121**, 2655 (2004)
6. B. C. Garrett, D. A. Dixon, *et al* "The Role of Water on Electron-Initiated Processes and Radical Chemistry: Issues and Scientific Advances", *Chemical Reviews* **106**, 355 (2005)

7. G. S. Fanourgakis, E. Aprà, W. A. de Jong, and S. S. Xantheas, "High-level *ab-initio* calculations for the four low-lying families of minima of (H₂O)₂₀: II. Spectroscopic signatures of the dodecahedron, fused cubes, face-sharing and edge-sharing pentagonal prisms hydrogen bonding networks", *Journal of Chemical Physics* **122**, 134304 (2005)
8. A. Lagutschenkov, G. S. Fanourgakis, G. Niedner-Schatteburg and S. S. Xantheas, "The spectroscopic signature of the "all-surface" to "internally solvated" structural transition in water clusters in the *n*=17-21 size regime", *Journal of Chemical Physics* **122**, 194310 (2005)
9. S. Hirata, M. Valiev, M. Dupuis and S. S. Xantheas, S. Sugiki and H. Sekino, "Fast electron correlation methods for molecular clusters in the ground and excited states", *Molecular Physics* (R. J. Bartlett special issue) **103**, 2255 (2005)
10. S. S. Xantheas, "Interaction potentials for water from accurate cluster calculations" in *Structure and Bonding: Intermolecular Forces and Clusters II*, Springer-Verlag Berlin Heidelberg, D. J. Wales (Editor), vol. **116**, pp. 119-148 (2005)
11. S. S. Xantheas, W. Roth, I. Fischer, "Competition between van der Waals and Hydrogen Bonding Interactions: The structure of the trans-1-Naphthol/N₂ cluster", *Journal of Physical Chemistry A* **109**, 9584 (2005)
12. G. S. Fanourgakis and S. S. Xantheas, "The flexible, polarizable, Thole-type interaction potential for water (TTM2-F) revisited" *Journal of Physical Chemistry A* **110**, 4100 (2006)
13. G. S. Fanourgakis and S. S. Xantheas, "The bend angle of water in ice Ih and liquid water: The significance of implementing the non-linear monomer dipole moment surface in classical interaction potentials" *Journal of Chemical Physics* **124**, 174504 (2006)
14. K. A. Ramazan, L. M. Wingen, Y. Miller, G. M. Chaban, R. B. Gerber, S. S. Xantheas and B. J. Finlayson-Pitts, "New Experimental and Theoretical Approach to the Heterogeneous Hydrolysis of NO₂: Key Role of Molecular Nitric Acid and Its Complexes", *Journal of Physical Chemistry A* **110**, 6886 (2006)
15. S. S. Xantheas, T. A. Blake, "The Structure, Anharmonic Spectra and Puckering Barrier of Cyclobutane: A Theoretical Study", *Journal of Physical Chemistry A* **110**, 10487 (2006)
16. G. S. Fanourgakis, V. Tipparaju, J. Nieplocha and S. S. Xantheas, "An efficient parallelization scheme for molecular dynamics simulations with many-body, flexible, polarizable empirical potentials: Application to water" *Theoretical Chemistry Accounts* (2006). Published online July 13, 2006. DOI: 10.1007/s00214-006-0145-x
17. S. S. Xantheas, "Anharmonic vibrational spectra of hydrogen bonded clusters: Comparison between higher energy derivative and mean-field grid based methods", Roger E. Miller memorial issue (invited), *International Reviews in Physical Chemistry* (in press, 2006)
18. S. Bulusu, S. Yoo, E. Aprà, S. S. Xantheas, X. C. Zeng, "The lowest energy structures of water clusters (H₂O)₁₁ and (H₂O)₁₃" *Journal of Physical Chemistry A*, Letter to the Editor (in press, 2006)
19. G. S. Fanourgakis, G. K. Schenter and S. S. Xantheas, "A quantitative account of quantum effects in liquid water" *Journal of Chemical Physics*, Communication to the Editor (in press, 14 October 2006)

Progress Report for DE-FG02-00ER15072
Experimental and Theoretical Studies of Conformational Dynamics of Proteins and
Nonequilibrium Steady State of Biochemical Reactions

PI: Sunney Xie

Department of Chemistry and Chemical Biology, Harvard University

xie@chemistry.harvard.edu

Abstract

We investigate the protein conformational fluctuations experimentally and theoretically. Our single molecule experiments lead to the discovery of a remarkable power law memory kernel spanning from 10^{-3} s to 10 s. The implication of this memory kernel for biochemical reactions is studied in the framework of Kramers' theory by stochastic simulations of generalized Langevin dynamics that naturally accounts for the experimentally observed dynamic disorder in enzymatic reactions. The microscopic origin of multiple timescale fluctuations of protein is also investigated with a polymer chain model. In studying nonequilibrium steady-state thermodynamics of biochemical reactions, we have developed a methodology for determining the thermodynamic driving force from nonequilibrium turnover time traces of single enzymes.

Recent Progress

Single molecule electron transfer experiment probing protein conformational fluctuations [1] (Wei Min and Guobion Luo, graduate students, Prof. Binny Cherayi, on sabbatical from Indian Institute of Science, Prof. Sam Kou, collaborator at Harvard's Statistics)

Protein conformational dynamics at biologically relevant timescales is crucial to the understanding of various protein functions. Such dynamics is usually masked in the ensemble measurements. To circumvent this difficulty, we have developed a technique to study one molecule at a time. In this study, we monitor a protein complex formed between fluorescein (FL) and monoclonal anti-fluorescein (anti-FL) (Fig. 1). While free FL molecules in solution exhibit a mono-exponential fluorescence decay, the FL/anti-FL complex has a shorter fluorescence lifetime, with a multi-exponential fluorescence decay due to electron transfer (ET) from a nearby tyrosine residue (gray) to the excited FL (red). The fluorescence lifetime of a single fluorescein anti-fluorescein complex, dominated by ET, was monitored as a function of time. Shown in Fig. 1 is the fluctuation of the donor-acceptor distance, $x(t)$, based on the exponential dependence of ET rate on $x(t)$. The autocorrelation function of the donor-acceptor distance, $C_x(t)$, is shown in Fig. 2, which decays over a broad range of time scales from millisecond to hundreds of seconds.

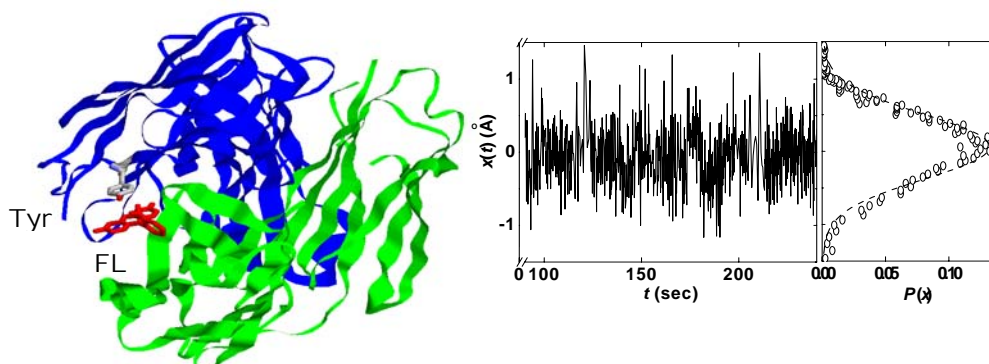


Fig. 1. Left panel: Structure of the FL and anti-FL complex. The tyrosine donor (Tyr) and fluorescein acceptor (FL) for the photo-induced electron transfer reaction are highlighted. Right panel: A trajectory of the donor acceptor distance fluctuation x , within a single complex, with a Gaussian distributed probability of $P(x)$, giving a harmonic potential of mean force $U(x) = -kT \ln P(x)$.

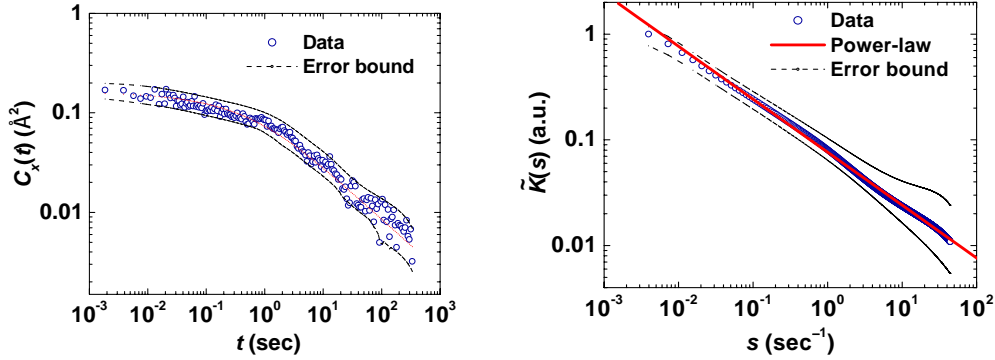


Fig. 2. Left: Autocorrelation function of $x(t)$ is highly stretched multi-exponential decay, indicating fluctuations on a broad range of time scales. Right: Within the frame work of GLE, the memory kernel $\tilde{K}(s)$ is experimentally determined to be a power law.

We model $x(t)$ as the coordinate of a fictitious particle diffusing in a harmonic potential. The generalized Langevin equation (GLE) governs its dynamical evolution:

$$m \frac{d^2 x(t)}{dt^2} = -\zeta \int_0^t d\tau K(t-\tau) \frac{dx(\tau)}{d\tau} - \frac{dU(x)}{dx} + F(t)$$

where m is the mass of the particle, $U(x)$ is the potential, ζ is the friction coefficient, $F(t)$ is the random force with a certain memory function $K(t, \tau)$ that is in turn related to $F(t)$ by fluctuation-dissipation theorem, $\langle F(t)F(\tau) \rangle = k_B T \zeta K(t-\tau)$. In the over-damped limit, where the inertial term can be neglected, we have shown that $\tilde{K}(s)$, the Laplace transform of $K(t)$, exhibits a simple power-law decay, $\tilde{K}(s) \propto s^\alpha$, with $\alpha = -0.49 \pm 0.07$ over at least four decades of time (Fig. 2). The inverse Laplace transform gives $K(t) = t^{-\alpha-1} \propto t^{-1/2}$, which is remarkably simple. To the best of our knowledge, this is the first time that the memory kernel for conformational fluctuation has been determined for protein molecules [1].

Polymer model to understand the power law memory kernel [4] (Prof. Binny Cherayi, on sabbatical from Indian Institute of Science)

We have recently proposed a microscopic model to account for the power law memory kernels based on the dynamics of a continuum semiflexible polymer chain. Time-dependent fluctuations in the distance $x(t)$ between two segments along a polymer are one measure of its overall conformational dynamics. The dynamics of $x(t)$, modeled as the coordinate of a particle moving in a one-dimensional potential well in thermal contact with a reservoir, is treated with a GLE

whose memory kernel $K(t)$ can be calculated from the time-correlation function of distance fluctuations $C_x(t)$. We compute $C_x(t)$ for a semiflexible

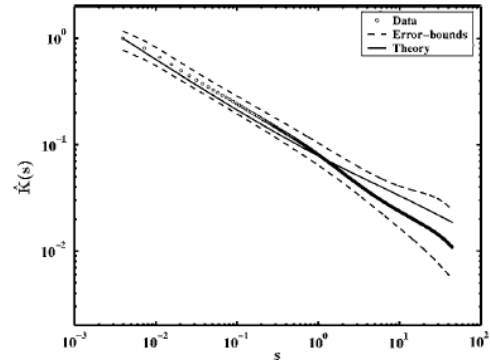


Fig. 3. The comparison of memory kernel (in the Laplace domain) between experiments and polymer chain model. They agree very well within the experimental error bounds.

continuum model of the polymer and use it to determine $K(t)$ via the GLE. The calculations demonstrate that $C_x(t)$ is well approximated by a Mittag-Leffler function and $K(t)$ by a power-law decay on time scales spanning several decades. Both functions depend on a number of parameters characterizing the polymer, including chain length, degree of stiffness, and the number of intervening residues between the two segments. The calculations are compared with the recent observation of a nonexponential $C_x(t)$ and a power law $K(t)$ in the conformational dynamics within single molecule proteins (shown in Fig 3).

Kramers' model with dynamic disorder [7] (Wei Min, graduate student, Prof. Binny Cherayi, on sabbatical from Indian Institute of Science)

To bridge the multi-time-scale conformational fluctuations within a single protein molecule to the dispersed kinetics and dynamic disorder observed in single enzyme turnover experiments [5], we generalized the Kramers model for the rate of chemical reactions in condensed phases by incorporating the newly observed power-law friction kernel into the generalized Langevin equation for a one-dimensional reaction coordinate.

We study this by stochastic simulation of a particle diffusing in a double potential well as shown in Fig. 4a. The first passage time distributions are constructed under different friction constants ζ (Fig. 4b). The friction constant reflects the coupling strength between the reaction coordinate and the other degrees of motions. The deviation of the decay from single exponential behavior is significant when the coupling strength increases.

Determination of thermodynamic driving force from nonequilibrium turnover time traces of single enzymes [6, 9] (Wei Min, graduate student, in collaboration with Professor Hong Qian, University of Washington)

A single enzyme molecule in a living cell usually undergoes biochemical reactions in a nonequilibrium steady state condition. The thermodynamic driving force, $\Delta\mu$, is an important quantity that determines how far the reaction is from equilibrium. Traditionally, this driving force is obtained by measuring substrate and product concentrations and rate constants in ensemble experiments. In contrast, we have recently shown that this driving force for an enzymatic reaction can be determined from the nonequilibrium time traces of enzymatic turnovers of individual enzyme molecules, which can now be experimentally recorded by single molecule techniques (Fig. 5).

We have developed three different $\Delta\mu$ estimators from the principles of nonequilibrium

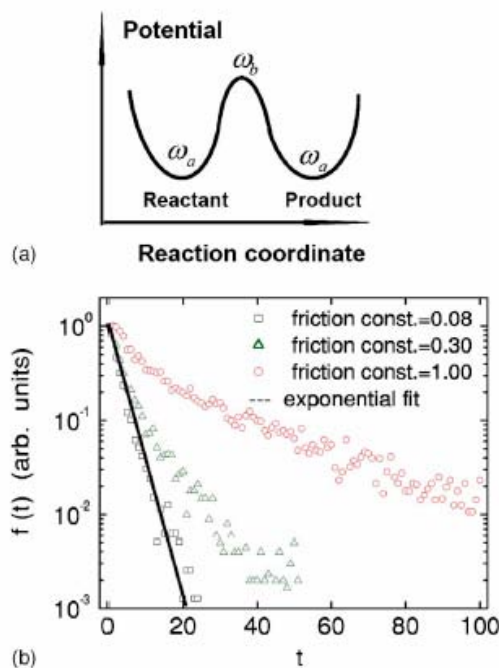


Fig. 4. (a) Symmetric double well potential with well frequency ω_a , barrier frequency ω_b , and barrier height E_a for simulations of barrier crossing. (b) Stochastic simulation of the first passage time distribution for a particle escaping a barrier with power law memory kernel.

statistical mechanics: fluctuation theorem, Kawasaki identity, and fluctuation dissipation theorem,. In particular, a Maximum Likelihood Estimation of $\Delta\mu$ has been derived based on the fluctuation theorem. The statistical precisions of these three $\Delta\mu$ estimators are analyzed and compared for experimental time traces with finite lengths. We believe that this work could provide a general methodology for single-molecule nonequilibrium enzymatic dynamics in living systems.

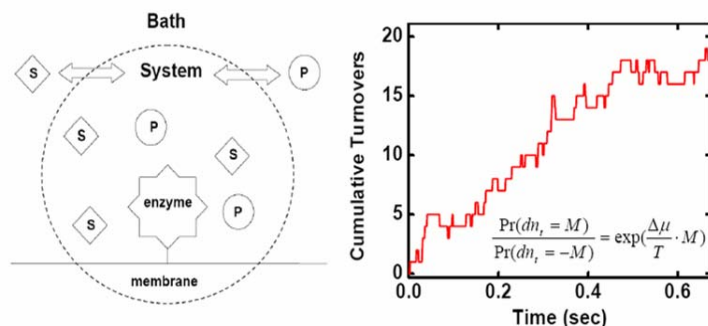


Fig. 5. Illustration of single-molecule enzymatic turnovers under nonequilibrium steady state (NESS). A single enzyme molecule attached on a membrane, surrounded by substrates and products molecules, undergoes catalytic turnovers. The dashed circle denotes an open thermodynamic system, in which substrates are continuously converted to products but their concentration [S] and [P] are held constant due to the exchange with the bath. The right panel shows the Monte-Carlo simulation of the stochastic reaction trajectory, together with the fluctuation theorem relation $\frac{\Pr(dn_t = M)}{\Pr(dn_t = -M)} = \exp\left(\frac{\Delta\mu}{T} \cdot M\right)$.

Publications in 2005-2006 supported by DOE/BES

- (9) Qian, Hong; Xie, X. Sunney "Generalized Haldane Equation and Fluctuation Theorem in The Steady-state Cycle Kinetics of Single Enzymes," *Phys. Rev. E*, **74**, 010902(R) (2006).
- (8) Luo, Guobin; Andricioaei, Ioan; Xie, X. Sunney; Karplus, Martin "Dynamic Distance Disorder in Proteins Is Caused by Trapping," *J. Phys. Chem. B*, **110**, 9363-9367 (2006).
- (7) Min, Wei; Xie, X. Sunney "Kramers Model with a Power-law Friction Kernel: Dispersed Kinetics and Dynamic Disorder of Biochemical Reactions," *Phys. Rev. E* **73**, 010902 (2006).
- (6) Min, Wei; Jiang, Liang; Yu, Ji; Kou, S.C.; Qian, Hong; Xie, X. Sunney "Nonequilibrium Steady State of a Nanometric Biochemical System: Determining the Thermodynamic Driving Force from Single Enzyme Turnover Time Traces," *Nano Lett.* **5**, 2373-2378 (2005).
- (5) Min, Wei; English, Brian P.; Luo, Guobin; Cherayil, Binny J.; Kou, S.C.; Xie, X. Sunney "Fluctuating Enzymes: Lessons from Single-Molecule Studies," *Acc. Chem. Res.* **38**, 923-931 (2005).
- (4) Debnath, Pallavi; Min, Wei; Xie, X. Sunney; Cherayil, Binny J. "Multiple Time Scale Dynamics of Distance Fluctuations in a Semiflexible Polymer: A One-dimensional Generalized Langevin Equation Treatment," *J. Chem. Phys.* **123**, 204903 (2005).
- (3) Krug II, John T.; Sánchez, Erik J. ; and Xie, X. Sunney "Fluorescence Quenching in Tip-enhanced Nonlinear Optical Microscopy," *Appl. Phys. Lett.* **86**, 233102 (2005).
- (2) Kou, S.C.; Xie, X. Sunney; Liu, Jun S. "Bayesian Analysis of Single-molecule Experimental Data," *Appl. Statist.* **54**, 469 (2005).
- (1) Min, Wei; Luo, Guobin; Cherayil, Binny J.; Kou, S.C.; Xie, X. Sunney "Observation of a Power-Law Memory Kernel for Fluctuations within a Single Protein Molecule," *Phys. Rev. Lett.* **94**, 198302 (2005).

*Author
Index*

Author Index

Ahmed, M.	30	Ho, G. S.	1
Anderson, S.	72	Huang, P.	1
Armentrout, P.	76	Jackson, B.	155
Balasubramanian, K.	38	Jackson, K.	128
Bartels, D.	80	Jellinek, J.	128
Beck, K. M.	147	Johnson, M.	159
Camillone, N.	60	Joly, A.G.	147
Carter, E.	1,143	Jordan, K.	159
Castleman, Jr., A. W.	84	Kathmann, S.	52
Ceyer, S. T.	88	Kay, B.	163
Chandler, D.	91	Kimmel, G.	167
Chelikowsky, J.	143	Laverne, J. A.	12
Chipman, D.	46,80	Lee, J.R.I.	9
Cook, A. R.	68,93	Leone, S. R.	30
Cowin, J.	97	Lignères, V.	1
Crowell, R.	56,198	Lim, E.	64
Dang, L.	101	Louie, S.G.	143
De Yoreo, J.J.	9	Lu, H. P.	171
Dove, P.	9	Lymar, S. V.	68,175
Dohnalek, Z.	163	Meisel, D.	179
Duncan, M.	106	Miller, J. R.	68,93
Dupuis, M.	50	Morse, M.D.	34
Eisenthal, K.	110	Morse, D.	9
Ellison, G. B.	114	Ogut, S.	128
Elhadj, S.	9	Osgood, R.	182
El-Sayed, M.	18	Petek, H.	186
Evans, J.	115	Petrik, N. G.	167
Fayer, M.I.	120	Qiu, R.	9
Fenter, P.	10	Ratner, M. A.	5,128
Fu, G.	9	Salter, A.	9
Garrett, B.	42	Saykally, R.	190
Geissler, P.	16	Schatz, G.C.	5,128
Gordon, M.	124	Schenter, G.	194
Gosztola, D.	56,198	Shkrob, I.	56,198
Gray, S.	128	Smith, R.S.	163
Han, Y.	9	Steimle, T.	202
Harris, C.	135	Stockman, M.	128,206
Harris, A.	60	Sverjensky, D.A.	11
Harrison, I.	139	Thompson, W.	210
Hayden, C.	26	Tokmakoff, A.	214
Head-Gordon, M.	143	Tully, J.C.	218
Head-Gordon, T.	22	Wang, D.	9
Hess, W.	147	Wang, L-S.	222
Ho, W.	151	Wang, L.-W.	143

Wesolowski, D.J.	8
White, M.	60
Wierzbicki, A.	9
Wilson, K.R.	30
Wishart, J.	228
Wodtke, A.	230
Xantheas, S.	231
Xie, S.	235
Yang, H.	26

Participants

Participants

Ahmed, Musahid
Lawrence Berkeley National Laboratory
MS 6-2100, 1 Cyclotron road
Berkeley, CA 94720
E-Mail: mahmed@lbl.gov
Phone:(510)486-6355

Armentrout, Peter
University of Utah
Chemistry Dept
315 S. 1400 E. Rm 2020
Salt Lake City, UT 84112
E-Mail: armentrout@chem.utah.edu
Phone:(801)581-7885

Bartels, David
Notre Dame Radiation Laboratory
University of Notre Dame
Notre Dame, IN 46556
E-Mail: bartels.5@nd.edu
Phone:(574)631-5561

Carmichael, Ian
Notre Dame Radiation Laboratory
University of Notre Dame
Notre Dame, IN 46556
E-Mail: carmichael.1@nd.edu
Phone:(574)631-4502

Castleman, Jr., A. Welford
Pennsylvania State University
104 Chemistry Building
University Park, PA 16802
E-Mail: awc@psu.edu
Phone:(814)865-7242

Chandler, David
University of California, Berkeley
208 Gilman Hall, Dept. of Chemistry
Berkeley, CA 94720
E-Mail: chandler@cchem.berkeley.edu
Phone:(510)643-6821

Cook, Andrew
Brookhaven National Lab
Bldg. 555 Chemistry
Upton, NY 11973
E-Mail: acook@bnl.gov
Phone:(631)344-4782

Anderson, Scott
University of Utah
Chemistry Dept/315 S.
1400 E. Rm2020
Salt Lake City, UT 84112
E-Mail: anderson@chem.utah.edu
Phone:(801)585-7289

Balasubramanian, Krishnan
Lawrence Livermore National Laboratory
PO Box 808, L-268
Livermore, CA 94550
E-Mail: balu@csueastbay.edu
Phone:(925)422-4984

Camillone, Nicholas
Brookhaven National Laboratory
Chemistry Department, Bldg 555
Upton, NY 11973
E-Mail: nicholas@bnl.gov
Phone:(631)344-4412

Carter, Emily
Princeton University
Dept. Mechanical & Aerospace Engineering,
EQUAD, Suite D404A, Olden Street
Princeton, NJ 08544
E-Mail: eac@princeton.edu
Phone:(609)258-5391

Ceyer, Sylvia
Massachusetts Institute of Technology
Department of Chemistry, 6-217
77 Mass Ave
Cambridge, MA 02139
E-Mail: stceyer@mit.edu
Phone:(617)253-4537

Chipman, Daniel
Notre Dame Radiation Laboratory
University of Notre Dame
Notre Dame, IN 46556
E-Mail: chipman.1@nd.edu
Phone:(574)631-5562

Cowin, James
Pacific Northwest National Laboratory
M/S K8-88
Richland, WA 99352
E-Mail: jp.cowin@pnl.gov
Phone:(509)376-6330

Participants

Crowell, Robert
Argonne National Laboratory
Chemistry Division
Argonne, IL 60439
E-Mail: rob_crowell@anl.gov
Phone:(630)252-8089

Dang, Liem
Pacific Northwest National Laboratory
PO Box 999, K1-83
Richland, WA 99352
E-Mail: liem.dang@pnl.gov
Phone:(509)375-2557

De Yoreo, Jim
Lawrence Livermore National Laboratory
L-003, PO Box 808
Livermore, CA 94551
E-Mail: deyoreo1@llnl.gov
Phone:(925)423-4240

Duncan, Michael
University of Georgia
Department of Chemistry
Athens, GA 30602
E-Mail: maduncan@uga.edu
Phone:(706)542-1998

Dupuis, Michel
Pacific Northwest National Laboratory
PO Box 999, K1-83
Richland, WA 99352
E-Mail: Michel.Dupuis@pnl.gov
Phone:(509)375-2617

Eisenthal, Kenneth
Columbia University
Department of Chemistry
3000 Broadway, MC 3107
New York, NY 10027
E-Mail: kbe1@columbia.edu
Phone:(212)854-3175

Ellison, Barney
University of Colorado
Department of Chemistry
Boulder, CO 80309
E-Mail: barney@jila.colorado.edu
Phone:(303)492-8603

El-Sayed, Mostafa A.
Georgia Institute of Technology
School of Chemistry and Biochemistry
770 State Street
Atlanta, GA 30332
E-Mail: melsayed@gatech.edu
Phone:(404)894-0292

Evans, James
Ames Laboratory - USDOE
315 Wilhelm Hall
Iowa State University
Ames, IA 50011
E-Mail: evans@ameslab.gov
Phone:(515)294-1638

Fayer, Michael
Stanford University
Department of Chemistry
Stanford, CA 94305
E-Mail: fayer@stanford.edu
Phone:(650)723-4446

Felmy, Andy
Pacific Northwest National Laboratory
PO Box 999, MS K8-96
Richland, WA 99352
E-Mail: ar.felmy@pnl.gov
Phone:(509)376-4079

Fenter, Paul
Argonne National Laboratory
9700 South Cass Avenue
Argonne, IL 60439
E-Mail: fenter@anl.gov
Phone:(630)252-7053

Fiechtner, Gregory
DOE/Basic Energy Sciences
19901 Germantown Road
Germantown, MD 20874
E-Mail: gregory.fiechtner@science.doe.gov
Phone:(301)903-5809

Gaffney, Kelly
SSRL/SLAC
2575 Sand Hill Road
Menlo Park, CA 94025
E-Mail: kgaffney@slac.stanford.edu
Phone:(650)926-2382

Participants

Garrett, Bruce
Pacific Northwest National Laboratory
PO Box 999, MSIN K9-90
Richland, WA 99352
E-Mail: bruce.garrett@pnl.gov
Phone:(509)372-6344

Geissler, Phillip
University of California, Berkeley
207 Gilman Hall, Dept. of Chemistry
Berkeley, CA 94720
E-Mail: pgeissler@cchem.berkeley.edu
Phone:(510)652-8716

Gordon, Mark
Ames National Laboratory
201 Spedding Hall
Iowa State University
Ames, IA 50011
E-Mail: mark@si.fi.ameslab.gov
Phone:(515)294-0452

Gosztola, David
Argonne National Laboratory
9700 S. Cass Ave.
Argonne, IL 60439
E-Mail: gosztola@anl.gov
Phone:(630)252-3541

Gray, Stephen
Argonne National Laboratory
Chemistry Division
Argonne National Laboratory
Argonne, IL 60439
E-Mail: gray@tcg.anl.gov
Phone:(630)252-3594

Harris, Alex
Brookhaven National Laboratory
Chemistry Department, Building 555
PO Box 5000
Upton, NY 11973
E-Mail: alexh@bnl.gov
Phone:(631)344-4301

Harris, Charles
Lawrence Berkeley National Laboratory
Chemical Science Division
Berkeley, CA 94720
E-Mail: cbharris@berkeley.edu
Phone:(510)642-2814

Harrison, Ian
University of Virginia
Department of Chemistry
P.O. Box 400319
Charlottesville, VA 22904
E-Mail: harrison@virginia.edu
Phone:(434)924-3639

Hayden, Carl
Sandia National Laboratories
P.O. Box 969, MS 9055
Livermore, CA 94551
E-Mail: cchayde@sandia.gov
Phone:(925)294-2298

Head-Gordon, Teresa
LBNL and University of California, Berkeley
Calvin 204
Berkeley, CA 94720
E-Mail: TLHead-Gordon@lbl.gov
Phone:(510)486-7365

Hess, Wayne
Pacific Northwest National Laboratory
902 Battelle Blvd
Richland, WA 99352
E-Mail: wayne.hess@pnl.gov
Phone:(509)376-9907

Hilderbrandt, Richard
DOE/BES SC22.1
19901 Germantown Rd.
Germantown, MD 20874
E-Mail: Richard.Hilderbrandt@science.doe.gov
Phone:(301)903-0035

Ho, Wilson
University of California, Irvine
Department of Physics and Astronomy
Irvine, CA 92697
E-Mail: wilsonho@uci.edu
Phone:(949)824-5234

Jackson, Bret
University of Massachusetts
Dept of Chemistry
Amherst, MA 01003
E-Mail: jackson@chem.umass.edu
Phone:(413)545-2583

Participants

Jellinek, Julius
Argonne National Laboratory
Chemistry Division
9700 S. Cass Ave.
Argonne, IL 60439
E-Mail: jellinek@anl.gov
Phone:(630)252-3463

Jordan, Kenneth
University of Pittsburgh
Dept. of Chemistry
Pittsburgh, PA 15260
E-Mail: jordan@pitt.edu
Phone:(412)624-8690

Kay, Bruce
Pacific Northwest National Laboratory
Mail Stop K8-88, PO Box 999
Richland, WA 99352
E-Mail: bruce.kay@pnl.gov
Phone:(509)376-0028

LaVerne, Jay
University of Notre Dame
314 Radiation Laboratory
Notre Dame, IN 46556
E-Mail: laverne.1@nd.edu
Phone:(574)631-5563

Linne, Mark
Sandia National Labs
P.O. Box 969, MS 9055
Livermore, CA 94551
E-Mail: mlinne@sandia.gov
Phone:(925)294-3704

Lymar, Sergei
Brookhaven National Laboratory
Chemistry Department, BLDG 555,
Upton, NY 11973
E-Mail: lymar@bnl.gov
Phone:(631)344-4333

Meisel, Dan
University of Notre Dame
Radiation Laboratory
Notre Dame, IN 46556
E-Mail: dani@nd.edu
Phone:(574) 631-5457

Johnson, Mark
Yale University
Sterling Chemistry Lab
P.O. Box 208107
New Haven, CT 06520
E-Mail: mark.johnson@yale.edu
Phone:(203)432-5226

Kathmann, Shawn
Pacific Northwest National Laboratory
PO Box 999, K1-83
Richland, WA 99352
E-Mail: shawn.kathmann@pnl.gov
Phone:(509)375-2870

Kimmel, Greg
Pacific Northwest National Laboratory
MSIN K8-88, PO Box 999
Richland, WA 99352
E-Mail: gregory.kimmel@pnl.gov
Phone:(509)376-2501

Lim, Edward
The University of Akron
Knight Chemical Laboratory
Akron, OH 44325
E-Mail: elim@uakron.edu
Phone:(330)972-5297

Lu, H. Peter
Bowling Green State University
Department of Chemistry and
Center for Photochemical Sciences
Bowling Green, OH 43403
E-Mail: hplu@bgnet.bgsu.edu
Phone:(419)372-1840

Marceau, Diane
US DOE Office of Basic Energy Sciences/SC-22.1
19901 Germantown Road
Germantown, MD 20874
E-Mail: diane.marceau@science.doe.gov
Phone:(301)903-0235

Meza, Juan
Lawrence Berkeley National Laboratory
1 Cyclotron Rd. MS 50B4230
Berkeley, CA 94720
E-Mail: jcmeza@lbl.gov
Phone:(510)486-7684

Participants

Miller, John
Brookhaven National Lab
Bld 555A
Upton, NY 11973
E-Mail: jrmiller@bnl.gov
Phone:(631)344-4354

Morse, Michael
University of Utah
Department of Chemistry
315 S. 1400 East, Room 2020
Salt Lake City, UT 84112
E-Mail: morse@chem.utah.edu
Phone:(801)581-8319

Mundy, Chris
Pacific Northwest National Laboratory
PO Box 999, K1-83
Richland, WA 99352
E-Mail: donna.sturdevant@pnl.gov
Phone:(509)372-6151

Osgood, Richard
Columbia University
500 West 120th Street
New York, NY 10027
E-Mail: osgood@columbia.edu
Phone:(212)854-4462

Petek, Hrvoje
University of Pittsburgh
Department of Physics and Astronomy
3941 O'hara St.
Pittsburgh, PA 15260
E-Mail: Petek@pitt.edu
Phone:(412)624-3599

Rohlfing, Eric
US DOE Office of Basic Energy Sciences/SC-22.1
19901 Germantown Road
Germantown, MD 20874
E-Mail: eric.rohlfing@science.doe.gov
Phone:(301)903-8165

Saykally, Rich
University of California
Department of Chemistry
Berkeley, CA 94720
E-Mail: saykally@berkeley.edu
Phone:(510)642-8269

Schatz, George
Northwestern University
Department of Chemistry
Evanston, IL 60208
E-Mail: schatz@chem.northwestern.edu
Phone:(847)491-5657

Schenter, Gregory
Pacific Northwest National Laboratory
PO Box 999, K1-83
Richland, WA 99352
E-Mail: gregory.schenter@pnl.gov
Phone:(509) 375-4334

Shkrob, Ilya
Argonne National Laboratory
9700 South Cass Avenue
Argonne, IL 60439
E-Mail: shkrob@anl.gov
Phone:(630)252-9516

Steimle, Timothy
Arizona State University
Department of Chemistry
Tempe, AZ 85287
E-Mail: tsteimle@asu.edu
Phone:(480)965-3265

Stockman, Mark
Georgia State University
Department of Physics and Astronomy
Atlanta, GA 30303
E-Mail: mstockman@gsu.edu
Phone:(404)651-2779

Sverjensky, Dimitri
The Johns Hopkins University
Department of Earth & Planetary Sciences
Baltimore, MD 21218
E-Mail: sver@jhu.edu
Phone:(410)516-8568

Thompson, Ward
University of Kansas
Department of Chemistry
Lawrence, KS 66045
E-Mail: wthompson@ku.edu
Phone:(785)-864-3980

Participants

Tokmakoff, Andrei
Massachusetts Institute of Technology
Department of Chemistry
77 Massachusetts Ave., Room 6-225
Cambridge, MA 02139
E-Mail: tokmakof@mit.edu
Phone:(617)253-4503

Tully, John
Yale University
Dept of Chemistry
PO Box 208107
New Haven, CT 06520
E-Mail: john.tully@yale.edu
Phone:(203)432-3934

Wang, Lai-Sheng
Washington State University/PNNL
2710 University Drive
Richland, WA 99354
E-Mail: ls.wang@pnl.gov
Phone:(509)376-8709

White, Michael
Brookhaven National Laboratory and
Stony Brook University
Chemistry Department
Upton, NY 11973
E-Mail: mgwhite@bnl.gov
Phone:(631)344-4345

Wishart, James
Brookhaven National Laboratory
Chemistry Department
Upton, NY 11973
E-Mail: wishart@bnl.gov
Phone:(631)344-4327

Xantheas, Sotiris
Pacific Northwest National Laboratory
PO Box 999, K1-83
Richland, WA 99352
E-Mail: sotiris.xantheas@pnl.gov
Phone:(509)375-3684

Tully, Frank
US DOE Office of Basic Energy Sciences/SC-22.1
19901 Germantown Road
Germantown, MD 20874
E-Mail: frank.tully@science.doe.gov
Phone:(301)903-5998

Wagner, Albert
Argonne National Laboratory
Chemistry Division
9700 S. Cass Avenue, Bldg. 200
Argonne, IL 60439
E-Mail: wagner@tcg.anl.gov
Phone:(630)252-3570

Wesolowski, David J.
Oak Ridge National Laboratory
P.O. Box 2008
Oak Ridge, TN 37831
E-Mail: wesolowskid@ornl.gov
Phone:(865)574-6903

Windus, Theresa
Iowa State University
Department of Chemistry
1651 Gilman Hall
Ames, IA 50010
E-Mail: theresa@fi.ameslab.gov
Phone:(515)294-6134

Wodtke, Alec
University of California, Santa Barbara
Chemistry Department
Santa Barbara, CA 93106
E-Mail: wodtke@chem.ucsb.edu
Phone:(805)893-8085

Xie, Xiaoliang
Harvard University
Department of Chemistry
12 Oxford Street
Cambridge, MA 02138
E-Mail: xie@chemistry.harvard.edu
Phone:(617)495-9925